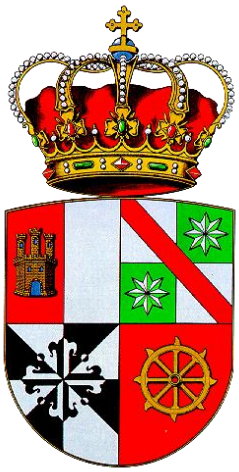

UNIVERSITY OF CASTILLA-LA MANCHA

FACULTY OF CHEMICAL SCIENCES AND TECHNOLOGIES

Department of Inorganic, Organic Chemistry and Biochemistry

SYNTHESIS OF BIODEGRADABLE POLYMERIC MATERIALS CATALYSED BY GROUP 13 METAL COMPLEXES

Dissertation submitted by

MARC MARTÍNEZ DE SARASA BUCHACA

To apply for the degree of

International Doctor in Chemical Sciences

Ciudad Real, July 2021

D. AGUSTÍN LARA SÁNCHEZ, Inorganic Chemistry Professor at University of Castilla-La Mancha.

D. JOSÉ ANTONIO CASTRO OSMA, Inorganic Chemistry Doctor at University of Castilla-La Mancha.

CERTIFY:

That the present research project: **"SYNTHESIS OF BIODEGRADABLE POLYMERIC MATERIALS CATALYSED BY GROUP 13 METAL COMPLEXES"** represents the Dissertation Marc Martínez de Sarasa Buchaca presents to apply for the International Doctorate Degree by the University of Castilla-La Mancha, has been performed under their management in the Inorganic, Organic Chemistry and Biochemistry Department, fulfilling all the necessary requirements.

And as evidence thereof, this certificate is issued and signed in Ciudad Real, in June 2021.

Fdo.: **Prof. Agustín Lara Sánchez** Fdo.: **Dr. José Antonio Castro Osma**

Table of contents

Abbreviations

Å	Angstrom
ACEN	N,N'-ethylenbis(acetylacetoneiminate)
aNHC	abnormal N-heterocyclic carbene
Ar	Aryl
ATR	Attenuated total reflectance
BBL	*β*-butyrolactone
BGDC	1,4-butanediol bis(glycidyl ether carbonate)
BGDE	1,4-butanediol bis-glycidyl ether
BGLBC	bis(glutaryl carbonate)
bdmpzm	Bis(3,5-dimethylpyrazol-1-yl)methane
bdmtzm	Bis(3,5-dimethyltriazol-1-yl)methane
Bn	Benzyl
bpzm	Bis(pyrazol-1-yl)methane
btzm	Bis(triazol-1-yl)methane
bptzom	1,1'-((2-methoxyphenyl)methylene)bis(4-phenyl-1H-1,2,3-triazole)
bptzpm	1,1'-((4-methoxyphenyl)methylene) bis(4-phenyl-1H-1,2,3-triazole)
bttzom	1,1'-((2-methoxyphenyl)methylene)bis(4-(trimethylsilyl)-1H-1,2,3-triazole)
bttzpm	1,1'-((4-methoxyphenyl)methylene)bis(4-(trimethylsilyl)-1H-1,2,3-triazole)
bptz(NMe_2)om	1,1'-((4-methoxyphenyl)methylene)bis(3-methyl-4-phenyl-1H-1,2,3-triazol-3-ium) triflate
bttz(NMe_2)pm	1,1'-((2-methoxyphenyl)methylene)bis(3-methyl-4-(trimethylsilyl)-1H-1,2,3-triazol-3-ium)triflate
bptzombeH	1-(1-((2-methoxyphenyl)(4-phenyl-1H-1,2,3-triazol-1-yl)methyl)-4-phenyl-1H-1,2,3-triazol-5-yl)-2,2-dimethylpropan-1-ol
bptzomteH	2-(2-methoxyphenyl)-2,2-bis(4-phenyl-1H-1,2,3-triazol-1-yl)-1-(p-tolyl)ethan-1-ol
bptzpmbeH	1-(1-((4- methoxyphenyl)(4-phenyl-1H-1,2,3-triazol-1-yl)methyl)-4-phenyl-1H-1,2,3-triazol-5-yl)-2,2-dimethylpropan-1-ol
bptzpmmabzeH	1- (4-(dimethylamino)phenyl)-2-(4-methoxyphenyl)-2,2-bis(4-phenyl-1H-1,2,3-triazol-1-yl)ethan-1-ol]
bptzpmteH	2- (4-methoxyphenyl)-1-(p-tolyl)-2,2-bis(4-(trimethylsilyl)-1H1,2,3-triazol-1-yl) ethan-1-ol
bpzappeH	(2,2-bis(3,5-dimethyl-1H-pyrazol-1-yl)-1-(4-(dimethylamino)phenyl)-1phenylethan-1-ol
bpzbeH	(1,1-bis(3,5-dimethyl-1H-pyrazol-1-yl)-3,3-dimethylbutan-2-ol
bpzFerrH	(2,2-bis(3,5-dimethyl-1H-pyrazol-1-yl)-1-ferrocenyl)ethan-1-ol
bpzteH	(2,2-bis(3,5-dimethyl-1H-pyrazol-1-yl)-1-*p*-tolyl)ethan-1-ol
bttzombeH	1- (1-((2-methoxyphenyl)(4-(trimethylsilyl)-1H-1,2,3-triazol-1-yl)methyl)-4-(trimethylsilyl)-1H-1,2,3-triazol-5-yl)- 2,2-dimethyl propan-1-ol
bttzomteH	2- (2-methoxyphenyl)-1-(p-tolyl)-2,2-bis(4-(trimethylsilyl)-1H-1,2,3-triazol-1-yl)ethan-1-ol
bttzpmbeH	1- (1-((4-methoxyphenyl)(4-(trimethylsilyl)-1H-1,2,3-triazol-1-yl)methyl)-4-(trimethylsilyl)-1H-1,2,3-triazol-5-yl)-2,2-dimethylpropan-1-ol

bttzpmmabzeH	1-(4-(dimethylamino)phenyl)-2,2-bis(4-(trimethylsilyl)-1H-1,2,3-triazol-1-yl)ethan-1-ol
bttzpmteH	2-(4-methoxyphenyl)-1-(p-tolyl)-2,2-bis(4-(trimethylsilyl)-1H1,2,3-triazol-1-yl) ethan-1-ol
BDA	1,4-Diaminobutane
Bu	Butyl
c	Concentration
c	Correction factor
CA	Camphoric anhydride
CABE	Carvyl acetate bis-epoxide
CABC	Carvyl acetate bis(cyclic carbonate)
CHC	Cyclohexene carbonate
CHD	Cyclohexanediol
CHO	Cyclohexene oxide
CL	*ε*-caprolactone
CO_2	Carbon dioxide
Cp	Cyclopentadienyl
CPrA	Cyclopropene 1,2-dicarboxylic anhydride
CSBO	Carbonated soybean oil
CSFO	Carbonated sunflower oil
Da	Daltons
DBU	1,8-Diazabicyclo(5.4.0)undec-7-ene
DL	*ε*-decalactone
DMAP	4-(dimethylamino)pyridine
DMC	Dimethyl carbonate
DMSO	Dimethyl sulfoxide
DSC	Differential Scanning Calorimetry
E_a	Activation energy
EDA	Ethanediamine
Et	Ethyl
EtOAc	Ethyl Acetate
EtOH	Ethanol
DETA	Diethylenetriamine
GPC	Gel Permeation Chromatography
HDMA	1,6-hexanediamine
IPDA	Isophorone diamine
^{i}Pr	Iso-propyl
^{i}PrOH	Iso-propanol
k	Rate constant
k_B	Boltzmann constant
k_{obs}	Observed rate constant
L	Ligand

L-LA	*L*-Lactide
LO	Limonene oxide
m	*meta* position in an aromatic ring
M	Metal
MA	Maleic anhydride
MALDI-ToF	Matrix Assisted Laser Desorption Ionisation Time-of-Flight
Me	Methyl
MeOH	Methanol
M_n	Average molecular weight in number
M_w	Average molecular weigth
N	Number of molecules
NA	Norborene anhydride
NHC	N-heterocyclic carbene
NIPU	Non-isocyanate polyurethane
NMI	*N*-methyl imidazole
NNN	Heteroscorpionate ligand with a coordination capacity through three nitrogen atoms
NNO	Heteroscorpionate ligand with a coordination capacity through two nitrogen atoms and one oxygen atom
Nu	Nucleophile
o	*ortho* position in an aromatic ring
ORTEP	Oak Ridge Termal Ellipsoid Plot
p	*para* position in an aromatic ring
PA	Phthalic anhydride
PC	Polycarbonate
PCHC	Poly(cyclohexene carbonate)
PCHO	Poly(cyclohexene oxide)
PCL	Poly(ε-caprolactone)
PDL	Poly(ε-decalactone)
PDI	Polidispersity index or molecular weight distribution
PE	Polyester
Ph	Phenyl
PHB	Poly(hydroxybutyrate)
PHU	Polyhydroxyurethane
PLA	Polylactide
PLC	Poly(limonene carbonate)
PLCO	Poly(limonene carbonate) oxide
PLDC	Poly(limonene dicarbonate)
PLO	Poly(limonene oxide)
PO	Propylene oxide
PPC	Poly(propylene carbonate)
PPDA	Paraphenylenediamine
PPNBr	bis(triphenylphosphine)iminium bromide

PPNCl	bis(triphenylphosphine)iminium chloride
PPNDNP	bis(triphenylphosphine)iminium 2,4-dinitrophenolate
PPNI	bis(triphenylphosphine)iminium iodide
Py	Pyridine
pz	Pirazolyl
R^2	Regression coeficient
ROCOP	Ring-Opening Copolymerisation
ROP	Ring-Opening Polymerisation
r.t.	room temperature
SALAN	N,N'-bis(salicylidene)ethyleneaniline
SALCY	N,N'-bis(salicylidene)cyclohexylenediamine
SALEN	N,N'-bis(salicylidene)ethylenediamine
SALOPHEN	N,N'-bis(salicylidene)phenylenediamine
SO	Styrene oxide
T	Temperature
TBAB	tetrabutylammonium bromide
TBAC	tetrabutylammonium chloride
TBAI	tetrabutylammonium iodide
TBD	1,5,7-Triazabicyclodec-5-ene
^{t}Bu	*tert*-butyl
T_g	Glass transition temperature
TGA	Thermogravimetric analysis
THF	Tetrahydrofurane
TMS	tetramethylsilane
TOF	Turnover frequency
TON	Turnover number
VCHO	Vinylcylohexene oxide
v	rate of a reaction
X	Alkyl, aryl or halide ligand
Z	Cell unit
τ	Trigonality index
α	Angle
β	Angle
μ_n	Bridge
κ^n	Denticity

Abbreviations employed in spectroscopy

Brs	Broad singlet
DOSY	Diffusion-Ordered NMR Spectroscopy
g-HSQC	Gradient-Heteronuclear Sensitive Quantum Correlation
Hz	Hertz

IR	Infrared
J	Coupling constant
NOESY	Nuclear Overhauser Enhancement Spectroscopy
ppm	parts per million
NMR	Nuclear magnetic resonance
^{1}H-NMR	proton NMR
^{1}H-^{13}C-*g*-HSQC	Proton and Carbon Heteronuclear correlation experiments
^{1}H-^{13}C-HMBC	Long distance proton and carbon heteronuclear correlation experiments
^{13}C-NMR	Carbon NMR
^{13}C-{^{1}H}-NMR	proton decoupled carbon NMR
VT NMR	Variable temperature nuclear magnetic resonance
δ	Chemical shift
ν	Tension's vibration
d	Doublet
m	Multiplet
s	Singlet
t	Triplet

General procedures

The synthesis of organometallic compounds has been carried out under inert atmosphere, using N-50 type nitrogen, supplied by Air Liquide (O_2 < 2 ppm; H_2O < 2 ppm; CO/CO_2 < 0.5 ppm). In order to maintain these conditions, the synthesis of organometallic complexes has been carried out in a vacuum line provided of a double shut-off valves (vacuum/inert gas), employing Schlenk or GloveBox techniques. The synthesis of organic compounds under catalytic conditions has been carried out either using inert atmosphere or under O_2 atmosphere.

The solvents employed for all the preparations have been purified and dried according to the methods described in bibliography (*Perrin, D. D.; Armarego, W. L. F.; Perrin, D. R. "Purification of laboratory Chemicals" 2ª Ed. Pergamon Press Ltd. Oxford,* ***1980***), distilled and stored under inert atmosphere prior to their use.

STRUCTURAL CHARACTERISATION TECHNIQUES

1. Elemental carbon, hydrogen, and nitrogen analysis

The quantitative elemental analysis of carbon, hydrogen and nitrogen of all the compounds described in this dissertation was performed by "Servicio Interdepartamental de Investigación de la Facultad de Ciencias de la Universidad Autónoma de Madrid" and, in some cases, by the "Servicio Instrumental de la Universidad de Alcalá".

2. MALDI-ToF mass spectrometry

Mass spectrometry was carried out using a Bruker Autoflex II TOF/TOF of the "Departamento de Química Inorgánica, Orgánica y Bioquímica de la Facultad de Ciencias y Tecnologías Químicas de la Universidad de Castilla-La Mancha", employing dithranol and sodium acetate as matrix. The excitement of the sample (1:100 ratio with respect to the matrix) was performed in a positive mode.

3. Infrared spectroscopy

Infrared spectra were aquired using a Fourier transform infrared spectrophotometer (FT-IR) Simadzu IR Prestige-21, which incorporates an ATR (attenuated total

reflectance) with a ZnSe lens. The most characteristic bands for each compound are given.

4. Nuclear magnetic resonance spectrometry

NMR spectra were acquired in three different spectrometers: VARIAN GEMINI FT-400 (400 MHz for ^{1}H-NMR and 100 MHz for ^{13}C-NMR), VARIAN INOVA FT-500 (500 MHz for ^{1}H-NMR and 125 MHz for ^{13}C-NMR) and Bruker Ascend TM-500 (500 MHz for ^{1}H-NMR and 125 MHz for ^{13}C-NMR).

Chemical shifts (δ) are expressed in ppm with respect to TMS, taking as internal reference the deuterated solvent signals. Coupling constants (J) are expressed in Hz.

5. X-Ray Diffraction Analysis

The determination of the X-Ray Crystal structures presented in this dissertation were carried out by Dra. Ana Mª Rodríguez Fernández-Pacheco, from the "E.T.S. de Ingenieros Industriales de la UCLM", within the "Departamento de Química Inorgánica, Orgánica y Bioquímica" and by Dr. Antonio Rodríguez Diéguez from "Universidad de Granada", within the "Departamento de Química Inorgánica". For this, two different diffractometers were used:

- Bruker X8 APPEX II, of the "Departamento de Química Inorgánica, Orgánica y Bioquímica de la Facultad de Ciencias y Tecnologías Químicas de la Universidad de Castilla-La Mancha".
- Bruker D8 VENTURE, of the "Departamento de Química Inorgánica de la Universidad de Granada".

6. Gel permeation chromatography (GPC)

The molecular weight determination and the polydispersity values of the poly(cyclohexene carbonate) and the terpolymers samples have been performed using a Shimadzu LC-20A GPC model, equipped with a TSK-Gel G3000H_{XL} 30 cm x 7.8 mm ID column and a RID-20A refractive index detector model, using THF as eluent at 25 ºC temperature. On the other hand, the determination of the molecular weight and dispersity values for the polyurethane samples has been carried out using a Waters 1515 model, equipped with three different columns: 1x PSS GRAM precolumn 10μm 8x50 mm, 1x PSS GRAM column 10μm 30 Å 8x300 mm and 1x PSS GRAM column

10μm 1000 Å 8x300 mm and a Waters 2414 Refractive Index Detector model, using N,N-dimethylacetamide as solvent at 25 ºC temperature.

7. Thermogravimetric analysis (TGA) and differential scanning calorimetry (DSC)

The thermogravimetric analysis of the synthesised polymers was carried out using a TGA-Q50 instrument, with a heating rate for the sample of 10 ºC/min and a nitrogen flow of 60 mL/min. As for the determination of the glass transition temperature (T_g), a DSC-Q20 instrument was employed. Samples were weighed in aluminium cresol (5 mg) and were subjected to two heating cycles with a heating rate of 10 ºC/min.

General introduction and objectives

At the beginning of the 21st century, around six billion people lived on earth, and this cypher continues to grow with time, reaching almost eight billion people nowadays. Because of this massive increase, humanity is facing serious problems such as food shortage, deficiencies in resources and energy, climate change and global environmental pollution. Science and technology have worked together throughout history and made astonishing progress during the last century to improve our life. In this context, a wide range of synthetic polymers have been developed and used as synthetic fibres, plastics and synthetic rubbers replacing the traditionally used natural fibres, woods, and natural rubbers. These polymeric materials are present in our daily life and find use in a wide range of fields such as transportation, packaging and clothing industry, construction, biomedical (drug delivery systems, tissue engineering), agrochemical, etc. Nowadays, around 370 million tons of plastics are produced annually worldwide, and the production and consumption continue to increase. However, most of these polymeric materials are petroleum-based, and the constant increase on their demand causes the increase in oil consumption. Besides, and more importantly, their higher durability compared to the natural occurring polymers aggravates the environmental situation because of the wasted and undegraded polymers.

In light of this situation, different strategies have been taken to solve this problem. Firstly, governments from all over the world have taken action and applied stronger policies into the recycling of wasted plastics. According to Plastics Europe, around 10 million tons of plastic from post-consumer waste and 7.5 million tons of plastic from the packaging industry were recycled in the European Union in 2018. In fact, Spain is among the countries which recycles the most along with Czech Republic and the Netherlands, with recycling rates over 40% of the plastics generated yearly. However, this recycling policy is not enough to stop the plastic contamination and pollution problem, since the 25 and the 18.5% of the plastic collected post-consumer waste and from packaging industry are destined to landfill. This is because, in the context of plastic recycling processes, regardless it is material recycling or chemical recycling, it consumes a lot of thermal energy and plastics can not be recycled forever, meaning that they have a life cycle and eventually are destined to burn or be buried in land. After having exposed this enormous issue, it is easy to understand why biodegradable polymers are needed.

During the last few decades, the scientific community has focused on the synthesis of biodegradable polymers as an alternative to petroleum-based polymers. We have designed new synthetic routes to generate these polymers using CO_2 and bio-derived compounds as feedstocks. Taking this into account, the main objectives of this dissertation have been:

1. The synthesis and characterisation of new group 13 metal complexes supported by heteroscorpionate ligands and their use as catalysts in polymerisation processes.
2. The synthesis and characterisation of biodegradable polymers using CO_2 and biomass derived compounds as feedstocks by Ring-Opening Polymerisation (ROP), Ring-Opening Copolymerisation (ROCOP) and polyaddition processes.

For that purpose and in order to obtain the International Ph.D. degree, this dissertation has been organised in five Chapters. Each chapter has been divided in four different parts including an introduction, a results and discussion section, an experimental section and the bibliographic references. Finally, a conclusion section at the end collects the most relevant results obtained.

Chapter 1 is focused on the synthesis and characterisation of new homo and heterobimetallic group 13 metal complexes supported by alkoxide heteroscorpionate ligands base on bis(pyrazol-1-yl)methane moieties. Chloride, alkyl, alkoxide and amido complexes have been prepared. In addition, their activity for the synthesis of polycarbonate and terpolymers by ring opening polymerisation has been tested.

Chapter 2 contains the results of the synthesis and characterisation of biodegradable polyesters materials prepared by ROCOP of epoxides and cyclic anhydrides catalysed by heteroscorpionate aluminium complexes. Different polyesters, including a newly synthesised poly(limonene succinate), have been prepared.

Chapter 3 describes the results of the synthesis and characterisation of biodegradable polycarbonates by ROCOP of epoxides and CO_2 and terpolymers by ROCOP and ROP processes of epoxides, CO_2 and *L*-lactide using the group 13 metal complexes previously described in Chapter 1 as catalysts.

Chapter 4 contains the results of the synthesis and characterisation of polyurethanes by polyaddition reaction of bis(cyclic carbonates) and diamines. The Chapter has been divided into two different sections depending on the nature of the bis(cyclic carbonate) employed.

Finally, Chapter 5 focuses on the synthesis and characterisation of new nitrogen ligands functionalised with alcohol groups based on bis(1,2,3-triazol-1-yl)methane moieties and their coordination to aluminium and zinc atoms. Also, quaternisation of the bis(1,2,3-triazol-1-yl)methane precursors and further preparation of *abnormal* N-heterocyclic carbene (*a*NHC) iridium complexes has been performed.

Chapter 1.

Group 13 metal complexes supported by heteroscorpionate ligands

Introduction

The catalysts designed to study the catalytic processes described in this dissertation contain heteroscorpionate ligands derived from the bis(3,5-dimethylpyrazol-1-yl) methane (bdmpzm) moiety. Thus, this first section of Chapter 1 will be aimed to review the most important features of these type of ligands and their coordination to group 13 metals.

1. General considerations of heteroscorpionate ligands

Scorpionate ligands represent one of the most versatile tridentate ligands with the general structure $[RR'B(pz)_2]^-$, where pz is either an unsubstituted or C-substituted pyrazolyl group that can coordinate to metals to give rise to complexes with the formula $[M\{RR'B(\mu\text{-}pz)_2\}L_n]$. This type of ligands can coordinate to a wide variety of elements, being known compounds either for main group metals or for early to late transition metals.[1] In these complexes, a six-membered ring is formed and, in most instances, exhibits a boat conformation where the pseudo-axial R' group is directed towards the metal, as shown in Figure 1.

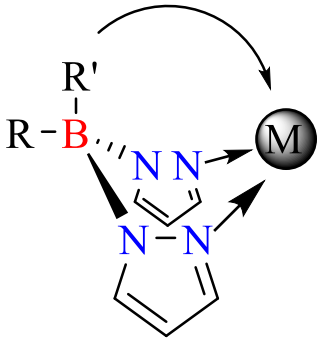

R' = -H, -OR, -SR, -NR_2, -pz, C-H agosthic

Figure 1

If R' is a pyrazole ring identical to the bridging pyrazole groups, the ligand contains a C_{3v} symmetry, $[RB(pz)_3]^-$. These ligands are referred to as "homoscorpionate" or "scorpionate" in the literature. If neither R nor R' is a pyrazole group, but hydrogen, alkyl, aryl, alkoxide, amido etc., then the ligands are described as "heteroscorpionate", a description that also includes ligands where R' is a pyrazolyl group different from the two bridging pyrazolyl units. There is a wide array of other types of heteroscorpionate ligands described in the literature in which the boron atom is replaced by other elements such as aluminium, indium, gallium, carbon, silicon etc. Such a change can either preserve or alter the charge of the ligand.

1.1. Heteroscorpionate ligands derived from bis(pyrazol-1-yl)methane

In this section, the chemistry of a specific class of heteroscorpionate ligands derived from the bis(pyrazol-1-yl)methane[2] moiety with general formula $[RR'C(pz)_2]^-$ will be revised. In this type of ligands the R–B–R' moiety has been substituted for R–C–R' as shown in Figure 2.

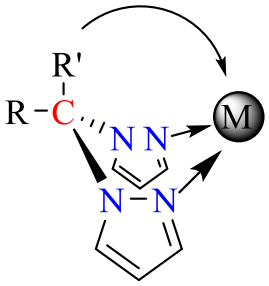

R'= -H, -OR, -SR, $-NR_2$, -pz, C-H agosthic

Figure 2

This class of ligands exhibits a series of advantages such as easy synthetic procedure, versatility in its coordination mode, and, after deprotonation, monoanionic character. This section will describe the synthetic methodologies to prepare this type of ligands, focusing specially on one of the processes which was firstly developed by our research group.

1.1.1. Preparative methods for heteroscorpionate ligands

Heteroscorpionate ligands derived from the bis(pyrazol-1-yl)methane have been prepared using four different synthetic routes:

a.- Reaction of aldehydes or ketones with carbonyl pyrazole or sulfonyl pyrazole using 1% mol $CoCl_2 \cdot 6H_2O$ as a catalyst (Scheme 1). This synthetic route was introduced by Peterson *et al.* in the seventies,[3] although other research groups have used this route to develop new heteroscorpionate ligands.[3d,4] Thus, as an example, 2-hydroxyphenylbis(pyrazol-1-yl)methane (NNO) derivatives can be obtained by reacting bis(pyrazol-1-yl)ketone with salicylaldehyde.

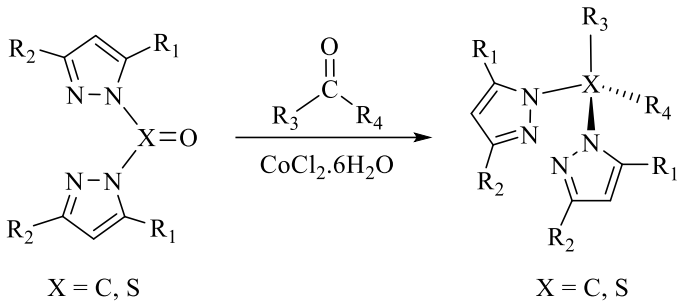

Scheme 1

b.- Reaction of two pyrazole rings with gem-dihalides, acetals or aldehydes, incorporating the R' moiety with coordination capacity within their structure.[5]

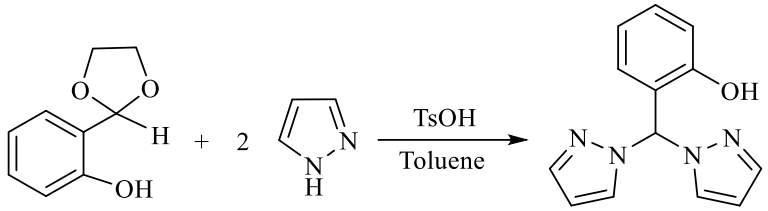

Scheme 2

A wide range of heteroscorpionate ligands featuring mainly phenol and thiol groups has been synthesised using these two methods (Figure 3).

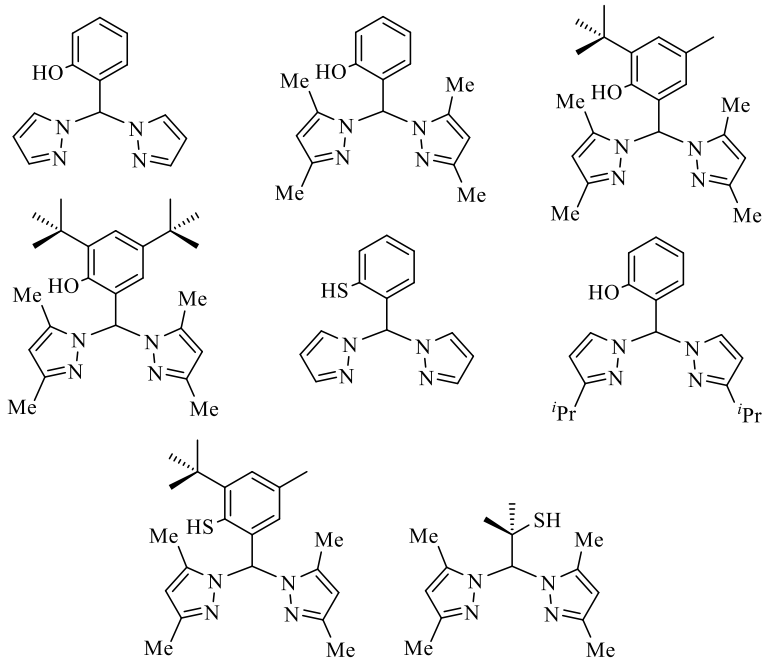

Figure 3. *Heteroscorpionate ligands functionalised with phenol and thiol groups*.

c.- A third synthetic method, firstly described by our research group, consists in the lithiation of bis(pyrazol-1-yl)methane, followed by the addition of an electrophile, which introduces the "E" group with coordination ability in the methylene bridging group (Scheme 3).[6,7] In this case, the use of C5-substituted pyrazole rings is necessary in order to avoid deprotonation at the C5 position. Using this synthetic route, a wide range of heteroscorpionate ligands have been synthesised.

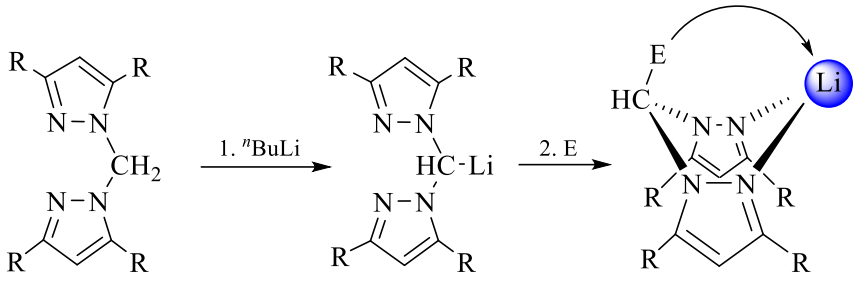

Scheme 3

Some examples for the preparation of ligands following this synthetic route are collected in Figure 4. Thus: **i**) By reaction with carbon dioxide or carbon disulfide, heteroscorpionate ligands functionalised with acetate or dithioacetate groups were obtained.[6,7,8] **ii**) By reduction of these, heteroscorpionate ligands functionalised with ethoxide or thioetoxide groups were prepared.[7a] **iii**–***v***) By reaction of the lithiated bis(pyrazol-1-yl)methane adduct with imines followed by hydrolysis with water, amine functionalised ligands were generated.[9] They can also be synthesised by reaction of the organolithiated adduct with an electrophile reagent such as Me_2SiCl_2 followed by reaction with $^{i}PrNH_2$ with elimination of HCl.[10] Recently, ligands functionalised with an amine group have also been prepared by reaction of the lithiated adduct on ketenimines derivatives.[11] ***vi***) By insertion of heterocumulenes, such as carbodiimides, isocyanates or thioisocyanates in the organolithiated adduct, heteroscorpionate ligands bearing amidinate, acetamidate or thioacetamidate groups were obtained.[12] Some of these compounds have been isolated as enantiomerically pure derivatives, when optically active isocyanate or thioisocyanate compounds were used. ***vii***) From lithiated bis(pyrazol-1-yl)methane adducts followed by the addition of $SO_3{\cdot}Et_3N$, the corresponding heteroscorpionate ligands with a sulfonate group were obtained.[13] These compounds are specially interesting due to the possibility to generate water soluble compounds. ***viii***) When a fulvene derivative was reacted with the

organolithiated adduct, a mixed scorpionate/cyclopentadienyl ligand featuring a cyclopentadienyl group was developed.[14] **ix**) By reaction of the organolithiated bis(pyrazol-1-yl)methane with organotin derivatives, heteroscorpionate ligands with organotin groups were obtained.[15] **x**) Reaction of the lithiated derivative from bis(pyrazol-1-yl)methane with aldehydes or ketones, such as 1(*R*)-(−)-myrtenal, followed by reduction reaction, the corresponding enantiomerically pure heteroscorpionate ligand functionalised with an alcohol group was prepared.[16,17]

This kind of ligands represents an interesting alternative to tris(pyrazolyl)borates (Tp) and cyclopentadienyl (Cp) ligands for the preparation of organometallic complexes, because not only act as tripods occupying three coordination positions, but it is also possible to fine tune their steric and electronic properties. Furthermore, the synthesis of the lithiated or the neutral specie is easy, obtaining the corresponding product in high yield in a two-step reaction.

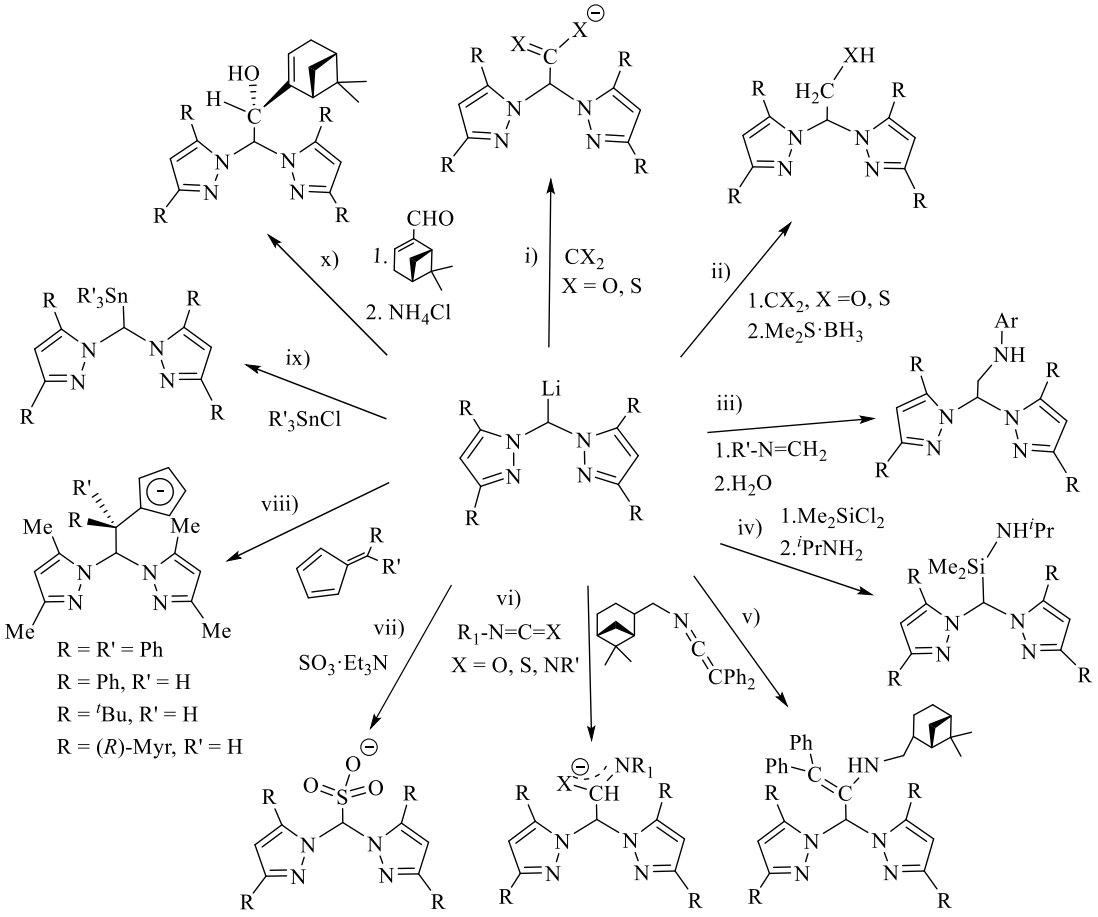

Figure 4. *Synthesis of heteroscorpionate ligands prepared by lithiation and electrophile addition*.

d.- An alternative for the preparation of heteroscorpionate ligands with acetate groups is based on the double Michael addition of a pyrazole ring to an activated alkyne, in this case, methyl propionate, which acts as the third coordination moiety R' (Scheme 4).[18]

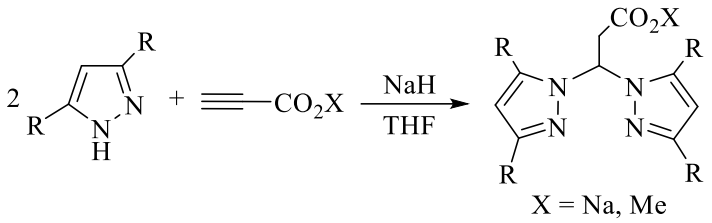

Scheme 4

2. Aluminium complexes containing scorpionate ligands

During the last few decades, an extensive chemistry of organometallic aluminium complexes has been developed since this metal provides a high Lewis acidity to its compounds. This feature makes aluminium complexes interesting in catalysis, so they have been used as catalysts in a range of catalytic transformations such as polymerisation of olefins,[19] Ring-Opening Polymerisation (ROP) of cyclic esters[20] and in different asymmetric catalytic processes.[21] Although the great majority of the aluminium compounds tested are neutral species, cationic and zwitterionic aluminium complexes have received great attention[22] due to the increase in the Lewis acidity, which is translated in an increase of the catalytic activity in the polymerisation of propylene oxide,[23] cyclic esters[24] and olefins,[19a,25] and in the synthesis of cyclic carbonates from epoxides and CO_2.[26]

2.1. Aluminium complexes containing scorpionate ligands derived from (pirazol-1-yl)borate

The first aluminium complex featuring scorpionate ligands was reported in the late 80's.[27] At that time, there was a lot of interest in the synthesis of cationic compounds from metallocene derivatives with general formula $[MCp_2][AlX_4]$, where M is a group 13 metal and X is a group 17 element. Due to the analogy between the cyclopentadienyl (Cp) ligands and scorpionate ligands, ionic compounds containing

tris(3,5-dimethylpyrazol-1-yl)borate (Tp*) scorpionate ligands with the formula $[AlTp^*_2]^+[AlCl_4]^-$ were synthesised (Scheme 5).[27]

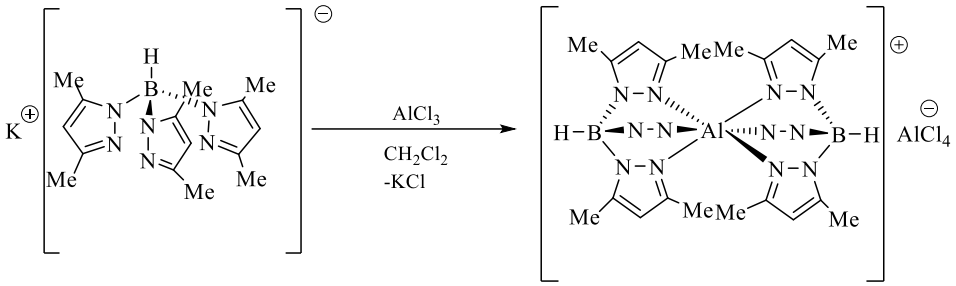

Scheme 5

Sometime later, organometallic aluminium complexes containing only one scorpionate ligand within the coordination sphere were prepared for the first time.[28] These were alkyl derivatives with $[AlR_2Tp^*]$ stoichiometry, in which the aluminium centre exhibited a coordination index of 5, with the scorpionate ligand coordinated in a tridentate manner. Initially, three pyrazole rings were believed to be coordinated to the aluminium centre, leaving the Tp* group coordinated in a tridentate monofacial manner. However, the X-ray structure showed that the Tp* ligand was coordinated in a bidentate κ^2-NN manner to the aluminium centre, which adopted a distorted tetrahedral geometry (Scheme 6). [29] Besides, a fluxional process of exchange between the two pyrazole rings was observed at room temperature.

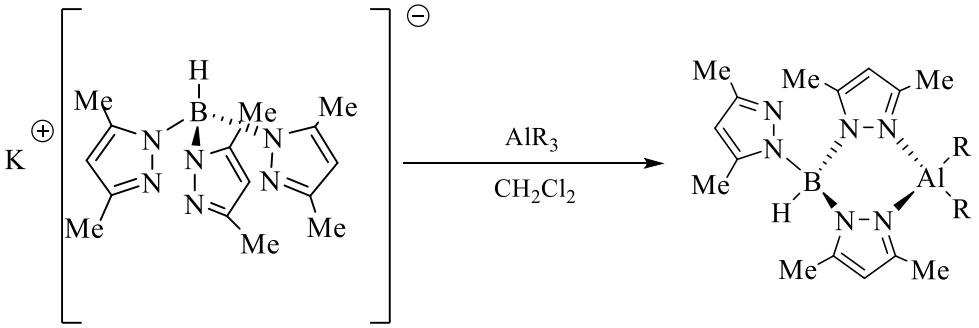

Scheme 6

On the other hand, when a bulkier scorpionate ligand such as tris(3-*tert*-butyl-pyrazol-1-yl)borate (Tp') was used, a compound with stoichiometry $[AlMe_2Tp']$ was obtained. The scorpionate ligand was coordinated to the metal centre in a bidentate manner κ^2-NN. In this case, there was no fluxional process of exchange between the

pyrazole rings due to the steric hindrance produced by the bulkier *tert*-butyl substituent on the 3 position of the pyrazole ring (Scheme 7).[30]

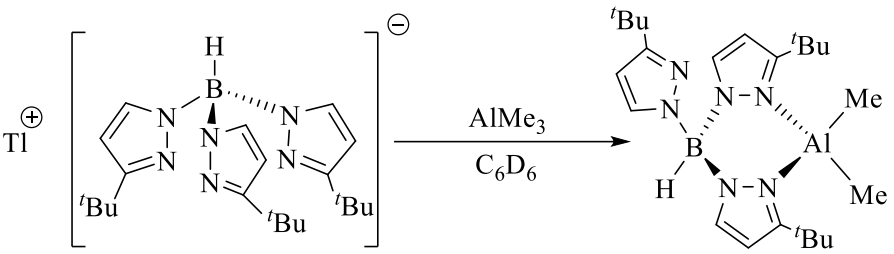

Scheme 7

Other scorpionate ligands similar to Tp, in which the pyrazole rings are replaced by other heterocycles like oxazoline[31] were employed as precursors to obtain complexes with stoichiometry [$AlMe_2(\kappa^2$-$To^M)$], where the ligand was coordinated in a κ^2-NN bidentate manner (Scheme 8).[32]

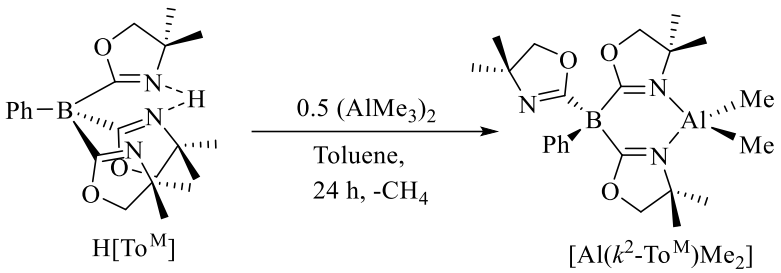

Scheme 8

2.2. Aluminium complexes containing heteroscorpionate ligands derived from bis(pyrazol-1-yl)methane

A broad range of aluminium complexes featuring heteroscorpionate ligands derived from bis(pirazol-1-yl)methane have been developed in the last 15 years. The first reported aluminium compounds were prepared by reaction between tris(pyrazol-1-yl)methane (tpzm) with trialkyl aluminium derivatives, such as $AlMe_3$.[27] The resulting complex showed a stoichiometry $[HC(pz)_3][Al(CH_3)_3]_3$, instead of the expected mononuclear aluminium complex with the tpzm ligand coordinated in a tridentate manner. However, the first aluminium complex with a heteroscorpionate ligand derived from the bis(pyrazol-1-yl)methane moiety was synthesised in 2006.[33] Thus, by reacting 2,4-*ditert*-butyl-6-{bis(3,5-dimethylpyrazol-1-yl)methyl}phenol

(bpzmpH) with AlR_3 (R = Me, Et, ^{t}Bu) in toluene, the corresponding mononuclear complexes with stoichiometry [AlR_2(κ^2-bpzmp)] were obtained (Scheme 9).

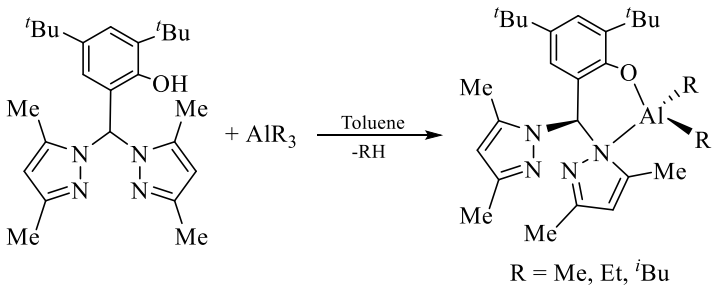

Scheme 9

In these complexes, the aluminium centre exhibits a distorted tetrahedral geometry with C_1 symmetry and the heteroscorpionate ligand is coordinated in a κ^2-NO manner through the oxygen atom of the phenol substituent and through the pyridinic nitrogen atom of one of the pyrazole rings, leaving the other pyrazole ring uncoordinated. These complexes can be used as precursors to prepare cationic aluminium complexes by abstraction of one of the methyl groups (Figure 5). It is worth noting that, in this case, the heteroscorpionate ligand is coordinated to the aluminium centre in a κ^3-NNO coordination mode.[33]

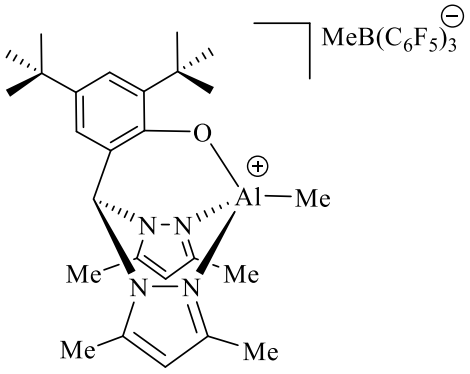

Figure 5. *Cationic aluminium complex with [Al(bpzmp)Me]$^+$[MeB(C_6F_5)$_3$]$^-$ stoichiometry.*

During the last decade, our research group has developed a wide range of heteroscorpionate aluminium complexes. The first family of heteroscorpionate aluminum complexes contained a ligand functionalised with acetamidate or thioacetamidate groups.[12] The ligand precursors exhibit different tautomers depending on the position in which the NCE group is protonated.[12b,34] This behaviour gives these

ligands a great versatility regarding their coordination ability to the metal centre (Figure 6).

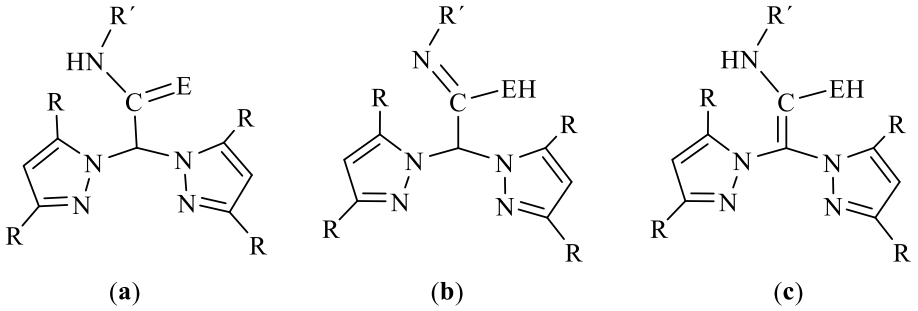

Figure 6. *Possible tautomers of acetamide and thioacetamide ligand precursors.*

These ligands were reacted with trialkylaluminium precursors to prepare the corresponding aluminium complexes with a scorpionate ligand functionalised with acetamidate or thioacetamidate groups. These complexes showed a tetrahedral geometry in which the thioacetamidate ligand was coordinated in a κ^2-NN fashion, whereas the acetamidate derivatives showed a κ^2-NO coordination mode to the aluminium centre. In these complexes, a fluxional exchange between the coordinated and the non-coordinated pyrazole rings was observed (Figure 7).[12g]

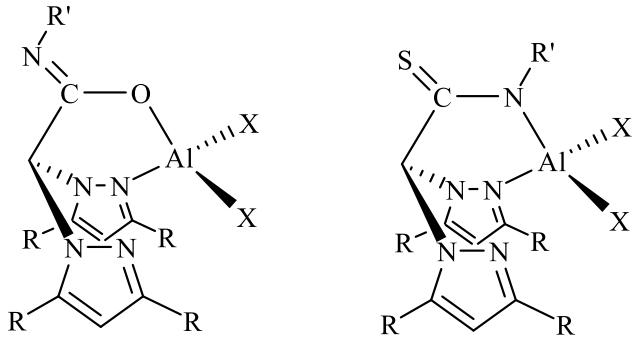

Figure 7. *Aluminium complexes with acetamidate and thioacetamidate ligands.*

Five-coordinate alkyl aluminium complexes containing two scorpionate ligands functionalised with acetamidate groups were also synthesised. In this case, the heteroscorpionate ligands were coordinated in a bidentate κ^2-NO manner with a pseudo-trigonal-bipyramidal structure around the aluminium atom (Figure 8).[12e]

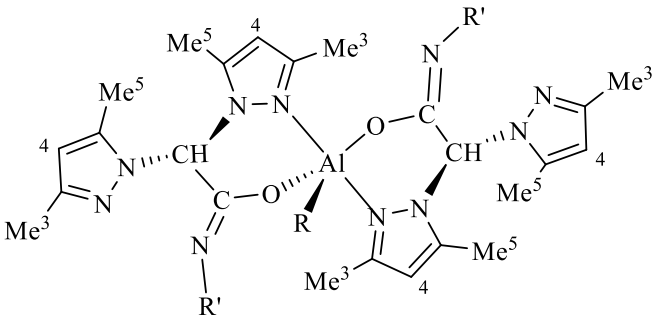

Figure 8. *Five-coordinated aluminium complexes with acetamidate ligands.*

As previously mentioned, the presence of tautomer *c* in the ligand precursors (Figure 6), allows these ligands to have a great versatility regarding the coordination mode. Thus, the activation of the methine proton bridge to both pyrazole rings allows these ligands to coordinate in a bridging manner to two or three aluminium centres (Figure 9),[12c,f] in which the steric restrictions generate a helical structure and these complexes can be isolated with helical chirality (Figure 10).[12c,f]

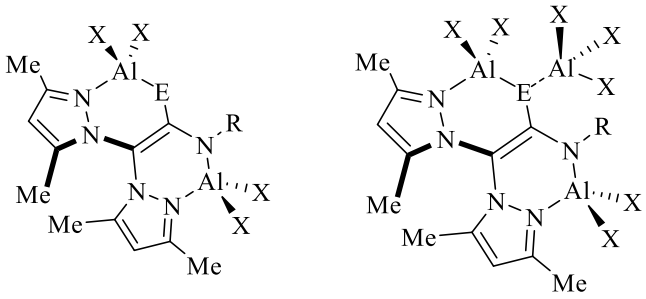

Figure 9. *Dinuclear and trinuclear acetamidate and thioacetamidate aluminium complexes.*

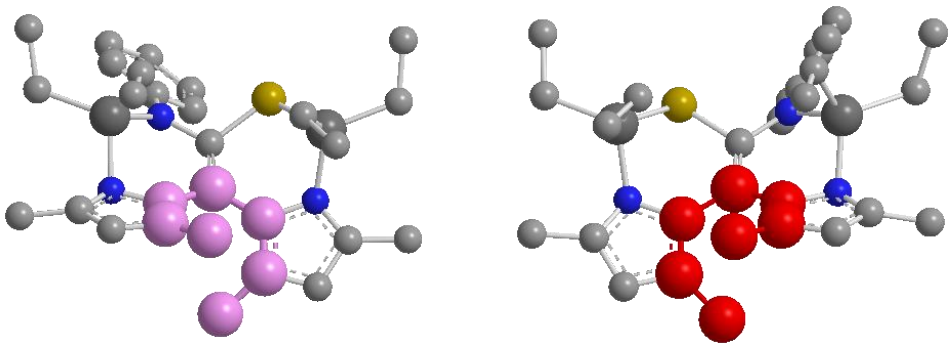

Figure 10. *Graphic representation of the helical structures P (left) and M (right) of complex [Al₂(μ-pbptam)Et₄].*

Following this approach, our research group has also synthesised a great variety of heteroscorpionate ligands functionalised with an alkoxide group by reacting bis(pyrazol-1-yl)methane with an aldehyde or a ketone.[26a,c,d,35] Thus, the reaction of the corresponding alcohol ligand precursors with trialkylaluminium derivatives afforded monometallic aluminium complexes with the scorpionate ligand exhibiting a κ^2-NO coordination mode (Figure 11).[26d,35] Surprisingly, when the ligand containing a *p*-tolyl moiety was used as the precursor, a bimetallic structure was obtained with the oxygen atom from the alkoxide moiety acting as a bridge between the aluminium centres, which exhibited a pseudo-trigonal-bipyramidal conformation with a κ^2-NO μ–O coordination mode (Figure 11).[35] These complexes were tested for the ROP of ε-caprolactone and *L*-lactide obtaining the corresponding biodegradable polyester materials with remarkable control on the M_n and M_w/M_n,[35] the synthesis of terpene-bioderived cyclic carbonates from different natural resources such as carvone, carvyl acetate, terpinene-4-ol, etc.[26d] and the Ring-Opening Copolymerisation (ROCOP) of epoxides and cyclic anhydrides to afford polyesters.[35]

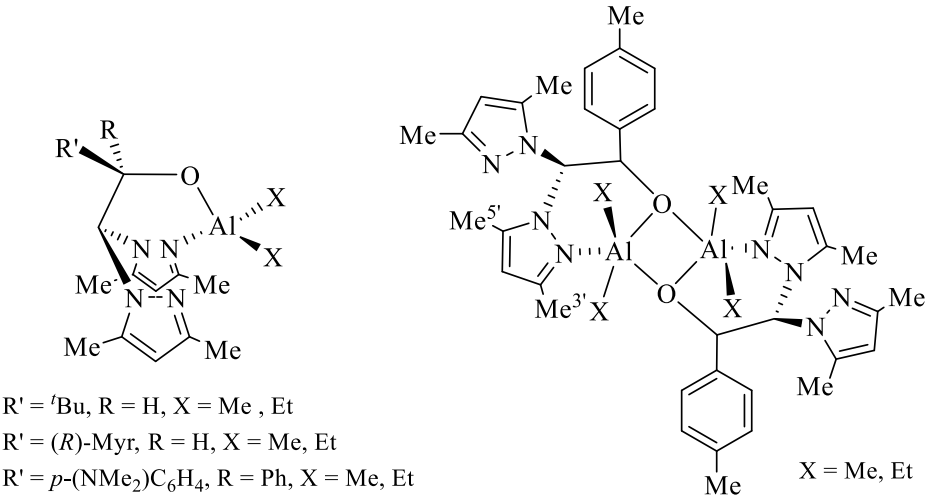

Figure 11. *Mono- and bimetallic heteroscorpionate alkoxide aluminium complexes.*

When the alcohol heteroscorpionate neutral precursors were reacted with two equivalents of trialkylaluminium derivatives, bimetallic heteroscorpionate aluminium complexes were prepared.[26a] In this case, one aluminium centre exhibited a distorted tetrahedral environment with the scorpionate ligand coordinated in a κ^2-NO coordination manner while the second aluminium centre was coordinated to the oxygen from the alkoxide group from the scorpionate ligand through a coordinate

dative bond and to three alkyl groups (Figure 12). These complexes were tested as catalysts along with different co-catalysts for the synthesis of a wide range of monosubstituted and disubstituted cyclic carbonates.[26a] The synthesis of disubstituted cyclic carbonates required harsher conditions of temperature and pressure (50-100 ºC, 10-50 bar) reaching TOF values up to 0.78 h^{-1}.

In addition, aluminium complexes featuring zwitterionic heteroscorpionate ligands have also been synthesised as bifunctional catalysts for the CO_2 fixation into cyclic carbonates. These complexes acted as one-component catalysts, where the aluminium centre and the bromide or iodide co-catalyst were present in the same moiety as shown in Figure 13.[26b,c] Thus, cyclic carbonates were obtained from their corresponding terminal, internal and bio-derived epoxides and carbon dioxide.[26c] In addition, it was shown that the halide counterion not only had a positive effect on the stability of the zwitterionic ligands, but also played a key role on the catalytic performance of the aluminium heteroscorpionate complex.[26b,c]

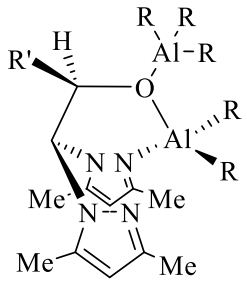

R' = ^{t}Bu, R = Me , Et
R' = (*R*)-Myr, R = Me, Et
R' = *p*-(NMe_2)C_6H_4, R = Me, Et

Figure 12. *Dinuclear heteroscorpionate alkoxide aluminium complexes.*

X-Ray diffraction studies confirmed the zwitterionic character of these complexes with a pseudo-tetrahedral geometry around the aluminium centre with the heteroscorpionate ligand coordinated in a κ^2-NO fashion and two alkyl groups. The halide anions were also shown to be within the structure (Figure 14).[26c]

More recently, mono- and bimetallic helical alkyl aluminium complexes featuring ketiminate ligands have also been developed by our group an tested in the ROP of cyclic esters and the preparation of a wide variety of cyclic carbonates (Figure 15).[36,37]

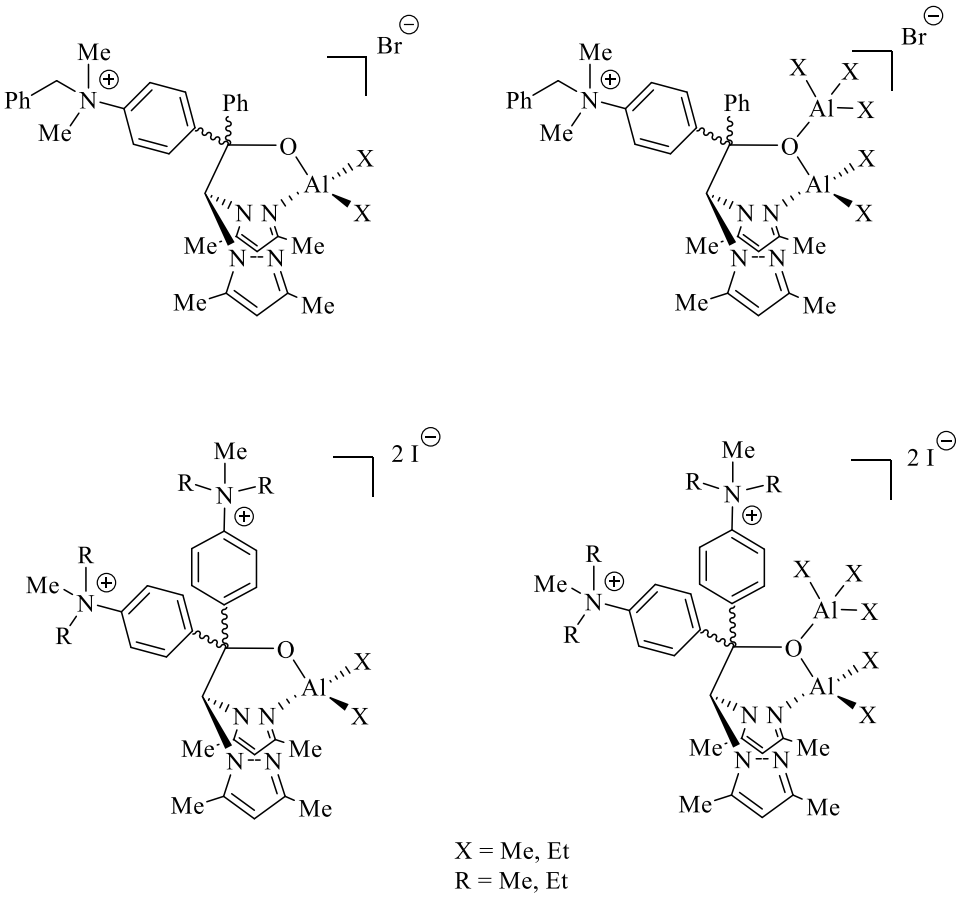

Figure 13. *Zwitterionic heteroscorpionate alkoxide aluminium complexes.*

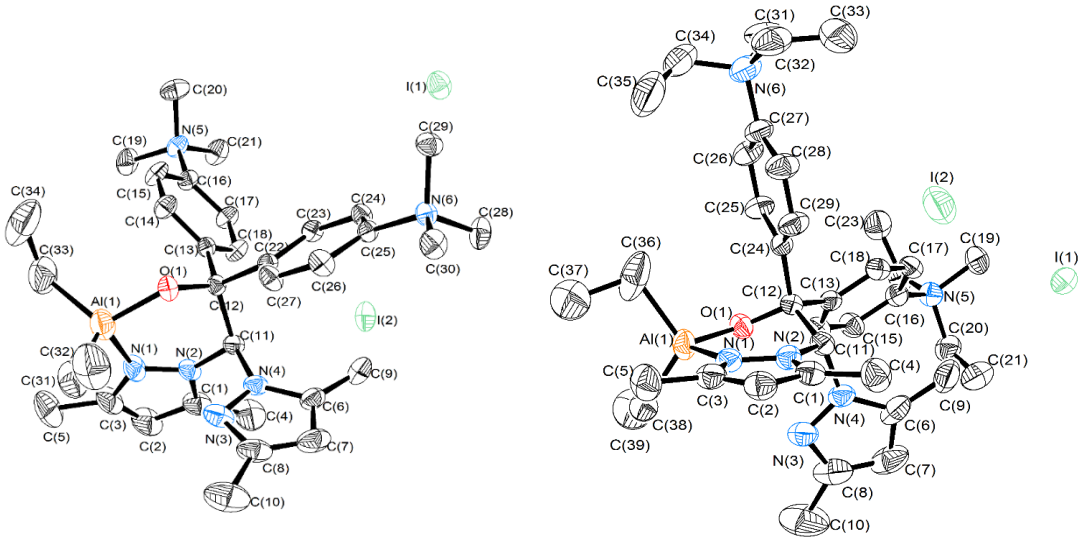

Figure 14. *ORTEP diagrams for zwitterionic heteroscorpionate aluminium complexes.*

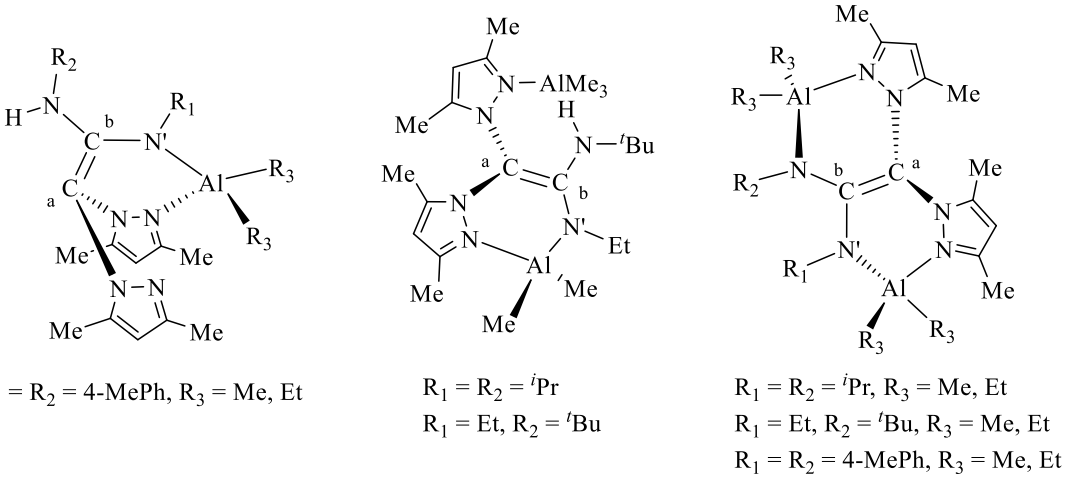

Figure 15. *Mono- and bimetallic helical heteroscorpionate alkyl aluminium complexes.*

3. Gallium complexes containing scorpionate ligands

Currently, the use of well-defined group 13 metal species in catalysis remains essentially dominated by Al(III) derivatives as a result of their stronger Lewis acidity and the low cost of the Al metal source, and thus, its ready availability. However, the use of Ga(III) derivatives in catalysis has recently attracted attention due to its biocompatibility and the specific properties of such gallium salts, in particular their π-Lewis acidity.[38] Gallium complexes have been found to be active for the ROP of cyclic ethers, esters and carbonates, the activation and reduction of alkenes and alkynes through hydrogen transfer, and alkyne and alkene hydroamination processes.[38] Cationic gallium complexes have also been developed and tested in a wide range of catalytic processes including polymerisation of olefins, hydrosilylation reactions and alcohol activation.[39]

The first (pyrazol)borate gallium complex reported was prepared from an equimolar mixture of KTp* and $GaCl_3$ in THF.[28] X-Ray crystallography showed the formation of a salt-type $[GaTp^*_2]^+[GaCl_4]^-$, with the Ga^{3+} ion coordinated in a close to regular octahedral geometry (Scheme 10). When KTp* was reacted with $GaCl_2Me$, the product obtained depended on the stoichiometry of the reaction.[40] Using one equivalent of the Tp* ligand, the mononuclear complex [Ga(Tp*)MeCl] was obtained (Scheme 11). However, when two equivalents of Tp* were used, the mononuclear trigonal-bipyramidal gallium complex $[Ga(Tp^*)_2Me]$ was obtained (Scheme 11).

Alkyl complexes with formula [Ga(Tp*)Me_2] were also synthesised by reacting the precursor $GaMe_2Cl$ and KTp* ligand (Scheme 11). X-ray structure for the latter is shown in Figure 16a. It showed a tetrahedral environment for the gallium centre with the scorpionate Tp* ligand coordinated in a κ^2-NN fashion and two methyl groups.

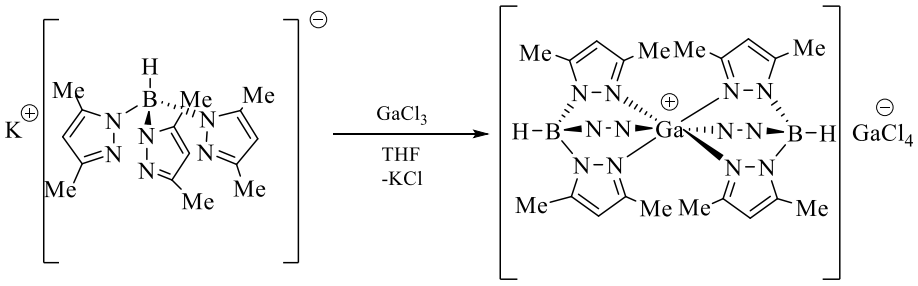

Scheme 10. *Synthesis of $[GaTp^*_2]^+[GaCl_4]^-$ complex.*

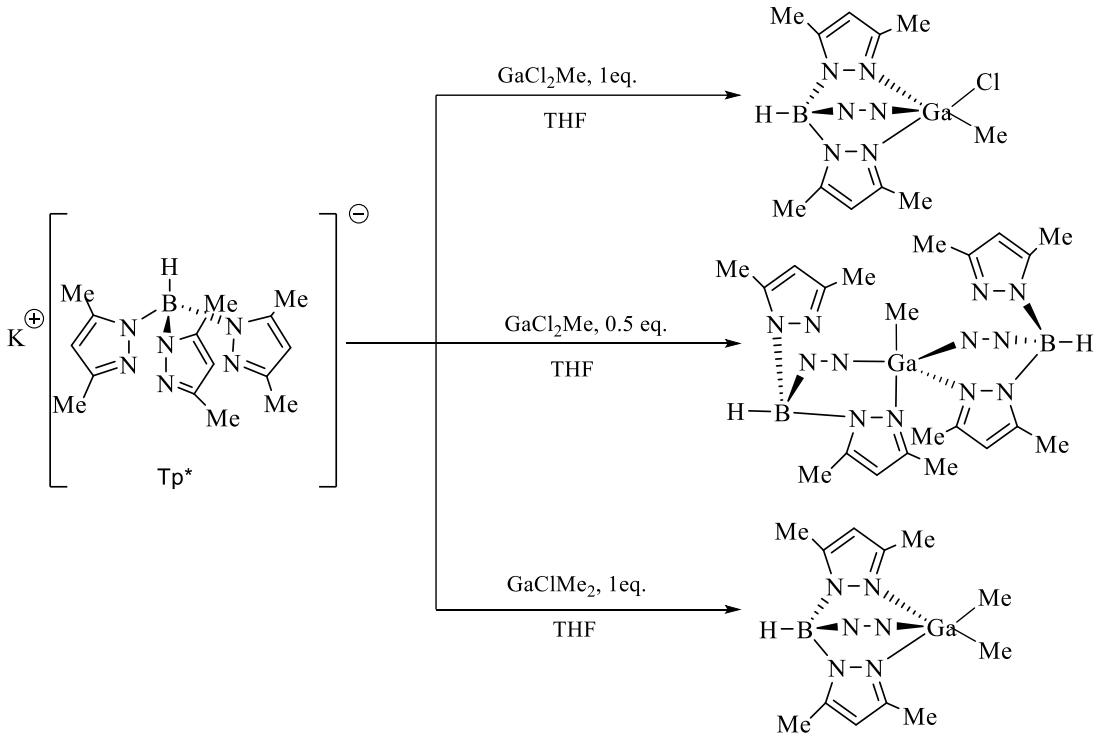

Scheme 11. *Synthesis of [Ga(Tp*)MeCl], [Ga(Tp*)$_2$Me] and [Ga(Tp*)Me_2] complexes.*

Shortly after, gallium complexes derived from bis(pyrazol-1-yl)borate (Bp) were also synthesised.[41,42] When using a 1:1 molar ratio, X-Ray structure confirmed the formation of salt-type $[GaBp_2]^+[GaCl_4]^-$ compounds in accordance to previous results.[38] However, when using a 2:1 or 3:1 molar ratio, the corresponding neutral gallium complexes $[Ga(Bp)_2Cl]$ and $[Ga(Bp)_3]$ were obtained respectively.[42] X-Ray

crystallographic analysis for complex [Ga(Bp)$_2$Cl] showed a trigonal bipyramidal geometry for the gallium atom (Figure 16b). On the other hand, spectroscopic studies indicated that the gallium centre presented an octahedral geometry in complex [Ga(Bp)$_3$]. The reactions of the Bp ligand with alkyl gallium(III) precursors have also been studied.[41] Thus, the reaction between the gallium precursor GaCl$_2$Me and KBp in a 1:2 molar ratio afforded the formation of the neutral complex [Ga(Bp)$_2$Me] for which the structure is presumably analogous to the corresponding chloride complex. Likewise, the reaction with only one equivalent of KBp gave rise to the monomeric gallium complex [Ga(Bp)MeCl] in which the gallium centre showed a 4-coordinate structure. The reaction between [Ga(Bp)MeCl] with MeLi, or the reaction between the GaMe$_2$Cl with KBp yielded to the formation of the alkyl gallium complex [Ga(Bp)Me$_2$].

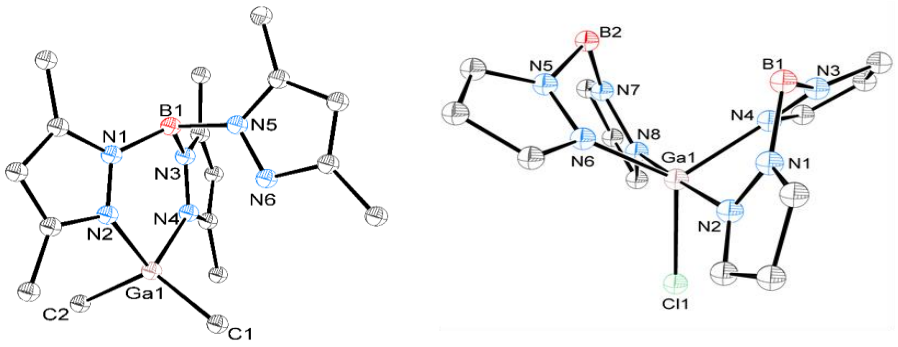

Figure 16. *X-Ray structures of a) [Ga(Tp*)Me$_2$] and b) [Ga(Bp)$_2$Cl].*

4. Indium complexes containing scorpionate ligands

Indium organometallic complexes have recently arisen a great interest within the scientific and industrial communities due to its biocompatibility, lower Lewis acidity compared to their aluminium and gallium analogues and higher stability of their precursors than their organoaluminium/gallium counterparts. They have been tested in a wide range of catalytic processes, especially for the ROP of cyclic esters,[43] in which they have found to be more active than their gallium analogues[44] and the co-polymerisation of epoxides and CO_2 to obtain polycarbonates.[45] As their aluminium and gallium counterparts, indium cationic catalysts have also been synthesised and used as catalysts for other catalytic processes such as the coupling of epoxides and

lactones, hydroarylation of alkynes and transfer hydrogenation of alkenes or the cyclisation of alkenes and alkynes.[39]

The first reported indium scorpionate complex resulted from the reaction of $InCl_3$ with KTp* in THF.[27] After recrystallisation in MeCN, X-Ray analysis confirmed the formation of $[In(Tp^*)Cl_2(NCMe)]$, in which the indium centre exhibited an octahedral geometry with a facially capping κ^3-coordinated Tp* ligand, two chloride ligands and an acetonitrile molecule in the coordination sphere (Figure 17). The reaction of InI_3 and KTp* in a 1:2 molar ratio at low temperature in toluene afforded the sandwich complex $[In(Tp^*)_2]I$. X-Ray diffraction analysis confirmed a regular N_6 coordination sphere around the indium atom (Figure 18a).[46] However, although crystal structure confirmed the formation of a "sandwich" complex, elemental and mass spectrum analysis were inconsistent with this observation. The data suggested that partial hydrolysis of the indium complex could occur on exposure to air or moisture.[47] To study the influence of water in the reaction mixture, complex $[In(Tp^*)_2]I$ was refluxed overnight in wet acetonitrile. The resulting complex was a dimeric species $[\{In(Tp^*)\}_2(\mu\text{-}pz^{Me})_2(\mu\text{-}OH)]I$ bridged by two pyrazole ligands derived from the hydrolysis of the Tp* ligand, and a hydroxide ligand, in which each indium centre displayed an octahedral geometry with a N_5O coordination environment (Figure 18b).

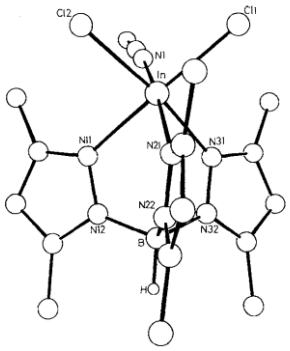

Figure 17. *X-Ray Crystal structure of [In (Tp*)(NCMe)Cl$_2$].*

Reactions using other (pyrazolyl)borate precursors such as Bp have also been extensively studied using $InCl_3$, $MeInCl_2$ and Me_2InCl.[48] Thus, reaction of KBp with $InCl_3$, yielded to the formation of $[In(Bp)Cl(\mu\text{–}Cl)]_2$, which in contrast to the majority of indium scorpionate complexes, is extremely susceptible to decomposition. Its limited solubility hinted to a dimeric structure (Scheme 12). Reactions using 2:1 or 3:1

ligand to metal molar ratios yielded [In(Bp)$_2$Cl] and [In(Bp)$_3$] respectively, the former with a trigonal bipyramidal geometry, while the latter displayed an octahedral structure with the ligand coordinated in a κ^3-NNN manner (Scheme 12).[49] The analogous [In(Bp)$_2$Me] was prepared using InCl$_2$Me as precursor with two equivalents of the ligand. Reaction of InCl$_2$Me with only one equivalent of ligand gave [In(Bp)MeCl], which exhibited a tetrahedral structure. The monomeric indium complex [In(Bp)Me$_2$] was prepared from KBp and InClMe$_2$, and displayed a distorted tetrahedral geometry.

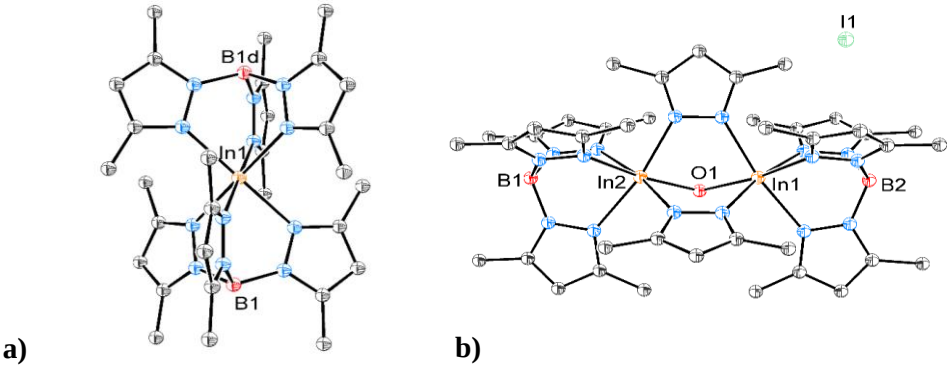

a) **b)**

Figure 18. *X-Ray Crystal structure of a) [In(Tp*)$_2$]I and b) [{In(Tp*)}$_2$(μ -pz^{Me})$_2$(μ-OH)]I.*

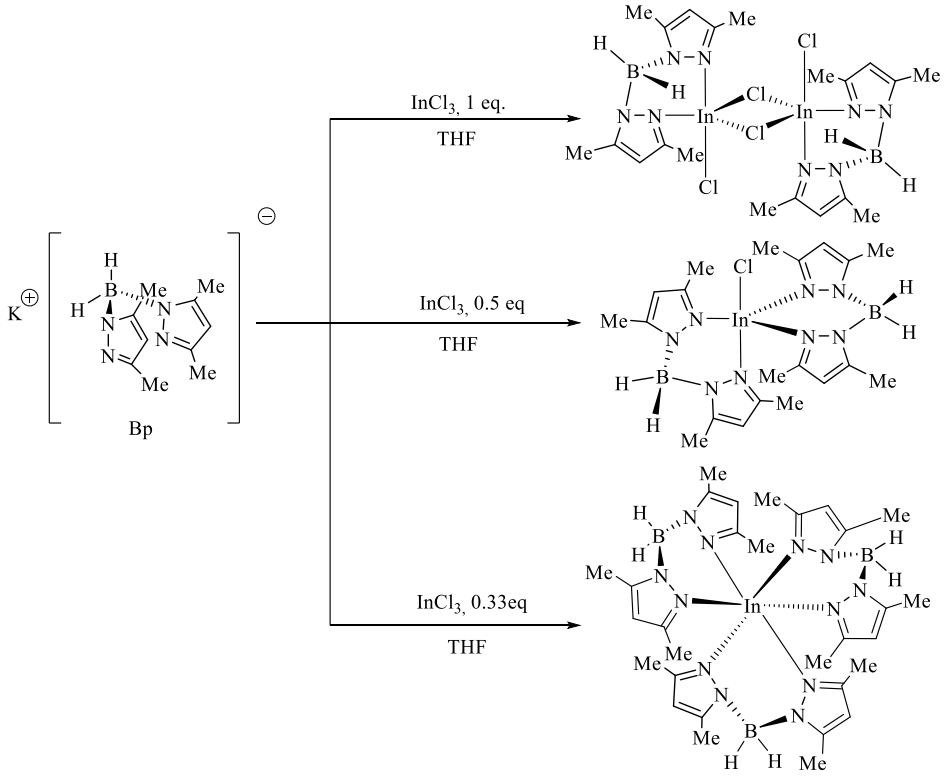

Scheme 12. *Synthesis of [In{Bp}Cl(μ–Cl)]$_2$, [In{Bp}$_2$Cl] and [In{Bp}$_3$] complexes.*

Results and discussion

In this section of Chapter 1, the synthesis of a wide range of chloride, alkyl, alkoxide and amido group 13 metal complexes, which will be further tested as catalysts for the preparation of polymeric materials, will be described.

1. Synthesis of ligand precursors

For the synthesis of group 13 metal complexes supported by heteroscorpionate ligands functionalised with alkoxide groups described in this chapter, neutral precursor compounds derived from bis(pyrazol-1-yl)methane: bpzbeH, [(1,1-bis(3,5-dimethyl-1H-pyrazol-1-yl)-3,3-dimethylbutan-2-ol], bpzteH [(2,2-bis(3,5-dimethyl-1H-pyrazol-1-yl)-1-*p*-tolyl)ethan-1-ol], bpzappeH [(2,2-bis(3,5-dimethyl-1H-pyrazol-1-yl)-1-(4-(dimethylamino)phenyl)-1phenylethan-1-ol] and bpzFerrH [(2,2-bis(3,5-dimethyl-1H-pyrazol-1-yl)-1-ferrocenyl)ethan-1-ol] (**1**) have been employed (Figure 19). Some of these ligands have been previously prepared and characterised by our research group as it has been previously discussed in the introduction,[16] while compound **1** has been prepared for the first time in this work.

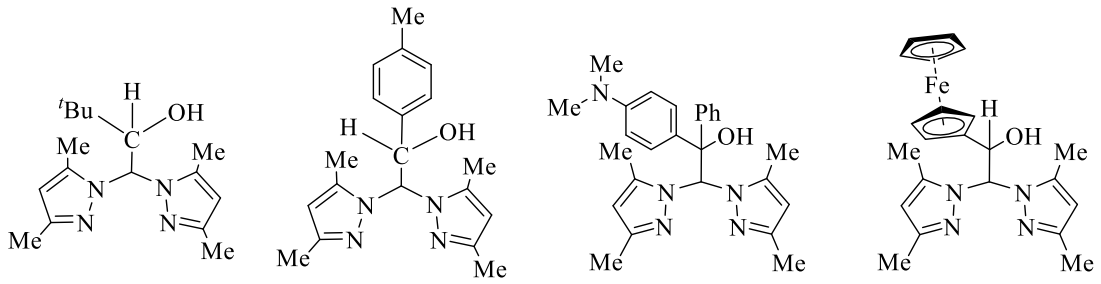

Figure 19. *Heteroscorpionate ligand precursors.*

The synthesis of these compounds was carried out by reaction of bis(pyrazol-1-yl)methane with ^{n}BuLi in 1:1 molar ratio and subsequent addition of the corresponding aldehyde/ketone derivative. Finally, the protonolysis reaction of the generated lithiated adduct with saturated aqueous NH_4Cl afforded the corresponding heteroscorpionate neutral precursor in good yield after the appropriate workup (Scheme 13).

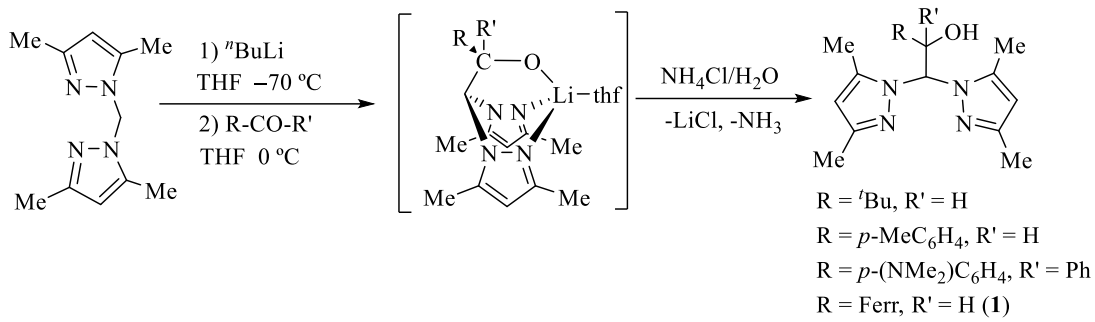

Scheme 13.

The spectroscopic data obtained for compound **1** in solution (Tables 1 and 2) confirmed the proposed structure (Scheme 13). ^{1}H-NMR and ^{13}C{^{1}H}-NMR spectra for compound **1** (Figures 20 and 21 respectively) showed two singlets for each of the H^{4}, Me^{3} and Me^{5} pyrazole protons and carbons, indicating the existence of two types of pyrazole rings due to the presence of a stereogenic centre in the heteroscorpionate ligand (C^{a}).

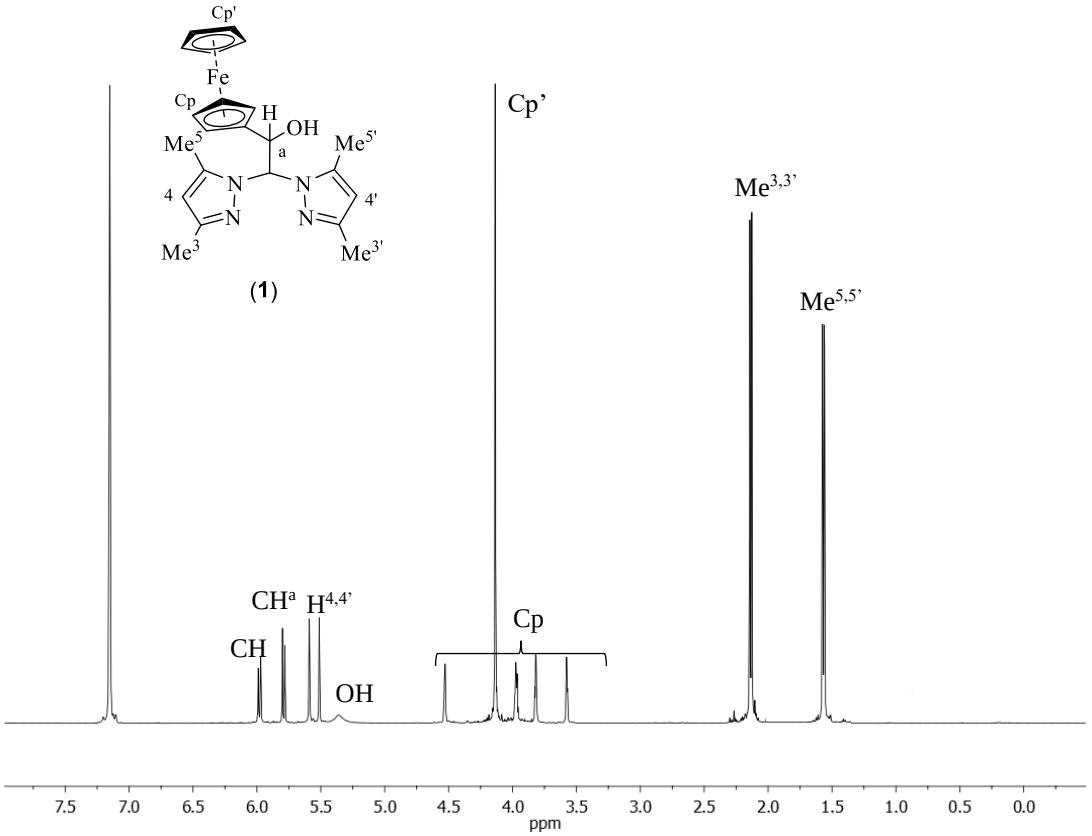

Figure 20. *^{1}H-NMR spectrum for bpzFerrH (**1**) in C_6D_6.*

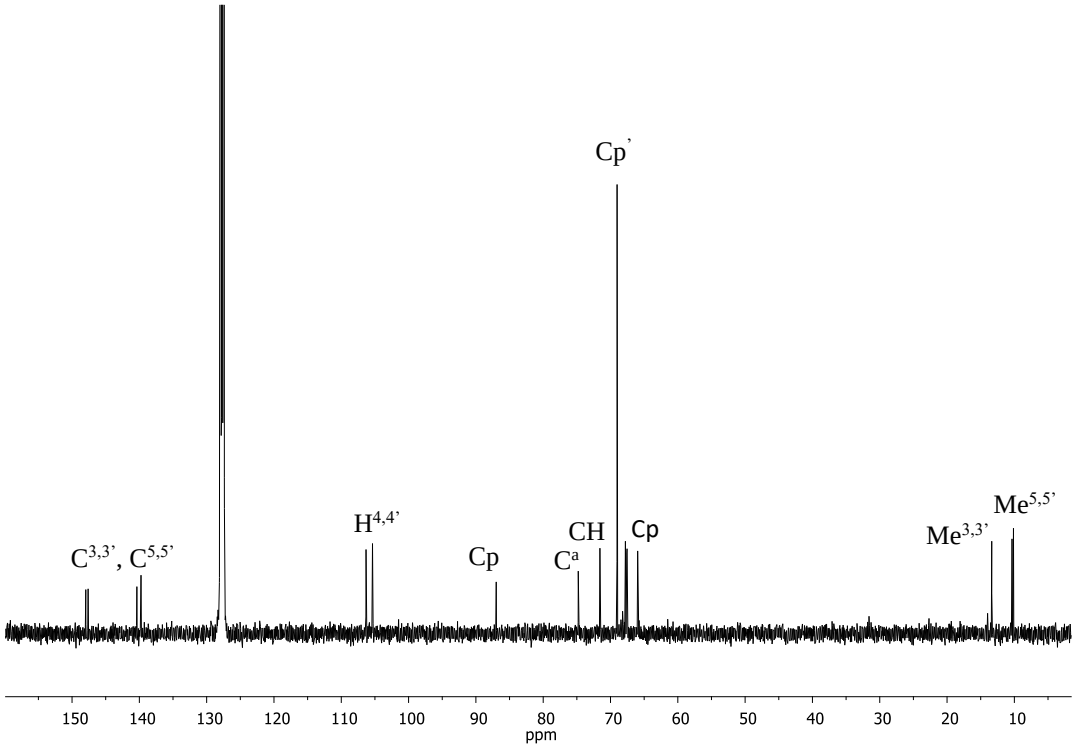

Figure 21. *$^{13}C\{^{1}H\}$-NMR spectrum for bpzFerrH (**1**) in C_6D_6.*

Table 1. *^{1}H-NMR data for compound **1** in C_6D_6.*

Compound	CH	C^a-H	H^4, $H^{4'}$	Me^3, $Me^{3'}$	Me^5, $Me^{5'}$	Ferr
bpzFerrH (**1**)	5.99 (d, J_{HH} = 7.6 Hz, 1H)	5.79 (d, J_{HH} = 7.6 Hz, 1H)	5.51 (s, 1H) 5.59 (s, 1H)	2.13 (s, 3H) 2.14 (s, 3H)	1.56 (s, 3H) 1.57 (s, 3H)	3.58 (m, 1H, Cp) 3.82 (m, 1H, Cp) 3.97 (m, 1H, Cp) 4.13 (s, 5H, Cp') 4.53 (m, 1H, Cp)

Table 2. *$^{13}C\{^{1}H\}$-NMR data for compound **1** in C_6D_6.*

Compound	CH	C^a	$C^{3,3'}$, $C^{5,5'}$	C^4, $C^{4'}$	Me^3, $Me^{3'}$	Me^5, $Me^{5'}$	Ferr
bpzFerrH (**1**)	71.6	74.8	147.6 148.0 139.8 140.4	104.4 106.3	13.4 13.5	10.1 10.4	66.0 (Cp) 67.5 (Cp) 67.6 (Cp) 67.8 (Cp) 69.0 (Cp') 87.0 (Cp)

2. Synthesis of chloride group 13 metal complexes

2.1. Synthesis of chloride aluminium and gallium complexes

The synthesis of chloride aluminium and gallium complexes was carried out in a two-step reaction as shown in Scheme 14. In the first step, the corresponding neutral heteroscorpionate ligand precursor was deprotonated using ^{n}BuLi in THF at −78 ºC for one hour. Then, the lithiated adduct was transferred to a pre-cooled suspension at 0 ºC of MCl_3 (M = Al, Ga) in THF. The resulting mixture was stirred overnight at room temperature to afford the corresponding chloride aluminium/gallium salt complexes $[Al(\kappa^2\text{-bpzbe})_2]^+[AlCl_4]^-$ (**2**), $[Al(\kappa^2\text{-bpzte})_2]^+[AlCl_4]^-$ (**3**), $[Al(\kappa^2\text{-bpzappe})_2]^+[AlCl_4]^-$ (**4**), $[Al(\kappa^2\text{-bpzFerr})_2]^+[AlCl_4]^-$ (**5**), $[Ga(\kappa^3\text{-bpzbe})_2]^+[GaCl_4]^-$ (**6**), $[Ga(\kappa^3\text{-bpzte})_2]^+[GaCl_4]^-$ (**7**), $[Ga(\kappa^3\text{-bpzappe})_2]^+[GaCl_4]^-$ (**8**) and $[Ga(\kappa^3\text{-bpzFerr})_2]^+[GaCl_4]^-$ **(9)** as white (**2**-**4**, **6**-**8**) or pale yellow (**5** and **9**) solids after the appropriate work-up procedure. All complexes were obtained in yields between 80-90% and are soluble in polar solvents such as CH_2Cl_2 and MeCN. These results are in accordance with previously reported chloride aluminium and gallium complexes derived from (pirazol-1-yl)borate scorpionate ligands as discussed previously in the introduction section.[27]

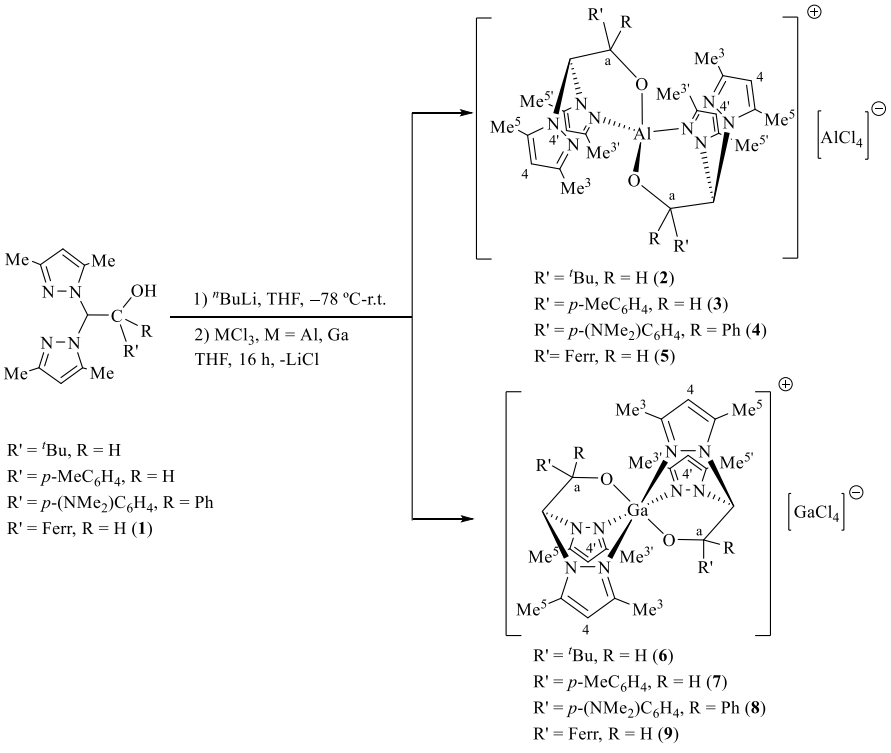

Scheme 14. *Synthesis of chloride aluminium **(2-5)** and gallium **(6-9)** complexes.*

Structural Characterisation

The structural characterisation of complexes **2-9** was performed by ^{1}H-NMR and ^{13}C{^{1}H}-NMR spectroscopy (Tables 3 and 4). ^{1}H-NMR and ^{13}C{^{1}H}-NMR spectra exhibited two distinct sets of pyrazole resonances, showing two singlets for the H$^{4,4'}$, Me$^{3,3'}$and Me$^{5,5'}$ pyrazole protons and carbons due to the presence of the C^{a}-H stereogenic group from the alkoxide ligand, one singlet for the methine group, and the signals corresponding to the different moieties of the heteroscorpionate ligands (Figure 22). The NMR results are consistent with the salt-type $[ML_2]^+[MCl_4]^-$ structure proposed for complexes **2-9** featuring a tetrahedral environment for the cationic aluminium centre in complexes **2-5** coordinated to two heteroscorpionate ligands in a κ^2-NO fashion and an octahedral environment for the cationic gallium centre in complexes **6-9**, in which the two heteroscorpionate ligands are coordinated in a κ^3-NNO coordination mode. It is worth noting that a new stereogenic centre is generated in the *CH* methine group bridging both pyrazole rings due to the κ^2-NO coordination of the heteroscorpionate ligand to the aluminium centre for complexes **2-5**. Thus, up to eight diastereoisomers could be obtained for each aluminium complex (**2-5**). This explains why complexes **2** and **5** exhibit several diastereoisomers in solution. In the case of gallium complexes, the coordination mode of the ligands could generate two diastereoisomers. The ^{1}H-NMR spectrum for complex **4** and ^{13}C{^{1}H}-NMR for complex **6** are given in Figures 22 and 23 respectively.

NOESY-1D experiments were performed for the assignment of most ^{1}H NMR resonances and ^{1}H-^{13}C heteronuclear correlation (g-HSQC) experiments were carried out to assign the resonances corresponding to C^{4}, Me^{3} and Me^{5} of the pyrazole rings. Figure 24 shows the correlation spectrum for complex $[Al(\kappa^2\text{-bpzFerr})_2]^+[AlCl_4]^-$ (**5**).

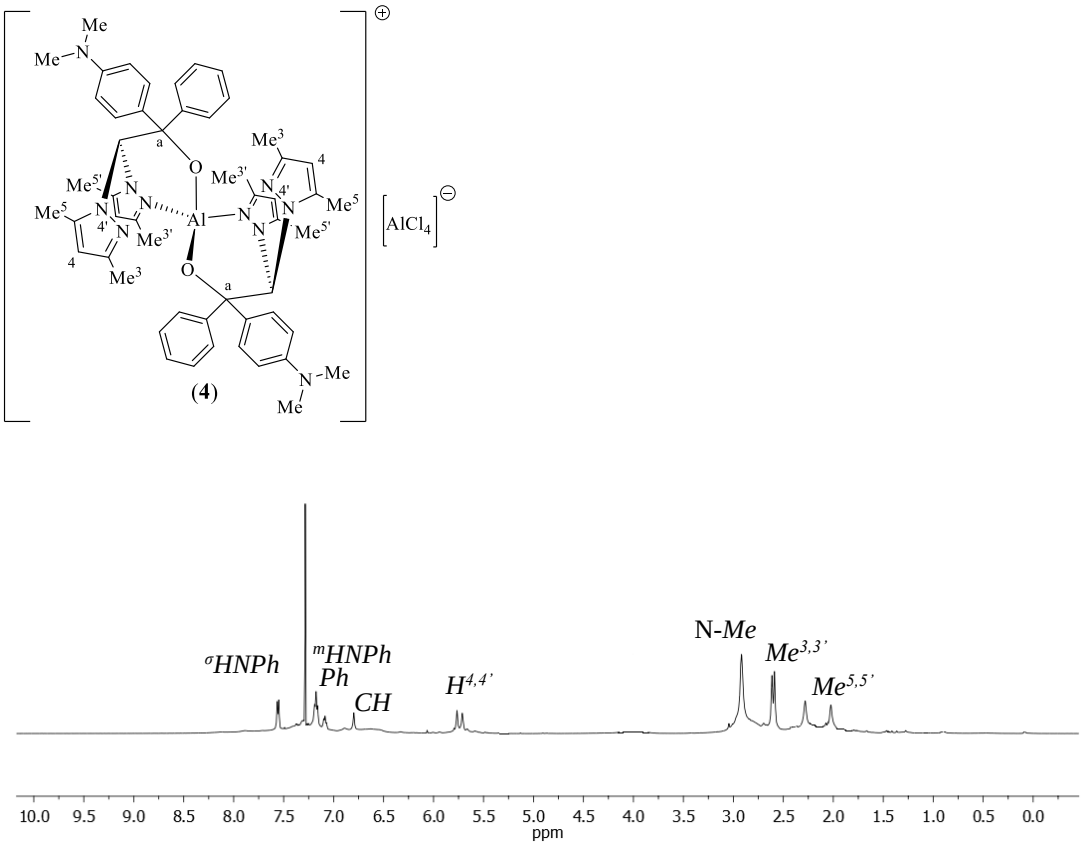

Figure 22. *^{1}H-NMR spectrum for complex [Al{κ^{2}-bpzappe}$_2$]$^+$[AlCl$_4$]$^-$(**4**) in CDCl$_3$.*

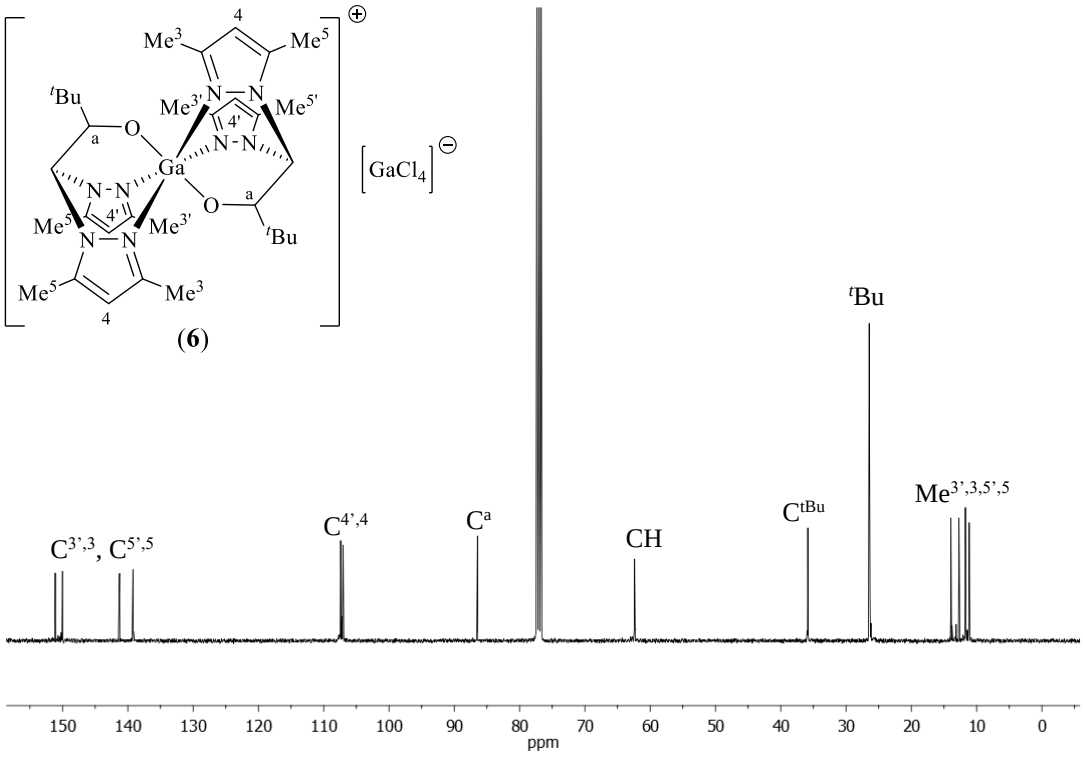

Figure 23. *^{13}C{^{1}H}-NMR spectrum for complex [Ga(κ^{3}-bpzbe)$_2$]$^+$[GaCl$_4$]$^-$(**6**) in C$_6$D$_6$.*

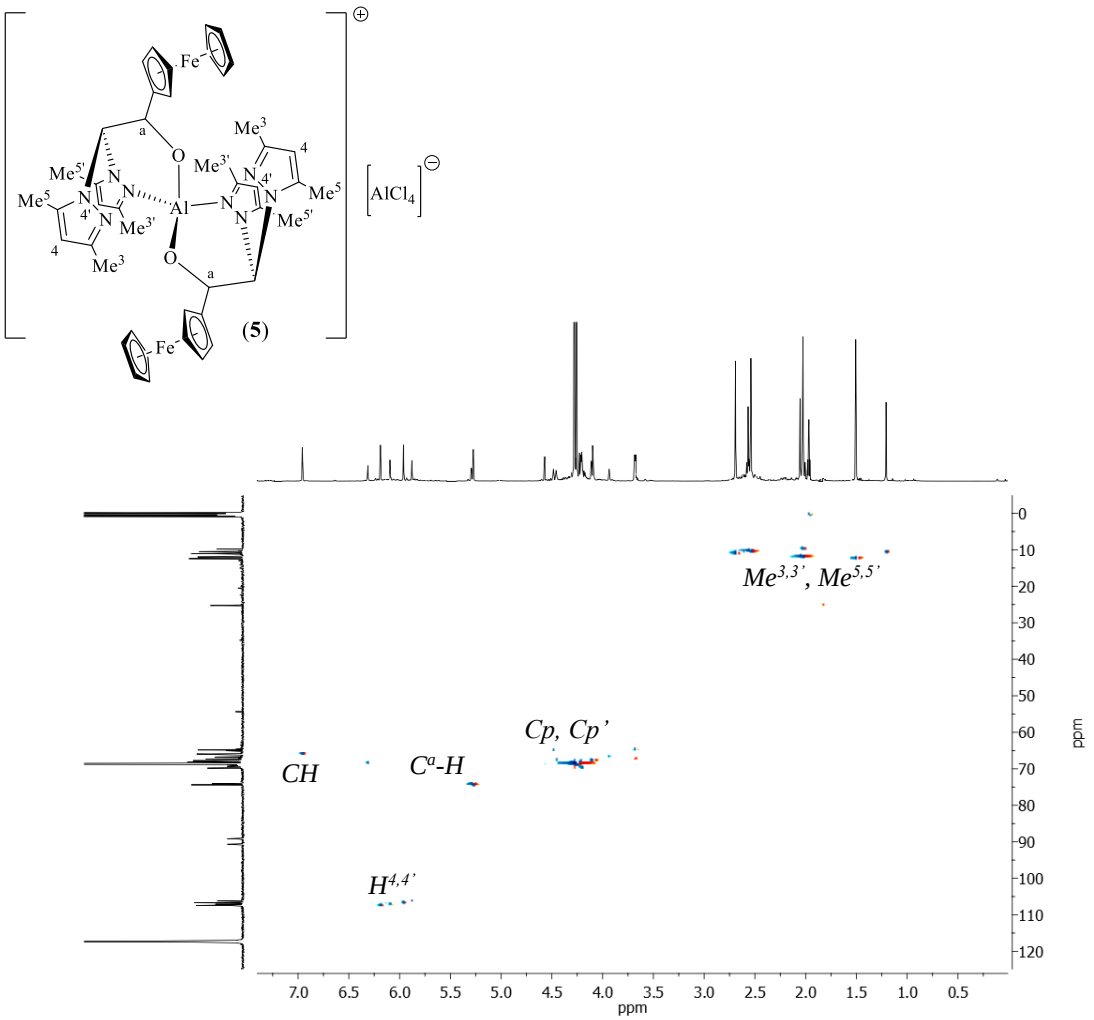

Figure 24. *^{1}H-^{13}C-g-HSQC spectrum for complex [Al(κ^{2}-bpzFerr)$_2$]$^{+}$[AlCl$_4$]$^{-}$(**5**) in CD$_3$CN.*

Table 3. *^{1}H-NMR data for complexes **2**-**9**.*

Compound	CH	CH[a]	H$^{4,4'}$	R, R'	Me$^{3,3'}$	Me$^{5,5'}$
[Al(κ^2-bpzbe)$_2$]$^+$[AlCl$_4$]$^-$ (**2**)	6.40 (s, 1H)	3.68 (s, 1H)	5.94 (s, 1H) 6.04 (s, 1H)	0.68 (s, 9H, ^{t}*Bu*)	2.34 (s, 3H) 2.45 (s, 3H)	2.39 (s, 3H) 2.41 (s, 3H)
[Al(κ^2-bpzte)$_2$]$^+$[AlCl$_4$]$^-$ (**3**)	6.35 (s, 1H)	4.12 (s, 1H)	5.77 (s, 1H) 6.03 (s, 1H)	6.96 (d, J_{HH} = 8.0 Hz, 2H, ^{m}*H*Ph) 7.20 (d, J_{HH} = 7.8 Hz, 2H, ^{o}*H*Ph) 2.23 (s, 3H, *Me*Ph)	2.14 (s, 3H) 2.50 (s, 3H)	1.06 (s, 3H) 1.91 (s, 3H)
[Al(κ^2-bpzappe)$_2$]$^+$[AlCl$_4$]$^-$ (**4**)	6.80 (s, 1H)	-	5.71 (s, 1H) 5.77 (s, 1H)	7.18 (d, J_{HH} = 7.3 Hz, 2H, ^{m}*H*NPh) 7.56 (d, J_{HH} = 7.6 Hz, 2H, ^{o}*H*NPh) 6.60 (m, 1H, ^{p}*H*Ph) 7.09 (m, 2H, ^{m}*H*Ph) 7.18 (m, 2H, ^{o}*H*Ph) 2.92 (s, 6H, N*Me*$_2$)	2.59 (s, 3H) 2.61 (s, 3H)	2.02 (s, 3H) 2.28 (s, 3H)
*[Al(κ^2-bpzFerr)$_2$]$^+$[AlCl$_4$]$^-$ (**5**)	6.96 (s, 1H)	5.27 (s, 1H)	5.96 (s, 1H) 6.19 (s, 1H)	3.68 (m, 1H, Cp) 4.11 (m, 1H, Cp) 4.21 (m, 1H, Cp) 4.28 (s, 5H, Cp') 4.49 (s, 1H, Cp)	1.51 (s, 3H) 2.03 (s, 3H)	2.54 (s, 3H) 2.69 (s, 3H)

*Spectra were recorded in $CDCl_3$ and CD_3CN (**5**).* Chemical shifts corresponding to the major isomer in solution.*

Table 3. *^{1}H-NMR data for complexes **2-9** (continued).*

Compound	CH	CH[a]	H$^{4,4'}$	R, R'	Me$^{3,3'}$	Me$^{5,5'}$
[Ga(κ^3-bpzbe)$_2$]$^+$[GaCl$_4$]$^-$ (**6**)	6.44 (s, 1H)	3.78 (s, 1H)	6.01 (s, 1H) 6.09 (s, 1H)	0.97 (s, 9H, ^{t}*Bu*)	2.09 (s, 3H) 2.10 (s, 3H)	2.43 (s, 3H) 2.57 (s, 3H)
[Ga(κ^3-bpzte)$_2$]$^+$[GaCl$_4$]$^-$ (**7**)	6.28 (s, 1H)	4.21 (s, 1H)	5.85 (s, 1H) 6.17 (s, 1H)	7.05 (d, J_{HH} = 7.0 Hz, 2H, ^{m}*H*Ph) 7.19 (d, J_{HH} = 6.8 Hz, 2H, ^{o}*H*Ph) 2.29 (s, 3H, *Me*Ph)	2.15 (s, 3H) 2.63 (s, 3H)	1.35 (s, 3H) 1.77 (s, 3H)
[Ga(κ^3-bpzappe)]$^+$[GaCl$_4$]$^-$ (**8**)	7.30 (s, 1H)	-	5.52 (s, 1H) 5.86 (s, 1H)	6.50 (d, J_{HH} = 8.6 Hz, 2H, ^{m}*H*NPh) 7.77 (d, J_{HH} = 8.2 Hz, 2H, ^{o}*H*NPh) 7.18 (m, 2H, ^{m}*H*Ph) 7.13 (m, 1H, ^{p}*H*Ph) 7.80 (d, J_{HH} = 7.6 Hz, 2H, ^{o}*H*Ph) 2.77 (s, 6H, N*Me$_2$*)	1.51 (s, 3H) 2.63 (s, 3H)	1.16 (s, 3H) 2.20 (s, 3H)
[Ga(κ^3-bpzFerr)]$^+$[GaCl$_4$]$^-$ (**9**)	6.15 (s, 1H)	4.71 (s, 1H)	5.84 (s, 1H) 5.98 (s, 1H)	4.07 (s, 1H, Cp) 4.11 (s, 1H, Cp) 4.23 (s, 1H, Cp) 4.29 (s, 5H, Cp') 4.42 (s, 1H, Cp)	1.98 (s, 3H) 2.50 (s, 3H)	1.31 (s, 3H) 2.08 (s, 3H)

Spectra recorded in $CDCl_3$.

Table 4. *^{13}C-{^{1}H}-NMR data for complexes **2-9**.*

Compound	CH	C^{a}	$C^{3,3'}$, $C^{5,5'}$	$C^{4,4'}$	R, R'	$Me^{3,3'}$	$Me^{5\,5'}$
$[Al(\kappa^2\text{-bpzbe})_2]^+[AlCl_4]^-$ (**2**)	64.0	83.7	139.2, 141.3 149.7, 151.7	107.2 107.9	25.3 (^{t}Bu) 35.6 (*C*-^{t}Bu)	12.9 14.2	10.7 11.1
$[Al(\kappa^2\text{-bpzte})_2]^+[AlCl_4]^-$ (**3**)	68.4	79.9	138.4, 140.6 150.2, 150.9	106.4 107.1	141.5-137.8 ($C^{ipso,p}$-Ph) 126.7 (C^{o}-Ph) 129.1 (C^{m}-Ph) 21.7 *Me*Ph	11.7 12.5	10.1 11.5
$[Al(\kappa^2\text{-bpzappe})_2]^+[AlCl_4]^-$ (**4**)	69.0	83.0	138.8 151.0	107.4	107.5 (C^{o}-NPh) 128.1 (C^{m}-NPh) 144.7-126.3 (Ph) 40.2 N*Me*$_2$	14.7	11.1 11.2
*$[Al(\kappa^2\text{-bpzFerr})_2]^+[AlCl_4]^-$ (**5**)	66.0	74.4	140.4, 142.2 150.6, 150.8	106.7 107.4	68.6 (Cp') 68.1-64.8 (Cp)	11.1 12.4	10.5 12.0

*Spectra were recorded in $CDCl_3$ and CD_3CN (**5**).* Chemical shifts corresponding to the major isomer in solution.*

Table 4. *^{13}C-{^{1}H}-NMR data for complexes **2-9** (continued).*

Compound	CH	C^{a}	$C^{3,3'}$, $C^{5,5'}$	$C^{4,4'}$	R, R'	$Me^{3,3'}$	$Me^{5\ 5'}$
[Ga(κ^3-bpzbe)$_2$]$^+$[GaCl$_4$]$^-$ (**6**)	62.4	86.4	139.2, 141.3 150.0, 151.1	107.0 107.4	26.5 (^{t}Bu) 35.9 (*C*-^{t}Bu)	12.7 13.9	11.1 11.7
[Ga(κ^3-bpzte)$_2$]$^+$[GaCl$_4$]$^-$ (**7**)	68.0	79.4	138.7, 141.9 149.8, 150.6	106.8 108.1	126.4 (C^o-Ph) 128.3 (C^m-Ph) 138.7-140.8 (C^{ipso,p}-Ph) 21.2 *Me*Ph	11.5 12.6	10.3 11.7
[Ga(κ^3-bpzappe)]$^+$[GaCl$_4$]$^-$ (**8**)	69.0	78.5	140.0, 141.0 148.6, 149.7	105.6 106.8	111.0 (C^o-NPh) 127.0 (C^m-NPh) 125.1-145.2 (Ph) 39,8 NMe$_2$	11.4 11.8	10.4 10.6
[Ga(κ^3-bpzFerr)]$^+$[GaCl$_4$]$^-$ (**9**)	66.9	75.5	140.6, 141.7 149.1, 150.7	106.8 107.5	65.2-71.0 (Cp, Cp') 91.7 (Cp)	11.4 12.4	10.9 11.7

Spectra were recorded in $CDCl_3$.

Complexes **2-9** were further characterised by Matrix Assisted Laser Desorption/Ionisation Time of Flight Mass Spectrometry (MALDI-ToF). The spectra for complexes **2-9** showed ions for metal complexes containing two heteroscorpionate ligands with the general formula $[M(L)_2]^+$. As an example, the MALDI-ToF spectrum for complex $[Al(\kappa^2\text{-bpzbe})_2]^+[AlCl_4]^-$ (**2**) is shown in Figure 25a. As it can be seen, the mass spectrum shows a single peak at m/z 605.509 which corresponds to a cationic aluminium complex supported by two heteroscorpionate ligands with the molecular formula $[Al(\kappa^2\text{-bpzbe})_2]^+$. Furthermore, the isotopic distribution matches the simulated spectrum (Figure 25b). These results confirm the molecular structure proposed on the basis of solution-state NMR spectroscopy, in which the aluminium centre exhibits a pseudo-tetrahedral environment with two heteroscorpionate ligands coordinated in a κ^2-NO manner.

The proposed structure for these compounds was further confirmed by X-Ray diffraction analysis of complex $[Ga(\kappa^3\text{-bpzbe})_2]^+[GaCl_4]^-$ (**6**). The corresponding ORTEP diagram is given in Figure 26. This complex shows an ionic structure with two gallium centres. The cationic gallium moiety adopts an octahedral geometry with two heteroscorpionate ligands coordinated in a tridentate κ^3-NNO manner to the metal centre through the pyridinic nitrogen atoms of the pyrazole rings and the oxygen atoms from the alkoxide groups in a *trans* disposition. In addition, the second gallium centre is coordinated to four chloride ligands as an anionic tetrahedral counterion. The structure in solid state is consistent with that proposed in Scheme 14 on the basis of solution-state NMR spectroscopy. Complex **6** crystallises in solid state as a racemic mixture of a single diastereoisomer *SR/RS*. The structure of enantiomer *SR* for complex **6** is depicted in Figure 26.

Bond distances between gallium centre and nitrogen atoms from the pyrazole rings (Table 5) present values of 2.091(7) Å and 2.149(7) Å, which are similar to the ones found for other chloride gallium complexes supported by scorpionate ligands described in literature.[27] On the other hand, the bond distance between the oxygen atom from the alkoxide moiety and the gallium atom (Table 5) of 1.867(5) Å, is slightly higher compared to other gallium alkoxide complexes previously reported.[42]

Bond angles (Table 5) confirm a distorted octahedral geometry for the gallium cationic moiety. Thus, the maximum distortion is observed for the angle between

N(1^{i})–Ga(1)–N(3^{i})/N(1)–Ga(1)–N(3) with a value of 83.8(3)º and N(1)–Ga(1)–N(3^{i})/ N(1^{i})–Ga(1)–N(3) with a value of 96.2(3)º. The geometry at the anionic gallium moiety Ga(2) is distorted tetrahedral, with the dihedral angle between the Cl(1)–Ga(2)–Cl(1^{ii}) and Cl(2)–Ga(2)–Cl(2^{ii}) planes of 87.8º.

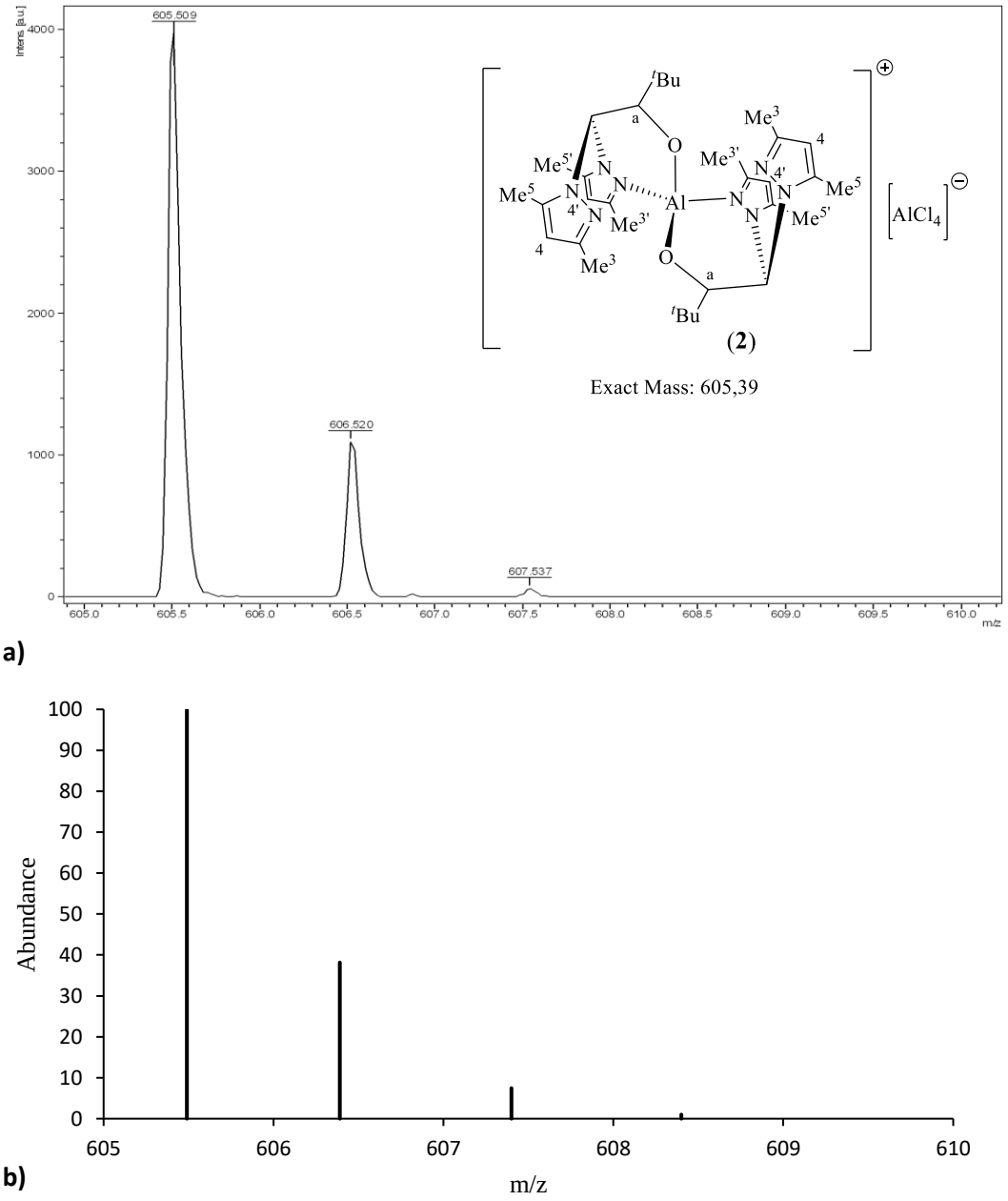

Figure 25. *a) MALDI-ToF spectrum obtained for complex **2**. b) Simulated MALDI-TOF spectrum for complex **2**.*

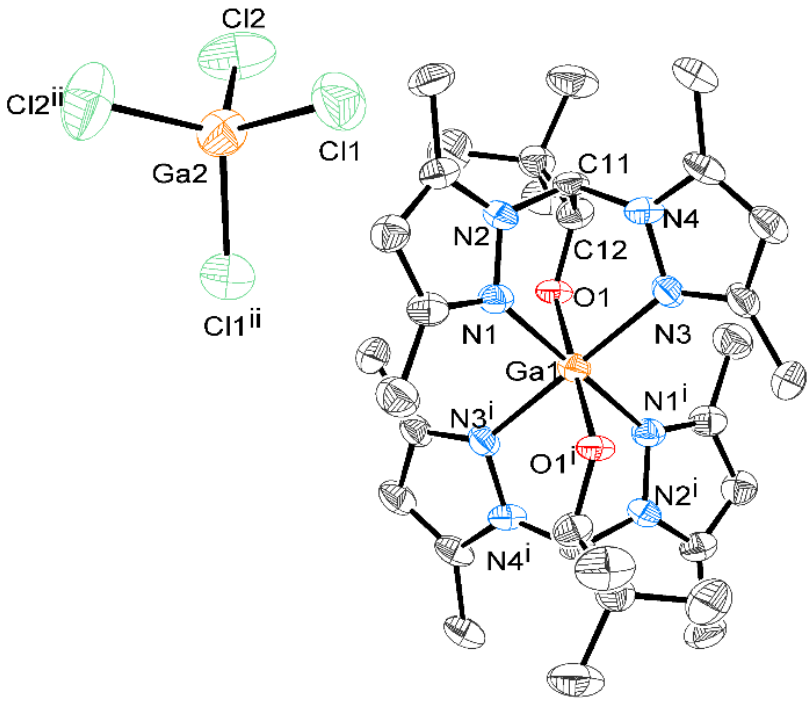

Figure 26. *ORTEP diagram for complex [Ga(κ^3-bpzbe)$_2$]$^+$[GaCl$_4$]$^-$ (**6**).*

Table 5. *Bond distances and angles for complex [Ga(κ^3-bpzbe)$_2$]$^+$[GaCl$_4$]$^-$ (**6**).*

Distances (Å)		**Angles (º)**	
[Ga(κ^3-bpzbe)$_2$]$^+$[GaCl$_4$]$^-$ (**6**)			
Ga(1)–O(1)	1.867(5)	O(1)–Ga(1)–N(1^i)	94.1(3)
Ga(1)–O(1^i)	1.867(5)	O(1^i)–Ga(1)–N(1^i)	85.9(3)
Ga(1)–N(1^i)	2.091(7)	N(1^i)–Ga(1)–N(3^i)	83.8(3)
Ga(1)–N(1)	2.091(7)	N(1)–Ga(1)–N(3^i)	96.2(3)
Ga(1)–N(3^i)	2.149(7)	O(1)–Ga(1)–N(3^i)	89.9(2)
Ga(1)–N(3)	2.149(7)	O(1)–Ga(1)–N(3)	90.1(2)
Ga(2)–Cl(2)	2.145(3)	O(1)–Ga(1)–O(1^i)	180.0
Ga(2)–Cl(2^{ii})	2.145(3)	N(1^i)–Ga(1)–N(1)	180.0
Ga(2)–Cl(1^{ii})	2.152(3)	N(3^i)–Ga(1)–N(3)	180.0(3)
Ga(2)–Cl(1)	2.152(3)	N(1)–Ga(1)–N(3)	83.8(3)
		Cl(2)–Ga(2)–Cl(2^{ii})	112.3(2)
		Cl(2)–Ga(2)–Cl(1^{ii})	107.73(12)
		Cl(2)–Ga(2)–Cl(1)	109.82(14)
		Cl(1^{ii})–Ga(2)–Cl(1)	109.44(19)

2.2. Synthesis of chloride indium complexes

The synthesis of chloride indium complexes was carried out following the same procedure as their chloride aluminium and gallium analogues described previously (Scheme 14), obtaining the corresponding chloride indium complexes $[InCl_2\{(\kappa^3\text{-bpzbe})(\mu\text{-O})\}]_2$ (**10**), $[InCl_2\{(\kappa^3\text{-bpzte})(\mu\text{-O})\}]_2$ (**11**), $[InCl_2\{(\kappa^3\text{-bpzappe})(\mu\text{-O})\}]_2$ (**12**) and $[InCl_2\{(\kappa^3\text{-bpzFerr})(\mu\text{-O})\}]_2$ (**13**). These copounds were isolated as white (**10**-**12**) and pale yellow (**13**) solids after the appropriate work-up (Scheme 15). All complexes were obtained in good yields (85-90%) and are soluble in polar solvents such as MeCN and slightly soluble in halogenated solvents such as CH_2Cl_2 or $CHCl_3$.

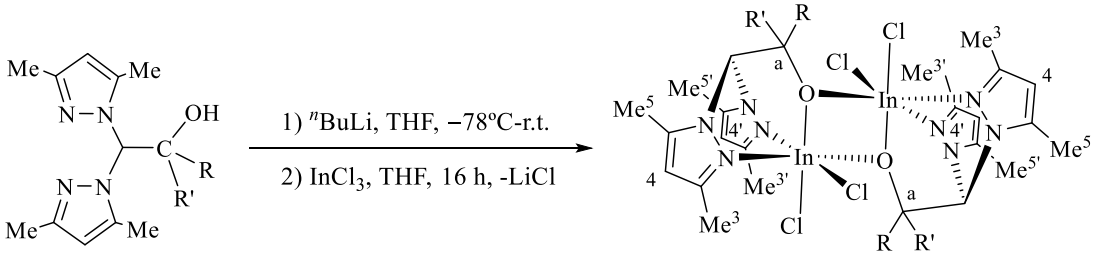

R' = ^{t}Bu, R = H
R' = *p*-MeC_6H_4, R = H
R' = *p*-$(NMe_2)C_6H_4$, R = Ph
R'= Ferr, R = H (**1**)

R' = ^{t}Bu, R = H (**10**)
R' = *p*-MeC_6H_4, R = H (**11**)
R' = *p*-$(NMe_2)C_6H_4$, R = Ph (**12**)
R' = Ferr, R = H (**13**)

Scheme 15. *Synthesis of heteroscorpionate chloride indium complexes.*

Structural Characterisation

Characterisation of complexes **10**-**13** was performed by ^{1}H and $^{13}C\{^1H\}$-NMR spectroscopy. ^{1}H-NMR spectra for complexes **10**-**13** exhibited two distinct sets of pyrazole resonances, showing two singlets for the $H^{4,4'}$, $Me^{3,3'}$and $Me^{5,5'}$ pyrazole protons, one singlet for the methine group, and the signals corresponding to the R and R' moieties of the heteroscorpionate ligands. Figure 27a,b shows the ^{1}H-NMR and $^{13}C\{^1H\}$-NMR spectra respectively for complex **10** in CD_3CN.

NOESY-1D experiments were performed for the assignment of most ^{1}H NMR resonances and ^{1}H-^{13}C heteronuclear correlation (g-HSQC) experiments were carried out to assign the resonances corresponding to C^4, Me^3 and Me^5 of the pyrazole rings.

Figure 28 shows the correlation spectrum for complex $[InCl_2\{(\kappa^3\text{-bpzappe})(\mu\text{-O})\}]_2$ (**12**).

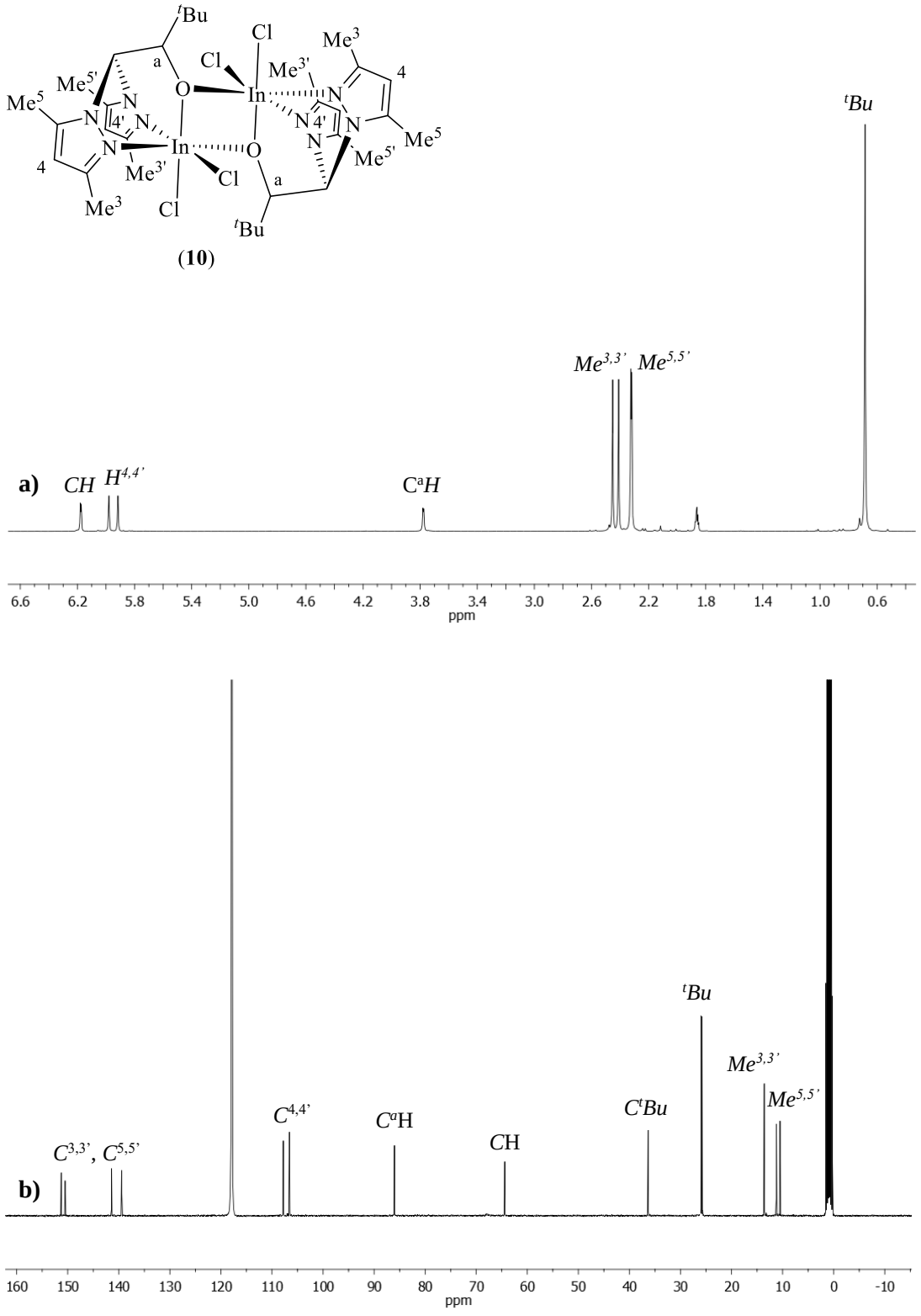

Figure 27. *a) ^{1}H-NMR spectrum and b) ^{13}C{^{1}H}-NMR spectrum for complex $[InCl_2\{(\kappa^3\text{-bpzbe})(\mu\text{-O})\}]_2$ (**10**) in CD_3CN.*

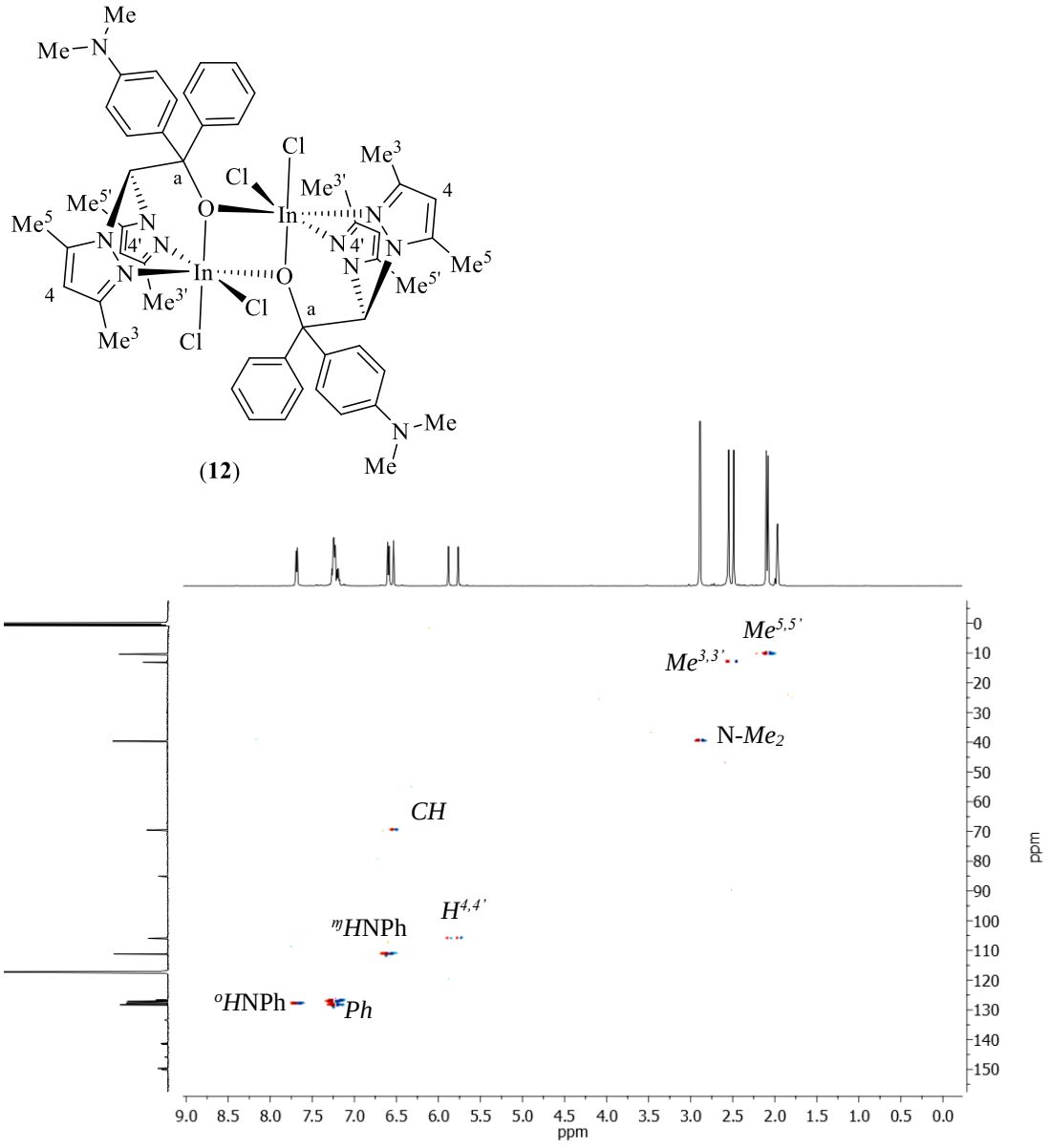

Figure 28. *^{1}H-^{13}C-gHSQC spectrum for complex $[InCl_2\{(\kappa^3\text{-bpzappe})(\mu\text{-}O)\}]_2$ (**12**) in CD_3CN.*

Table 6. *^{1}H-NMR data for complexes **10-14**.*

Compound	CH	CH[a]	H$^{4,4'}$	R, R'	Me$^{3,3'}$	Me$^{5,5'}$
$[InCl_2\{(\kappa^3\text{-bpzbe})(\mu\text{-O})\}]_2$ (**10**)	6.18 (d, J_{HH} = 2.4 Hz, 1H)	3.78 (d, J_{HH} = 2.3 Hz, 1H)	5.92 (s, 1H) 5.98 (s, 1H)	0.68 (s, 9H, ^{t}Bu)	2.41 (s, 3H) 2.45 (s, 3H)	2.32 (s, 3H) 2.32 (s, 3H)
$[InCl_2\{(\kappa^3\text{-bpzte})(\mu\text{-O})\}]_2$ (**11**)	6.18 (s, 1H)	5.50 (s,1H)	5.76 (s, 1H) 6.08 (s, 1H)	7.07 (d, J_{HH} = 7.7 Hz, 2H, ^{m}HPh) 7.42 (d, J_{HH} = 7.7 Hz, 2H, ^{o}HPh) 2.29 (s, 3H, *Me*Ph)	2.54 (s, 3H) 2.58 (s, 3H)	2.47 (s, 3H) 2.29 (s, 3H)
$[InCl_2\{(\kappa^3\text{-bpzappe})\}(\mu\text{-O})\}]_2$ (**12**)	6.53 (s, 1H)	-	5.76 (s, 1H) 5.88 (s, 1H)	6.59 (d, J_{HH} = 8.4 Hz, 2H, ^{m}HNPh) 7.68 (d, J_{HH} = 7.3 Hz, 2H, ^{o}HNPh) 7.24 (m, 5H, *Ph*) 2.89 (s, 6H, NMe_2)	2.50 (s, 3H) 2.55 (s, 3H)	2.08 (s, 3H) 2.10 (s, 3H)
$[InCl_2\{(\kappa^3\text{-bpzFerr})(\mu\text{-O})\}]_2$ (**13**)	6.03 (d, J_{HH} = 3.4 Hz, 1H)	5.34 (d, J_{HH} = 3.2 Hz, 1H)	5.75 (s, 1H) 6.07 (s, 1H)	3.89 (s, 1H, Cp) 4.03 (s, 1H, Cp) 4.18 (s, 5H, Cp') 4.28 (s, 1H, Cp) 4.63 (s, 1H, Cp)	2.48 (s, 3H) 2.56 (s, 3H)	2.05 (s, 3H) 2.48 (s, 3H)
$[\{InCl_2(\kappa^3\text{-bpzbe})\}_2(\mu\text{-}H_2O)]$* (**14**)	6.24 (d, J_{HH} = 2.8 Hz, 1H)	4.26 (d, J_{HH} = 2.5 Hz, 1H)	5.98 (s, 1H) 6.14 (s, 1H)	0.80 (s, 9H, ^{t}Bu)	2.45 (s, 3H) 2.65 (s, 3H)	2.38 (s, 3H) 2.43 (s, 3H)

*Spectra recorded in CD_3CN and CD_2Cl_2 (**14**)**

Table 7. *^{13}C-{^{1}H}-NMR data for complexes **10-14**.*

Compound	CH	C^{a}	$C^{3,3'}$, $C^{5,5'}$	$C^{4,4'}$	R, R'	$Me^{3,3'}$	$Me^{5\ 5'}$
$[InCl_2\{(\kappa^3\text{-bpzbe})(\mu\text{-O})\}]_2$ (**10**)	64.4	86.0	139.4, 141.4 150.5, 151.3	106.6 107.8	26.1 (^{t}Bu) 36.3 (*C*-^{t}Bu)	13.6	11.1 11.7
$[InCl_2\{(\kappa^3\text{-bpzte})(\mu\text{-O})\}]_2$ (**11**)	67.7	79.2	137.4, 138.0 151.6, 152.1	106.2 107.0	126.9 (C^{o}-Ph) 128.8 (C^{m}-Ph) 139.8-141.6 ($C^{ipso,p}$-Ph) 20.9 *Me*Ph	13.3 13.9	9.9 10.9
$[InCl_2\{(\kappa^3\text{-bpzappe})\}(\mu\text{-O})\}]_2$ (**12**)	69.5	85.0	141.2, 141.5 149.9, 150.0	105.9 106.0	111.2 (C^{o}-NPh) 127.7 (C^{m}-NPh) 126.7-149.7 (Ph) 39.6 NMe_2	13.1 13.2	10.4
$[InCl_2\{(\kappa^3\text{-bpzFerr})(\mu\text{-O})\}]_2$ (**13**)	68.0	76.4	140.0, 141.3 150.1, 150.2	105.8 106.2	64.1-68.5 (Cp,Cp') 91.3 (Cp)	13.0 13.1	10.1
$[\{InCl_2(\kappa^3\text{-bpzbe})\}_2(\mu\text{-}H_2O)]$* (**14**)	63.5	88.2	138.9, 140.8 150.2, 151.7	107.3 108.2	27.4 (^{t}Bu) 38.5 (*C*-^{t}Bu)	13.4 15.2	10.6 11.8

*Spectra recorded in CD_3CN and CD_2Cl_2 **(14)****

The solid-state structure of complex **10** was confirmed by X-Ray diffraction studies (Figure 29). This complex shows a dimeric structure in which each indium centre exhibits a distorted octahedral geometry with the heteroscorpionate ligand coordinated in a κ^3-NNO fashion, two chloride atoms and the last position of the coordination sphere occupied by the oxygen atom from the alkoxide group, which also acts as bridging atom between both indium centres. The crystal structure is consistent with the one proposed in Scheme 15 on the basis of solution-state NMR spectroscopy. In solid-state, complex **10** crystallises as a racemic mixture of a single diastereoisomer *RR/SS* and the structure for enantiomer *RR* is depicted in Figure 29.

Bond distances (Table 8) between the indium and chloride atoms are quite similar, with values of 2.407 and 2.415 Å and are slightly lower than the ones found for other indium chloride complexes.[50] Also, bond distances between the indium and oxygen atoms are also quite similar, with values of 2.156 and 2.171 Å, which are slightly higher than the ones found for other alkoxide indium complexes.[50] Finally, bond distances between the indium and nitrogen atoms are 2.267 Å for the In(1)–N(1) bond and 2.372 Å for the In(1)–N(3) bond, which are slightly higher than those found for other indium complexes with scorpionate ligands.[47,48] Bond angles (Table 8) confirmed the distorted octahedral structure proposed, with the maximum distorted value of 162.20(16)º observed for the O(1A)–In(1)–N(1) angle.

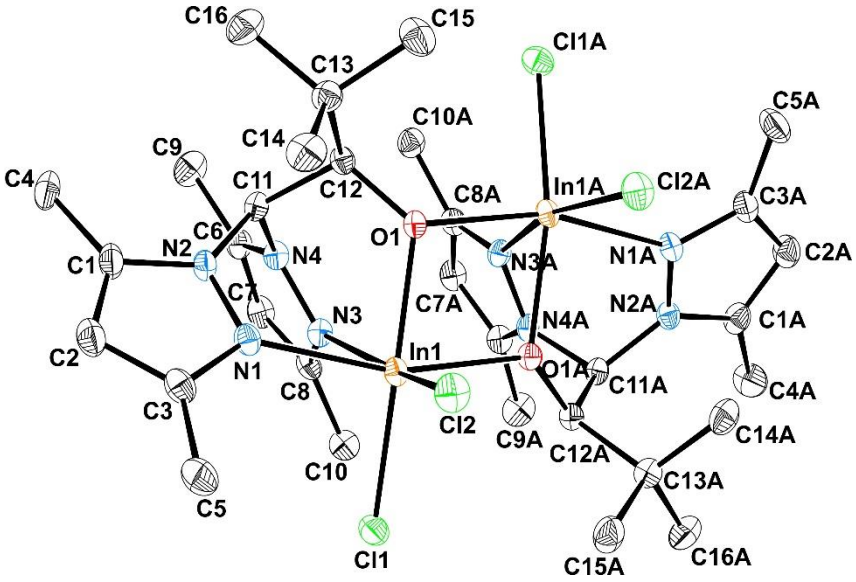

Figure 29. *ORTEP diagram for complex [InCl$_2${(κ^3-bpzbe)(μ-O)}]$_2$ (**10**).*

Complex **10** was found to be stable under inert atmosphere in different solvents. However, in an attempt to crystallise complex **10** in CH_2Cl_2, a new dinuclear complex [{$InCl_2(\kappa^3$-bpzbe)}$_2(\mu$-H_2O)] (**14**) with one water molecule bridging both indium centres was obtained (Scheme 16). This was attributed to the presence of small traces of water in the solvent. The structure proposed for complex **14** was further confirmed by X-Ray diffraction studies. The ORTEP diagram for this complex is shown in Figure 30. In this complex, the indium atom exhibits a distorted octahedral environment with the heteroscorpionate ligand coordinated in a κ^3-NNO fashion, two chloride atoms and a molecule of water bridging both metal centres. In the solid-state, complex **14** crystallises as a racemic mixture of a single diastereoisomer *RR/SS* and the structure for enantiomer *RR* is depicted in Figure 30.

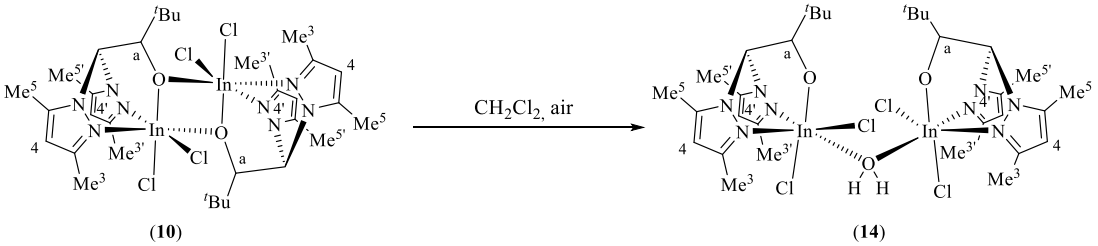

Scheme 16. *Formation of complex **14** from complex **10**.*

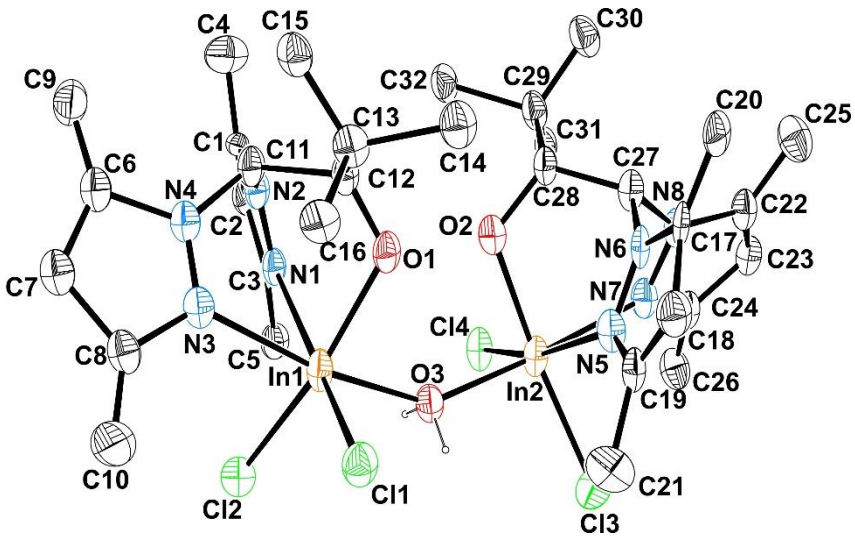

Figure 30. *ORTEP diagram for complex [{$InCl_2(\kappa^3$-bpzbe)}$_2(\mu$-H_2O)] (**14**).*

Bond distances (Table 8) between indium and chloride atoms adopt values between 2.418(10) Å and 2.441(12) Å and are quite similar than the ones found for other indium chloride complexes.[50,51] Also, bond distances between indium and oxygen atoms from

the alkoxide moiety In(1)–O(1) and In(2)–O(2) of 2.13(3) Å and 2.19(3) Å respectively were found to be larger than the distance between indium and oxygen atoms from the water bridging molecule of In(1)–O(3) and In(2)–O(3) of 2.09(2) Å and 2.11(2) Å respectively. Bond angles (Table 8) confirmed the distorted octahedral structure proposed, with the maximum distortion value observed for the O(1)–In(1)–Cl(2) and O(2)–In(2)–Cl(3) angles with 162.5(6)º and 165.3(6)º, respectively.

Table 8. *Bond distances and angles for complexes complex [$InCl_2\{(\kappa^3$-bpzbe)(μ-O)$\}]_2$ (**10**) and [$\{InCl_2(\kappa^3$-bpzbe)$\}_2(\mu$-H_2O)] (**14**).*

Distances (Å)		**Angles (º)**	
[$InCl_2\{(\kappa^3$-bpzbe)(μ-O)$\}]_2$ (**10**)			
In(1)–O(1)	2.156(4)	O(1A)–In(1)–N(1)	162.20(16)
In(1)–O(1A)	2.171(4)	O(1)–In(1)–N(3)	78.13(15)
In(1)–N(1)	2.267(5)	O(1A)–In(1)–N(3)	96.10(15)
In(1)–N(3)	2.372(5)	N(1)–In(1)–N(3)	76.35(16)
In(1)–Cl(1)	2.4068(16)	O(1)–In(1)–Cl(1)	165.83(10)
In(1)–Cl(2)	2.4150(16)	O(1A)–In(1)–Cl(1)	97.98(11)
		N(1)–In(1)–Cl(1)	98.04(13)
		N(3)–In(1)–Cl(1)	89.53(13)
		O(1)–In(1)–Cl(2)	95.64(10)
		N(1)–In(1)–Cl(2)	90.50(12)
		Cl(1)–In(1)–Cl(2)	97.92(6)
[$\{InCl_2(\kappa^3$-bpzbe)$\}_2(\mu$-H_2O)] (**14**)			
In(1)–O(3)	2.09(2)	O(3)–In(1)–O(1)	84.5(9)
In(1)–O(1)	2.13(3)	O(3)–In(1)–N(3)	169.7(11)
In(1)–N(3)	2.29(3)	O(1)–In(1)–Cl(2)	162.5(6)
In(1)–Cl(1)	2.418(10)	O(1)–In(1)–N(1)	73.0(9)
In(1)–Cl(2)	2.441(12)	N(3)–In(1)–N(1)	77.1(10)
In(1)–N(1)	2.45(3)	O(3)–In(2)–O(2)	84.8(9)
In(2)–O(3)	2.11(2)	O(3)–In(2)–N(7)	169.5(10)
In(2)–O(2)	2.19(3)	O(2)–In(2)–N(5)	76.5(10)
In(2)–N(7)	2.21(3)	N(7)–In(2)–N(5)	77.6(10)
In(2)–N(5)	2.35(3)	O(2)–In(2)–Cl(3)	165.3(6)

3. Synthesis of alkyl group 13 metal complexes

3.1. Synthesis of alkyl aluminium complexes

One of the most effective routes to synthesise alkyl aluminium complexes is by protonolysis reaction of the neutral heteroscorpionate ligand precursors with trialkyl aluminium derivatives.[26b,d,33a] Thus, the synthesis of alkyl aluminium complexes was carried out by reacting the corresponding neutral heteroscorpionate precursor bpzFerrH (**1**) with alkyl aluminium derivatives AlX_3 (X = Me, Et) in toluene for two hours at 0 ºC in a 1:1 molar ratio (Scheme 17). The corresponding dialkyl aluminium complexes supported by heteroscorpionate ligands functionalised with alkoxide groups [$AlMe_2(\kappa^2$-bpzFerr)] (**15**) and [$AlEt_2(\kappa^2$-bpzFerr)] (**16**) were obtained in 90% yield and were isolated as orange solids. These complexes are soluble in aliphatic and aromatic hydrocarbons and are thermally stable.

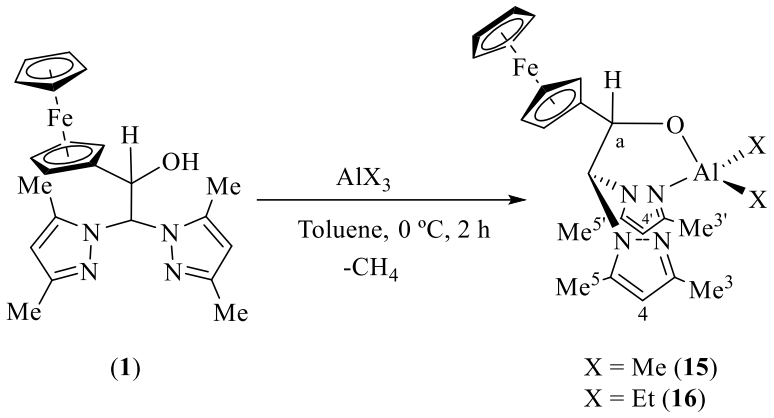

Scheme 17. *Synthesis of alkyl aluminium complexes **15** and **16**.*

Structural Characterisation

The solution-state structures of complexes **15** and **16** were characterised by spectroscopic methods. The ^{1}H-NMR and $^{13}C\{^1H\}$-NMR spectra (Tables 9 and 10) exhibited two sets of signals for the pyrazole rings and the alkyl groups, which indicated that the pyrazole rings are not equivalent (Figures 31 and 32). It is worth noting that some pyrazole proton signals appeared as broad resonances at room temperature (Figure 31), which can indicate the existence of a fluxional process due to an exchange between a coordinated and a non-coordinated pyrazole ring.

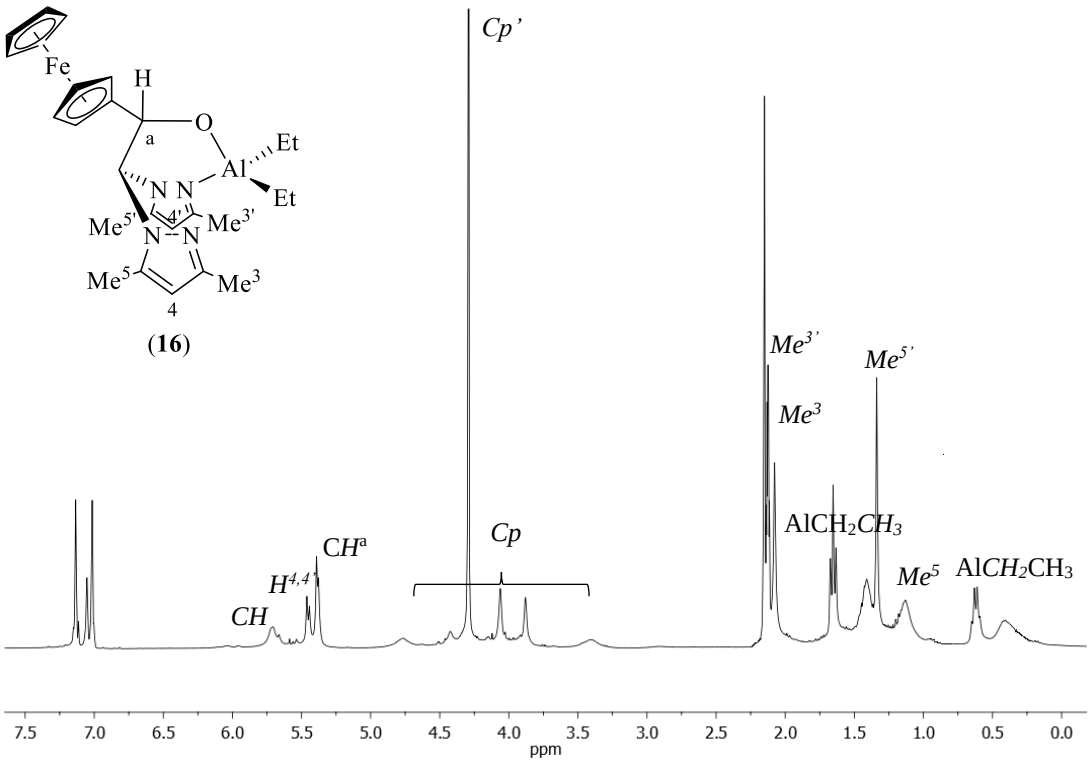

Figure 31. *^{1}H-NMR spectrum for complex [AlEt$_2$(κ^2-bpzFerr)] (**16**) in toluene-d$_8$.*

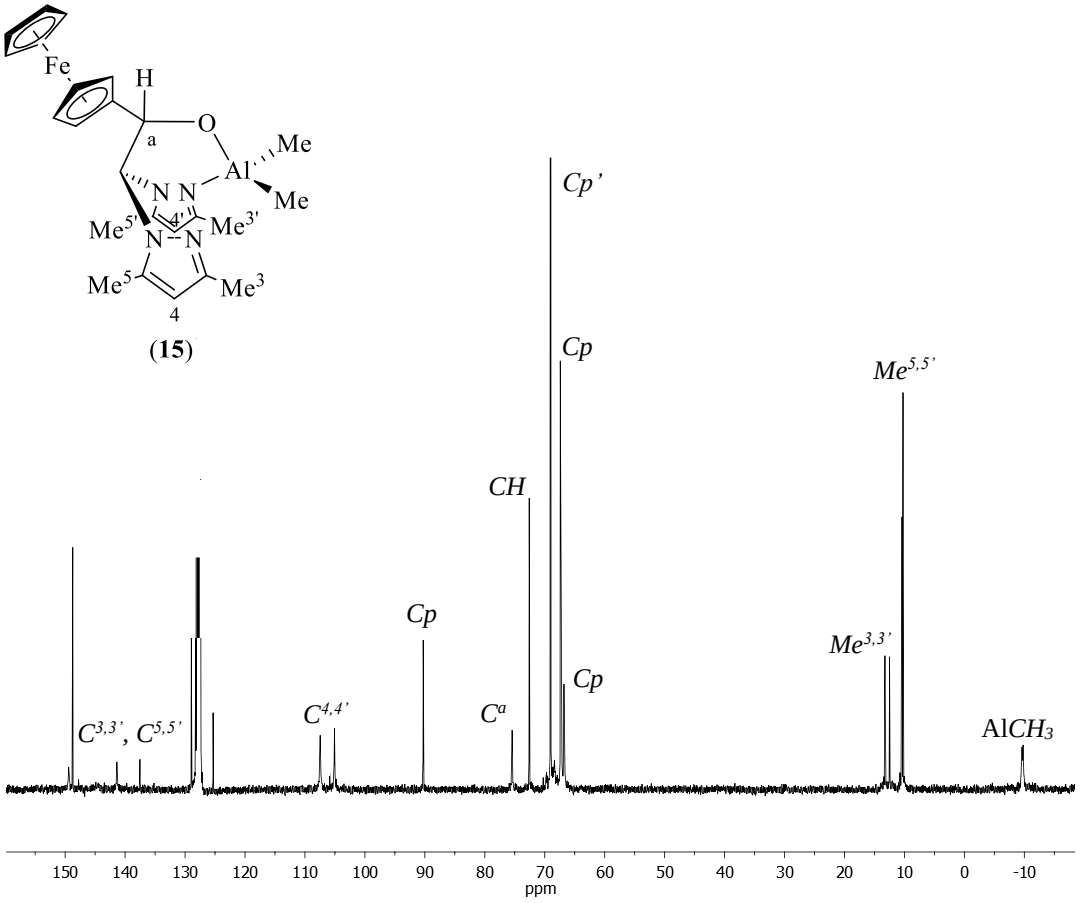

Figure 32. *^{13}C{^{1}H}-NMR spectrum for complex [AlMe$_2$(κ^2-bpzFerr)] (**15**) in C$_6$D$_6$.*

The spectroscopic data in solution is consistent with a tetrahedral environment for the aluminium atom, in which the heteroscorpionate ligand is coordinated to the metal centre in a κ^2-NO coordination mode for compounds **15** and **16**.

NOESY-1D experiments allowed the unequivocal assignment of the pyrazole and alkyl groups resonances. The assignment of the $^{13}C\{^1H\}$-NMR signals was carried out by heteronuclear correlation ^1H-^{13}C-g-HSQC experiments. Figure 33 shows the correlation spectrum for complex [$AlMe_2(\kappa^2$-bpzFerr)] (**15**).

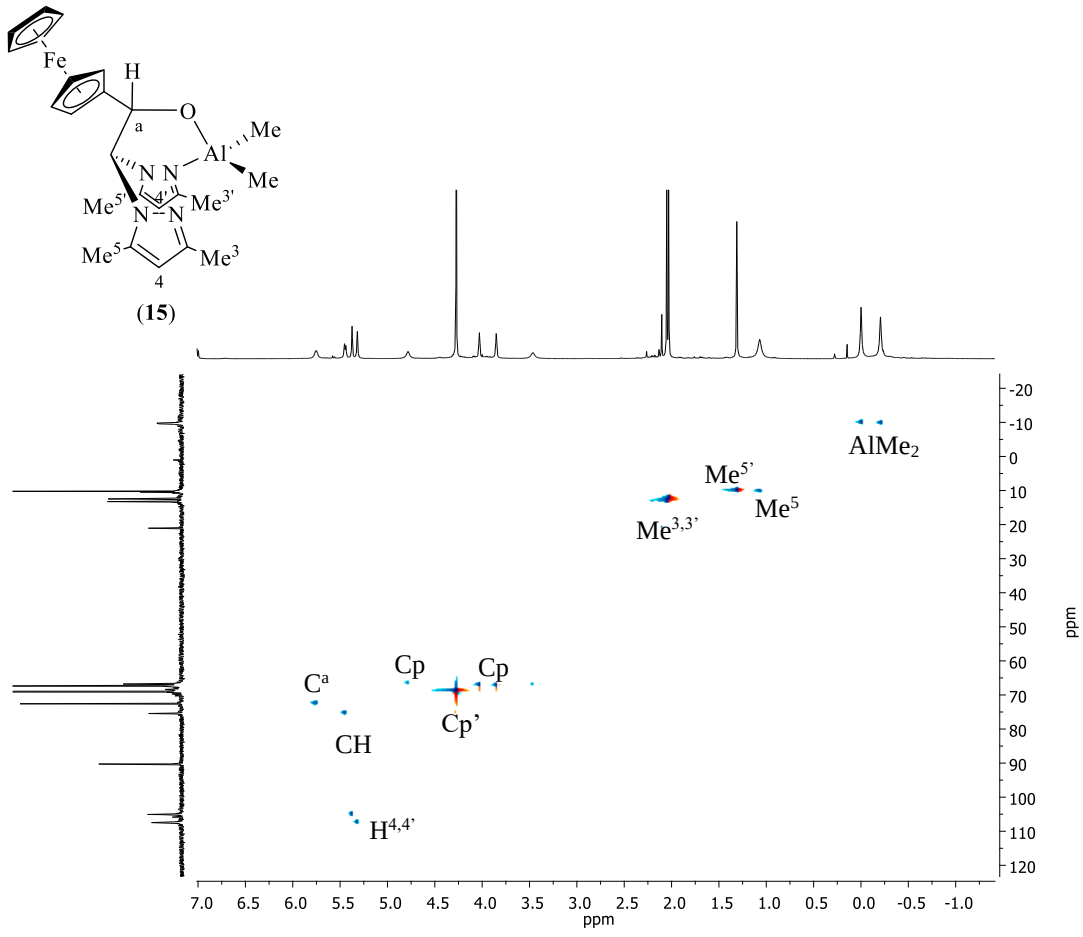

Figure 33. *^1H-^{13}C-gHSQC spectrum for complex [$AlMe_2(\kappa^2$-bpzFerr)] (**15**) in C_6D_6.*

Fluxional process

As it has been previously mentioned, broad signals for some proton and carbon resonances are observed in the NMR spectra at room temperature for complexes **15** and **16**, which is thought to be due to the existence of a fluxional process of rapid exchange process between a coordinated and a non-coordinated pyrazole ring. To study the dynamic behaviour of complexes **15** and **16**, variable-temperature (VT)

NMR experiments were carried out. The VT NMR study for compound **16** in the region of the $Me^{3,3'}$ and $Me^{5,5'}$ groups from the pyrazole rings and the ethyl groups coordinated to the aluminium centre is shown in Figure 34. As can be seen, the resonances of the alkyl groups bonded to the aluminium atom, as well as those of the pyrazole rings become resolved into two peaks which correspond to a single diastereoisomer at −60 °C (Figure 34), supporting that there is no fluxional process between both pyrazole rings at room temperature and only one of them is coordinated to the metal centre. Thus, the temperature was increased in order to reach the coalescence temperature in which the fluxional process of both pyrazole rings starts. The coalescence temperature was reached at 80 ºC, when the ethyl groups resonances broaden. These results are not in agreement with the tendency observed for other alkyl aluminium complexes with heteroscorpionate ligands functionalised with alkoxide groups previously reported by our group, where, at room temperature, exhibited a fast fluxional process between the two pyrazole rings.[34]

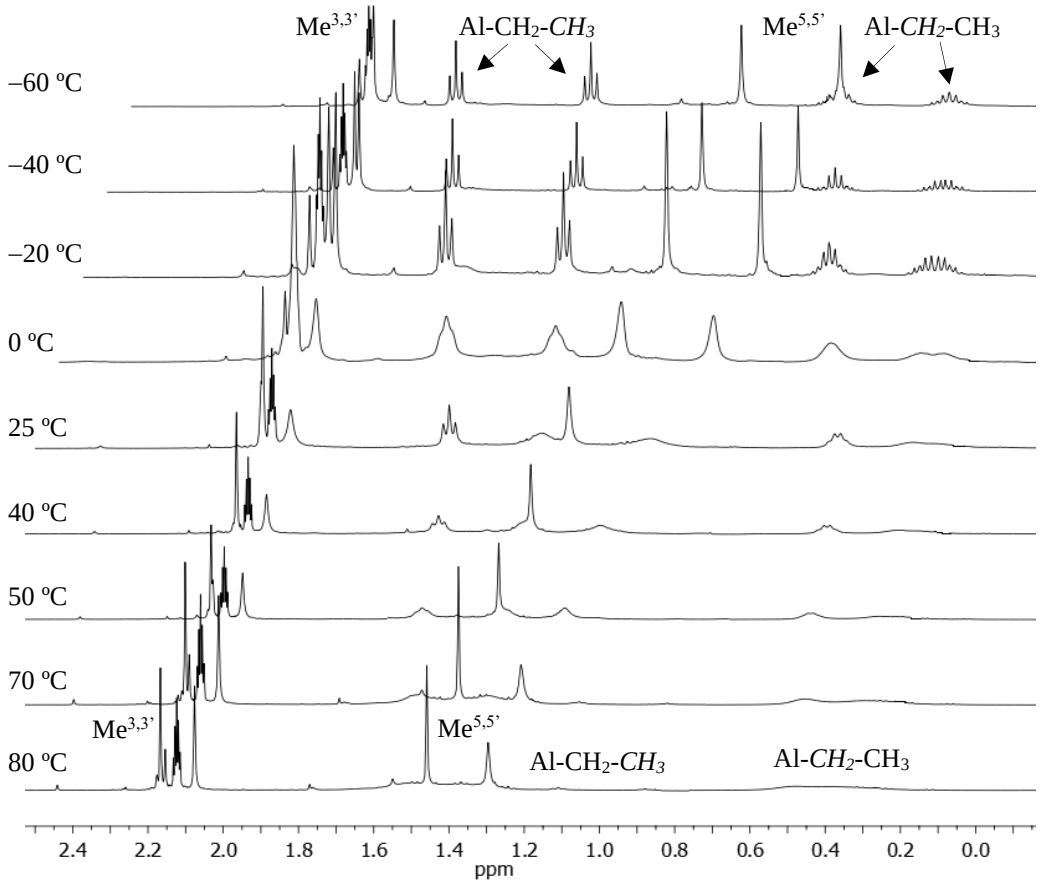

Figure 34. *Variable temperature ^{1}H-NMR study for complex [AlEt$_2$(κ^2-bpzFerr)] (**16**) in toluene-d$_8$.*

Therefore, the presence of two chiral carbon atoms in the heteroscorpionate ligand (C^a and CH bridging both pyrazole rings) leads to the presence of four different stereoisomers (two diastereoisomers) in solution for complexes **15** and **16** which contain a racemic heteroscorpionate ligand (Scheme 18).

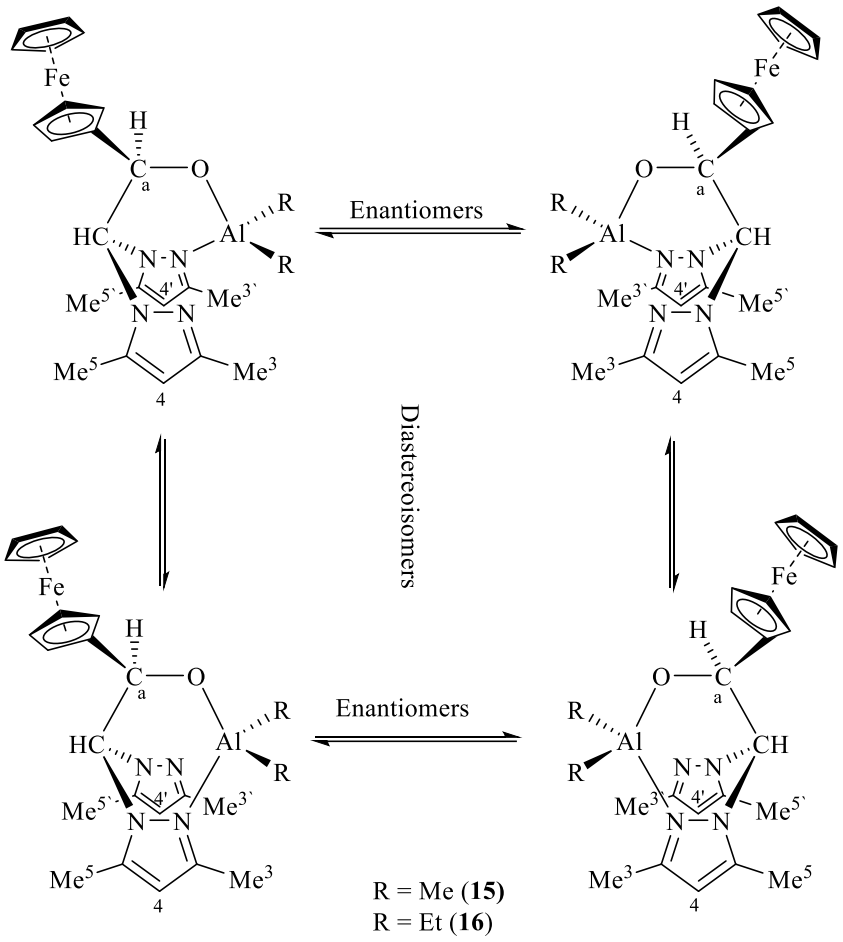

Scheme 18. *Fluxional process for complexes **15-16**.*

Table 9. *^{1}H-NMR data for complexes **15** and **16**.*

Compound	CH	CH[a]	H[4,4']	Ferr	Me[3,3']	Me[5,5']	Al–X
[$AlMe_2$(κ^2-bpzFerr)] (**15**)	5.75 (s, 1H)	5.45 (d, J_{HH} = 7.1Hz, 1H)	5.37 (s, 1H) 5.32 (s, 1H)	3.46 (s, 1H, Cp) 3.85 (s, 1H, Cp) 4.00 (s, 1H, Cp) 4.27 (s, 5H, Cp') 4.78 (s, 1H, Cp)	2.03 (s, 3H) 2.05 (s, 3H)	1.07(s, 3H) 1.31 (s, 3H)	0.00 (s, 3H, AlCH_3) –0.21 (s, 3H, AlCH_3)
[$AlEt_2$(κ^2-bpzFerr)]* (**16**)	5.69 (s, 1H)	5.45 (d, J_{HH} = 7.3Hz, 1H)	5.38 (s, 2H)	3.41 (s, 1H, Cp) 3.88 (s, 1H, Cp) 4.06 (s, 1H, Cp) 4.39 (s, 5H, Cp') 4.76 (s, 1H, Cp)	2.08 (s, 3H) 2.15 (s, 3H)	1.13 (s, 3H) 1.34 (s, 3H)	0.41 (s, 2H, AlCH_2CH_3) 0.62 (q, J_{H-H} = 8.3 Hz; 2H, AlCH_2CH_3) 1.41 (s, 3H, $AlCH_2CH_3$) 1.65 (t, J_{H-H} = 8.1 Hz; 3H, $AlCH_2CH_3$)

*Spectra were recorded in C_6D_6 (**15**) and tol-d_8 (**16**)*.*

Table 10. *^{13}C-{^{1}H}-NMR data for complexes **15** and **16**.*

Compound	CH	C[a]	C[3,3'], C[5,5']	C[4,4']	Ferr	Me[3,3']	Me[5,5']	Al–X
[$AlMe_2$(κ^2-bpzFerr)] (**15**)	72.6	75.5	138.6, 140.3 150.4, 150.8	105.1 107.5	66.8 (Cp) 67.2, 67.3 (Cp) 67.4, 90.3 (Cp) 69.0 (Cp')	12.5 13.2	10.2 10.4	–9.9 (AlCH_3) –9.6 (AlCH_3)
[$AlEt_2$(κ^2-bpzFerr)]* (**16**)	72.7	75.8	138.4, 139.7 150.7, 150.9	104.9 107.6	66.6 (Cp) 67.2 67.3 (Cp) 90.6 (Cp) 69.0 (Cp')	12.4 13.1	9.4 10.4	0.1 (AlCH_2CH_3) 10.1 ($AlCH_2CH_3$) 0.5 (AlCH_2CH_3) 10.4 ($AlCH_2CH_3$)

*Spectra were recorded in C_6D_6 (**15**) and tol-d_8 (**16**)*.*

3.2. Synthesis of alkyl gallium and indium complexes

The synthesis of alkyl gallium and indium complexes was carried out in a two-step reaction as shown in Schemes 19 and 20. In the first step, the corresponding chloride metal precursor MCl_3 (M = Ga, In) was reacted with MeLi in a 1:3.3 (Scheme 19) molar ratio. Then, a solution of the corresponding neutral heteroscorpionate ligand precursor in Et_2O was transferred via cannula and the resulting suspension was stirred overnight at room temperature. The incomplete reaction of the MCl_3 precursors with MeLi allowed the synthesis of heterobimetallic complexes [{Li(κ^3-bpzFerr)(Et_2O)}(μ-O){$GaMe_2Cl$}] (**17**) [{Li(κ^3-bpzbe)(Et_2O)}(μ-O){$InMe_2Cl$}] (**18**), [{Li(κ^3-bpzte)(Et_2O)(μ-O){$InMe_2Cl$}] (**19**), [Li(κ^3-bpzFerr)(Et_2O)}(μ-O){$InMe_2Cl$}] (**20**) in good yields (Scheme 19) after the appropriate work-up procedure.

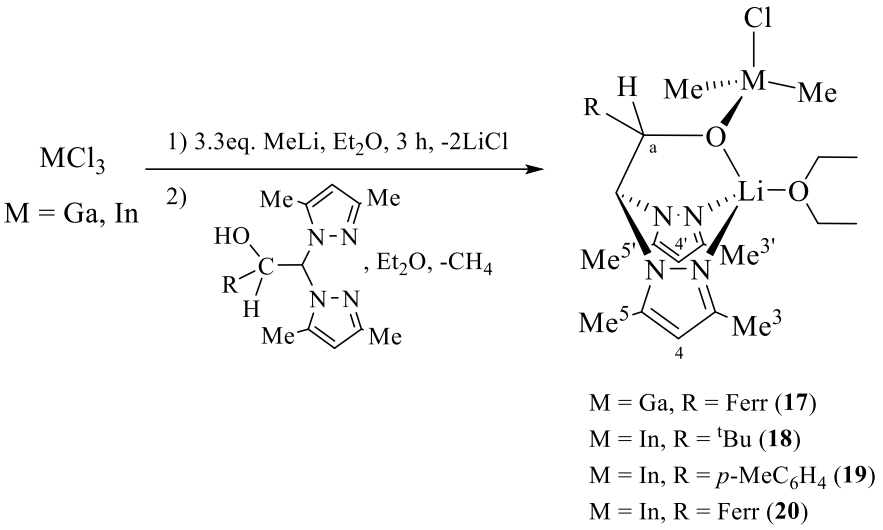

Scheme 19. *Synthesis of heterobimetallic alkyl-chloride complexes **17-20**.*

To avoid the formation of the heterobimetallic derivatives **17-20**, the MCl_3 precursors were reacted with two equivalents of MeLi (Scheme 20). The addition of the ligand precursors led to the synthesis of the mixed methyl-chloride gallium and indium complexes [GaMeCl(κ^3-bpzbe)] (**21**), [GaMeCl(κ^3-bpzte)] (**22**), [$InMe_2Cl$(κ^3-bpzbeH)] (**23**) and [$InMe_2Cl$(κ^3-bpzappeH)] (**24**) (Scheme 20) in moderate yields after the appropriate work-up procedure.

These alkyl complexes were isolated as white (**18**-**19**, **21**-**24**) or orange (**17**, **20**) solids. These complexes are very soluble in aromatic hydrocarbons and slightly soluble in aliphatic hydrocarbons.

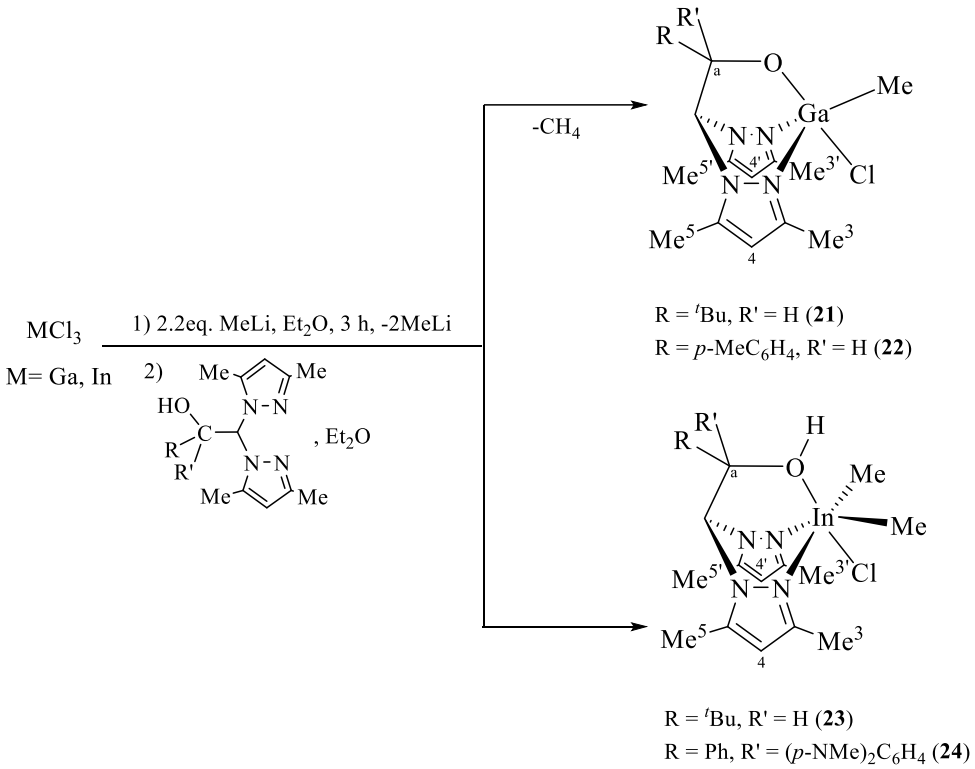

Scheme 20. *Synthesis of alkyl-chloride gallium and indium complexes **21-24**.*

Attempts to synthesise the fully alkyl-derivate analogues complexes were carried out by reacting the lithiated adduct of bpzbeH with $InMe_2Cl$ (generated *in situ* by reacting $InCl_3$ with 2.2 equivalents of MeLi) (Scheme 21). However, the reaction afforded, once again, the formation of [{Li(κ^3-bpzbe)(Et_2O)}(μ-O){$InMe_2Cl$}] (**18**).

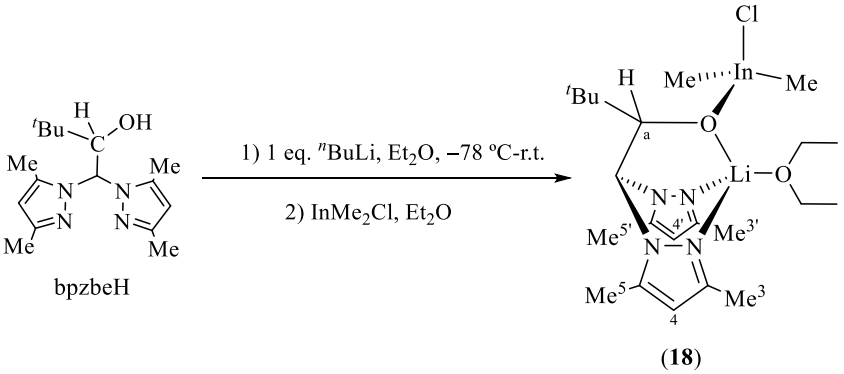

Scheme 21. *Synthesis of complex [{Li(κ^3-bpzbe)(Et_2O)}(μ-O){$InMe_2Cl$}] (**18**) by reaction of the lithiated adduct of bpzbeH and $InMe_2Cl$.*

Structural Characterisation

Complexes **17-24** were characterised by ^{1}H-NMR and ^{13}C{^{1}H}-NMR spectroscopy (Tables 11 and 12) and X-Ray diffraction studies. The study of the ^{1}H-NMR and

$^{13}C\{^{1}H\}$-NMR spectra for complexes **17**-**24** confirmed that both pyrazole rings are not equivalent since two set of signals for the protons and carbons of both pyrazole rings are observed. ^{1}H-NMR spectra for heterobimetallic complexes **17**-**20** showed two singlets in the alkyl region, confirming the formation of the alkyl metal complexes (Figure 35). These findings would fit the proposed structure in Scheme 19, consisting of a heterobimetallic compound in which the heteroscorpionate ligand is coordinated in a κ^3-NNO manner to a lithium atom, which adopts a tetrahedral geometry, with the fourth position occupied by an Et_2O molecule. The gallium/indium atom also adopts a tetrahedral geometry coordinated to two alkyl groups, a chloride ligand, and the oxygen atom from the alkoxide group of the heteroscorpionate ligand through a coordinate covalent or dative bond. This proposed structure was further confirmed by X-Ray crystallography for complex **18**.

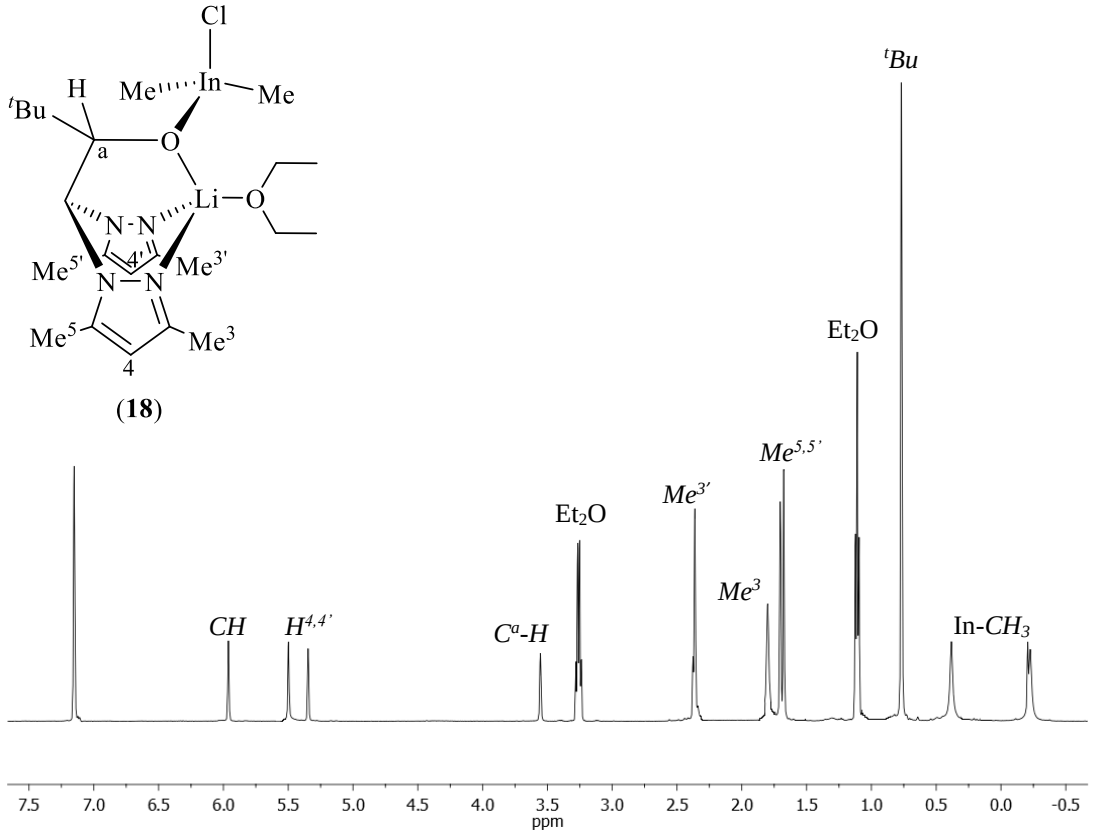

Figure 35. *^{1}H-NMR spectrum for [Li{(κ^3-bpztbe)(Et_2O)}(μ-O){$InMe_2Cl$}] (**18**) complex in C_6D_6.*

On the other hand, only one signal for the methyl group is observed for monometallic complexes **21**-**24**, confirming the formation of the alkyl-chloride specie (Figure 36). In case of indium complexes **23** and **24**, the methyl group signal integrates

for six protons, and another signal corresponding to the O–H proton from the alcohol moiety from the heteroscorpionate ligand is also observed (Figure 37). These findings are consistent with the proposed structures in which the gallium centre in complexes **21** and **22** exhibits a penta-coordinated environment with the heteroscorpionate ligand coordinated in a monoanionic κ^3-NNO fashion, while the indium centre in complexes **23** and **24** exhibits an octahedral geometry with the heteroscorpionate ligands coordinated in a neutral κ^3-NNO fashion.

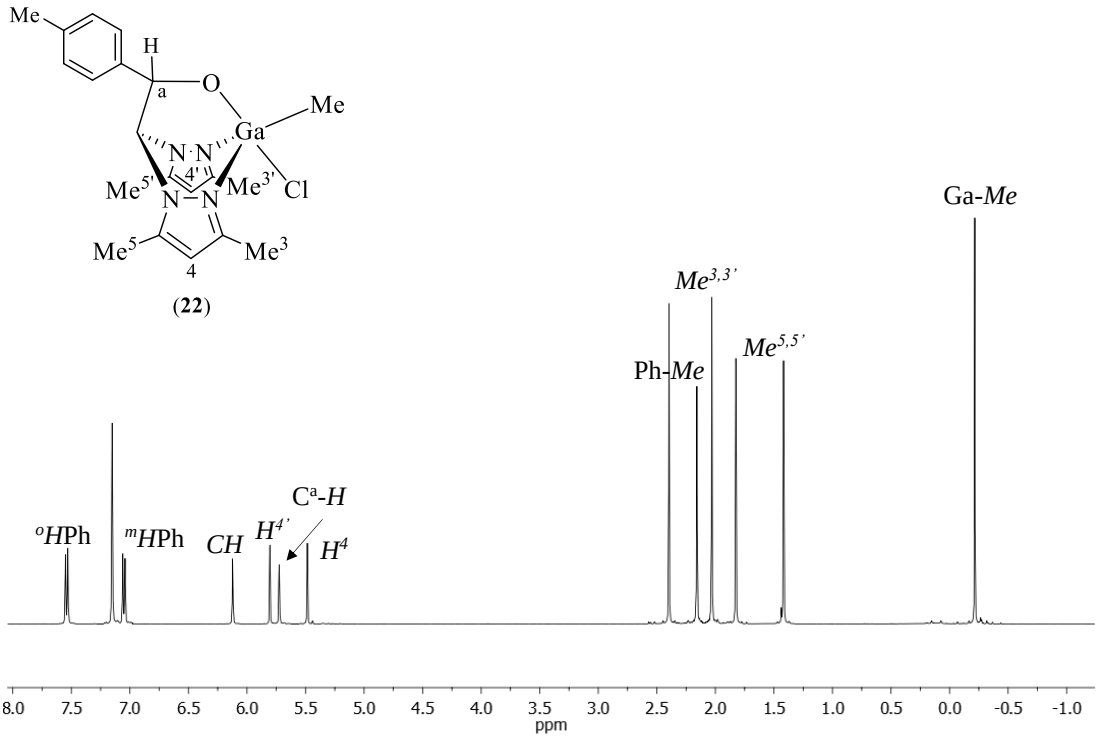

Figure 36. *^{1}H-NMR spectrum for complex [GaMeCl{κ^3-bpzte}] (**22**) in C_6D_6.*

1D NOESY NMR experiments afforded the unequivocal assignment for the NMR resonances of $Me^{3,3'}$ and $Me^{5,5'}$ and $H^{4,4'}$ protons of the pyrazole rings and protons corresponding to the methyl ligand bonded to the metal centre. Figure 38 shows the NOESY-1D experiments performed for complex [$InMe_2Cl(\kappa^3$-bpzbeH)] (**23**). Thus, when irradiating the frequency of the $H^{4,4'}$ protons (noesy 1), a response from the methyl groups $Me^{3,3'}$ and $Me^{5,5'}$ of the pyrazole rings was observed. The irradiation of the alkyl group (noesy 2) protons rose response from the methyl groups from the *tert*-butyl group of the ligand, the O-H and C^a-H proton and with much less intensity from the methyl groups in 3,3' from the pyrazole rings. Finally, the irradiation of the CH

group (noesy 3, Figure 39), gave response from the $Me^{5',5}$ from the pyrazole rings, the CH and the methyl protons from the *tert*-butyl group of the ligand.

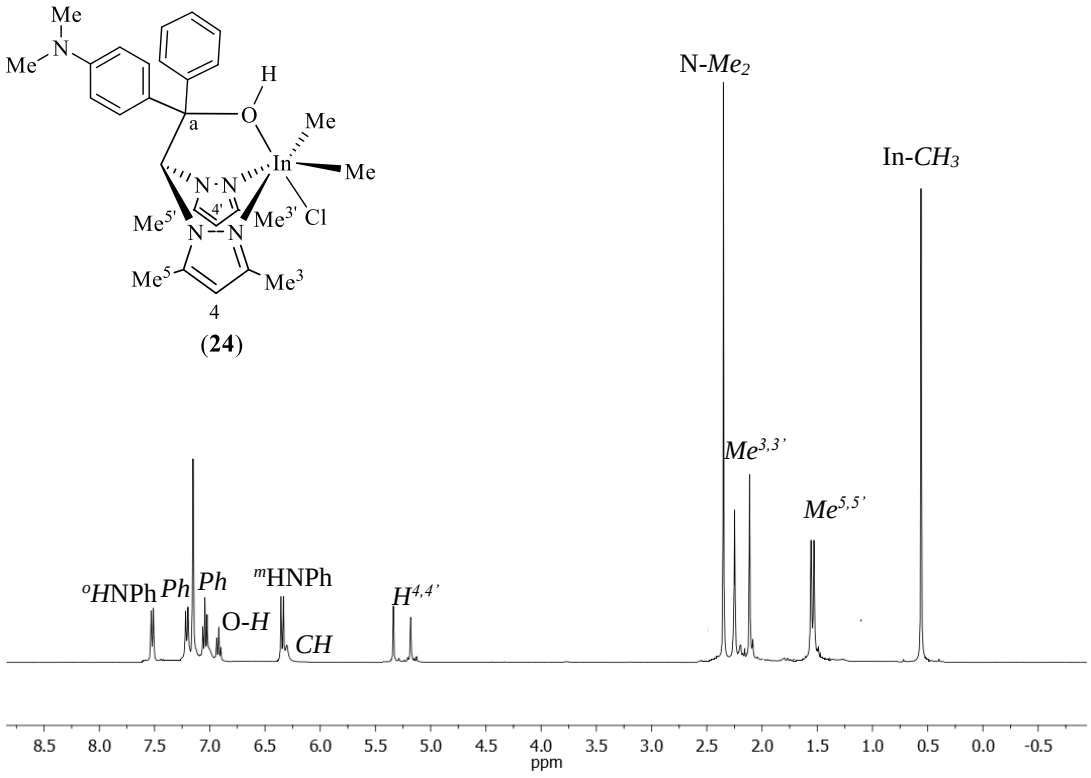

Figure 37. *^{1}H-NMR spectrum for complex [InMe$_2$Cl(κ^3-bpzappeH)] (**24**) in C_6D_6.*

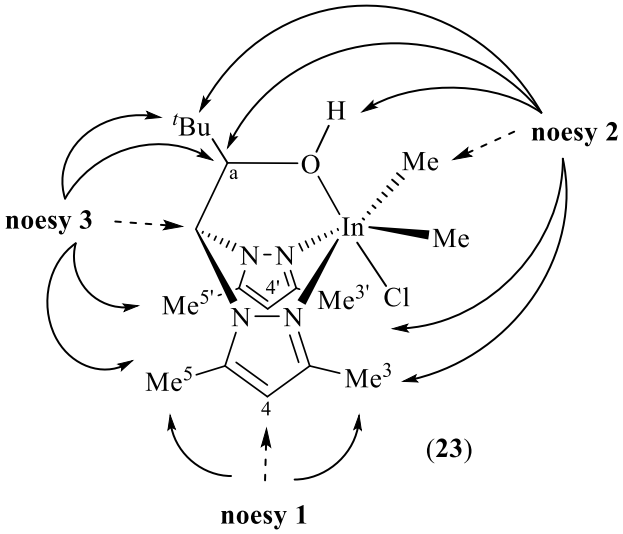

Figure 38. *NOESY-1D experiments performed for complex [InMe$_2$Cl(κ^3-bpzbeH)] (**23**).*

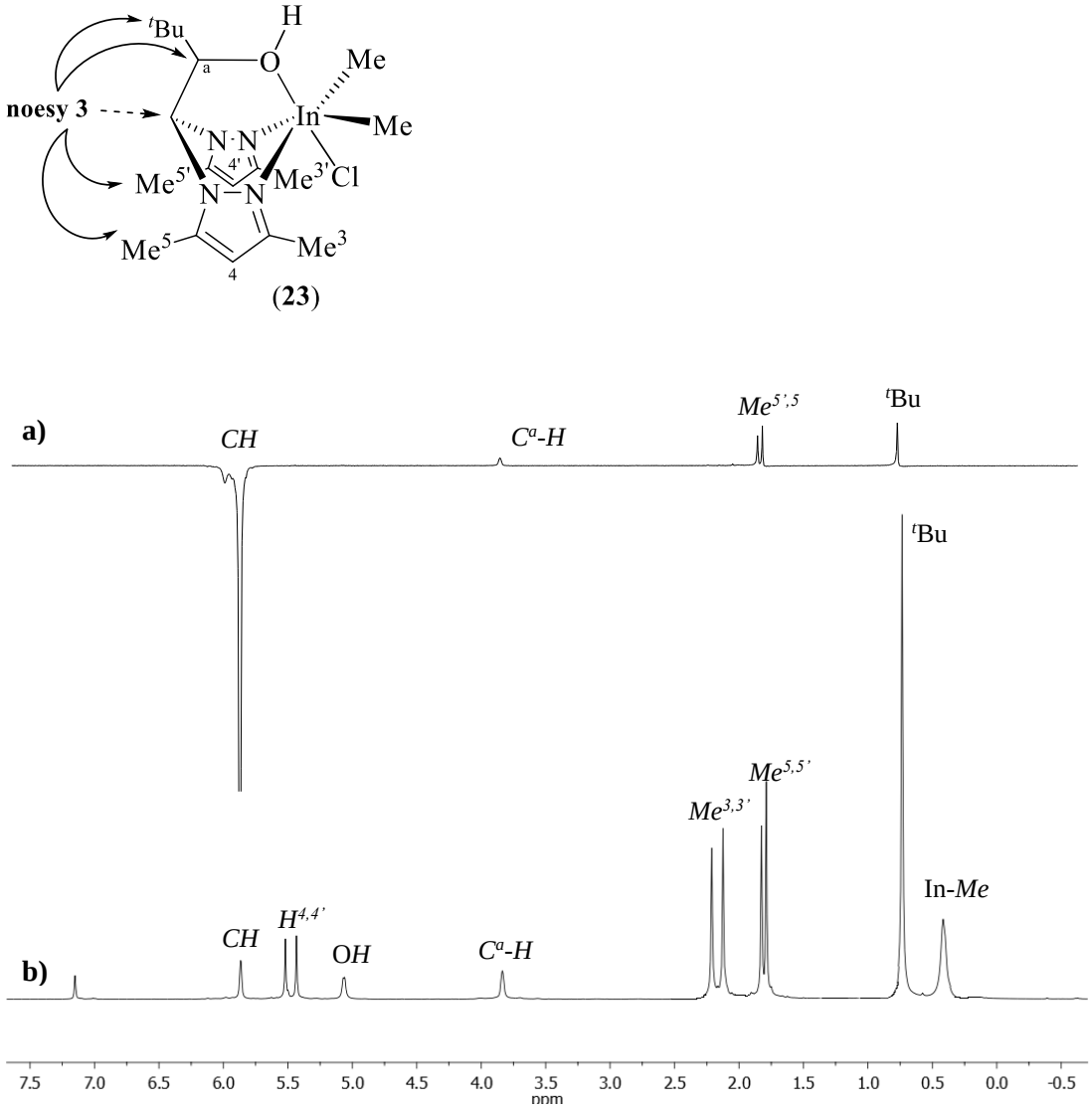

Figure 39. *a) NOESY-1D effect when irradiating the methine group CH. b) ^{1}H-NMR spectrum for complex [GaMeCl{κ^2-bpzbe}] (**21**) in C_6D_6.*

The assignment of the $^{13}C\{^{1}H\}$ NMR signals was carried out by heteronuclear ^{1}H-^{13}C g-HSQC NMR experiments. As an example, Figure 40 shows the ^{1}H-^{13}C g-HSQC NMR correlation spectrum for complex [$InMe_2Cl(\kappa^3$-bpzbeH)] (**23**).

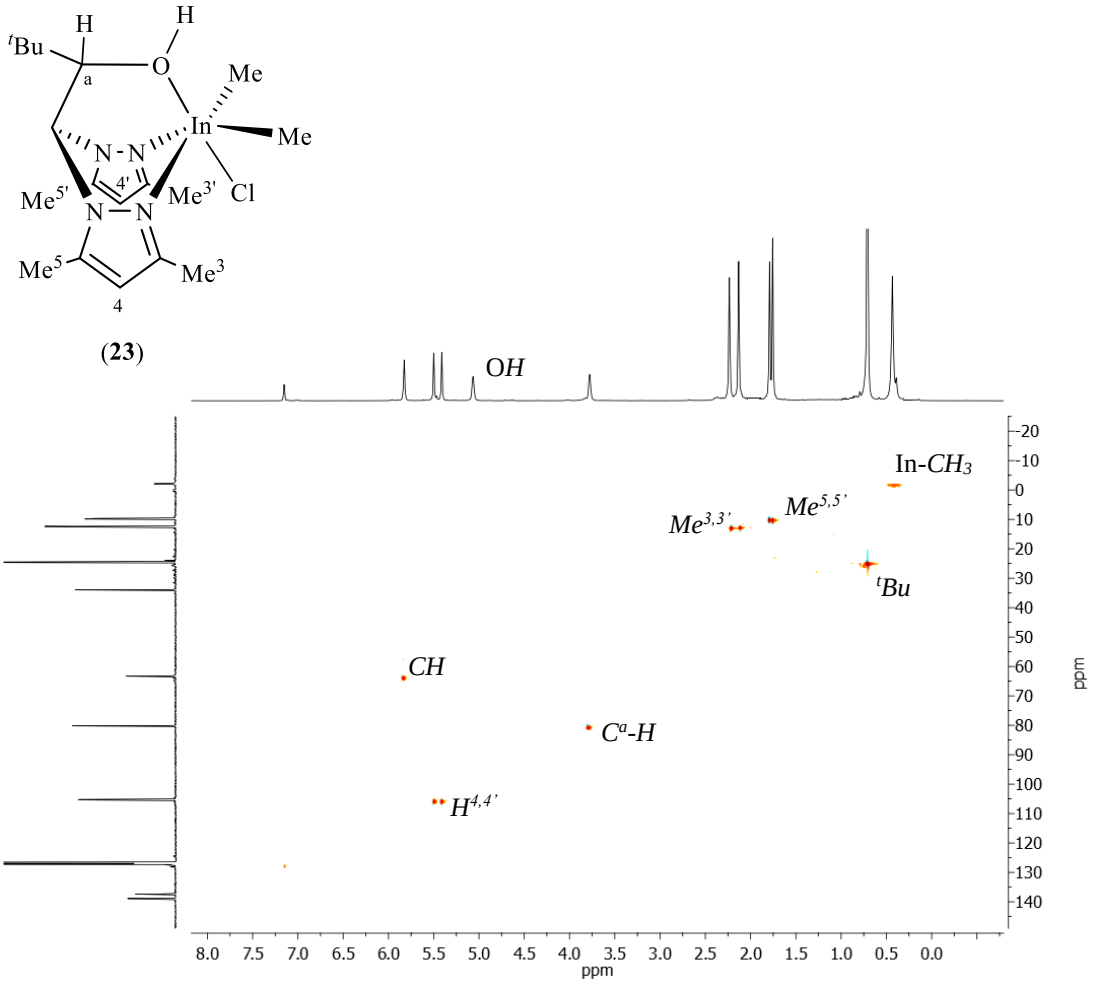

Figure 40. *^{1}H-^{13}C-gHSQC spectrum for complex (**23**) in C_6D_6.*

Table 11. *^{1}H-NMR data for complexes **17-24**.*

Compound	CH	CH[a]	H$^{4,4'}$	R	Me$^{3,3'}$	Me$^{5,5'}$	M-Me
[Li{(κ^2-bpzFerr)(Et_2O)}(μ-O){$GaMe_2Cl$}] (**17**)	5.51 (s, 1H)	6.02 (s, 1H)	5.51 (s, 1H) 5.74 (s, 1H)	3.91 (s, 1H, Cp) 3.99 (s, 1H, Cp) 4.01 (s, 1H, Cp) 4.30 (s, 5H, Cp') 4.72 (s, 1H, Cp)	1.89 (s, 3H) 2.22 (s, 3H)	1.71 (s,3H) 1.86 (s,3H)	0.00 (s, 3H) 0.25 (s, 3H)
[Li{(κ^3-bpzbe)(Et_2O)}(μ-O){$InMe_2Cl$}] (**18**)	5.96 (s, 1H)	3.55 (s, 1H)	5.35 (s, 1H) 5.50 (s, 1H)	0.77 (s, 9H, ^{t}*Bu*)	1.80 (s, 3H) 2.36 (s, 3H)	1.68 (s, 3H) 1.70 (s, 3H)	–0.23 (s, 3H) 0.38 (s, 3H)
[{Li(κ^3-bpzte)(Et_2O)}(μ-O){$InMe_2Cl$}] (**19**)	5.29 (s, 1H)	5.71 (s, 1H)	5.34 (s, 1H) 5.50 (s, 1H)	6.91 (d, J_{HH} = 7.3 Hz, 2H, ^{m}*H*Ph) 7.00 (d, J_{HH} = 7.4 Hz, 2H, ^{o}*H*Ph) 2.51 (s, 3H, *Me*Ph)	2.27 (s, 3H) 2,41 (s, 3H)	1.14 (s, 3H) 1.69 (s, 3H)	–0.03 (s, 3H) 0.15 (s, 3H)
[Li(κ^3-bpzFerr)(Et_2O)}(μ-O){$InMe_2Cl$}] (**20**)	5.55 (s, 1H)	5.95 (s, 1H)	5.53 (s, 1H) 5.74 (s, 1H)	4.04 (s, 2H, Cp) 4.05 (s, 1H, Cp) 4.29 (s, 5H, Cp') 4.66 (s, 1H, Cp)	1.79 (s, 3H) 2.31 (s, 3H)	1.69 (s, 3H) 1.90 (s, 3H)	–0.09 (s, 3H) 0.30 (s, 3H)

**Spectra were recorded in C_6D_6.*

Table 11. *^{1}H-NMR data for complexes **17-24** (continued).*

Compound	CH	CH[a]	H[4,4']	OH	R, R'	Me[3,3']	Me[5,5']	M-Me
[GaMeCl(κ^2-bpzbe)] (**21**)	6.20 (s,1H)	3.92 (s,1H)	5.62 (s, 1H) 5.72 (s, 1H)	-	1.02 (s, 9H, ^{t}Bu)	2.02 (s, 3H) 2.32 (s, 3H)	1.88 (s,3H) 1.94 (s,3H)	–0.37 (s, 1H, Ga-*Me*)
[GaMeCl(κ^2-bpzte)] (**22**)	6.12 (s, 1H)	5.72 (s, 1H)	5.48 (s, 1H) 5.80 (s, 1H)	-	7.05 (d, J_{HH} = 7,8 Hz, 2H, ^{m}*H*Ph) 7.54 (d, J_{HH} = 7,8 Hz, 2H, ^{o}*H*Ph) 2.16 (s, 3H, *Me*Ph)	2.03 (s, 3H) 2.40 (s, 3H)	1.42 (s,3H) 1.82 (s,3H)	–0.22 (s, 1H, Ga-*Me*)
[$InMe_2Cl(\kappa^3$-bpzbeH)] (**23**)	5.83 (s, 1H)	3.78 (s, 1H)	5.41 (s, 1H) 5.50 (s, 1H)	5.07 (s, 1H)	0.71 (s, 9H, ^{t}*Bu*)	2.13 (s, 3H) 2.23 (s, 3H)	1.76 (s, 3H) 1.79 (s, 3H)	0.43 (s, 6H, In-*Me*)
[$InMe_2Cl(\kappa^3$-bpzappeH)] (**24**)	6.30 (s, 1H)	-	5.18 (s, 1H) 5.34 (s, 1H)	7.03 (s, 1H)	6.34 (d, J_{HH} = 8.6 Hz, 2H, ^{m}*H*NPh) 7.52 (d, J_{HH} = 7.5 Hz, 2H, ^{o}*H*NPh) 6.92 (t, J_{HH} = 7.5 Hz, 1H, *Ph*) 7.04 (t, J_{HH} = 7.8 Hz, 2H, *Ph*) 7.21 (t, J_{HH} = 8.8 Hz, 2H, *Ph*) 2.35 (s, 6H, NMe_2)	2.11 (s, 3H) 2.25 (s, 3H)	1.53 (s, 3H) 1.56 (s, 3H)	0.56 (s, 6H, In-*Me*)

**Spectra were recorded in C_6D_6*

Table 12. *^{13}C-{^{1}H}-NMR data for complexes **17-24**.*

Compound	CH	C^{a}	$C^{3,3'}$, $C^{5,5'}$	$C^{4,4'}$	R	$Me^{3,3'}$	$Me^{5\ 5'}$	M-Me
[Li{(κ^2-bpzFerr)(Et_2O)}(μ-O){$GaMe_2Cl$}] (**17**)	71.6	75.6	136.6, 138.8 147.9, 148.2	104.5 104.9	64.2 (Cp) 65.5 (Cp) 66.8 (Cp) 67.0 (Cp) 68.8 (Cp') 95.1 (Cp)	12.7 13.7	10.6 10.7	–7.6
[Li{(κ^3-bpzbe)(Et_2O)}(μ-O){$InMe_2Cl$}] (**18**)	65.6	86.5	136.4, 138.8 148.5, 149.1	105.3 105.6	26.1 (^{t}Bu) 35.8 (*C*-^{t}Bu)	12.9 13.4	10.2 10.8	–2.7
[{Li(κ^3-bpzte)(Et_2O)}(μ-O){$InMe_2Cl$}] (**19**)	72.5	77.3	137.7, 138.4 148.5, 148.9	104.7 105.1	144.6-134.7 ($C^{ipso,p}$-Ph) 128.1 (C^{o}-Ph) 128.9 (C^{m}-Ph) 21.6 (*Me*Ph)	13.5 14.5	10.3 10.5	–2.8
[Li(κ^3-bpzFerr)(Et_2O)}(μ-O){$InMe_2Cl$}] (**20**)	72.5	76.8	136.8, 138.3 147.4, 148.5	104.3 104.7	64.4 (Cp) 66.8 (Cp) 67.0 (Cp) 68.3 (Cp) 68.7 (Cp') 96.5 (Cp)	12.6 13.8	10.2 10.6	–8.2

**Spectra were recorded in C_6D_6.*

Table 12. *^{13}C-{^{1}H}-NMR data for complexes **17-24** (continued).*

Compound	CH	C^{a}	$C^{3,3'}$, $C^{5,5'}$	$C^{4,4'}$	R	$Me^{3,3'}$	$Me^{5\ 5'}$	M-Me
[GaMeCl(κ^2-bpzbe)] (**21**)	65.4	84.9	135.7, 138.2 147.8, 147.9	104.9 105.2	27.1 (^{t}Bu) 36.4 (*C*-^{t}Bu)	12.9 14.0	10.7 11.1	–8.70
[GaMeCl(κ^2-bpzte)] (**22**)	71.8	77.8	137.3, 138.9 148.1, 148.3	104.4 105.0	126.7 (C^{o}-Ph) 128.6 (C^{m}-Ph) 143.5-135.8 ($C^{ipso,p}$-Ph) 20.8 *Me*Ph	13.0 14.0	10.1 10.6	–8.60
[$InMe_2Cl$(κ^3-bpzbeH)] (**23**)	63.3	80.2	137.4, 138.9 149.2, 149.3	105.2 105.3	24.6 (^{t}Bu) 34.0 (*C*-^{t}Bu)	12.4 12.5	9.7 9.9	–2.1
[$InMe_2Cl$(κ^3-bpzappeH)] (**24**)	65.5	83.2	139.9, 140.3 149.9, 150.0	105.4	111.2 (C^{o}-NAr) 127.7 (C^{m}-NAr) 149.8-126.7 (Ar) 39.6 N*Me*$_2$	13.2 13.4	10.4	–1.2

**Spectra were recorded in C_6D_6.*

The solid-state structure of complex [{Li(κ^3-bpzFerr)(Et$_2$O)}(μ-O){InMe$_2$Cl}] (**18**) was confirmed by X-Ray diffraction analysis. The corresponding ORTEP diagram is represented in Figure 41. This complex exhibits a heterobimetallic lithium-indium structure, in which both lithium and indium centres adopt a pseudo-tetrahedral geometry with the heteroscorpionate ligand coordinated in a tridentate κ^3-NNO fashion to the lithium atom and a molecule of diethyl ether occupying the fourth position. The indium centre is coordinated in a dative fashion to the oxygen atom from the alkoxide group of the heteroscorpionate ligand, two methyl groups and a chloride ligand. The crystal structure is in good agreement with the one proposed in Scheme 19 on the basis of solution-state NMR spectroscopy. In the solid state, complex **18** crystallises as a racemic mixture and the structure for enantiomer *R* is depicted in Figure 41.

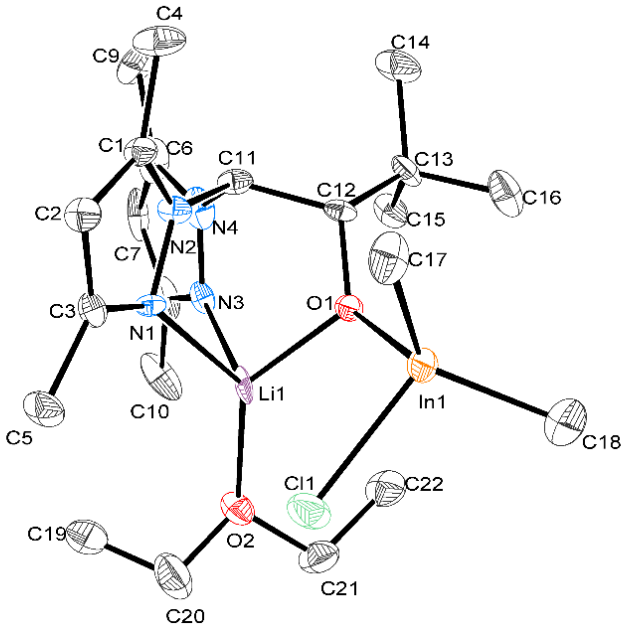

Figure 41. *ORTEP diagram for complex [{Li(κ^2-bpzbe)(Et$_2$O)}(μ-O){InMe$_2$Cl}] (**18**).*

Bond distances (Table 13) between the lithium centre and the nitrogen atoms from both pyrazole rings are 2.080 and 2.173 Å for the N(3)–Li(1) and N(1)–Li(1) bonds respectively, which are slightly shorter than other lithium heteroscorpionate complexes previously reported.[7,14e] Also, the bond distance between the lithium centre and the oxygen atom from the alkoxide group from the heteroscorpionate ligand O(1)–Li(1) of 1.911(17) Å, is slightly longer compared to previously reported lithium

heteroscorpionate complexes.[7] On the other hand, bond distance between the indium atom and the oxygen from the alkoxide moiety of the heteroscorpionate ligand In(1)–O(1) of 2.132(7) Å, is shorter than the one found for complex **10**, where the oxygen is coordinated in an anionic fashion to one indium centre and acting as a bridge to the other indium centre, while for complex **18**, it is coordinated to the indium centre in a dative fashion. Finally, bond angles confirmed the distorted tetrahedral structure proposed, with the major distortion observed in the O(2)–Li(1)–N(1) bond angle with a value of 135.5(9)º for the lithium atom and C(17)–In(1)–C(18) bond angle with a value of 128.3(7)º for the indium centre.

Table 13. *Bond distances and angles for complex [{Li(κ²-bpzbe)(Et₂O)}(μ-O){InMe₂Cl}] (**18**).*

Distances (Å)		**Angles (º)**	
[{Li(κ²-bpzbe)(Et₂O)}(μ-O){InMe₂Cl}] (**18**)			
In(1)–O(1)	2.132(7)	O(1)–In(1)–C(17)	105.5(4)
In(1)–C(17)	2.163(14)	O(1)–In(1)–C(18)	109.2(6)
In(1)–C(18)	2.171(19)	C(17)–In(1)–C(18)	128.3(7)
In(1)–Cl(1)	2.458(4)	O(1)–In(1)–Cl(1)	93.9(2)
In(1)–Li(1)	3.300(19)	C(17)–In(1)–Cl(1)	107.9(5)
Li(1)–Cl(1)	3.300(2)	C(18)–In(1)–Cl(1)	106.7(6)
O(1)–Li(1)	1.911(17)	O(1)–Li(1)–O(2)	131.4(10)
Li(1)–O(2)	2.05(2)	O(1)–Li(1)–N(3)	93.9(9)
Li(1)–N(1)	2.173(19)	O(2)–Li(1)–N(3)	102.3(9)
Li(1)–N(3)	2.08(2)	O(1)–Li(1)–N(1)	90.0(8)
		O(2)–Li(1)–N(1)	135.5(9)
		N(3)–Li(1)–N(1)	88.1(9)

4. Synthesis of alkoxide aluminium complexes

One of the challenges of this dissertation was the synthesis of alkoxide aluminium heteroscorpionate complexes, since only one alkoxide aluminium complex supported by scorpionate ligands has been previously reported.[52] Thus, neutral heteroscorpionate ligand precursors bpzbeH and bpzFerrH (**1**) were used for the synthesis of alkoxide aluminium complexes by reaction with $Al(O^iPr)_3$ in toluene at 80 ºC for 7 days. Complexes $[Al(O^iPr)(\kappa^2\text{-bpzbe})_2]$ (**25**) and $[Al(O^iPr)(\kappa^2\text{-bpzFerr})_2]$ (**26**) were synthesised in moderate yields (50-60%) after the appropriate work-up procedure as a white and pale orange solids respectively (Scheme 22). These complexes are soluble in aromatic hydrocarbons and slightly soluble in aliphatic hydrocarbons.

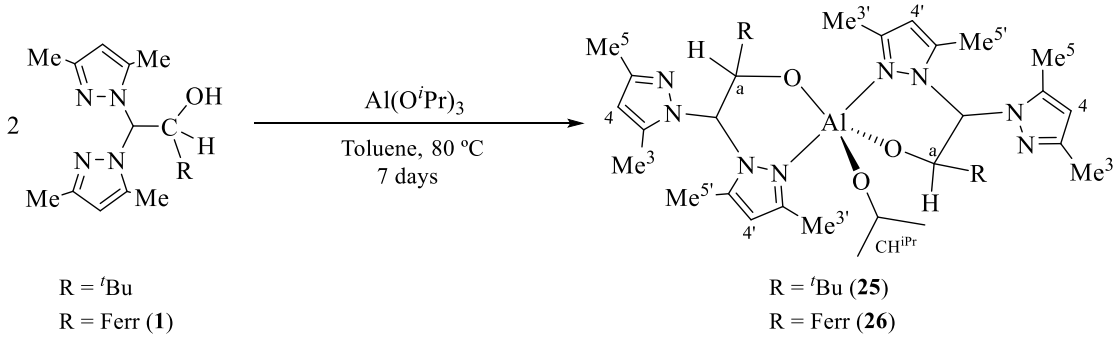

Scheme 22. *Synthesis of complexes **25** and **26**.*

Structural Characterisation

Complexes **25** and **26** were characterised by nuclear magnetic resonance spectroscopy and X-Ray diffraction studies. The ^{1}H-NMR and $^{13}C\{^1H\}$-NMR spectra of these complexes (Tables 14 and 15) exhibit broad signals at room temperature for protons and carbons of pyrazole rings (Figure 42). This fact is indicative of a fluxional behaviour due to a quick exchange between the two pyrazole rings in complexes **25** and **26**, similarly to what was discussed previously for alkyl aluminium complexes **15** and **16**. The NMR results are consistent with the structures proposed for complexes **25** and **26** (Scheme 22) featuring a penta-coordinated structure for the aluminium centre with two heteroscorpionate complexes coordinated in a κ^2-NO fashion.

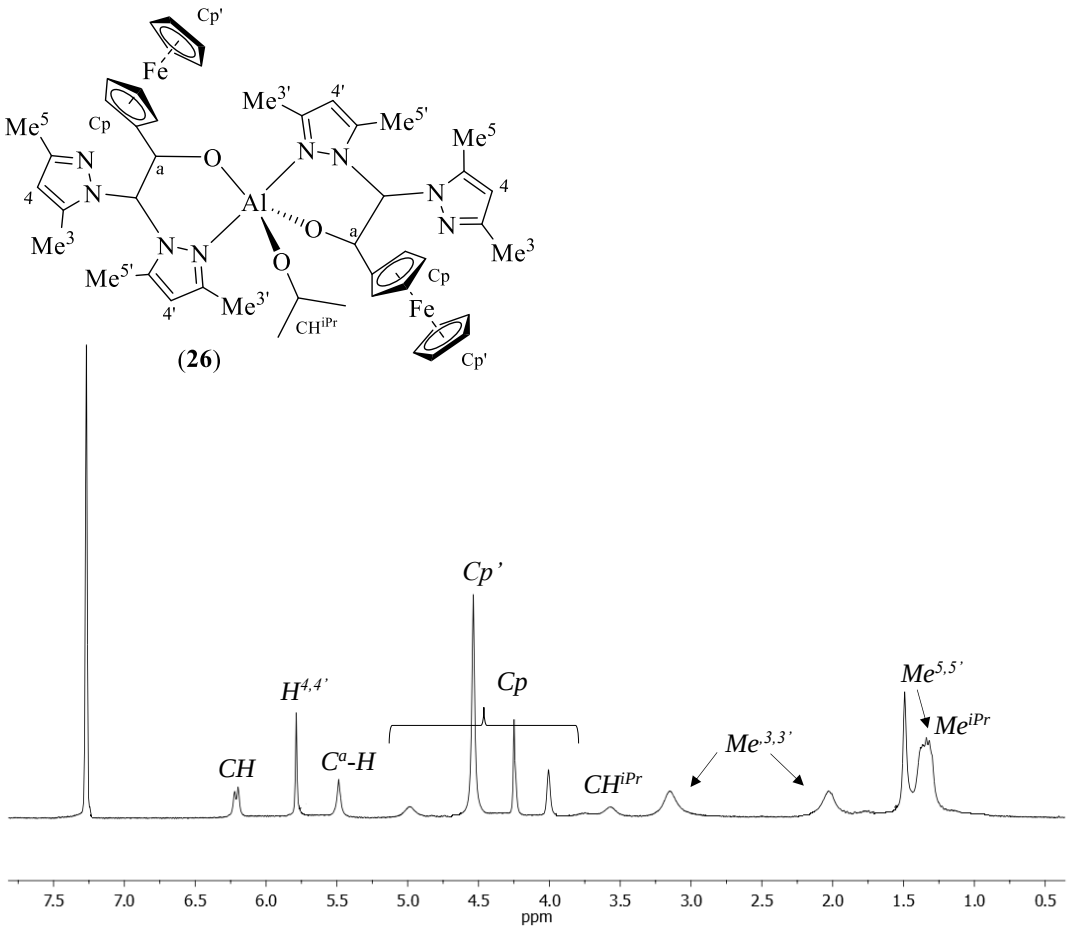

Figure 42. *^{1}H-NMR spectrum for complex [Al(O^{i}Pr)(κ^{2}-bpzFerr)$_2$] (**26**) in C_6D_6.*

1D NOESY NMR experiments afforded the unequivocal assignment for the NMR resonances of $Me^{3,3'}$ and $Me^{5,5'}$ and $H^{4,4'}$ protons of the pyrazole rings and protons corresponding to the isopropoxide ligand bonded to the aluminium centre. $^{13}C\{^{1}H\}$ NMR signals were assigned by ^{1}H-^{13}C g-HSQC NMR experiments. Figure 43 shows the ^{1}H-^{13}C-g-HSQC spectrum for complex **25**.

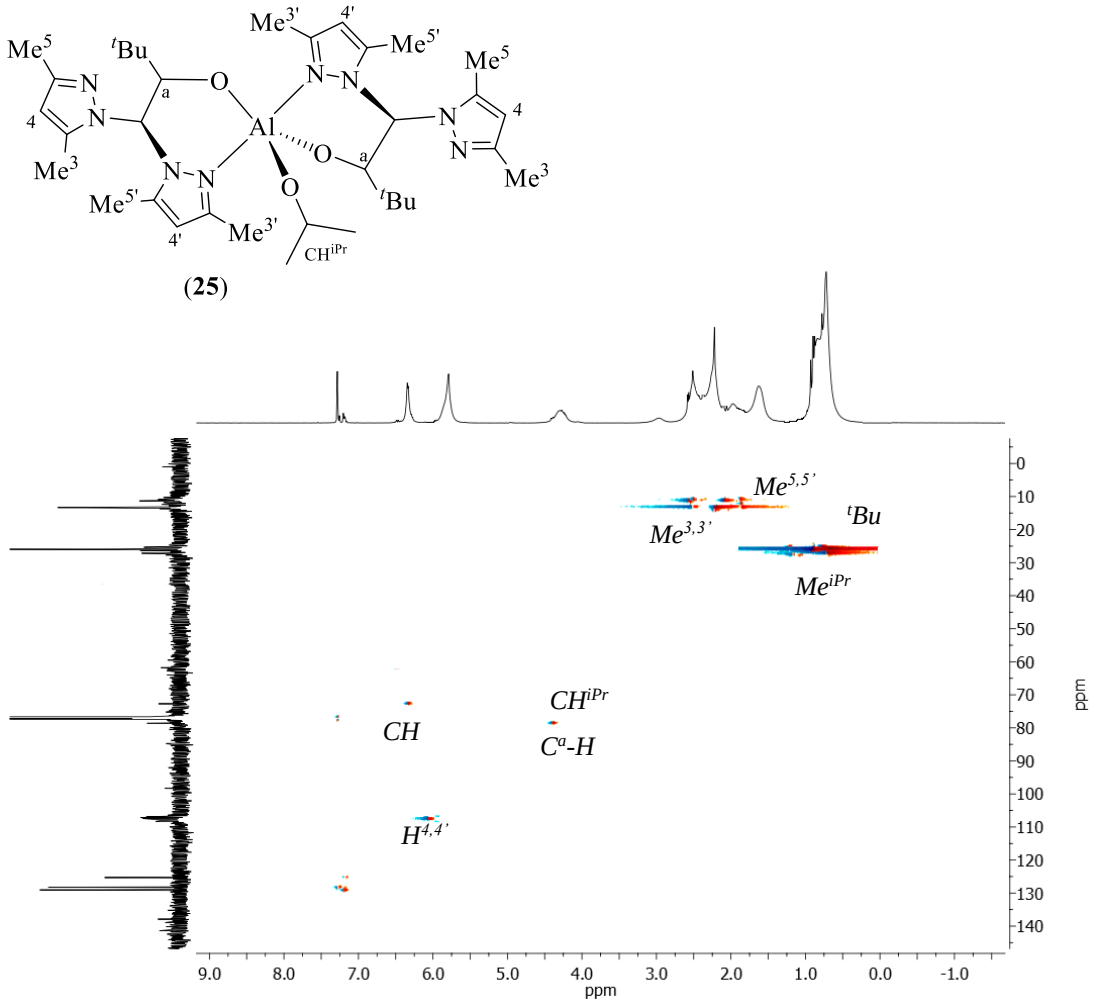

Figure 43. *Correlation spectrum ^{1}H-^{13}C-gHSQC for complex [Al(O^{i}Pr)(κ^2-bpzbe)$_2$] (**25**) in $CDCl_3$.*

Fluxional process

As it has been previously commented, the fact that at room temperature some proton and carbon resonances for complexes **25** and **26** appear as broad signals, indicates the possibility of the existence of a fluxional process of rapid exchange between both pyrazole rings (Figure 42). Therefore, VT ^{1}H-NMR experiments were carried out. When decreasing the temperature, different sets of signals are observed, corresponding to the different diasteroisomers (up to 8 diastereisomers, 16 enantiomers), that can be generated when stopping the exchange of the pyrazole rings, which generates a new chiral centre at the methine group bridgining both pyrazole rings.

The variable temperature ^{1}H-NMR spectra for complex [Al(O^{i}Pr)(κ^2-bpzbe)$_2$] (**25**) in the region corresponding to the H$^{4,4'}$ protons of the pyrazole ring, the methine group

(CH) bridging both pyrazole rings and methine group (C^a-H) is shown in Figure 44. As can be seen from Figure 44, the coalescence temperature is reached at room temperature. When the temperature is decreased down to –80 ºC, the broad signals become resolved into two different sets of signals for the CH, C^a-H and $H^{4,4'}$ protons for each of the different diastereomers present in solution. These results allowed us to propose a trigonal bipyramidal structure at low temperatures, in which the pyrazole rings would not be equivalent, where one of them is not coordinate to the aluminium centre.

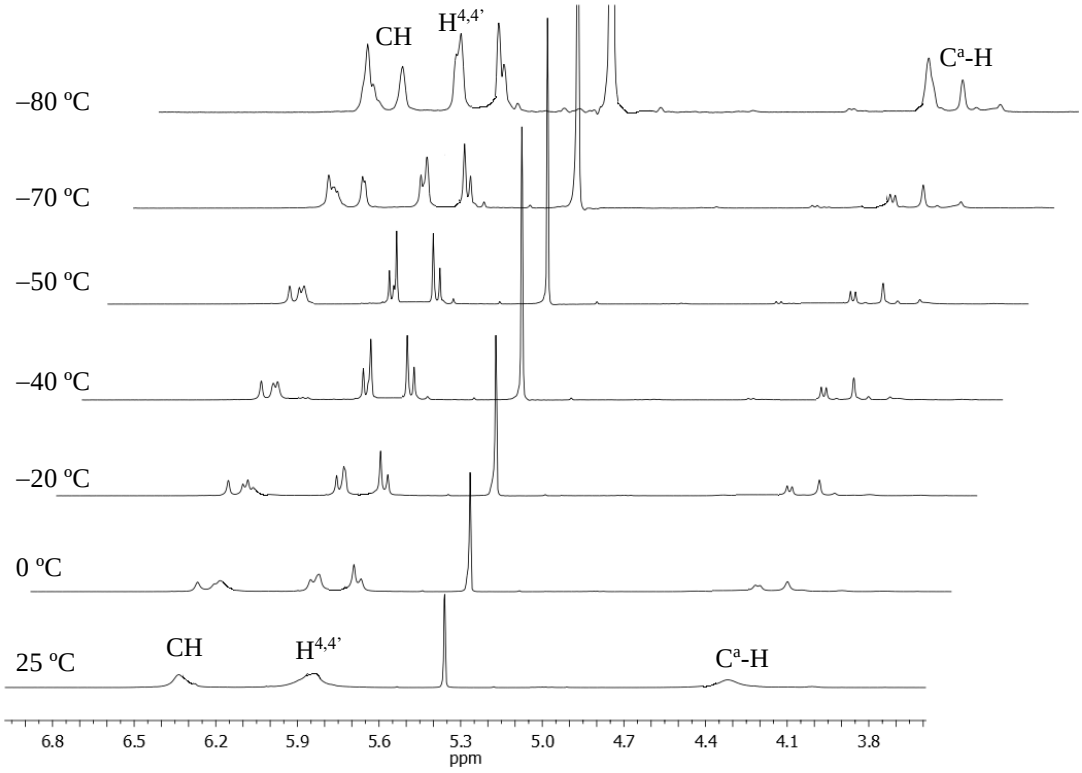

Figure 44. *Variable temperature ^{1}H-NMR study for complex [Al(O^{i}Pr)(κ^2-bpzbe)$_2$] (**25**) in CD_2Cl_2.*

Similarly, the variable temperature ^{1}H-NMR spectra for complex [Al(O^{i}Pr)(κ^2-bpzFerr)$_2$] (**26**) was performed in the region corresponding to the methyl groups from both pyrazole rings and the isopropoxide ligand (Figure 45). As can be seen, the coalescence temperature is reached at room temperature following the same tendency as it analogous complex **25**. When the temperature is increased to 60 ºC, the broad signals become more resolved and four different signals for the methyl groups

for both pyrazole rings and two different doublets for the methyl groups of the isopropoxide group are observed.

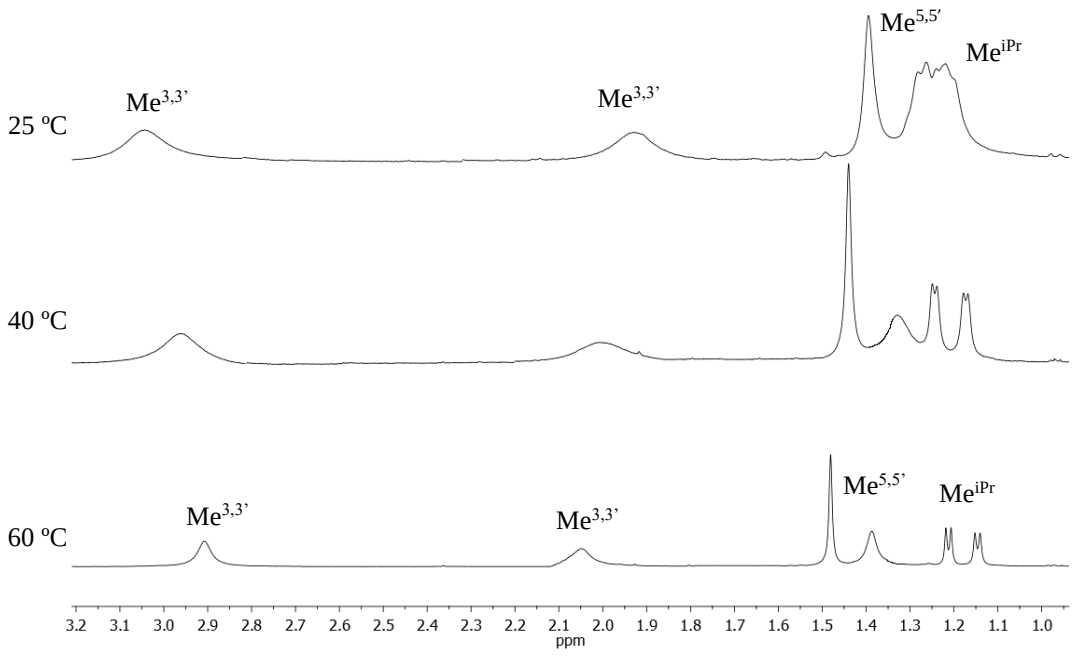

Figure 45. *Variable temperature ^{1}H-NMR study for complex [Al(O^{i}Pr)(κ^{2}-bpzFerr)$_2$] (**26**) in $CDCl_3$.*

Table 14. *^{1}H-NMR data for complexes **25** and **26**.*

Compound	CH	CH^{a}	H$^{4,4'}$	R	Me$^{3,3'}$	Me$^{5,5'}$	Al-O^{i}Pr
[Al(O^{i}Pr)(κ^2-bpzbe)$_2$] (**25**)	6.35 (s, 1H)	4.22 (s, 1H)	5.80 (s, 2H)	0.88 (s, 9H, ^{t}Bu)	2.22 (s, 3H) 2.51 (s, 3H)	1.63 (s, 3H) 2.98 (s, 3H)	0.72 (s, 3H, Me^{iPr}) 2.96 (s, 0.5H, CH-^{i}Pr)
[Al(O^{i}Pr)(κ^2-bpzFerr)$_2$] (**26**)	6.15 (d, $J_{H\text{-}H}$ = 7.8 Hz, 1H)	5.49 (s, 1H)	5.70 (s, 2H)	3.91 (s, 1H, Cp) 4.15 (s, 1H, Cp) 4.43 (s, 1H, Cp) 4.44 (s, 5H, Cp') 5.01 (s, 1H, Cp)	2.01 (s, 3H) 3.05 (s, 3H)	1.40 (s, 6H)	1.45 (s, 3H, Me^{iPr}) 3.51 (s, 0.5H, CH-^{i}Pr)

Spectra were recorded in $CDCl_3$

Table 15. *^{13}C-{^{1}H}-NMR data for complexes **25** and **26**.*

Compound	CH	C^{a}	C$^{3,3'}$, C$^{5,5'}$	C$^{4,4'}$	R	Me$^{3,3'}$	Me$^{5\ 5'}$	Al-O^{i}Pr
[Al(O^{i}Pr)(κ^2-bpzbe)$_2$] (**25**)	62.0	78.6	137.5, 140.1 146.5, 148.2	106.4 107.0	26.0 (^{t}Bu) 36.3 (*C*-^{t}Bu)	13.3 13.4	10.4 10.6	34.8, 35.5 (Me^{iPr}) 72.7 (CH-^{i}Pr)
[Al(O^{i}Pr)(κ^2-bpzFerr)$_2$] (**26**)	70.1	81.5	137.2, 139.6 148.2, 149.3	106.2 107.1	64.2 (Cp) 65.9 (Cp) 66.3 (Cp) 68.0 (Cp) 68.5 (Cp') 92.1 (Cp)	12.2 13.7	10.1 10.8	33.5, 34.6 (Me^{iPr}) 73.5 (CH-^{i}Pr)

Spectra were recorded in $CDCl_3$

The solid-state structure of complexes [Al(O^{i}Pr)(κ^2-bpzbe)$_2$] (**25**) and [Al(O^{i}Pr)(κ^2-bpzFerr)$_2$] (**26**) were confirmed by X-Ray diffraction analysis. The corresponding ORTEP diagrams are represented in Figure 46 and 47 respectively. These complexes exhibit a monomeric structure in which two heteroscorpionate ligands are coordinated to the metal centre in a bidentate κ^2-NO manner, through the nitrogen atom of one pyrazole ring and the oxygen atom from the alkoxide group, with the other pyrazole ring non-coordinated to the metal centre. In addition, the aluminium centre is coordinated to one isopropoxide ligand. Thus, the aluminium atom exhibits a penta-coordinate environment, in which the geometry can be either square pyramidal or trigonal bipyramidal. The crystal structures are consistent with those proposed in Scheme 22 on the basis of solution-state NMR spectroscopy. In the solid state, complex **25** crystallises as a single enantiomer *SSRR*, while complex **26** crystallises as a racemic mixture of a single diastereoisomer *SSRR/RRSS*. The structures of enantiomer *SSRR* for complexes **25** and **26** are depicted in Figure 46 and 47 respectively.

The angular structural parameter τ, has been reported as a quantitative tool to determine the extent to which five coordination geometries are more trigonal-bipyramidal or square-pyramidal.[53] The τ parameter is defined as $\tau = (\beta-\alpha)/60$, where β and α are the bond angles of the molecule, which, in an ideal square-pyramidal geometry, both angles adopt 180º, and therefore, $\tau = 0$, while in an ideal trigonal-bipyramidal geometry , $\beta = 180^o$ and $\alpha = 120^o$, in which $\tau = 1$ (Figure 48).

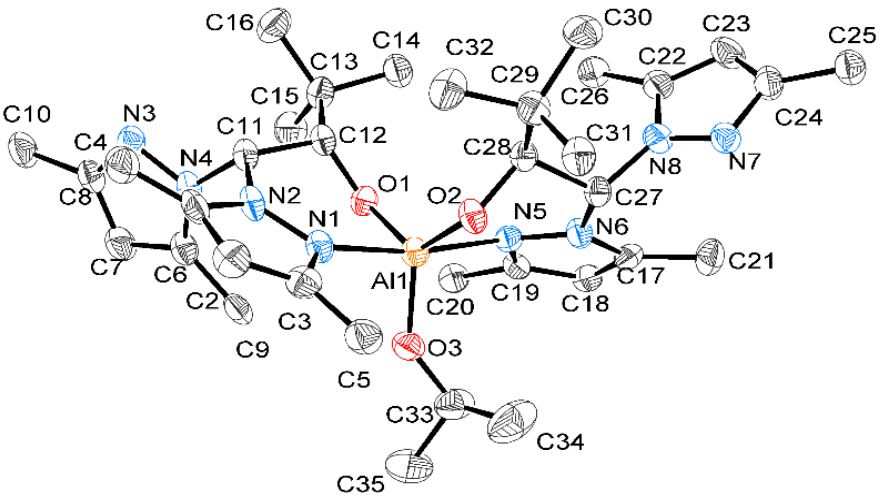

Figure 46. *ORTEP diagram for complex [Al(O^{i}Pr)(κ^2-bpzbe)$_2$] (**25**).*

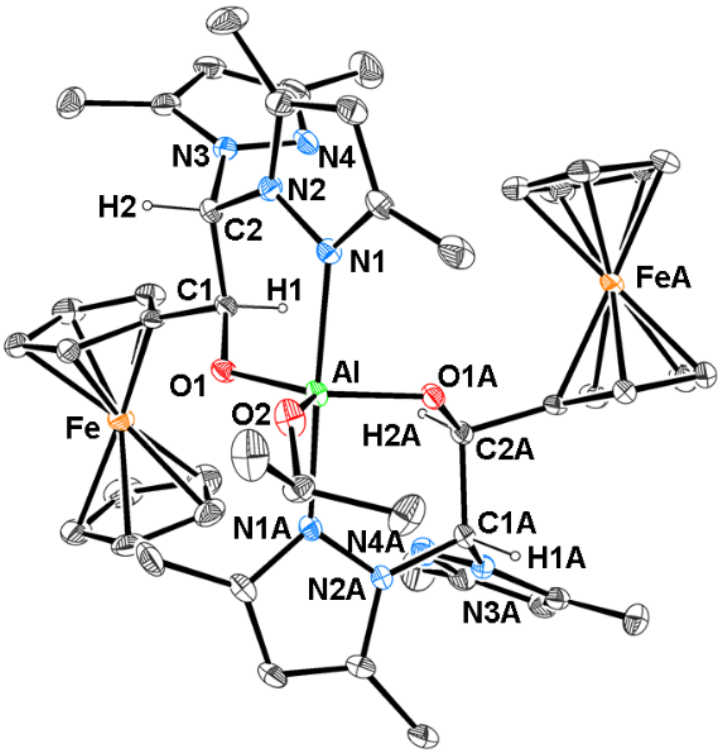

Figure 47. *ORTEP diagram for complex [Al(O^{i}Pr)(κ^{2}-bpzFerr)$_2$] (**26**).*

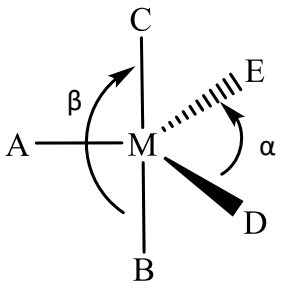

Figure 48. *α,β angles which define the geometry of five-coordinate complexes.*

The τ value for complex **25** is 0.74, which indicates that the geometry around the aluminium centre can be described as a distorted trigonal-bipyramid, with the highest distortion at the N(1)–Al(1)–N(5) angle (Table 16) with a value of 170.3º with respect the 180º of a perfect trigonal-bipyramid. Similarly, τ value for complex **26** is 0.67, which indicates that the geometry around the aluminium centre can be described as a distorted trigonal-bipyramid as well, with the highest distortion observed at the N(1)–Al(1)–N(1A) angle (Table 16) with a value of 169.3(13)º. The bond distance (Table 16) between the aluminium centre of complex **25** and the oxygen atom from the isopropoxide ligand of 1.718(11) Å for Al(1)–O(3) is slightly shorter than that found for complex **26** of 1.731(28) Å for Al(1)–O(2), probably due to the steric

requirements of the ferrocene moiety. Also, these same distances between the aluminium centres of complexes **25** and **26** and the oxygen atoms from the isopropoxide ligands are slightly longer than those found for other aluminium isopropoxide complexes previously reported.[54]

Table 16. *Bond distances and angles for complexes **25** and **26**.*

Distances (Å)		**Angles (º)**	
[Al(O^{i}Pr)(κ^2-bpzbe)$_2$] (**25**)			
Al(1)–O(1)	1.736(11)	O(3)-Al(1)-O(1)	116.1(6)
Al(1)–O(2)	1.746(10)	O(3)-Al(1)-O(2)	118.2(6)
Al(1)–O(3)	1.718(11)	O(1)-Al(1)-O(2)	125.7(6)
Al(1)–N(1)	2.038(16)	O(3)-Al(1)-N(1)	93.5(6)
Al(1)–N(5)	2.094(16)	O(1)-Al(1)-N(1)	87.5(6)
O(1)–C(12)	1.389(16)	O(2)-Al(1)-N(1)	88.7(6)
O(2)–C(28)	1.389(16)	O(3)-Al(1)-N(5)	96.2(6)
O(3)–C(33)	1.39(2)	O(1)-Al(1)-N(5)	89.1(6)
		O(2)-Al(1)-N(5)	86.0(6)
		N(1)-Al(1)-N(5)	170.3(6)
[Al(O^{i}Pr)(κ^2-bpzFerr)$_2$] (**26**)			
Al(1)–O(1)	1.757(17)	O(1)–Al(1)–O(1A)	129.2(13)
Al(1)–O(2)	1.731(28)	O(1)–Al(1)–O(2)	115.4(7)
Al(1)–N(1)	2.087(21)	O(2)–Al(1)–N(1)	95.4(6)
O(1)–C(1)	1.381(30)	O(1)–Al(1)–N(1)	87.1(8)
		N(1)–Al(1)–N(1A)	169.3(13)

5. Synthesis of amido indium complexes

For the synthesis of the indium amido complex described in this section, the amido precursor [InCl{N(SiMe$_3$)$_2$}$_2$pyr] (**27**), which was synthesised as shown in Scheme 23, was used. Thus, reaction of **27** with the neutral heteroscorpionate ligand precursor bpzbeH in toluene for two hours, afforded the corresponding chloride-amido indium complex [InCl{N(SiMe$_3$)$_2$}{(κ^3-bpzbe)(μ-O)}]$_2$ (**28**) with elimination of the corresponding amine NH(SiMe$_3$)$_2$ (Scheme 24). Complex **28** was isolated as a white solid in 80% yield. This complex is soluble in aromatic hydrocarbons and partially soluble in aliphatic hydrocarbons. Besides, it is thermically unstable.

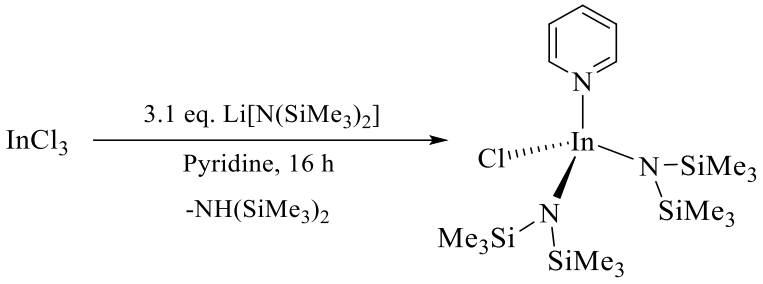

Scheme 23. *Synthesis of precursor [InCl{N(SiMe$_3$)$_2$}$_2$pyr] (**27**).*

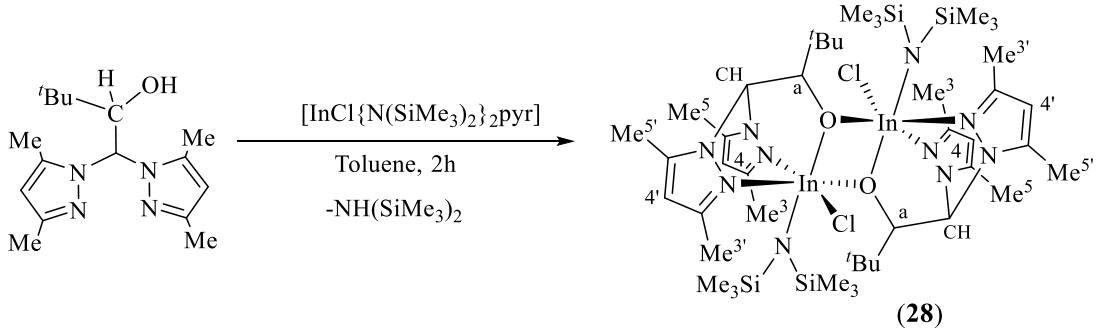

(**28**)

Scheme 24. *Synthesis of amido-chloride indium (**28**).*

<u>Structural Characterisation</u>

Indium precursor **27** and complex **28** were characterised by ^{1}H-NMR and ^{13}C{^{1}H}-NMR spectroscopy (Tables 17 and 18) and X-ray diffraction studies (Figures 52 and 53 respectively). The study of the ^{1}H-NMR and ^{13}C{^{1}H}-NMR spectra for complex **28** shows the presence of two isomers, due to the presence of a chiral carbon in the

ligand. Two singlets for the $H^{4,4'}$, $Me^{3,3'}$and $Me^{5,5'}$ pyrazole protons are observed indicating the non-equivalence of both pyrazole rings. Besides, two singlets corresponding to the methyl group from the silyl-amido ligands are also observed (Figure 49). The NMR results are consistent with the structure proposed in Scheme 24, following the same tendency as its chloride analogue (Scheme 15), with each indium centre featuring an octahedral environment with the ligand coordinated in a κ^3-NNO fashion, one chloride atom, one bis(trimethyl-silyl)amide group and the oxygen from the alkoxide moiety bridging both indium centres.

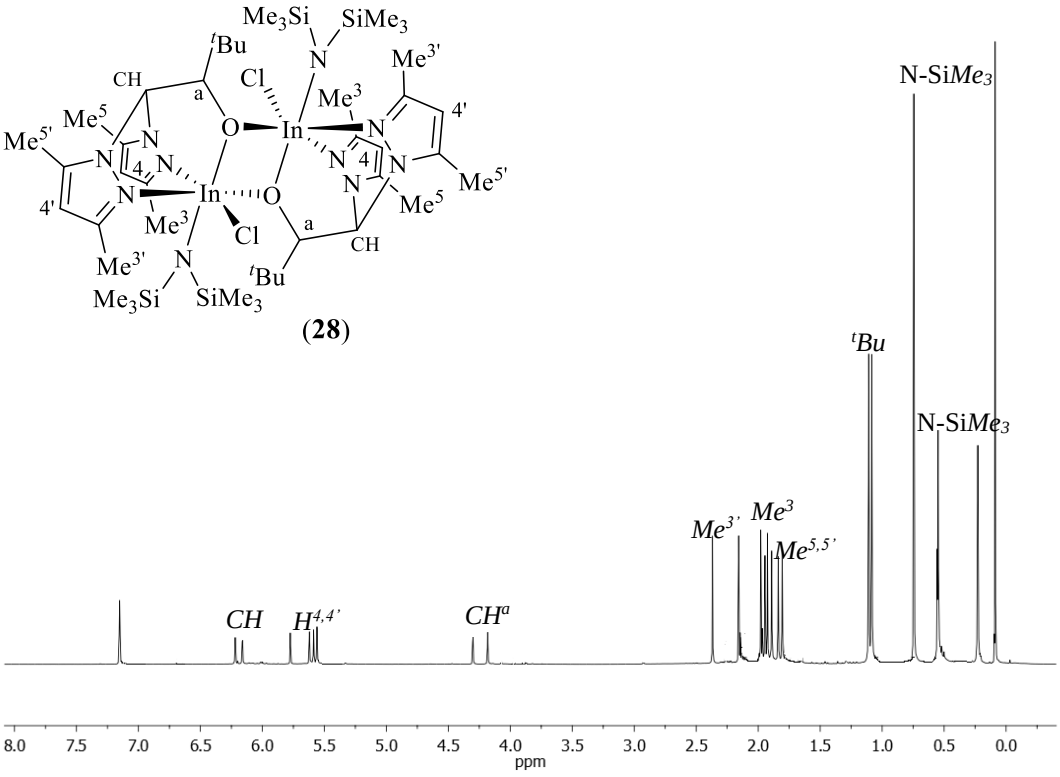

Figure 49. *^{1}H-NMR spectrum for complex **28** in C_6D_6.*

NOESY-1D experiments allowed the unequivocal assignment of the pyrazole and amide groups resonances. The assignment of the $^{13}C\{^1H\}$-NMR signals was carried out by heteronuclear correlation ^1H-^{13}C-g-HSQC experiments. Figure 50 shows the correlation spectrum for complex $[InCl\{N(SiMe_3)_2\}\{(\kappa^3\text{-bpzbe})(\mu\text{-O})\}]_2$ (**28**).

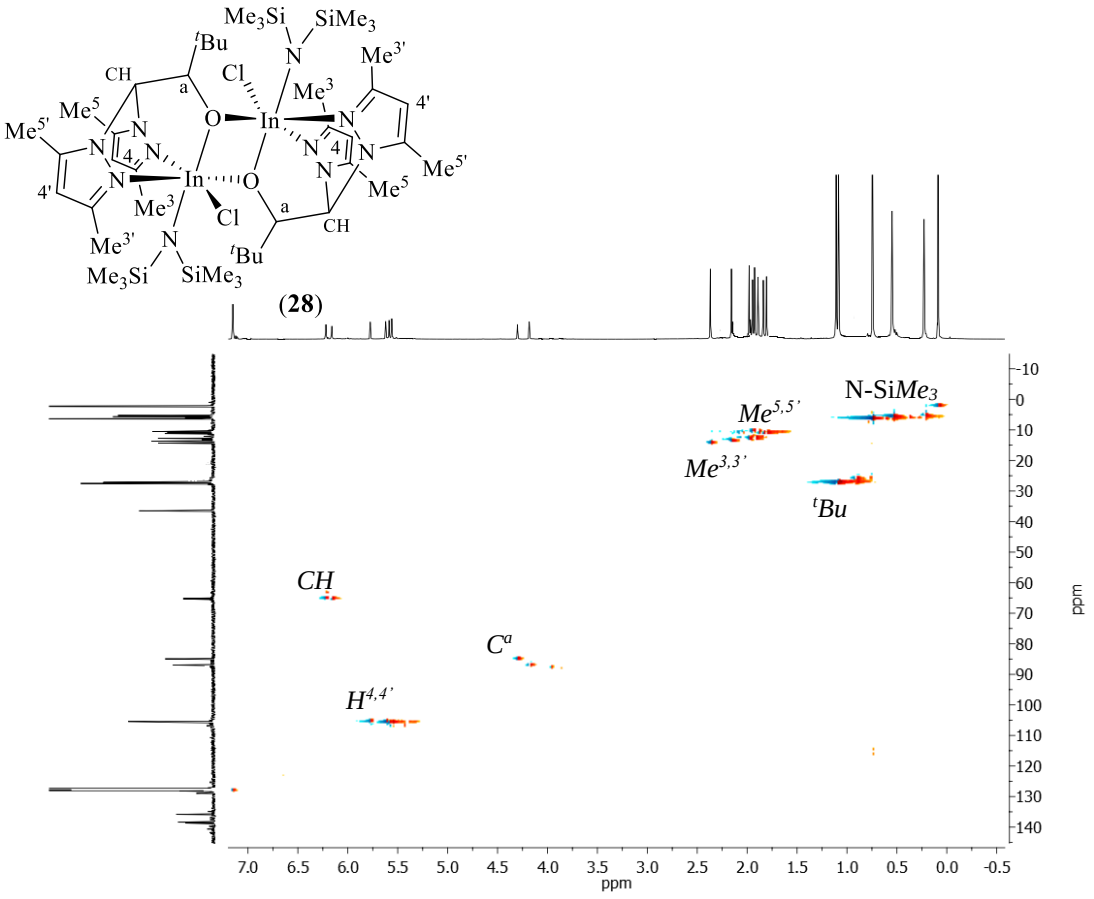

Figure 50. *Correlation spectrum ^{1}H-^{13}C-gHSQC for complex **28** in C_6D_6*

As previously mentioned, complex **28** was found to be unstable in solution and slowly evolved into the salt-type complex **29** (Scheme 25), which structure was further confirmed by X-Ray diffraction studies. Figure 51 shows the ^{1}H-NMR and $^{13}C\{^{1}H\}$-NMR spectra for complex $[In(\kappa^3\text{-bpzbe})_2]^+[InCl_2\{N(SiMe_3)_2\}_2]^-$ (**29**).

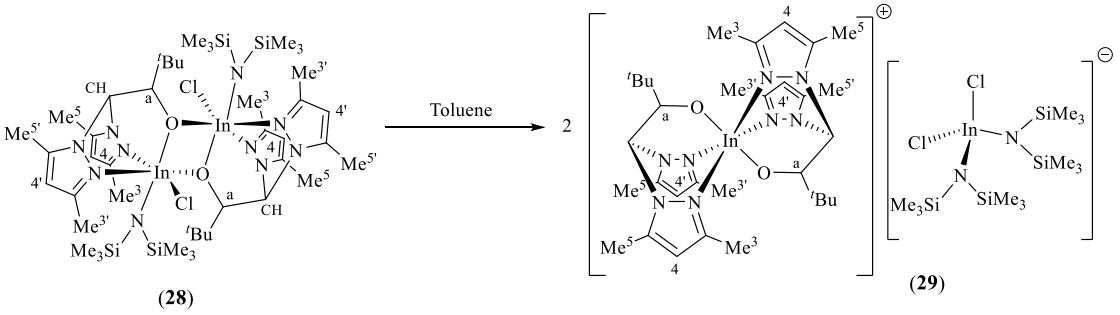

Scheme 25. *Formation of complex **29** from decomposition of complex **28** in solution.*

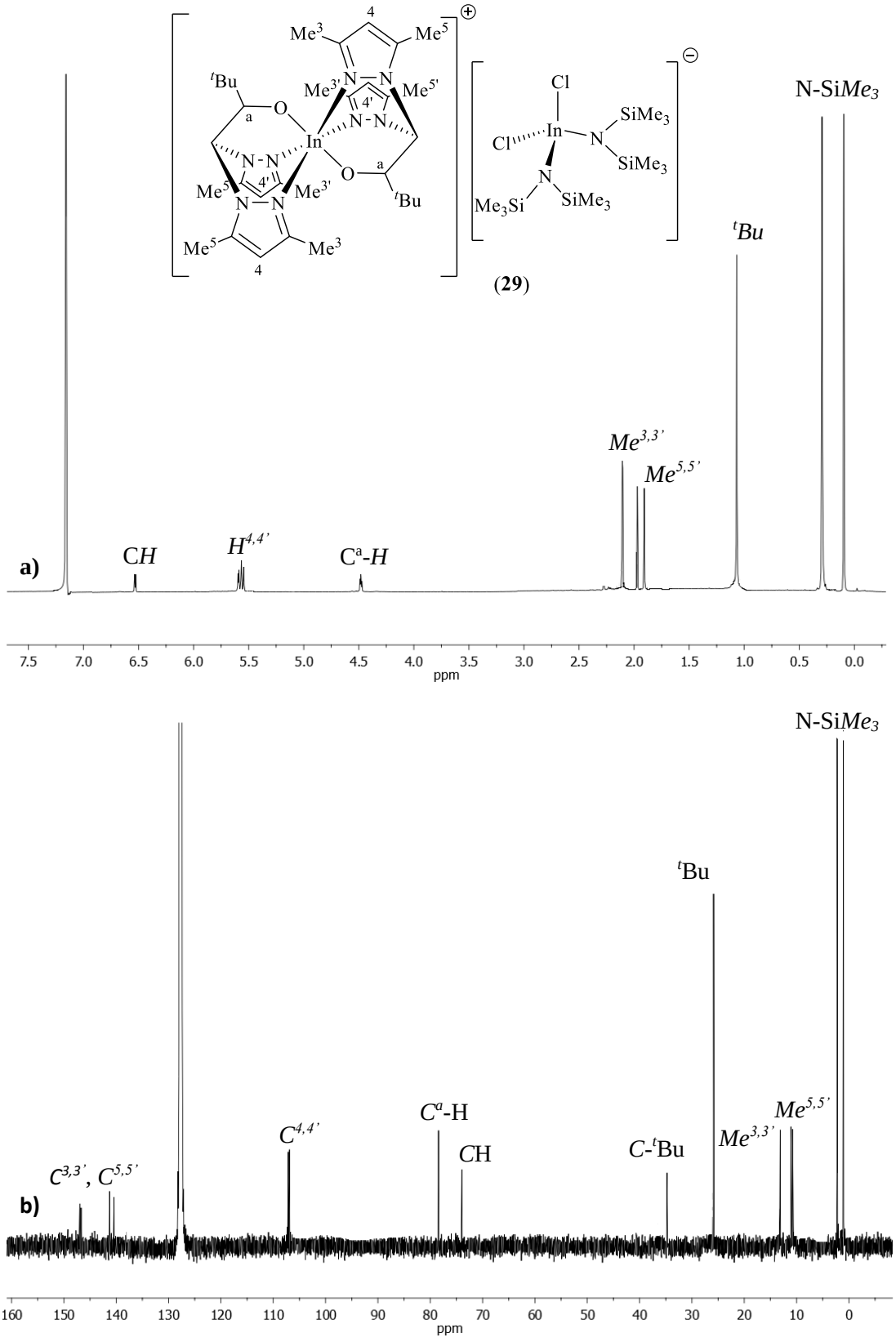

Figure 51. *a) ^{1}H-NMR and b) ^{13}C{^{1}H}-NMR spectra for complex **29** in C_6D_6, respectively.*

Table 17. *^{1}H-NMR data for complexes **28** and **29**.*

Compound	CH	CH[a]	H[4,4']	^{t}Bu	Me[3,3']	Me[5,5']	N-SiMe$_3$
[InCl{N(SiMe$_3$)$_2$}(κ^3-bpzbe)(μ-O)]$_2$ (**28**)	4.18 (d, J_{HH} = 1.0 Hz, 1H)	6.22 (s, 1H)	5.56 (s, 1H) 5.59 (s, 1H)	1.08 (s, 9H, ^{t}Bu)	2.16 (s,3H) 2.37 (s,3H)	1.89 (s,3H) 1.95 (s,3H)	0.09 (s, 9H) 0.74 (s, 9H)
[In(κ^3-bpzbe)$_2$]$^+$ [InCl$_2$\{N(SiMe$_3$)$_2$\}$_2$]$^-$ (**29**)	4.49 (d, J_{HH} = 4.2 Hz, 1H)	6.53 (d, J_{HH} = 4.7 Hz, 1H)	5.59 (s,1H) 5.54 (s, 1H)	1.07 (s, 9H, ^{t}Bu)	2.11 (s,3H) 2.10 (s,3H)	1.97 (s,3H) 1.91 (s,3H)	0.10 (s, 9H) 0.29 (s, 9H)

**Spectra were recorded in C_6D_6. Chemical shifts corresponding to the major isomer in solution.*

Table 18. *^{13}C-{^{1}H}-NMR data for complexes **28** and **29**.*

Compound	CH	C[a]	C[3,3'], C[5,5']	C[4,4']	^{t}Bu	Me[3,3']	Me[5 5']	N-SiMe$_3$
[InCl{N(SiMe$_3$)$_2$}\{(κ^3-bpzbe)(μ-O)\}]$_2$ (**28**)	65.3	84.9	135.8, 138.7 148.4, 148.8	105.6 105.7	27.5 (^{t}Bu) 36.5 (*C*-^{t}Bu)	13.7 14.3	10.5 11.1	2.3 6.4
[In(κ^3-bpzbe)$_2$]$^+$ [InCl$_2$\{N(SiMe$_3$)$_2$\}$_2$]$^-$ (**29**)	73.9	78.4	140.4-147.0	106.7 107.1	26.1 (^{t}Bu) 34.6 (*C*-^{t}Bu)	13.1 13.2	10.8 11.1	1.0 2.3

**Spectra were recorded in C_6D_6. Chemical shifts corresponding to the major isomer in solution.*

The structures for precursor **27** and complex **29** were confirmed by X-Ray diffraction analysis (Figures 52 and 53). The ORTEP diagram for precursor **27** is shown in Figure 52. This compound exhibits a monomeric structure in which the indium centre adopts a pseudo-tetrahedral geometry coordinated to two bis-trimethylsilyl amido ligands, one chloride ligand and a pyridine molecule.

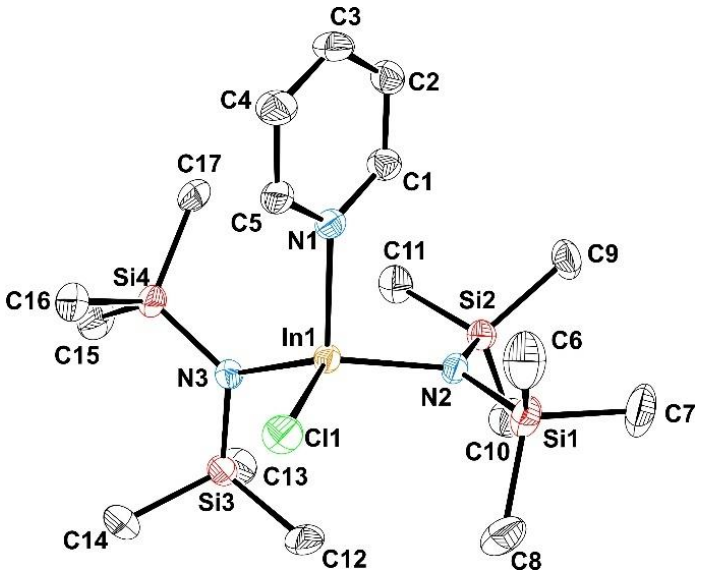

Figure 52. *ORTEP diagram for precursor [InCl{(N(SiMe$_3$)$_2$}$_2$pyr] (27).*

The ORTEP diagram for complex **29** is depicted in Figure 53. The X-Ray diffraction study of complex **29** confirmed the salt-type structure proposed with two ions with the indium atoms being the central atoms of the anion and the cation moieties. One of the indium centres exhibits an octahedral geometry with two heteroscorpionate ligands coordinated in a κ^3-NNO coordination mode. In addition, the second indium centre is coordinated to two chloride and two bis(trimethyl-silyl) amide ligands in an anionic tetrahedral counterion (**29**). Complex **29** crystallises in solid state as a racemic mixture of one of the diastereoisomer *SR/RS*. The structure of enantiomer *SR* for complex **29** is depicted in Figure 56.

Bond distances (Table 19) between the indium centre and nitrogen atoms from the pyrazole rings exhibit values ranging from 2.249(15) to 2.330(14) Å, which are slightly shorter than the ones found for the indium chloride complex **10**. Similarly, bond distances between the indium centre and the oxygen atom from the alkoxide moiety present values of 2.018(13) and 2.055(12) Å for the In(1)–O(1) and In(1)–O(2) bonds respectively, which are also slightly shorter than the ones found for complex **10**. Angle

bonds (Table 19) confirm the octahedral structure proposed for the cationic moiety, with distorted values with respect to a perfect octahedron. Thus, the major distortion is observed for the N(5)–In(1)–N(1) angle with a 101.0(5)º. On the other hand, the geometry at the anionic indium moiety In(2) is distorted tetrahedral, with the dihedral angle between the Cl(1)-In(2)-Cl(2) and the N(9)-In(2)-N(10) planes of 85.0 º.

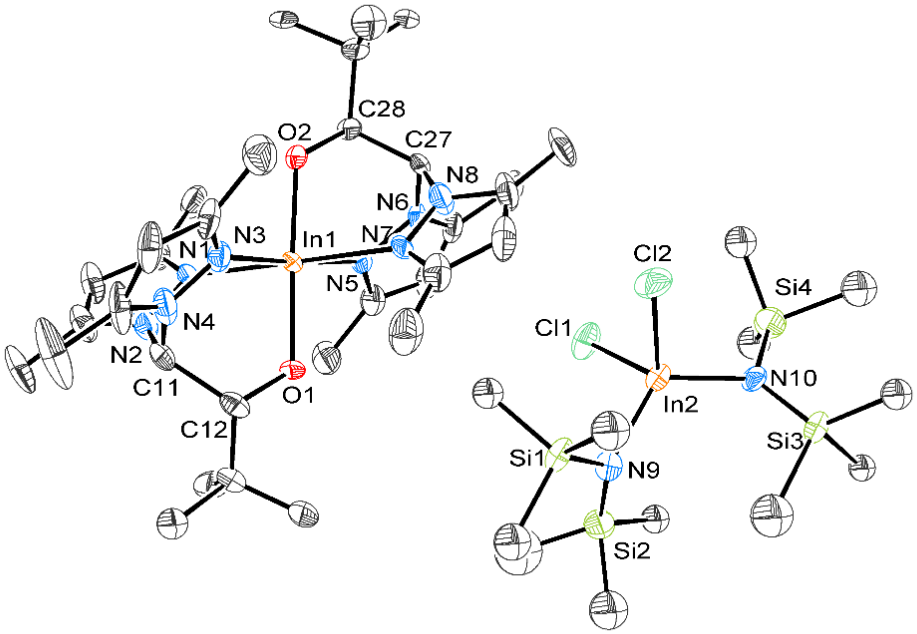

Figure 53. *ORTEP diagram for complex* $[In(\kappa^3\text{-bpzbe})_2]^+[InCl_2\{N(SiMe_3)_2\}_2]^-$ ***(29)***.

Table 19. *Bond distances and angles for precursor [InCl{(N(SiMe$_3$)$_2$}$_2$pyr] (**27**) and complex [In{κ^3-bpzbe}$_2$]$^+$[InCl$_2${N(SiMe$_3$)$_2$}$_2$]$^-$ (**29**).*

Distances (Å)		**Angles (º)**	
[InCl{(N(SiMe$_3$)$_2$}$_2$pyr] (**27**)			
In(1)–N(2)	2.068(4)	N(2)–In(1) –N(3)	126.28(16)
In(1)–N(3)	2.072(4)	N(2)–In(1)–N(1)	98.11(16)
In(1)–N(1)	2.250(5)	N(3)–In(1)–N(1)	113.57(17)
In(1)–Cl(1)	2.3941(17)	N(2)–In(1)–Cl(1)	114.77(12)
		N(3)–In(1)–Cl(1)	105.81(12)
		N(1)–In(1)–Cl(1)	93.25(13)
[In{κ^3-bpzbe}$_2$]$^+$[InCl$_2${N(SiMe$_3$)$_2$}$_2$]$^-$ (**29**)			
In(1)–O(2)	2.018(13)	O(2)–In(1)–N(5)	83.2(5)
In(1)–O(1)	2.055(12)	O(1)–In(1)–N(5)	95.3(5)
In(1)–N(5)	2.249(15)	O(2)–In(1)–N(1)	95.9(5)
In(1)–N(1)	2.268(14)	O(1)–In(1)–N(1)	86.2(5)
In(1)–N(3)	2.306(16)	N(5)–In(1)–N(1)	101.0(5)
In(1)–N(7)	2.330(14)	O(2)–In(1)–N(3)	94.0(5)
In(2)–N(10)	2.037(15)	O(1)–In(1)–N(3)	87.5(6)
In(2)–N(9)	2.121(18)	N(1)–In(1)–N(3)	81.2(6)
In(2)–Cl(1)	2.416(6)	O(2)–In(1)–N(7)	84.1(5)
In(2)–Cl(2)	2.414(7)	O(1)–In(1)–N(7)	93.7(5)
In(2)–N(10)	2.037(15)	N(5)–In(1)–N(7)	80.1(6)
		N(3)–In(1)–N(7)	97.6(6)
		N(10)–In(2)–N(9)	122.5(7)
		N(10)–In(2)–Cl(2)	105.1(5)
		N(9)–In(2)–Cl(2)	112.4(5)
		N(10)–In(2)–Cl(1)	109.8(5)

Experimental section

EXPERIMENTAL SECTION

1. Synthesis of precursors

The starting materials bis(3,5-dimethyl-pyrazol-1-yl)methane (bdmpzm) and heteroscorpionate alkoxide neutral ligands bpzbeH, bpzteH and bpzappeH have been prepared as previously described in bibliography.[16, 17, 55]

*1.1. Synthesis of bpzFerrH (**1**)*

In a 250 cm^3 Schlenk tube, bdmpzm (2.50 g, 12.25 mmol) was dissolved in 70 mL of dry THF and cooled down to −78 ºC. Then, a solution of ^{n}BuLi (1.6M in hexanes, 8.05 mL, 12.86 mmol) was added dropwise and the mixture was maintained at −78 ºC during one hour. After that time, the lithiated-adduct suspension was cannulated to a pre-cooled solution of ferrocenecarboxaldehyde (2.75 g, 12.86 mmol) in 20 mL of THF and the resulting mixture was left stirring for one hour at room temperature. The suspension was then quenched with a satured aqueous solution of NH_4Cl and a white-yellowish solution was obtained. The organic layer was extracted, dried over $MgSO_4$ for two hours and filtered. The solvent was removed *in vacuo*, and an orange-reddish sticky oil was obtained. The oil was washed with *n*-hexane for 16 hours and an orange solid corresponding to bpzFerrH (**1**) was isolated in 80% yield.

Analysis found:	C: 63.4 %	H: 6.5 %	N: 13.1 %
Calculated:	C: 63.2 %	H: 6.3 %	N: 13.4 %

2. Synthesis of chloride group 13 metal complexes

2.1. Synthesis of chloride aluminium and gallium complexes

*2.1.1. Synthesis of $[Al(\kappa^2\text{-bpzbe})_2]^+[AlCl_4]^-$ (**2**)*

In a 100 cm^3 Schlenk tube, bpzbeH (1.00 g, 3.45 mmol) was dissolved in 30 mL of dry THF and cooled down to −78 ºC. Then, a solution of ^{n}BuLi (1.6M in hexanes, 2.30 mL, 3.62 mmol) was added dropwise and the mixture was maintained at −78 ºC during one hour. After that time, the lithiated adduct was transferred *via* cannula to a precooled suspension of $AlCl_3$ (0.48 g, 3.62 mmol) in 20 mL of THF. The resulting mixture was warmed to room temperature and left stirring overnight. Solvent was then removed *in vacuo* and the remaining solid was taken up in Et_2O and filtered through

celite to eliminate the LiCl salt generated. Solvent was again removed under vacuum affording a white solid corresponding to complex **2** in 80% yield.

Analysis found:	C: 49.8 %	H: 6.6 %	N: 14.2 %
Calculated:	C: 49.6 %	H: 6.5 %	N: 14.5 %

*2.1.2. Synthesis of $[Al(\kappa^2\text{-bpzte})_2]^+[AlCl_4]^-$ (**3**)*

The synthesis of complex **3** was carried out following the same experimental procedure as complex **2** using bpzteH (1.00 g, 3.10 mmol), ^{n}BuLi (2.00 mL, 3.24 mmol) and $AlCl_3$ (0.43 g, 3.24 mmol). Complex **3** was obtained as a white solid in 85% yield.

Analysis found:	C: 54.4 %	H: 5.6 %	N: 16.4 %
Calculated:	C: 54.2 %	H: 5.5 %	N: 16.8 %

*2.1.3. Synthesis of $[Al(\kappa^2\text{-bpzappe})_2]^+[AlCl_4]^-$ (**4**)*

The synthesis of complex **4** was carried out following the same experimental procedure as complex **2** using bpzappeH (1.00 g, 2.33 mmol), ^{n}BuLi (1.53 mL, 2.44 mmol) and $AlCl_3$ (0.33g, 2.44 mmol). Complex **4** was obtained as a white solid in 85% yield.

Analysis found:	C: 59.6 %	H: 5.9 %	N: 13.0 %
Calculated:	C: 59.3 %	H: 5.7 %	N: 13.3 %

*2.1.4. Synthesis of $[Al(\kappa^2\text{-bpzFerr})_2]^+[AlCl_4]^-$ (**5**)*

The synthesis of complex **5** was carried out following the same experimental procedure as complex **2,** using bpzFerrH (**1**) (1.00 g, 2.39 mmol), ^{n}BuLi (1.55 mL, 2.51 mmol) and $AlCl_3$ (0.33 g, 2.51 mmol). Complex **5** was obtained as an orange solid in 85% yield.

Analysis found:	C: 51.5 %	H: 5.1 %	N: 10.6 %
Calculated:	C: 51.3 %	H: 4.9 %	N: 10.9 %

*2.1.5. Synthesis of $Gal(\kappa^3\text{-bpzbe})_2]^+[GaCl_4]^-$ (**6**)*

The synthesis of complex **6** was carried out following the same experimental procedure as complex **2**, using bpzbeH (1.00 g, 3.45 mmol), ^{n}BuLi (2.0 mL, 3.62 mmol) and $GaCl_3$ (0.64 g, 3.62 mmol). Suitable crystals for X-Ray analysis were

obtained at –25 ºC from an Et_2O solution. Complex **6** was obtained as a white crystalline solid in 85% yield.

Analysis found:	C: 44.4 %	H: 6.0 %	N: 12.9 %
Calculated:	C: 44.1 %	H: 5.6 %	N: 13.3 %

*2.1.6. Synthesis of Gal(κ^3-bpzte)$_2$]$^+$[GaCl$_4$]$^-$ (**7**)*

The synthesis of complex **7** was carried out following the same experimental procedure as complex **6**, using bpzteH (1.00 g, 3.10 mmol), ^{n}BuLi (2.00 mL, 3.24 mmol) and $GaCl_3$ (0.57 g, 3.24 mmol). Complex **7** was obtained as a white solid in 82% yield.

Analysis found:	C: 49.0 %	H: 5.1 %	N: 12.0 %
Calculated:	C: 48.7 %	H: 4.8 %	N: 12.3 %

*2.1.7. Synthesis of Gal(κ^3-bpzappe)$_2$]$^+$[GaCl$_4$]$^-$ (**8**)*

The synthesis of complex **8** was carried out following the same experimental procedure as complex **6,** using bpzappeH (1.00 g, 2.33 mmol), ^{n}Buli (1.53 mL, 2.44 mmol) and $GaCl_3$ (0.43 g, 2.44 mmol). Complex **8** was obtained as a white solid in 78% yield.

Analysis found:	C: 54.8 %	H: 5.5 %	N: 12.2 %
Calculated:	C: 54.5 %	H: 5.1 %	N: 12.5 %

*2.1.8. Synthesis of Gal(κ^3-bpzFerr)$_2$]$^+$[GaCl$_4$]$^-$ (**9**)*

The synthesis of complex **9** was carried out following the same experimental procedure as complex **6,** using bpzFerrH (**1**) (1.00 g, 2.39 mmol), ^{n}BuLi (1.55 mL, 2.51 mmol) and $GaCl_3$ (0.44 g, 2.51 mmol) were used. Complex **9** was obtained as an orange solid in 82% yield.

Analysis found:	C: 49.0 %	H: 5.1 %	N: 12.0 %
Calculated:	C: 48.7 %	H: 4.8 %	N: 12.3 %

2.2. Synthesis of chloride indium complexes

*2.2.1. Synthesis of [$InCl_2${(κ^3-bpzbe)(μ-O)}]$_2$ (**10**)*

In a 100 cm^3 Schlenk tube, bpzbeH (1.00 g, 3.45 mmol) was dissolved in 30 mL of dry THF and cooled down to −78 ºC. Then, a solution of ^{n}BuLi (1.6M in hexanes, 2.30 mL, 3.62 mmol) was added dropwise and the mixture was maintained at −78 ºC during one hour. After that time, the lithiated adduct was transferred *via* cannula to a pre-cooled slurry of $InCl_3$ (0.80 g, 3.62 mmol) in THF. The resulting mixture was warmed to room temperature and left stirring overnight. The white solid precipitated was filtered and dried *in vacuo* for two hours to afford complex **10** in 80% yield. Suitable crystals for X-Ray analysis were obtained from a CH_2Cl_2 solution at room temperature.

Analysis found:	C: 42.0 %	H: 5.7 %	N: 11.1 %
Calculated:	C: 41.8 %	H: 5.4 %	N: 11.5 %

*2.2.2. Synthesis of [$InCl_2${(κ^3-bpzte)(μ-O)}]$_2$ (**11**)*

The synthesis of complex **11** was carried out following the same experimental procedure as complex **10**, using bpzteH (1.00 g, 3.10 mmol), ^{n}BuLi (2.00 mL, 3.24 mmol) and $InCl_3$ (0.72 g, 3.24 mmol). Complex **11** was obtained as a white solid in 70% yield.

Analysis found:	C: 45.9 %	H: 4.8 %	N: 10.6 %
Calculated:	C: 45.5 %	H: 4.5 %	N: 10.9 %

*2.2.3. Synthesis of [$InCl_2${(κ^3-bpzappe)(μ-O)}]$_2$ (**12**)*

The synthesis of complex **12** was carried out following the same experimental procedure as complex **10**, using bpzappeH (1.00 g, 2.33 mmol), ^{n}BuLi (1.53 mL, 2.44 mmol) and $InCl_3$ (0.54 g, 2.44 mmol). Complex **12** was obtained as a white solid in 70% yield.

Analysis found:	C: 52,0 %	H: 5,3 %	N: 10,9 %
Calculated:	C: 51,7 %	H: 5,0 %	N: 11,2 %

*2.2.4. Synthesis of [$InCl_2${(κ^3-bpzFerr)(μ-O)}]$_2$ (**13**)*

The synthesis of complex **13** was carried out following the same experimental procedure as complex **10**, using bpzFerrH (**1**) (1.00 g, 2.40 mmol), ^{n}BuLi (1.57 mL,

2.51 mmol) and $InCl_3$ (0.56 g, 2.51 mmol). Complex **13** was obtained as an orange solid in 76% yield.

Analysis found:	C: 52.0 %	H: 5.3 %	N: 10.9 %
Calculated:	C: 51.7 %	H: 5.0 %	N: 11.2 %

3. Synthesis of alkyl group 13 metal complexes

3.1. Synthesis of alkyl aluminium complexes

*3.1.1. Synthesis of [$AlMe_2(\kappa^2$-bpzFerr)] (**15**)*

In a 100 cm^3 Schlenk tube, bpzFerrH (**1**) (1.00 g, 2.39 mmol) was dissolved in 20 mL of dry toluene and cooled down to 0 ºC. Then, a solution of $AlMe_3$ (2M in hexanes, 1.25 mL, 2.51 mmol) was added dropwise and the mixture was allowed to warm up to room temperature and left stirring for two hours. After that time, solvent was removed *in vacuo* and complex **15** was obtained as an orange solid in 89% yield.

Analysis found:	C: 58.2 %	H: 4.9 %	N: 13.1 %
Calculated:	C: 58.0 %	H: 4.6 %	N: 13.5 %

*3.1.2 Synthesis of [$AlEt_2(\kappa^2$-bpzFerr)] (**16**)*

The synthesis of complex **16** was carried out following the same experimental procedure as complex **15**, using bpzFerrH (**1**) (1.00 g, 2.39 mmol) and $AlEt_3$ (1M in hexanes, 2.50 mL, 2.50 mmol). Complex **16** was obtained as an orange solid in 87% yield.

Analysis found:	C: 60.2 %	H: 5.5 %	N: 12.4 %
Calculated:	C: 59.8 %	H: 5.2 %	N: 12.7 %

3.2. Synthesis of alkyl gallium and indium complexes

*3.2.1. Synthesis of [{Li(κ^3-bpzFerr)(Et_2O)}(μ-O){$GaMe_2Cl$}] (**17**)*

In a 100 cm^3 Schlenk tube, $GaCl_3$ (0.50 g, 2.83 mmol) was dissolved in 20 mL of dry Et_2O. Then, a solution of MeLi (1.6M in hexanes, 5.84 mL, 9.34 mmol) was added dropwise and the suspension was stirred for three hours. A solution of bpzFerrH (**1**) (0.78 g, 2.70 mmol) in Et_2O was then transferred *via* cannula and the resulting mixture was left stirring overnight. After that time, the suspension was left decanting and

filtered thorough celite to eliminate the LiCl salt generated. Solvent was then removed *in vacuo* affording complex **17** as an orange solid in 75% yield.

Analysis found:	C: 53.4 %	H: 6.9 %	N: 8.6 %
Calculated:	C: 53.1 %	H: 6.5 %	N: 8.8 %

*3.2.2. Synthesis of [{Li(κ^3-bpzbe)(Et_2O)}(μ-O){$InMe_2Cl$}] (**18**)*

The synthesis of complex **18** was carried out following the same experimental procedure as complex **17,** using $InCl_3$ (0.50 g, 2.26 mmol), MeLi (4.67 mL, 7.46 mmol) and bpzbeH (0.62 g, 2.15 mmol). Complex **18** was obtained as a white solid in 77% yield.

Analysis found:	C: 48.2 %	H: 7.8 %	N: 9.8 %
Calculated:	C: 48.0 %	H: 7.5 %	N: 10.2 %

*3.2.3. Synthesis of [{Li(κ^3-bpzte)(Et_2O)}(μ-O){$InMe_2Cl$}] (**19**)*

The synthesis of complex **19** was carried out following the same experimental procedure as complex **17,** using $InCl_3$ (0.50 g, 2.26 mmol), MeLi (4.67 mL, 7.46 mmol) and bpzteH (0.70 g, 2.15 mmol). Complex **19** was obtained as a white solid in 77% yield.

Analysis found:	C: 51.5 %	H: 7.0 %	N: 9.5 %
Calculated:	C: 51.3 %	H: 6.7 %	N: 9.6 %

*3.2.4. Synthesis of [{Li(κ^3-bpzFerr)(Et_2O)}(μ-O){$InMe_2Cl$}] (**20**)*

The synthesis of complex **20** was carried out following the same experimental procedure as complex **17**, using $InCl_3$ (0.50 g, 2.26 mmol), MeLi (4.67 mL, 7.46 mmol) and bpzFerrH (**1**) (0.90 g, 2.15 mmol). Complex **20** was obtained as a white solid in 73% yield.

Analysis found:	C: 49.9 %	H: 6.5 %	N: 8.1 %
Calculated:	C: 49.6 %	H: 6.1 %	N: 8.3 %

*3.2.5. Synthesis of [GaMeCl(κ^3-bpzbe)] (**21**)*

The synthesis of complex **21** was carried out following the same experimental procedure as complex **17**, using $GaCl_3$ (0.50 g, 2.83 mmol), MeLi (3.89 mL, 6.23

mmol) and bpzFerrH (**1**) (0.90 g, 2.15 mmol). Complex **21** was obtained as a white solid in 73% yield.

Analysis found:	C: 50.2 %	H: 7.2 %	N: 13.4 %
Calculated:	C: 49.9 %	H: 6.9 %	N: 13.7 %

*3.2.6. Synthesis of [GaMeCl(κ^3-bpzte)] (**22**)*

The synthesis of complex **22** was carried out following the same experimental procedure as complex **17**, using $GaCl_3$ (0.50 g, 2.83 mmol), MeLi (3.89 mL, 6.23 mmol) and bpzteH (0.88 g, 2.70 mmol). Complex **22** was obtained as a white solid in 78% yield.

Analysis found:	C: 54.5 %	H: 6.2 %	N: 12.3 %
Calculated:	C: 54.2 %	H: 5.9 %	N: 12.6 %

*3.2.7. Synthesis of [$InMe_2Cl(\kappa^3$-bpzbeH)] (**23**)*

The synthesis of complex **23** was carried out following the same experimental procedure as complex **17**, using $InCl_3$ (0.50 g, 2.26 mmol), MeLi (3.10 mL, 4.97 mmol) and bpzteH (0.88 g, 2.15 mmol). Complex **23** was obtained as a white solid in 82% yield.

Analysis found:	C: 50.2 %	H: 7.2 %	N: 11.5 %
Calculated:	C: 45.9 %	H: 6.9 %	N: 11.9 %

*3.2.8. Synthesis of [$InMe_2Cl(\kappa^3$-bpzappeH)] (**24**)*

The synthesis of complex **24** was carried out following the same experimental procedure as complex **17**, using $InCl_3$ (0.50 g, 2.26 mmol), MeLi (3.10 mL, 4.97 mmol) and bpzappeH (0.92 g, 2.15 mmol). Complex **24** was obtained as a white solid in 77% yield.

Analysis found:	C: 55.2 %	H: 6.3 %	N: 11.3 %
Calculated:	C: 55.1 %	H: 6.1 %	N: 11.5 %

4. Synthesis of alkoxide aluminium complexes

*4.1. Synthesis of complex [Al(O^{i}Pr)(κ^2-bpzbe)$_2$] (**25**)*

In a 100 cm^3 Schlenk tube, bpzbeH (0.80 g, 2.75 mmol) and Al(O^{i}Pr)$_3$ (0.28 g, 1.38 mmol) were dissolved in 25 mL of dry toluene and the solution was warmed up to 80 ºC and left stirring for 7 days. After that time, the solution was concentrated down, filtered and kept in the freezer at −25 ºC. Suitable crystals for X-Ray analysis were obtained from the solution. Complex **25** was isolated as a white solid in 60% yield.

Analysis found:	C: 63.6 %	H: 8.9 %	N: 16.5 %
Calculated:	C: 63.2 %	H: 8.6 %	N: 16.9 %

*4.2. Synthesis of complex [Al(O^{i}Pr)(κ^2-bpzFerr)$_2$] (**26**)*

The synthesis of complex **26** was carried out following the same experimental procedure as complex **25**, using bpzFerrH (**1**) (0.80 g, 1.91 mmol) and Al(O^{i}Pr)$_3$ (0.20 g, 0.96 mmol). Suitable crystals were obtained from a concentrated solution of *n*-hexane at −25 ºC. Complex **26** was isolated as an orange solid in 57% yield.

Analysis found:	C: 61.6 %	H: 6.5 %	N: 11.9 %
Calculated:	C: 61.3 %	H: 6.2 %	N: 12.2 %

5. Synthesis of amido indium complexes

*5.1. Synthesis of [InCl{N(SiMe$_3$)$_2$}$_2$pyr] (**27**)*[56]

In a 100 cm^3 Schlenk tube, InCl$_3$ (0.60 g, 2.70 mmol) was dissolved in 30 mL of pyridine. Another solution containing LiN(SiMe$_3$)$_2$ (1.36 g, 8.14 mmol) in pyridine (20 mL) was prepared and transferred dropwise to the first one. The resulting mixure was left stirring overnight. After that time, solvent was removed *in vacuo* affording a reddish sticky oil, which was held *in vacuo* for four hours. The remaining oil was extracted with 2x20 mL of hexane and filtered through celite. Suitable crystals for X-Ray analysis were obtained from the solution at −25 ºC. Compound **27** was obtained as a white crystalline solid in 70% yield.

Analysis found:	C: 37.4 %	H: 7.8 %	N: 7.4 %
Calculated:	C: 37.1 %	H: 7.5 %	N: 7.6 %

*5.2. Synthesis of [InCl{N(SiMe$_3$)$_2$}{(κ^3-bpzbe)(μ-O)}]$_2$ (**28**)*

In a 100 cm^3 Schlenk tube, [InCl{(N(SiMe$_3$)$_2$)$_2$pyr}] (**27**) (0.30 g, 0.54 mmol) was dissolved in 10 mL of toluene and cooled down to 0 ºC. Another solution containing bpzbeH (0.15 g, 0.52 mmol) in 10 mL of toluene was prepared and transferred dropwise to the first one. The resulting mixture was warmed to room temperature and left stirring for two hours. After that time, solution was concentrated down to 5 mL, filtered and cooled down to −25 ºC. Suitable crystals for X-Ray analysis were obtained from the solution. Compound **28** was isolated as a white crystalline solid in 73% yield.

Analysis found:	C: 44.4 %	H: 7.5 %	N: 11.5 %
Calculated:	C: 44.0 %	H: 7.2 %	N: 11.7 %

Bibliography

BIBLIOGRAPHY

(1) *(a)* S. Trofimenko, "Scorpionate, The Coordination Chemistry of Polypyrazolylborate Ligands", Imperial College Press, London, **1998**; *(b)* C. Pettinari, "Scorpionate II: Chelating Borate Ligands", Imperial College Press, London, **2008**.

(2) *(a)* A. Otero, J. Fernández-Baeza, A. Antiñolo, J. Tejeda, A. Lara-Sánchez, *Dalton Trans.*, **2004**, 1449; *(b)* C. Pettinari, R. Pettinari, *Coord. Chem. Rev.*, **2005**, *249*, 663; *(c)* A. Otero, J. Fernández-Baeza, A. Lara-Sánchez, J. Tejeda, L. F. Sánchez-Barba, *Eur. J. Inorg. Chem.*, **2008**, 5309; *(d)* A. Otero, J. Fernández-Baeza, A. Lara-Sánchez, L. F. Sánchez-Barba, *Coord. Chem. Rev.*, **2013**, *257*, 1806.

(3) *(a)* K. I. The, L. K. Peterson, *Can. J. Chem.*, **1973**, *51*, 422; *(b)* K. I. The, L. K. Peterson, E. Kiehlmann, *Can. J. Chem.*, **1973**, *51*, 2448; *(c)* L. K. Peterson, E. Kiehlmann, A. R. Sanger, K. I. The, *Can. J. Chem.*, **1974**, *52*, 2367; *(d)* T. C. Higgs, C. J. Carrano, *Inorg. Chem.*, **1997**, *36*, 291.

(4) *(a)* T. C. Higgs, R. Czernuszewicz, B. F. Matnauke, V. Schunemann, A. X. Trantwein, M. Helliwell, W. Ramirez, C. J. Carrano, *Inorg. Chem.*, **1998**, *37*, 2383; *(b)* U. Brand, M. Rombach, C. J. Carrano, H. Vahrenkamp, *Chem. Commun.*, **1998**, 2717; *(c)* B. S. Hammes, C. J. Carrano, *Inorg. Chem.*, **1999**, *38*, 4593; *(d)* G. A. Santillan, C. J. Carrano, *Inorg. Chem.*, **2007**, 46, 1751; *(e)* G. A. Santillan, C. J. Carrano, *Dalton Trans.*, **2009**, 6599.

(5) D. L. Jameson, S. E. Hilgen, C. E. Hummel, S. L. Pichla, *Tetrahedron Lett.*, **1989**, *30*, 1609.

(6) A. Otero, J. Fernández-Baeza, J. Tejeda, A. Antiñolo, F. Carrillo-Hermosilla, E. Díez-Barra, A. Lara-Sánchez, M. Fernández-López, M. Lanfranchi, M. A. Pellinghelli, *J. Chem. Soc., Dalton Trans.*, **1999**, 3537.

(7) *(a)* A. Otero, J. Fernández-Baeza, A. Antiñolo, E. Díez-Barra, F. Carrillo-Hermosilla, J. Tejeda, A. Lara-Sánchez, M. Fernández-López, *J. Chem. Soc., Dalton Trans.*, **2000**, 2367; *(b)* A. Otero, J. Fernández-Baeza, A. Antiñolo, F. Carrillo-Hermosilla, J. Tejeda, A. Lara-Sánchez, L. Sánchez-Barba, M. Fernández-López, A. M. Rodríguez, I. López-Solera, *Inorg. Chem.*, **2002**, *41*,

5193.

(8) G. Türkoglu, C. P. Ulldemolins, R. Müller, E. Hübner, F. W. Heinemann, M. Wolf, N. Burzlaff, *Eur. J. Inorg. Chem.*, **2010**, 2962.

(9) *(a)* J. C. Huffman, D. J. Mindiola, G. Zhao, F. Basuli, J. Tomaszewski, D. Adhikari, *Inorg. Chem.*, **2006**, *45*, 1604; *(b)* A. Otero, J. Fernández-Baeza, J. Tejeda, A. Lara-Sánchez, S. Franco, J. Martínez-Ferrer, M. P. Carrión, I. López-Solera, A. M. Rodriguez, *Inorg. Chem.*, **2011**, *50*, 1826.

(10) R. G. Howe, C. S. Tredget, S. C. Lawrence, S. Subongkoj, A. R. Cowley, P. Mountford, *Chem. Commun.*, **2006**, 223.

(11) M. Honrado, S. Sobrino, J. Fernández-Baeza, L. F. Sánchez-Barba, A. Garcés, A. Lara-Sánchez, A. M. Rodríguez, *Chem. Commun.*, **2019**, *55*, 8947.

(12) *(a)* A. Otero, J. Fernández-Baeza, A. Antiñolo, J. Tejeda, A. Lara-Sánchez, L. Sánchez-Barba, M. Sánchez-Molina, S. Franco, M. I. López-Solera, A. M. Rodríguez, *Eur. J. Inorg. Chem.*, **2006**, 707; *(b)* A. Otero, A. Lara-Sánchez, J. Fernández-Baeza, E. Martínez-Caballero, I. Márquez-Segovia, C. Alonso-Moreno, L. F. Sánchez-Barba, A. M. Rodríguez, *Dalton. Trans.*, **2010**, *39*, 930; *(c)* A. Otero, A. Lara-Sánchez, C. Alonso-Moreno, J. Tejeda, J. A. Castro-Osma, I. Márquez-Segovia, L. F. Sánchez-Barba, A. M. Rodríguez, M. V. Gómez, *Chem. Eur. J.*, **2010**, *16*, 8615; *(d)* A. Otero, A. Lara-Sánchez, J. Fernández-Baeza, C. Alonso-Moreno, J. A. Castro-Osma, I. Márquez-Segovia, L. F. Sánchez-Barba, A. M. Rodríguez, J. C. García-Martínez, *Organometallics*, **2011**, *30*, 1507; *(e)* J. A. Castro-Osma, C. Alonso-Moreno, I. Márquez-Segovia, A. Otero, A. Lara-Sánchez, J. Fernández-Baeza, A. M. Rodríguez, L. F. Sánchez-Barba, J. C. García-Martínez, *Dalton Trans.*, **2013**, *42*, 9325; (*f)* J. A. Castro-Osma, C. Alonso-Moreno, M. V. Gómez, I. Márquez-Segovia, A. Otero, A. Lara-Sánchez, J. Fernández-Baeza, L. F. Sánchez-Barba, A. M. Rodríguez, *Dalton Trans.*, **2013**, *42*, 14240; *(g)* J. A. Castro-Osma, C. Alonso-Moreno, A. Lara-Sánchez, A. Otero, J. Fernández-Baeza, L. F. Sánchez-Barba, A. M. Rodriguez, *Dalton Trans.*, **2015**, *44*, 12388.

(13) *(a)* M. Ortiz, A. Díaz, R. Cao, A. Otero, J. Fernández-Baeza, *Inorg. Chim. Acta*, **2004**, *357*, 19; *(b)* M. Porchia, G. Papini, G. G. Lobbia, M. Pellei, F. Tisato, G. Bandoli, A. Dolmella, *Inorg. Chem.*, **2005**, *44*, 4045.

(14) *(a)* A. Otero, J. Fernández-Baeza, A. Antiñolo, A. Lara-Sánchez, E. Martínez-Caballero, J. Tejeda, L. F. Sánchez-Barba, C. Alonso-Moreno, I. López-Solera, O*rganometallics*, **2008**, *27*, 976; *(b)* A. Otero, J. Fernández-Baeza, A. Lara Sánchez, A. Antiñolo, J. Tejeda, E. Martínez-Caballero, I. Márquez-Segovia, I. López-Solera, L. F. Sánchez-Barba, C. Alonso-Moreno, *Inorg. Chem.*, **2008**, *47*, 4996; *(c)* A. Garcés, L. F. Sánchez-Barba, C. Alonso-Moreno, M. Fajardo, J. Fernández-Baeza, A. Otero, A. Lara-Sánchez, I. López-Solera, A. M. Rodríguez, *Inorg. Chem.*, **2010**, *49*, 2859; *(d)* M. Honrado, A. Otero, J. Fernández-Baeza, L. F. Sánchez-Barba, A. Lara-Sánchez, M. P. Carrión, J. Martínez-Ferrer, A. Garcés, A. M. Rodriguez, *Organometallics*, **2013**, *32*, 3437. *(e)* M. Honrado, A. Otero, J. Fernández-Baeza, L. F. Sánchez-Barba, A. Gracés, A. Lara-Sánchez, J. Martínez-Ferrer, S. Sobrino, A. M. Rodríguez, *Organometallics*, **2015**, *34*, 3196.

(15) *(a)* L. F. Tang, S. B. Zhao, W. L. Jia, Z. Yang, D. T. Song, J. T. Wang, *Organometallics*, **2003**, *22*, 3290; *(b)* J. T. Lu, M. Du, L. F. Tang, *J. Chem. Crystallogr.*, **2010**, *40*, 668.

(16) *(a)* A. Otero, J. Fernández-Baeza, A. Antiñolo, J. Tejeda, A. Lara-Sánchez, L. F. Sánchez-Barba, M. Sanchez-Molina, S. Franco, I. Lopez-Solera, A. M. Rodríguez, *Inorg*. *Chem.*, **2007**, *46*, 8475; *(b)* A. Otero, J. Fernández-Baeza, J. Tejeda, A. Lara-Sánchez, M. Sanchez-Molina, S. Franco, I. Lopez-Solera, A. M. Rodríguez, L. F. Sánchez-Barba, S. Morante-Zarcero, A. Garcés, *Inorg*. *Chem.*, **2009**, *48*, 5540.

(17) Z. Zhang, D. Cui, A. A. Trifonov, *Eur. J. Inorg. Chem.*, **2010**, 2861.

(18) *(a)* E. Díez-Barra, J. Guerra, V. Hornillos, S. Merino, J. Tejeda, *Tetrahedron Lett.*, **2004**, *45*, 6937; *(b)* M. Bhanuchandra, M. R. Kuram, A. K. Sahoo, *J. Org. Chem.*, **2013**, *78*, 11824.

(19) *(a)* M. Bochmann, D. M. Dawson, *Angew. Chem. Int. Ed.*, **1996**, *35*, 2226; *(b)* A. Rodriguez-Delgado, E. Chen, *J. Am. Chem. Soc.*, **2005**, *127*, 961; *(c)* Q. Liu, Y. X. Wu, Y. Zhang, P. F, Yan, R. W. Xu, *Polymer*, **2010**, *51*, 5960; *(c)* Z. Flisak, G. P. Spaleniak, M. Bremmek, *Organometallics*, **2013**, *32*, 3870; *(d)* C.

Boulho, H. S. Zijlstra, S. Harder, *Eur. J. Inorg. Chem.,* **2015**, 2132; *(e)* R. Tanaka, T. Hirosi, Y. Nakayama, T. Shiono, *Polym J.*, **2016**, *48*, 67.

(20) *(a)* T. M. Ovitt, G. W. Coates, *J. Am. Chem. Soc*., **1999**, *121*, 4072; *(b)* C. R. Radano, G. L. Baker, M. R. Smith, *J. Am. Chem. Soc*., **2000**, *122*, 1552; *(c)* N. Nomura, R. Ishii, M. Akakura, K. Aoi, *J. Am. Chem. Soc*., **2002**, *124*, 5938; *(d)* Z. Zhong, P. Dijkstra, J. Feijen, *J. Am. Chem. Soc*., **2003**, *125*, 1291; *(e)* K. Majerska, A. Duda, *J. Am. Chem. Soc*., **2004**, *126*, 1026; *(f)* Z. Tang, X. Chen, Y. Yang, X. Pang, J. Sun, X. Zhuang, X. Jing, *J. Polym. Sci. Part A: Polym. Chem.*, **2004**, *42*, 5974; *(g)* M. H. Chisholm, J. C. Gallucci, K. T. Quisenberry, Z. Zhou, *Inorg. Chem.*, **2008**, *47*, 2613; *(h)* C. A.Wheaton, P. G. Hayes, B. J. Ireland, *Dalton Trans*., **2009**, 4832; *(i)* H. Du, A. H. Velders, P. J. Dijkstra, J. Sun, Z. Zhong, X. Chen, J. Feijen, *Chem. Eur. J.,* **2009**, *15*, 9836; *(j)* M. Bouyahyi, T. Roisnel, J. F. Carpentier, *Organometallics*, **2010**, *29*, 491; *(k)* M. Bouyahyi, T. Roisnel, J. F. Carpentier, *Organometallics*, **2012**, *31*, 1458; *(l)* C. Romain, C. Fliedel, S. Bellemin-Laponnaz, S. Dagorne, *Organometallics*, **2014**, *33*, 5730; *(m)* A. Pilone, N. D. Maio, K. Press, V. Venditto, D. Pappalardo, M. Mazzeo, C. Pellecchia, M. Kol, M. Lamberti, *Dalton Trans.*, **2015**, *44*, 2157.

(21) *(a)* J. P. Abell, H. Yamamoto, *J. Am. Chem. Soc.*, **2009**, *131*, 15118; *(b)* P. Sumrit, P. Hormnirun, *Macromol. Chem. Phys.,* **2013**, *214*, 1845; *(c)* H. Itoh, H. Maeda, S. Yamada, Y. Hori, T. Mino, M. Sakamoto, *Org. Biomol. Chem.,* **2015**, *13*, 5817; *(d)* O. V. Fedorova, Y. A. Titova, A. Y. Vigorov, M. S. Toporova, O. A. Alisienok, A. N. Murashkevich, V. P. Krasnov, G. L. Rusinov, V. N. Charushin, *Catal. Lett.*, **2016**, *146*, 493.

(22) *(a)* D. A. Atwood, *Chem. Rev.,* **2008**, *108*, 4037; (*b)* N. Nakata, Y. Saito, A. Ishii, *Organometallics*, **2014**, *33*, 1840; *(c)* S. Verma, R.I. Kureshy, T. Roi, M. Kumar, A. Das, N. H. Khan, S. H. R. Abdi, H. C. Bajaj, *Catal. Commun.,* **2015**, *61*, 78; *(d)* L. L. Cao, E. Daley, T. C. Johnstone, D. W. Stephan, *Chem. Commun.,* **2016**, *52*, 5305

(23) *(a)* X. Sheng,W. Wu, Y. Qin, X. Wang, F. Wang, *Polym. Chem.,* **2015**, *6*, 4719; *(b)* N. J. Van Zee, G. W. Coates, *Angew. Chem. Int. Ed.,* **2015**, *54*, 2665; *(c)* N. J. Van Zee, M. J. Sandford, G. W. Coates, *J. Am. Chem. Soc.,* **2016**, *138*, 2755

(24) *a)* R. Olejník, J. Bazantova, Z. Ruzickova, J. Merna, Z. Hostalek, A. Ruzicka, *Inorg. Chem. Commun.*, **2015**, *55*, 161; *(b)* S. Tabthong, T. Nanok, P. Sumrit, P. Kongsaeree, S. Prabpai, P, Chuawong, P. Hornnirum, *Macromolecules*, **2015**, *48*, 684.

(25) B. Lian, H. Ma, T. P. Spaniol, J. Okuda, *Dalton Trans.*, **2009**, 9033.

(26) *(a)* J. Martinez, J. A. Castro-Osma, A. Earlam, C. Alonso-Moreno, A. Otero, A. Lara-Sanchez,M. North, A. Rodriguez-Dieguez, *Chem. Eur. J.*, **2015**, *21*, 9850; *(b)* J. Martinez, J. A. Castro-Osma, C. Alonso-Moreno, A. Rodriguez-Dieguez, M. North, A. Otero, A. Lara-Sanchez, *ChemSusChem*, **2017**, *10*, 1175; *(c)* F. De La Cruz-Martinez, J. Martínez, M. A. Gaona, J. Fernandez-Baeza, L. F. Sanchez-Barba, A. M. Rodríguez, J. A. Castro-Osma, A. Otero, A. Lara-Sanchez, *ACS Sustainable Chem. Eng*., **2018**, 6, 5322; *(d)* F. de la Cruz-Martínez, M. Martínez de Sarasa Buchaca, J. Martínez, J. Fernandez-Baeza, L. F. Sanchez-Barba, A. Rodríguez-Dieguez, J. A. Castro-Osma, A. Lara-Sanchez, *ACS Sustainable Chem. Eng*., **2019**, 7, 20126; *(e)* J. A. Castro-Osma, C. Alonso-Moreno, A. Lara-Sánchez, J. Martínez, M. North, A. Otero, *Catal. Sci. Technol*., **2014**, *4*, 1674

(27) A. H. Cowley, C. J. Carrano, R. L. Geerts, R. A. Jones, C. M. Nunn, *Angew. Chem. Int. Ed.*, **1988**, *27*, 277.

(28) *(a)* R. Han, A. Looney, G. Parkin, *J. Am. Chem. Soc.*, **1989**, *111*, 7276; *(b)* A. Looney, G. Parkin, *Polyhedron*, **1990**, *9*, 265

(29) J. Koller, G. Bergman, *Organometallics*, **2012**, *31*, 2530.

(30) M. H. Chisholm, N. W. Eilerts, J. C. Huffman, *Inorg. Chem*., **1996**, *35*, 445.

(31) *(a)* B. Baird, A. V. Pawlikowski, J. Su, J. W. Wiench, M. Pruski, A. D. Sadow, *Inorg. Chem.*, **2008**, *47*, 10208; *(b)* J. F. Dunne, J. C. Su, A. Ellern, A. D. Sadow, *Organometallics*, **2008**, *27*, 2399.

(32) J. F. Dunne, K. Manna, J. W. Wiench, A. Ellern, M. Pruski, A. D. Sadow, *Dalton Trans*., **2010**, *39*, 641.

(33) *(a)* S. Milione, F. Grisi, R. Centore, A. Tuzi, *Organometallics*, **2006**, *25*, 266; *(b)* A. Silvestri, F. Grisi, S. Milione, *J. Polym. Sci.: Polym. Chem.*, **2010**, *48*,

3632; *(c)* S. Milione, G. Milano, L. Cavallo, *Organometallics*, **2012**, *31*, 8498; *(d)* F. Grisi, V. Bertolasi, S. Milione, *J. Organomet. Chem.*, **2014**, *749*, 174.

(34) A. Otero, J. Fernández-Baeza, A. Lara-Sánchez, C. Alonso-Moreno, I. Márquez-Segovia, L. F. Sánchez-Barba, A. M. Rodríguez, *Angew. Chem. Int. Ed.*, **2009**, *48*, 2176.

(35) J. Martínez, M. Martínez de Sarasa Buchaca, F. de la Cruz-Martínez, C. Alonso-Moreno, L. F. Sánchez-Barba, J. Fernández-Baeza, A. M. Rodríguez, A. Rodríguez-Diéguez, J. A. Castro Osma, A. Otero and A. Lara-Sánchez, *Dalton Trans*., **2018**, *47*, 7471.

(36) A. Garcés, L. F. Sánchez-Barba, J. Fernández-Baeza, A. Otero, I. Fernández, A. Lara-Sánchez, A. M. Rodríguez, *Inorg. Chem*., **2018**, *57*, 12132.

(37) M. Navarro, L. F. Sánchez-Barba, A. Garcés, J. Fernández-Baeza, I. Fernández, A. Lara-Sánchez, A. M. Rodríguez, *Catal. Sci. Technol*., **2020**, *10*, 3265.

(38) S. Dagorne, R. Wehmschulte, *ChemCatChem*, **2018**, *10*, 2509.

(39) H-J. Jung, Y. Cho, D. Kim, P.Merkhodavandi, *Catal. Sci. Technol.*, **2021**, *11*, 62.

(40) D. L. Reger, Y. Ding, *Organometallics*, **1993**, *12*, 4485.

(41) D. L. Reger, S. J. Knox, L. Lebioda, *Inorg. Chem*., **1989**, *28*, 3092.

(42) D. L. Reger, S. J. Knox, L. Lebioda, *Organometallics*, **1990**, *9*, 2218.

(43) K. M. Osten, P. Mehrkhodavandi, *Acc. Chem. Res.*, **2017**, *50*, 2861.

(44) A. B. Kremer, R. J. Andrews, M. J. Milner, X. R. Zhang, T. Ebrahimi, B. O. Patrick, P. L. Diaconescu, P. Mehrkhodavandi, *Inorg. Chem.*, **2017**, *56*, 1375.

(45) A. Thevenon, A. Cyriac, D. Myers, A. J. P. White, C. B. Durr, C. K. Williams, *J. Am. Chem. Soc.*, **2018**, *140*, 6893.

(46) A. Frazer, B. Piggott, M. Harman, M. Mazid, M. B. Hursthouse, *Polyhedron*, **1992**, *11*, 3013.

(47) A. Frazer, B. Piggott, J. *Chem. Soc., Dalton Trans.*, **1999**, 3483.

(48) D. L. Reger, S. J. Knox, A. L. Rheingold, B. S. Heggerty, *Organometallics*, **1990**, *9*, 2581.

(49) B. K. Nicholson, R. A. Thomson, F. D. Watts, *Inorg. Chem. Acta*, **1988**, *148*, 101.

(50) A. F. Douglas, B. O. Patrick, P. Mehrkhodavandi, *Angew. Chem. Int. Ed.* **2008**, *47*, 2290.

(51) M. Hu, M. Wang, P. Zhang, L. Wang, F. Zhu, L. Sun, *Inorg. Chem. Commun.* **2010**, *13*, 968.

(52) J. Lewinski, J. Zachara, P. Gós, E. Grabska, T. Kopéc, I. Madura, W. Marciniak, I. Prowotorow, *Chem. Eur. J.*, **2000**, *6***,** 3215.

(53) *a)* M. A. Muñoz-Hernandez, T. S. Keizer, P. Wei, S. Parkin, D. A. Atwood, *Inorg. Chem.*, **2001**, *40*, 6782; *(b)* J. Muller and R. Boese, *J. Mol. Struct.*, **2000**, *520*, 215; *(c)* A. W. Addison, T. N. Rao, J. Reedijk, K. J. Van Rijn, G. C. Verschoor, *J. Chem. Soc., Dalton Trans.*, **1984**, 1349.

(54) C. T. Altaf, H. Wang, M. Keram, Y. Yang, H. Ma, *Polyhedron.*, **2014**, *81*, 11.

(55) I. Alkorta, R. M. Claramunt, E. Diez-Barra, J. Elguero, A. de la Hoz, C. López, *Coord. Chem. Rev.*, **2017**, *339*, 153.

(56) J. Kim, S. G. Bott, D. M. Hoffman, *Inorg. Chem.* **1998**, *37*, 3835.

Chapter 2.

Preparation of biodegradable polyesters catalysed by heteroscorpionate aluminium complexes

Introduction

In this Chapter, the results obtained in the synthesis of biodegradable polyesters by Ring-Opening Copolymerisation (ROCOP) of epoxides and cyclic anhydrides will be described. Before discussing the results obtained, a brief introduction about this process will be covered.

Polyesters are a category of polymers which include an ester group (–O–CO–) in their main chain. They are amongst the most used oxygenated polymers and are often obtained by step growth polymerisation either by direct esterification between a diacid and a diol or by self-condensation of a hydroxy carboxylic acid (Scheme 1).[1] In this mechanism, bifunctional or multifunctional monomers react between themselves to form dimers, trimers, tetramers, oligomers, and eventually long-chain polymers.

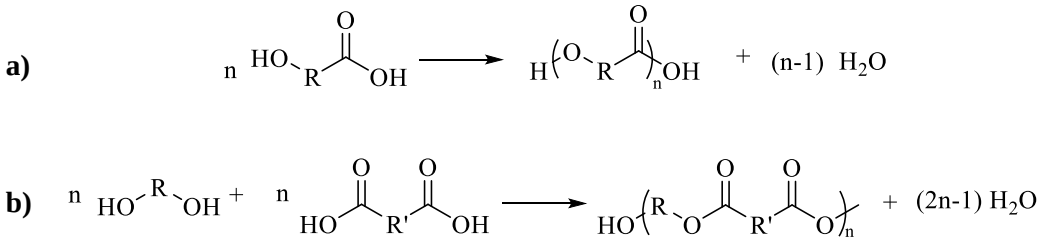

Scheme 1. *Synthesis of polyesters by a) self-condensation of a hydroxy carboxylic acid and b) polycondensation of a diacid and a diol.*

Polyesters can be broadly divided in two different types: semiaromatic and aliphatic polyesters. Semiaromatic polyesters include those polymers which have a rigid or a cyclic group within their backbone. This structure gives them unique physical and chemical properties such as good mechanical strength, toughness, fatigue resistance as well as good chemical, hydrolytic and solvent resistance, which make them perfect for a wide range of applications including packaging, fibres, rigid plastics and engineering materials.[1] They have also found application as liquid crystalline polymers.[2,3]

Among this type of polyesters, polyethylene terephthalate (PET) is the most produced worldwide. It was firstly synthesised and patented by the British chemists John Rex Whinfield and James Tennant Dickson in 1941 and started being commercialised in 1953.[1] PET can be synthesised by two different routes: the first one is based on the use of dimethyl terephthalate (DMT), obtained from the reaction between methanol and terephthalic acid, and the second one, based on the polycondensation reaction of terephthalic acid (TA) with ethylene glycol (Scheme 2).[1]

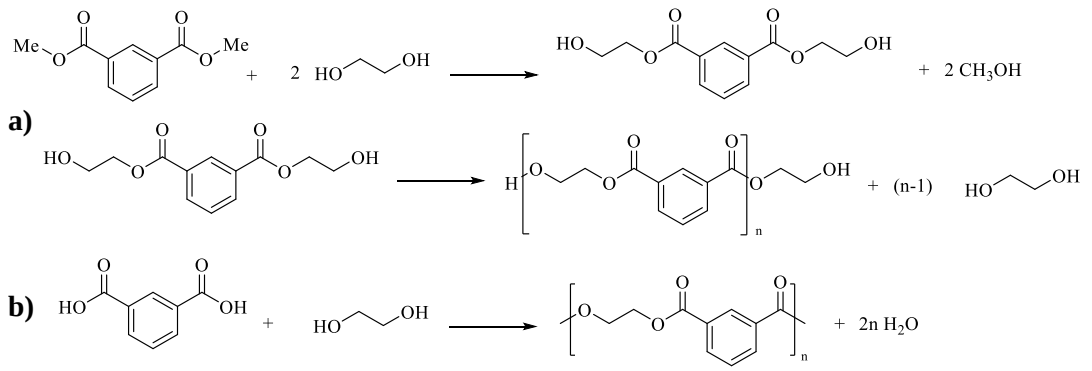

Scheme 2. *Synthesis of polyethylene terephthalate: a) from methanol and terephthalic acid and b) by polycondensation of terephthalic acid and ethylene glycol*

Another class of semiaromatic polyester is poly(ethylene 2,6-naphthalate), which is produced from ethylene glycol and 2,6-naphthalic acid. The rigidity of the naphthalene ring results in increased strength, heat stability, and barrier properties compared to PET. Among its applications are photographic and electronic films, and food and beverage bottles that require filling at higher temperatures.[4,5]

On the other hand, aliphatic polyesters have received attention as potential sustainable alternatives to petroleum-based polymers because of their numerous renewable sources and high biocompatibility.[6–8] As a result, they have been used in applications ranging from biomedical devices to bulk packaging.[9–11] Three different mechanisms of polymerisation can be implemented to synthesise aliphatic polyesters: (1) the Ring-Opening Polymerisation (ROP) of cyclic ketene acetals,[12–14] (2) the step-growth polymerisation of lactones and (3) the ROP of lactones (Scheme 3).[15] During the last few years, many scientific groups have focused their efforts on the development of this type of polymers due to their potential biodegradability. Poly(lactic acid) (PLA) is the most studied polyester which is produced from renewable resources and can be a good alternative to replace petrol-based polymers in applications such as packaging, fibers, medical equipment and drug delivery systems.[16–18] PLA can be obtained by two different synthetic procedures: the polycondensation of lactic acid, and the ROP of lactide.

Other lactones that have been polymerised by ROP to produce biodegradable polyesters are ε-caprolactone (ε-CL) and β-butyrolactone (Scheme 4). The most widely used is ε-CL, whose polymer was first reported in 1934 by Carothers and co-workers.[19] Nowadays, the production of poly(ε-caprolactone) (PCL) is implemented on industrial

scale. PCL is a semicrystalline polyester with a melting temperature of 60 °C and a glass transition temperature of –60 °C which it is commonly used in the polyurethane industry to increase water, oil, solvent, and chlorine resistance.[15] Besides, it also finds applications in the biomedical industry and as carrier for drug delivery systems.[20,21]

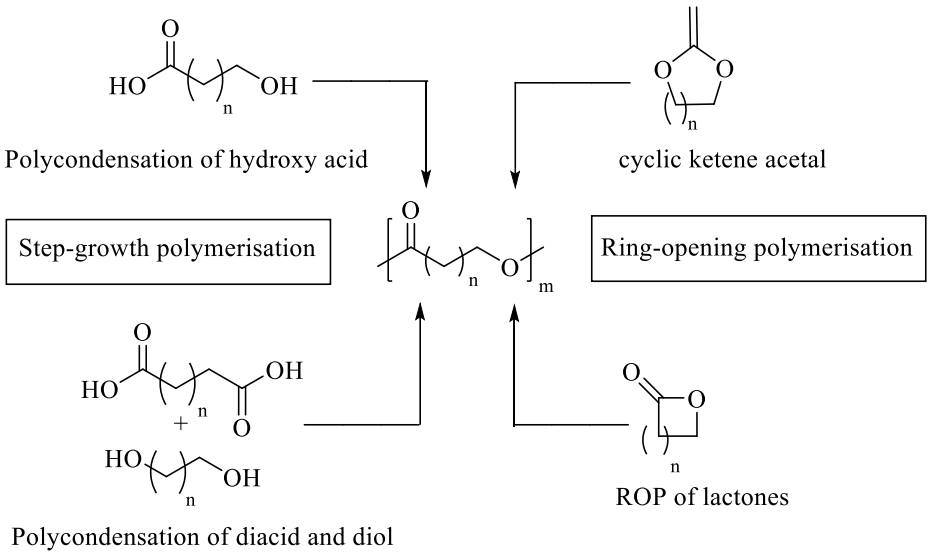

Scheme 3. *Synthesis of aliphatic polyesters.*

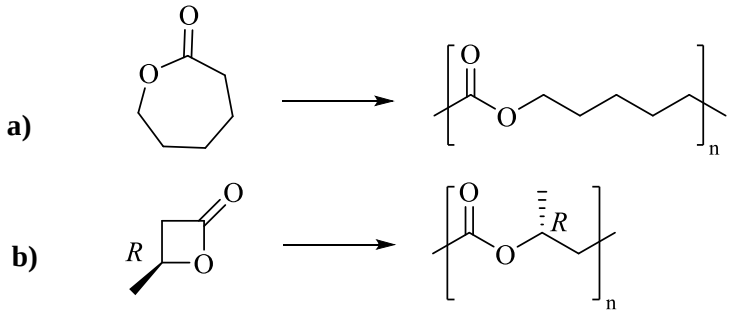

Scheme 4. *ROP of a) ε-caprolactone and b) β-butyrolactone.*

The mechanism for the ROP of lactones (Scheme 5) can be divided in five categories:

a.- Anionic polymerisation, in which the initiator is a nucleophilic alkoxide.[22–24]

b.- Coordination-insertion polymerisation, in which organometallic complexes act as initiators.[25–32]

c.- Cationic polymerisation, in which the catalyst is a cation such as alkylating or acylating agents, or Lewis or Brönsted acids and which has received less attention due to the poor control of the molecular weight parameters.[33–35]

d.- Organocatalytic polymerisation, in which N-heterocyclic carbenes, amines such as 1,5,7-triazabicyclo[4.4.0]dec-5-ene (TBD) or phosphazenes bases such as

2- tertbutylimino-2-diethylamino-1,3-dimethylperhydridro-1,3,2-diazaphosphorine (BEMP), can initiate the polymerisation process.[36–39]

e.- Enzymatic polymerisation, where lipases, enzymes of the hydrolase family, act as catalysts for the polymerisation.[40–43]

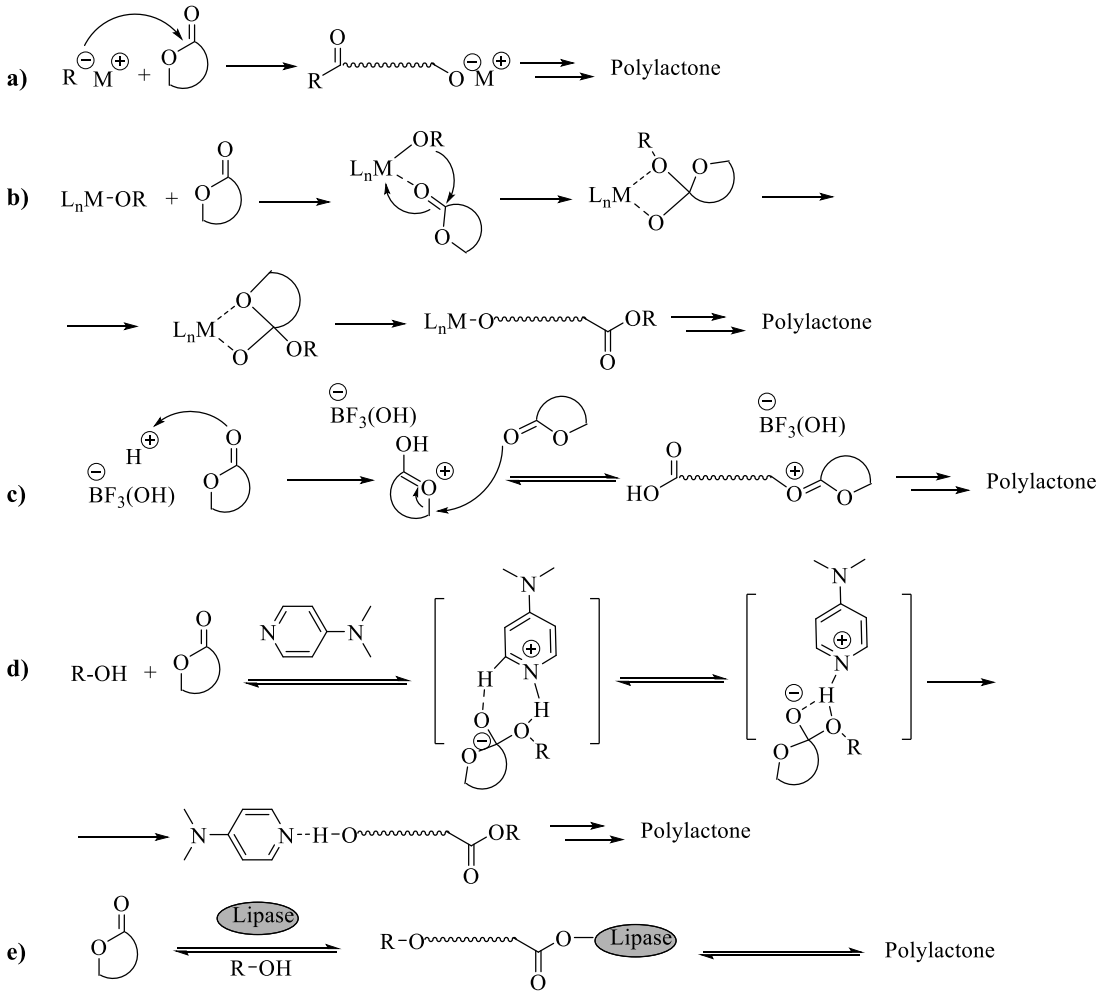

Scheme 5. *a) anionic, b) coordination-insertion, c) cationic, d) organocatalytic and e) enzymatic polymerisations mechanisms for the ROP of lactones.*

However, the design of new biodegradable polyester architectures with improved properties by ROP is seriously restricted due to the limited number of commercially available cyclic esters. Thus, scientific, and industrial community have focused on the development of other catalytic processes for this purpose. In this context, a promising alternative to ROP is the Ring-Opening Copolymerisation (ROCOP) of epoxides and cyclic anhydrides. This methodology could expand the scope of biodegradable polyesters due to the large number of epoxides and cyclic anhydrides available.

1. Ring-opening copolymerisation between epoxides and cyclic anhydrides

During the last few decades, the scientific community and industry have focused their efforts on the development of new alternatives to the ROP of cyclic esters to expand the number of bio-degradable aliphatic and aromatic polyesters. The ROCOP of epoxides and cyclic anhydrides (Scheme 6) is the most promising synthetic methodology since the use of two different monomers broads the synthetic possibilities and allows for facile tuning of polymer properties and post-functionalisation.[44]

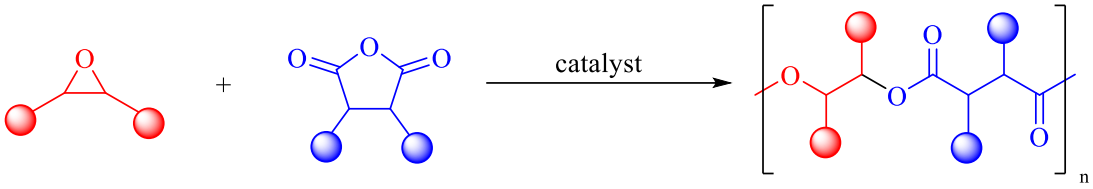

Scheme 6. *ROCOP of epoxides and cyclic anhydrides.*

This process requires the use of a catalyst, or an initiator. The catalyst is often a metal complex of the form LMX, where L is the ancillary ligand, X is the initiator, and M is the metal site in which the catalysis takes place. Scheme 7 shows the general mechanism for the ROCOP of anhydrides and epoxides. The initiation occurs when the MX initiator reacts with the monomers to generate a metal alkoxide-carboxylate intermediate. Then, the alternative insertion of epoxides and cyclic anhydrides into the growing chain takes place in the propagation step. In this step, the alkoxide species attacks the cyclic anhydride to generate a metal-carboxylate intermediate, which, attacks and ring-opens the epoxide to regenerate the metal-alkoxide intermediate. The process usually ends by the addition of water or acids, which act as chain transfer agents. Side reactions such as the sequential insertion of epoxides to generate polyether chains can also occur (Scheme 7).[45] Many renewable monomers for epoxide/anhydride copolymerisation have been explored, resulting in a broad range of renewably sourced aliphatic/aromatic polyester materials with desired properties (Figure 1).

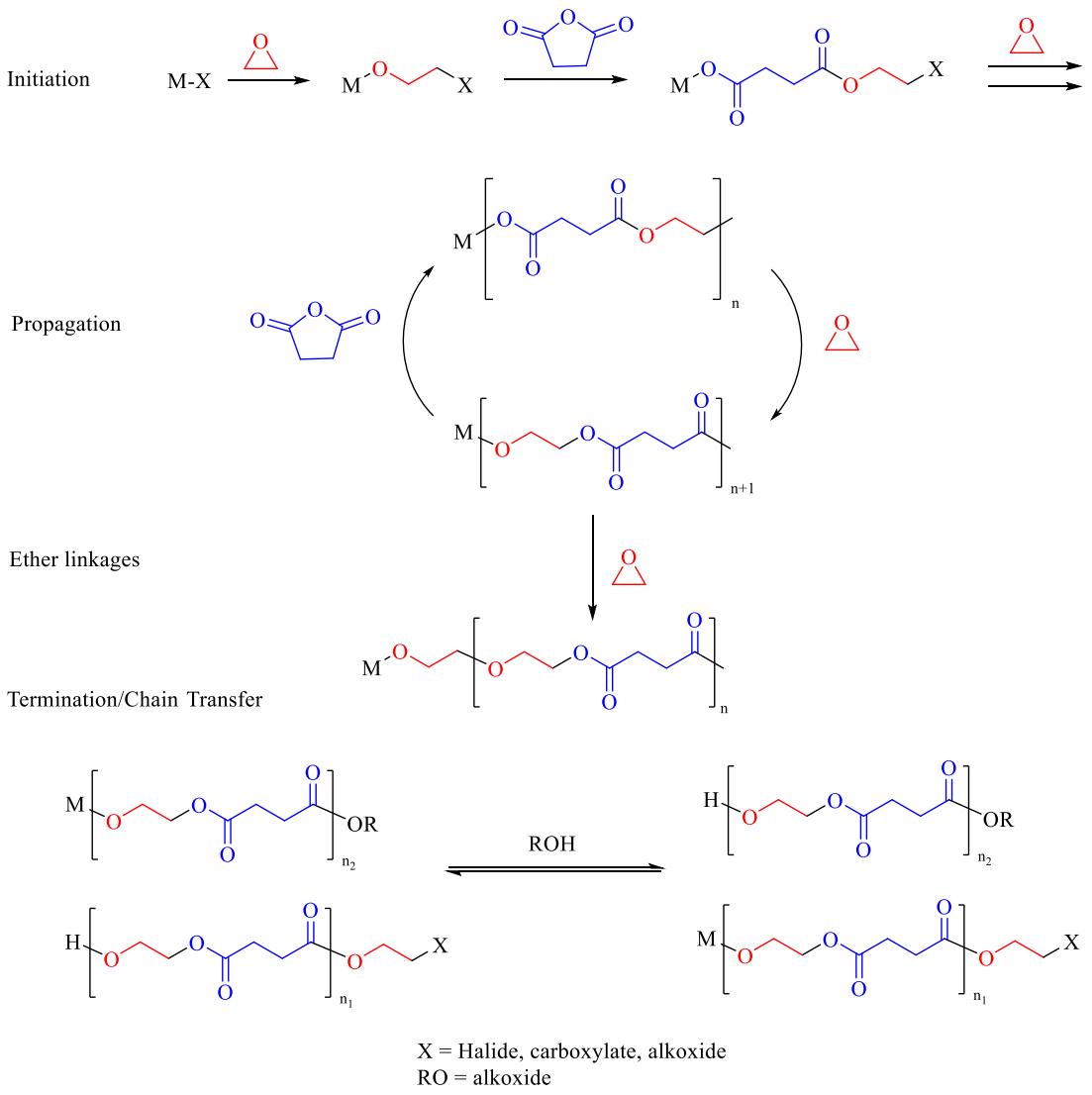

Scheme 7. *General mechanism for the ROCOP of epoxides and anhydrides.*

The first alternating copolymerisation of epoxides and anhydrides was reported in the 1960s by Fischer.[46] In the mid-60s, Inoue and co-workers reported the use of organometallic initiators for the preparation of polyesters by ROCOP.[47–49] Since then, a wide range of metal complexes including zinc, chromium, magnesium, cobalt, manganese, iron, aluminium, and nickel, have been developed as catalysts for this process. Although some of them can catalyse the ROCOP by themselves, the addition of a co-catalyst leads to higher catalytic activities and selectivies. Thus, the use bis-(triphenylphospine)iminium salts ([PPN]X), 4-dimethylaminopiridine (DMAP), phosphines and ammonium salts has been reported.[50,51]

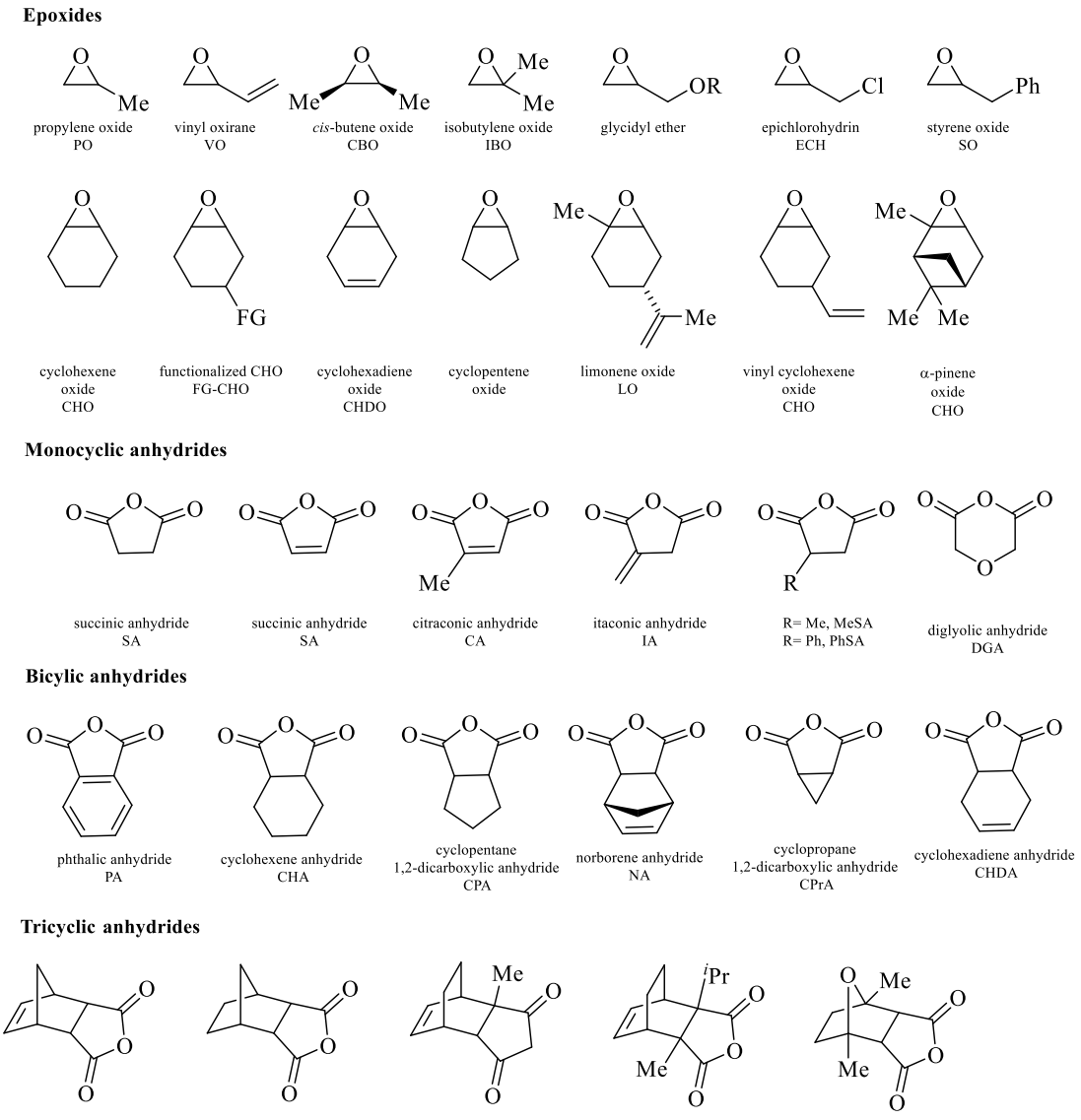

Figure 1. *Common epoxides and anhydrides used for ROCOP.*

The first well controlled copolymerisation between epoxides and anhydrides was reported by Inoue and Aida in 1985 using PO (or SO, CHO and butylene oxide) and PA as substrates and an aluminium porphyrin complex in combination with quaternary phosphonium/ammonium salts as the catalytic system.[52,53] The catalytic system afforded the synthesis of the corresponding polyester material with high selectivity and molecular weights between 2000 and 6000 g mol^{-1} with narrow polydispersities.

This system led to the discovery of related porphyrin and corrole metal catalysts (Figure 2).[54–57] A range of Cr, Co and Mn porphyrin TPP complexes (Figure 2a) was investigated as catalysts in combination with DMAP as co-catalyst for the copolymerisation of SO with different cyclic anhydrides such as SA, MA, CA CPrA,

CPA and PA. Among the metal complexes developed, the porphyrin chromium catalyst was the most active.[54] Nozaki and co-workers reported the use of corrole metal complexes (Figure 2b) as catalyst for the copolymerisation of PO with glutaryl anhydride, SA and MA using [PPN]$OBzF_5$ as co-catalyst. It was shown that the FeCl corrole complex was the most active catalyst even though low molecular weight (8000 g mol^{-1}) polyester materials were obtained.[57]

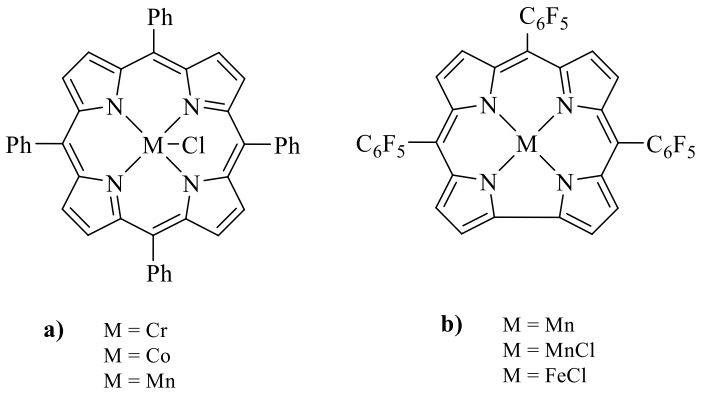

Figure 2. *Porphyrin and corrole catalysts.*

Since these initial catalyst developments, metal-SALEN type complexes have become one of the most widely used catalysts for the ring-opening copolymerisation of cyclic anhydrides and epoxides. Among these, the N,N'-bis(salicylidene) cyclohexanediamine (SALCY) ligand (Figure 3) has been widely used for the synthesis of SALCY metal complexes.[50,58–70] The SALCY chromium complex (Figure 3a) displayed the highest catalytic activity, obtaining TOF values up to 246 h^{-1} for the copolymerisation of CHO and PA in the absence of a co-catalyst.[66] Enantiopure SALCY complexes (Figure 3b) have also been reported as catalysts for the stereoselective ROCOP of epoxides and cyclic anhydrides in order to obtain stereoregular polymers.[62,69] Coates and co-workers reported the use of enantiopure SALCY cobalt complexes with a range of substituents on the phenol ring (Figure 3b) for the synthesis of poly(propylene succinate), obtaining the corresponding polyester materials with a regioregularity of 96-97%.[62] Finally, bifunctional catalysts in which the metal centre and the co-catalyst functionality are comprised within the same molecule have also been studied (Figure 3c, d).[63,65] Kim and co-workers reported for the first time the use of a bifunctional SALCY cobalt complex (Figure 3d) for the copolymerisation of PO and PA and the terpolymerisation of PO, norborene anhydride

(NA) and CO_2 with high selectivities. No ether linkages were formed in either of the polymerisation processes, obtaining poly(1,2-propylene phthalate) or poly(1,2-propylene phthalate-*co*-carbonate) respectively with 99% selectivity.[63]

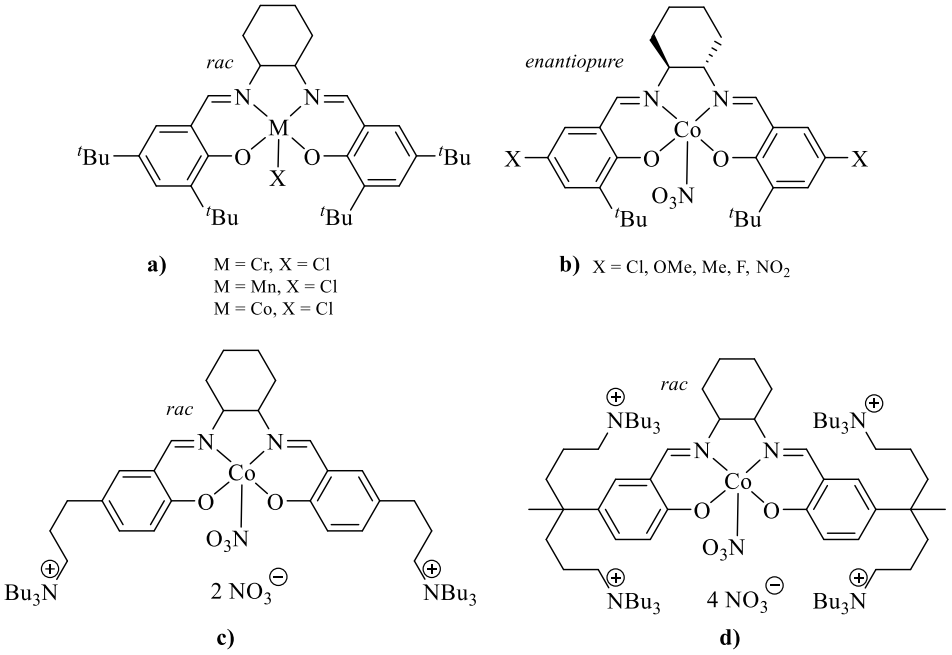

Figure 3. *N,N'-Bis-(salicylidene)cyclohexanediamine (SALCY) metal catalysts.*

Metal complexes supported by N,N'-bis(salicylidene)-phenyldiamine (SALPH)[50,54,60,61,71–76] (Figure 4a) and N,N'-bis(salicylidene)-ethylenediamine (SALEN)[60,61] (Figure 4b) ligands and Cr complexes supported by SALAN[77] (Figure 4c) and tetradentate sulphur-based ligands (OSSO) (Figure 4d) have also been reported.[78] Studies comparing the use of different SALEN-type ligands for the same metal centre were performed resulting the SALCY ligand-based complex, the most active catalyst in comparison to the SALPH and SALEN counterparts.[50,60]

The activity of a serie of SALPH Mn(III) complexes with different substituents in the phenol moiety has been recently studied (Figure 4a). The introduction of electron donating groups (OMe) in the *ortho* position and electron withdrawing groups in the *para* position of the phenoxide group resulted in the catalyst with the best performance, due to the combination of steric and electronic effects. Thus, polyesters were obtained with high selectivities, molecular weights up to 15600 g mol^{-1} and narrow polydispersities (1.09-1.27).[76]

Similarly, the catalytic activity of different SALAN chromium complexes for the copolymerisation of terminal epoxides with MA and SA, without the use of a co-

catalyst has been compared. The results showed that the dinuclear SALAN chromium complex (Figure 4c) was the most active catalyst, obtaining TOF values up to 7.4 h^{-1}, due to an intramolecular synergetic effect. [77]

Finally, different chromium complexes bearing sulphur tetradentate ligands for the copolymerisation of PA and various epoxides using DMAP as co-catalyst have been reported.[78] Polyesters with molecular weights up to 22100 g mol^{-1} and polydispersities ranging from 1.27 to 2.33 were obtained. The chromium complex containing a cyclohexane moiety (Figure 4d) turned out to be the most active, as previously reported with other metals.[50,76]

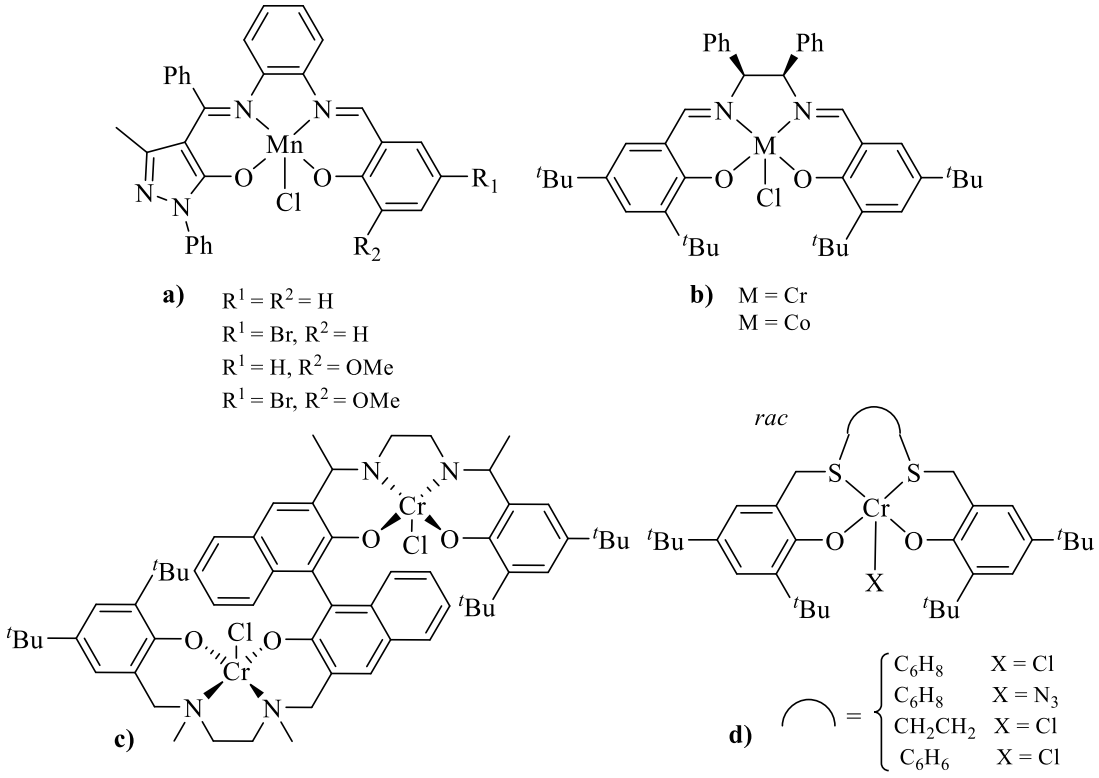

Figure 4. *a) N, N'-Bis(salicylidene)phenyldiamine (SALPH) catalyst; b) N, N'-bis(salicylidene)ethylendiamine (SALEN) catalyst; c) SALAN catalyst; d) sulphur (OSSO) catalysts.*

Multinuclear heterobimetallic complexes have also been extensively studied by Williams,[79–85] Ko,[86] and Lü[87–89] and represent a potential alternative to SALEN-based catalysts. In this context, it is worth highlighting the highly active zinc and magnesium heterobimetallic catalyst reported by Williams and co-workers (Figure 5a) for the copolymerisation of CHO and PA, obtaining TOF values up to 188 h^{-1}.[83] The high

catalytic activity displayed by this heterobimetallic catalyst is due to the synergistic effect between the two metal centres. The Lewis acidic Zn enhanced epoxide coordination while the labile Mg-carbonate accelerated carbonate attack, increasing the reaction rate.[83] A bimetallic zinc complex featuring 2,2-dimethyl propylene backbone (Figure 5b) has also been reported for CHO and PA copolymerisation, which was found to be the most active ever reported by Williams for ROCOP processes with a TOF value of 198 h^{-1}.[82]

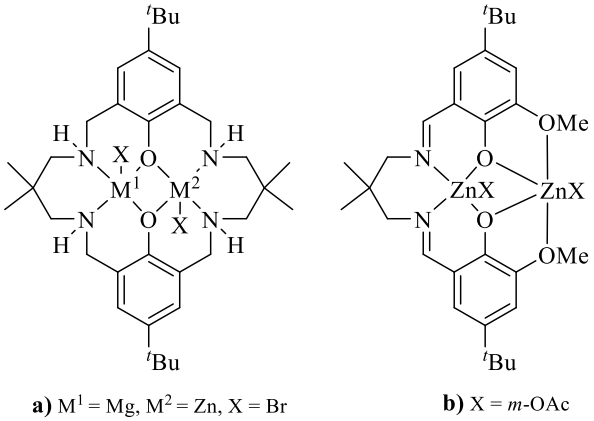

Figure 5. *Multinuclear and SALEN catalysts with pendant functionality.*

Other important catalysts include *β*-diiminate zinc acetate [Zn(BDI)OAc], aminotriphenolate metal complexes and alkoxide magnesium complexes reported by Coates, Kleij and Mazzeo respectively (Figure 6).[73,90,91] Kleij and co-workers have also reported a series of aminotriphenolate bifunctional Co, Mn and Co complexes (Figure 6c), for which the Cr analogue displayed the highest catalytic activity with TOF values of 4.8, 5.3 and 21.3 h^{-1} respectively.[92]

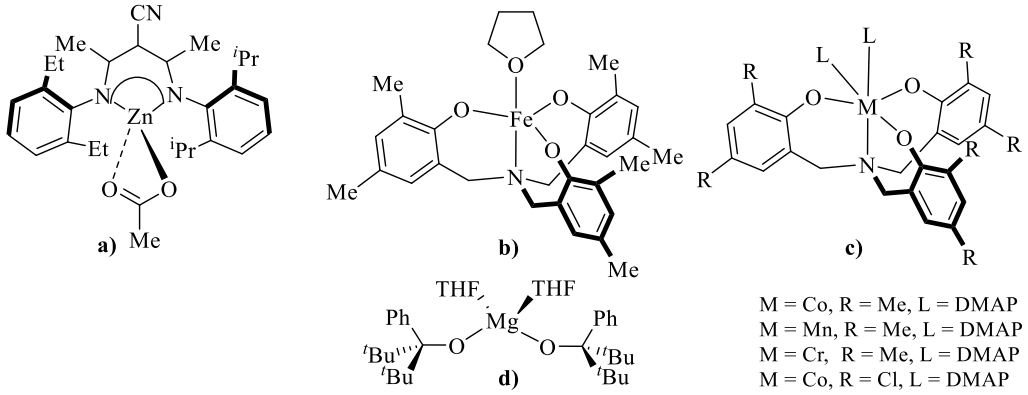

Figure 6. *β-diiminate zinc acetate, aminotriphenolate and magnesium alkoxide metal catalysts.*

1.1. Aluminium catalysts for the ROCOP of epoxides and cyclic anhydrides

As mentioned before, the first well controlled copolymerisation between epoxides and cyclic anhydrides was reported by Inoue and Aida in 1985 using a porphyrin aluminium catalyst (Figure 7a).[52,53] Coates also tested this Al porphyrin complex as catalyst for the copolymerisation of MA with a broad range of epoxides to produce unsaturated polyesters.[93] However, it showed low catalytic activity by itself and produced polymeric materials with high polyether content. Chisholm and co-workers compared the catalytic activity between different aluminium porphyrin complexes (Figure 7a). The results showed that the tetraphenyl porphyrin (TPP) aluminium complex was the most active catalysts obtaining a TOF value of 19 h^{-1}, followed by octaethyl porphyrin (OEP) and tri(pentafluorophenyl)porphyrin (TPFP) complexes with TOF values of 9 and 8 h^{-1} respectively.[56]

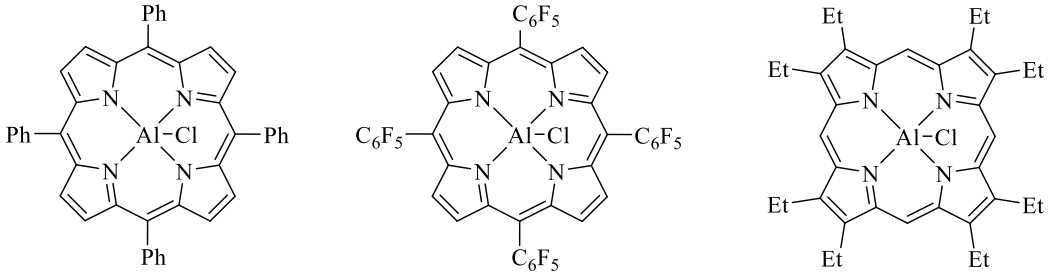

Figure 7. *Aluminium porphyrin complexes.*

SALEN-type aluminium complexes (Figure 8) have also been employed for the ROCOP of cyclic anhydrides and epoxides.[54,61,64,72–75] Thomas and co-workers reported the use of a SALCY aluminium complex (Figure 8a) along with its chromium, cobalt, and manganese analogues (Figure 3a) in combination with PPNCl for the tandem synthesis of polyesters from renewable resources.[64] Aluminium SALCY complex afforded the cyclisation of several diacids to generate the corresponding cyclic anhydrides (pimelic and camphoric anhydrides with TOF values of 194 and 100 h^{-1} respectively). These cyclic anhydrides were further reacted with epoxides to generate the corresponding polyester materials with molecular weights up to 27700 g mol^{-1} and narrow polydispersities ranging from 1.2-1.6. Also, renewable polyesters from LO and CA, and the first reported polyester from pinene oxide were synthesised. Duchateau and co-workers performed an extensive study comparing the catalytic

activity of SALCY, SALPH, SALEN, and diphenyl SALEN aluminium complexes as catalysts for the ROCOP of CHO with cyclic anhydrides (Figure 8) using DMAP as co-catalyst.[54] Among them, SALPH aluminium complex (Figure 8b) displayed the highest catalytic activity, obtaining TOF values up to 100 h^{-1} followed by the SALCY aluminium complex (Figure 8a) with TOF values up to 94 h^{-1}. The meso-diphenyl SALEN Al complex (Figure 8e) and the less sterically demanding ethylenediamine SALEN complex (Figure 8d) showed the lowest catalytic activity with TOF values of 80 and 25 h^{-1} respectively. Thus, different polyesters with molecular weights up to 13900 g mol^{-1} and polydisperisities values ranging from 1.1-2.3 were obtained.

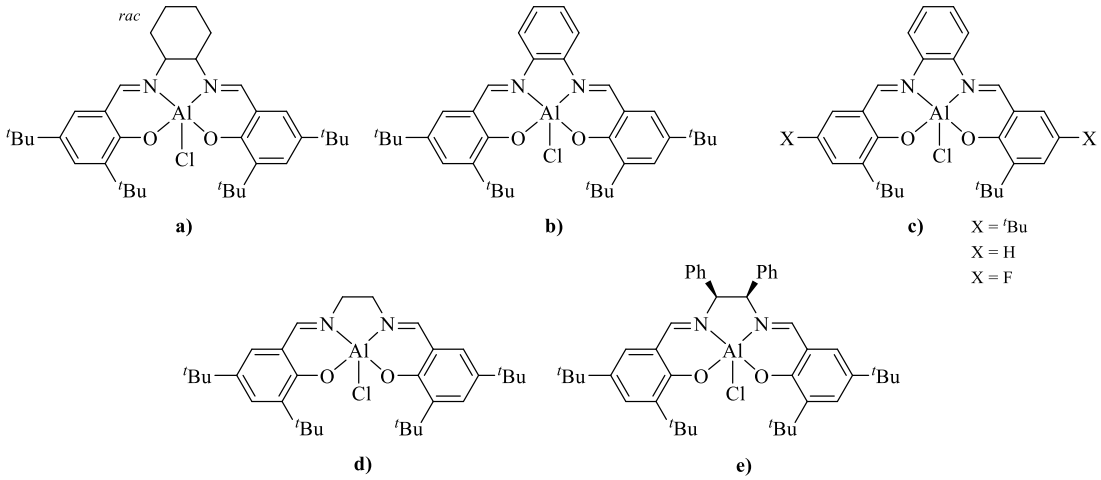

Figure 8. *Aluminium SALEN-type complexes.*

SALPH aluminium complex (Figure 8b) has also been investigated in the copolymerisation of PO with bio-renewable terpene-based anhydrides using PPNCl as co-catalyst,[74] which showed to be highly regioselective in the ring-opening of the epoxide at the methylene carbon. Following these results, they investigated the combination of several SALPH aluminium complexes (Figure 8c) and PPNCl as catalyst system for the copolymerisation of PO with tricyclic anhydrides to study the electronic effects on the catalytic activity, obtaining TOF values ranging between 63 and 185 h^{-1}.[73] Several polyesters with molecular weights up to 7400 g mol^{-1} and narrow polydispersities were synthesised. The study showed that the more electron deficient the catalyst, the lower the catalytic activity observed, obtaining TOF values of 88, 80, 49 h^{-1} for ^{t}Bu, H, and F substituted, respectively. Even though the F containing aluminium complex did not display the highest catalytic activity, it was the most selective catalyst, obtaining the corresponding polyester materials without any

signs of transesterification or epimerisation reactions, due to its enhanced Lewis acidity.

A series of enantiopure bimetallic aluminium complexes (Figure 9) have also been developed for the copolymerisation of different epoxides with cyclic anhydrides using PPNCl as co-catalyst.[94] A first screening was performed to evaluate the catalysts' activity in the ROCOP of CHO and PA. It was shown a significant steric effect of the substituents in *ortho* position of the phenolate moiety (Figure 9a) on the catalytic activity and product enantioselectivity. Thus, it was observed that neither low (methyl) nor highly hindered (TMS) substituents were beneficial for the asymmetric copolymerisation of epoxides and cyclic anhydrides. Therefore, the aluminium complex (*R,R,R,R*) or (*S,S,S,S*) containing ^{t}Bu groups in the phenol rings proved to be the most active and enantioselective catalyst, with TOF values up to 750 h^{-1} and 71% of enantiomeric excess (*ee*).

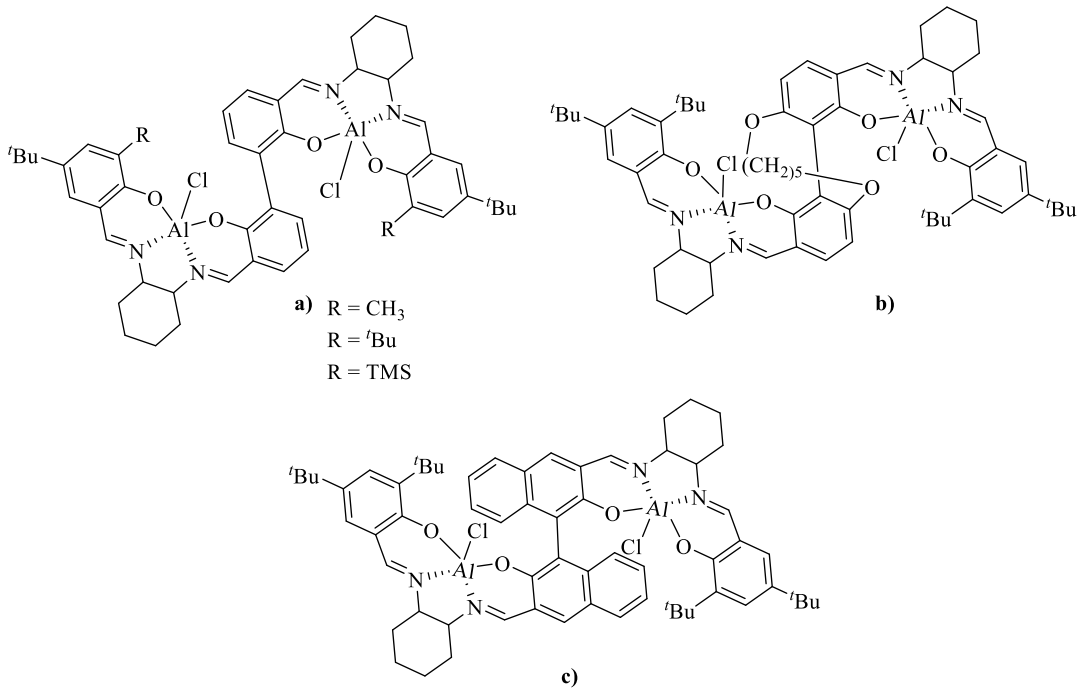

Figure 9. *Enantiopure bimetallic aluminium complexes*.

SALEN alkyl aluminium complexes with a diamine containing an alkyl backbone of different length (Figure 10a) and their mononuclear counterparts have been studied for the copolymerisation of CHO or LO with SA, MA and PA using different salts as co-catalysts.[95] The bimetallic SALEN aluminium bearing a propylene backbone (Figure 10a) was tested for the CHO and SA copolymerisation. This complex showed

higher catalytic activity than monometallic SALEN aluminium complexes previously investigated,[61] obtaining TOF values up to 250 h^{-1}. Monometallic SALCY, SALPH, SALEN, and di-phenyl SALEN aluminium complexes (Figure 8a, b, d, e) showed lower catalytic activities under the same reaction conditions, obtaining TOF values ranging from 25 to 100 h^{-1}, depending on the diamine backbone.[61] Bimetallic aluminium complex (Figure 10a) was further investigated as catalyst for the ROP of different cyclic esters (*L*-lactide, *ε*-caprolactone and *β*-butyrolactone), copolymerisation between CHO and SA, and for the formation of block co-polymers poly(lactide)-poly(cyclohexene succinate).[96] Dinuclear SALPH alkyl aluminium complexes (Figure 10b) containing a dinaphtylimine backbone have been recently developed as catalysts for the ROP of lactides and lactones, the ROCOP of LO and PA and the formation of diblock polyesters.[97]

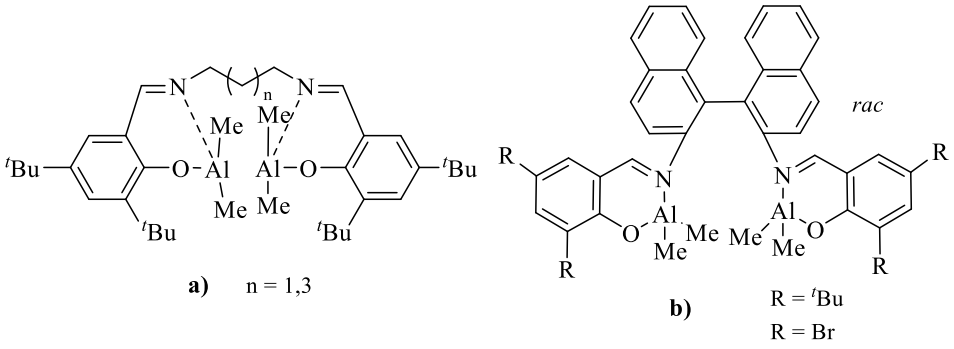

Figure 10. *Bimetallic aluminium SALEN-type catalysts.*

Coates and co-workers have recently reported innovative bifunctional aluminium complexes in which the SALEN-type catalyst and the aminocyclopropenium co-catalyst are covalently tethered (Figure 13).[98] Their catalytic activity was tested against their binary catalyst counterparts using PPNCl as co-catalyst. All catalytic systems afforded the formation of perfectly alternating polyesters with low polydispersities, which is indicative of a well-controlled polymerisation behaviour. The SALPH inspired bifunctional catalysts (Figure 11a, b) exhibited higher polymerisation rates (TOF values of 93 and 64 h^{-1} respectively) than the pyrrolidine (Figure 11c) analogue (TOF value of 14 h^{-1}). A similar trend was observed for their binary counterparts, obtaining TOF values of 112, 57 and 28 h^{-1}, respectively. When lowering the catalyst loading, bifunctional catalysts still maintained their catalytic activity (TOF values of 87, 24, 12 h^{-1} respectively), while their binary counterparts displayed lower activity

(TOF values of 22, 13, 8 h^{-1}). The kinetic behavior of both bifunctional and binary catalytic systems was investigated using Burés's time-normalised method.[99] The results showed that first order kinetics were obtained for both systems at high catalyst loadings. However, the reaction rate was found to be second order for the binary system at low catalyst loading, depending on the concentration of both catalyst and co-catalyst. On the other hand, first order with respect to the [catalyst] was observed for the bifunctional catalysts. These findings are in good agreement with the high catalytic activity displayed by bifunctional catalysts even at low catalyst concentration.

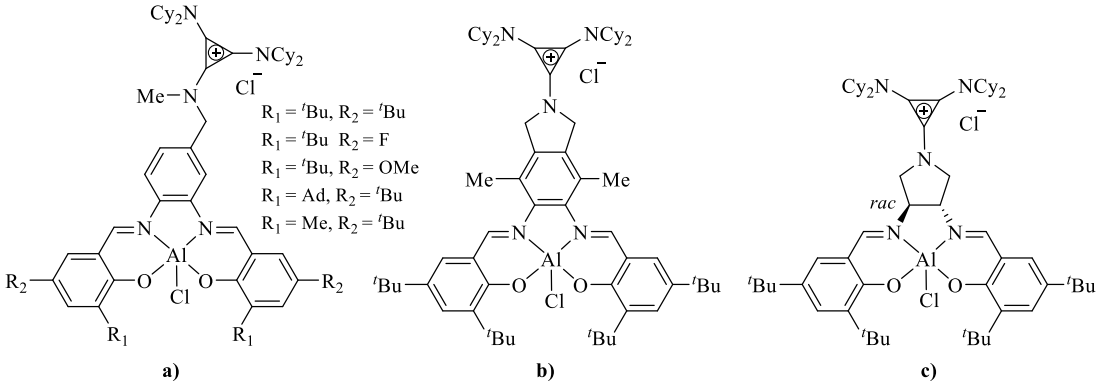

Figure 11. *Bifunctional aluminium complexes developed by Coates et al.* [98]

The mechanism for the ROCOP of cyclic anhydrides and epoxides catalysed by the combination of SALEN metal complexes and iminium salts as a catalytic system is shown in Scheme 8.[100] In this mechanism, the initiation occurs with the formation of a hexacoordinate bis-alkoxide species (AA) ([PPN][SALPH $M(OR)_2$] or [(SALPH)MOR/[PPN][OR]). The counterion of the SALEN complex ring-opens the epoxide and a pentacoordinate alkoxide complex is generated. Then, a molecule of epoxide can coordinate to the metal centre and the anion of the iminium salt ring-opens it to generate the bis-alkoxide hexacoordinate species (AA). This species reacts with a cyclic anhydride to yield the alkoxide-carboxylate intermediate (AC). This intermediate can undergo epoxide binding, activation, and ring-opening to regenerate the bis-alkoxide (AA) species (cycle 1) or can react with another molecule of anhydride to yield to the bis-carboxylate species (CC), which depending on the coordination sphere, acts as an active species or as a dormant species. It was found that the intermediate species AC, reacts 50 times faster with the anhydride rather than with the epoxide, indicating that cycle 2 is much preferred when the anhydride concentration is high enough. On the other hand, cycle one is only important when the

copolymerisation is almost complete, and an excess of epoxide was used. Accordingly, the rate determining step of the reaction was found to be the ring-opening of the epoxide by the CC species. Thus, enhancing the rate of epoxide opening by CC would increase the overall polymerisation rate.

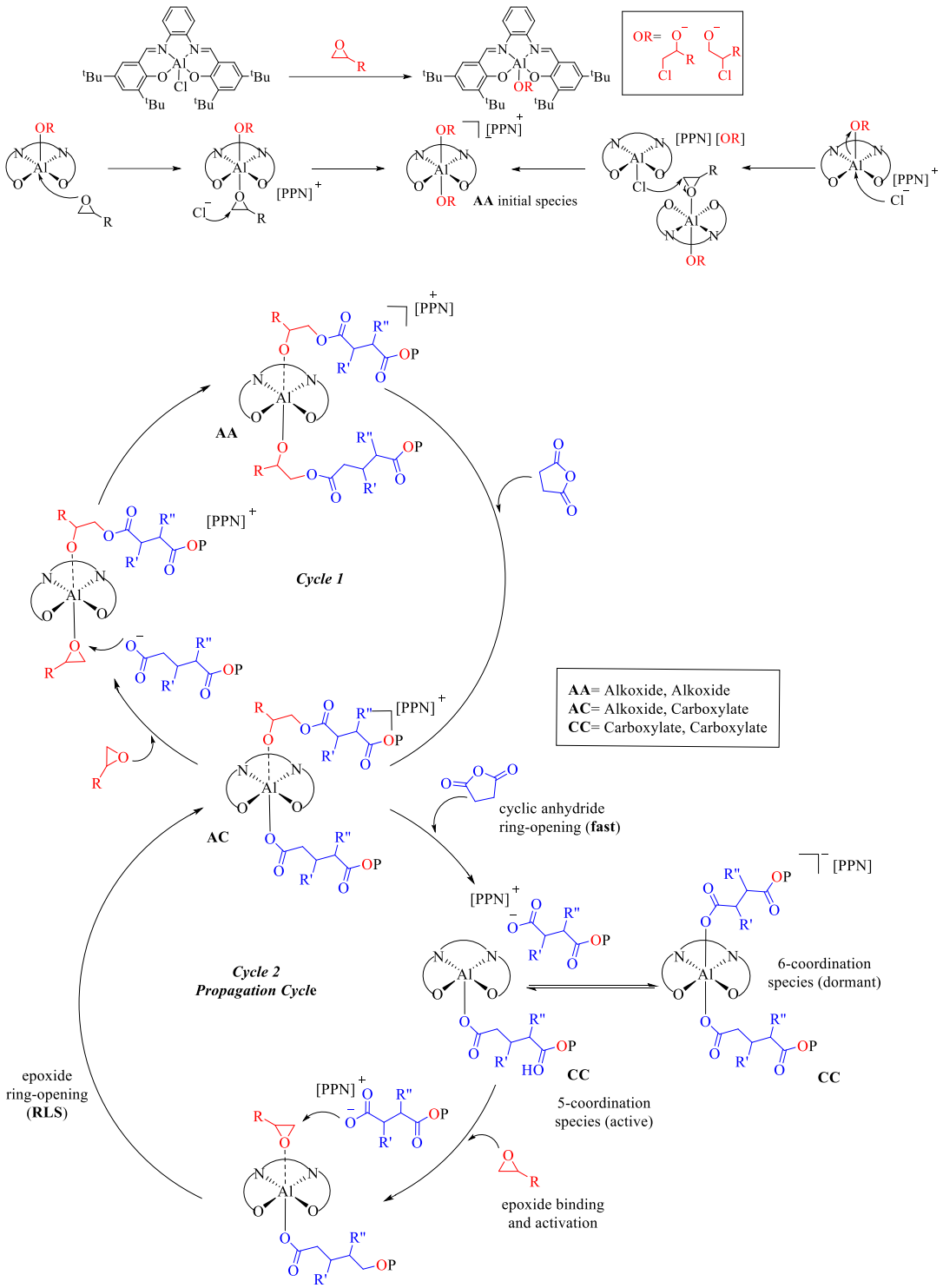

Scheme 8. *Proposed mechanism for the ROCOP of epoxides and cyclic anhydrides catalysed by SALEN-type MLX complexes.*

Results and discussion

1. Alternating copolymerisation of epoxides and cyclic anhydrides (ROCOP) for the synthesis of biodegradable polyesters

As it has been previously described in the introduction of this section, there is a growing interest within the industrial and scientific community to produce polyester materials from renewable resources. In this context, one of the most promising approaches is the ring-opening copolymerisation of epoxides and cyclic anhydrides (ROCOP). Thus, to contribute to this study, several polyesters from a range of epoxides and cyclic anhydrides have been synthesised using heteroscorpionate aluminium complexes previously reported by our research group.[101–103] This work represents the use of this type of complexes for the first time as catalysts for ROCOP processes.

As it has been discussed previously, aluminium complexes have shown to be one of the most active catalysts for the ROCOP of epoxides and cyclic anhydrides. In this section, the use of heteroscorpionate aluminium complexes funcionalised with alkoxide[101] and acetamidate[102,103] groups as catalysts for ROCOP processes is described.

1.1. Synthesis of polyesters catalysed by aluminium complexes with heteroscorpionate ligands functionalised with alkoxide groups

To carry out this study, previously reported aluminium complexes with heteroscorpionate ligands functionalised with alkoxide groups have been employed (Figure 12).[101]

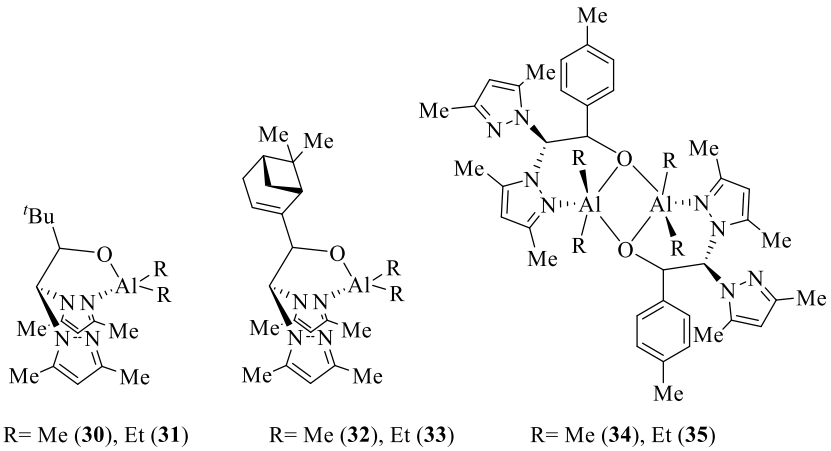

Figure 12. *Heteroscorpionate aluminium complexes used for the ROCOP of epoxides and cyclic anhydrides.*

Initially, preliminary studies were carried out to evaluate the catalytic activity of heteroscorpionate aluminium complexes **30**-**35** using cyclohexene oxide (CHO) and phthalic anhydride (PA) as substrates. The initial experiments were performed using 0.5-1 mol% of catalyst at 90 ºC for 6 hours and using toluene as solvent (Scheme 9). In order to compare the catalytic activity of bimetallic complexes **34** and **35** with the monometallic complexes **30**-**33**, the reactions were carried out using 0.5 mol% of complexes **34** and **35** in order to keep the concentration of aluminium constant to 1 mol% (Table 1, entries 5-6). As it is shown in Table 1, bimetallic complexes (entries 5-6) displayed higher activity than the monometallic ones (entries 1-4). Among the catalysts studied, complex **35** was the most active and selective catalyst for this process (Table 1, entry 6). On the other hand, the nature of the alkyl group on the initiators (Al–Me *versus* Al–Et) affects the catalytic activity, which increases for complexes containing ethyl groups, similar to what has been previously reported for other aluminium complexes, probably due to solubility reasons and lability of the Al–C bond.[104,105]

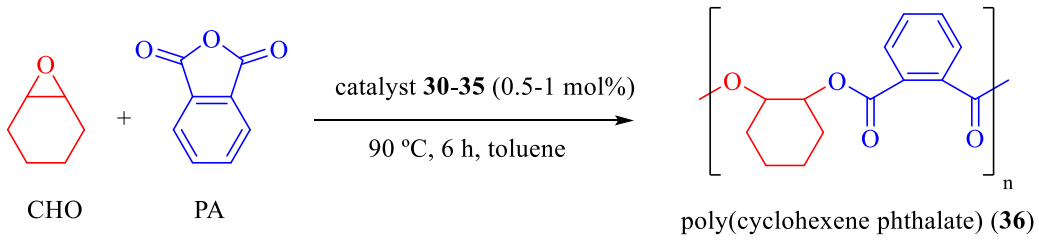

Scheme 9. *ROCOP of CHO and PA catalysed by complexes **30**-**35**.*

Since catalyst **35** was found to be the most active for the process, the optimisation of the reaction conditions for the copolymerisation process was carried out. Kinetic studies confirmed that the copolymerisation proceeded very rapidly reaching high conversion in six hours, which did not increase when the reaction was carried out for 16 hours (Figure 13).

Then, the effect of the solvent and the reaction temperature on the catalytic activity of complex **35** were investigated (Table 2). The results showed the copolymerisation proceeded faster in the absence of a solvent, with 92% of conversion achieved in 6 hours. However, the selectivity towards polyester formation was very low (51%) and high polyether content was observed (Table 2, entry 1). As can be seen in Table 2, the addition of a solvent was detrimental, and the catalytic activity was reduced (71-85%)

due to the lower concentration of the monomers in the reaction mixture. However, the selectivity of the process increased (68-79%) since the homopolymerisation of CHO to form polyether was also reduced (Table 2, entries 2-4).

Table 1. *Results obtained for the copolymerisation between CHO and PA catalysed by complexes **30**-**35**.*[a]

Entry	Catalyst (mol %)	T (ºC)	Conversion (%)[b]	Polyester (%)[b]
1	**30** (1)	90	74	70
2	**31** (1)	90	78	73
3	**32** (1)	90	72	68
4	**33** (1)	90	75	71
5	**34** (0.5)	90	80	74
6	**35** (0.5)	90	85	79

[a]*Copolymerisation conditions: 90 µmol of complex; 2 mL of toluene as solvent; 6 hours.* [b]*Determined by* ^{1}*H-NMR.*

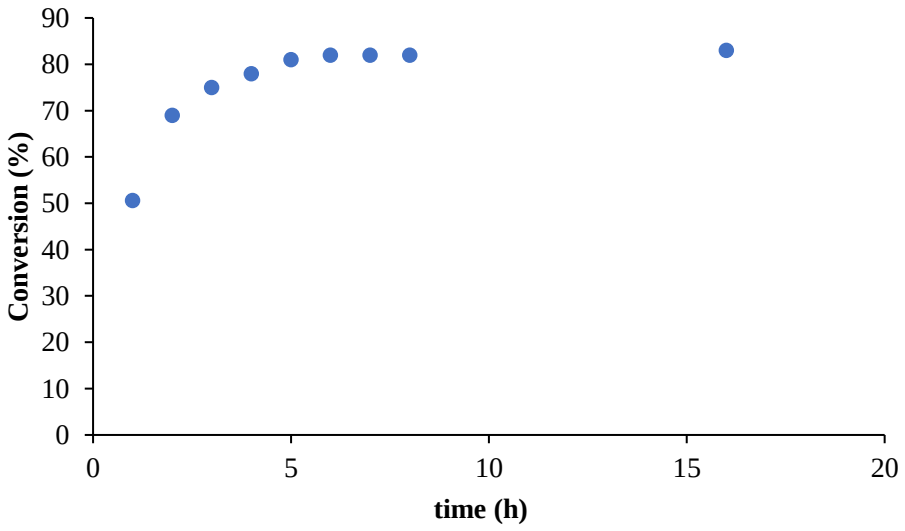

Figure 13. *Plot of conversion vs time for the ROCOP of CHO and PA catalysed by complex **35**.*

In order to study the influence of the reaction temperature on the catalytic activity of complex **35**, the ROCOP was studied at 50 ºC and 70 ºC. As expected, the catalytic activity decreased when the reaction temperature was decreased (Table 2, entries 5 and 6). On the other hand, the reaction temperature did not have any influence on the selectivity of the process toward polyester formation and remained almost constant at 80%.

Table 2. *ROCOP of CHO and PA catalysed by complex **35**.*[a]

Entry	Solvent	T (ºC)	Conversion (%) [b]	Ester linkage (%)[b]
1	Bulk	90	92	51
2	Toluene	90	85	79
3	THF	90	75	67
4	MeCN	90	71	65
5	Toluene	70	69	80
6	Toluene	50	47	77
7[c]	Toluene	90	82	>99
8[d]	Toluene	90	80	91
9[e]	Toluene	90	83	95
10[f]	Toluene	90	81	94

*[a]Copolymerisation conditions: 90 µmol of complex **35**; 2 mL of toluene as solvent, [PA]/[CHO]/[**35**]= 200:200:1, 6 hours. [b]Conversion relative to PA determined by ^{1}H-NMR spectroscopy of the crude reaction mixture. [c]1 equiv. of TBAB. [d]1 equiv. of TBAI. [e]1 equiv. of TBAC. [f]1 equiv. of PPNCl.*

The effect of adding a nucleophile as a co-catalyst to increase the catalytic activity and/or the selectivity of the process was studied (Table 2, entries 7-10). The addition of a nucleophile did not have a significant impact on the catalytic activity and conversions were not affected significantly. However, a marked increase in the selectivity was observed, similarly to what was observed for previously reported

aluminium catalysts.[95] Amongst all the additives tested, TBAB proved to be the most selective and produced polymeric materials with a selectivity towards the formation of polyester greater than 99%. Furthermore, amongst all the tetrabutylammonium salts, the selectivity was $Br^- > Cl^- > I^-$ (Table 2, entries 7-9), indicating that a good balance between nucleophilicity and leaving group ability was crucial in order to enhance the catalyst selectivity.

Having determined the optimal catalytic system and reaction conditions, several polyesters with a range of molecular weights were prepared (Table 3). The molecular weight (M_n) and the molecular weight distributions (M_w/M_n) were determined by gel permeation chromatography (GPC). As can be observed from the results in Table 3, the molecular weight of the synthesised polyester increased as the [PA]/[CHO]/[**35**] was gradually increased from 50:50:1 to 200:200:1, obtaining polymers with high ester linkages and narrow polydispersities in all cases.

Table 3. *ROCOP of CHO and PA in toluene catalysed by complex **35** and TBAB.*[a]

Entry	[PA]/[CHO]/ [35]/[TBAB]	Conv (%)[b]	Polyester (%)[b]	M_n(exp)[c]	PDI[c]	T_g[d]
1	200:200:1:1	82	>99	30297	1.24	103
2	150:150:1:1	89	>99	25599	1.16	102.5
3	100:100:1:1	95	>99	21158	1.06	102
4	50:50:1:1	99	>99	14744	1.04	101.6

*[a]Copolymerisation conditions: 90 µmol of complex **35** and 90 µmol of TBAB; 2mL of toluene as solvent, 90 ºC, 6 hours. [b]Conversion relative to PA determined by ^{1}H-NMR spectroscopy of the crude reaction mixture. [c]Determined by GPC. [d]Determined by differential scanning calorimetry.*

The poly(cyclohexene phthalate) copolymers microstructure was characterised by ^{1}H-NMR, ^{13}C-{^{1}H}-NMR and IR spectroscopies (Figure 14). ^{1}H-NMR spectrum (Figure 14a) exhibited a singlet at 5.20 ppm corresponding to the methine proton from the cyclohexane ring, two singlets at 7.62 and 7.43 ppm corresponding to the aromatic ring from the phthalate moiety and four different singlets between 2.36-1.40 ppm corresponding to the methylene protons of the cyclohexene ring. Similarly, it showed two other singlets with much less intensity at 4.95 and 2.99 ppm which were assigned to chain end groups. On the other hand, IR spectrum (Figure 16b) exhibited a sharp

band at 1720 cm^{-1} corresponding to the C=O stretching resonance from the ester group, and two sharp bands at 1260 and 1066 cm^{-1} which were assigned to the C–O stretching resonance from the ester group.

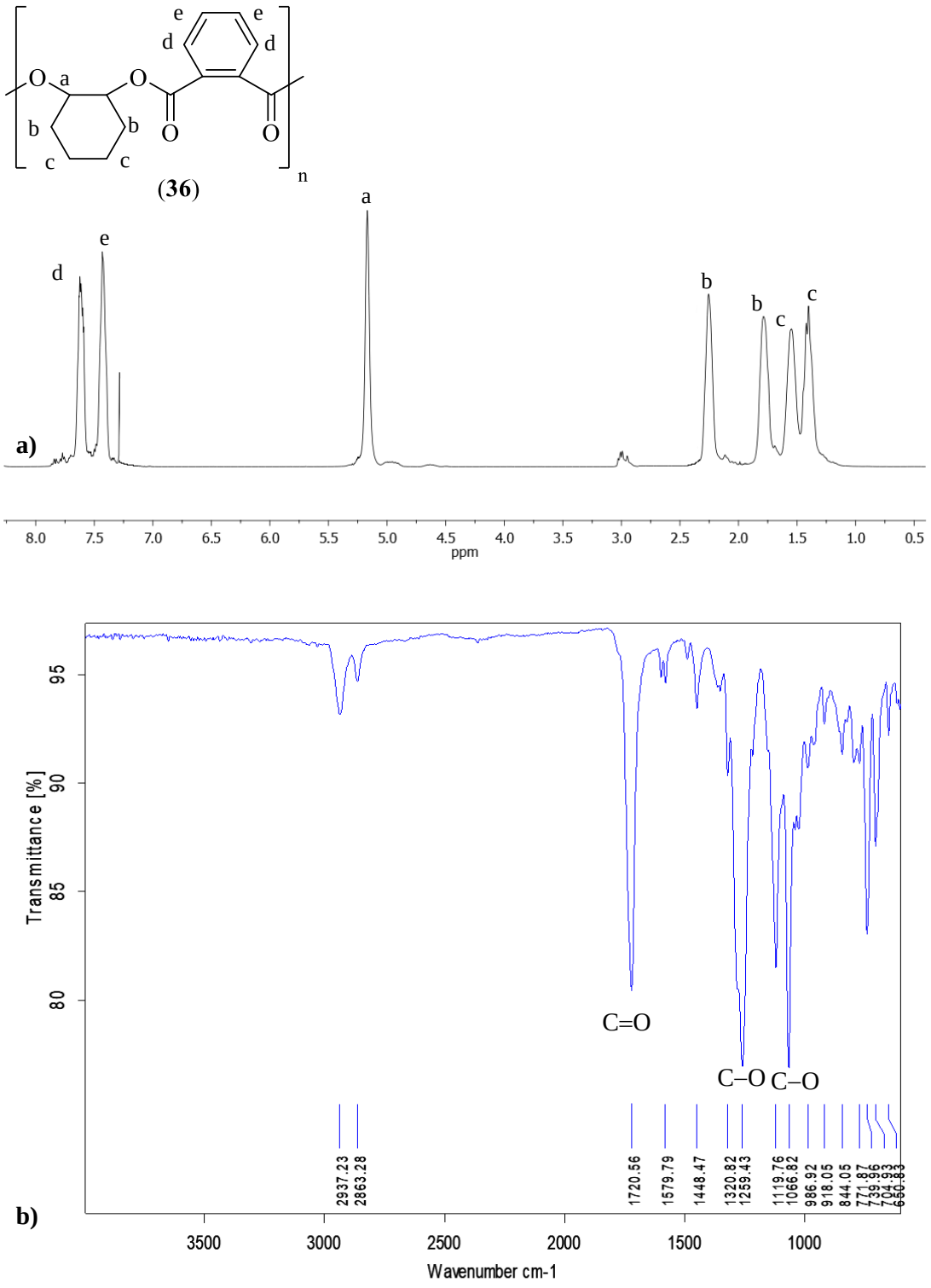

Figure 14. *a) ^{1}H-NMR spectrum for poly(cyclohexene phthalate in $CDCl_3$). b) IR spectrum for poly(cyclohexene phthalate).*

The resulting copolymers were also analysed by matrix-assisted laser desorption/ ionisation time-of-flight mass spectrometry (MALDI-ToF MS) in order to determine the end groups. The MALDI-ToF spectrum for poly(cyclohexene phthalate) showed two end-group series of peaks with an *m/z* interval of 246 mass units, indicating a controlled alternating microstructure (Figure 15). The major series (blue diamond) is in good agreement with a polymer chain with two hydroxyl end groups in the polyester containing *trans*-cyclohexanediol, and the second major series (green diamond) containing hydroxyl- and carboxylic acid end groups was also observed, indicating the existence of chain transfer agents during the copolymerisation.[71,95]

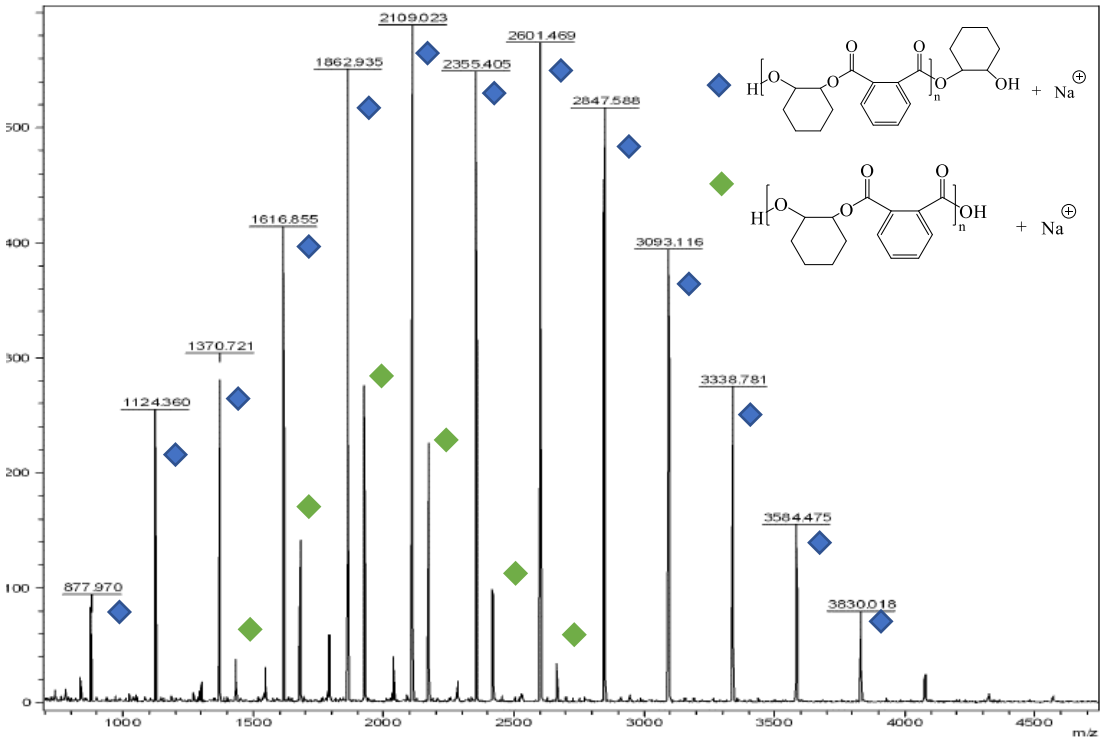

Figure 15. *MALDI-ToF analysis for poly(cyclohexene phthalate).*

The thermal properties of the copolymers were determined by thermogravimetric analysis (TGA) and differential scanning calorimetry (DSC). It was found that all polymers (Table 3) were stable in the range of temperatures from 0-200 ºC. The percentage weight loss increased from 250 to 350 ºC and after this temperature the remaining weight was almost constant until 800 ºC. The single glass temperature (T_g) for the polymeric materials shown in Table 3 exhibited very similar values ranging from 101-103 ºC, which is similar to those of some commercially available polymers.

Figure 16 shows the TGA (Figure 16a) and DSC (Figure 16b) analyses for the polymeric material obtained in Table 3, entry 4.

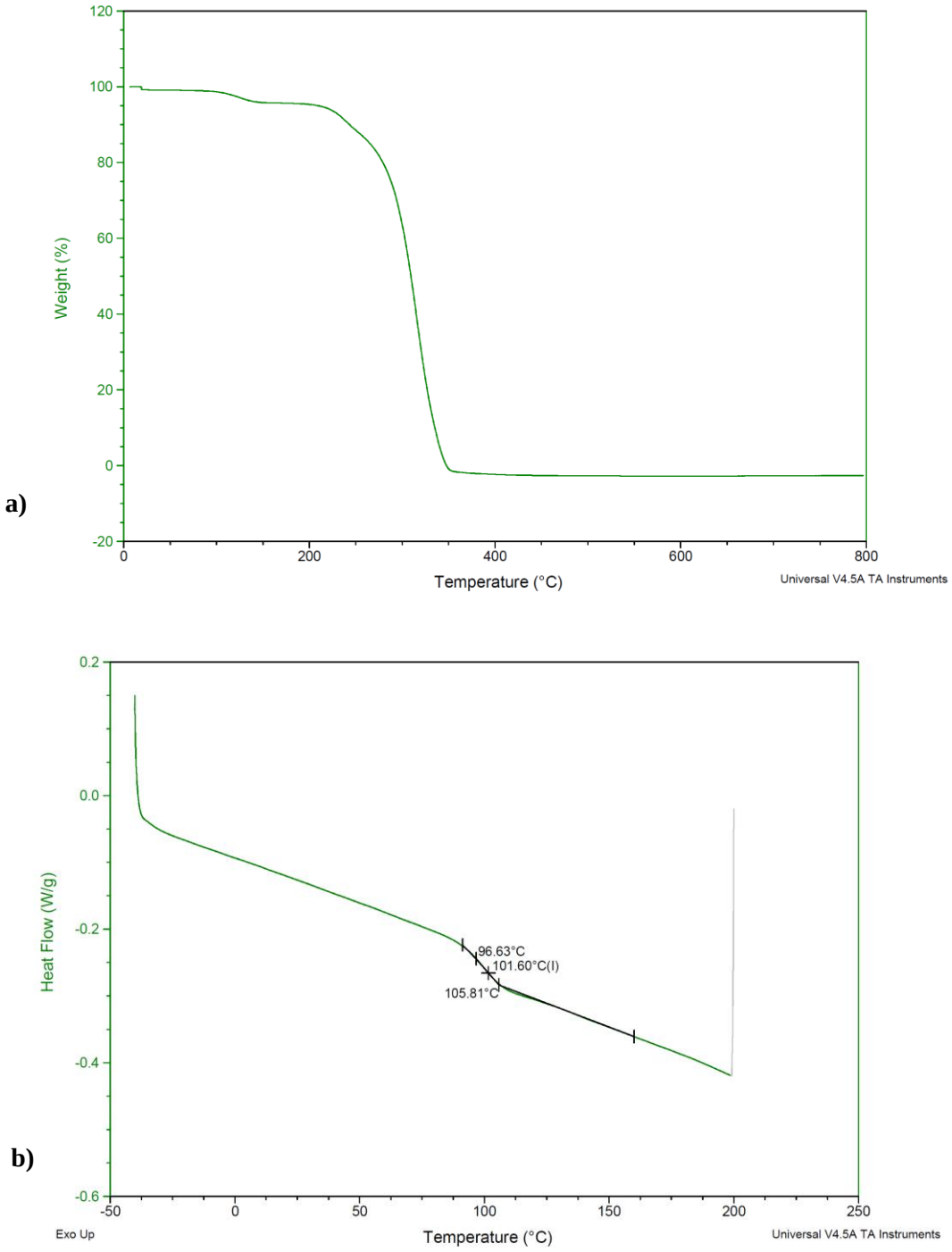

Figure 16. *a) TGA analysis for copolymer [PA]/[CHO]/[**35**] 50:50:1, b) DSC analysis for copolymer [PA]/[CHO]/[**35**] 50:50:1.*

1.2. Synthesis of polyesters catalysed by aluminium complexes with heteroscorpionate ligands functionalised with acetamidate groups

In this section, the use of mono- and bimetallic aluminium complexes with heteroscorpionate ligands functionalised with acetamidate groups (Figure 17) as catalysts for the ROCOP of different epoxides and cyclic anhydrides will be discussed. These complexes have been synthesised as previously described by our research group and have found different applications as catalysts for the ROP of cyclic esters (*ε*-caprolactone and *rac*-lactide) and for the synthesis of cyclic carbonates from epoxides and CO_2.[102,103]

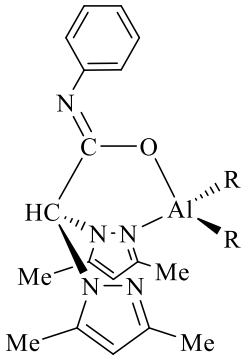

R = Me (**37**), Et (**38**)

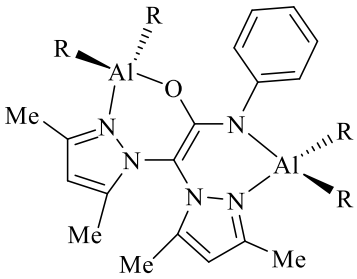

R = Me (**39**), Et (**40**)

Figure 17. *Mono- and bimetallic heteroscorpionate aluminium complexes for ROCOP of epoxides and cyclic anhydrides.*

Following the same approach for aluminium complexes with heteroscorpionate ligands functionalised with alkoxide groups, the catalytic activity of complexes **37-40** was evaluated for the ROCOP of CHO and succinic anhydride (SA) as substrates at 80 ºC in toluene, for 16 hours (Scheme 10). The initial experiments are shown in table 4.

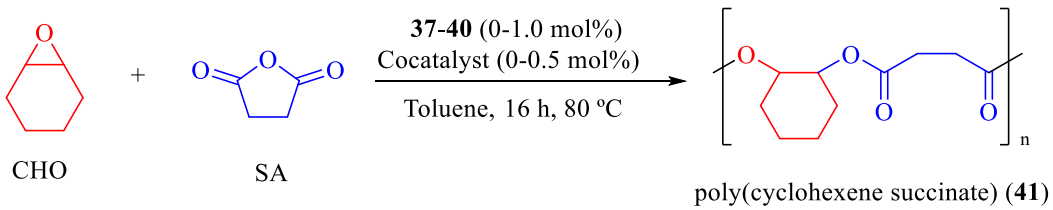

CHO SA poly(cyclohexene succinate) (**41**)

Scheme 10. *ROCOP of CHO and SA catalysed by complexes **37-40**.*

Firstly, the ROCOP process of CHO and SA catalysed by aluminium complexes was investigated in the absence of a co-catalyst (Table 4, entries 1-4). The results

showed that complexes **37**-**40** were highly active as catalysts for the ROCOP process and good conversions were achieved, although low selectivities were obtained. Since previous works confirmed that the addition of a co-catalyst increased the selectivity of the process,[73,95,100] the effect of adding tetrabutylammonium bromide (TBAB) as a co-catalyst was studied. As can be seen in Table 4, the selectivities towards the synthesis of the polyester increased up to 91% (Table 4, entries 5-9). These results also evidenced that bimetallic complexes **37**-**40** were more active for the ROCOP of CHO and SA than their monometallic counterparts **37**-**38**. On the other hand, the catalytic activity of ethyl derivatives **38** and **40** showed to be slightly higher than the methyl complexes **37** and **39**, due to a higher lability of the Al–C bond in ethyl complexes, which is in agreement with what previously observed for alkyl aluminium complexes functionalised with alkoxide groups.[101] A control test using TBAB as a catalyst showed that the co-catalyst itself could catalyse the process but less efficiently (Table 4, entry 9).

Table 4. *ROCOP of CHO and SA catalysed by complexes **37-40**.*[a]

Entry	Catalyst	Co-catalyst	Conversion (%) [b]	Polyester (%)[b]
1	**37**	-	71	50
2	**38**	-	74	43
3	**39**	-	81	52
4	**40**	-	83	50
5	**37**	TBAB	93	85
6	**38**	TBAB	93	88
7	**39**	TBAB	93	81
8	**40**	TBAB	100	91
9	**-**	TBAB	25	89

*[a]Reactions were carried out at 80 ºC in toluene for 16h using 1 mol% of aluminium complexes **37** and **38** or 0.5 mol% of aluminium complexes **39** and **40**. [b]Determined by NMR.*

^{1}H-NMR studies confirmed that the presence of a co-catalyst was crucial in order to increase the selectivity towards the synthesis of the polyester (Figure 18). A stoichiometric mixture of complex **40** and CHO in the absence of TBAB showed that 47% of CHO was converted into polyether at room temperature after five minutes (Figure 18a). However, when a stoichiometric amount of TBAB was added to the reaction mixture, no CHO was converted into polyether even after four hours of reaction at 80 ºC (Figure 18b).

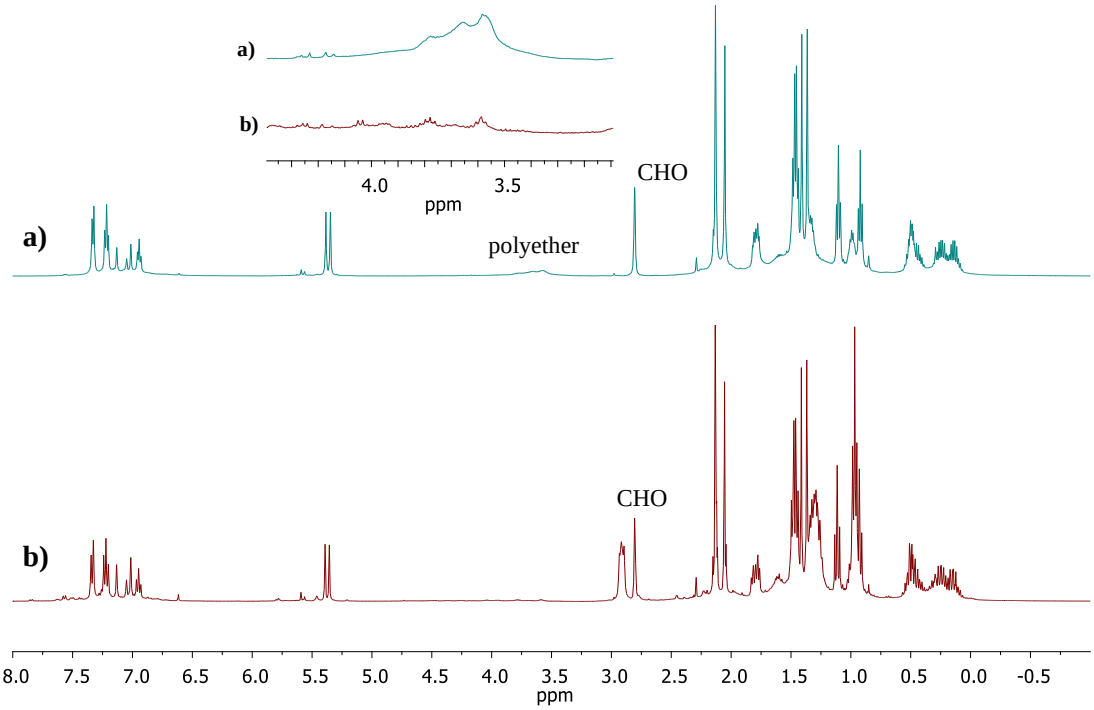

Figure 18. *(a) ^{1}H-NMR spectrum of complex **40** and CHO at t =5 min and 25 ºC in toluene-d_8. (b) ^{1}H-NMR spectrum of complex **40**, TBAB and CHO at t =4 h and 80 ºC in toluene-d_8.*

To optimise the catalytic system comprising complex **40**, the influence of the co-catalyst for the ROCOP of CHO and SA was next investigated (Figure 19). In general, tetrabutylammonium salts exhibited slightly higher catalytic activity and selectivity than their corresponding bis(triphenylphosphine)iminium ones (PPNX), and TBAB showed to be the optimal co-catalyst in terms of activity and selectivity. Bis(triphenylphosphine)iminium dinitrophenolate also showed good values of catalytic activity and selectivity. N-Methylimidazole (NMI) and dimehtylaminopyridine (DMAP) were also tested as co-catalysts, obtaining good selectivity but lower catalytic activity than that obtained when using TBAB. The

higher catalytic activity and selectivity obtained when using a bromide counterion can be due to the good balance between the nucleophilicity and the steric hindrance to ring-open the epoxide.

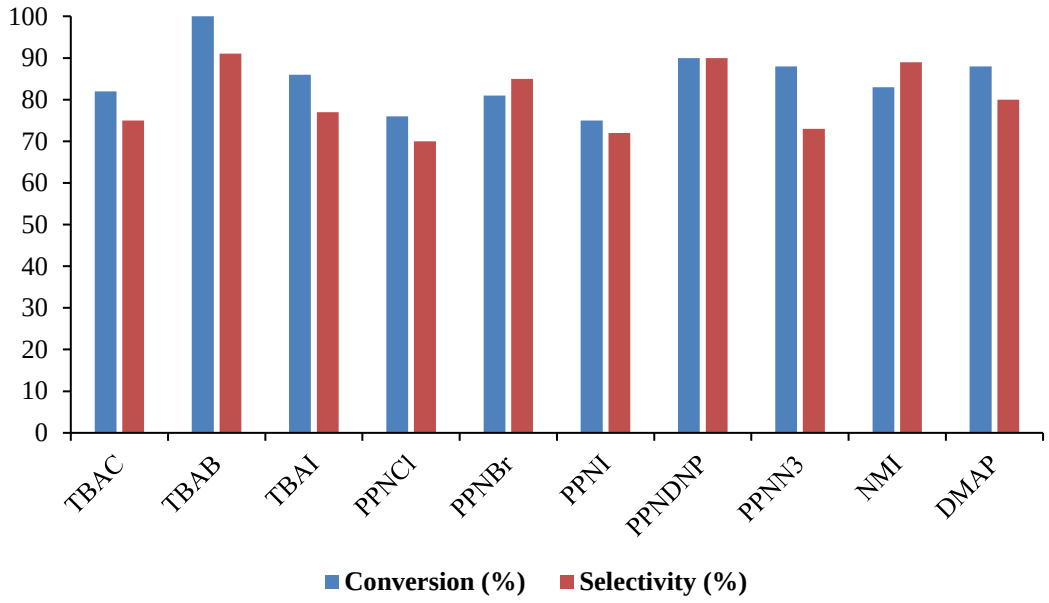

Figure 19. *Influence of the co-catalyst on the catalytic activity and selectivity of complex **40** in the ROCOP of CHO and SA at 80 ºC in toluene for 16vh using 0.5 mol% of complex **40**.*

The optimal catalytic system for the ROCOP of CHO and SA was found to be the combination of complex **40** and TBAB. Then, the solvent effect on the catalytic process was investigated (Table 5). The ROCOP of CHO and SA was first studied in the absence of a solvent to maximise the sustainability of the process but complete conversion of the starting materials to the formation of polyester was not achieved because of solidification of the reaction mixture due to the homopolymerisation of CHO which resulted in high polyether formation. Thus, the selectivity towards polyester formation decreased to 18% (Table 5, entry 1). The optimal catalytic system acted efficiently in a range of different solvents and the polarity of the solvent did not affect significantly on the selectivity of the process. However, when using hexane as the solvent for the process, the conversion decreased to 41% (Table 5, entry 5), due to the low solubility of the starting materials, which was translated into a heterogeneous mixture.

The versatility of the catalytic system was further tested towards the synthesis of a wide range of polyesters derived from the copolymerisation of CHO with SA, PA and

maleic anhydride (MA). Furthermore, the synthesis of bio-derived polyester materials from the ROCOP of limonene oxide (LO) with SA, PA and MA was also investigated (Figure 20).

Table 5. *Influence of the solvent in the ROCOP of CHO and SA catalysed by **40** and TBAB.*[a]

Entry	Solvent	Conversion (%)[b]	Polyester (%)[b]
1	Bulk	89	18
2	Toluene	100	91
3	THF	81	89
4	Acetonitrile	75	90
5[c]	Hexane	41	88

[a]*Reactions were carried out at 80 ºC in solvent for 16h using 0.5 mol% of aluminium complex **40** and 0.5 mol% of TBAB.* [b]*Determined by NMR.* [c]*The reaction mixture was not homogeneous.*

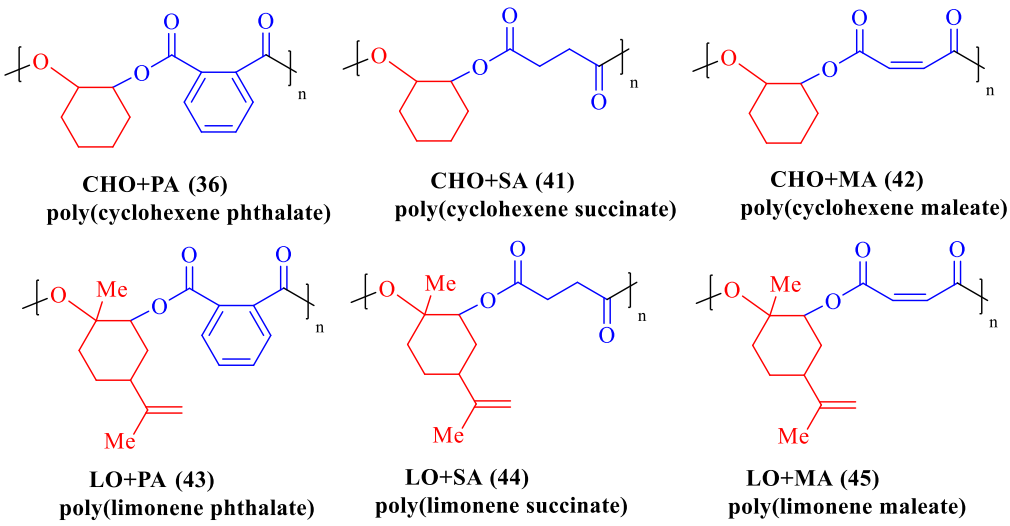

Figure 20. *Polyesters synthesised by complex **40** derived from CHO or LO and SA, PA or MA.*

The results for the copolymerisation of the different substrates catalysed by complex **40** are given in Table 6. Good selectivities toward the synthesis of the corresponding polyester were obtained in all cases, except for poly(cyclohexene maleate) (**42**), which showed high polyether content (Table 6, entry 2). The experimental molecular weights obtained for the copolymers were much lower than

the theoretical values, probably because of the presence of transesterification reactions or chain transfer agents. These results might be justified by the presence of traces of water or diols in the starting CHO or diacid from the hydrolysis of the corresponding cyclic anhydride.[95] It is worth noting that under the same reaction conditions, conversions were higher when using CHO (Table 6, entries 1-6) than those observed when using LO (Table 6, entries 7-9). These results showed that highly-substituted epoxides, such as LO, are much more challenging substrates for this reaction than disubstituted ones. The effect on the [monomers]/[**40**] ratio was also examined (Table 6, entries 3-6). Thus, the molecular weights of the copolymers obtained decreased when the [monomers]/[**40**] ratio decreased from 200 to 50. Also, it is worth highlighting that the activity of dinuclear acetamidate complex **40** towards the synthesis of poly(cyclohexene phthalate) (Table 6, entries 3-6) was slightly lower than its alkoxide analogue **35**, which performed similarly in terms of activity and selectivity, but only after 6 h under the same reaction conditions (Table 3).

Table 6. *GPC data for selected copolymers.*[a]

Entry	Epoxide/anhydride	Conv. (%)[b]	Polyester (%)[b]	$M_{n,exp}$[c]	PDI[c]
1	CHO/SA	100	91	1656	1.34
2	CHO/MA	97	62	2109	1.25
3	CHO/PA	100	95	3572	1.11
4	CHO/PA[d]	100	98	2088	1.09
5	CHO/PA[e]	100	95	2533	1.21
6	CHO/PA[f]	100	94	3114	1.16
7	LO/SA	47	92	1194	1.50
8	LO/MA	50	88	1536	1.49
9	LO/PA	59	93	2856	1.36

*[a]Reactions were carried out at 80 ºC in toluene for 16 h using [epoxide]/[anhydride]/[**40**]/[TBAB]= 200:200:1:1. [b]Determined by NMR. [c]Determined by GPC. [d][CHO]/[PA]/[**40**]/[TBAB]= 50:50:1:1. [e][CHO]/[PA]/[**40**]/[TBAB]= 100:100:1:1. [f][CHO]/[PA]/[**40**]/[TBAB]= 150:150:1:1.*

a) Copolymers Characterisation

All the synthesised polyesters were characterised by NMR and IR spectroscopy, gel permeation chromatography (GPC) and MALDI-ToF. The formation of polyester materials was confirmed by NMR analysis, showing that the ROCOP of epoxides and anhydrides takes place in a controlled manner. Figure 21 shows the ^{1}H-NMR spectrum for poly(cyclohexene succinate).

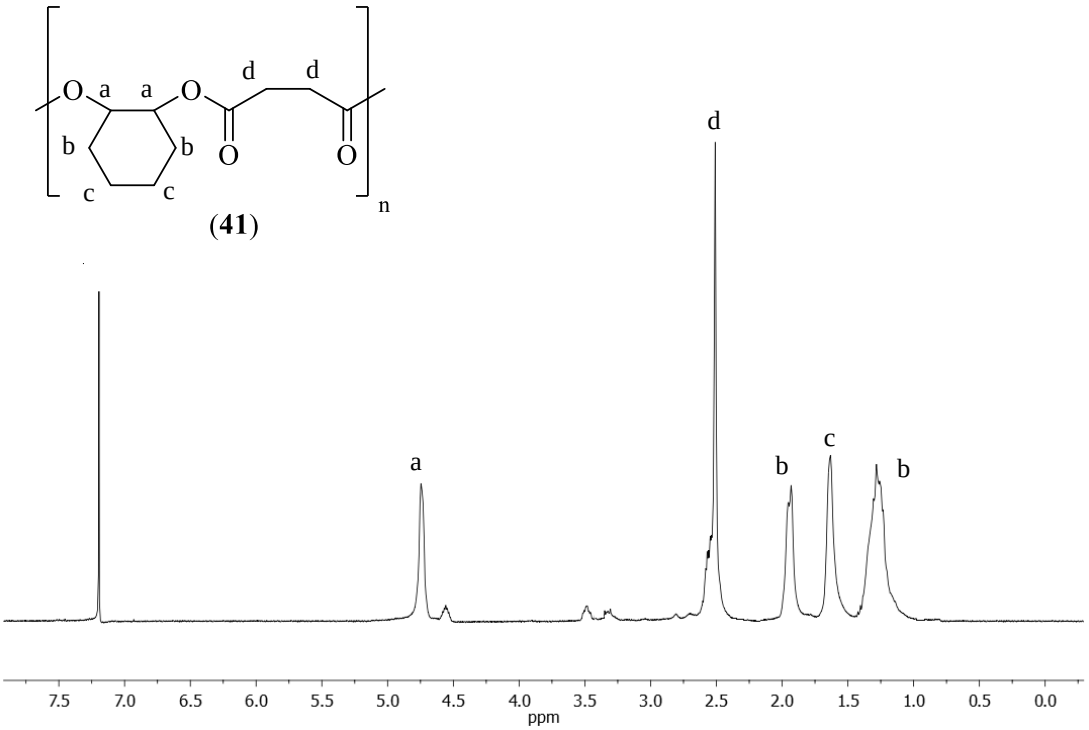

Figure 21. *^{1}H.NMR spectrum for poly(cyclohexene succinate) (**41**).*

The resulting copolymers were also analysed by MALDI-ToF MS in order to determine the chain-end groups. When a combination of complex **40** and TBAB was used as catalytic system for CHO and SA copolymerisation, the MALDI-ToF spectrum showed multiple end-group series of peaks with an *m/z* interval of 198 mass units, indicating a controlled alternating microstructure (Figure 22). The major series (blue diamond) is in good agreement with a polymer chain with two hydroxyl end groups in the polyester containing *trans*-cyclohexanediol, and the second major series (red diamond) containing hydroxyl- and carboxylic acid end groups was also observed, indicating the existence of chain transfer agents during the copolymerisation.[71,95] When DMAP was used as a co-catalyst, the MALDI-ToF spectrum (Figure 23) only showed one end-group series of peaks which corresponded to perfectly alternating

poly(cyclohexene succinate) chains with DMAP and a hydroxyl group as chain end, corroborating the previously reported results in which DMAP could act as initiator for ROCOP processes.[50,51]

Finally, analysis of the MALDI-ToF spectrum of the novel poly(limonene succinate) revealed the existence of three series of peaks with an interval between consecutive peaks of 252 (Figure 24). These series corresponded to chains with two hydroxy-limonene end groups (blue diamond) and chains with hydroxyl and carboxylic acid groups (red diamond). This observation can be explained by the presence of water and/or limonene-1,2-diol traces in the reaction mixture

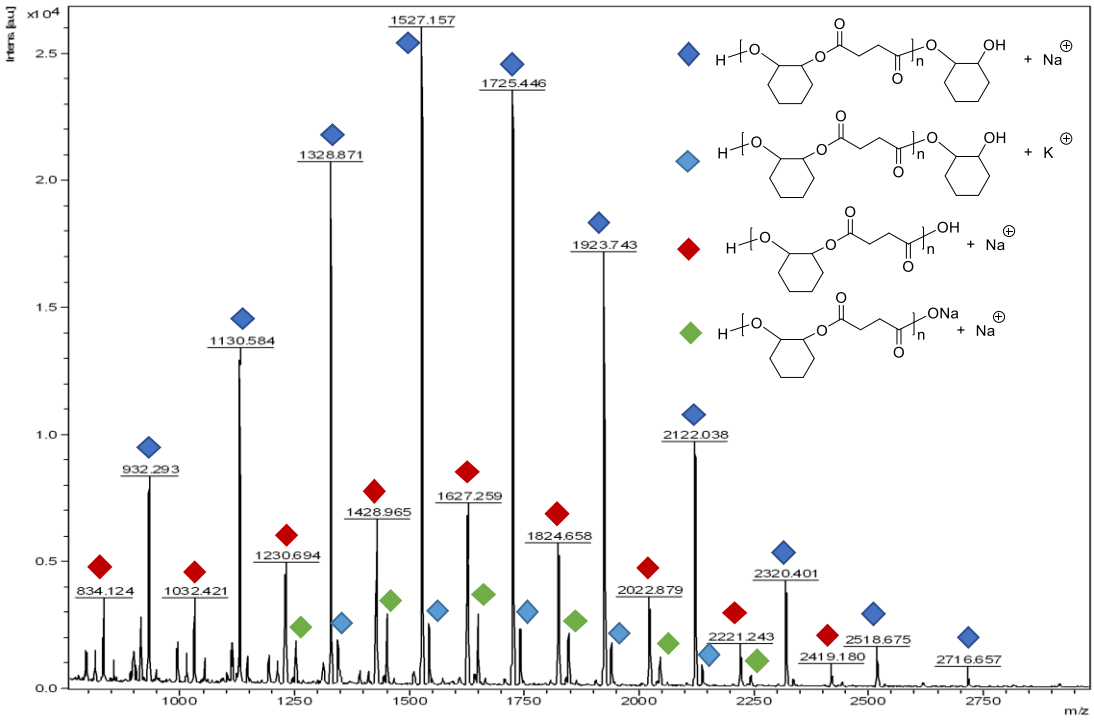

Figure 22. *MALDI-ToF spectrum of poly(cyclohexene succinate) (**41**) obtained using a combination of complex **40** and TBAB*

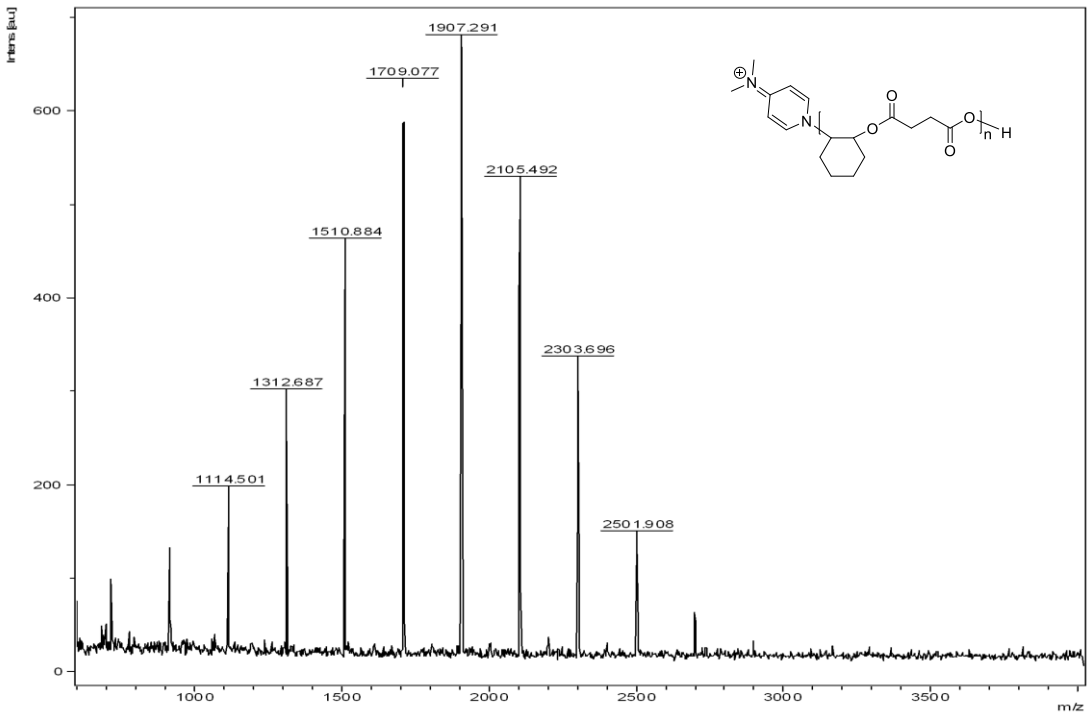

Figure 23. *MALDI-ToF spectrum of poly(cyclohexene succinate) (**41**) obtained using a combination of complex **40** and DMAP*

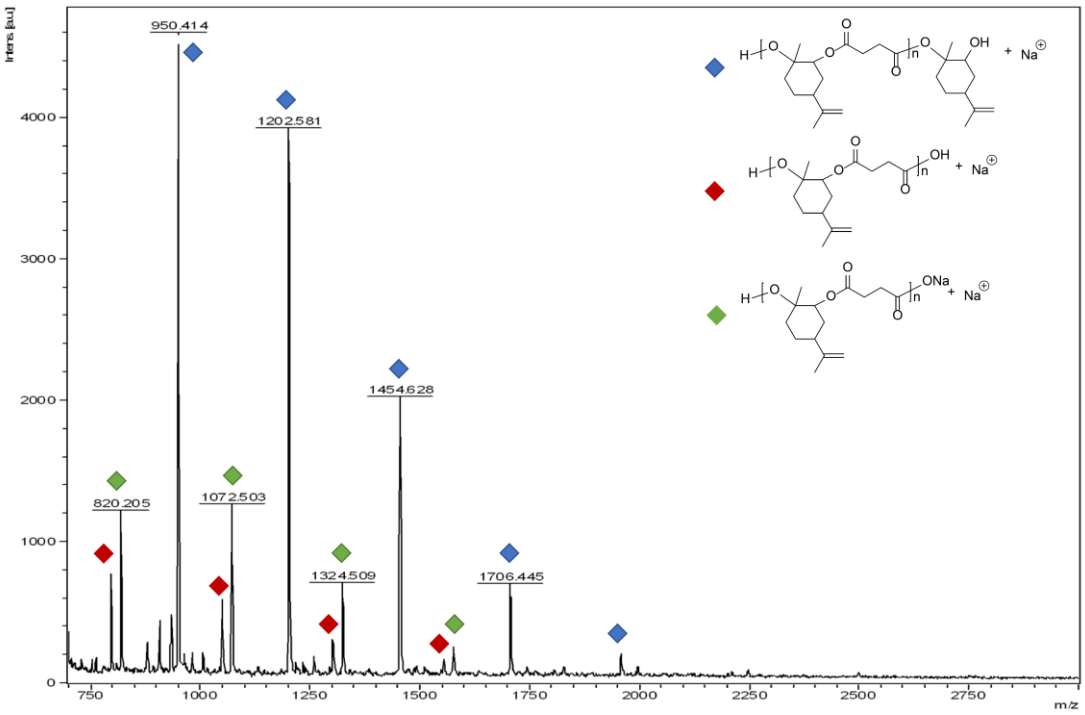

Figure 24. *MALDI-ToF spectrum of poly (limonene succinate) (**44**) obtained using a combination of complex **40** and TBAB.*

The thermal properties of the synthesised polyesters were analysed by DSC and TGA. The glass-transition temperatures (T_g's) of the polyesters prepared using the optimal catalytic system were determined by DSC and the results are shown in Table 7. Figure 25 shows the DSC and TGA analyses for poly(limonene phthalate) (**43**). As expected, in all cases, the T_g values for the polyesters derived from CHO (Table 7, entries 1-3) were higher than those observed when using LO (Table 7, entries 4-6). Similarly, when varying the cyclic anhydride, the T_g increased in the order PA>MA>SA. These results suggest an increase of the T_g values with the rigidity of the monomer used.[106] TGA analysis revealed that all polymers are stable in the range of temperatures from 10 to 200 ºC except poly(limonene maleate) (**45**), for which the range of temperatures was from 10 to 125 ºC.

Table 7. *DSC data for selected polyesters.*[a]

Entry	Polyester	$M_{n,exp}$[b]	T_g (ºC)[c]
1	poly(cyclohexene phthalate) (**36**)	3572	103
2	poly(cyclohexene succinate) (**41**)	1656	44
3	poly(cyclohexene maleate) (**42**)	2109	84
4	poly(limonene phthalate) (**43**)	2856	50
5	poly(limonene succinate) (**44**)	1194	26
6	poly(limonene maleate) (**45**)	1536	27

*[a]Reactions were carried out at 80 ºC in toluene for 16 h using 0.5 mol% of aluminium complex **40** and 0.5 mol% of TBAB. [b]Determined by GPC. [c]Determined by DSC during the second heating cycle.*

b) Kinetic studies and mechanism proposal

In order to gain insight into the copolymerisation process catalysed by complex **40** and TBAB, a kinetic study for the synthesis of poly(cyclohexene phthalate) was performed using complex **40** as catalyst and TBAB as co-catalyst. The experiments were performed in toluene at 80 ºC. Samples were taken from the copolymerisation reaction every hour and analysed by ^{1}H-NMR to determine the conversion of the starting materials into the corresponding polyester and the selectivity of the process.

Experiments carried out under these reaction conditions showed a good fit to first-order kinetics. The reaction rate equation can be defined as:

$$v = k\,[\mathbf{40}]^{a}[\mathrm{TBAB}]^{b}[\mathrm{CHO}]^{c}[\mathrm{PA}]^{d}$$

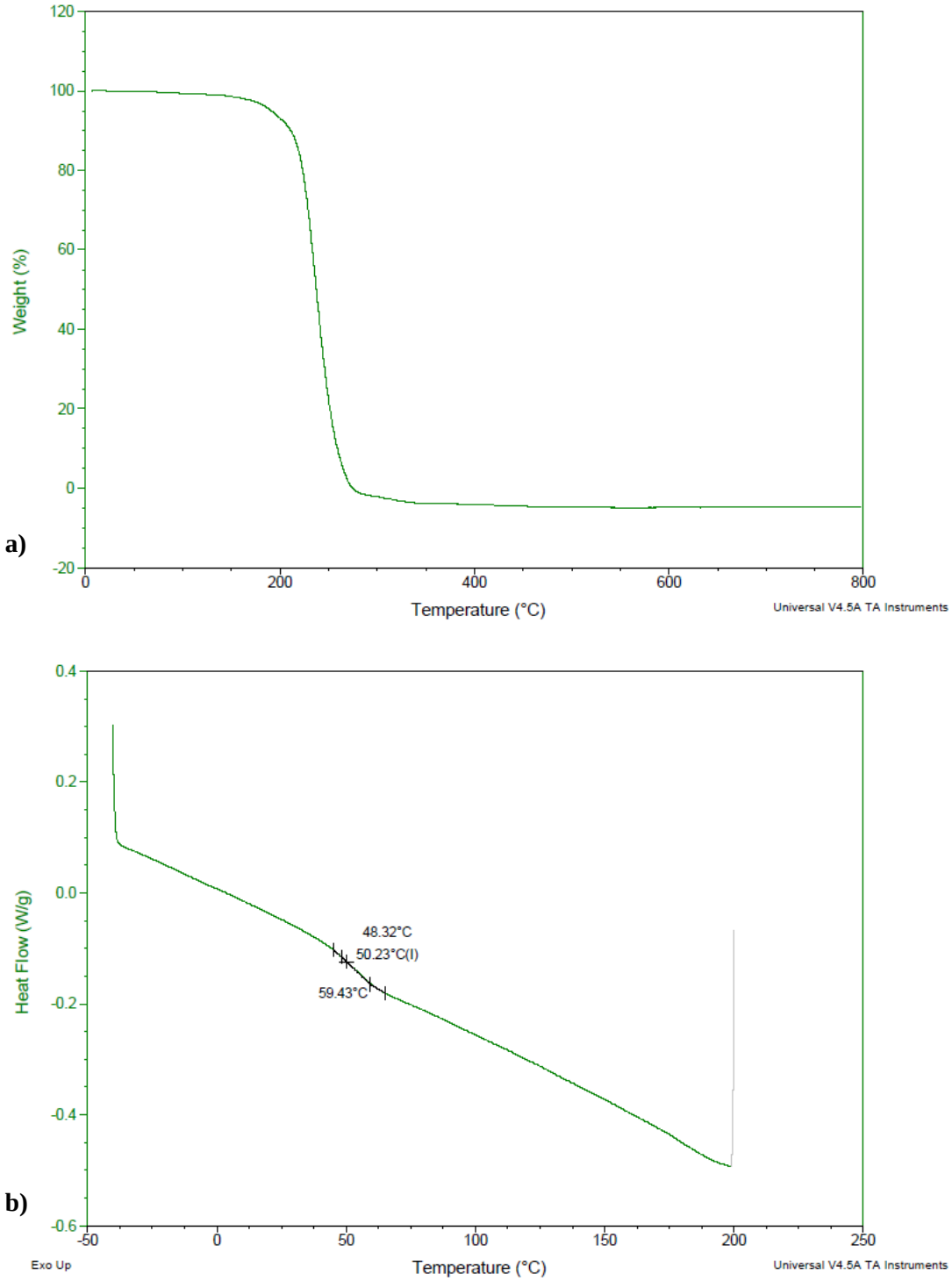

Figure 25. *a) TGA analysis for poly(limonene phthalate) (**43**). b) DSC analysis for poly(limonene phthalate) (**43**).*

Considering [CHO] and [PA] constants at the beginning of the process, the equation can be simplified to:

$$v = k_{obs}\,[\mathbf{40}]^{a}\,[TBAB]^{b}, \text{ where } k_{obs} = k[CHO]^{c}[PA]^{d}$$

First, the order with respect to the concentration of complex **40** was studied by carrying out reactions using different concentrations of complex **40**, [**40**] = 0.1–0.75 mol% whilst keeping constant the co-catalyst concentration, [TBAB] = 0.5 mol% (Table 8). The lineal correlation obtained when plotting log[**40**] vs log(k_{obs}) indicated that the reaction was first order with respect to the [**40**], with a slope value of 0.84 (Figure 26). This was further confirmed by plotting [**40**] vs k_{obs}, which also fitted to a straight line (Figure 27). Similarly, to determine the order with respect to the [TBAB], reactions were carried out at different concentration of co-catalyst, [TBAB] = 2–5 mol% whilst keeping constant the catalyst concentration, [**40**] = 2 mol% (Table 9). As can be seen in Figure 26, a linear correlation was obtained when plotting log[TBAB] vs log(k_{obs}), indicating that the reaction was also first order with respect to the [TBAB], with a slope value of 1.05 (Figure 28). Furthermore, this was also confirmed by plotting [TBAB] vs k_{obs} (Figure 29).

Thus, the equation rate for the copolymerisation process can be defined as:

$$v = k_{obs}\,[\mathbf{40}]^{1}\,[TBAB]^{1}, \text{ where } k_{obs} = k[CHO]^{c}[PA]^{d}$$

Table 8. *Effect of [40] on the reaction rate.*

[40] (mol%)	[40] (mol/L)	log [40]	k_{obs} (mol/L·s)	log k_{obs}
0.1	0.00203666	-2.69	0.004748	-1.36
0.25	0.00509165	-2.29	0.112960	-0.98
0.5	0.01018329	-1.99	0.188140	-0.75
0.75	0.01527494	-1.81	0.263520	-0.58

Table 9. *Effect of [TBAB] on the reaction rate.*

[TBAB] (mol%)	[TBAB] (mol/L)	log [TBAB]	k_{obs} (mol/L·s)	log k_{obs}
2	0.174736842	-0.75	0.191145	-0.72
3	0.262105263	-0.58	0.261760	-0.58
4	0.349473684	-0.46	0.386555	-0.41
5	0.436842105	-0.36	0.495095	-0.31

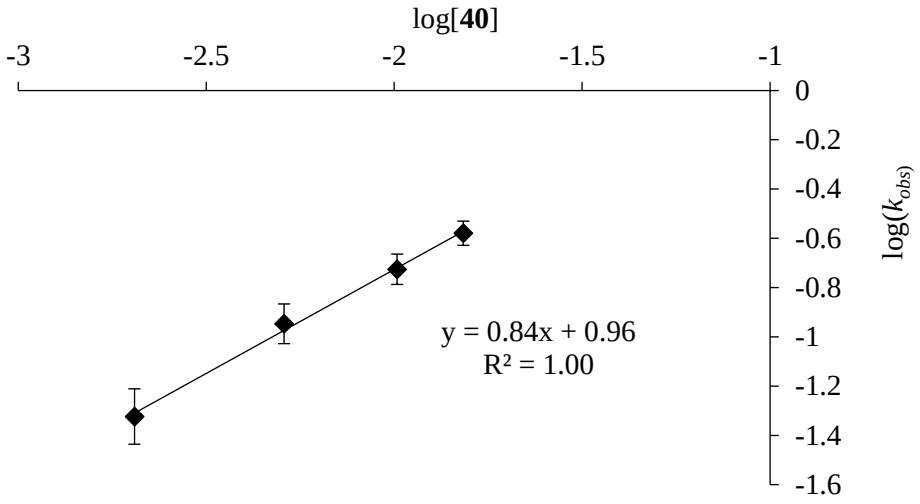

Figure 26. *Plot of log (k_{obs}) vs log [**40**] for the ROCOP of CHO and PA.*

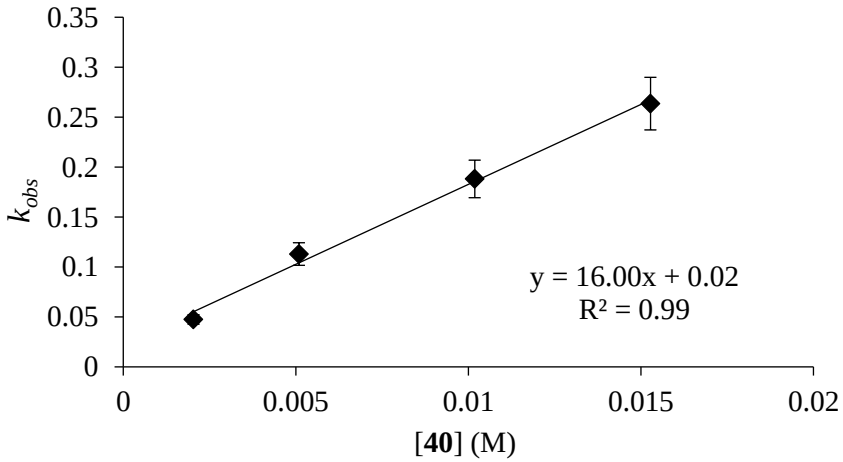

Figure 27. *Plot of k_{obs} vs [**40**] for the ROCOP of CHO and PA.*

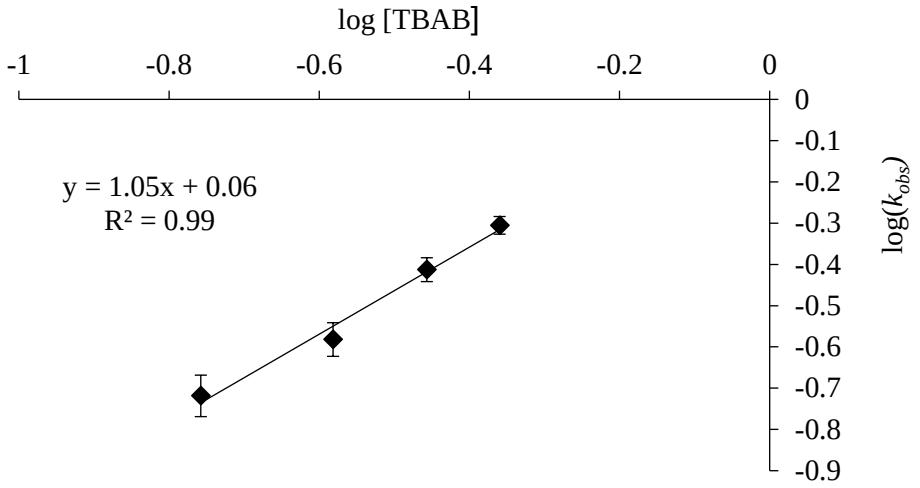

Figure 28. *Plot of log(k_{obs}) vs log[TBAB] for the ROCOP of CHO and PA.*

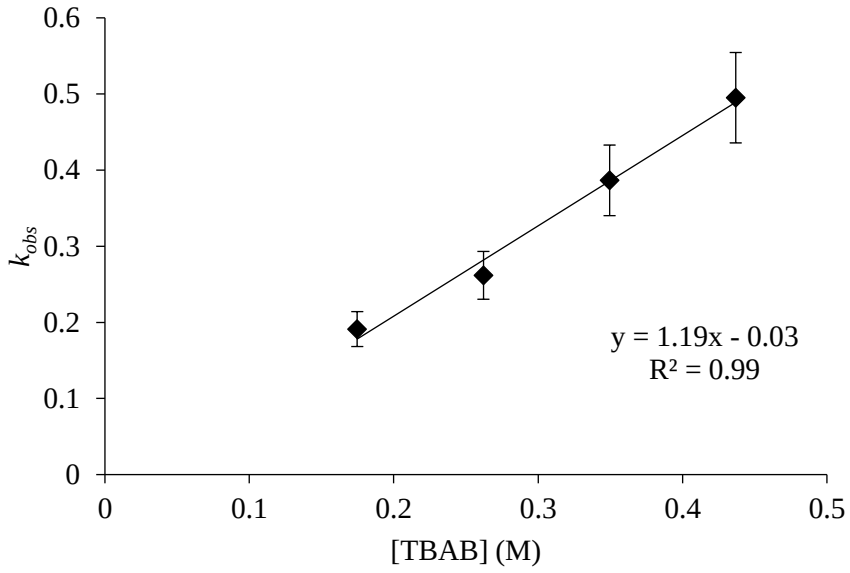

Figure 29. *Plot of k_{obs} vs [TBAB] for the ROCOP of CHO and PA.*

Following the results obtained, a plausible mechanism for the ROCOP catalysed by complex **40** and TBAB can be proposed (Scheme 11). In the first step of the mechanism, the coordination and activation of CHO by one of the aluminium metal centres of complex **40** would give rise to the intermediate **40a**. In a second step, the bromide anions of TBAB would ring-open the coordinated epoxide to the aluminium center to generate the alkoxide derivative **40b**. This step might be considered as the rate determining step of the reaction, since in this step both complex **40** and TBAB are involved, and according to the kinetic studies performed, the reaction rate was first order with respect to the [**40**] and [TBAB]. This alkoxide derivative **40b**, could ring-

open an activated monomer of PA coordinated to the second aluminium centre of complex **40** to yield the carboxylate specie **40c**, which could undergo successive alternating ring-opening reactions of epoxides and anhydrides to generate the desired polyester materials.

The polyether formation can be explained by the coordination of a second CHO monomer to the other aluminium centre of complex **40** and subsequent attack of the alkoxide derivate **40b'**, which could undergo successive ring-opening reactions to generate the undesired polyether material.

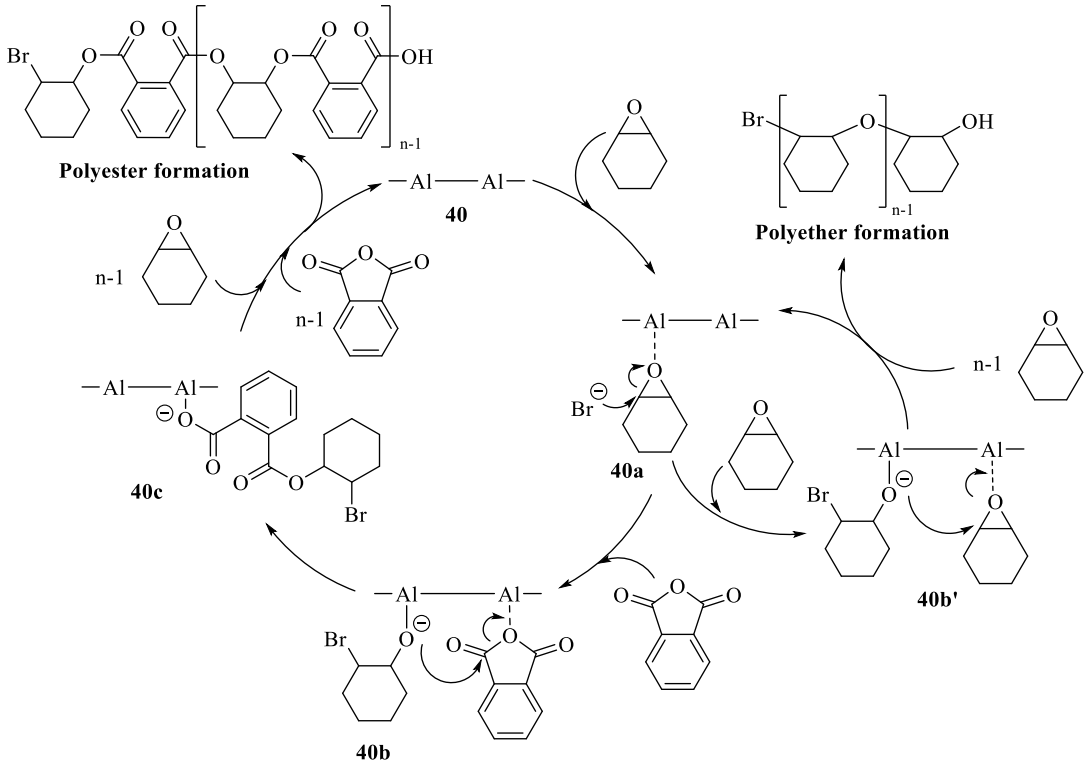

Scheme 11. *Proposed mechanism for the ROCOP catalysed by complex **40** and TBAB as co-catalyst.*

Experimental section

EXPERIMENTAL SECTION

1. Synthesis of starting materials

Most of the reagents used are commercially available, so in this section it will only be discussed the synthesis of the co-catalysts which were prepared.

Epoxides CHO and LO, which were purchased from Sigma Aldrich, were predried over calcium hydride, distilled under vacuum and stored in the glovebox under nitrogen prior to use. Similarly, anhydrides PA, SA an MA were also purchased from Sigma Aldrich and sublimed three times and stored in the glovebox prior to use. All the other reagents were purchased from common commercial sources and used as received.

1.1. Synthesis of co-catalysts

1.1.1. Synthesis of PPNBr[107]

Bis(triphenylphosphine)ammonium chloride (PPNCl) (1.00 g, 1.74 mmol) were dissolved in 50 mL of ethanol. Then, sodium bromide (2.06 g, 2.00 mmol) was added to the solution and the suspension was left stirring for 16 hours at room temperature. After that time, the suspension was left decanting, filtered and dried under vacuum, affording a white solid. The salt was recrystallised from a dichloromethane/ether mixture obtaining a crystalline white solid which was further dried under vacuum for 5 hours. The yield of the reaction is 81%.

1.1.2. Synthesis of PPNDNP[107]

PPNCl (1.00 g, 1.74 mmol) was dissolved in 50 mL of CH_2Cl_2. Then, sodium 2,4-dinitrophenolate (0.36 g, 1.74 mmol) was added and the suspension was left stirring for 24 hours. After that time, the suspension was left decanting and filtered. Finally, diethyl ether was added to the reaction mixture obtaining a yellow precipitate corresponding to the desired product. The yield of the reaction is 80%.

2. Synthesis of polyesters

2.1. Representative copolymerisation procedure

In the glovebox, complex **40** (20 μmol), co-catalyst (20 μmol), and a cyclic anhydride (4 mmol) were placed into a 10 mL Schlenk equipped with a small stir bar. Toluene (2 mL) was added, and the reaction mixture was stirred. Then, the reaction mixture was placed in a preheated oil bath at the desired temperature and the epoxide (4 mmol) was added. After the appropriate time, a small aliquot was taken from the reaction mixture for NMR analysis to determine the monomer conversion and process selectivity. The viscous mixture was then dissolved in the minimum amount of dichloromethane or toluene and precipitated in MeOH or pentane. The polymer was then dried and collected as a white or light-yellow solid.

2.2. Characterisation of polyesters

The synthesised polyesters were characterised by IR, ^{1}H-NMR, and ^{13}C-NMR spectroscopy, MALDI-ToF analysis, DSC and TGA.

Poly(cyclohexene phthalate) (36): Obtained as a white solid in 70% yield. ^{1}H-NMR ($CDCl_3$, 25 ºC): δ(ppm) = 7.62 (s, 2H); 7.43 (s, 2H); 5.17 (s, 2H); 2.26 (s, 2H); 1.79 (s, 2H); 1.55 (s, 2H); 1.41 (s, 4H). ^{13}C-{^{1}H}-NMR ($CDCl_3$, 25 ºC): δ(ppm) = 166.7; 132.1; 131.1; 129.0; 128.2; 125.3; 74.6; 29.9; 23.4. IR: ν (C=O) = 1720 cm^{-1}; ν (C–O) = 1259 cm^{-1}.

Poly(cyclohexene succinate) (41): Obtained as a light-yellow solid in 76% yield. ^{1}H-NMR ($CDCl_3$, 25 ºC): δ(ppm) = 4.75 (s, 2H); 2.51 (s, 2H); 1.94 (s, 2H); 1.64 (s, 2H); 1.30 (s, 4H). ^{13}C-{^{1}H}-NMR ($CDCl_3$, 25 ºC): δ(ppm) = 171.8; 73.8; 30.1; 29.2; 23.4. IR: ν (C=O) = 1729 cm^{-1}; ν (C–O) = 1142 cm^{-1}.

Poly(cyclohexene maleate) (42): Obtained as a light-yellow solid in 75% yield. ^{1}H-NMR ($CDCl_3$, 25 ºC): δ(ppm) = 6.22 (s, 2H); 4.92 (s, 2H); 1.97 (s, 2H); 1.69 (s, 2H); 1.28 (s, 4H). ^{13}C-{^{1}H}-NMR ($CDCl_3$, 25 ºC): δ(ppm) = 166.7; 131.1-125.3; 74.6; 30.0; 23.4. IR: ν (C=O) = 1725 cm^{-1}; ν (C–O) = 1207;1160 cm^{-1}.

Poly(limonene phthalate) (43): Obtained as a white solid in 78% yield. ^{1}H-NMR ($CDCl_3$, 25 ºC): δ(ppm) = 7.72 (s, 2H); 7.59 (s, 2H); 5.55 (s, 1H), 4.73 (s, 2H); 2.7-1.3 (s, 7H); 1.73 (s, 6H). ^{13}C-{^{1}H}-NMR ($CDCl_3$, 25 ºC): δ(ppm) = 166.6; 166.2;

148.8; 133.1–128.9; 109.2; 74.0; 72.7; 38.2–25.9; 21.8; 21.0. IR: ν (C=O) = 1720 cm^{-1}; ν (C–O) = 1260 cm^{-1}.

Poly(limonene succinate) (44): Obtained as a white solid in 69% yield. ^{1}H-NMR ($CDCl_3$, 25 ºC): δ (ppm) = 5.22 (s, 1H); 4.7 (s, 2H); 2.65 (s, 2H); 2.59 (s, 2H); 2.5-1.2 (s, 7H); 1.69 (s, 3H); 1.58 (s, 3H). ^{13}C-{^{1}H}-NMR ($CDCl_3$, 25 ºC): δ (ppm) = 171.2; 170.8; 148.9; 109.2; 75.8; 72.7; 69.9; 38.1–25.9; 21.8; 20.9. IR: ν (C=O) = 1730 cm^{-1}; ν (C–O) = 1155 cm^{-1}.

Poly(limonene maleate) (45): Obtained as a light-yellow solid in 58% yield. ^{1}H-NMR ($CDCl_3$, 25 ºC): δ (ppm) = 6.18 (s, 2H); 5.22 (s, 1H), 4.66 (s, 2H); 2.65 (s, 2H); 2.5-1.3 (s, 7H); 1.66 (s, 3H); 1.48 (s, 3H). ^{13}C-{^{1}H}-NMR ($CDCl_3$, 25 ºC): δ (ppm) = 164.3; 163.3; 148.8; 130.5; 129.8; 109.3; 82.5; 73.7; 37.5–25.7; 21.8; 21.1. IR: ν (C=O) = 1780 cm^{-1}; ν (C–O) = 1158 cm^{-1}.

2.3. Representative kinetic procedure

In the glovebox, complex **40** (2–15 μmol), TBAB (5–20 μmol), and PA (4 mmol), were placed into a 10 mL vial equipped with a small stir bar. Toluene (2 mL) was added and the vials were placed in a preheated multireactor at the desired temperature. Then, CHO (4 mmol) was added to the reaction mixture. Small aliquots were taken for NMR analysis to determine monomer conversions and reaction selectivities at the desired times.

Bibliography

BIBLIOGRAPHY

(1) K. Ravindranath, R. A. Mashelkar, *Chem. Eng. Sci.*, **1986**, *41*, 2197.

(2) B. Tylkowski, K. A. Bogdanowicz, V. Ambrogi, A. Lederer, V. Patroniak, M. Giamberini, *Polym. Int.*, **2014**, *63*, 315.

(3) M. Tokita, J. Watanabe, *Polym. J.*, **2006**, *38*, 611.

(4) I. Ouchi, I. Nakai, M. Ono, S. Kimura, *J. App. Polym. Sci.*, **2007**, *105*, 114.

(5) I. Ouchi, R. Miyamura, M. Sakaguchi, S. Hosaka, M. Kitagawa, *Polym. Adv. Technol.*, **1999**, *10*, 195.

(6) M. A. Hillmyer, W. B. Tolman, *Acc. Chem. Res.*, **2014**, *47*, 2390.

(7) M. Vert, *Biomacromolecules*, **2005**, *6*, 538.

(8) K. O. Siegenthaler, A. Künkel, G. Skupin, M. Yamamoto, *Adv. Polym. Sci.*, **2012**, *245*, 91.

(9) H. W. Engels, H. G. Pirkl, R. Albers, R. W. Albach, J. Krause, A. Hoffmann, H. Casselmann, J. Dormish, *Angew. Chem. Int. Ed.*, **2013**, *52*, 9422.

(10) A. P. Gupta, V. Kumar, *Eur. Polym. J.*, **2007**, *43*, 4053.

(11) R. Datta, M. Henry, *J. Chem. Technol. Biotechnol.*, **2006**, *81*, 1119.

(12) F. Sanda, T. Endo, *J. App. Polym. Sci. Part A: Polym. Chem.*, **2001**, *39*, 266.

(13) W. J. Bailey, *Polym. J.*, **1985**, *17*, 85.

(14) S. Agarwal, *Polym. Chem.*, **2010**, *1*, 953.

(15) P. Lecomte, C. Jérôme, *Adv. Polym. Sci.*, **2012**, *245*, 173.

(16) S. Inkinen, M. Hakkarainen, A. C. Albertsson, A. Södergård, *Biomacromolecules*, **2011**, *12*, 523.

(17) M. J. L. Tschan, E. Brulé, P. Haquette, C. M. Thomas, *Polym. Chem.*, **2012**, *3*, 836.

(18) R. H. Platel, L. M. Hodgson, C. K. Williams, *Polym. Rev.*, **2008**, *48*, 11.

(19) F. J. van Natta, J. W. Hill, W. H. Carothers, *J. Am. Chem. Soc.*, **1934**, *56*, 455.

(20) M. A. Woodruff, D. W. Hutmacher, *Prog. Polym. Sci.*, **2010**, *35*, 1217.

(21) V. R. Sinha, K. Bansal, R. Kaushik, R. Kumria, A. Trehan, *Int. J. Pharm.*, **2004**, *278*, 1.

(22) S. Penczek, M. Cypryk, A. Duda, P. Kubisa, S. Słomkowski, *Prog. Polym. Sci.*, **2007**, *32*, 247.

(23) M. Szwarc., Hazel Rossotti, *Nature*, **1969**, *222*, 303.

(24) O. Coulembier, P. Degée, J. L. Hedrick, P. Dubois, *Prog. Polym. Sci.*, **2006**, *31*, 723.

(25) M. Oshimura, A. Takasu, *Macromolecules*, **2010**, *43*, 2283.

(26) M. Honrado, A. Otero, J. Fernández-Baeza, L. F. Sánchez-Barba, A. Garcés, A. Lara-Sánchez, J. Martínez-Ferrer, S. Sobrino, A. M. Rodríguez, *Organometallics*, **2015**, *34*, 3196.

(27) H. Shere, P. McKeown, M. F. Mahon, M. D. Jones, *Eur. Polym. J.*, **2019**, *114*, 319.

(28) A. Kowalski, J. Libiszowski, K. Majerska, A. Duda, S. Penczek, *Polymer*, **2007**, *48*, 3952.

(29) E. Martin, P. Dubois, R. Jérŏme, *Macromolecules*, **2003**, *36*, 5934.

(30) I. Palard, A. Soum, S. M. Guillaume, *Macromolecules*, **2005**, *38*, 6888.

(31) E. Martin, P. Dubois and R. Jérŏme, *Macromolecules*, **2003**, *36*, 7094.

(32) H. R. Kricheldorf, *J. Polym. Sci. Part A: Polym. Chem.*, **2004**, *42*, 4723.

(33) R. L. D. Whitby, L. C. Smith, G. Dichello, T. Fukuda, T. Maekawa, S. V. Mikhalovsky, *Mater. Express*, **2014**, *4*, 242.

(34) M. Oshimura, T. Tang, A. Takasu, *J. Polym. Sci., Part A: Polym. Chem.*, **2011**, *49*, 1210.

(35) J. Jitonnom, W. Meelua, *J. Theo. Comp. Chem.*, **2017**, *16*, 1750003-1.

(36) V. Ladelta, J. D. Kim, P. Bilalis, Y. Gnanou, N. Hadjichristidis, *Macromolecules*, **2018**, *51*, 2428.

(37) M. K. Kiesewetter, E. J. Shin, J. L. Hedrick, R. M. Waymouth, *Macromolecules*, **2010**, *43*, 2093.

(38) J. U. Pothupitiya, N. U. Dharmaratne, T. M. M. Jouaneh, K. v. Fastnacht, D. N. Coderre, M. K. Kiesewetter, *Macromolecules*, **2017**, *50*, 8948.

(39) J. Undin, P. Olsén, J. Godfrey, K. Odelius, A. C. Albertsson, *Polymer*, **2016**, *87*, 17.

(40) J. Engel, A. Cordellier, L. Huang, S. Kara, *ChemCatChem*, **2019**, *11*, 4983.

(41) S. Kobayashi, A. Makino, *Chem. Rev.*, **2009**, *109*, 5288.

(42) A. C. Albertsson, R. K. Srivastava, *Adv. Drug Delivery Rev.*, **2008**, *60*, 1077.

(43) S. Kobayashi, *Macromol. Sym.*, **2006**, *240*, 178.

(44) J. M. Longo, M. J. Sanford, G. W. Coates, *Chem. Rev.*, **2016**, *116*, 15167.

(45) S. Paul, Y. Zhu, C. Romain, R. Brooks, P. K. Saini, C. K. Williams, *Chem. Commun.*, **2015**, *51*, 6459.

(46) R. F. Fischer, *J. Polym. Sci.*, **1960**, *44*, 155.

(47) S. Inoue, K. Kitamura, T. Tsuruta, *Makromol. Chem.*, **1969**, *126*, 250.

(48) T. Tsuruta, K. Matsuura, S. Inoue, *Makromol. Chem.*, **1964**, *75*, 211.

(49) K. Matsuura, T. Tsuruta, Y. Terada, S. Inoue, *Makromol. Chem.*, **1965**, *81*, 258.

(50) R. Mundil, Z. Hostálek, I. Šeděnková and J. Merna, *Macromol. Res.*, **2015**, *23*, 161.

(51) B. Han, L. Zhang, B. Liu, X. Dong, I. Kim, Z. Duan, P. Theato, *Macromolecules*, **2015**, ***48***, 3431.

(52) T. Aida, S. Inoue, *J. Am. Chem. Soc.*, **1985**, *107*, 1358.

(53) T. Aida, K. Sanuki, S. Inoue, *Macromolecules*, **1985**, *18*, 1049.

(54) E. Hosseini Nejad, A. Paoniasari, C. E. Koning, R. Duchateau, *Polym. Chem.*, **2012**, *3*, 1308.

(55) N. D. Harrold, Y. Li, M. H. Chisholm, *Macromolecules*, **2013**, *46*, 692.

(56) A. Bernard, C. Chatterjee, M. H. Chisholm, *Polymer*, **2013**, *54*, 2639.

(57) C. Robert, T. Ohkawara, K. Nozaki, *Chem. Eur. J.*, **2014**, *20*, 4789.

(58) D. J. Darensbourg, R. R. Poland, C. Escobedo, *Macromolecules*, **2012**, *45*, 2242.

(59) A. M. Diciccio, G. W. Coates, *J. Am. Chem. Soc.*, **2011**, *133*, 10724.

(60) D. Liu, Z. Zhang, X. Zhang, X. Lü, *Aust. J. Chem.*, **2016**, *69*, 47.

(61) E. Hosseini Nejad, C. G. W. van Melis, T. J. Vermeer, C. E. Koning, R. Duchateau, *Macromolecules*, **2012**, *45*, 1770.

(62) J. M. Longo, A. M. Diciccio, G. W. Coates, *J. Am. Chem. Soc.*, **2014**, *136*, 15897.

(63) J. Y. Jeon, S. C. Eo, J. K. Varghese, B. Y. Lee, *Beilstein J. Org. Chem.*, **2014**, *10*, 1787.

(64) C. Robert, F. de Montigny, C. M. Thomas, *Nature Commun.*, **2011**, *2*, 586.

(65) Z. Duan, X. Wang, Q. Gao, L. Zhang, B. Liu, I. Kim, *J. Polym. Sci. Part A: Polym. Chem.*, **2014**, *52*, 789.

(66) M. Winkler, C. Romain, M. A. R. Meier, C. K. Williams, *Green Chem.*, **2015**, *17*, 300.

(67) U. Biermann, A. Sehlinger, M. A. R. Meier, J. O. Metzger, *Eur. J. Lipid Sci. Tech.*, **2016**, *118*, 104.

(68) M. Proverbio, N. G. Galotto, S. Losio, I. Tritto, L. Boggioni, *Polymers*, **2019**, *11*, 1222.

(69) A. M. Diciccio, J. M. Longo, G. G. Rodríguez-Calero, G. W. Coates, *J. Am. Chem. Soc.*, **2016**, *138*, 7107.

(70) T. Stöber, G. S. Sulley, G. L. Gregory, C. K. Williams, *Nature Commun.*, **2019**, *10*, 2668.

(71) S. Huijser, E. Hosseininejad, R. Sablong, C. de Jong, C. E. Koning, R. Duchateau, *Macromolecules*, **2011**, *44*, 1132.

(72) E. H. Nejad, A. Paoniasari, C. G. W. van Melis, C. E. Koning, R. Duchateau, *Macromolecules*, **2013**, *46*, 631.

(73) M. J. Sanford, L. Peña Carrodeguas, N. J. van Zee, A. W. Kleij, G. W. Coates, *Macromolecules*, **2016**, *49*, 6394.

(74) N. J. van Zee, M. J. Sanford, G. W. Coates, *J. Am. Chem. Soc.*, **2016**, *138*, 2755.

(75) N. J. van Zee, G. W. Coates, *Angew. Chem. Int. Ed.*, **2015**, *54*, 2665.

(76) D. F. Liu, L. Q. Zhu, J. Wu, L. Y. Wu, X. Q. Lü, *RSC Adv.*, **2015**, *5*, 3854–3859.

(77) J. Liu, Y. Y. Bao, Y. Liu, W. M. Ren, X. B. Lu, *Polym. Chem.*, **2013**, *4*, 1439.

(78) G. Si, L. Zhang, B. Han, Z. Duan, B. Li, J. Dong, X. Li, B. Liu, *Polym. Chem.*, **2015**, *6*, 6372.

(79) P. K. Saini, C. Romain, Y. Zhu, C. K. Williams, *Polym. Chem.*, **2014**, *5*, 6068.

(80) M. Winkler, C. Romain, M. A. R. Meier, C. K. Williams, *Green Chem.*, **2015**, *17*, 300.

(81) Y. Zhu, C. Romain, C. K. Williams, *J. Am. Chem. Soc.*, **2015**, *137*, 12179.

(82) A. Thevenon, J. A. Garden, A. J. P. White, C. K. Williams, *Inorg. Chem.*, **2015**, *54*, 11906.

(83) J. A. Garden, P. K. Saini, C. K. Williams, *J. Am. Chem. Soc.*, **2015**, *137*, 15078.

(84) C. Romain, Y. Zhu, P. Dingwall, S. Paul, H. S. Rzepa, A. Buchard, C. K. Williams, *J. Am. Chem. Soc.*, **2016**, *138*, 4120.

(85) P. K. Saini, G. Fiorani, R. T. Mathers, C. K. Williams, *Chem. Eur. J.*, **2017**, *23*, 4260.

(86) C. Y. Yu, H. J. Chuang, B. T. Ko, *Cat. Sci. Technol.*, **2016**, *6*, 1779.

(87) L. Zhu, D. Liu, L. Wu, W. Feng, X. Zhang, J. Wu, D. Fan, X. Lü, R. Lu, Q. Shi, *Inorg. Chem. Commun.*, **2013**, *37*, 182.

(88) D. F. Liu, L. Y. Wu, W. X. Feng, X. M. Zhang, J. Wu, L. Q. Zhu, D. di Fan, X. Q. Lü, Q. Shi, *J. Mol. Catal. A Chem.*, **2014**, *382*, 136.

(89) L. Y. Wu, D. di Fan, X. Q. Lü, R. Lu, *Chinese J. Polym. Sci.*, **2014**, *32*, 768.

(90) R. C. Jeske, A. M. DiCiccio, G. W. Coates, *J. Am. Chem. Soc.*, **2007**, *129*, 11330.

(91) D. Wannipurage, T. S. Hollingsworth, F. Santulli, M. Cozzolino, M. Lamberti, S. Groysman, M. Mazzeo, *Dalton Trans.*, **2020**, *49*, 2715.

(92) C. Martín, A. Pizzolante, E. C. Escudero-Adán, A. W. Kleij, *Eur. J. Inorg. Chem.*, **2018**, *18*, 1921.

(93) A. M. Diciccio, G. W. Coates, *J. Am. Chem. Soc.*, **2011**, *133*, 10724.

(94) J. Li, Y. Liu, W. M. Ren, X. B. Lu, *J. Am. Chem. Soc.*, **2016**, *138*, 11493.

(95) F. Isnard, M. Lamberti, C. Pellecchia, M. Mazzeo, *ChemCatChem*, **2017**, *9*, 2972.

(96) F. Isnard, M. Carratù, M. Lamberti, V. Venditto, M. Mazzeo, *Cat. Sci. Technol.*, **2018**, *8*, 5034.

(97) F. Santulli, I. D'Auria, L. Boggioni, S. Losio, M. Proverbio, C. Costabile, M. Mazzeo, *Organometallics*, **2020**, *39*, 1213.

(98) B. A. Abel, C. A. L. Lidston, G. W. Coates, *J. Am. Chem. Soc.*, **2019**, *141*, 12760.

(99) J. Burés, *Angew. Chem. Int. Ed.*, **2016**, *128*, 16318.

(100) M. E. Fieser, M. J. Sanford, L. A. Mitchell, C. R. Dunbar, M. Mandal, N. J. van Zee, D. M. Urness, C. J. Cramer, G. W. Coates, W. B. Tolman, *J. Am. Chem. Soc.*, **2017**, *139*, 15222.

(101) J. Martínez, M. Martínez De Sarasa Buchaca, F. de La Cruz-Martínez, C. Alonso-Moreno, L. F. Sánchez-Barba, J. Fernandez-Baeza, A. M. Rodríguez, A. Rodríguez-Diéguez, J. A. Castro-Osma, A. Otero, A. Lara-Sánchez, *Dalton Trans.*, **2018**, *47*, 7471.

(102) A. Otero, A. Lara-Sánchez, J. Fernández-Baeza, C. Alonso-Moreno, J. A. Castro-Osma, I. Márquez-Segovia, L. F. Sánchez-Barba, A. M. Rodríguez, J. C. Garcia-Martinez, *Organometallics*, **2011**, *30*, 1507.

(103) J. A. Castro-Osma, C. Alonso-Moreno, M. V. Gómez, I. Márquez-Segovia, A. Otero, A. Lara-Sánchez, J. Fernández-Baeza, L. F. Sánchez-Barba, A. M. Rodríguez, *Dalton Trans.*, **2013**, *42*, 14240.

(104) F. de La Cruz-Martínez, M. Martínez De Sarasa Buchaca, J. Martínez, J. Fernández-Baeza, L. F. Sánchez-Barba, A. Rodríguez-Diéguez, J. A. Castro-Osma, A. Lara-Sánchez, *ACS Sustain. Chem. Eng.*, **2019**, *7*, 20126.

(105) J. Martínez, J. A. Castro-Osma, C. Alonso-Moreno, A. Rodríguez-Diéguez, M. North, A. Otero, A. Lara-Sánchez, *ChemSusChem*, **2017**, *10*, 1175.

(106) D. J. Darensbourg, S. B. Fitch, *Inorg. Chem.*, **2008**, *47*, 11868.

(107) G. P. Wu, S. H. Wei, X. B. Lu, W. M. Ren, D. J. Darensbourg, *Macromolecules*, **2010**, *43*, 9202.

Chapter 3.

Synthesis of polycarbonates and terpolymers catalysed by group 13 metal complexes

Introduction

Polycarbonates (PCs) are a type of polymer with carbonate group (–O–CO_2R–) repeat units within their main backbone. During the last few years, polycarbonates have arisen a great interest within the scientific and industrial community due to their wide range of applications and properties. Polycarbonate materials can be divided into aliphatic and aromatic polycarbonates. Aliphatic polycarbonates exhibit poor mechanical properties which restrict their use to packaging, as a binder in ceramics or as polyols for the formulation of PHUs foams.[1] On the other hand, aromatic polycarbonates are used as engineering plastics in automotive, electrical and electronic devices and in construction due to their high impact resistance, stiffness, toughness, good thermal stability, transparency, and flame retardancy. In addition, their biodegradability and biocompatibility make them useful candidates in the biomedical sector.[1] Thus, as an example, the aromatic polycarbonate derived from bisphenol-A, 2,2-bis-(4-hydroxyphenyl)propane, is widely used as "engineering plastic" in different industries such as automotive, mobile, laptops, photo and video camera, home appliances, etc. According to Plastics Europe, almost 5 million tons of this polycarbonate are produced annually worldwide.[2]

Traditionally, polycarbonates have been prepared on industrial scale from the polycondensation of a diol, such as bisphenol-A, and phosgene, a highly toxic gas, whose use is being more restricted (Scheme 1). However, companies such as Covestro, SABIC, Mitsubishi and LOTTE are currently using this method.[3]

The development and industrialisation of new processes for the production of this polymeric materials is a current challenge for the chemical community. Thus, in 2002, the Japanese company Asahi Kasei, developed the first industrial process of phosgene-free polycarbonate production based on the reaction between bisphenol-A and diphenyl carbonate (Scheme 1).[4] Since the development of this process, the chemical industry and the scientific community have focused their efforts on the design of new processes for the synthesis of polycarbonates employing CO_2 as chemical feedstock. Thus, new synthetic routes have been developed for the production of polycarbonates bearing aromatic or aliphatic substituents. Some of the most important are shown in Scheme 2.

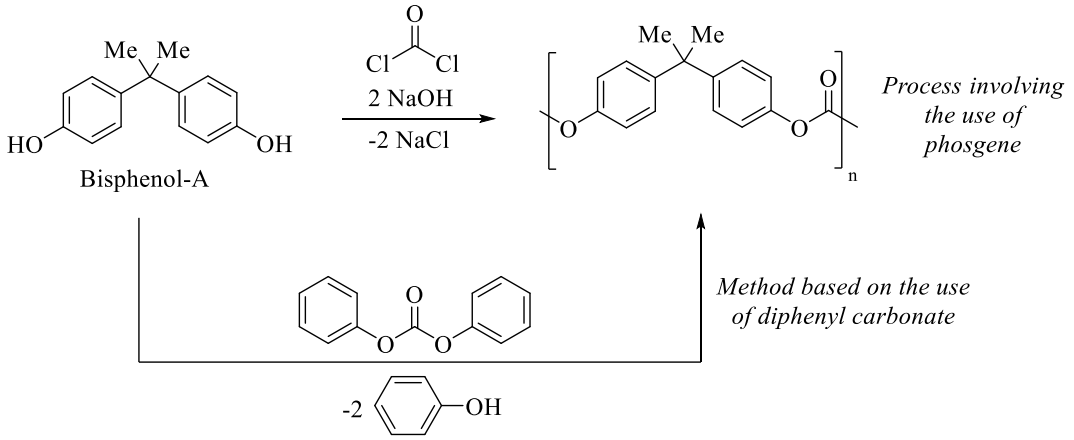

Scheme 1. *Synthesis of aromatic polycarbonate using phosgene or diphenyl carbonate.*

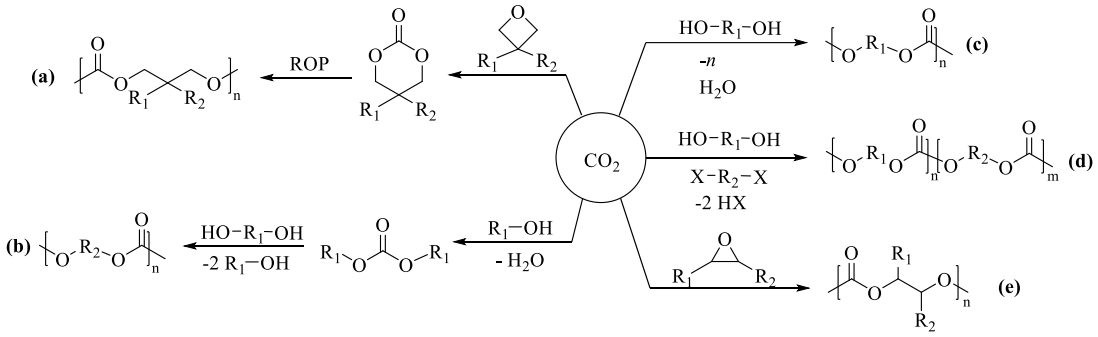

Scheme 2. *New synthetic routes for the synthesis of polycarbonates.*

The Ring-Opening Polymerisation (ROP) of a cyclic carbonate as monomer (Scheme 2a) represents an ideal method for the preparation of high molecular weight polycarbonate materials. This process requires the use of six-, seven- or eight-membered cyclic carbonates as monomers in order to perform the reaction under mild reaction conditions. On the other hand, the polymerisation of most common five-membered cyclic carbonates is not thermodynamically favoured, and, thus, require harsher reaction conditions.[1,5] Currently, many research groups are focused on the design of new catalytic systems for the obtention of polycarbonate materials *via* ROP of five-membered cyclic carbonates.[6]

Another strategy for the synthesis of polycarbonates is the polycondensation reaction between dialkyl/diaryl carbonates, prepared from CO_2 and diols (Scheme 2b). In this process, the PC materials are generated from the transcarbonation reaction between a carbonate and a diol. The polycondensation reaction is performed under atmospheric pressure at moderate temperatures, in the range of 80-140 ºC, to remove the generated volatile alcohols (such as MeOH or EtOH) by distillation. In a second

step, high molecular weight PCs are produced by applying higher temperatures to induce melt chain extension of the oligomers under vacuum so as to allow the elimination of the co-produced volatile alcohol.[1,7] The inherent advantage of this process *versus* the ROP of 5- and 6-membered cyclic carbonates is the access to a larger variety of both aliphatic and aromatic PCs with tuneable properties. However, the control over the molecular weight of the polymeric materials obtained and the design of functional polymeric architectures are more challenging.[1]

The synthesis of polycarbonates by polycondensation between diols and CO_2 (Scheme 2c) shares conceptual similarities and comparable bottlenecks as generally observed for the synthesis of 5- and 6-memebred cyclic carbonates from diols, with the major difference being the proper selection of diol reagents.[1,8] The polycondensation reaction can be carried out either by dehydration employing a desiccant agent,[9] or by alkylation using an alkylating reagent and an excess of base.[10] Alternatively, terpolymerisation of dihalides, diols and CO_2 (Scheme 2d) has also been used to synthesize PCs. However, this process requires the use of a base and is highly dependent on the nature of the dihalide employed.[11,12]

1. Ring-opening copolymerisation of epoxides and CO_2

Despite the enormous progress that has been made on the development of CO_2-sourced PCs obtained from CO_2-derived building blocks, environmentally more friendly and economical synthetic routes have been explored to avoid the additional steps associated with the preparation of CO_2-sourced monomers that decrease time and resource efficiency. Among these strategies, the CO_2/epoxide copolymerisation has been the most studied process in the last 20 years.[1,13,14] The formation of cyclic carbonate and polyether fragments as subproducts is usually observed in this process (Scheme 3). Thus, the design of catalytic systems has been focused not only to increase the catalytic activity, but also the selectivity to polycarbonate formation.

The ring-opening copolymerisation of epoxides and CO_2 requires the use of a catalyst. This catalyst is often a metal complex of the form L_nMX, where M is a metal centre acting as a Lewis acid, L is the ancillary ligand coordinated to the metal atom providing stability to the complex, and X is the initiating group in the catalytic process. The latest can also be an external nucleophile, such as DMAP or PPNCl, which are amongst the most used co-catalysts in these reactions.[14]

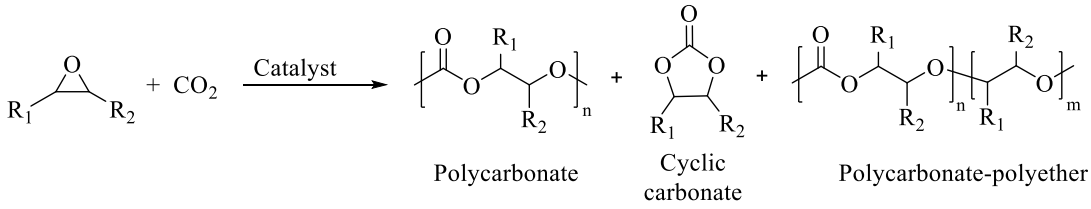

Scheme 3. *Copolymerisation of CO_2 and epoxides to obtain polycarbonates.*

The copolymerisation process generally proceeds through a well-established coordination-insertion mechanism (Scheme 4).[1,15] Firstly, a Lewis acidic metal centre activates the epoxide through coordination, after which the activated monomer undergoes ring-opening *via* nucleophilic attack of the initiating species (X). The resulting metal-alkoxide is then transformed into a metal carbonate by a formal CO_2 insertion (Scheme 4, initiation). In a second step, chain propagation occurs by repetitive and sequential insertion of epoxides and CO_2 leading to fully alternating PCs. Depending on the metal centre, the ligand and/or epoxide structure, the chain propagation is accompanied by potential reactions which may include: (i) two or more consecutive chain enchainments that involve epoxide monomers resulting thus in the formation of ether linkages (Scheme 4, propagation); (ii) intramolecular back-biting reactions that involve alkoxide- or carbonate-terminated chain-ends producing thermodynamically more stable five-membered cyclic carbonates as by-products; (iii) the presence of protic impurities (such as H_2O) may induce chain transfer reactions that affect the molecular weights and the polydispersity values of the produced PCs.

The PC properties are also influenced by the regioselectivity of the epoxide ring-opening and the stereochemistry of the carbonate sequences. The ring-opening of terminal epoxides depends on several factors such as the type and the stereochemistry of the catalyst as well as the presence and structure of co-catalysts. Thus, depending on the regioselectivity in terminal epoxide ring-opening reactions, head-to-head (H-H) and tail-to-tail (T-T) carbonate linkages can be produced by sequential ring-opening of the epoxide with the substituents in consecutive carbon atoms, or head-to-tail (H-T) linkages, obtained by successive ring-opening reactions at the same carbon centre of the epoxide monomer.[1,16] The stereochemistry of the PC is also affected by the regiochemistry of the epoxide ring-opening. Thus, three different stereochemistries can be operative affording either isotactic, syndiotactic or atactic polymer domains (Scheme 5).[1,17]

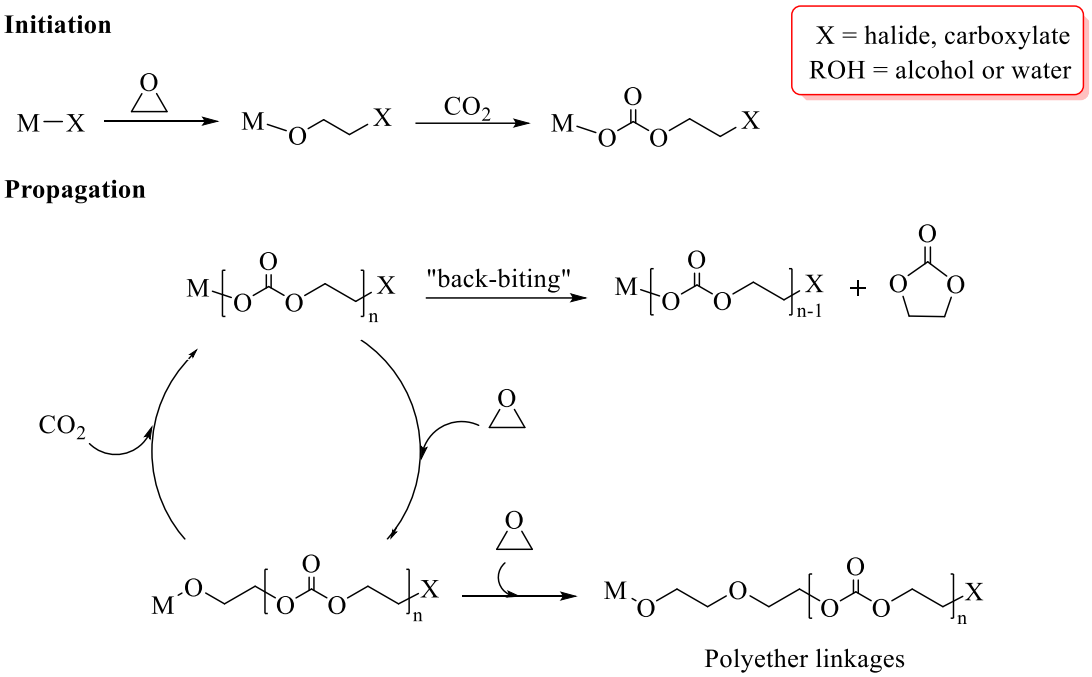

Scheme 4. *Coordination-insertion mechanism for the synthesis of polycarbonates from epoxides and CO_2.*

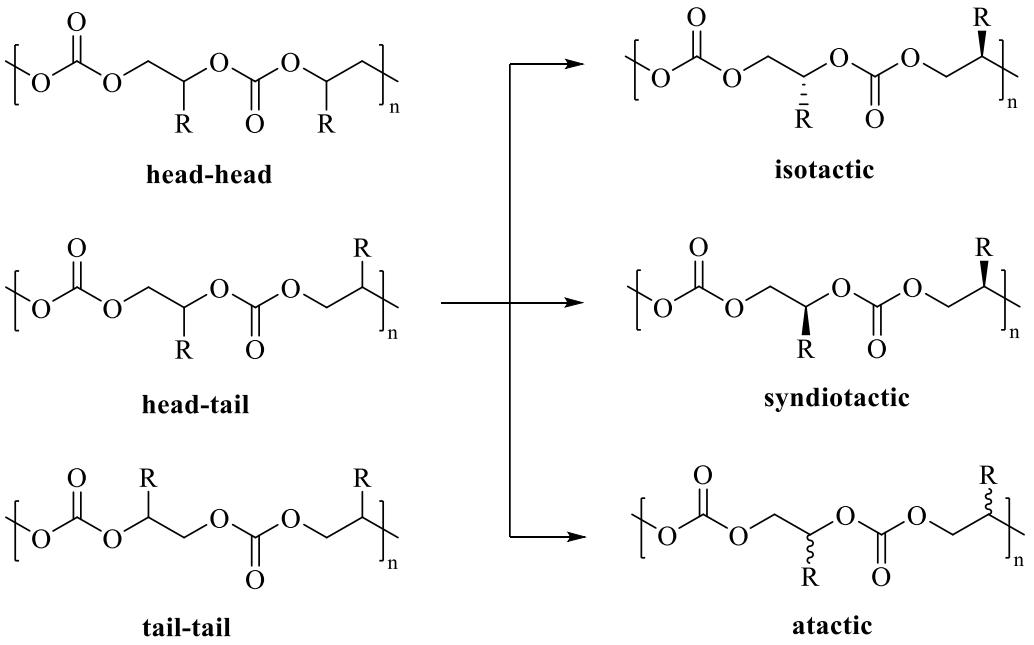

Scheme 5. *Regio- and stereoselectivity in the copolymerisation processes of epoxides and CO_2.*

The copolymerisation of CO_2 has been studied for a great number of epoxides. Propylene oxide (PO), cyclohexene oxide (CHO) and limonene oxide (LO) are the most commonly used, and to a lesser extent, styrene oxide (SO) (Figure 1). The copolymerisation of CHO and CO_2 to generate poly(cyclohexene carbonate) (PCHC) has been widely studied by a great number of research groups. A wide variety of catalysts has been reported to perform this copolymerisation under mild reaction conditions and the resulting polycarbonate shows very high CO_2 incorporation into the polymeric material.[13] On the other hand, the use of propylene oxide is more challenging since it is much more prone to the formation of cyclic carbonate. Hence, careful choice of reaction conditions and catalyst play a key role in the obtention of poly(propylene carbonate) (PPC).[14]

Currently, there is a great interest in the preparation of bio-derived polycarbonates from their corresponding epoxides to produce polycarbonate materials from renewable feedstocks. In this context, poly(limonene carbonate) (PLC) has been prepared from LO and CO_2 using different metal complexes as catalysts for the copolymerisation process.[18,19]

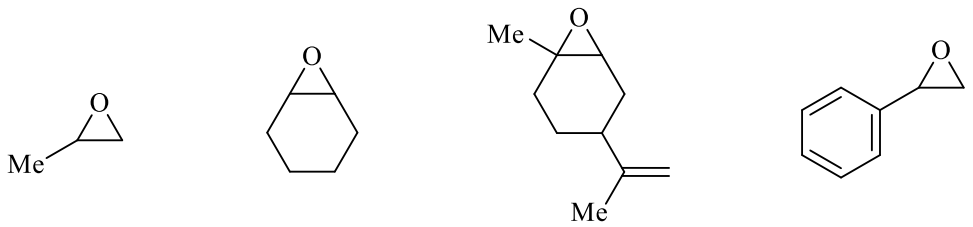

Figure 1. *Common epoxides used for the synthesis of polycarbonates by copolymerisation with CO_2.*

A wide range of Al(III), In(III), Co(III), Cr(III), Fe(III) and Zn(II) metal complexes has been developed as catalysts for the copolymerisation of epoxides and CO_2.[1,13,14,20] In this context, it is worth highlighting few Zn(II) complexes reported during the last decades, whose structure is depicted in Figure 2.

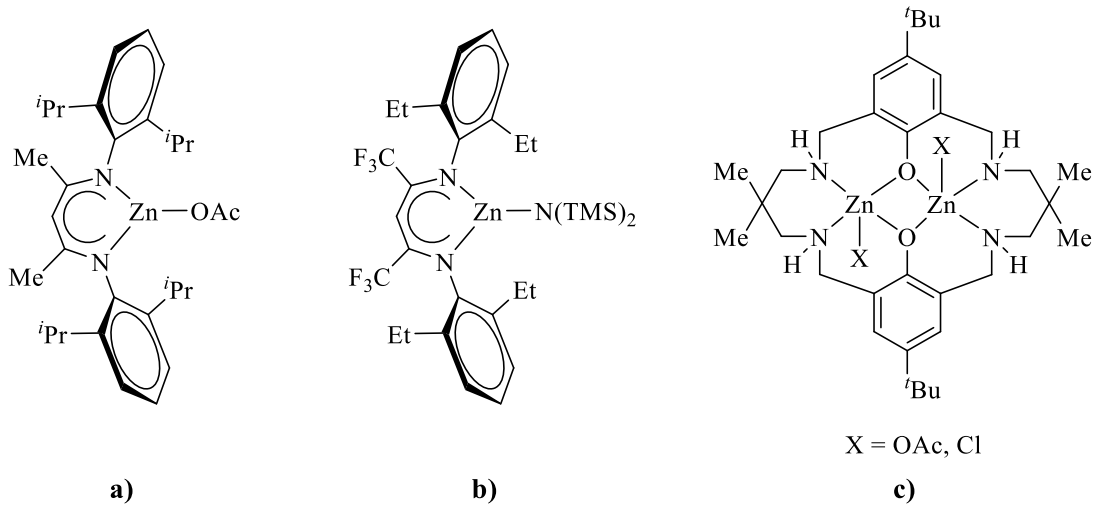

Figure 2. *Zn(II) catalysts for the copolymerisation of epoxides and CO_2*

Coates and co-workers reported in 1998 a highly active zinc acetate catalyst featuring a *β*-diiminate ligand (Figure 2a) for the copolymerisation of CHO and CO_2, obtaining PCHC with high selectivity and molecular weights up to 38 kg mol^{-1} under mild reaction conditions.[21] It was shown that the catalytic activity of these complexes was highly dependent on the steric and electronic properties of the *β*-diiminate ligand.[22–24] More recently, these complexes have also been used for the copolymerisation of PO and CO_2, affording polycarbonate materials with molecular weights up to 35 kg mol^{-1}.[25] Poly(limonene carbonate) was prepared for the first time using a *β*-diiminate zinc acetate catalyst, obtaining TOF values up to 33 h^{-1}, molecular weights up to 9.3 kg mol^{-1} and narrow polydispersities ranging from 1.13-1.34.[18]

More recently, Rieger and co-workers reported the use of another *β*-diiminate zinc complex featuring an amide ligand as initiating group (Figure 2b) for the copolymerisation of a wide range of epoxides and CO_2, demonstrating the great versatility of these complexes for this process.[26] This catalyst afforded the synthesis of PLC with a 100% selectivity under mild reaction conditions (40 ºC and 30 bar) obtaining polycarbonate materials with molecular weights up to 145 kg mol^{-1}. It is worth highlighting that this complex is the most active catalyst known so far for the copolymerisation of LO and CO_2.[26]

Williams and co-workers have described a broad range of air-stable dinuclear zinc complexes in which the two metal centres were supported by a bridging diphenolate ligand (Figure 2c).[27] These complexes exhibited high catalytic activity towards the

synthesis of PCHC at one bar CO_2 pressure in the absence of a co-catalyst.[28] The substituents on the *para* position of the phenol moiety showed to be decisive in the catalyst activity, being the *tert*-butyl analogue the most active. In addition, the synergy between both metal centres and the macrocyclic structure of the phenolate ligand also proved to play a key role in the catalytic activity of these complexes.[28]

1.1. Ring-opening copolymerisation of epoxides and CO_2 catalysed by group 13 metal complexes

As it has been previously discussed, the increasing growth in the polycarbonate's market has arisen a great interest for the development of new catalysts for the copolymerisation of epoxides and CO_2. In this context, metal complexes based on group 13 elements such as aluminium and indium have proven to be highly active as initiators for the synthesis of polycarbonates due to their Lewis acidity and their biocompatibility, which confer them an added value, since one of the applications of these materials lies within the biomedical industry.

Takeda and Inoue reported in 1978 the first aluminium porphyrin complex (Figure 3a) as catalyst for the copolymerisation of PO and CO_2. Reactions required 19 days to achieve complete conversion and only 40% carbonate linkages were found within PPC produced, with molecular weight of 3900 g mol^{-1} and polydispersity value of 1.15.[29] This system led to the discovery of related porphyrin aluminium catalysts (Figure 3b, c).[30–32] Wang and co-workers developed bifunctional aluminium porphyrin complexes possessing tethered quaternary ammonium salts.[31,32] The aluminium complex shown in Figure 3b exhibited the highest catalytic activity for poly(propylene carbonate) synthesis at 80 ºC and 30 bar pressure of CO_2 achieving a TOF value of 560 h^{-1} and molecular weight of 96 kg mol^{-1}. Several aluminium complexes containing shorter alkane linkers, different counterions and different functionalisation at the bromophenyl moiety were also investigated, exhibiting TOF values up to 485 h^{-1}, obtaining polycarbonates with molecular weights up to 36 kg mol^{-1}.[31] Recently, Ema and co-workers developed bifunctional porphyrin aluminium complexes featuring ammonium halides on the phenyl moieties and different aluminium halides for the copolymerisation of CHO and CO_2 (Figure 3c).[30] Both complexes showed TOF values up to 10000 h^{-1}, one of the highest values for the solvent-free copolymerisation of CHO and CO_2 among the monometallic catalysts reported so far. In addition, both

complexes displayed a selectivity higher than 99% towards the formation of poly(cyclohexene carbonate), obtaining the corresponding polymeric materials with molecular weights of 230 kg mol^{-1} and polydispersity values of 1.02.[30]

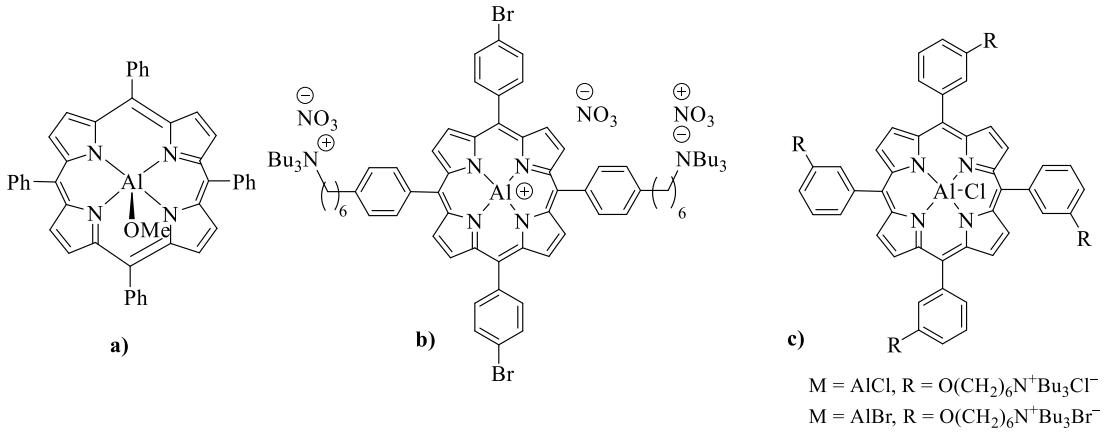

Figure 3. *Porphyrin aluminium catalysts for the copolymerisation of epoxides and CO_2.*

Other aluminium complexes that have been reported as catalysts for the copolymerisation of epoxides and CO_2 are depicted in Figure 4.

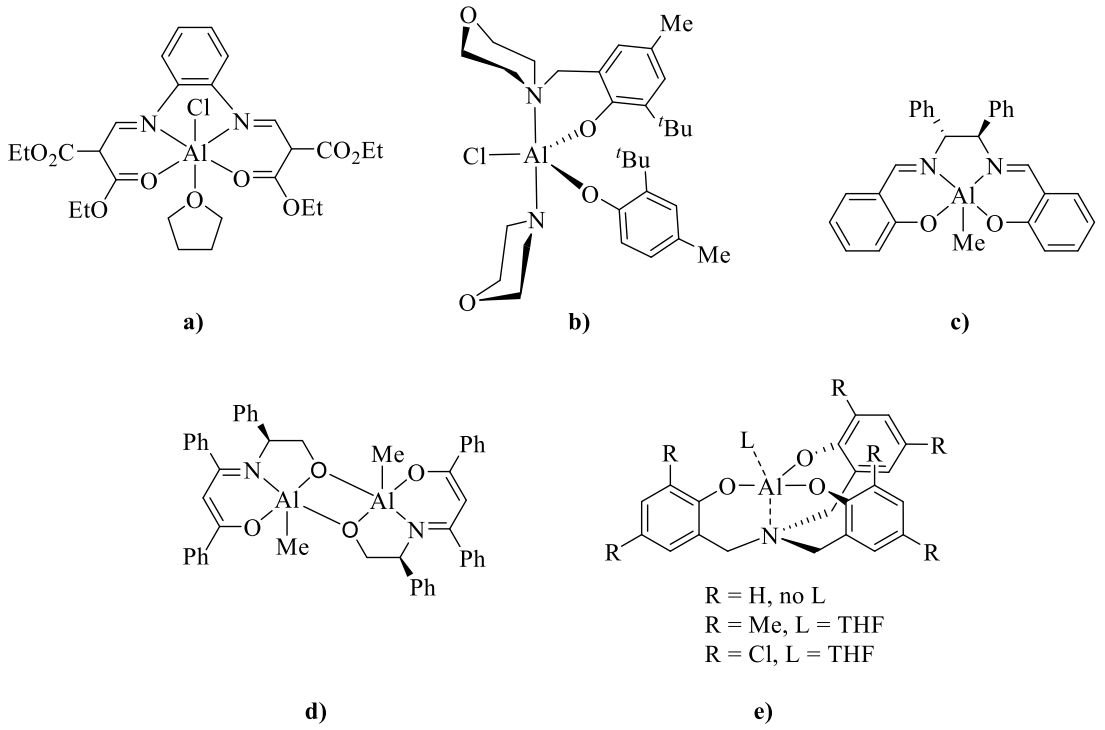

Figure 4. *Aluminium catalysts for the copolymerisation of epoxides and CO_2.*

Firstly, a chloride aluminium complex containing an N_2O_2 ligand (Figure 4a) in combination with tetrabutylammonium halide salts (TBAX, X = Br, Cl, I) or DMAP

as co-catalysts has been reported for the copolymerisation of CHO and CO_2.[33] The catalyst system allowed the production of PCHC in good yields at 80 ºC and 50 bar CO_2 after 20 hours. The polycarbonate materials obtained exhibited moderate molecular weights ranging from 11.1 to 14.5 kg mol^{-1} under these reaction conditions, with polydispersities between 1.47 and 1.63. TOF values were moderate (average of 23 h^{-1}) but polycarbonate content ranged from 98 to 100%. Copolymerisation was observed at lower CO_2 pressure while maintaining high carbonate linkage formation, but yields decreased significantly even after 48 h of reaction.

Bisaminophenolate chloride aluminium complexe (Figure 4b) bearing morpholinyl groups has also been found active for the copolymerisation of CO_2 and CHO in the absence of a co-catalyst.[34] Poly(cyclohexene oxide)-poly(cyclohexene carbonate) (PCHO-PCHC) was obtained in 67% conversion and with 54% carbonate linkages at 60 ºC and 40 bar CO_2 pressure using 0.2 mol% of catalyst loading. The polymeric materials obtained displayed molecular weight up to 29 kg mol^{-1} with broad polydispersity values of 3.16. In order to increase the selectivity towards polycarbonate formation, the aluminium complex was tested in combination with a co-catalyst, however, no catalytic activity was observed when a co-catalyst was added. This finding may be attributed to a strong coordination of the co-catalyst to the metal centre, blocking the active site. It was later reported that this type of catalysts and their derivatives were effective for the ROP of CHO yielding to polyethers with molecular weights up to 500 kg mol^{-1} and polydispersities values between 1.08 and 1.36, explaining the inhibition of polycarbonate formation.[35]

The asymmetric alternating copolymerisation of CHO and CO_2 has also been reported in literature using chiral, C_2–symmetric aluminium complexes containing SALEN-type Schiff base and ketoiminate ligands (Figure 4c, d).[36] Chiral SALEN aluminium complex (Figure 4c) in combination with $[Et_4N][OAc]$ as co-catalyst at 40-80 ºC and 50 bar of CO_2 afforded PCHC with moderate catalytic activity (TOF = 6.3 h^{-1}), obtaining PCHC with molecular weights up to 6800 g mol^{-1} and PDI values of 1.22. Several aluminium complexes were reported, including SALCY-type ligands varying the substitution at 3 and 5 positions of the phenolate groups. All polymers were obtained in 31 to 73% isolated yield after 24 h, containing more than 94% of carbonate linkages, but with low molecular weights (1.9-6.8 kg mol^{-1}) and

polydispersities in the range of 1.22-1.98. Stereochemical characterisation of the diols resulting from the hydrolysis of the polymers showed a moderate bias for the *R*,*R* isomer, obtaining the highest enantioselectivity when the aluminium complex depicted in Figure 4c was used. Achiral and chiral aluminium *β*-ketoiminate complexes (Figure 4d) were also investigated for the CHO/CO_2 copolymerisation. These complexes displayed slightly higher activities with TOF values ranging from 6.7-15 h^{-1} and the polycarbonate materials obtained showed high carbonate content (96-99%). Polymer molecular weights, polydispersity values and enantioselectivity were similar to those observed for the SALEN complexes. Isolated yields of the polymers were lower than those obtained for SALEN-type aluminium complexes, ranging from 16 to 36%.

Finally, a series of amino-tris(phenolate) aluminium complexes (Figure 4e) in combination with suitable nucleophiles as co-catalysts have also been described for the copolymerisation of LO and CO_2 to afford alternating PLC.[19] In general, the aluminium complex featuring methyl substituents on the phenyl moieties and a THF molecule coordinated to the aluminium centre was the most effective catalyst to produce PLC in combination with [PPN][X] (X = Cl, Br) as co-catalysts, with the Cl^- nucleophile giving higher percentage of *trans* polycarbonate units. Molecular weights of the copolymers ranged from 2.4 to 10.5 kg mol^{-1}, with narrow to moderate polidispersities from 1.3 to 1.6. The ability to maintain effective stirring of the reaction mixture was found to be important due to mass transfer issues, which arose from increasing viscosity during the polymerisation, and, thus, affected the molecular weights of the polycarbonate materials. The PLC obtained was epoxidised using 3-chloroperbenzoic acid (MCPBA) in CH_2Cl_2 to afford poly(limonene carbonate oxide) (PLCO) with no change in the polycarbonate backbone.[37] The epoxide groups of the PLCO were further coupled with CO_2 to afford poly(limonene dicarbonate), PLDC, using [PPN][Cl] or [PPN][Br] as catalyst. It is worth noting that the PLDC obtained exhibited glass transition temperatures (T_g) up to 180 ºC (Scheme 6).

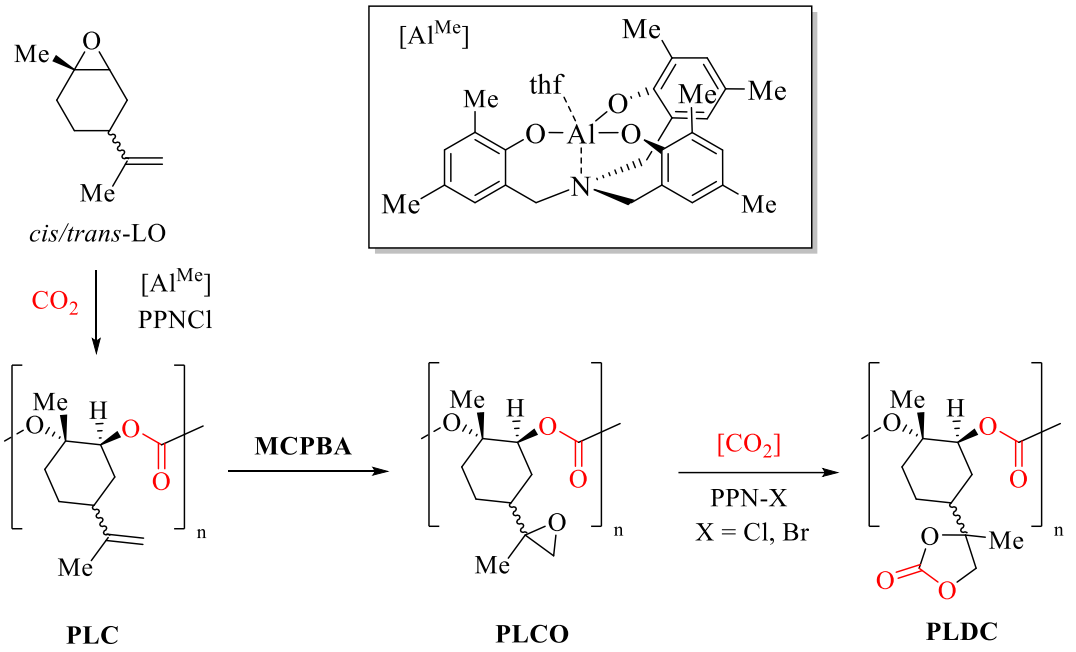

Scheme 6. *Sequential synthesis of PLDC.*

Recently, new heterobimetallic complexes Zn/M (M= Al, Ga, In) have also been developed for the copolymerisation of CHO and CO_2 in the absence of a co-catalyst, at 80 ºC and one bar CO_2 pressure for 2-3 days (Figure 5).[38] Heterobimetallic complexes Zn/M showed to be much less efficient than the homometallic counterparts Zn/Zn. All heteronuclear complexes showed high selectivity (88-95%) with low cyclic carbonate by-product formation. In terms of polymerisation selectivity, heterobimetallic complexes showed lower ether linkages when descending the group 13 series and Ga(III) and In(III) complexes showed reasonable to good selectivity (68-85%) towards the synthesis of PCHC. However, the cationic heterobimetallic Zn/In complex (Figure 5c) displayed a selectivity higher than 99% towards PCHO, which was attributed to the increased Lewis acidity of the In(III) site. Amongst them, heterobimetallic Zn/In complex (Figure 5a) proved to be the most active and selective catalyst for PCHC formation with a TOF value of 6 h^{-1} and molecular weight of 16.8 kg mol^{-1} followed by its analogue featuring a *p*-(trifluoromethyl)benzoate group (Figure 5b) with a TOF value of 3 h^{-1} and molecular weight of 11.2 kg mol^{-1}, and their Zn/Ga and Zn/Al counterparts (Figure 5a) with TOF values of 1 and 0.3 h^{-1} respectively.

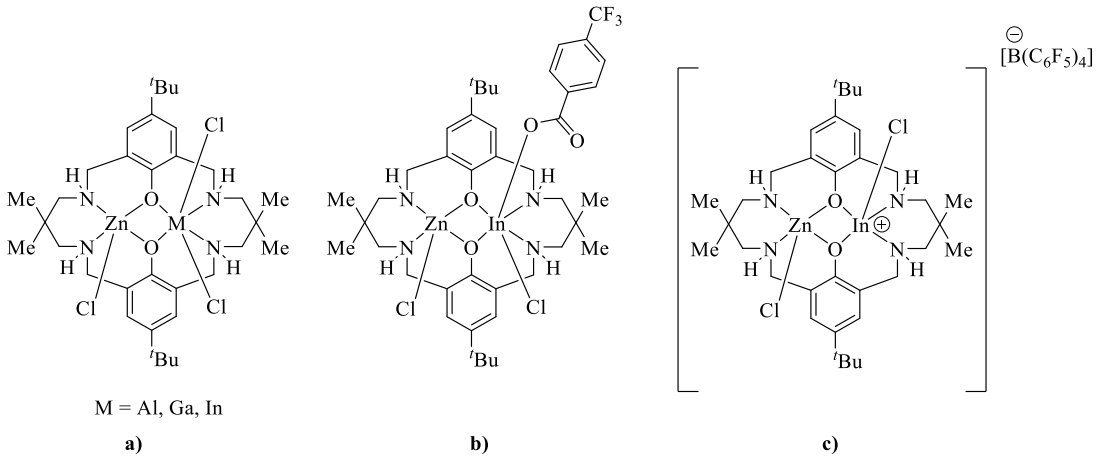

Figure 5 *Heterobimetallic Zn/M (M = Al, Ga, In) catalysts for CO_2 and epoxide copolymerisation.*

On the other hand, few examples have been reported on heavier group 13 metal complexes for the copolymerisation of CO_2 and epoxides to generate polycarbonates. In 2020, Williams and co-workers reported the use of indium SALEN and PHOSPHASALEN complexes as catalysts for the copolymerisation of CHO and CO_2 at 60 ºC and one bar CO_2 pressure using 0.1 mol% of catalyst loading (Figure 6).[39] In general, all catalysts displayed moderate to high selectivity towards the formation of polymer (60-95%), with high carbonate linkages (>99%) except for the chloride and nitro PHOSPHASALEN catalysts, with 66 and 61% carbonate linkages respectively. *Tert*-butoxide PHOSPHASALEN indium complex featuring cumyl substituents on the phenol moieties turned to be the most active catalyst, with a TOF value of 350 h^{-1}. Thus, PCHC was obtained with molecular weights up to 197 kg mol^{-1} and polydispersity values ranging from 1.2-2.0.

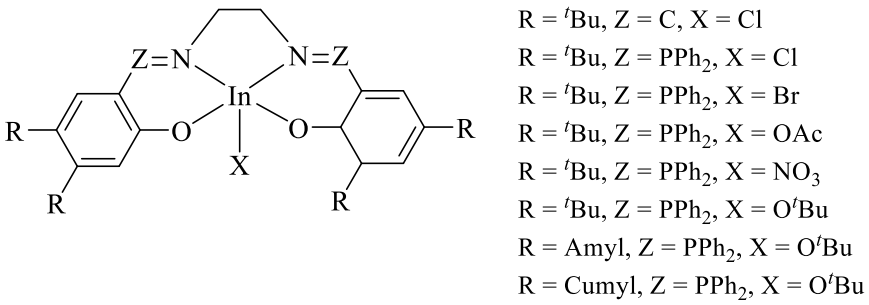

Figure 6. *SALEN/PHOSPHASALEN indium catalysts for CHO and CO_2 copolymerisation.*

As for the mechanism, an unexpected mononuclear pathway was proposed (Scheme 7).[39] The initiation occurs by the coordination of a cyclohexanediol (CHD) molecule to the indium centre. Since a dynamic gas atmosphere is applied, low levels of water ingress resulted in the hydrolysis of CHO to obtain CHD. The alkoxide intermediate In-CHD reacts rapidly with CO_2 to form a stable indium carbonate intermediate InO_2COCHD. Next, the indium carbonate intermediate coordinates a new epoxide molecule to form a monomer bound intermediate. Monomer coordination should occur *cis* to the carbonate group to enable carbonate attack and ring-opening to reform the alkoxide intermediate. After epoxide ring-opening, the five-coordinate alkoxide intermediate is regenerated and the catalytic cycle continues.

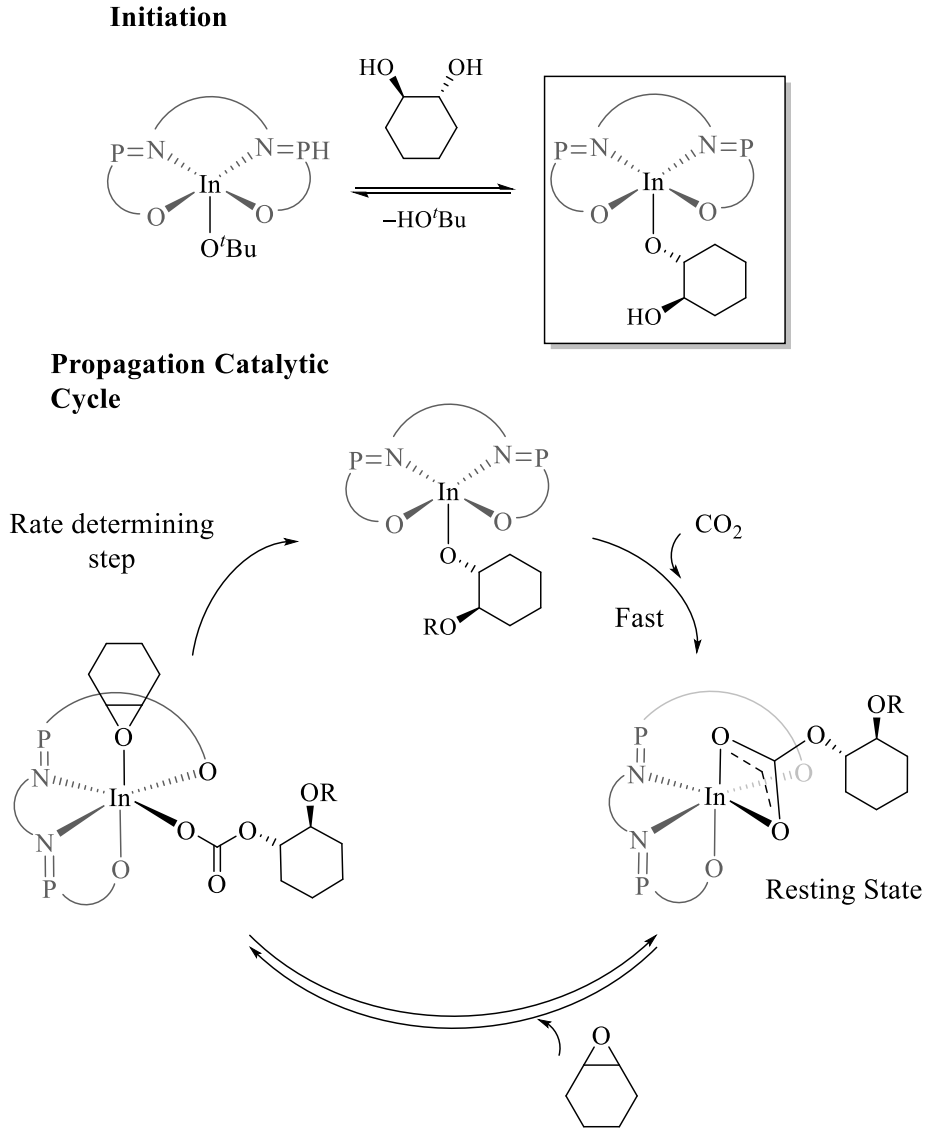

Scheme 7. *Proposed mononuclear mechanism for CO_2/epoxide ROCOP using indium catalysts. R = growing polymer chain.*

2. Catalytic processes for the synthesis of terpolymers

During the last few years, great advances have been made in the development of copolymerisation processes to obtain polymers with a specific composition and microstructure.[40,41] In this context, a great variety of new terpolymers have been developed, whose polymeric chain contains, at least, three different monomers. Therefore, the synthesis of new terpolymers allows the preparation of polymeric materials with enhanced mechanical and thermal properties, better behaviour towards biodegradability and better delivery of drugs compared to the corresponding homopolymers or copolymers obtained from two monomers. Two different structures can be obtained during terpolymerisation processes:

1. Random copolymerisation: The monomeric units are arbitrarily distributed along the polymeric chain (Figure 7a).
2. Block copolymerisation: The monomeric units are separated in different sections or blocks forming the polymeric chain (Figure 7b).

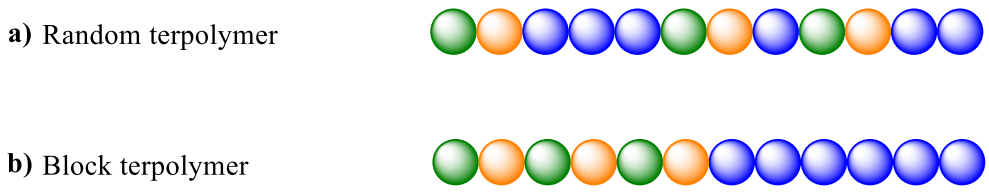

Figure 7. *Possible structures generated during terpolymerisation processes.*

The development of new block copolymers has recently arisen a great interest since the block structure has a strong influence on the morphology and the properties of the resulting polymeric material. Thus, the same terpolymer can be used in different applications such as the plastic, microelectronic and optic industries and as drug delivery systems, depending on the block structure.[42–44] As an example, acrylonitrile-butadiene-styrene (ABS) block terpolymer is widely used in the automotive industry due to its extraordinary rigidity and toughness.[42]

Traditionally, olefins have been employed for the preparation of terpolymers.[42] However, the low biodegradability of the obtained polymers as well as the increase of the CO_2 levels in the atmosphere, have directed the scientific community towards the synthesis of new polymeric materials using CO_2 as one of the monomers.[1,14,41,45] Generally, the copolymerisation between epoxides and CO_2 affords polymers with

poor mechanical properties. In this context, and as it has been previously commented, the addition of a third monomer might improve the mechanical and/or thermal properties of the resulting polymers and increase their applications in different fields. An example is the terpolymer recently synthesized by Rieger *et al*. using CHO, CO_2 and *β*-butyrolactone as monomers, which exhibited better mechanical properties than PCHC.[46]

Up to date, different terpolymers have been synthesised from CO_2, epoxides and a third monomer consisting of a cyclic ester, another epoxide, or a cyclic anhydride (Scheme 8).[1,45] Thus, the terpolymerisation of CO_2 with two different epoxides (Scheme 8a) has been explored in order to modify the properties of the polycarbonate materials, as well as to introduce a functional group within the main backbone such as alkenes or halogens, with the objective of post-functionalisation.[26,47,48] The choice of the catalyst employed for this process plays a key role to guarantee the incorporation of both monomers, especially if both of them exhibit different reactivity (*i.e.* CHO and PO).[47,49,50] The best results for terpolymerization processes have been obtained when using SALEN and aminotriphenolate metal catalysts.[49,51]

The terpolymerisation of CO_2, epoxides and cyclic esters (Scheme 8b) involves two different copolymerisation processes: the copolymerisation of CO_2 and epoxides (ROCOP) and the ring-opening polymerisation (ROP) of cyclic esters. As can be seen in Figure 8, two different terpolymers can be obtained during this terpolymerisation: a random microstructure with the monomers incorporated in the polymeric chain or a polymeric chain with a block polycarbonate-polyester microstructure. The formation of both structures is highly dependent on the reaction conditions, the catalytic system employed for the process and the synthetic method used.[45,52,53]

Finally, another method for the preparation of polycarbonate-polyester terpolymers is the use of cyclic anhydrides with epoxides and CO_2 (Scheme 8c). In this case, two copolymerisation processes which include the epoxide as monomer are combined. Scheme 9 shows the most common cyclic anhydrides used for the synthesis of terpolymers from CHO and PO. It is worth highlighting that the polymer properties are highly dependent on the cyclic anhydride used. Thus, the presence of bi- or tricyclic anhydrides often lead to more rigid and tougher polymeric structures with enhanced thermal properties.[41]

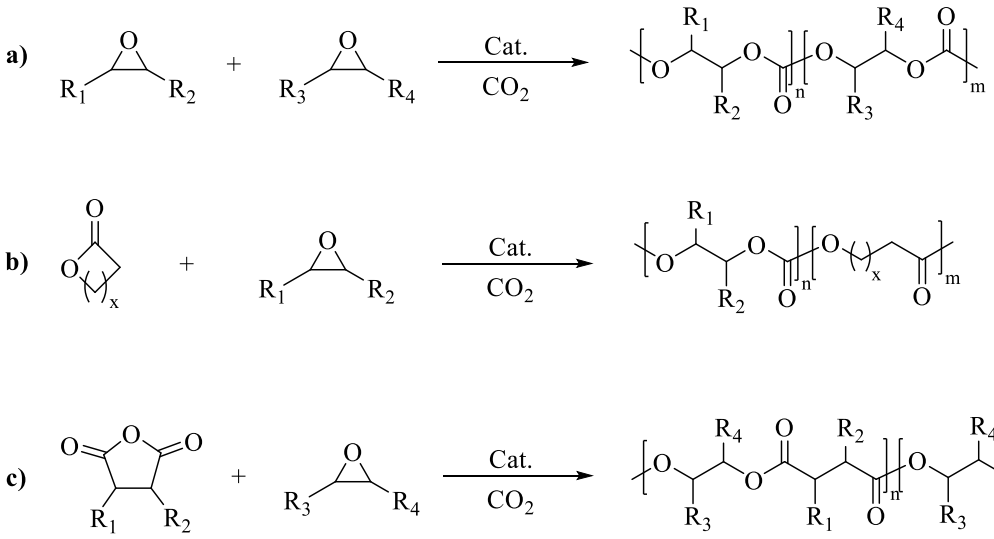

Scheme 8. *Terpolymer synthesis using CO_2, epoxide and: a) a cyclic ester, b) another epoxide, c) a cyclic anhydride.*

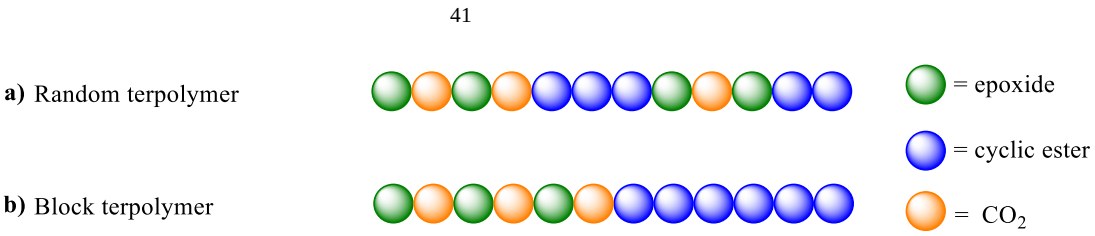

Figure 8. *Possible structures generated by terpolymerisation of epoxides, cyclic esters and CO_2.*

As it has been previously described, zinc and aluminium complexes are amongst the most effective and selective catalysts for the copolymerisation of CO_2 and epoxides. Besides, these complexes have also been proved to be highly active for the synthesis of terpolymers from a wide variety of monomers. Figure 9 shows some of the best catalyst reported for these processes.

A *β*-diiminate zinc catalyst (Figure 9a) has been recently reported for the one-pot terpolymerisation of *β*-butyrolactone (BBL), different epoxides (CHO or LO) and CO_2.[46] Two different polymerisation pathways during the terpolymerisation process were observed depending on the CO_2 pressure. At 40 bar CO_2 pressure, it was observed that the polymerisation began with the exclusive formation of PCHC and only when the CO_2 pressure was released, the ROP of BBL to afford poly(hydroxybutyrate) (PHB) started. On the other hand, when the CO_2 pressure was decreased to 3 bar, the two polymerisation processes proceeded at similar rates, thereby enabling a statistical

incorporation of both monomers. Statistical terpolymers were T_g-tunable whereas the block structures showed enhanced mechanical properties.

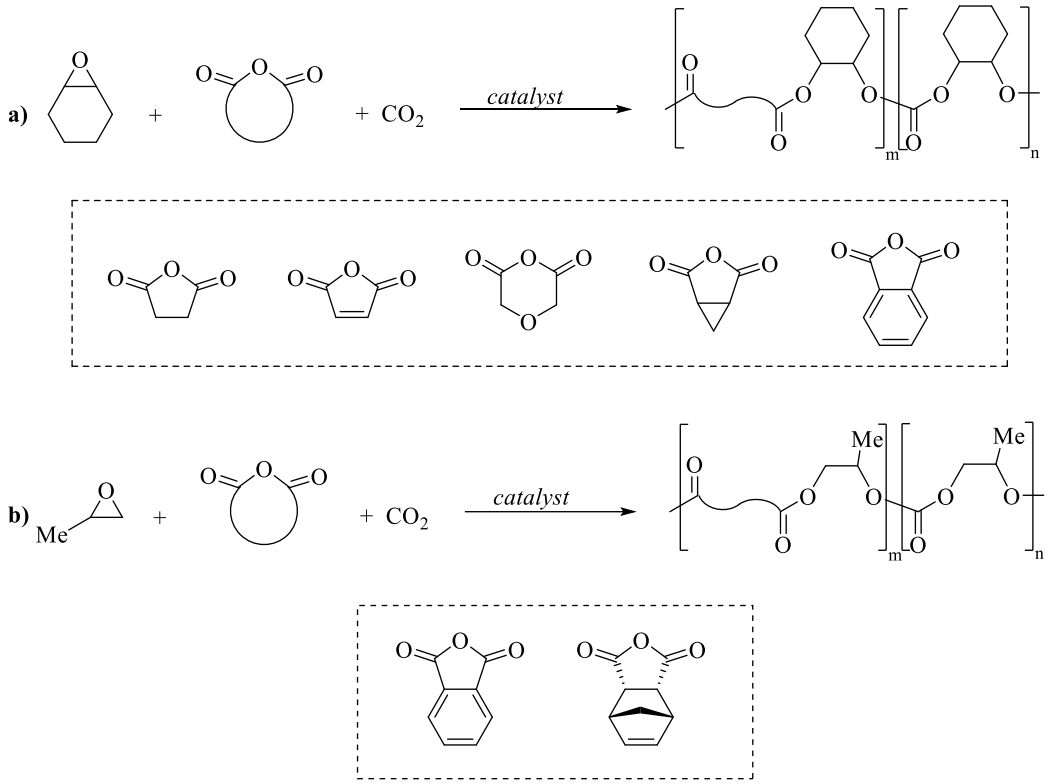

Scheme 9. *Most common anhydrides used for terpolymerisation processes using a) cyclohexene oxide (CHO); b) propylene oxide (PO).*

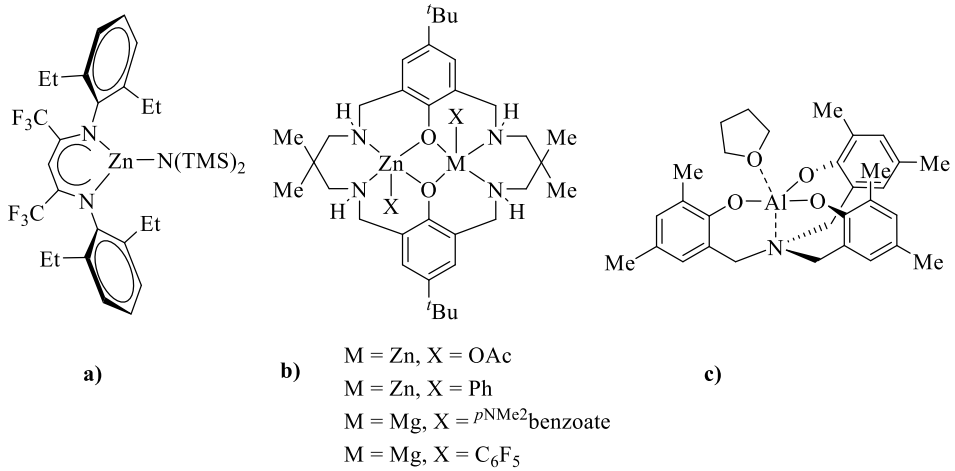

Figure 9. *Aluminium and zinc catalysts used in the synthesis of terpolymers.*

Similarly, different homobimetallic Zn-Zn and heterobimetallic Zn-Mg complexes (Figure 9b) have also been reported for the synthesis of terpolymers from different monomers (lactones, epoxides, anhydrides and CO_2).[53–58] As an example, bimetallic

Zn catalyst featuring phenyl ligands was reported for the terpolymerisation of CHO/VCHO, PA/NA, *ε*-decalactone (DL) and CO_2 to generate pentablock copolymers.[55] Initial experiments were carried out in the presence of the four monomers. However, the reaction only yielded a PC-PE-PC triblock polymer formed by ROCOP processes. To perform the ROP of DL, CO_2 was completely removed from the reaction mixture, however, poly(*ε*-decalactone) (PDL) was not observed even after long reaction times. Rather, the *trans*-cyclic carbonate by-product slowly evolved, evidencing that backbiting reactions from the metal alkoxide intermediate occured faster than the initiation of the ROP of DL. Thus, this problem was overcome by a simple change in monomer addition. First, the catalyst was reacted with PA/CHO/DL under N_2, forming the desired PDL-PE-PDL copolyester. Thereafter, the N_2 atmosphere was replaced with one bar of CO_2, resulting in the selective formation of PC-PDL-PE-PDL-PC pentablock copolymer, with molecular weights up to 22.7 kg mol^{-1} and polydispersity values ranging from 1.05-1.16. The mechanism proposed for the terpolymerisation is shown in Scheme 10.

As for aluminium complexes, an aminotriphenolate aluminium complex (Figure 9c) has been recently developed in combination with PPNCl for the terpolymerisation of CHO, LO and CO_2 to generate the di-block PCHC-PLC polymer.[51] The copolycarbonates obtained showed molecular weights up to 11.9 kg mol^{-1} and polydispersity values ranging from 1.24-1.49. In addition, the terpolymers obtained were further post-functionalised and cross-linked using 2,2'-azobis(2-methyl-propionitrile) (AIBN) obtaining polymeric materials with T_g ranging from 74-150 ºC.

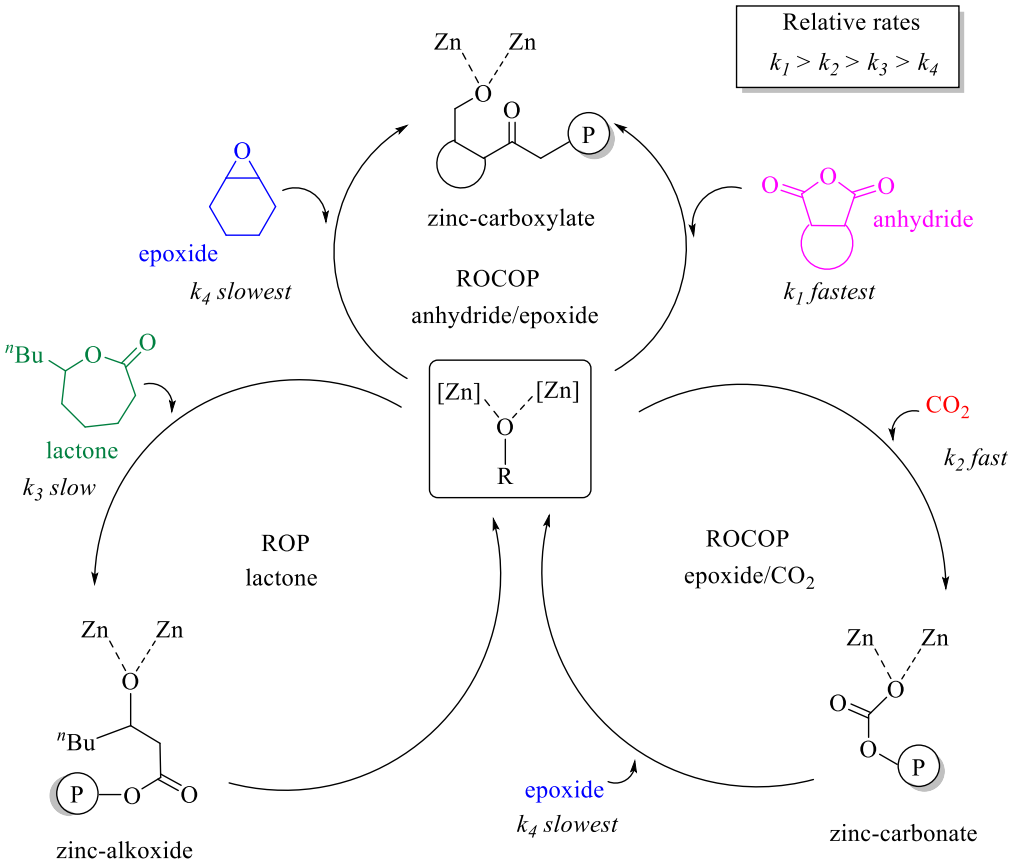

Scheme 10. *Proposed mechanism for the polymerisation of anhydride, epoxide, lactone and CO_2, highlighting the central role of the zinc alkoxide intermediate (P = growing polymer chain).*

Results and discussion

1. Alternating copolymerisation of epoxides and CO_2 catalysed by group 13 metal complexes

As it has been previously described in Chapter 1, one of the main objectives of the synthesis of group 13 metal complexes has been the study of their catalytic activity for the synthesis of polycarbonate materials by copolymerisation reaction between epoxides and CO_2. In this section, the results obtained for the synthesis of PCHC by copolymerisation reaction between CHO and CO_2 employing group 13 metal complexes described in Chapter 1 as catalysts, are presented.

A first screening using all the chloride group 13 metal complexes synthesized (Figure 10) was carried out in order to evaluate their catalytic activity for the synthesis of PCHC by copolymerisation reaction between CHO and CO_2 (Table 1). The initial experiments were performed using 0.5 mol% of metal complex at 60 ºC and 40 bar of CO_2 without the use of a co-catalyst under solvent-free conditions (Scheme 11). As it has been previously mentioned, the reaction is not always selective towards polycarbonate formation and *trans*-cyclic carbonate by-product and polyether chains can also be obtained.

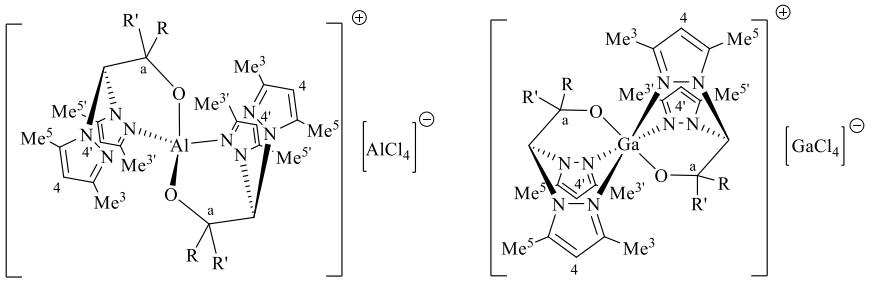

R' = ^{t}Bu, R = H (**2**)
R' = *p*-MeC$_6$H$_4$, R = H (**3**)
R' = *p*-(NMe$_2$)C$_6$H$_4$, R = Ph (**4**)
R' = Ferr, R = H (**5**)

R' = ^{t}Bu, R = H (**6**)
R' = *p*-MeC$_6$H$_4$, R = H (**7**)
R' = *p*-(NMe$_2$)C$_6$H$_4$, R = Ph (**8**)
R' = Ferr, R = H (**9**)

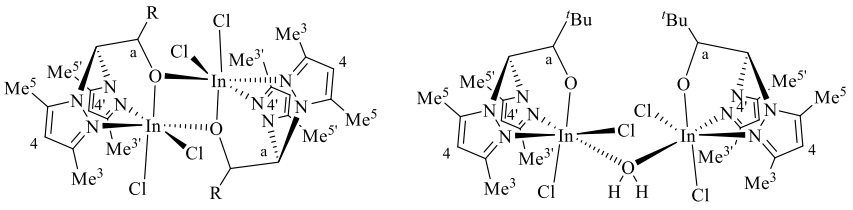

R' = ^{t}Bu, R = H (**10**)
R' = *p*-MeC$_6$H$_4$, R = H (**11**)
R' = *p*-(NMe$_2$)C$_6$H$_4$, R = Ph (**12**)
R' = Ferr, R = H (**13**)

(**14**)

Figure 10. *Chloride group 13 metal complexes tested as catalyst for the copolymerisation of CHO and CO_2.*

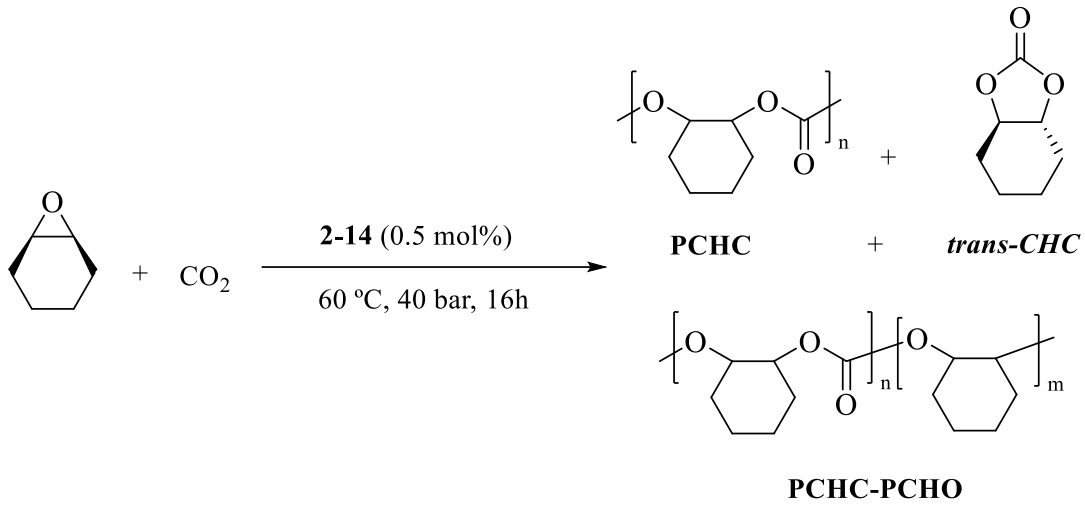

Scheme 11. *Synthesis of poly(cyclohexene carbonate) catalysed by chloride group 13 metal complexes **2-14**.*

As it can be seen from Table 1, complexes **2-14** displayed from low to good catalytic activity and selectivity towards the synthesis of polymeric materials in the absence of a co-catalyst, indicating the absence of back-biting reactions to generate the *trans*-cyclic carbonate by-product. Higher Lewis-acidic aluminium and gallium complexes containing non-planar alkoxide scorpionate ligands (Table 1, entries 1, 4, 5, 8) displayed lower selectivity towards the synthesis of poly(cyclohexene carbonate) than their analogous complexes featuring planar alkoxide ligands (Table 1, entries 2-3; 6-7), which exhibited higher selectivity values ranging from 92 to 99% towards the synthesis of PCHC. In contrast, lower Lewis acidic indium complexes (Table 1, entries 9-13) showed to be the best catalysts for this process, achieving good conversion and excellent selectivity values, except for complex **11** (Table 1, entry 11), which did not display catalytic activity, which was attributed to the low solubility of the catalyst in CHO. Bimetallic indium complexes **10**-**14** afforded the best conversion values, due to the synergetic effect between both metal centres, in agreement with previously reported results. Thus, indium complex **10** (Table 1, entry 9) was selected as the optimal catalyst for the copolymerisation of CHO and CO_2, reaching 72% conversion and 99% selectivity towards the synthesis of PCHC in 16 hours at 60 ^{o}C and 40 bar CO_2 pressure.

Table 1. *CO_2/CHO ROCOP catalysed by chloride group 13 metal complexes **2-14**.*[a]

Entry	Catalyst	Conv. (%)[b]	% carbonate linkages[b]	% polymer selectivity[b]
1	[Al{κ^2-bpzbe}$_2$]$^+$[AlCl$_4$]$^-$ (**2**)	41.5	71	>99
2	[Al{κ^2-bpzte}$_2$]$^+$[AlCl$_4$]$^-$ (**3**)	17	>99	>99
3	[Al{κ^2-bpzappe}$_2$]$^+$[AlCl$_4$]$^-$ (**4**)	17	>99	>99
4	[Al{κ^2-bpzFerr}$_2$]$^+$[AlCl$_4$]$^-$ (**5**)	50	75	>99
5	[Ga{κ^3-bpzbe}$_2$]$^+$[GaCl$_4$]$^-$ (**6**)	45	50	>99
6	[Ga{κ^3-bpzte}$_2$]$^+$[GaCl$_4$]$^-$ (**7**)	42	92	>99
7	[Ga{κ^3-bpzappe}]$^+$[GaCl$_4$]$^-$ (**8**)	55	93	>99
8	[Ga{κ^3-bpzFerr}]$^+$[GaCl$_4$]$^-$ (**9**)	21	37	>99
9	[{InCl$_2$(κ^3-bpzbe)}$_2$(μ-O)$_2$] (**10**)	77	>99	>99
10	[{InCl$_2$(κ^3-bpzte)}$_2$(μ-O)$_2$] (**11**)	-	-	-
11	[{InCl$_2$(κ^3-bpzappe)}$_2$(μ-O)$_2$] (**12**)	72	>99	>99
12	[{InCl$_2$(κ^3-bpzFerr)}$_2$(μ-O)$_2$] (**13**)	26	>99	>99
13	[{InCl$_2$(κ^3-bpzbe)}$_2$(μ-H$_2$O)] (**14**)	70	>99	>99

*[a]Copolymerisation conditions: 25 µmol of complex; [CHO]/[**complex**]= 200:1, 16 hours, 60 ºC, 40 bar CO_2. [b]Determined by ^{1}H-NMR spectroscopy of the crude reaction mixture.*

Once chloride indium complex **10** was found to be the most active and selective catalyst for the copolymerisation process, the catalytic activity of alkyl and amido indium complexes containing the same alkoxide ligand (Figure 11) was also investigated and the results are shown in Table 2. As can be seen in Table 2, chloride indium complex **10** proved to be the most active catalyst for the process. Trimethylsilylamide complex **28** (Table 2, entry 5) and alkyl heterobimetallic lithium-indium complex **18** afforded moderate conversions (54 and 48% respectively) and selectivity values higher than 99% towards the synthesis of PCHC, followed by the mononuclear chloride alkyl complex **23**, which afforded the lowest conversion of 20% (Table 2, entry 4).

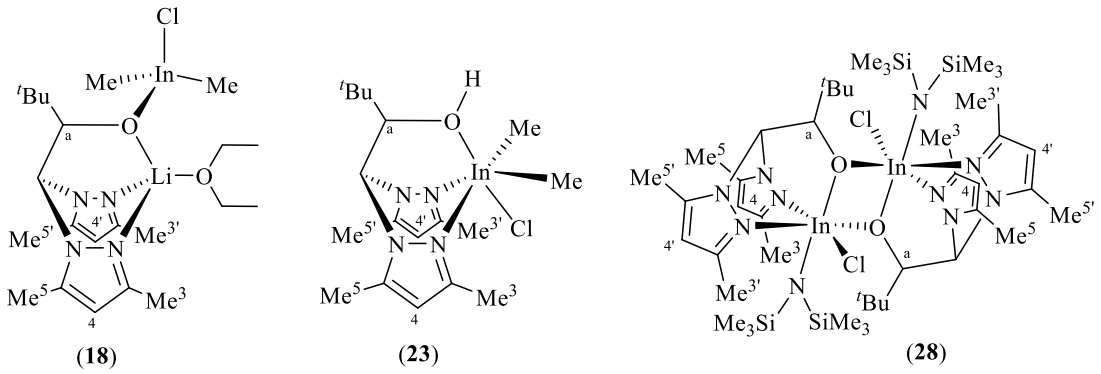

Figure 11. *Alkyl (**18** and **22**) and amido (**28**) indium complexes tested as catalyst for the CHO and CO_2 copolymerisation.*

Table 2. *CO_2/CHO ROCOP catalysed by indium metal complexes.*[a]

Entry	Catalyst	Conv. (%)[b]	% carbonate linkages[b]	% polymer selectivity[b]
1	[{$InCl_2(\kappa^3$-bpzbe)}$_2(\mu$-O)$_2$] (**10**)	77	>99	>99
2	[{$InCl_2(\kappa$-bpzbe)}$_2(\mu$-H_2O)] (**14**)	70	>99	>99
3	[Li(Et_2O){κ^3-bpzbe}(μ-O)$InMe_2Cl$] (**18**)	48	>99	>99
4	[$InMe_2Cl${κ^3-bpzbeH}] (**23**)	20	>99	>99
5	[$InCl(N(SiMe_3)_2)${κ^3-bpzbe}(μ-O)]$_2$ (**28**)	54	>99	>99

[a]*Copolymerisation conditions: 25 µmol of complex; [CHO]/[**complex**]= 200:1, 16 hours, 60 ºC, 40 bar CO_2.* [b]*Determined by ^{1}H-NMR spectroscopy of the crude reaction mixture.*

Once complex **10** was selected as the optimal catalyst for the copolymerisation process, the effect of the reaction temperature was studied, keeping constant the CO_2 pressure at 40 bar and the reaction time at 16 h. As it can be seen from Figure 12, the temperature showed to have a great influence in the catalytic performance of complex **10**. However, the selectivity of the process remained almost constant for all the range of temperatures tested, decreasing to 95% when increasing the reaction temperature to 100 ºC, at which the formation of *trans*-cyclohexene carbonate by-product is favoured. The catalytic activity of complex **10** remained almost constant in the range of temperatures 60-100 ºC. However, it decreased notably to 25 % when decreasing the temperature to 50 ºC.

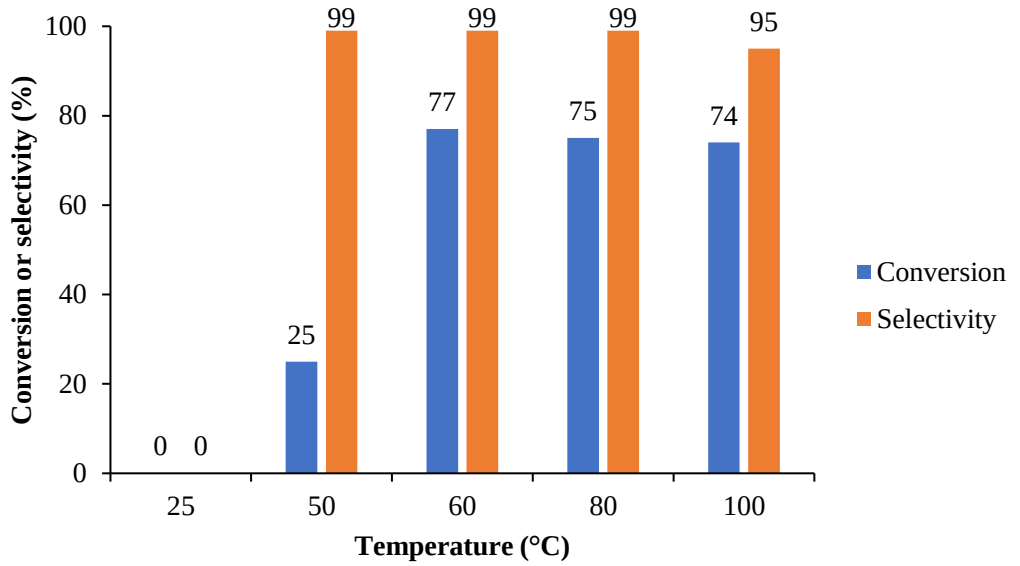

Figure 12. *Effect of the reaction temperature on the catalytic activity of complex **10**.*

The effect of the CO_2 pressure on the copolymerisation process was then investigated at the optimal reaction temperature of 60 ºC for 16 h (Figure 13, Table 3). It is worth highlighting that complex **10** showed to be active for the copolymerisation process even at one bar CO_2 pressure, achieving 47% conversion and a selectivity towards the formation of the polycarbonate material higher than 99%. The selectivity of the process remained constant for all the range of pressures tested and the catalytic performance of complex **10** increased as the pressure increased, reaching 77% conversion at 40 bar.

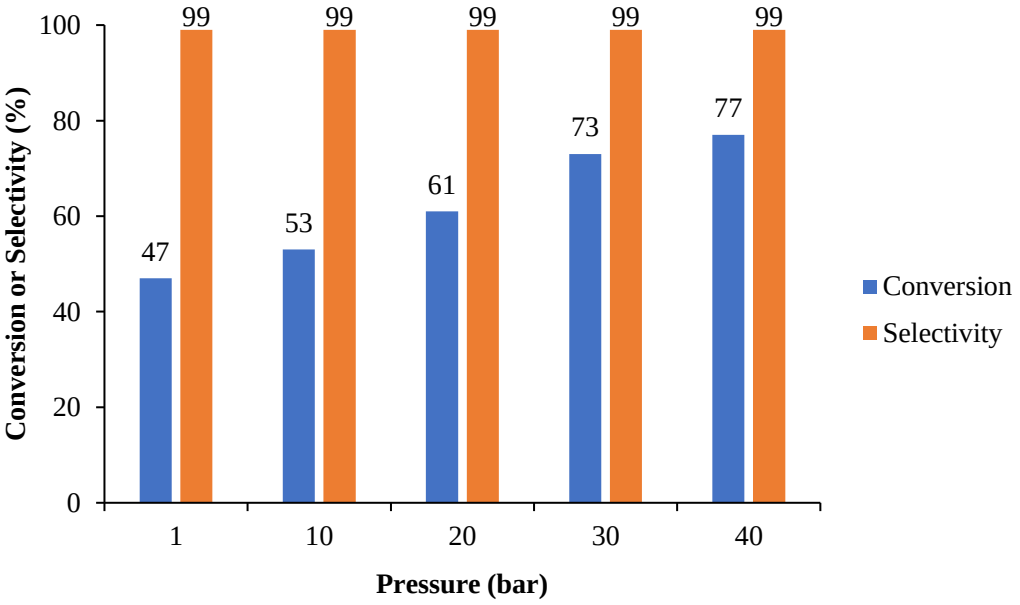

Figure 13. *Effect of the CO_2 pressure on the catalytic activity of complex **10**.*

Table 3. *Effect of the reaction pressure on the synthesis of PCHC catalysed by complex **10**.*[a]

Entry	Pressure (bar)	Conv (%)[b]	% PCHC	$M_{n,exp.}$[c]	PDI[c]
1	1	47	>99	2865	1.16
2	10	53	>99	2840	1.13
3	20	61	>99	2800	1.10
4	30	73	>99	2770	1.20
5	40	77	>99	2621	1.15

[a]*Copolymerisation conditions: 25 µmol of complex; [CHO]/[**complex**]= 200:1, 16 hours, 60 ºC.* [b]*Determined by ^{1}H-NMR spectroscopy of the crude reaction mixture.* [c]*Determined by GPC.*

As it can be seen from Table 3, the molecular weight of the polycarbonate material slightly increased when decreasing the reaction pressure while the polydispersity values remained almost constant ranging from 1.13 to 1.20. As an example, Figure 14 shows the GPC traces for PCHC synthesised at 1 bar and 40 bar CO_2 pressure after 16h time.

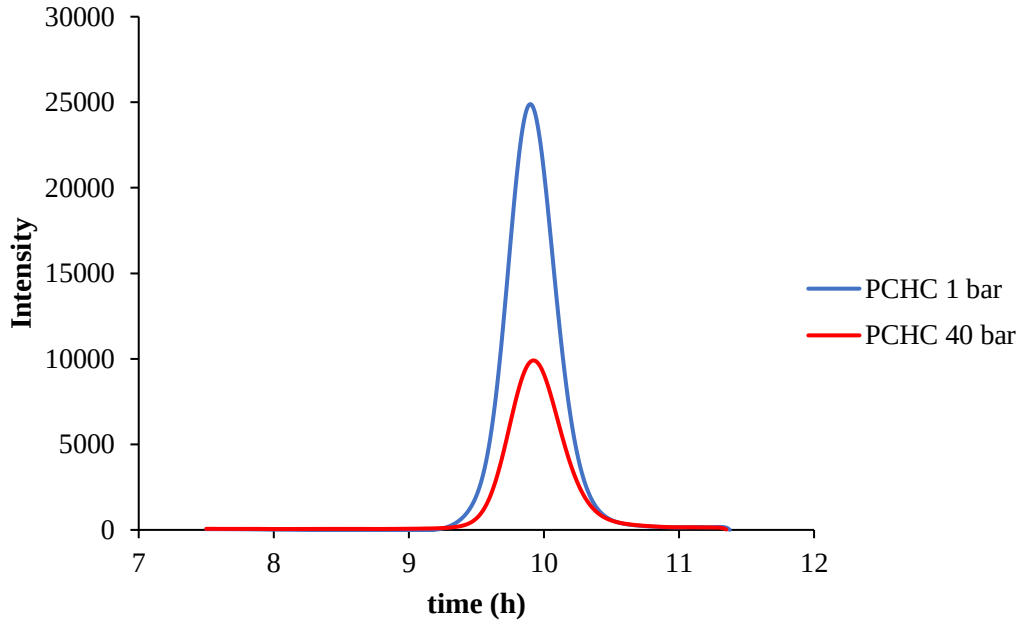

Figure 14. *GPC traces for poly(cyclohexene carbonate) at one (blue) and 40 bar (red) CO_2 pressure.*

In order to maximise the sustainability of the process and perform the copolymerisation process under the mildest reaction conditions, the reaction temperature and pressure were set at 60 ºC and one bar CO_2 pressure, respectively. Then, the effect of the reaction time on the copolymerisation process was also studied (Figure 15), obtaining TOF values ranging from 4 to 11 h^{-1} for reaction times between 2 and 24 hours (Table 4). It is worth highlighting that conversion increased linearly until reaching 42% after 8 hours. Then, the conversion increased much slower reaching 52% after 24 hours, which can be attributed to mass transfer issues, due to the increase of the viscosity of the reaction mixture. The molecular weights of the polycarbonate materials synthesised increased as the conversion of the copolymerisation process increased, obtaining in all cases narrow polydispersity values ranging from 1.15-1.20 (Figure 16). Generally, the molecular weights obtained for the polycarbonate materials proved to be approximately 5 times lower than the theoretical values calculated from the conversion obtained (Table 4), which was indicative of the presence of water or cyclohexenediol acting as chain-transfer agents, and, thus, reducing the molecular weight of the polycarbonates obtained. This was further confirmed by MALDI-ToF analysis.

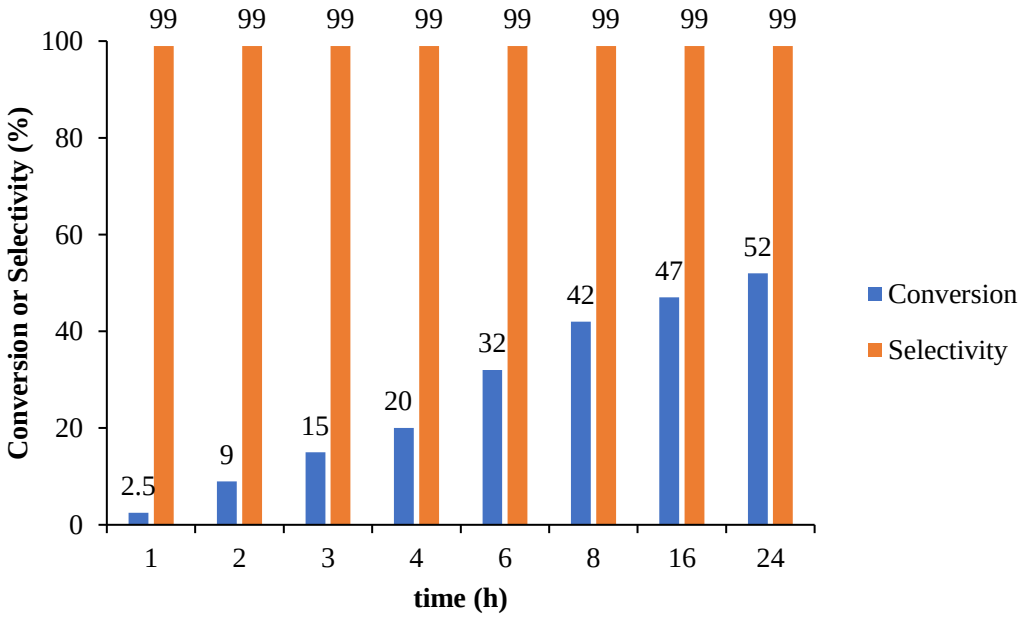

Figure 15. *Effect of the reaction time on the catalytic activity of complex **10**.*

Table 4. *Effect of the reaction time on the synthesis of poly(cyclohexene carbonate) catalysed by complex **10**.*[a]

Entry	t (h)	Conv (%)[b]	PCHC (%)[b]	TOF (h^{-1})[c]	$M_{n,theo}$[d]. (g/mol)	$M_{n,exp.}$[e] (g/mol)	PDI[e]
1	1	2.5	>99	4.6	653	-	-
2	2	9	>99	8.8	2556	-	-
3	3	15	>99	10	4260	850	1.21
4	4	20	>99	10.1	5680	1150	1.20
5	6	32	>99	10.7	9088	1800	1.20
6	8	42	>99	10.5	11928	2400	1.18
7	16	47	>99	6	13348	2865	1.16
8	24	52	>99	4.3	14768	3100	1.15

*[a]Copolymerisation conditions: 25 µmol of complex; [CHO]/[**complex**]= 200:1, 16 hours, 60 ºC. [b]Determined by ^{1}H-NMR from the reaction mixture; [c]TOF = (mol product) / (mol catalyst × time); [d]$M_{n,theo.}$ = (monomer/initiator) × (% conversion) × (M_w CHC). [e]Determined by GPC using polystyrene standards in THF.*

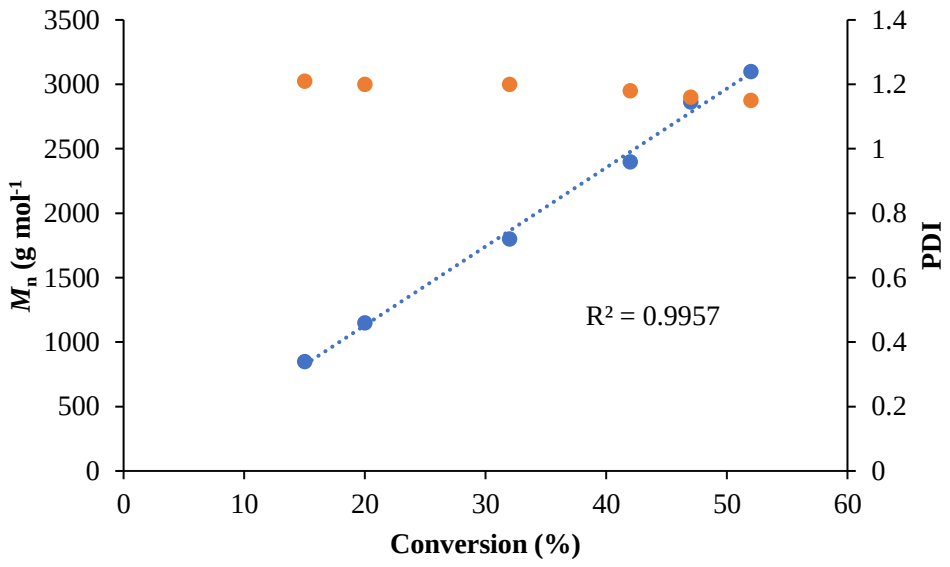

Figure 16. *Plot of molecular weight (M_n) of the polycarbonate vs conversion and polydispersity (M_w/M_n) vs conversion for reactions catalysed by complex **10**.*

The polycarbonate materials synthesised were characterised by IR, ^{1}H-NMR and ^{13}C-{^{1}H}-NMR spectroscopy, as well as MALDI-ToF mass spectrometry. The

determination of molecular weights was performed by gel permeation chromatography (GPC), while the thermal properties were evaluated by thermogravimetric analysis (TGA) and differential scanning calorimetry (DSC).

The polycarbonate microstructure was determined by ^{1}H-NMR and ^{13}C-{^{1}H}-NMR (Figures 17 and 18 respectively).[15] ^{1}H-NMR spectrum exhibited five signals with high intensity corresponding to the methylene and methine (CH_2, CH) groups of the cyclohexyl ring, and low intensity signals corresponding to chain-end groups (Figure 17). Similarly, ^{13}C-{^{1}H}-NMR study (Figure 18) allowed to determine the tacticity of the synthesised polycarbonate materials.[1] Thus, an atactic structure was proposed since both signals corresponding to the isotactic dyad at 153.8 ppm and syndiotactic dyad at 153.3 and 153.2 ppm, were observed.

The MALDI-ToF spectrum for PCHC showed two end-group series of peaks with a *m/z* interval of 142 mass units, indicating a controlled alternating microstructure (Figure 19). The major series (blue diamond) is in good agreement with a polymeric chain with two hydroxyl end-groups in the polycarbonate material. A second major series (green diamond) also containing two hydroxyl end groups corresponding to *trans*-cyclohexanediol was also observed, indicating the existence of chain transfer agents during the copolymerisation, as expected due to the low molecular weights obtained for the polycarbonate materials synthesised.

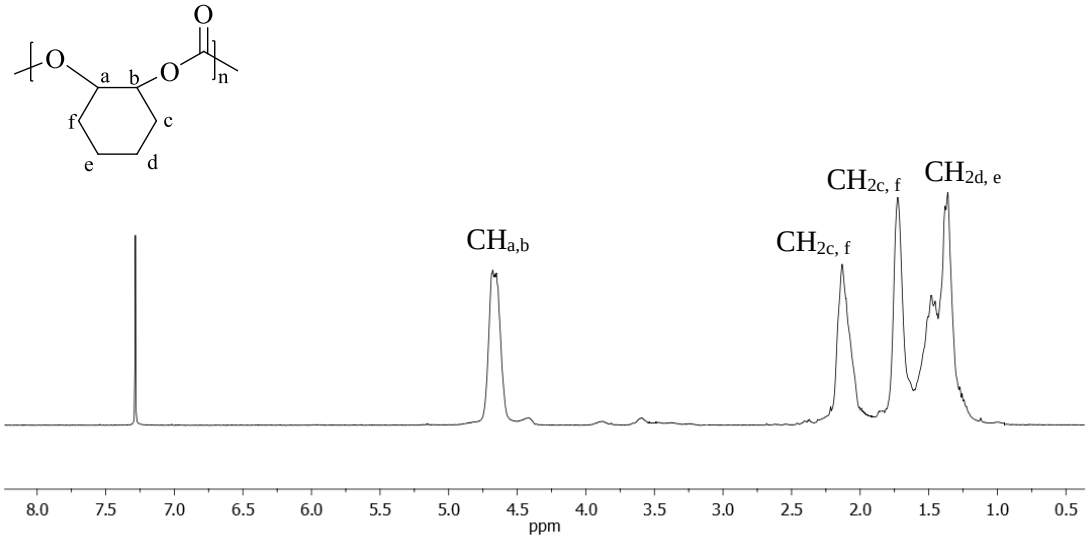

Figure 17. *^{1}H-NMR spectrum for poly(cyclohexene carbonate) in $CDCl_3$.*

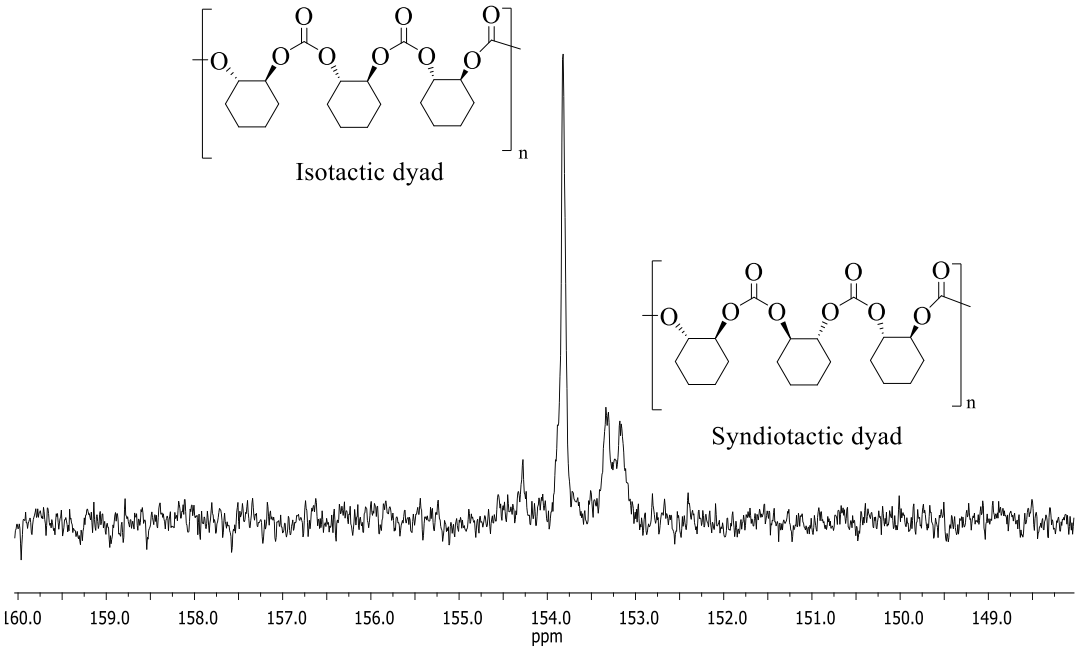

Figure 18. *^{13}C-{^{1}H}-NMR spectrum for poly(cyclohexene carbonate) in $CDCl_3$.*

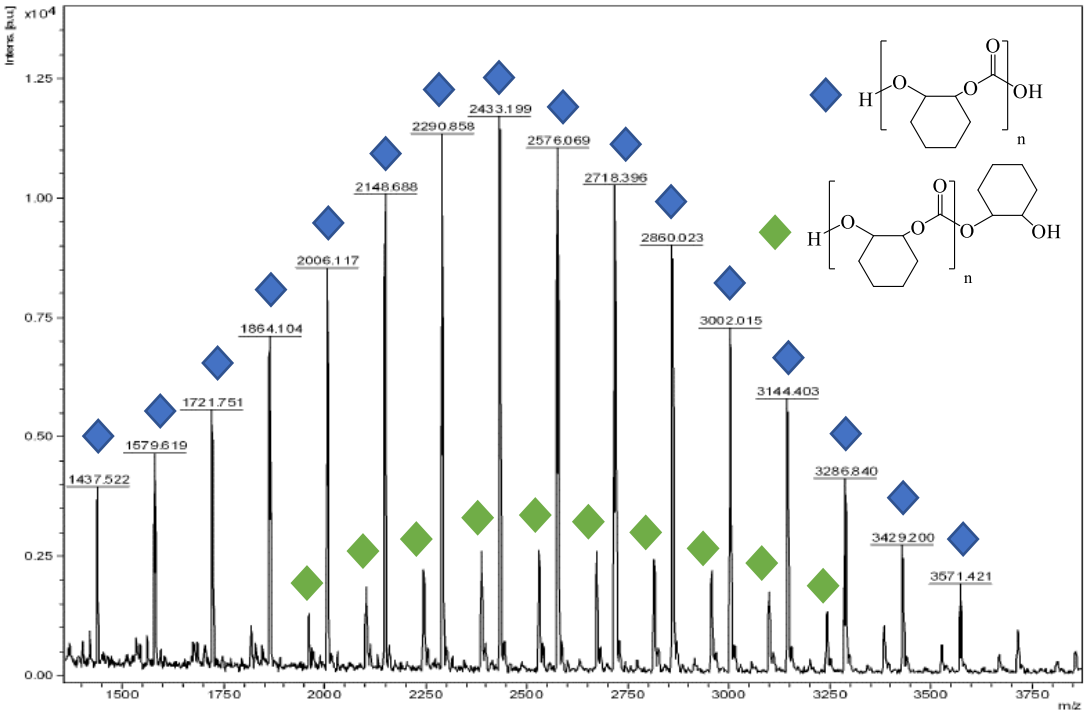

Figure 19. *MALDI-ToF spectrum for poly(cyclohexene carbonate) obtained employing complex **10**.*

Finally, the thermogravimetric analysis of PCHC showed that it is stable in the range of temperatures between 0-200 ºC (Figure 20), while the differential scanning

calorimetry (DSC) exhibited only one value of T_g at 65 ºC (Figure 21). This T_g value is slightly lower than others found in the literature for atactic PCHC, probably due to the low molecular weight of the PCHC obtained.[45]

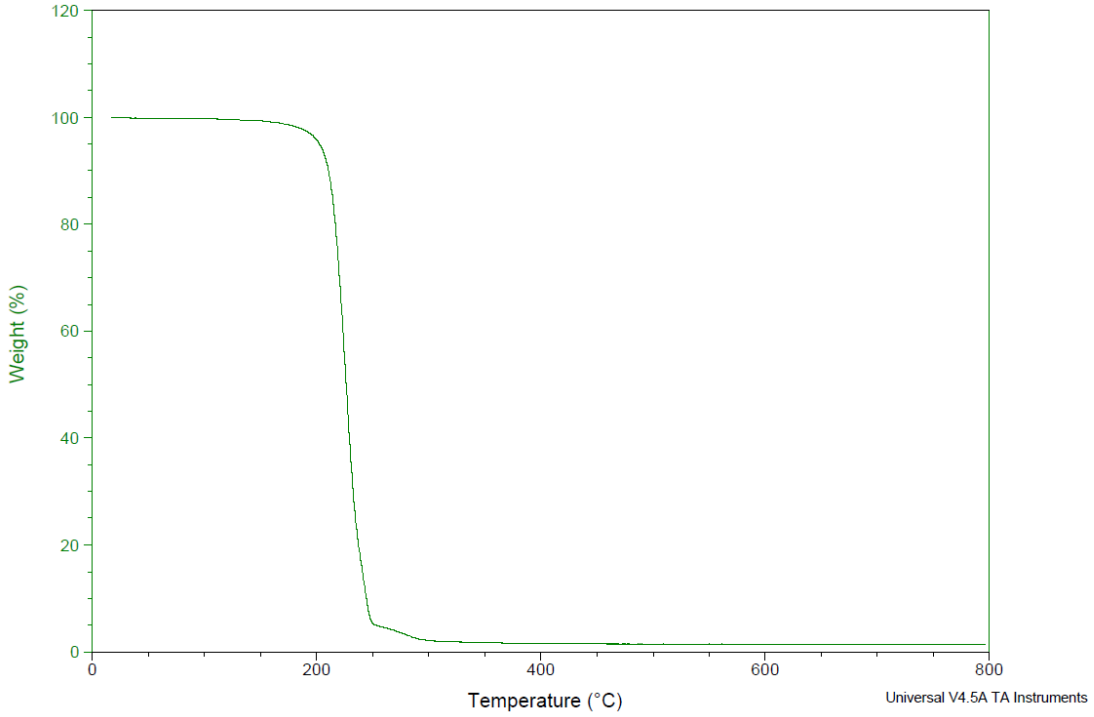

Figure 20. *TGA thermogram for poly(cyclohexene carbonate).*

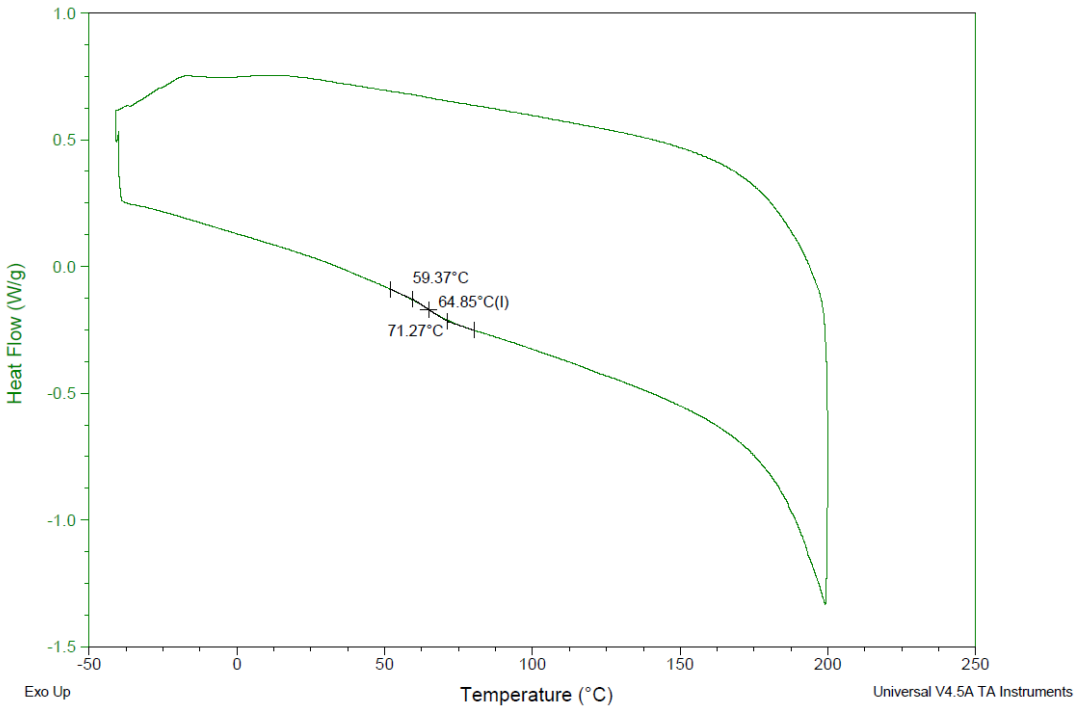

Figure 21. *DSC thermogram for poly(cyclohexene carbonate).*

2. Synthesis of terpolymers catalysed by complex 10

Once the catalytic activity of some of the group 13 metal complexes synthesised in this dissertation were tested for the copolymerisation process of CHO/CO_2 and complex **10** was determined to be the most active and selective for this process, the scope of application of this compound was further extended and was studied as catalyst for the synthesis of terpolymers. As it has been previosuly discussed, block terpolymers have received great attention during the last years since their composition has a strong influence on the morphology and properties of the resulting polymer, and, therefore, on their potential applications. In this section, the results obtained for the synthesis of terpolymers using complex **10** are presented.

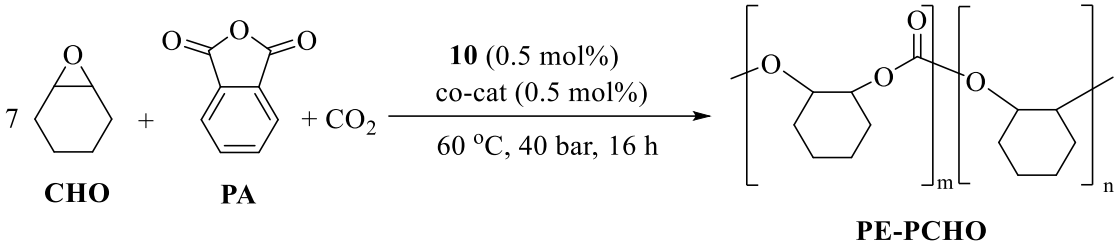

CHO **PA** **PE-PCHO**

Scheme 12. *Synthesis of terpolymers derived from CHO, PA and CO_2 catalysed by **10**.*

Firstly, the catalytic activity of complex **10** towards the synthesis of terpolymers derived from CHO, CO_2 and phthalic anhydride (PA) was investigated. Reactions were carried out in the absence of a solvent, at 60 ºC and 40 bar CO_2 pressure for 16 hours, and using **10**:co-catalyst:PA:CHO of 0.5:0.5:100:700 molar ratio (Scheme 12).

Initially, the catalytic activity of complex **10** for terpolymerisation processes was studied in the absence of a co-catalyst (Table 5, entry 1), obtaining 65 % selectivity towards the synthesis of PCHO and 35% selectivity towards the formation of poly(cyclohexene phthalate). No formation of the desired PCHC was observed. Thus, the addition of different co-catalysts was investigated next in order to increase the selectivity of the process towards the synthesis of polycarbonate (Table 5, entries 2-4). The selectivity towards the synthesis of polyester increased up to 100% when DMAP or KO^{t}Bu were used as co-catalysts, and to 65% when using PPNCl. However, PCHC formation was not detected. Finally, in order to determine whether the presence of CO_2 could influence and drive the homopolymerisation of CHO towards the formation of PCHO, two different experiments in the absence of CO_2 were carried out in neat

conditions (Table 5, entry 5) and using toluene as solvent (Table 5, entry 6). Both experiments showed similar selectivity towards the formation of polyester (PE) (33 and 36 % respectively), which followed the same trend as the experiment carried out in the presence of CO_2 (Table 5, entry 1), indicating that CO_2 did not affect the selectivity of the process towards the formation of PCHO.

In order to gain a further insight into the reaction mechanism and determine the catalytic active species for the terpolymerisation process, a stoichiometric reaction between complex **10**, CHO and PA was performed (Figure 22). The addition of one equivalent of CHO and PA resulted in the appearance of two signals at 7.45 and 7.36 ppm, indicating that the first step of the copolymerisation process is the coordination of the cyclic anhydride by the catalyst and possible ring-opening to generate a carboxylate species. On the other hand, the signal corresponding to the CHO remained unchanged. After warming up at the reaction mixture to 60 ºC during 16 h, new signals corresponding to the polyester (5.00 ppm) and polyether (3.55 ppm) moieties were observed.

Table 5. *Synthesis of terpolymers from CHO, CO_2 and PA catalysed by complex **10**.*[a]

Exp.	co-cat.	Conv. (%) CHO[b]	Conv. (%) PA[b]	PE (%)[b]	PCHO (%)[b]	PCHC (%)[b]
1	-	93	65	35	65	-
2	DMAP	22.5	100	100	-	-
3	PPNCl	52	73	74	26	-
4	KO^{t}Bu	19	100	100	-	-
5[c]	-	48	100	33	67	-
6[c, d]	-	70	100	36	64	-
7[c]	DMAP	23	100	100	-	-

[a]*Copolymerisation conditions: 25 μmol of complex **10**; [CHO]/[PA]/[**10**]/[co-cat.] = 700:100:0.5:0.5, 16 hours.* [b]*Determined by ^{1}H-NMR from the reaction mixture;* [c]*No CO_2 added;* [d]*2 mL toluene added and 1 eq. of CHO used.*

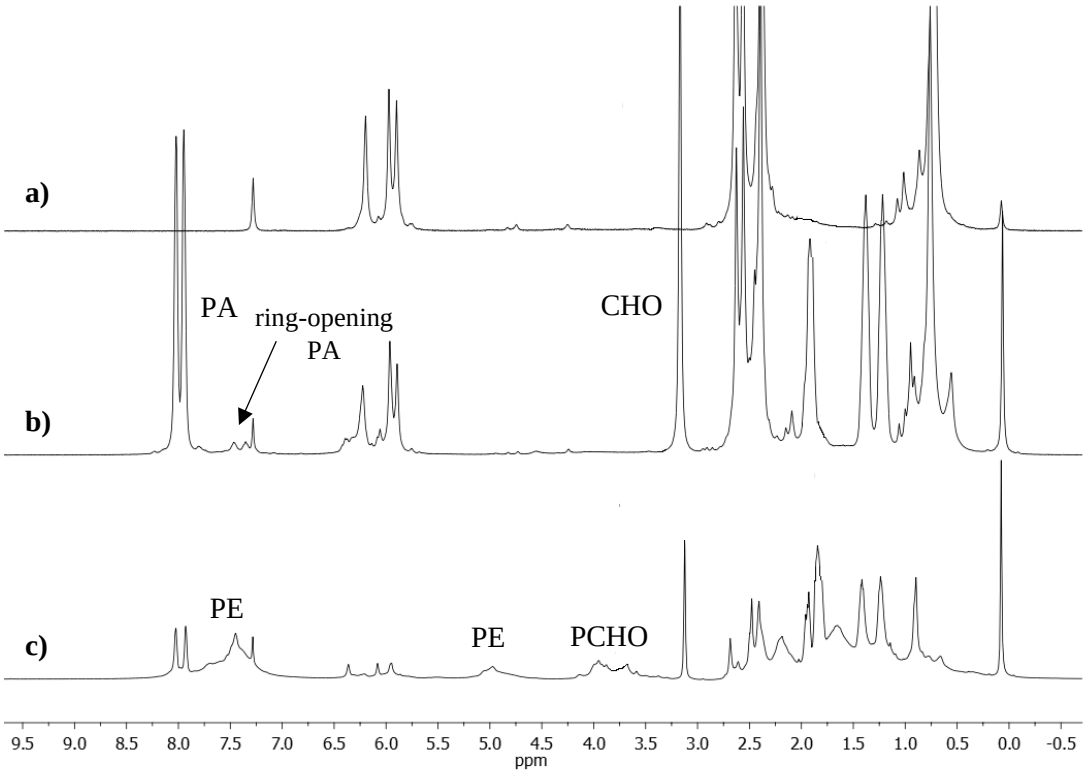

Figure 22. a) *^{1}H-NMR spectrum of complex **10** in $CDCl_3$; b) ^{1}H-NMR spectrum of complex **10** + CHO + PA at 25 ºC; c) ^{1}H-NMR spectrum of complex **10** + CHO + PA at 60 ºC after 16 h.*

Since complex **10** was not able to perform the terpolymerisation of CHO, CO_2 and PA, the terpolymerisation of CHO, CO_2 and *L*-lactide was also explored. First experiments were carried out in the absence of a solvent, at 60 ºC and 40 bar CO_2 pressure for 16 hours, using **10**:*L*-lactide:CHO of 0.5-1:100:700 molar ratio (Scheme 13) and the results are given in Table 6.

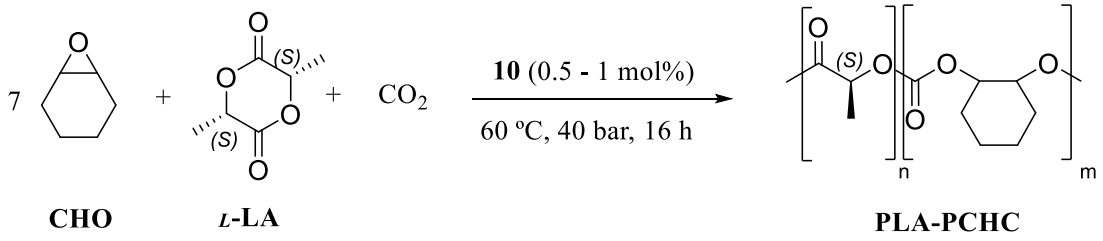

Scheme 13. *Synthesis of terpolymers derived from CHO, L-LA and CO_2 catalysed by complex **10**.*

As it can be seen in Table 6, an increase of the catalyst loading resulted in a higher CO_2 incorporation into the polymeric material, producing a higher PCHC content in

the terpolymer synthesised. On the other hand, the ROP of *L*-lactide to afford poly(*L*-lactide) (PLA) was achieved quantitatively in both scenarios. In addition, no homopolymerisation of CHO to produce PCHO was observed in any case.

Table 6. *Effect of the [**10**] on the synthesis of terpolymers derived from CHO, CO_2 and L-LA.*[a]

Exp.	cat (%).	Conv. (%) CHO[b]	Conv. (%) *L*-LA[b]	PLA (%)[b]	PCHO (%)[b]	PCHC (%)[b]
1	0.5	2.7	100	91	-	9
2	1	17	100	60	-	40

[a]Copolymerisation conditions: [CHO]/[L-LA] = 700:100, 16 hours, 60 ºC, 40 bar CO_2. [b]Determined by ^{1}H-NMR from the reaction mixture.

The effect of the reaction pressure on the terpolymerisation process was then investigated using both 0.5 and 1.0 mol% of catalyst loading, and the results are given in Tables 7 and 8. As it can be seen, the same trend was observed in both cases, with the highest PCHC content obtained at 10 bar CO_2 pressure. The increase of the reaction pressure resulted in a lower PCHC content in the resulting terpolymer. As discussed before, an increase of the [**10**] used resulted in PCHC content in the polymeric material, when the same reaction pressure was used (Figure 23).

Table 7. *Influence of the reaction pressure on the PCHC content in the resulting polymer using 0.5 mol% of complex **10**.*[a]

Entry	Pressure (bar)	Conv (%) CHO[b]	Conv (%) *L*-LA[b]	PLA (%)[b]	PCHO (%)[b]	PCHC (%)[b]
1	1	0	100	100	-	-
2	5	5.5	100	80	-	20
3	10	9	100	78	-	22
4	20	7.5	100	83	-	17
5	30	5.8	100	86	-	14
6	40	2.7	100	90	-	10

[a]Copolymerisation conditions: [CHO]/[L-LA]/[10] = 700:100:0.5, 16 hours, 60 ºC. [b]Determined by ^{1}H-NMR from the reaction mixture.

Table 8. *Influence of the reaction pressure on the PCHC content in the resulting polymer using 1 mol% of complex* ***10****.*[a]

Entry	Pressure (bar)	Conv (%) CHO[b]	Conv (%) L-LA[b]	PLA (%)[b]	PCHO (%)[b]	PCHC (%)[b]
1	1	0	100	100	-	-
2	5	16	100	60	-	40
3	10	27	100	42	-	58
4	20	23	100	48	-	52
5	30	20	100	54	-	46
6	40	17	100	60	-	40

[a]*Copolymerisation conditions: [CHO]/[L-LA]/[**10**] = 700:100:1, 16 hours, 60 ºC.* [b]*Determined by* ^{1}*H-NMR from the reaction mixture.*

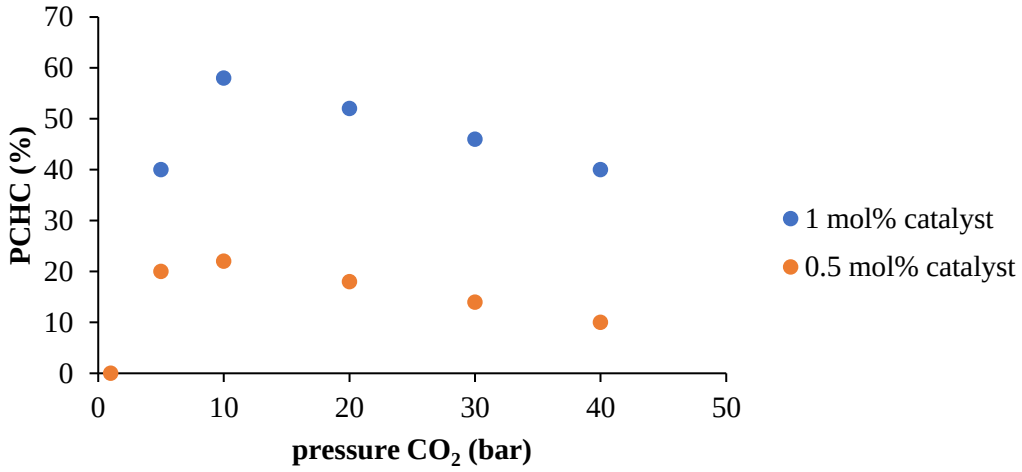

Figure 23. *Influence of the reaction pressure on the PCHC content in the terpolymer at 0.5 and 1.0 mol% content of complex* ***10****.*

Once the [**10**] and CO_2 pressure were optimised, the optimal ratio CHO:*L*-LA for the terpolymerisation process was investigated and the results are presented in Table 9. When the CHO:*L*-LA ratio used was 1:1, only 75 % conversion of *L*-LA toward the formation of PLA was achieved (Table 9, entry 1) with no formation of polycarbonate. This result led us to think of a mechanism in which the first step of the terpolymerisation would be the ROP of *L*-LA, and, only when all the *L*-LA monomer

is consumed, the ROCOP between CHO and CO_2, takes place. As expected, the increase in the CHO:*L*-LA ratio resulted in the complete consumption of *L*-LA towards the formation of PLA and the increase of the PCHC content in the resulting terpolymer (Figure 24). As can be seen in Figure 24, there is a linear correlation between the CHO:*L*-LA ratio and the PCHC content in the terpolymer, with the highest PCHC content of 60% when the CHO:*L*-LA ratio was 7:1.

Table 9. *Influence of the CHO:L-LA ratio on the PCHC content in the resulting terpolymer.*[a]

Entry	Ratio CHO: *L*-LA	Conv (%) CHO[b]	Conv (%) *L*-LA[b]	PLA (%)[b]	PCHO (%)[b]	PCHC (%)[b]
1	1:1	0	75	100	-	-
2	2:1	18	100	81	-	19
3	3:1	20	100	71	-	29
4	4:1	21	100	64	-	36
5	5:1	24	100	55	-	45
6	7:1	27	100	40	-	60

[a]*Copolymerisation conditions: 1 mol% complex **10**, 16 hours, 60 ºC.* [b]*Determined by ^{1}H-NMR from the reaction mixture.*

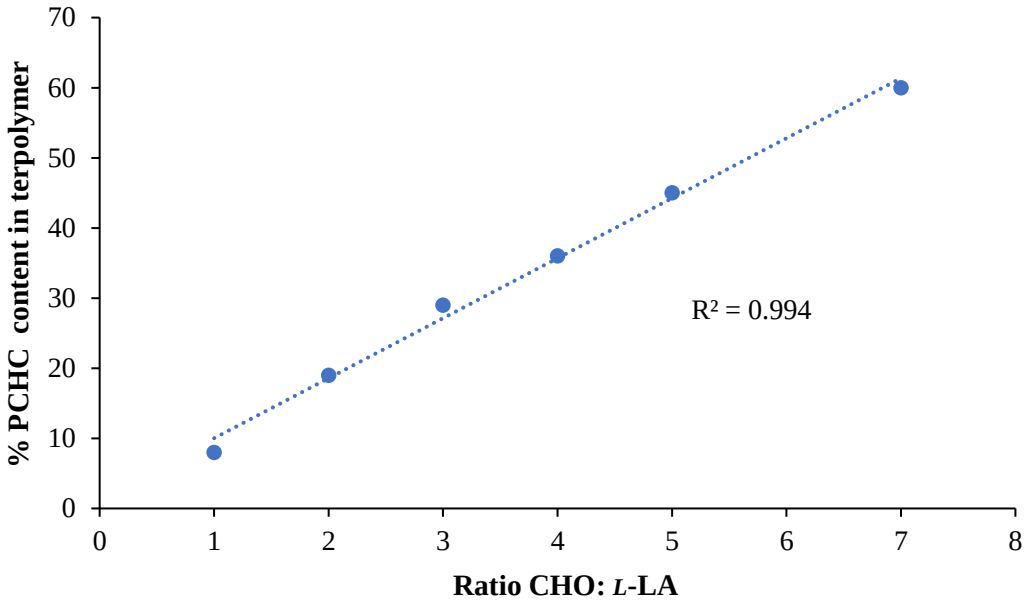

Figure 24. *Plot of % PCHC content in terpolymer vs ratio CHO:L-LA.*

Molecular weights and polydispersity values for the different terpolymers synthesised using different CHO: *L*-LA ratios are presented in Table 10. Figure 25 shows the GPC traces for different CHO:*L*-LA ratios employed. As it can be seen from Figure 25, the molecular weights of the resulting terpolymers slightly increased as the ratio CHO:*L*-LA increased due to the higher PCHC content in the resulting terpolymer.

Table 10. *Influence of the CHO:L-LA ratio on the molecular weight in the resulting terpolymer.*[a]

Entry	Ratio CHO:*L*-LA	$M_{n,\,exp.}$[b]	PDI[b]
1	1:1	5100	1.68
2	2:1	5295	1.80
3	3:1	5307	1.70
4	4:1	5344	1.67
5	5:1	5468	1.75
6	7:1	5523	1.60

[a]*Copolymerisation conditions: 1 mol% complex* ***10****, 16 hours, 60ºC.* [b]*Determined by GPC using polystyrene standards in THF.*

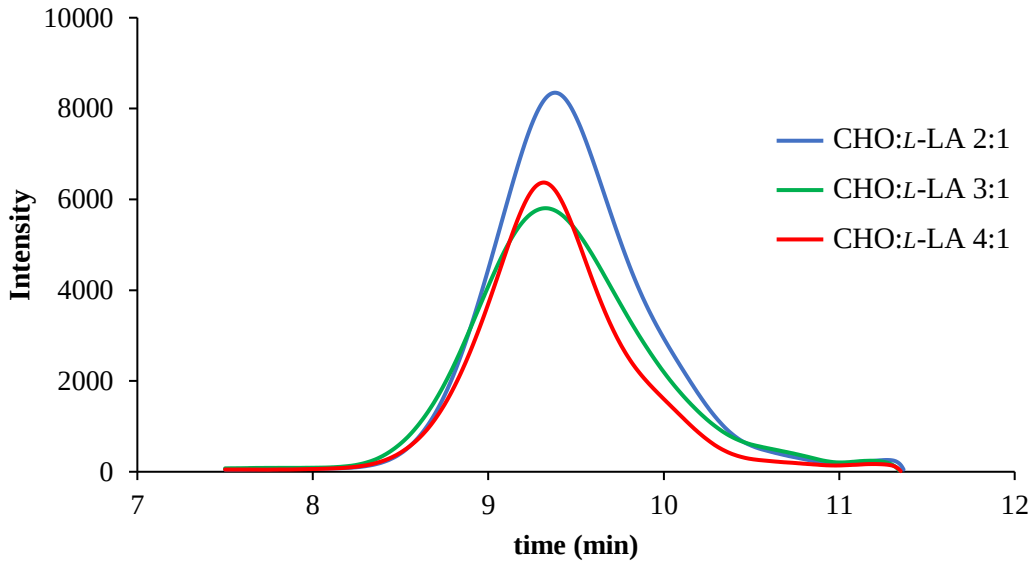

Figure 25. *GPC traces for terpolymers synthesised using different CHO:L-LA ratios.*

The terpolymer materials synthesised were characterised by ^{1}H-NMR and ^{13}C-{^{1}H}-NMR spectroscopy, as well as DOSY NMR studies. The determination of molecular weights was performed by gel permeation chromatography (GPC), while the thermal properties were evaluated by thermogravimetric analysis (TGA) and differential scanning calorimetry (DSC).

The microstructure of the terpolymeric materials was determined by NMR spectroscopy. ^{1}H-NMR spectrum (Figure 26) exhibited two different sets of signals with high intensity corresponding to the PLA and the PCHC moieties and low intensity signals corresponding to chain end and junction groups. PLA exhibited a quartet at 5.17 ppm corresponding to the methine proton *CH*^{a} and a doublet at 1.57 ppm corresponding to the methyl group. Following the same tendency, PCHC moiety exhibited five signals with high intensity corresponding to the methylene and methine (CH_2, CH) groups of the cyclohexyl ring. ^{13}C-{^{1}H}-NMR spectrum (Figure 27) suggested the formation of a block copolymer since different signals in the C=O region are observed, corresponding to both polycarbonate (169.6 ppm) and polyester (154.3, 153.8 ppm) blocks, in agreement with previously reported results.[46]

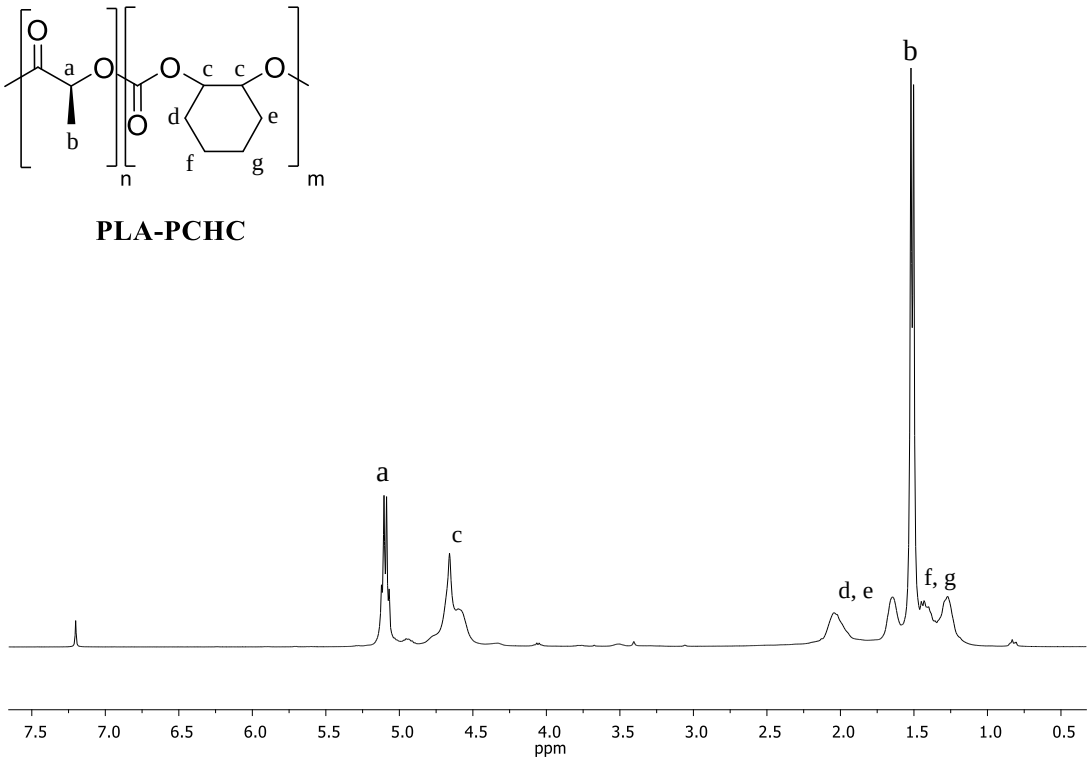

Figure 26. *^{1}H-NMR spectrum for poly(L-lactide)-poly(cyclohexene carbonate) (PLA-PCHC) terpolymer in $CDCl_3$.*

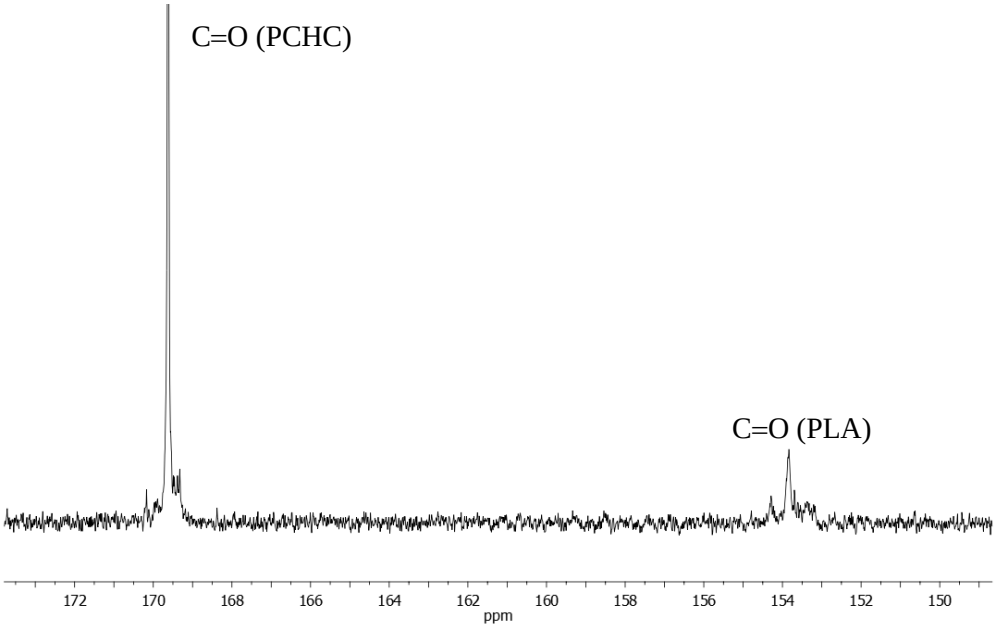

Figure 27. *^{13}C-{^{1}H}-NMR spectrum for poly(L-lactide)-poly(cyclohexene carbonate) (PLA-PCHC) terpolymer in $CDCl_3$.*

The formation of a block copolymer was also confirmed by 2D-DOSY NMR spectroscopy. As it can be seen from Figure 28, a single diffusion coefficient was observed for all signals, indicating the existence of only one block polyester-polycarbonate (PLA-PCHC) copolymer.

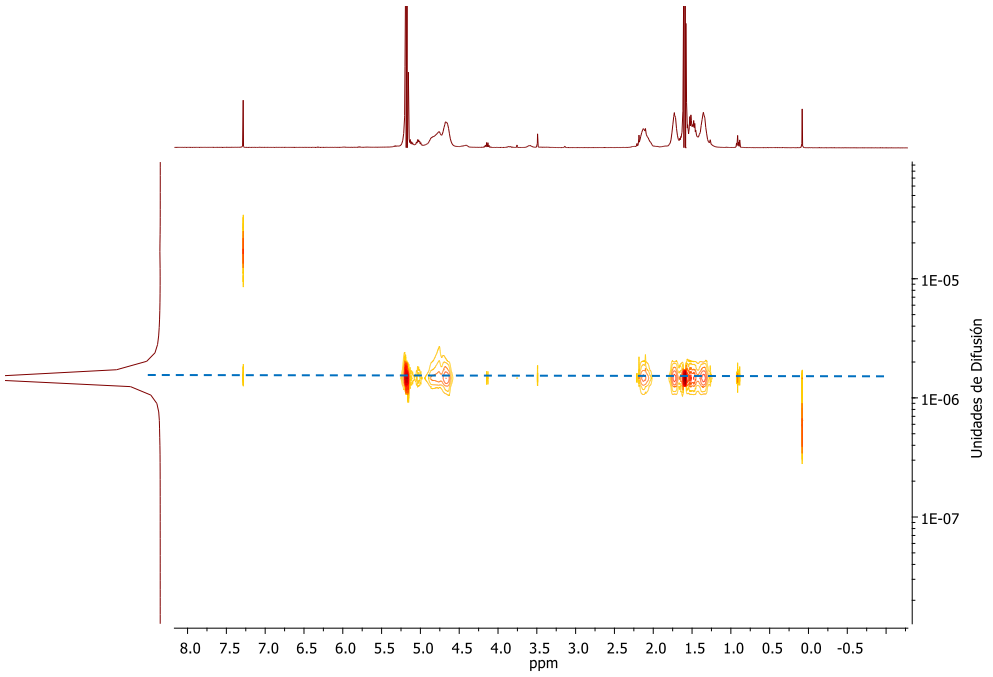

Figure 28. 2D-*DOSY-NMR spectrum for poly(L-lactide)-poly(cyclohexene carbonate) (PLA-PCHC) terpolymer in $CDCl_3$.*

Finally, the different terpolymers synthesised using different CHO:*L*-LA ratios were analysed by thermogravimetric analysis and differential scanning calorimetry. TGA analysis revealed that all terpolymers were stable in the range between 0-200 ºC. Terpolymer with the highest ratio CHO:*L*-LA (Table 11, entry 6) showed to be stable up to 244 ºC, due to the higher PCHC content. DSC studies revealed that the T_g obtained for each of the terpolymers increased as the ratio CHO:*L*-LA increased, and thus, with the polycarbonate content in the terpolymer, obtaining values ranging from 47 ºC and 74 ºC. As it can be seen from Table 11, the highest increase in the T_g is observed when increasing the ratio of CHO:*L*-LA from 5:1 to 7:1 (Table 11, entries 6 and 7), for which the polycarbonate content in the terpolymer increased from 45% to 60% exhibiting T_g values of 59 ºC and 74 ºC, respectively. On the other hand, the T_g remained almost constant when 3:1, 4:1 and 5:1 ratios were used (Table 11, entries 3-5), with T_g values of 58 ºC, 59 ºC and 59 ºC and 29%, 36% and 45% polycarbonate content respectively in the resulting terpolymer. As an illustrative example, Figure 29 shows the comparison of the DSC thermograms for terpolymers with CHO:*L*-LA ratios of 1:1, 4:1 and 7:1, and Figure 30 shows the TGA thermogram for terpolymer CHO:*L*-LA 7:1.

Table 11. *DSC and TGA data for selected terpolymers.*[a]

Entry	Ratio CHO:*L*-LA	T_g (ºC)[b]	$T_{d,5\%}$ (ºC)[c]
1	1:1	47	197
2	2:1	55	201
3	3:1	58	205
4	4:1	59	205
5	5:1	59	222
6	7:1	74	244

*[a]Copolymerisation conditions: 1 mol% complex **10**, 16 hours, 60ºC. [b]Determined by Different Scanning Calorimetry (DSC). [c]Determined by Thermal Gravimetric Analysis (TGA). Reported as temperature at 5% mass loss.*

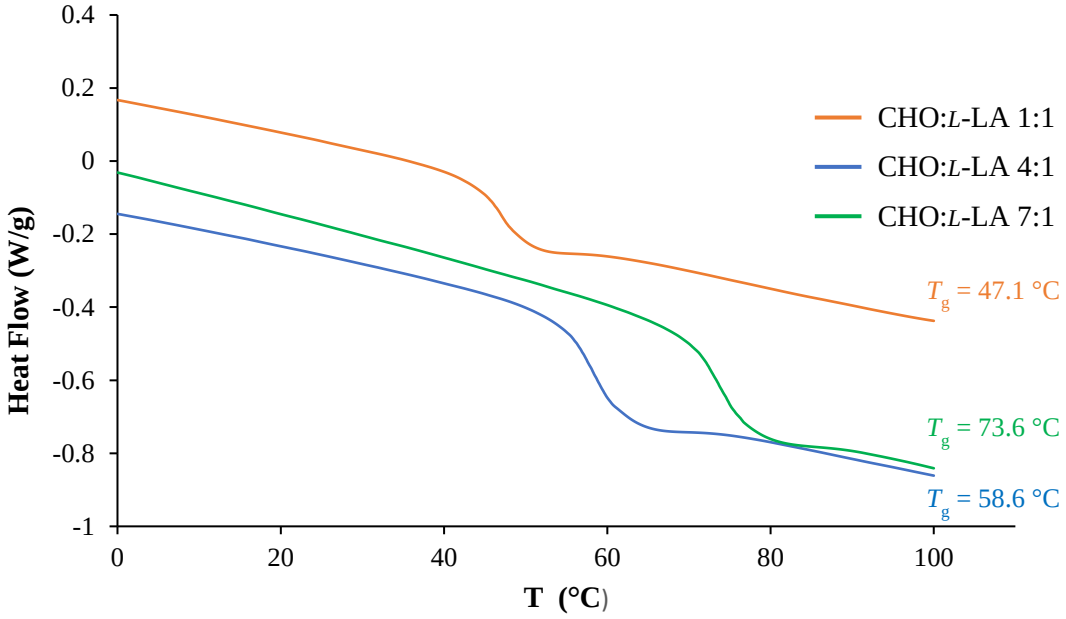

Figure 29. *DSC thermograms for terpolymers with CHO:L-LA ratios of 1:1, 4:1 and 1:7.*

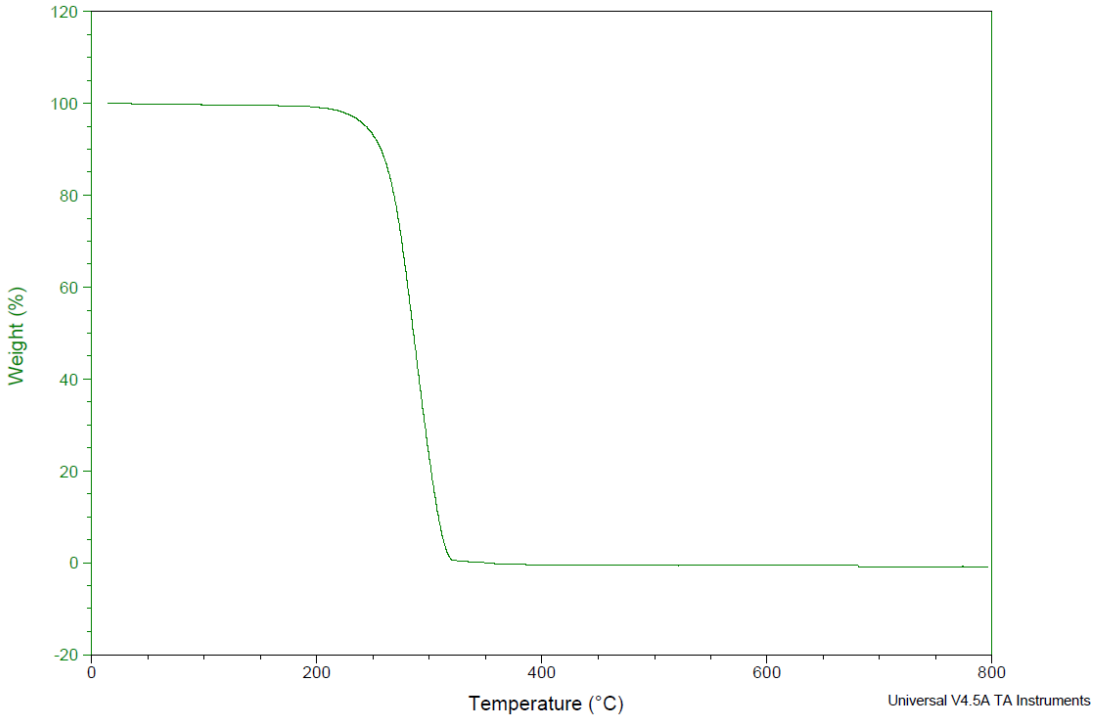

Figure 30. *TGA thermogram for terpolymer with CHO:L-LA ratio 1:7.*

Experimental section

EXPERIMENTAL SECTION

1. Synthesis of poly(cyclohexene carbonate) (PCHC)

As a mode of example, the synthesis of PCHC using chloride indium complex **10** is described. In a vial, freshly distilled cyclohexene oxide (0.50 g, 5.09 mmol) and complex **10** (24.0 mg, 25.0 μmol) were added. The reaction mixture was then placed in a stainless-steel reactor, pressurised at the desired CO_2 pressure, warmed up at the desired temperature and left stirring for 16 hours. After that time, an aliquot was taken for ^{1}H-NMR analysis and the conversion was calculated by integration of the remaining cyclohexene oxide, poly(cyclohexene oxide) and *trans*-cyclohexene carbonate. Once the conversion was determined, the polymeric materials obtained were purified using a MeOH/Hexane mixture, filtered, and dried over vacuum.

2. Synthesis of terpolymers

In a vial, freshly distilled cyclohexene oxide (0.75 g, 7.64 mmol), freshly sublimed *L*-LA (0.157 g, 1.09 mmol) and complex **10** (10.4 mg, 10.9 μmol) were added. The reaction mixture was then placed in a stainless-steel reactor, pressurised at the desired CO_2 pressure, warmed up at 60 ºC and left stirring for 16 hours. After that time, an aliquot was taken for ^{1}H-NMR analysis and the conversion was calculated by integration of the remaining cyclohexene oxide, *L*-LA and the signals corresponding to the terpolymeric material. Once the conversion was determined, the polymeric materials obtained were purified using a MeOH/Hexane mixture, filtered, and dried over vacuum.

Bibliography

BIBLIOGRAPHY

(1) B. Grignard, S. Gennen, C. Jérôme, A. W. Kleij, C. Detrembleur, *Chem. Soc. Rev.*, **2019**, *48*, 4466.

(2) *Plastics-the Facts 2019 An analysis of European plastics production, demand and waste data*. *https://www.plasticseurope.org* (access 05 May 2021)

(3) K. O. Siegenthaler, A. Künkel, G. Skupin, M. Yamamoto, *Adv. Polym. Sci.*, **2012**, *245*, 91.

(4) S. Fukuoka, M. Tojo, H. Hachiya, M. Aminaka, K. Hasegawa, *Polym. J.*, **2007**, *39*, 91.

(5) S. Tempelaar, L. Mespouille, O. Coulembier, P. Dubois, A. P. Dove, *Chem. Soc. Rev.*, **2013**, *42*, 1312.

(6) M. Azechi, K. Matsumoto, T. Endo, *J. Polym. Sci., Part A: Polym. Chem.*, **2013**, *51*, 1651.

(7) J. H. Park, J. Y. Jeon, J. J. Lee, Y. Jang, J. K. Varghese, B. Y. Lee, *Macromolecules*, **2013**, *46*, 3301.

(8) T. M. McGuire, E. M. López-Vidal, G. L. Gregory, A. Buchard, *J. CO_2 Utilis.*, **2018**, *27*, 283.

(9) Y. Gu, K. Matsuda, A. Nakayama, M. Tamura, Y. Nakagawa, K. Tomishige, *ACS Sustain. Chem. Eng.*, **2019**, *7*, 6304.

(10) S. Bian, C. Pagan, A. A. Andrianovaartemyeva, G. Du, *ACS Omega*, **2016**, *1*, 1049.

(11) Z. Chen, N. Hadjichristidis, X. Feng, Y. Gnanou, *Polym. Chem.*, **2016**, *7*, 4944.

(12) D. Pati, Z. Chen, X. Feng, N. Hadjichristidis, Y. Gnanou, *Polym. Chem.*, **2017**, *8*, 2640.

(13) S. J. Poland, D. J. Darensbourg, *Green Chem.*, **2017**, *19*, 4990.

(14) C. M. Kozak, K. Ambrose, T. S. Anderson, *Coord. Chem. Rev.*, **2018**, *376*, 565.

(15) M. R. Kember, A. Buchard, C. K. Williams, *Chem. Commun.*, **2011**, *47*, 141.

(16) X. B. Lu, D. J. Darensbourg, *Chem. Soc. Rev.*, **2012**, *41*, 1462.

(17) W. M. Ren, Y. Liu, G. P. Wu, J. Liu, X. B. Lu, *J. Polym. Sci., Part A: Polym. Chem.*, **2011**, *49*, 4894.

(18) C. M. Byrne, S. D. Allen, E. B. Lobkovsky, G. W. Coates, *J. Am. Chem. Soc.*, **2004**, *126*, 11404.

(19) L. Peña Carrodeguas, J. González-Fabra, F. Castro-Gómez, C. Bo, A. W. Kleij, *Chem. Eur. J.*, **2015**, *21*, 6115.

(20) A. J. Kamphuis, F. Picchioni, P. P. Pescarmona, *Green Chem.*, **2019**, *21*, 406.

(21) M. Cheng, E. B. Lobkovsky, G. W. Coates, *J. Am. Chem. Soc.*, **1998**, *120*, 11018.

(22) D. R. Moore, M. Cheng, E. B. Lobkovsky, G. W. Coates, *J. Am. Chem. Soc.*, **2003**, *125*, 11911.

(23) D. R. Moore, M. Cheng, E. B. Lobkovsky, G. W. Coates, *Angew. Chem. Int. Ed.*, **2002**, *41*, 12.

(24) M. Cheng, D. R. Moore, J. J. Reczek, B. M. Chamberlain, E. B. Lobkovsky, G. W. Coates, *J. Am. Chem. Soc.*, **2001**, *123*, 8738.

(25) S. D. Allen, D. R. Moore, E. B. Lobkovsky, G. W. Coates, *J. Am. Chem. Soc.*, **2002**, *124*, 14284.

(26) M. Reiter, S. Vagin, A. Kronast, C. Jandl, B. Rieger, *Chem. Sci.*, **2017**, *8*, 1876.

(27) P. K. Saini, C. Romain, C. K. Williams, *Chem. Commun.*, **2014**, *50*, 4164.

(28) M. R. Kember, P. D. Knight, P. T. R. Reung, C. K. Williams, *Angew. Chem. Int. Ed.*, **2009**, *48*, 931.

(29) N. Takeda and S. Inoue, *Makromol. Chem.*, **1978**, *179*, 1377.

(30) J. Deng, M. Ratanasak, Y. Sako, H. Tokuda, C. Maeda, J. Y. Hasegawa, K. Nozaki, T. Ema, *Chem. Sci.*, **2020**, *11*, 5669.

(31) W. Wu, X. Sheng, Y. Qin, L. Qiao, Y. Miao, X. Wang, F. Wang, *J. Polym. Sci., Part A: Polym. Chem.*, **2014**, *52*, 2346.

(32) X. Sheng, Y. Wang, Y. Qin, X. Wang, F. Wang, *RSC Adv.*, **2014**, *4*, 5404.

(33) M. A. Fuchs, C. Altesleben, T. A. Zevaco, E. Dinjus, *Eur. J. Inorg. Chem.*, **2013**, 4541.

(34) N. Ikpo, S. M. Barbon, M. W. Drover, L. N. Dawe, F. M. Kerton, *Organometallics*, **2012**, *31*, 8145.

(35) H. Plommer, I. Reim, F. M. Kerton, *Dalton Trans.*, **2015**, *44*, 12098.

(36) K. Nishioka, H. Goto, H. Sugimoto, *Macromolecules*, **2012**, *45*, 8172.

(37) N. Kindermann, À. Cristòfol, A. W. Kleij, *ACS Catal.*, **2017**, *7*, 3860.

(38) A. C. Deacy, C. B. Durr, C. K. Williams, *Dalton Trans.*, **2019**, *49*, 223.

(39) A. Thevenon, A. Cyriac, D. Myers, A. J. P. White, C. B. Durr, C. K. Williams, *J. Am. Chem. Soc.*, **2018**, *140*, 6893.

(40) G. L. Gregory, E. M. López-Vidal, A. Buchard, *Chem. Commun.*, **2017**, *53*, 2198.

(41) J. M. Longo, M. J. Sanford, G. W. Coates, *Chem. Rev.*, **2016**, *116*, 15167.

(42) N. Hadjichristidis, M. Pitsikalis, H. Iatrou, *Adv.Polym. Sci.*, **2005**, *189*, 1.

(43) H. C. Kim, S. M. Park, W. D. Hinsberg, I. R. Division, *Chem. Rev.*, **2010**, *110*, 146.

(44) A. Hirao, Y. Matsuo, R. Goseki, *J. Polym. Res.*, **2019**, *26*.

(45) S. Paul, Y. Zhu, C. Romain, R. Brooks, P. K. Saini, C. K. Williams, *Chem. Commun.*, **2015**, *51*, 6459.

(46) S. Kernbichl, M. Reiter, J. Mock, B. Rieger, *Macromolecules*, **2019**, *52*, 8476.

(47) L. Shi, X. B. Lu, R. Zhang, X. J. Peng, C. Q. Zhang, J. F. Li, X. M. Peng, *Macromolecules*, **2006**, *39*, 5679.

(48) D. J. Darensbourg, Y. Wang, *Polym. Chem.*, **2015**, *6*, 1768.

(49) J. E. Seong, S. J. Na, A. Cyriac, B. W. Kim, B. Y. Lee, *Macromolecules*, **2010**, *43*, 903.

(50) G. P. Wu, P. X. Xu, Y. P. Zu, W. M. Ren, X. B. Lu, *J. Polym. Sci., Part A: Polym. Chem.*, **2013**, *51*, 874.

(51) C. Martín, A. W. Kleij, *Macromolecules*, **2016**, *49*, 6285.

(52) S. Kernbichl, M. Reiter, F. Adams, S. Vagin, B. Rieger, *J. Am. Chem. Soc.*, **2017**, *139*, 6787.

(53) S. Paul, C. Romain, J. Shaw, C. K. Williams, *Macromolecules*, **2015**, *48*, 6047.

(54) D. C. Romain, C. K. Williams, *Angew. Chem. Int. Ed.*, **2014**, *53*, 1607.

(55) T. T. D. Chen, Y. Zhu, C. K. Williams, *Macromolecules*, **2018**, *51*, 5346.

(56) Y. Zhu, C. Romain, C. K. Williams, *J. Am. Chem. Soc.*, **2015**, *137*, 12179.

(57) C. Romain, Y. Zhu, P. Dingwall, S. Paul, H. Rzepa, A. Buchard, C. K. Williams, *J. Am. Chem. Soc.*, **2016**, *138*, 4120.

(58) G. S. Sulley, G. L. Gregory, T. T. D. Chen, L. Peña Carrodeguas, G. Trott, A. Santmarti, K. Y. Lee, N. J. Terrill, C. K. Williams, *J. Am. Chem. Soc.*, **2020**, *142*, 4367.

Chapter 4.

Synthesis of poly(hydroxyurethane)s by polyaddition reaction of bis(cyclic carbonates) and diamines.

Introduction

Polyurethanes (PUs) are a type of polymer which include a urethane group (–O–CO–NH–) within their structure. In the last few years, the plastic industry has seen a growing interest in the development of novel polyurethane materials. According to *PlasticsEurope*, 51.2 million tons of plastics were produced in Europe in 2018, from which, 4 million tons were polyurethanes.[1] Currently, PUs are one of the most common and researched materials in the world. These materials combine the durability and toughness of metals with the elasticity of rubbers, making them suitable to replace metals, plastics, and rubbers in several engineered products.[2] Thanks to their physical properties such as hardness, elongation, strength, abrasion resistance, light weight etc., they have been widely used in biomedical, building and construction applications, automotive, textiles and several other industries.[2–7] They also find applications as coatings due to their specific properties.[8,9]

Due to the wide variety of starting materials from which PUs can be synthesised and given the broad range of different applications for which they can be used, they can be divided in different classes depending on their properties: rigid, flexible, thermoplastic, waterborne, binders, coatings, adhesives, sealants, and elastomers (Figure 1). [10]

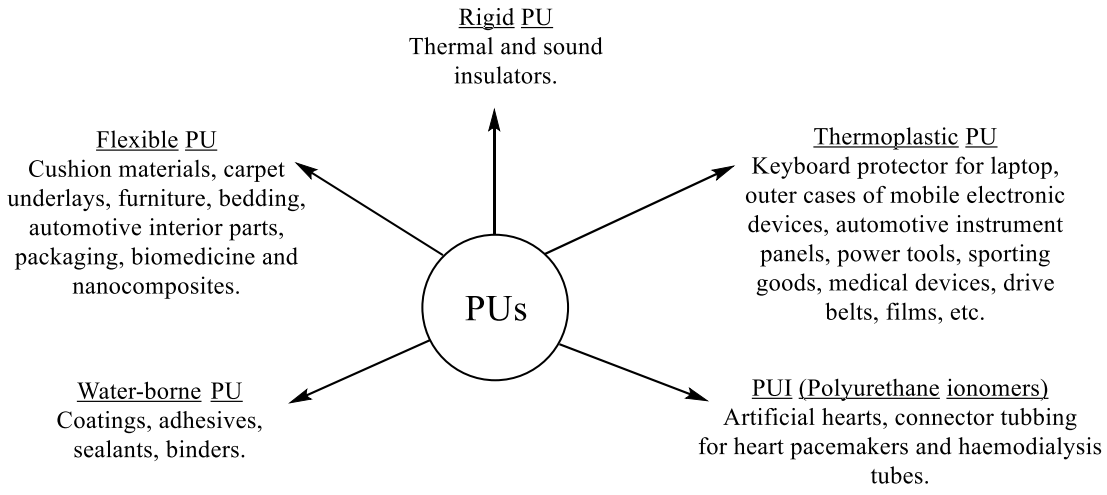

Figure 1. *Important types of polyurethanes and common examples of their uses and applications.*

Polyurethane materials can be obtained in multiple ways. Professor Otto Bayer *et al.* reported the first route for their synthesis in the late 1940's consisting in the polyaddition of a diol (or polyol) onto a diisocyanate (or poly isocyanate).[11] However,

isocyanates are known to be highly toxic,[12] since they are directly produced from the corresponding amine and phosgene, a gas which is highly toxic too. Therefore, alternative pathways for PU synthesis involving greener intermediates and processes have become more and more attractive for industrial and academic research. Figure 2 presents an overview of the main synthetic routes to polyurethanes according to their dependence on phosgene and isocyanates.[13] They can broadly be divided into six different categories: polycondensation, Ring-Opening Polymerisation (ROP), rearrangement reactions, polyaddition of diamines into cyclic carbonates, transurethanisation and reductive carbonylation of nitro compounds. Polycondensation routes,[14,15] have found difficulties for industrialisation since the synthesis of the PU precursors involved the use of phosgene or derivatives. Besides, the need of a catalyst to perform the reaction and the high temperatures required (c.a. 150-220 °C) together with the release of side products, such as alcohols and HCl, are other obstacles that have restricted the extension of polycondensation processes to industrial scale. Another method to synthesise non-isocyanate polyurethanes (NIPU) is the Ring-Opening Polymerisation of cyclic carbamates.[16,17] Although no side by-products are formed using this pathway, the cyclic carbamates precursors are often synthesised from phosgene and the reactions are performed at high temperature. Recently, new strategies for the synthesis of five and six-membered cyclic carbamates have been reported by reaction of alkylene diamines or aminoalcohols with reagents, such as dialkyl carbonates,[18,19] or with pressurised carbon dioxide in the absence of catalysts.[20] However, not all these cyclic carbamates are easy to synthesise, and the ones that are easily generated are thermodynamically stable, and thus, less reactive for polymerisation.

A phosgene-free method frequently used for the synthesis of PUs is the rearrangement reaction, in which a carboxylic acid derivative is transformed ultimately into a carbamate, which, in presence of a diol, gives rise to the desired PU. However, this method also uses isocyanates, even if they are generated in situ, but more importantly, other toxic reactants such as acyl azides, carboxiamides and hydroxamic azides.[21–27]

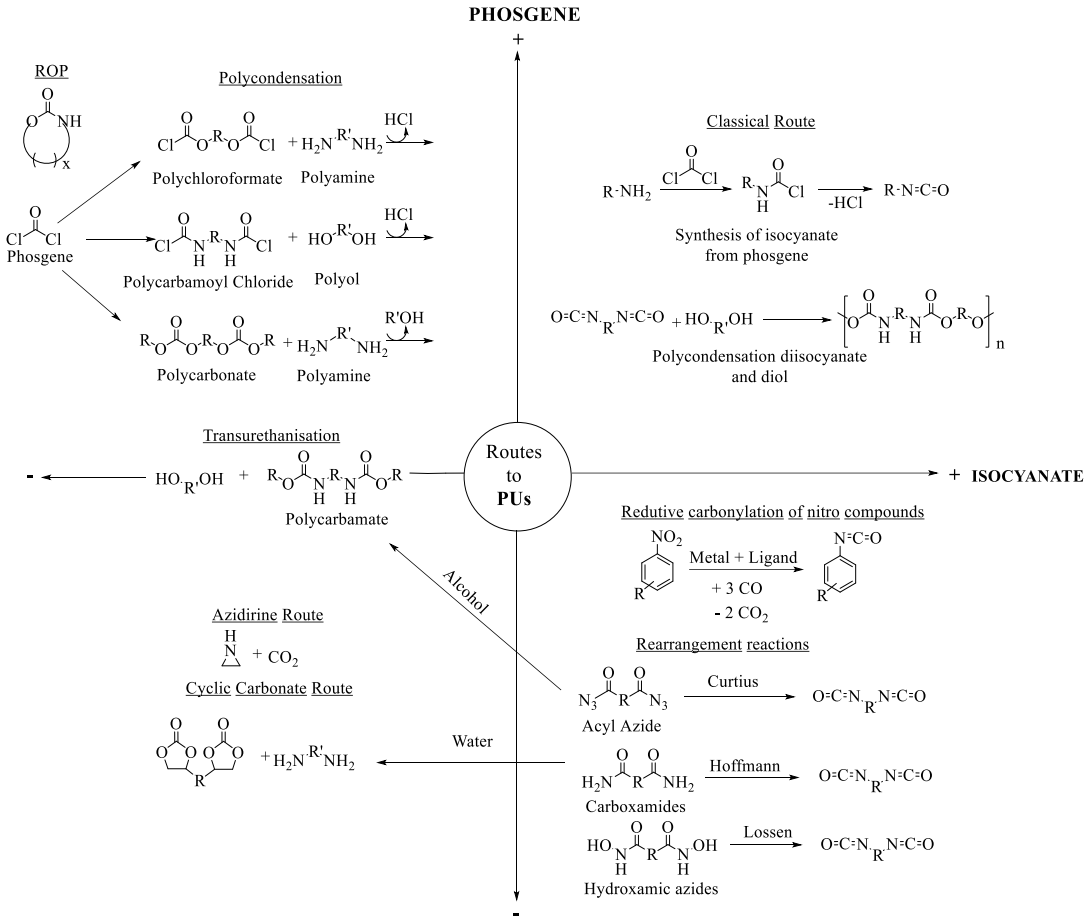

Figure 2. *Overview of synthetic routes to polyurethanes.*

A promising and a more sustainable pathway for the obtention of aryl isocyanates is the reductive carbonylation of nitro compounds.[28,29] It was firstly reported by Hardy and Benett in 1967, who described the direct conversion of aromatic nitro compounds with carbon monoxide at high pressure and temperatures using Rh/C as catalyst.[30] The reaction is thermodynamically favoured and is highly exothermic. Normally, non-toxic transition metals are applied, but also sulphur, selenium, and tellurium compounds catalyse this reaction.[29] However, highly-toxic catalyst residues were detected among the final products and, thus, this route became inapplicable for and industrial polyurethane synthesis.

The greenest pathways for the synthesis of NIPUs are the transurethanisation polycondensation between a bis-carbamate and a diol,[31–35] the copolymerisation between aziridines and CO_2[36–38] and the polyaddition of bis(cyclic carbonates) and diamines.[39,40]

Transurethanisation processes are condensation reactions of diols onto carbamates. Three different types of carbamates can be distinguished using phosgene-free routes for their synthesis: bis-alkyl carbamates, bis-hydroxyalkylcarbamates, and AB-type synthons (Scheme 1).

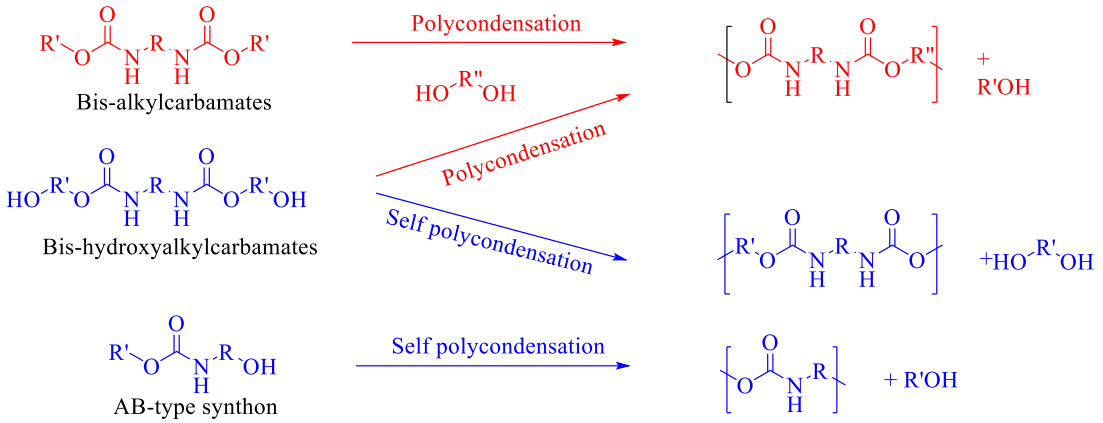

Scheme 1. *Three main routes to PU via transurethanisation processes*.

Bis-alkyl carbamates can be synthesised by reacting diisocyanates with alcohols, such as methanol or phenol.[41] To avoid the use of diisocyanates, bis-alkylcarbamates can also be prepared reacting dialkylcarbonates with diamines (Scheme 2). Dimethylcarbonate (DMC) is the most used dialkylcarbonate, which was originally synthesised by phosgenation of methanol. Nowadays, DMC is synthesised via a phosgene-free route from carbon monoxide (CO), methanol and dioxygen,[42] although it can also be synthesised using carbon dioxide (CO_2) and methanol.[43] Other alkyl-carbamates have been synthesised, such as ethyl carbamates and phenyl carbamates, using similar reaction conditions to dimethyl carbonate.[44–46]

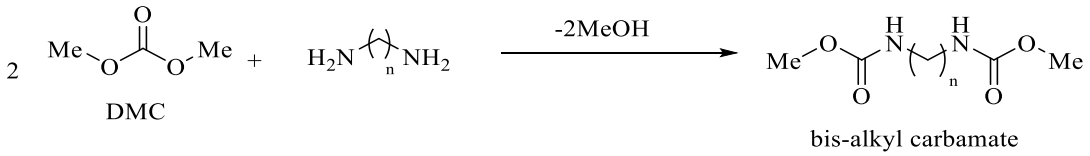

Scheme 2. *Methoxycarbonylation of diamines with dimethylcarbonate.*

Bis-hydroxyalkylcarbamates (BHCs) can be easily generated by the addition of a diamine on cyclic carbonates such as ethylene or propylene carbonate (Scheme 3).[47]

Ethylene carbonate is an attractive precursor to use since it can be easily obtained from ethylene oxide and CO_2. The reaction is catalyst-free and highly exothermic.

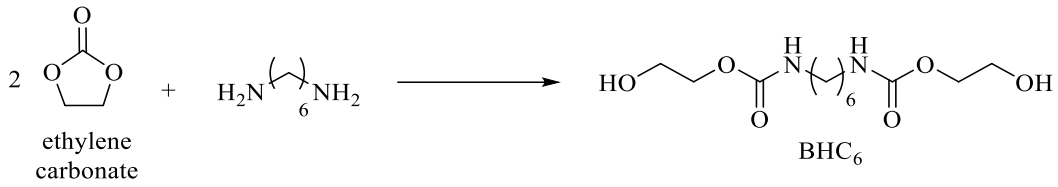

Scheme 3. *Synthesis of a bis-hydroxyalkylcarbamate from ethylene carbonate and 1,6-hexanediamine.*

BHCs can be self-polymerised to synthesise polyurethanes since they bear both bis-alcohol and bis-carbamate functionalities.[48] On the other hand, their reaction with diols allows the fine-tuning of the properties of the resulting PU to bring hard or soft segments, and thus, modify the T_g and the crystallinity of the PU depending on the needs and the future application.[48–50]

As it has been described, difunctional monomers are needed to perform the polymerisation. An interesting route to prepare PUs is the synthesis of AB-type monomers bearing both carbamate and alcohol functionalities. The advantage of such monomers is that the stoichiometry between both functionalities is always achieved, and thus, the polymerisation is not limited by the stoichiometry. There are few examples of these monomers in literature (Figure 3).[45,46,51]

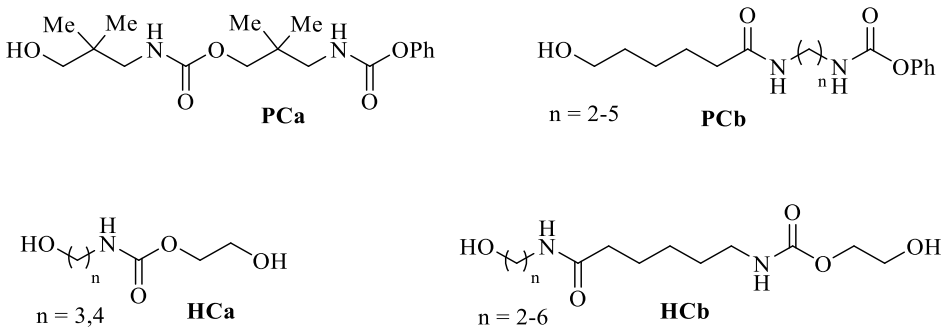

Figure 3. *AB-type monomers: phenylcarbamates and hydroxycarbamates.*

There are not many examples in the literature of bio-based polyurethanes obtained by transurethanisation processes. In this context, Meier *et al.* used limonene as bio-based raw material for the synthesis of bis-methylcarbamates and diols (Figure 4).[52]

The replacement of phosgene by CO_2, which is abundant, renewable, and environmentally friendly, is another emerging route for the synthesis of NIPUs. Aziridines, nitrogen analogues of epoxides, can react with supercritical CO_2 to give cyclic urethanes, and polymers containing urethane and amine units. This pathway is one of the least dependent in terms of phosgene and isocyanate content. However, the toxicity of aziridines still remains an issue.[37]

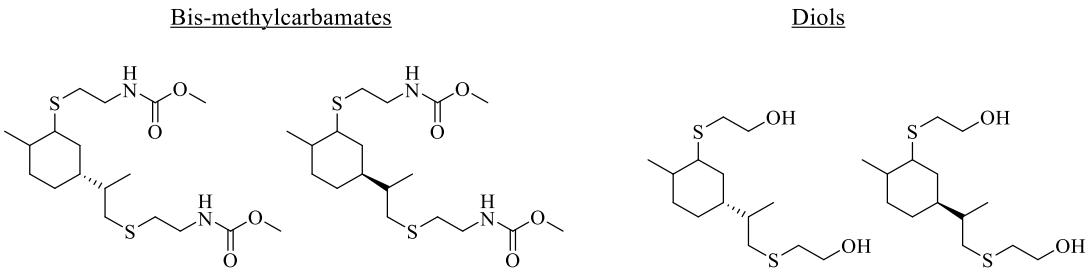

Figure 4. *Limonene-based monomers for fully bio-based PU synthesis.*

1. Polyaddition reaction of bis(cyclic carbonates) and diamines

Amongst the greenest and most-studied pathways for the synthesis of PUs, the polyaddition reaction of bis(cyclic carbonate)s and diamines is the most studied process (Scheme 4).[13] This reaction leads to the formation of linear poly-(hydroxyurethane)s (PHUs) with primary or secondary alcohols within the main polymer chain.

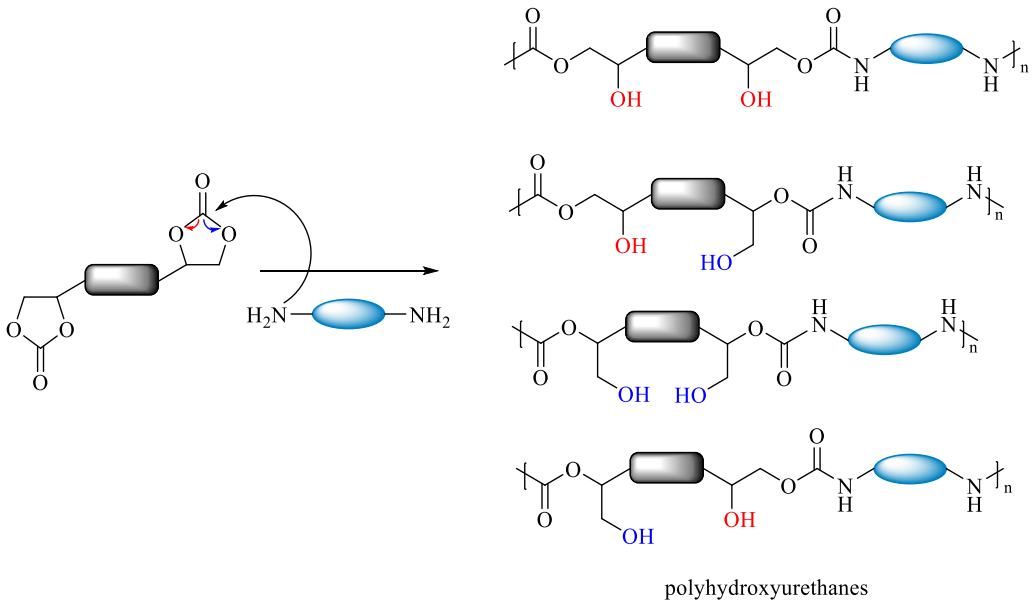

Scheme 4. *Synthesis of poly(hydroxyurethane)s from bis(cyclic carbonates) and diamines.*

One of the pioneers in this field were Grozsos *et al.*, who patented the preparation of oligo hydroxyl-urethanes by the reaction of bis(cyclic carbonates), diamines and urea in 1957.[53] Since then, several reviews on the synthesis of polyurethanes have been reported by several research groups.[31,33–35,39,40,54] The PHUs obtained using this route present various advantages such as the bypass of isocyanates and phosgene as starting materials, making the process safer and greener since the synthesis of cyclic carbonates allows CO_2 capture. Besides, the presence of hydroxyl groups in the structure gives specific chemical and physical properties to the polymer.[34,54] Moreover, the reactive pendant hydroxyl groups enable the polymer to undergo post-functionalisation reactions with chemical and biological functionalities.[55]

Different routes have been developed to synthesise bis(cyclic carbonates) precursors for the obtention of poly(hydroxyurethane)s by polyaddition reactions (Scheme 5). Amongst them, the most used and well-studied route is the insertion of CO_2 into epoxides.[56–58]

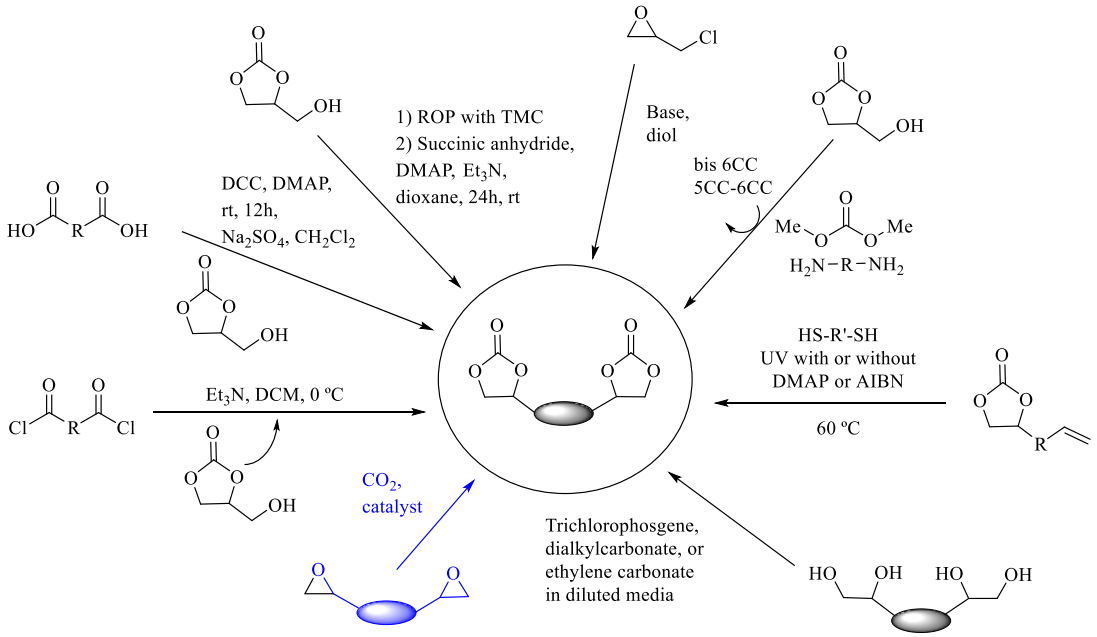

Scheme 5. *Synthesis of 5-membered bis(cyclic carbonates).*

The reactivity of cyclic carbonates with amines have been studied to have a better understanding of the nucleophilic addition and the mechanism of the reaction. Thus, a three-step reaction involving a tetrahedral intermediate has been proposed. (Scheme 6).[59–61]

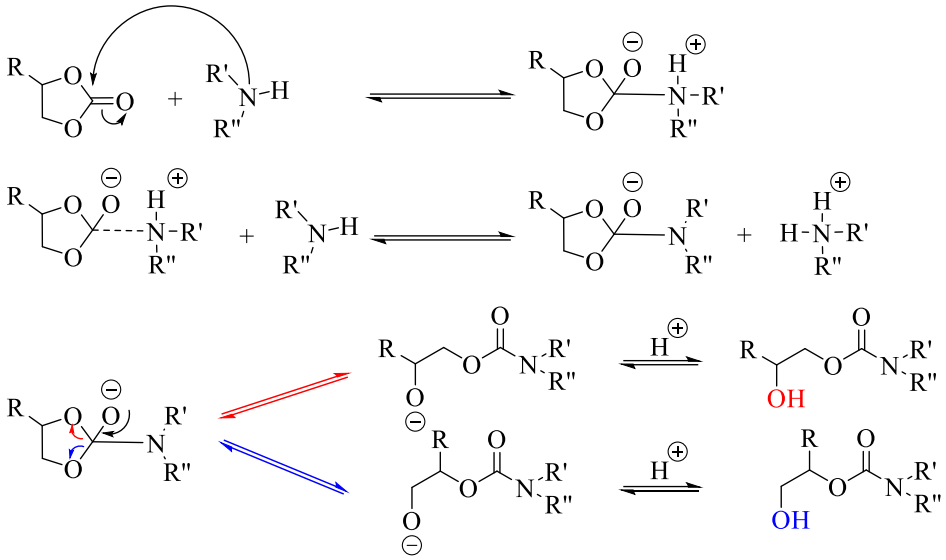

Scheme 6. *Mechanism involving a tetrahedral intermediate for the reaction between 5-membered cyclic carbonates and amines.*

In general, the ring-opening reaction of the cyclic carbonate by the amine takes place without the use of a catalyst. However, the reaction rate can be accelerated through activation of the monomers. For this purpose, either weakly Lewis acid or oxophilic additives may be added to increase the electrophilicity of the cyclic carbonate group.[62] Basic additives can be used to increase the nucleophilicity of the amine or even deprotonate it. Another option is the use of a Lewis Base to attack the carbonyl group of the cyclic carbonate.

Although Garipov *et al*. reported that the aminolysis reaction performed better using protic solvents,[60,61] the polyaddition of cyclic carbonates onto diamines is mostly carried out in polar aprotic solvents such as DMF, DMSO, DMAC etc. due to the better solubility of the starting materials.[55,63–65] Nevertheless, some research groups have also prepared the NIPUs in bulk conditions, to obtain higher molecular weights (M_n).[66–68]

The temperature also has an influence on the outcome of the polyaddition reaction. Endo *et al.* studied deeply this influence and quantified the effect of the temperature on the polymerisation process.[69,70] It was observed that higher yields were obtained when increasing the reaction temperature and calculated the effect of the temperature on the reaction rate constant. The higher rate at higher temperatures was explained by the decrease of the viscosity of the reaction mixture when the temperature was increased.[70]

As it has been previously discussed in Scheme 4, the polyaddition reaction of bis(cyclic carbonates) and diamines leads to the formation of poly(hydroxyurethane)s with pending primary and secondary hydroxyl groups along the polymeric chain. In all reported examples in literature, authors have found that more secondary alcohols are generated during the polymerisation rather than their primary alcohols counterparts. Ratios between primary and secondary alcohols ranged from 38:62 to 6:94.[55,63,71] However, only a few studies have reported or investigated the potential side products generated during the reaction (Scheme 7).[72–76]

The use of bis(cyclic carbonates) containing ester functionalities can lead to amidation reactions if the diamine reacts with the ester moiety instead of the carbonyl group of the cyclic carbonate. Thus, urea groups can be generated. Cramail *et al.* observed that the formation of amide groups depended on the structure of the diamine used.[74] The same group reported a complete study showing the formation of ureas, oxazolidinones synthesis by dehydration processes and amidification products when undecanoic bis(cyclic carbonate) ester and hexylamine (Scheme 7) were used.[76] Finally, and following the previous studies, Sardon, Cramail *et al.* reported a new mechanism for the formation of urea derivatives using 1,5,7-triazabicyclo[4.4.0]dec-5-ene (TBD) as catalyst, which is different to the well-established amidation side-reaction of hydroxyurethane with primary amine.[75]

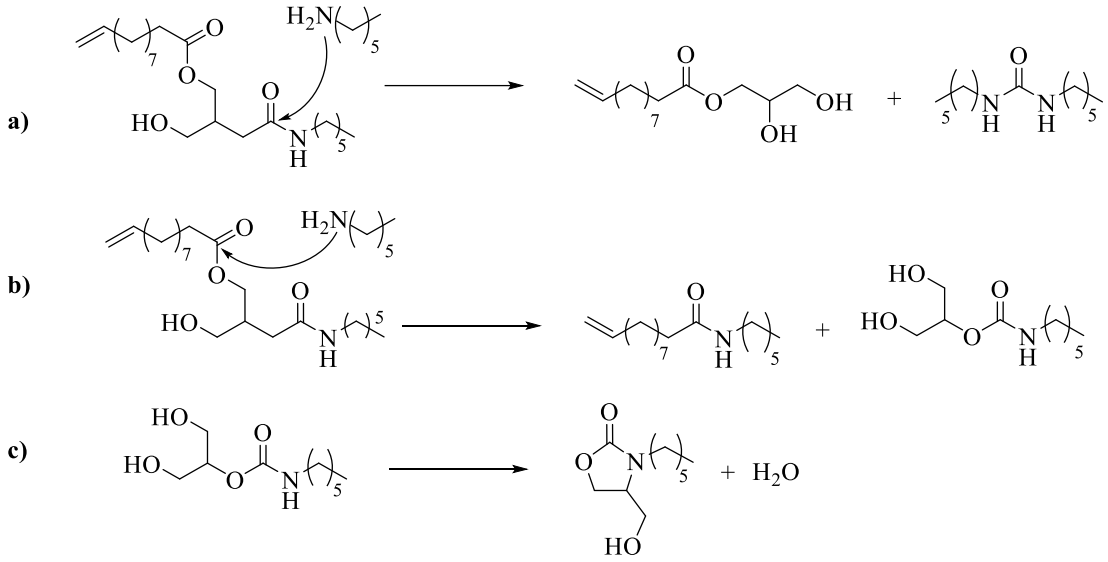

Scheme 7. *Possible side reactions between UndCC-ester and hexylamine: (a) urea formation, (b) amidification and (c) dehydration.*

1.1. Towards bio-based poly(hydroxyurethane)s

The depletion of fossil resources has provoked a growing interest within the scientific community and research groups in developing new routes for the synthesis of cyclic carbonates from bio-based resources. Thus, biomass-derived wastes including vegetable oils, lignin or polysaccharides represent an attractive source for producing polymers. In this context, several research groups have worked on the synthesis of poly(hydroxyurethane)s from bio-based cyclic carbonates to replace petroleum-based PHUs, using fatty acids and glycerol from transesterification of vegetable oils or other interesting natural molecules such as limonene, furane, *D*-mannitol or sorbitol.

Glycerol carbonate derivatives have been used as precursors for the synthesis of 5-membered bis(cyclic carbonates). For instance, Carpentier and co-workers used *α,ω*-dyhydroxy telechelic prepolymers such as poly(propyleneglycol) (PPG), poly(ethyleneglycol) (PEG) and polybutadiene (PB) and further reacted them with tosylated-glycerol carbonate (GC) in alkaline conditions to obtain bis(cyclic carbonate) prepolymers (Scheme 8). Polyaddition reactions onto different grade Jeffamines afforded the corresponding PHUs with the highest molecular weights ever reported (M_n= 68000 g mol^{-1}).[66]

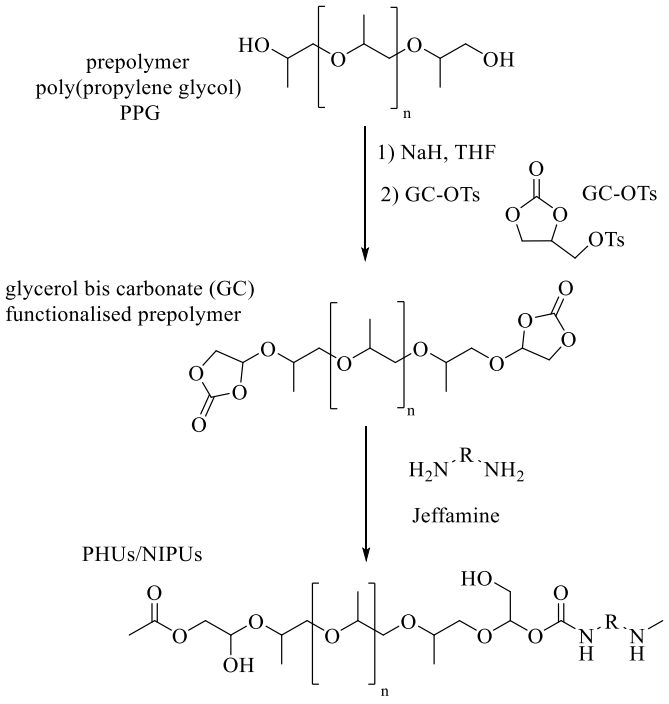

Scheme 8. *Synthesis of NIPUs derived from PPG functionalised with GC.*

Vegetable oils can also be used as raw materials to produce carbonated oils and therefore they are potential building blocks for NIPU synthesis (Scheme 9). However, the uncontrolled functionality of triglycerides restrains the control of PHUs structure and properties. Thus, the use of such poly(cyclic carbonates) can lead to thermosets PHUs when the cross-linking density is high. In this context, several vegetable oils have been used for the synthesis of PHUs.[77–82]

The first example of a vegetable oil-derived NIPU was reported by Wilkes *et al.* in 2003. Carbonated soybean oil (CSBO) was firstly synthesised and further reacted with several alkyl diamines to produce a range of PHUs.[77] Dubois *et al.* used CSBO (carbonated at 30%, 40% and 100%) and monomeric or oligomeric diamines to achieve thermosets or thermoplastic PHUs, depending on the carbonate/amine ratio used.[80] When the NIPUs were prepared from 100% CSBO and short diamines, the materials exhibited low mechanical properties attributed to a high cross-linking density due to the high cyclic carbonate functionality of CBSO. However, when using amino-telechelic oligoamides, NIPUs kept softness with T_g values close to 0 °C and a thermoplastic behaviour due to the limited reactivity of partial carbonated soybean oil.

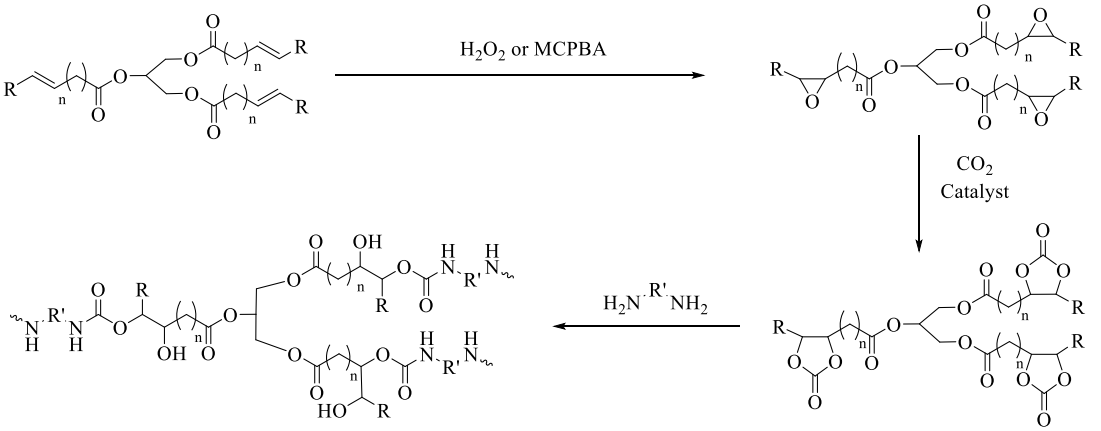

Scheme 9. Generic synthesis of PHUs from vegetable oils.

Sunflower oil has also been used as a precursor for PHU synthesis. Dolui *et al*. reported the bulk polyaddition of carbonated sunflower oil (CSFO) onto ethanediamine (EDA), diethylenetriamine (DETA) and isophorone diamine (IPDA).[81] As expected, the structure of the diamine and the carbonate/amine ratio affected the properties of the resulting PHU. In all CSFO/amine compounds, along with the ester and urethane groups, an amide group was present due to the hydrolysis of ester groups

along with the ester and urethane groups, except for IPDA, in accordance to previously studies reported studies.[74]

Finally, the synthesis of carbonated canola oil and its polyaddition reaction onto different diamines such as EDA, 1,6-hexanediamine (HDMA), IPDA and paraphenylenediamine (PPDA) has also been reported.[82] Thermal stability, mechanical strength and chemical resistance studies were performed to the produced PHUs. The TGA analysis for the different samples revealed that the NIPU from EDA showed the best thermal stability. Tensile strength was found to be higher when aliphatic amines were used. Chemical resistance for the obtained NIPUs was studied by observing its swelling behaviour in toluene and water. The least swelling was observed in case of EDA-based polyurethane. The formulation containing aromatic moieties showed lesser extent to solvent uptake as compared to the formulation having a cyclic amine.

To overcome the ill-defined cross-linked PHUs obtained from high carbonated triglycerides, well-defined bis-carbonated vegetable-based fatty acids have emerged as an alternative for the synthesis of linear PHUs. In this context, the first example was reported by Cramail *et al*. in 2010.[74] The fatty acid-based 5-membered bis(cyclic carbonate) was synthesised in a three-step process composed of (i) a transesterification reaction of fatty acid methyl esters, (ii) an epoxidation of the double bonds, and (iii) a carbonation of the resulting epoxides. Two 5-membered bis(cyclic carbonates), internal and terminal carbonated fatty acid diester were prepared from methyl oleate and methyl undecenoate and polymerised with EDA or IPDA to obtain linear PHUs with hydroxyl moieties. More recently, the same group reported the synthesis of several fatty acid-based 5-membered bis(cyclic carbonates) following the already mentioned epoxidation/carbonation strategy.[67]

As it has been previously mentioned, other natural products have also been employed for the synthesis of NIPUs. In this context, *D*-mannitol has been used to obtain bis carbonated derivatives which were later reacted with aliphatic diamines to afford NIPUs with molecular weights up to 87000 g mol^{-1}.[63] Similarly, North *et al.* reported the synthesis of sorbitol-derived bis carbonate and subsequent reaction with simple diamines such as cadaverine to generate NIPU foams.[83]

Other research groups have converted limonene into a bis(cyclic carbonate) by epoxidation/carbonation strategy (Scheme 10).[84,85] Novel linear and cross-linked NIPUs and prepolymers were obtained by reaction with aliphatic diamines and isophorone diamine. T_g values as high as 70 ºC were obtained when the two polymerised monomers were cycloaliphatic.

More recently, isosorbide diglycidyl ether oligomers have been synthesised by reaction of epichlorohydrin on the hydroxyl functions of the bio-based diol. Carbonation afforded an isosorbide-based bis(cyclic carbonate) which was further reacted with different diamines to obtain the corresponding NIPUs (Scheme 11).[86]

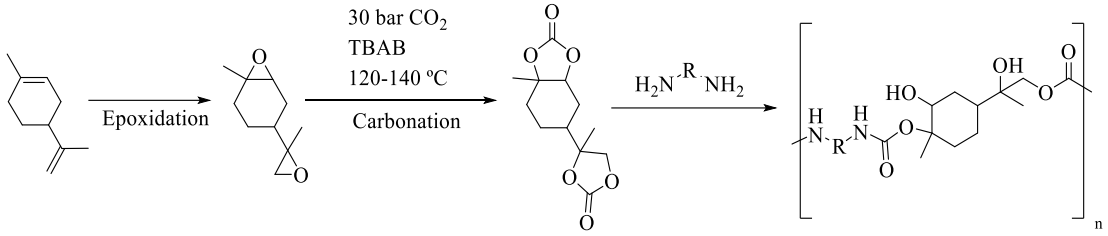

Scheme 10. *Limonene-based NIPUs synthesis.*

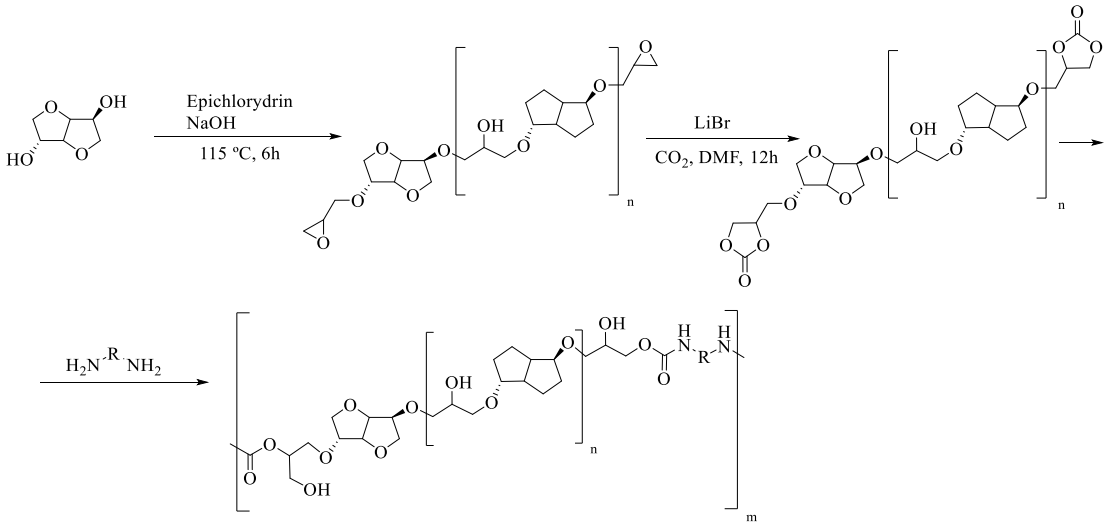

Scheme 11. *Isosorbide-based NIPUs synthesis.*

Despite the ongoing interest for the development of biopolymers, the cyclic carbonate/amine routes suffer from a lack of bio-based amines, and more specifically, vegetable-oil based diamines, restraining the access to fully bio-based PHUs.

Results and discussion

1. Polyaddition of 5-membered bis(cyclic carbonates) and diamines for the synthesis of non-isocyanate polyurethanes

As it has been discussed in the introduction of this section, one of the main applications of cyclic carbonates is their use as chemical intermediates to produce high-value added industrial products such as polyurethanes. These polymers exhibit multiple applications and can be easily obtained by polyaddition reactions of bis(cyclic carbonates) onto diamines. In this section, the synthesis of PHUs from either petroleum-based or fully bio-based bis(cyclic carbonates) will be described.

1.1. Synthesis of NIPUs from petroleum-based bis(cyclic carbonates)

In this section, the synthesis of PHUs derived from the polyaddition reaction of 1,4-butanediol bis(glycidyl ether carbonate) (BGDC) onto a range of diamines will be discussed.

Firstly, the commercially available 1,4-butanediol bis-glycidyl ether (BGDE) was carbonated using 1% of the previously reported hydroxy-containing imidazole organocatalyst designed by our group at 10 bar of CO_2 and 80 ºC for 2 hours.[87] Under these reaction conditions, 1,4-butanediol bis(glycidyl ether carbonate) (**46**) was synthesised in 90% yield as shown in Scheme 12.

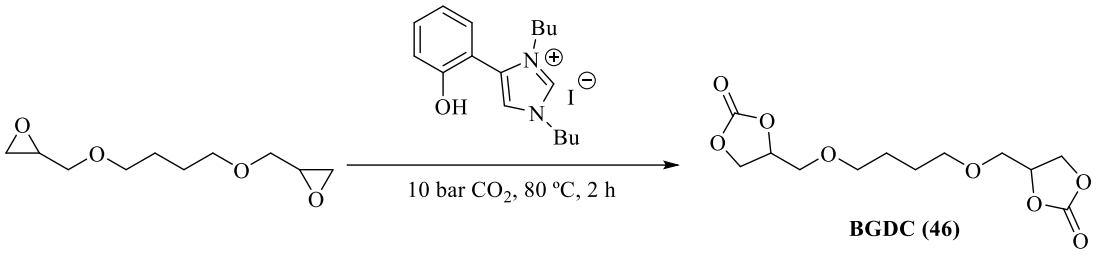

Scheme 12. *Synthesis of 1,4-butanediol bis(glycidyl ether carbonate) (**46**).*

Initially, the reaction conditions to synthesise NIPUs were optimised using BGDC and 1,4-diaminobutane (BDA) as substrates in a 1:1 molar ratio (Scheme 13). Firstly, the solvent effect on the conversion was investigated (Table 1, entries 1-4). However, all solvents afforded the desired PHU quantitatively. Amongst them, MeCN was chosen as the optimal solvent to perform the polyaddition reactions due to its low toxicity, high polarity to increase the solubility of the starting materials and easy accessibility. The effect of the reaction temperature was also studied (Table 1, entries 5-9). As expected, the conversion decreased as the temperature was descreased.

Polyaddition of BGDC to BDA at room temperature afforded the corresponding PHU in 67% conversion after 16 h of reaction (Table 1, entry 7). Since previous works confirmed the addition of strong bases catalysed the process,[88] the addition of TBD was also investigated (Table 1, entries 8-9), showing the conversion toward the synthesis of the NIPU increased to 93% at room temperature.

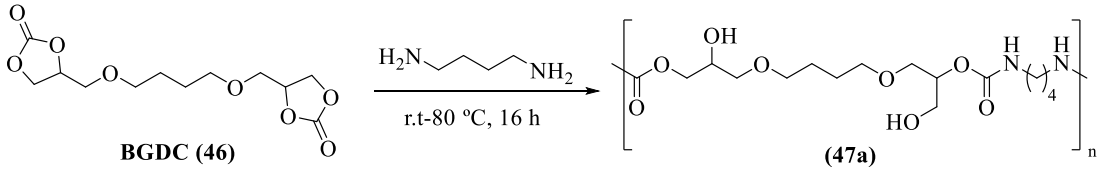

Scheme 13. *Synthesis of PHU **47a**.*

Table 1. *Optimisation of reaction conditions for the polyaddition of BGDC and 1,4-diaminobutane.*

Entry	Solvent	t (h)	T (ºC)	Conversion (%)[a]
1	DMF	16	80	100
2	MEK	16	80	100
3	EtOAc	16	80	100
4	MeCN	16	80	100
5	MeCN	16	60	93
6	MeCN	16	40	83
7	MeCN	16	r.t.	67
8[b]	MeCN	16	r.t.	92
9[c]	MeCN	16	r.t.	93

[a]Determined by NMR. [b]5 mol% of TBD was added. [c]10 mol% of TBD was added.

Once the optimal conditions for the polyaddition of BGDC to BDA were determined to be 80 ºC and MeCN as solvent for 16 hours, several PHUs were prepared using a wide range of commercial diamines to obtain a variety of polymers with different physical properties (Scheme 14) and the results are given in Table 2.

All PHUs were obtained quantitatively after 16 h (Table 2, entries 1-6), except when *L*-lysine was used, in which case, no reaction was observed (Table 2, entry 7). This result can be explained based on the low nucleophilicity of *L*-lysine, which is not able to ring-open the cyclic carbonate, and no polyaddition occurs. Thus, the addition of DBU or TBD as a catalyst to the reaction mixture resulted in the obtention of the desired PHU (Table 2, entries 8 and 9). However, the presence of strong bases led to the formation of PHU-polyurea materials, as has been previously observed in similar reactions.[75]

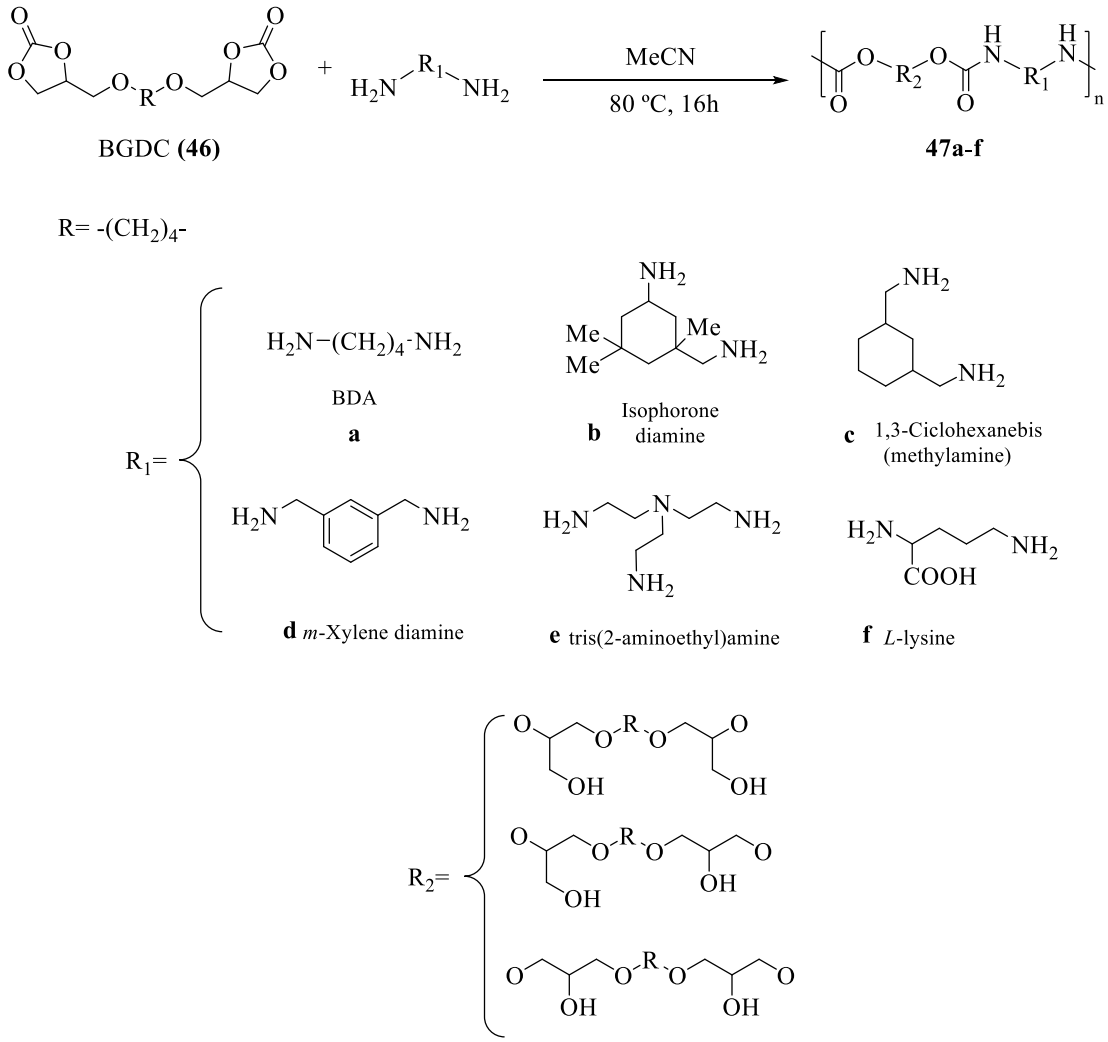

Scheme 14. *Synthesis of poly(hydroxyurethane)s (**47a-f**).*

In order to synthesise a cross-linked polyurethane, the reaction of 1 eq. of BGDC (**46**) with 0.66 eq. of tris(2-aminoethyl)amine was carried out (Table 2, entry 6). The formation of the cross-linked PHU was confirmed by the increase on the glass

transition temperature of the obtained PHU, due to the increased rigidity and crystallinity of the resulting polymer.

Table 2. *GPC data obtained for selected PHUs*[a].

Entry	Diamine	Conv. (%)[b]	Primary OH: Secondary OH[b]	$M_{n,exp}$[c]	PDI[c]
1	1,4-diaminobutane (**47a**)	100	32:68	5350	3.2
2	Isophorone diamine (**47b**)	100	36:64	6520	3.5
3	1,3-cyclohexanebis(methylamine) (**47c**)	100	36:64	6740	3.6
4	*m*-Xylene diamine (**47d**)	100	38:62	9050	2.2
5	tris(2-aminoethyl)amine (**47e**)	100	28:72	5720	3.1
6[d]	tris(2-aminoethyl)amine (**47e**)	100	-	-	-
7	*L*-lysine (**47f**)	0	-	-	-
8[e]	*L*-lysine (**47f**)	88	.	39200	4.1
9[f]	*L*-lysine (**47f**)	90	-	40325	4.2

[a]Reactions were carried out at 80 ºC in MeCN for 16h. [b]Determined by NMR. [c]Determined by GPC. [d]0.66 eq. of tris(2-aminoethyl)amine were used. [e]1 eq. of DBU was used. [f]1 eq. of TBD was used.

The chemical structures of PHUs were characterised by ^{1}H-NMR, ^{13}C-{^{1}H}-NMR, Diffusion Ordered Spectroscopy (DOSY) NMR and IR spectroscopy, MALDI-ToF analysis and Gel Permeation Chromatography (GPC). Figure 5 shows the FT-IR spectra of BGDC (**46**) and PHUs **47c** and **47f**. Bis(glycidyl ether carbonate) (**46**) exhibited two characteristic bands at 1781 and 1050 cm^{-1} corresponding to the cyclic carbonate groups. However, those signals disappeared in the PHUs IR spectra, and two new bands were observed at 1695 and 1537 cm^{-1} and 1699 and 1538 cm^{-1} for PHUs **47c** and **47f**, respectively, confirming the formation of urethane groups. However, a band at 1646 cm^{-1} was observed for PHU **47f** which corresponds to the C=O stretching vibration of the urea group, indicating the formation of polyurethane-polyurea chains.[75] The ^{1}H-NMR spectrum of the PHU **47a** synthesised from BGDC and 1,4-diaminobutane is shown in Figure 6. The signals at 7.11 ppm and 6.74 ppm were

assigned to the protons of the urethane groups, confirming the urethane structure of the final product. The pair of resonances at 2.95 ppm; 1.37 ppm and 3.39 ppm; 1.52 ppm were assigned to the methylene protons of the alkyl groups of the diamine and the BGDC respectively. As it has been previously mentioned, it is known that both primary and secondary hydroxyl groups can be formed in the PHU backbone depending on the ring-opening pathway of the cyclic carbonate moiety. In Figure 6, two signals are observed at 4.89 and 4.75 ppm, corresponding to the formation of the secondary and primary hydroxyl groups, respectively. Following previously reported results,[55,63,71] the PHUs synthesised in this work exhibited a primary:secondary OH ratio ranging from 28:72-38:62 (Table 2, entries 1-5).

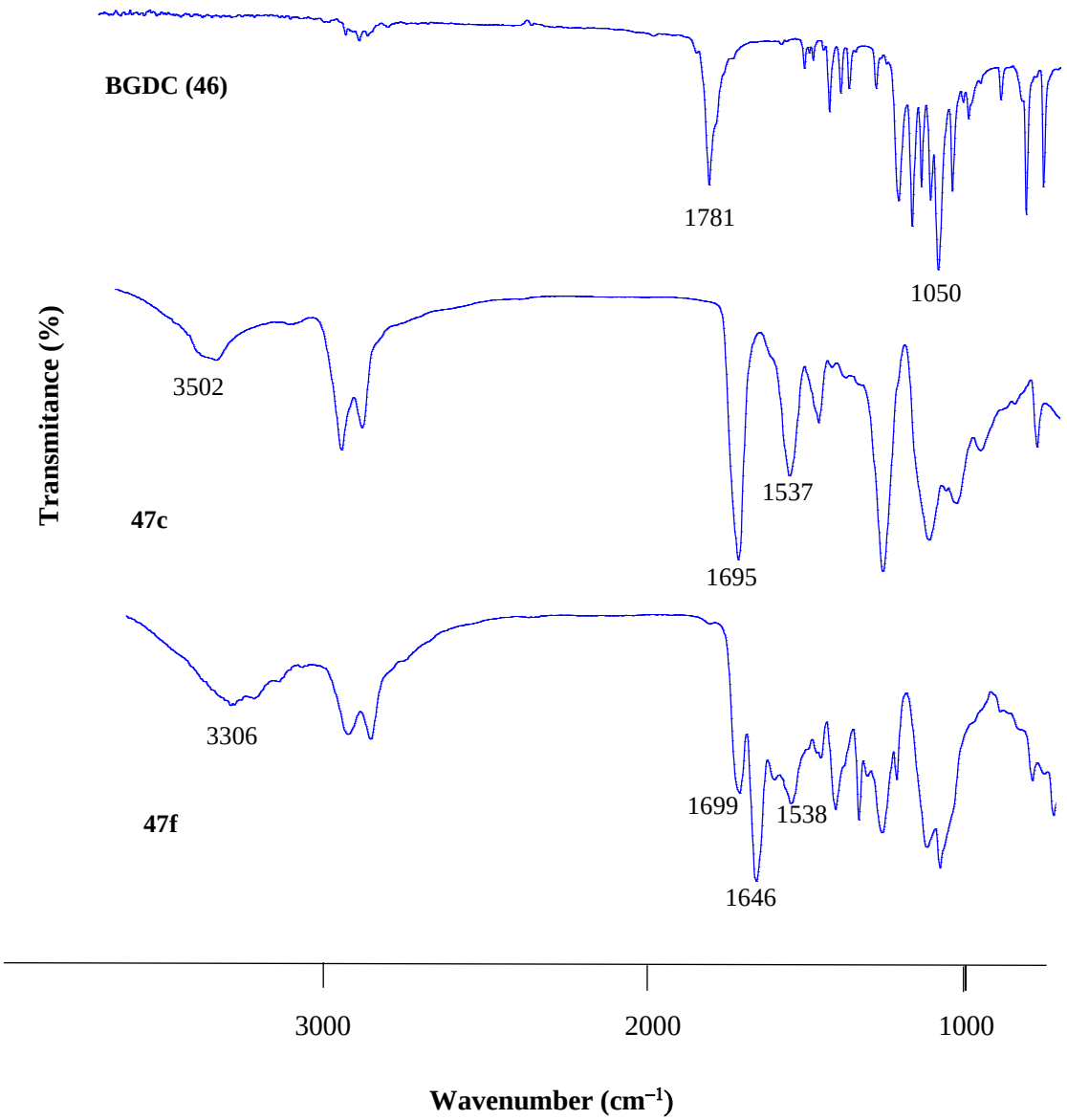

Figure 5. *IR spectra for BGDC and PHUs **47c** and **47f**.*

As can be seen from Table 2, molecular weights obtained for PHUs **47a-e** exhibited values between 5350 and 9050 g mol^{-1} with high polydispersity values ranging from 2.2 to 3.6. This was attributed to the fact that no catalyst was used during the polymerisation process. Thus, there is not a good control over the polyaddition reaction and multiple chains with different molecular weights can be generated, hence, the high PDI values obtained. On the other hand, molecular weight increased notably for PHU **47f**, since DBU/TBD were used as catalysts for the polyaddition process, with values of 39200 g mol^{-1} and 40325 g mol^{-1} respectively. As an example, Figure 7 shows the GPC trace for PHU **47d**.

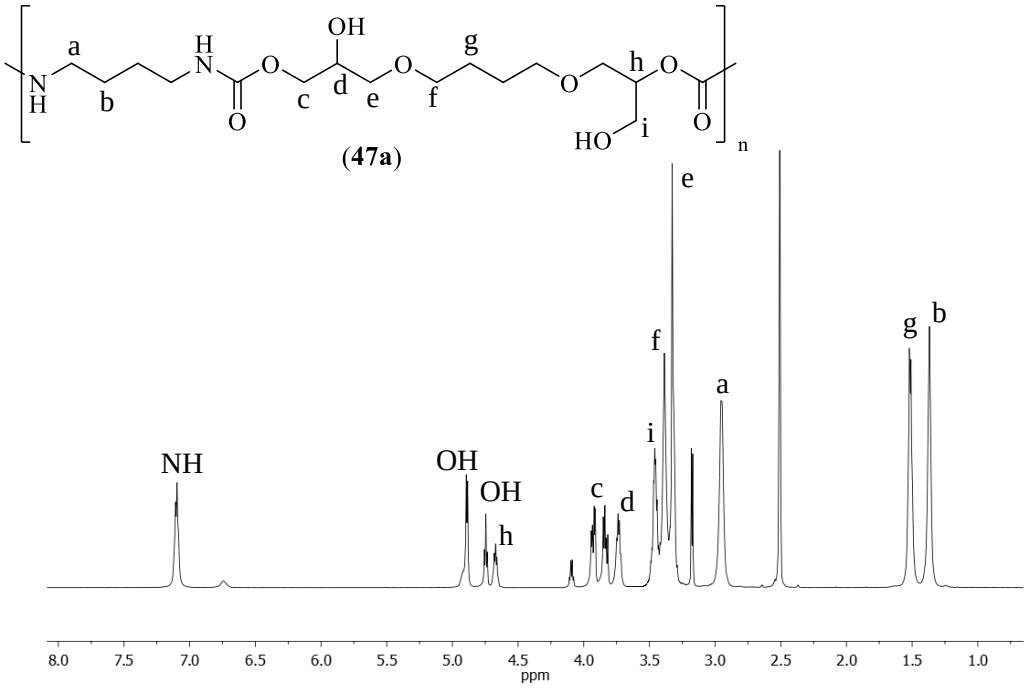

Figure 6. *^{1}H-NMR spectrum for poly(hydroxyurethane) **47a** in DMSO-d_6.*

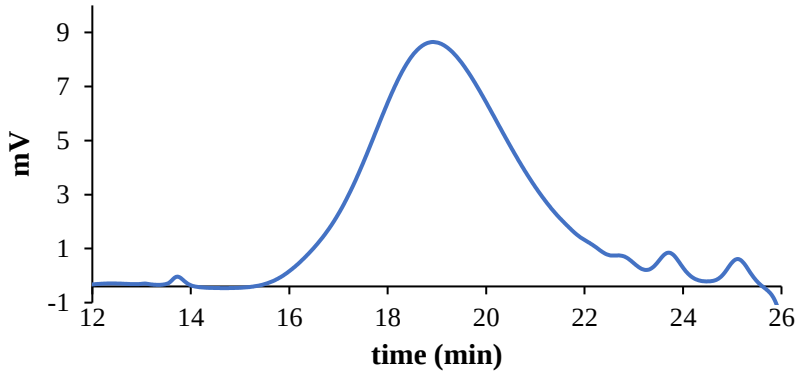

Figure 7. *GPC trace for PHU **47d**.*

MALDI-ToF mass spectrometry was used to determine the end groups of the obtained PHUs. Figure 8 exhibits the MALDI-ToF spectrum for PHU **47b**. It showed a series of peaks with an *m/z* interval of 460 mass units, indicating a controlled alternating microstructure, which is in good agreement with a polymer chain with one isophorone diamine group in one end and a protonated urethane group in the other end of the polymeric chain.

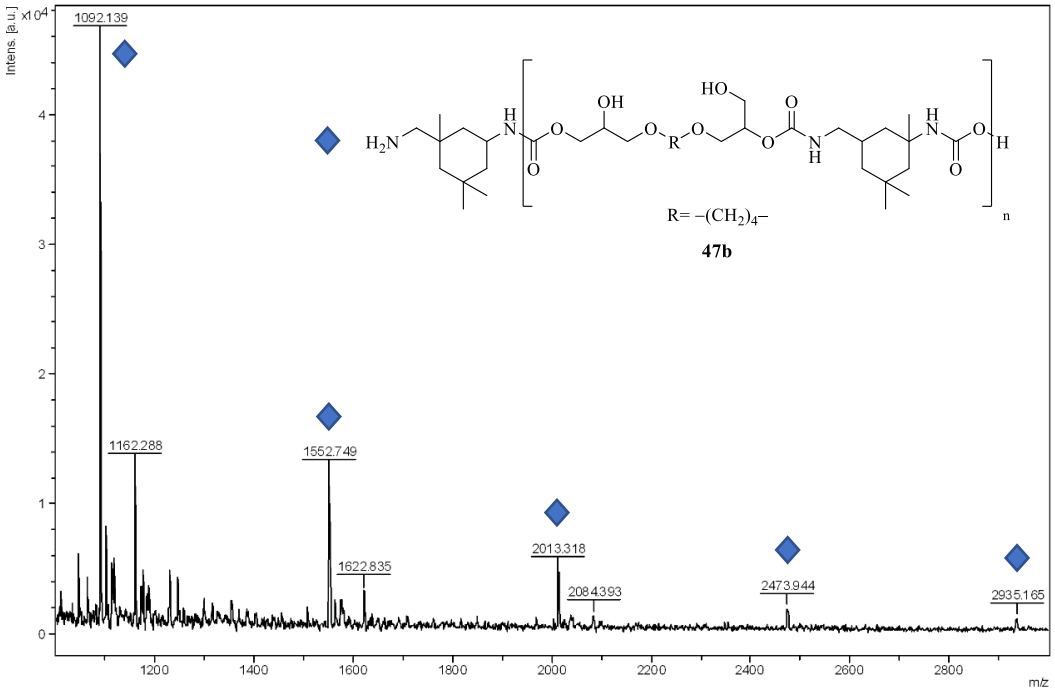

Figure 8. *MALDI-Tof spectrum for PHU **47b**.*

2D-DOSY NMR studies were also carried out to further confirm the obtention of PHUs. As an example, Figure 9 shows the DOSY-NMR spectrum for PHU **47f**. As it is shown in Figure 9, three diffusion coefficients were observed, corresponding to the solvent, DBU, and the polymer chain. This indicated that, even polyurea was formed during the polymerisation process, only one segmented poly(hydroxyurea-urethane) polymer was obtained.

The effect of the [diamine]/[BGDC] ratio on the polyaddition reaction of BGDC onto 1,4-diaminobutane was also studied (Scheme 15). Thus, when 0.5 eq. of 1,4-diaminobutane were used, a hydroxycarbamate with two cyclic carbonate ending groups was obtained (**48**). On the other hand, when 2 eq. of diamine were added, a hydroxycarbamate with two amine ending groups was obtained (**49**). The structures for compounds **48** and **49** were characterised by NMR spectroscopy, IR and MALDI-

ToF analysis. Figure 10 shows the ^{1}H-NMR spectrum for compound **48**. The resonances at 4.92 ppm, 4.52 ppm and 4.27 ppm confirmed the presence of cyclic carbonate groups. Besides, the IR spectrum for hydroxycarbamate **48** exhibited two bands at 1787 and 1048 cm^{-1}, which correspond to the cyclic carbonate groups as well as two bands at 1692 and 1525 cm^{-1} corresponding to the urethane group generated. MALDI-ToF spectrum for compound **48** is shown in Figure 11. A single peak with a *m/z* of 691 mass units is observed, which corresponds to the molecular weight of hydroxycarbamate **48** and Na^{+}.

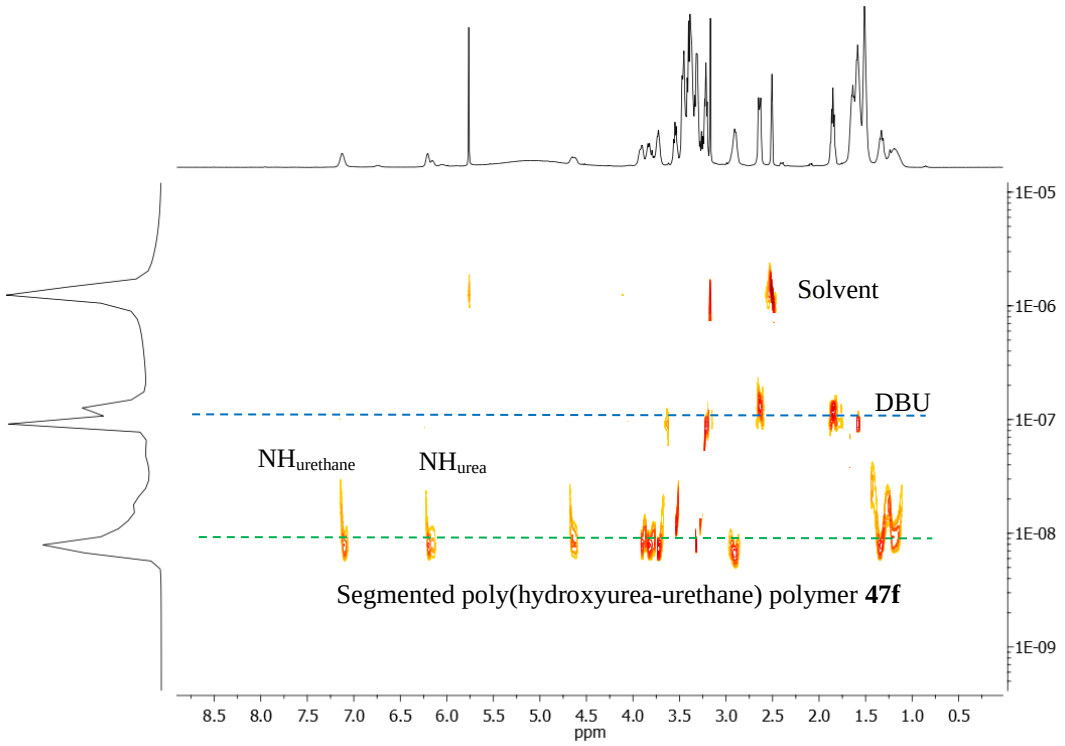

Figure 9. *DOSY NMR spectrum for PHU **47f** in DMSO-d_6.*

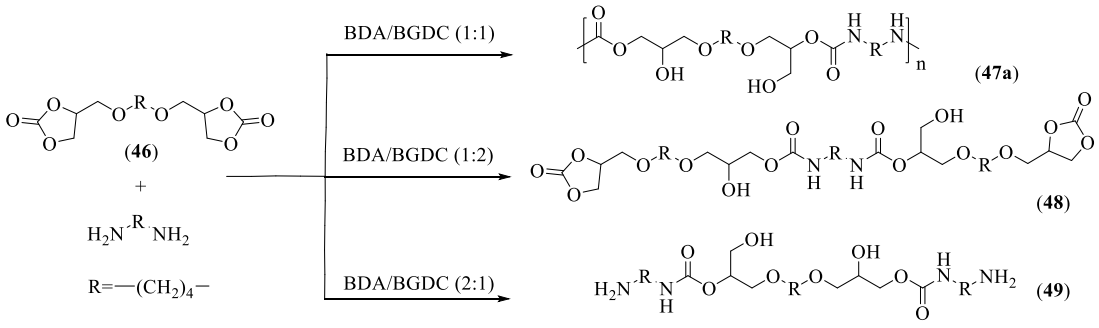

Scheme 15. *Synthesis of hydroxycarbamates **48** and **49** and PHU **47a**.*

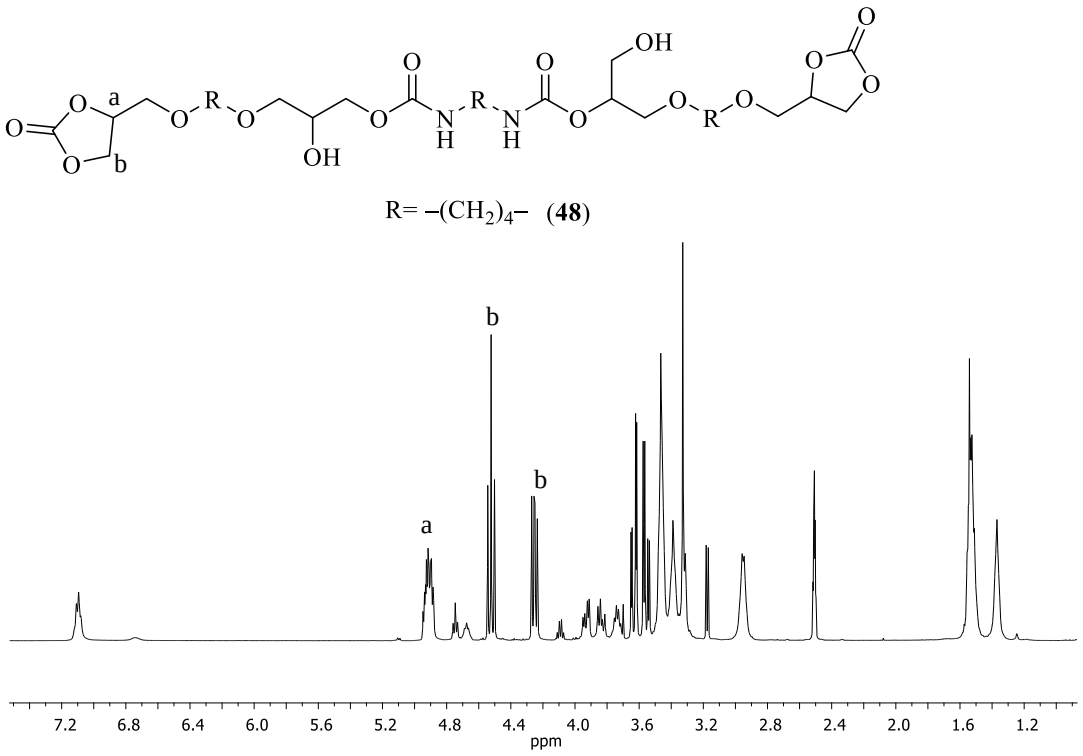

Figure 10. *^{1}H-NMR spectrum for hydroxycarbamate **48** in DMSO-d_6.*

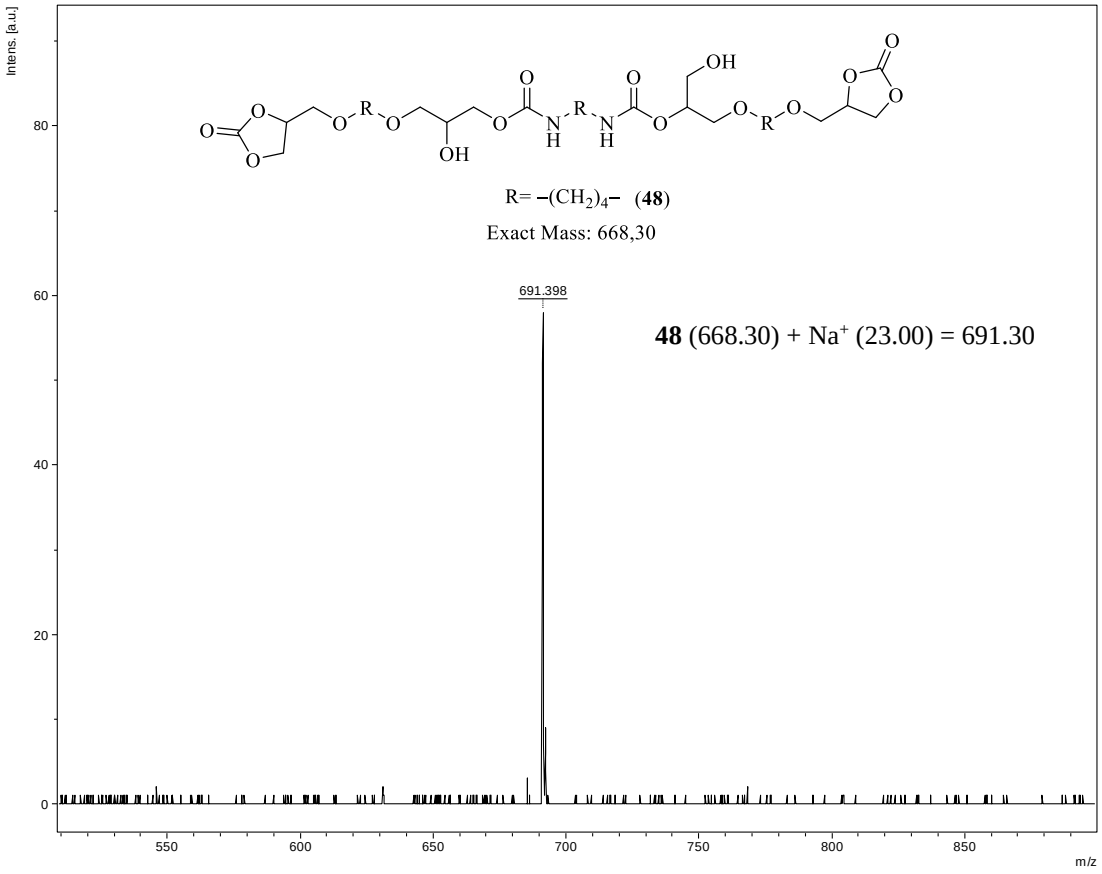

Figure 11. *MALDI-ToF spectrum for hydroxycarbamate **48**.*

Table 3. *DSC and TGA analyses for selected PHUs.*

Entry	Diamine	T_g (ºC)[a]	$T_{d,\,5\%}$ (ºC)[b]
1	1,4-diaminobutane (**47a**)	11	252
2	Isophorone diamine (**47b**)	22	272
3	1,3-cyclohexanebis(methylamine) (**47c**)	22	263
4	*m*-Xylene diamine (**47d**)	22	231
5	tris(2-aminoethyl)amine (**47e**)	–3	229
6[c]	tris(2-aminoethyl)amine (**47e**)	43	261
7	*L*-lysine (**47f**)	–13	128

[a]Determined by Different Scanning Calorimetry (DSC). [b]Determined by Thermal Gravimetric Analysis. (TGA). Reported as temperature at 5% mass loss. [c]0.66 eq. of tris(2-aminoethyl)amine were used.

Thermal properties of the PHUs synthesised from BGDC and diamines were investigated by DSC and TGA analyses (Table 3). TGA showed that all PHUs were stable in the range of temperatures from 0 ºC to 230 ºC (Table 3), except for the PHU derived from *L*-lysine (Table 3, entry 7), which was found to be stable between 0 ºC and 128 ºC. The glass transition phenomenon was observed in the DSC thermograms. As can be observed from Table 3, the T_g of the PHUs ranged from –13 to 43 ºC (Table 3, entries 1-7), depending on the chemical structure of the diamines used. Most studies agreed that high molecular flexibility between the hydroxyurethane groups led to lower T_g of PHUs.[89–91] Thus, PHUs derived from rigid amines such as isophorone diamine (Table 3, entry 2), 1,3-cyclohexanebis (methylamine) (Table 3, entry 3) or *m*-xylene diamine (Table 3, entry 4) exhibited higher T_g values than PHUs derived from aliphatic diamines such as BDA (Table 3, entry 1), tris(2-aminoethyl)amine (Table 3, entry 5) or *L*-lysine (Table 3, entry 7). On the other hand, the cross-linked PHU derived from tris(2-aminoehtyl)amine exhibited the highest T_g due to the formation of a polymeric structure with higher rigidity and crystallinity (Table 3, entry 6). For instance, Figure 12 shows the DSC thermogram for PHU **47e** and Figure 13 exhibits the TGA thermogram for PHU **47d**.

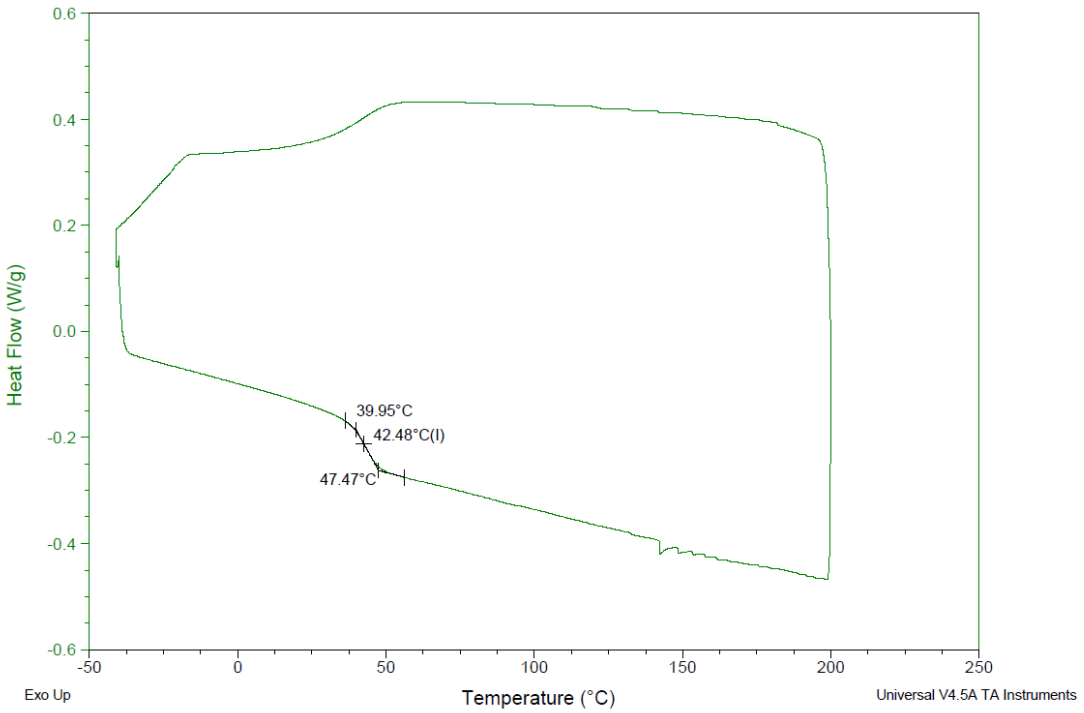

Figure 12. *DSC thermogram for PHU **47e** using 0.66 eq. of tris(2-aminoethyl)amine.*

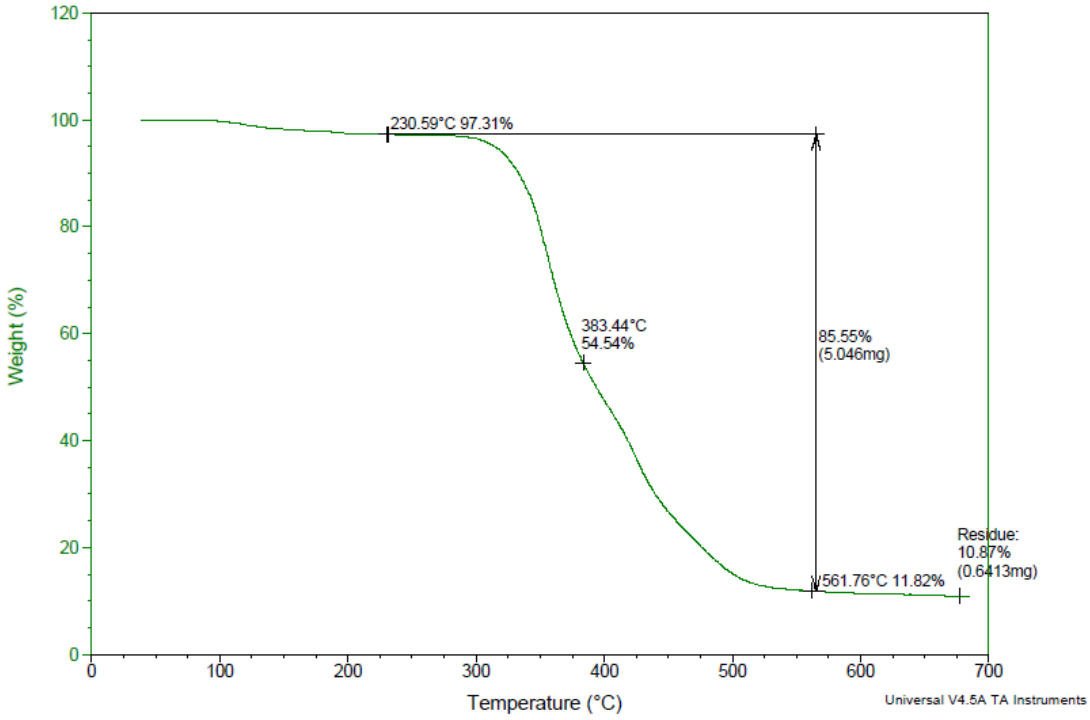

Figure 13. *TGA thermogram for PHU **47d**.*

After the successful multi-step synthesis of PHUs **47a-f**, their direct synthesis from BGDE, TBAB, CO_2 and a diamine in a one-pot process was investigated. For that purpose, BDA, 1,3-cyclohexanebis(methylamine) and *m*-xylene diamines were used as starting materials. In all cases, full conversion of BGDE to BGDC (**46**) and subsequent polyaddition onto the corresponding diamine to generate the corresponding NIPU was achieved under the same reaction conditions previously mentioned. However, the obtained polymeric materials were insoluble in all standard solvents Notably, the formation of cross-linked poly(aminoalcohols) from bis-epoxides and diamines in the absence of CO_2 has been previously reported.[92,93] Additionally to the polymer, a white precipitate was also obtained and was identified as the corresponding carbamate salt from the corresponding diamine and CO_2 (Scheme 16).[94]

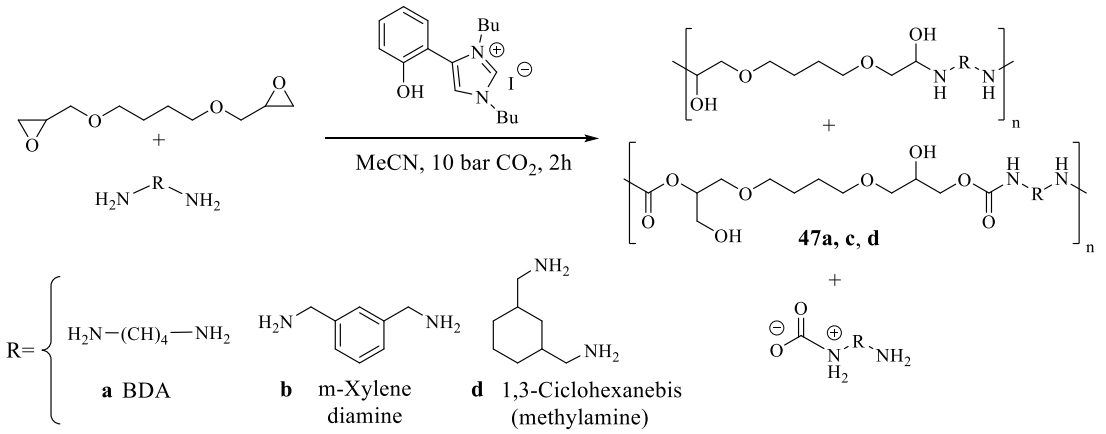

Scheme 16. *One-pot synthesis of PHUs **47a**, **c**, **d**.*

IR analysis of the resulting mixture confirmed the presence of poly(aminoalcohol), carbamate salt and poly(hydroxyurethane). Figure 14 shows the comparison of the IR spectra of a blank sample containing 1,4-diaminobutane and BGDE (Figure 14a), 1,4-diaminobutane and CO_2 (Figure 14b), and the one-pot reaction mixture (Figure 14c). As it can be observed from Figure 14, the one-pot reaction mixture (Figure 14c) shows a sharp band at 3315 cm^{-1} corresponding to the frequency of the carbamate salt as well as bands at 1555 and 1326 cm^{-1} which correspond to the N–H bending and C–N stretching frequencies of the amine group, confirming the presence of the carbamate salt. Similarly, the presence of poly(aminoalcohol) was confirmed by the presence of two peaks at 1108 and 1454 cm^{-1} corresponding to the C–O stretching and O–H bending from the alcohol group. The obtention of the PHU was confirmed by the presence of a band at 1699 cm^{-1} corresponding to the urethane moiety.

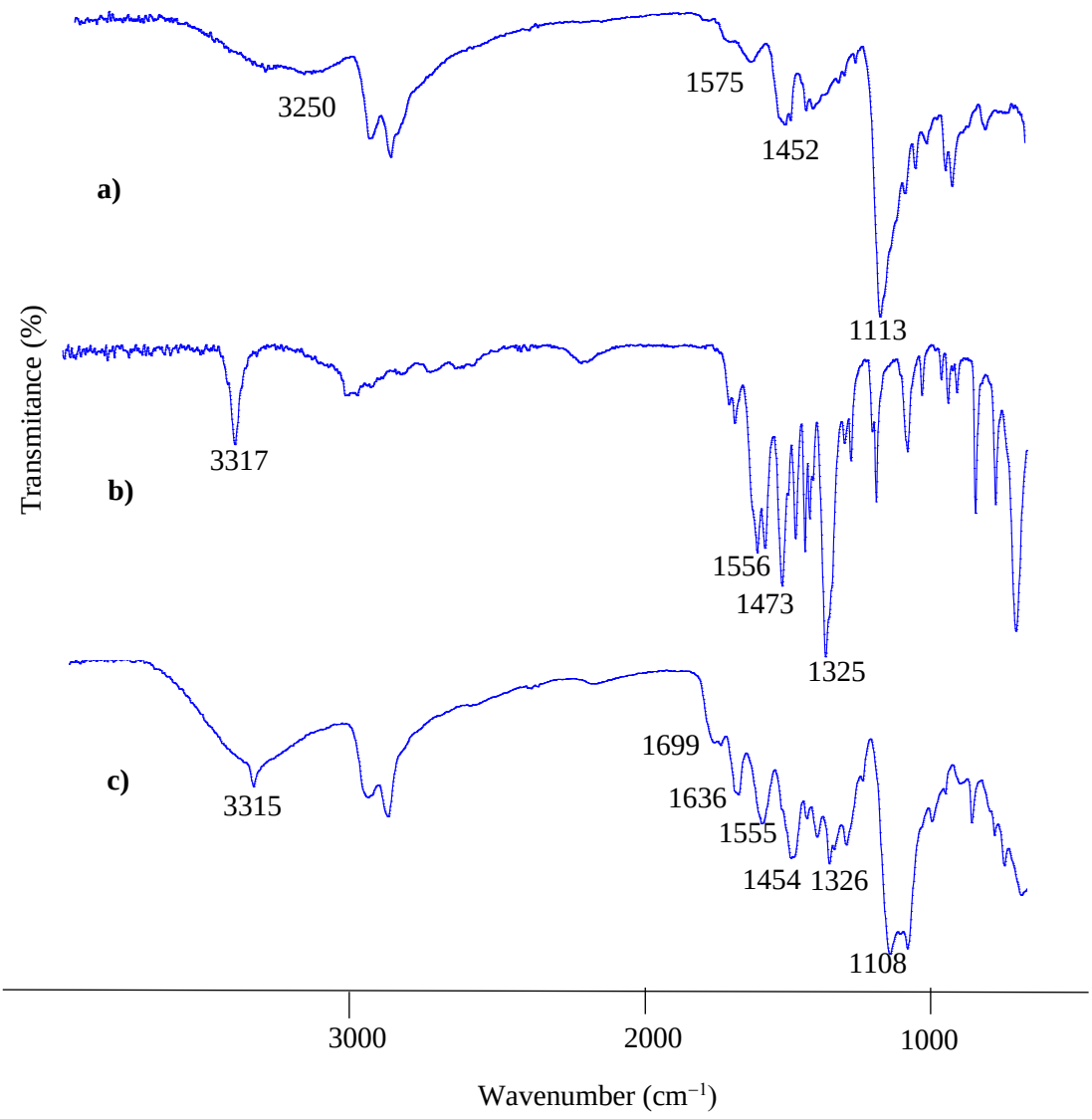

Figure 14. *IR spectra for a) 1,4-diaminobutane + BGDE, b) 1,4-diaminobutane + CO_2 and c) one pot synthesis of PHU* **47b**.

Finally, to avoid undesired reactions such as the formation of poly(aminoalcohol) or carbamate salt, a sequential one-pot method was developed for the synthesis of PHUs. Therefore, bis(cyclic carbonate) BGDC (**46**) was prepared from BGDE as shown in Scheme 12. Subsequent addition of the corresponding diamine to the reaction mixture afforded the formation of PHUs **47a**,**c**,**d**. It is worth noting that polyurea formation was observed by NMR and IR when using primary and less steric hindered diamines such as 1,4-diaminobutane and 1,3-cyclohexanebis(methylamine). This can be attributed to the presence of the hydroxy-containing imidazole organocatalyst, used for the carbonation of BGDE, in the reaction mixture, which could act in the same manner as TBD, and, thus, produce the formation of polyurea.

1.2. Synthesis of NIPUs from bio-based bis(cyclic carbonates)

In this section, the synthesis of PHUs derived from the polyaddition reaction of bio-based glutaryl- and carvyl-derived bis(cyclic carbonates) and a range of diamines will be discussed.

Firstly, bis(oxiran-2-ylmethyl) glutarate (**50**) and carvyl acetate bis-epoxide (CABE, **51**) were synthesised as shown in Scheme 17. Commercially available glutaryl chloride was reacted with glycidol in dichloromethane at 0 ºC for 16 hours, and after the appropriate work up, afforded compound **50** in high yield. On the other hand, bis-epoxide **51** was synthesised by reacting commercially available (–)-carvyl acetate with 3-chloroperbenzoic acid (MCPBA) in dichloromethane at 0 ºC for 24 hours, and after the appropriate work up, carvyl acetate bis-epoxide was obtained in good yield.

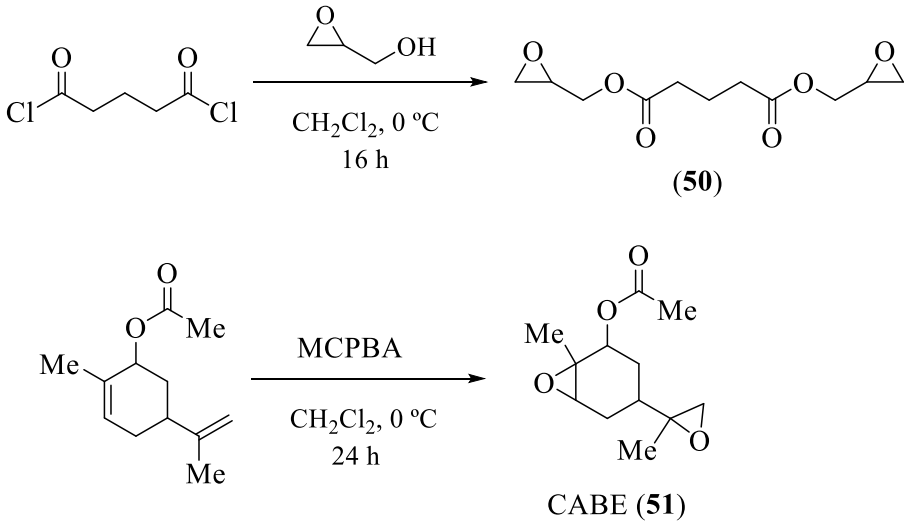

Scheme 17. *Synthesis of bis(oxiran-2-ylmethyl) glutarate (**50**) and carvyl acetate bis-epoxide (**51**).*

Then, glutaryl bis(cyclic carbonate) (BGLBC, **52**) and carvyl acetate-derived bis(cyclic carbonate) (CABC, **53**) were synthesised as shown in Scheme 18.[95] Compounds **50** and **51** were carbonated using the previously reported heteroscorpionate aluminium complex [$AlMe_2(\kappa^2$-bpzbdeape)] in combination with TBAB as the catalytic system at 80 ºC and 10 bar of CO_2 for 3 hours to synthesise BGLBC (**52**) or 66 hours for CABC (**53**).[95]

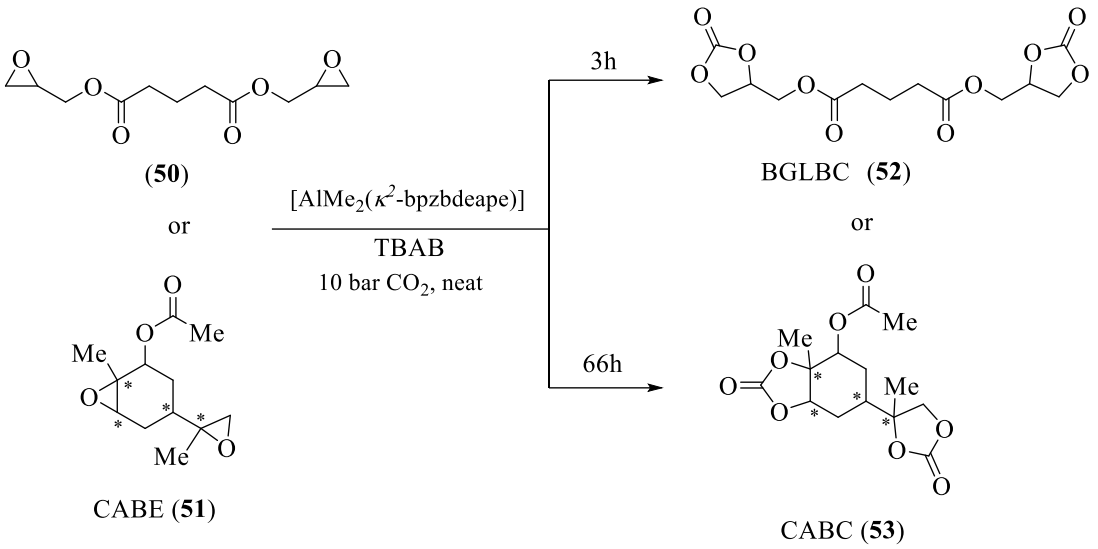

Scheme 18. *Synthesis of bioderived bis(cyclic carbonates)* ***52*** *and* ***53****.*

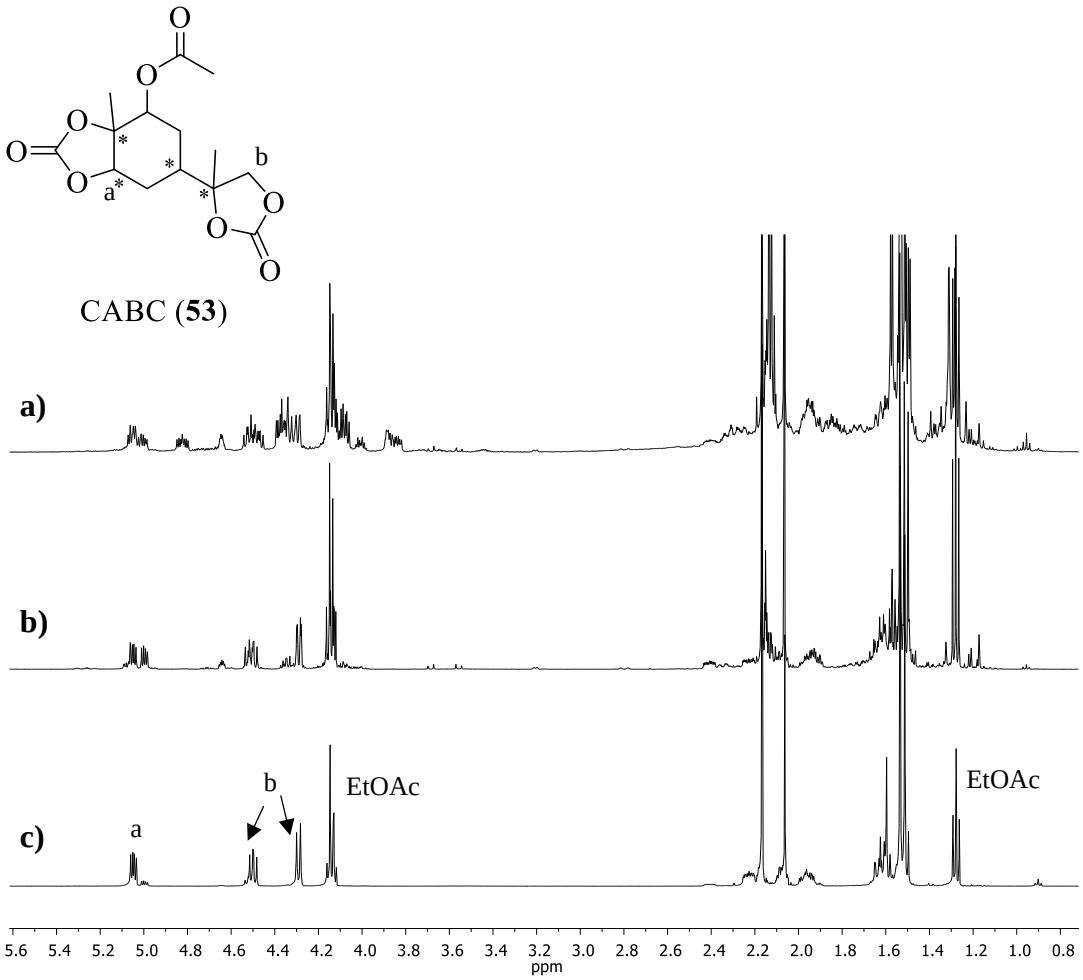

Figure 15. *^{1}H-NMR of CABC (****53****) a) 8 diasteroisomers b) 4 diasteroisomers c) single diastereoisomer obtained by crystallization in $CDCl_3$.*

The structural characterisation of bis(cyclic carbonates) BGLBC (**52**) and CABC (**53**) was performed by ^{1}H-NMR and ^{13}C{^{1}H}-NMR spectroscopy and X-Ray Diffraction Crystallography. As can be seen from Scheme 18, CABC (**53**) exhibits four different stereogenic centres. Thus, up to 16 stereoisomers (8 pairs of diastereoisomers) can be obtained. During its purification procedure by flash chromatography, three different fractions of CABC (**53**) were obtained, corresponding to different mixtures of diastereoisomers. Figure 15 shows the ^{1}H-NMR spectra for the different fractions of CABC obtained during its purification. White crystals of CABC (**53**) were obtained by slow evaporation from a solution of Hex/EtOAc (2:1) and the ORTEP diagram is represented in Figure 18. In solid state, CABC (**53**) crystallizes as an enantiopure estereoisomer *RSSR* and its structure is depicted in Figure 16.

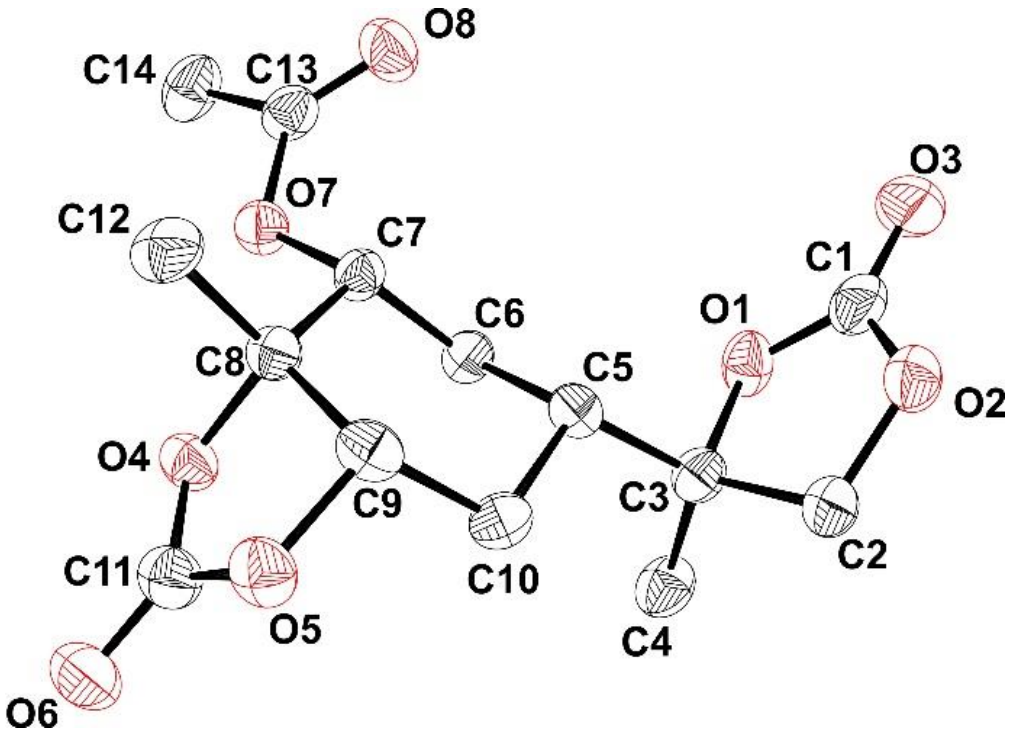

Figure 16. *ORTEP diagram for CABC (53).*

Once BGLBC (**52**) and CABC (**53**) were synthesised, they were used as building blocks for the preparation of different PHUs using a wide range of commercial diamines with different physical and electronic properties (Scheme 19). The optimised reaction conditions for the synthesis of PHUs derived from BGDC (**46**) previously described were firstly used as standard conditions. However, due to the low solubility of BGLBC (**52**) in MeCN, reactions to synthesise PHUs **54a-e** were carried out in

dimethylformamide (DMF). The results are given in Tables 4 and 5. All PHU's were obtained in 100% conversion after 16 h. It is worth highlighting that all the NIPUs **54a-e** and **55a,c-f** from bio-derived bis(cyclic carbonates) have been firstly synthesised in this work.

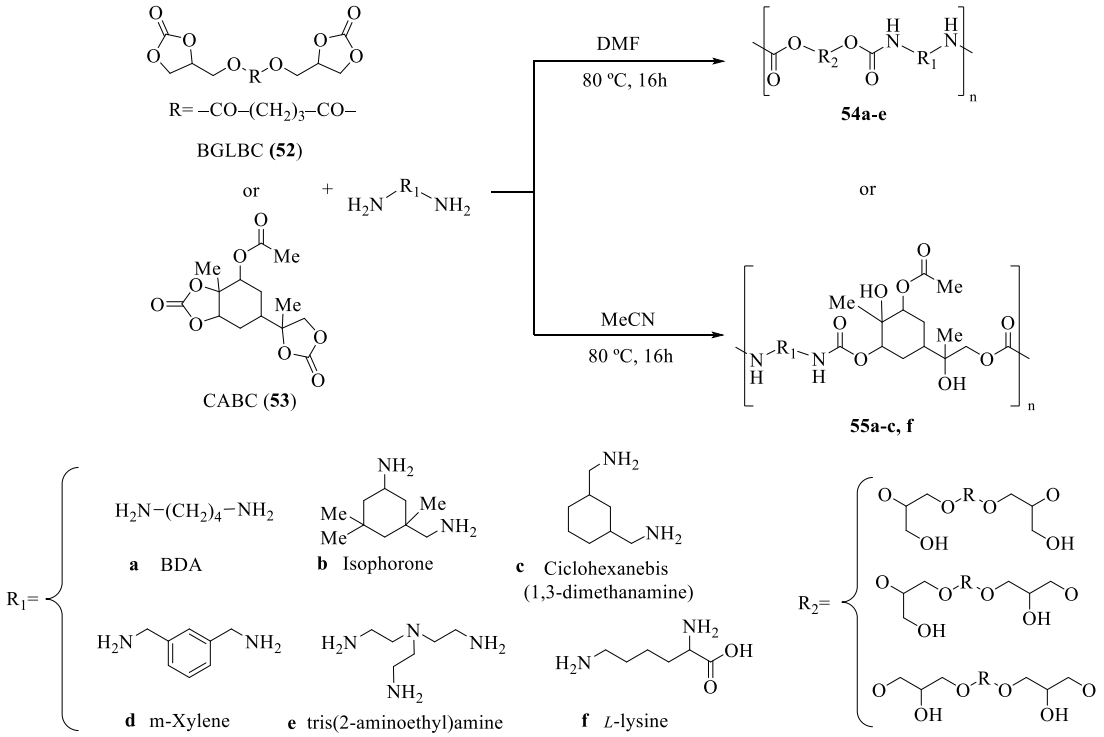

Scheme 19. *Synthesis of PHUs **54a-e** and **55a,c-f**.*

The chemical structures of all PHUs were characterised by ^{1}H-NMR, ^{13}C-{^{1}H}-NMR, 2D-DOSY-NMR, and IR spectroscopy, and GPC analysis. Figure 17 shows the FT-IR spectra of BGLBC (**52**) (Figure 17a) and PHU **54e** (Figure 17b). The spectrum for BGLBC (**52**) exhibited two characteristic bands at 1780 and 1737 cm^{-1} corresponding to the C=O vibration of the cyclic carbonate and the ester group respectively. Similarly, two bands were observed at 1047 and 1146 cm^{-1} corresponding to the C–O stretching vibration. However, in the PHU spectrum, two new bands at 1652 and 1542 cm^{-1} corresponding to the urethane/urea groups were observed. In addition, the obtention of PHU **54e** was confirmed by the observation of a broad band at 3294 cm^{-1}, corresponding to the O–H vibration after the ring-opening of the cyclic carbonate groups. The presence of a band at 1723 cm^{-1} corresponds to the amide group due to the presence of amidification byproducts. Similarly, Figure 18 shows the FT-IR spectra of CABC (**53**) and PHU **55e**. CABC (**53**) exhibited two characteristic bands

at 1791 and 1050 cm^{-1} corresponding to the C=O vibrations of the cyclic carbonate groups and acetate groups respectively. In addition, two bands at 1240 and 1027 cm^{-1} corresponding to the C–O stretching frequencies were also observed. However, those bands disappeared in the IR spectrum for PHU **55c** (Figure 18b), and two new bands at 1700 and 1534 cm^{-1} appeared, which correspond to the urethane group, confirming the formation of the poly(hydroxyurethane) chain.

Table 4. *GPC data for selected PHUs derived from BGLBC (**52**).*[a]

Entry	Diamine	Conv. (%)[b]	Primary OH: Secondary OH[b]	$M_{n,exp}$[c]	PDI[c]
1	1,4-diaminobutane (**54a**)	100	32:68	4800	2.8
2	Isophorone diamine (**54b**)	100	-	5370	3.0
3	1,3-cyclohexanebis (methylamine) (**54c**)	100	-	5260	3.1
4	*m*-Xylene diamine (**54d**)	100	36:64	7430	2.4
5	tris(2-aminoethyl)amine (**54e**)	100	36:64	4680	2.7

[a]*Reactions were carried out at 80 ºC in DMF for 16h.* [b]*Determined by NMR.* [c]*Determined by GPC.*

Table 5. *GPC data for selected PHUs derived from CABC (**53**).*[a]

Entry	Diamine	Conv. (%)[b]	Primary OH: Secondary OH	$M_{n,exp}$[c]	PDI[c]
1	1,4-diaminobutane (**55a**)	100	-	2500	2.1
2[d]	1,4-diaminobutane (**55a**)	100	-	2460	2.2
2	*m*-Xylene diamine (**55d**)	100	-	3500	2.7
3	tris(2-aminoethyl)amine (**55e**)	100	-	4630	2.5
4	*L*-lysine (**55f**)	100	-	-	-
5[e]	*L*-lysine (**55f**)	100	-	43900	2.8
6[f]	*L*-lysine (**55f**)	100	-	42650	2.9

[a]*Reactions were carried out at 80 ºC in MeCN for 16h.* [b]*Determined by NMR.* [c]*Determined by GPC.* [d]*Diastereoisomerically enriched CABC was used.* [e]*1 eq. of DBU was used.* [f]*1 eq. of TBD was used.*

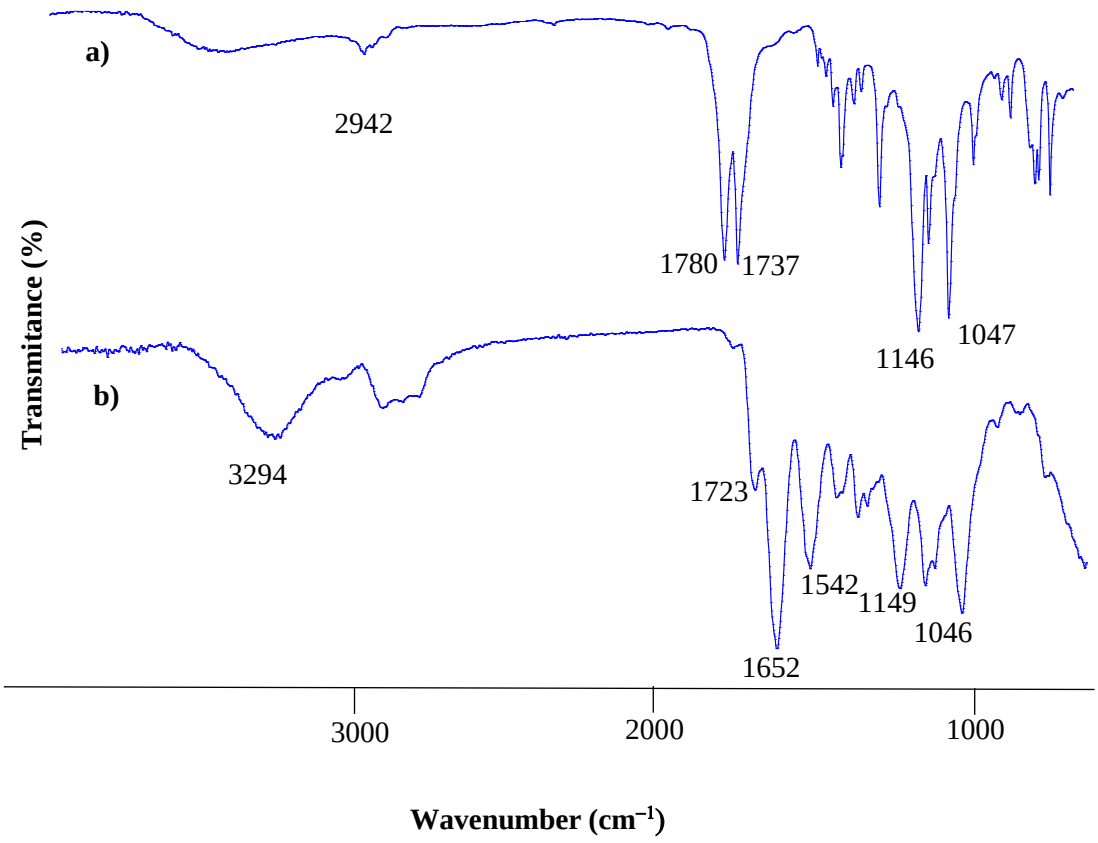

Figure 17. *IR spectrum for a) BGLBC (**52**), b) PHU* **54e**.

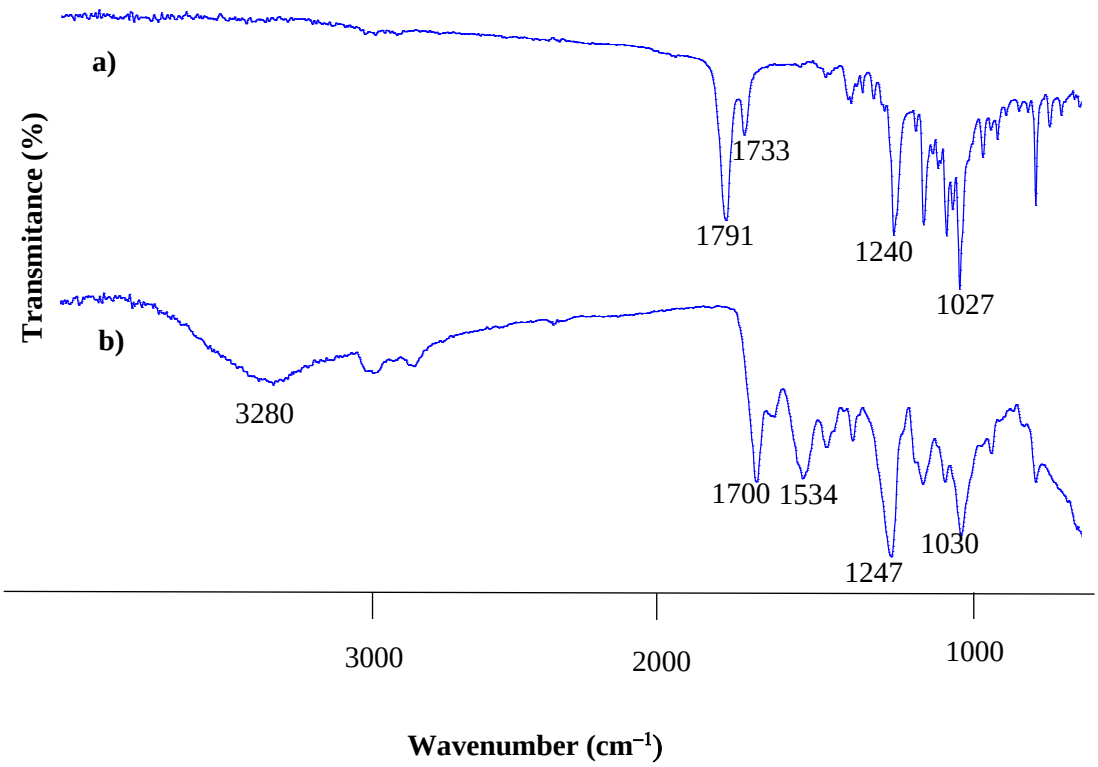

Figure 18. *IR spectrum for a) CABC (**53**), b) PHU **55c.***

The ^{1}H-NMR spectra of the PHU derived from BGLBC and 1,4-diaminobutane (**54a**) and the PHU derived from the diastereoisomerically enriched CABC and 1,3-diaminobutane (**55a**) are collected in Figures 19 and 20, respectively. As can be seen from Figure 19, three resonances at 7.11 ppm, 7.09 ppm and 6.79 ppm are observed, which were assigned to the protons of the urethane groups, confirming the urethane structure of the final product. The resonance pairs at 2.96 ppm; 1.37 ppm and 2.37 ppm; 1.78 ppm were assigned to the methylene protons of the alkyl groups from the diamine and the BGLBC (**52**) respectively. As it has been previously mentioned, it is known that both primary and secondary hydroxyl groups can be formed in the PHU backbone depending on the ring-opening pathway of the cyclic carbonate moiety. In Figure 19, two resonances were observed at 5.18 ppm and 4.91 ppm, corresponding to the formation of the secondary and primary hydroxyl groups, respectively. Amidification reaction, taking place during the BGLBC (**52**) polymerisation, was detected with the characteristic labile protons at 7.76 ppm and 7.99 ppm as well as the formation of urea with the characteristic proton at 5.76 ppm.[76] Similarly, the ^{1}H-NMR spectrum of the PHU synthesised from diastereoisomerically enriched CABC and 1,4-diaminobutane (**55a**) (Figure 20) followed the same pattern as its analogous **54a**. The signals at 7.13 ppm and 6.84 ppm were assigned to the protons of the urethane groups, confirming the formation of polyurethane **55a**. Resonances at 3.02 ppm and 1.61 ppm were assigned to the methylene protons of the alkyl groups from 1,4-diaminobutane and signals at 2.11 ppm, 1.46 ppm and 1.06 to the methyl groups from the carvyl acetate-derived bis(cyclic carbonate). In this case, signals corresponding to amidification byproducts and urea formation were also detected with the labile protons at 7.85 ppm and 7.53 ppm as well as at 5.88 ppm respectively.[76]

As an illustrative example, Scheme 20 shows the possible byproducts that can be generated during the polyaddition reaction of BGLBC (**52**) onto the different diamines employed to synthesise the corresponding PHUs **54a-e**.

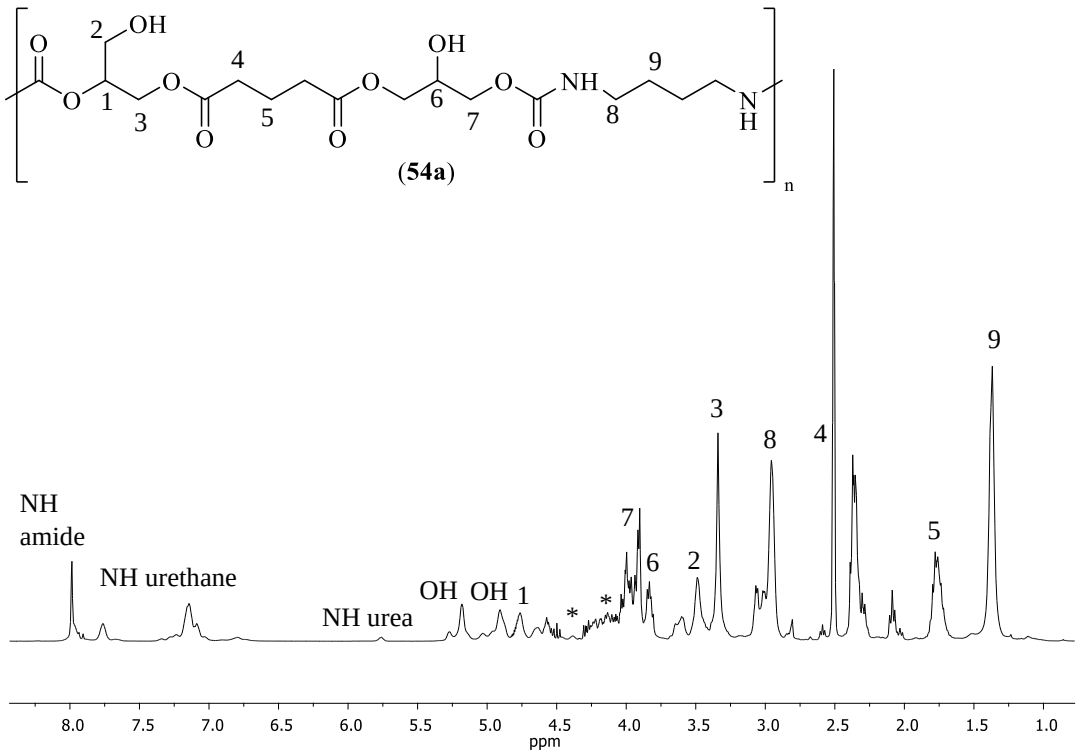

Figure 19. *^{1}H-NMR spectrum for PHU **54a** in DMSO-d_6.*: Residual monomers and chain ends.*

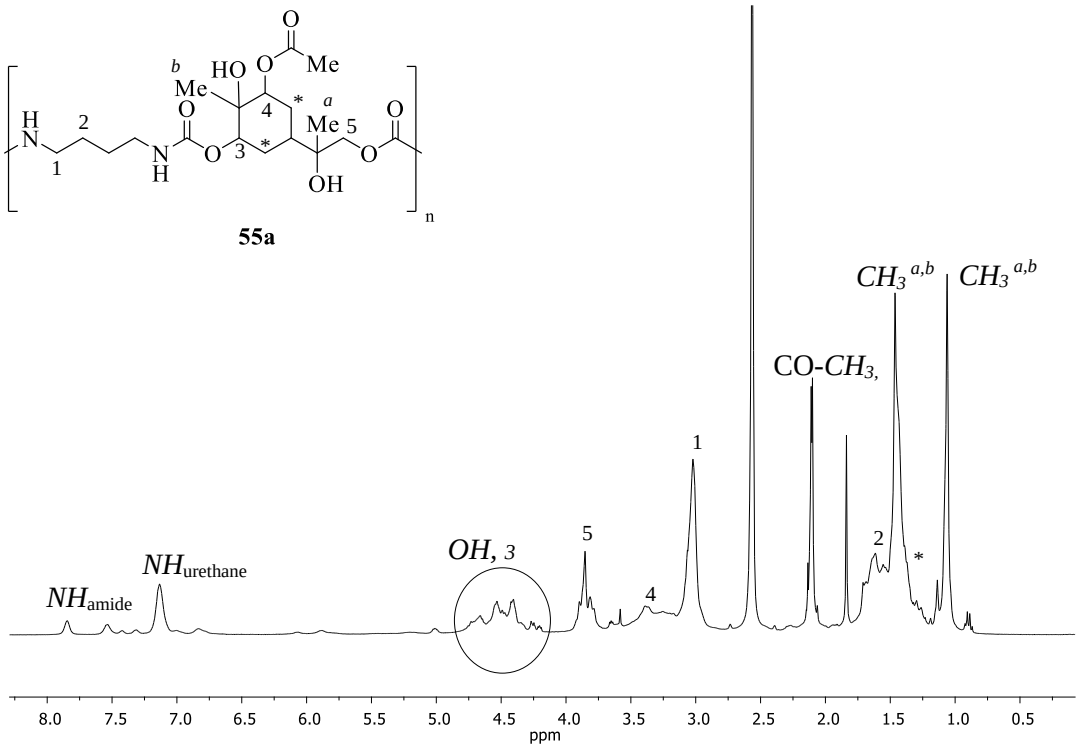

Figure 20. *^{1}H-NMR spectrum for PHU **55a** using diastereoisomerically enriched CABC **(53)** in DMSO-d_6.*

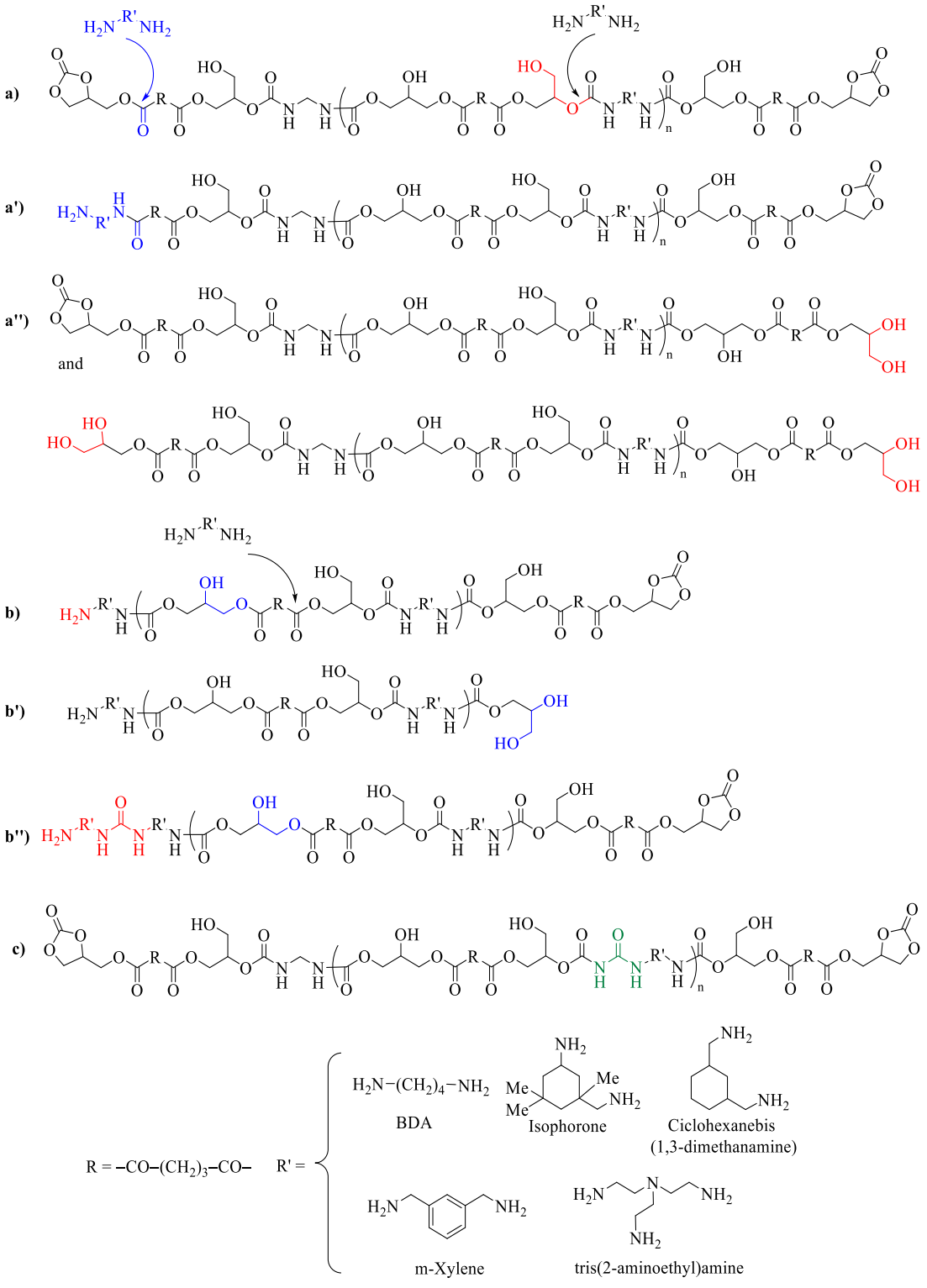

Scheme 20. *Possible products generated during polymerisation: a) Polyaddition: urethane formation; a') transamidification at the chain end or by cyclisation; a'') urea formation intra-chain resulting in the formation of hydroxyl groups at the chain end; b) polyaddition: urethane formation; b') transamidification intra-chain; b'') urea formation at the chain end; c) urea linkages within the chain.*

The molar masses for PHUs **54a-e** and **55a-c,f** were determined by GPC and their results are presented in Tables 4 and 5. As it can be seen, the molecular weight values range from 2460 to 7430 g mol^{-1} except for PHU **55f**, with molecular weights of 42650 and 43900 g mol^{-1} (Table 5, entries 5 and 6), which was attributed to the fact that a catalyst (TBD and DBU respectively) was used for the polymerisation process. Generally, PHUs synthesised from BGLBC (Table 4) exhibited higher molecular weights than their analogues synthesised from CABC (**53**) (Table 5). In terms of polydispersity, PHUs exhibited values between 2.1 and 3.1. These high dispersity values were attributed to the low control of the polymerisation since it proceeds without a catalyst. For instance, the GPC chromatogram for PHU **54d** is shown in Figure 21.

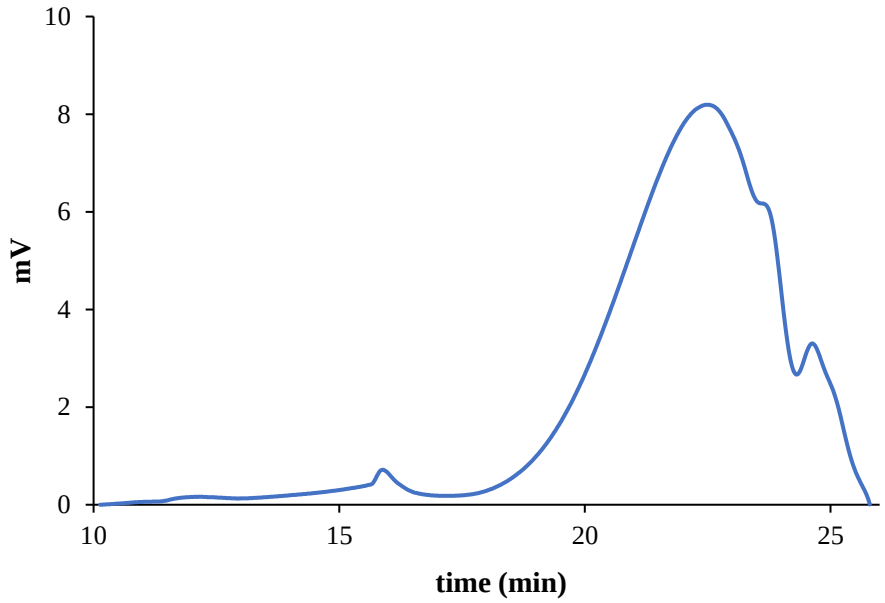

Figure 21. *GPC trace for PHU **54d**.*

Diffusion Ordered Spectroscopy NMR studies were also carried to further confirm the obtention of PHUs. Figures 22 and 23 show the DOSY-NMR spectrum for PHU **54d** and **55a**. As it can be observed from the spectrum, three diffusion coefficients are present for PHU **54d**, which correspond to the solvent, and two different polymers which exhibited very similar diffusion coefficients. As it can be deduced from the spectrum, a major polymeric chain contained amide, urea and urethane linkages, while the other polymeric chain exhibited only amide-urethane groups. On the other hand, a single diffusion coefficient is present in PHU **55a** which corresponds to a single polymeric chain containing amide, urea and urethane linkages.

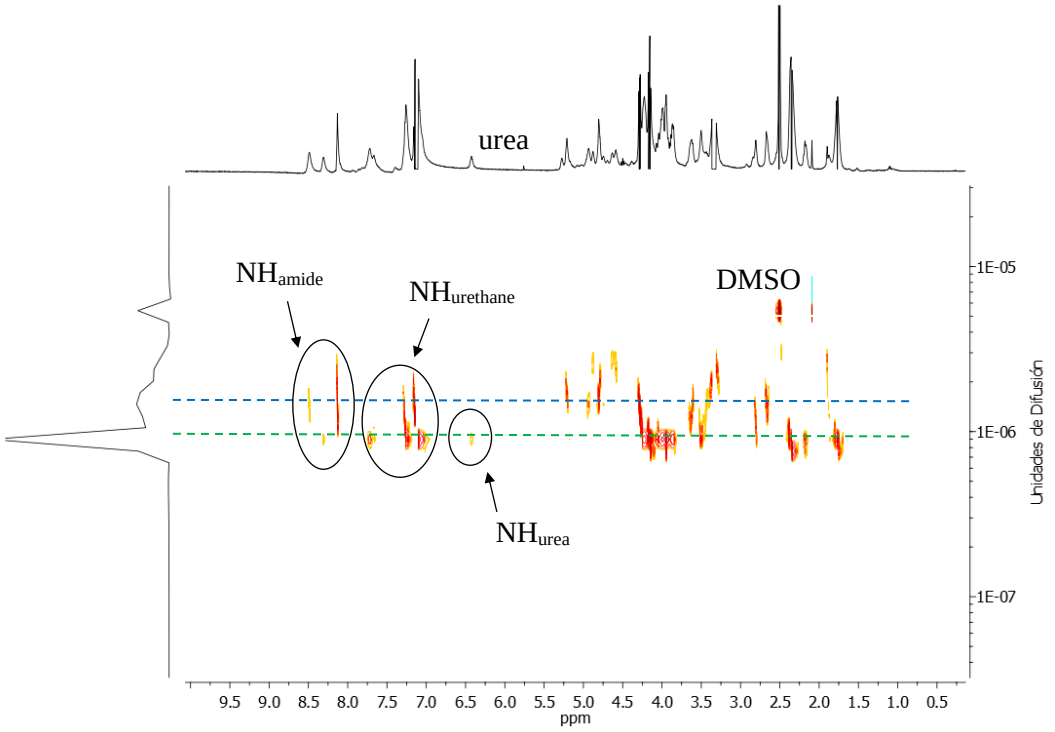

Figure 22. *DOSY NMR spectrum for PHU **54d** in DMSO-d_6.*

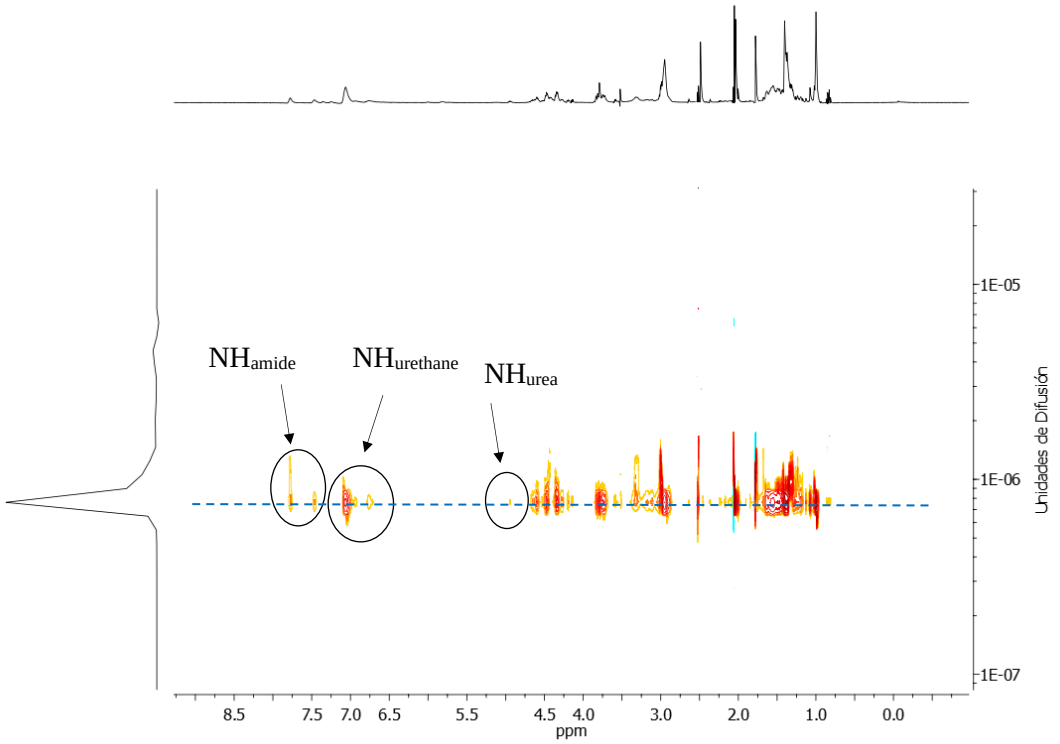

Figure 23. *^{1}H-NMR spectrum for PHU **55a** using diastereoisomerically enriched CABC (**53**) in DMSO-d_6.*

The effect of the [diamine]/[BGDC] ratio was also studied for the polyaddition of CABC (**53**) onto different diamines (Scheme 21). Thus, when 0.5 eq. of the corresponding diamine were used, hydroxycarbamate products with two cyclic carbonates ending groups were obtained (**56a**,**d**). On the other hand, when 2 eq. of diamine were used, hydroxycarbamate products with two amine ending groups were obtained (**57a**,**d**,**e**). The structures for these compounds were characterised by ^{1}H-NMR, ^{13}C-{^{1}H}-NMR and IR spectroscopy and MALDI-ToF analysis. Figure 24 shows the ^{1}H-NMR for compound **56a**. Resonances at 5.11 ppm; 5.02 ppm and 4.50 ppm; 4.25 ppm confirm the presence of cyclic carbonate ending groups. On the other hand, the ^{1}H-NMR spectrum for compound **57d** (Figure 25) exhibited resonances at 7.20 ppm and 4.16 ppm for the aromatic and methylene protons of the corresponding ending *m*-xylene diamine moieties.

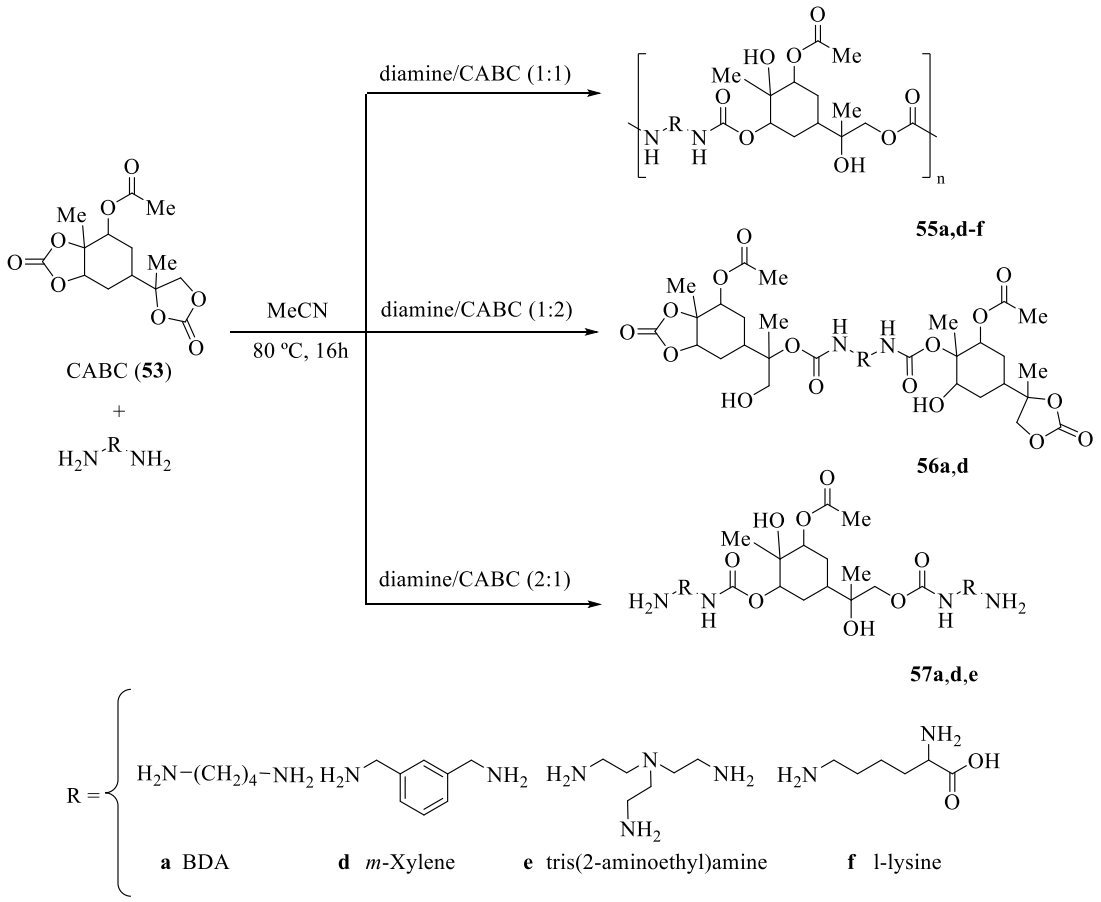

Scheme 21. *Synthesis of hydroxycarbamates **56a**,**d** and **57a**,**d**,**e**.*

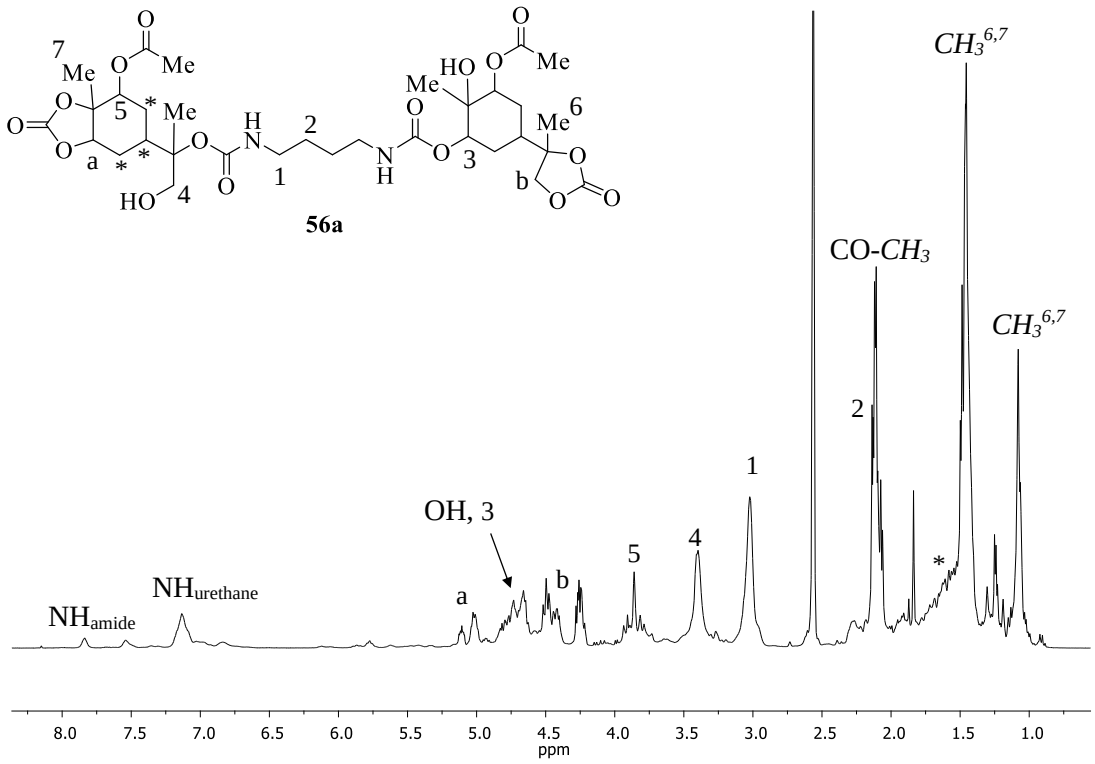

Figure 24. *[1]H-NMR spectrum for hydroxycarbamate **56a** in DMSO-d6.*

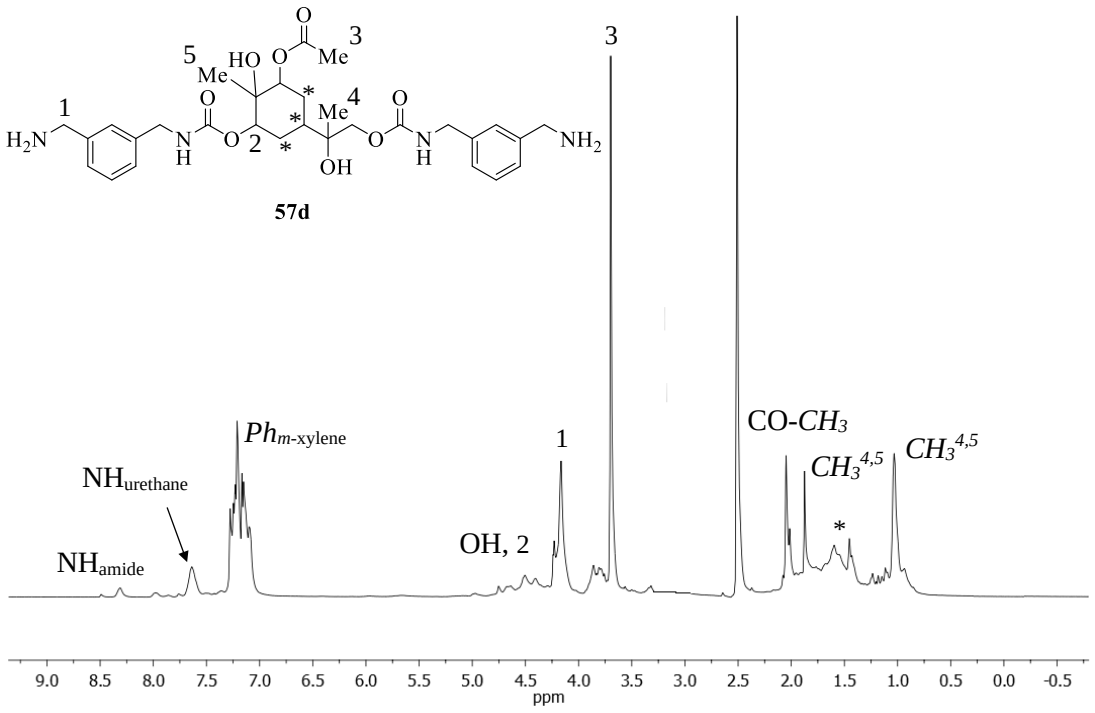

Figure 25. *[1]H-NMR spectrum for hydroxycarbamate **57d** in DMSO-d6.*

The MALDI-ToF spectrum for compound **57e** is shown in Figure 26. Different peaks with different *m/z* mass units are observed, corresponding to the fragmentation of compound **57e**. The peak with *m/z* of 607.65 was attributed to compound **57e**. On the other hand, the peak at *m/z* of 565.6 was assigned to a new compound obtained from the fragmentation and hydrolysis of the acetate group and the peak at *m/z* of 393.5 to a new compound obtained from the hydrolysis of both acetate and urethane groups.

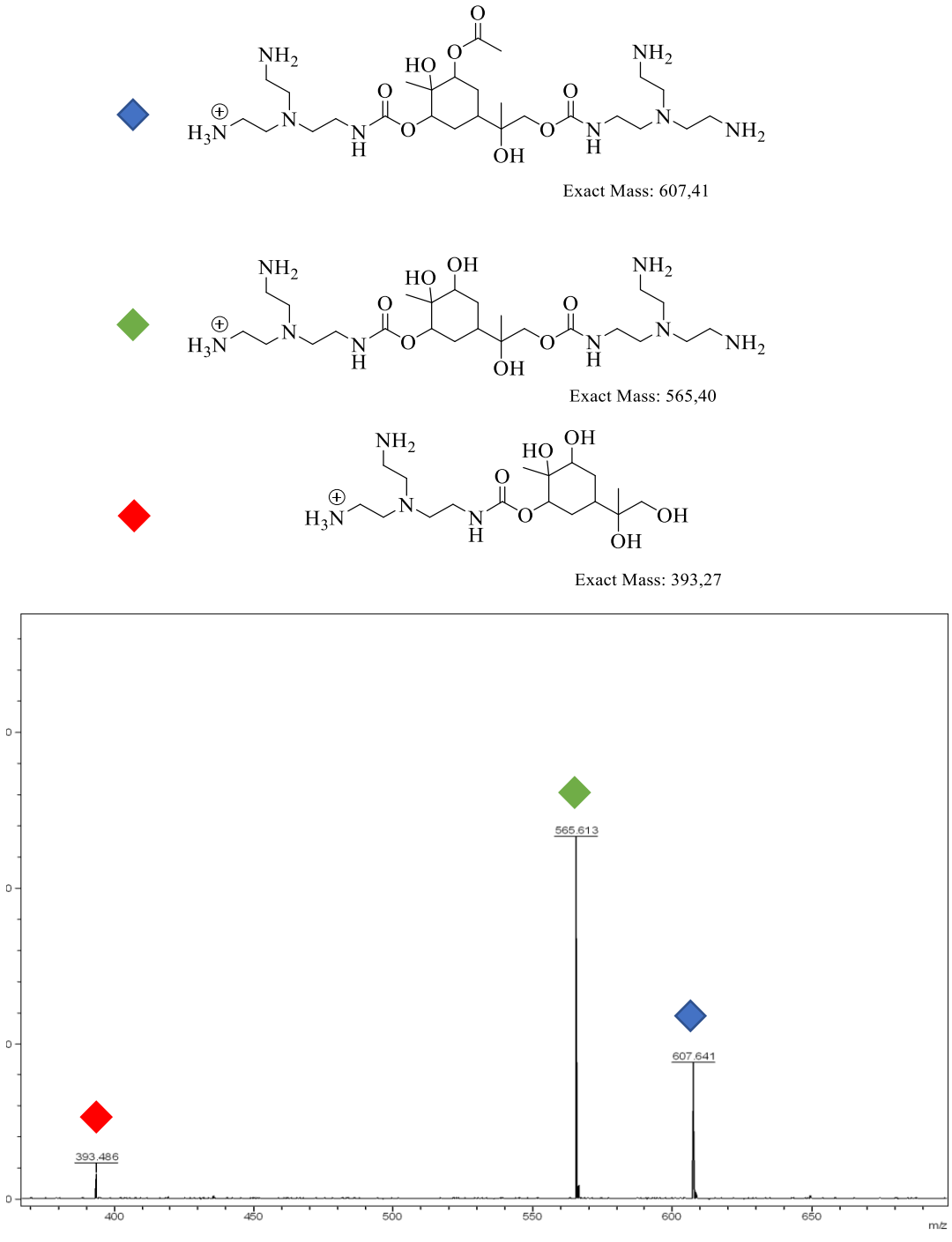

Figure 26. *MALDI-ToF spectrum for hydroxycarbamate **57e**.*

Thermal properties of the PHUs synthesised from BGLDC (**51**) or CABC (**53**) and diamines were investigated by DSC and TGA analyses (Tables 6 and 7). In both cases, TGA thermograms showed that less rigid PHUs derived from aliphatic diamines (Table 6, entries 1 and 5; Table 7, entries 1 and 4) were stable in a lower range of temperatures than their more rigid PHUs counterparts derived from aromatic/cyclic diamines (Table 6, entries 2-4, Table 7, entry 3). However, PHU **55a** derived from diastereisomerically enriched CABC and 1,4-diaminobutane (Table 7, entry 2) exhibited a higher value than its PHU **55d** analogue derived from *m*-xylene diamine (Table 7, entry 3), due to the higher crystallinity of the enantiomerically pure CABC employed. In general terms, PHUs **54a-e** derived from BGLBC exhibited higher stability against decomposition than their PHUs **55a**,**d-f** derived from CABC analogues since they exhibited higher molecular weights.

The glass transition phenomenon was observed in the DSC thermograms. As can be observed from Table 6, PHUs derived from BGLBC exhibited T_g values between 7 ºC and 49 ºC depending on the chemical structure of the diamines used. As previously mentioned, several studies agreed that the high molecular flexibility between the hydroxyurethane groups leads to lower T_g of PHUs.[88–90] Thus, PHUs derived from rigid amines such as isophorone diamine (Table 6, entry 2), 1,3-cyclohexanebis(methylamine) (Table 6, entry 3) or *m*-xylene diamine (Table 6, entry 4) exhibited higher T_g than PHUs derived from aliphatic diamines such as BDA (Table 6, entry 1) or tris(2-aminoethyl)amine (Table 6, entry 5). Similarly, the same tendency was observed for PHUs derived from CABC (Table 7). Therefore, PHUs derived from aliphatic diamines 1,4-diaminobutane (Table 7, entry 1) and *L*-lysine (Table 7, entry 5) exhibited lower T_g values than their PHUs counterparts derived from more rigid diamines such as *m*-xylene diamine (Table 7, entry 3), except for PHU **55e** derived from tris(2-aminoethyl)amine (Table 7, entry 4), which exhibited a slightly higher T_g of 62 ºC, probably due to a light cross-linking of the polymeric chains. Finally, PHU derived from diasteroisomerically enriched CABC and 1,4-diaminobutane exhibited the highest T_g with a value of 64 ºC, which was attributed to the higher crystallinity of the CABC used. In general terms, PHUs **54a-e** derived from BGLBC (**52**) exhibited lower T_g values than their PHUs analogues **55a**,**d-f** derived from CABC (**53**) with values ranging from 7-49 ºC and 42-64 ºC respectively, probably due to the higher rigidity and crystallinity of the cyclic CABC compared to the aliphatic BGLBC. As an

example, Figures 27 and 28 show a comparison between the T_g obtained for PHUs **54a-e** and PHUs **55a,d-f** respectively, and Figures 29 and 30 exhibit the thermogravimetric analysis for PHU **54b** and **55d** respectively.

Table 6. *DSC and TGA analyses for selected PHUs derived from BGLBC (**52**).*

Entry	Diamine	T_g (ºC)[a]	$T_{d,\,5\%}$ (ºC)[b]
1	1,4-diaminobutane (**54a**)	7	177
2	Isophorone diamine (**54b**)	49	228
3	1,3-cyclohexanebis(methylamine) (**54c**)	28	226
4	*m*-Xylene diamine (**54d**)	17	220
5	tris(2-aminoethyl)amine (**54e**)	11	96

[a]Determined by Different Scanning Calorimetry (DSC). [b]Determined by Thermal Gravimetric Analysis (TGA). Reported as temperature at 5% mass loss.

Table 7. *DSC and TGA analyses for selected PHUs derived from CABC (**53**).*

Entry	Diamine	T_g (ºC)[a]	$T_{d,\,5\%}$ (ºC)[b]
1	1,4-diaminobutane (**55a**)	57	119
2[c]	1,4-diaminobutane (**55a**)	64	184
3	*m*-xylene diamine (**55d**)	58	152
4	tris(2-aminoethyl)amine (**55e**)	62	111
5	*L*-lysine (**55f**)	42	163

[a]Determined by Different Scanning Calorimetry (DSC). [b]Determined by Thermal Gravimetric Analysis (TGA). Reported as temperature at 5% mass loss. [c]Crystals of BCDC used. [d]0.66 eq. of tris(2-aminoethyl)amine were used.

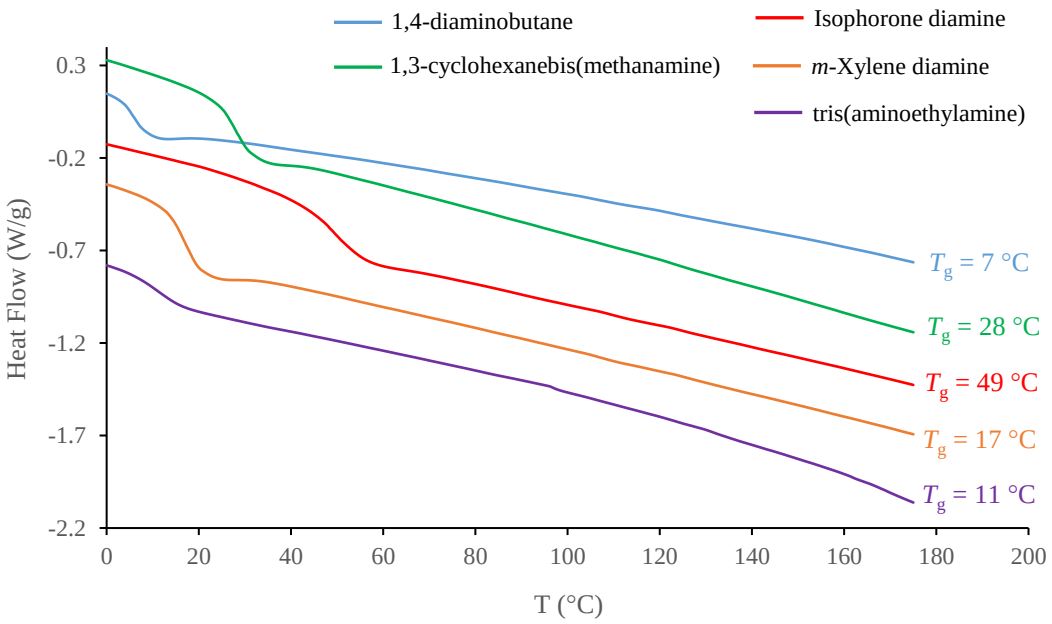

Figure 27. *DSC thermograms for PHUs **54a-e**.*

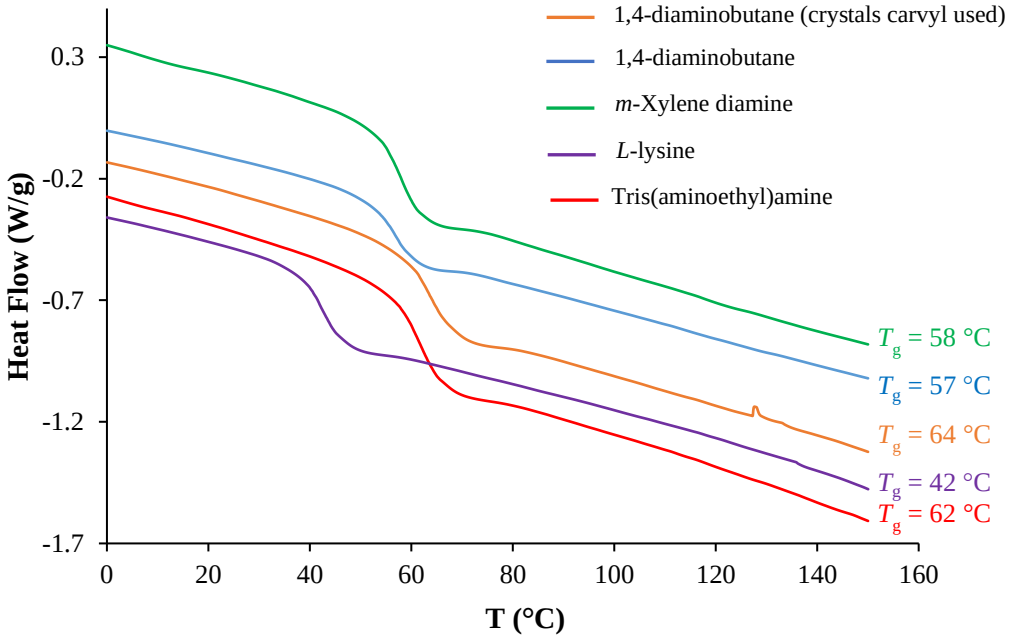

Figure 28. *DSC thermograms for PHUs **55a**,**d-f**.*

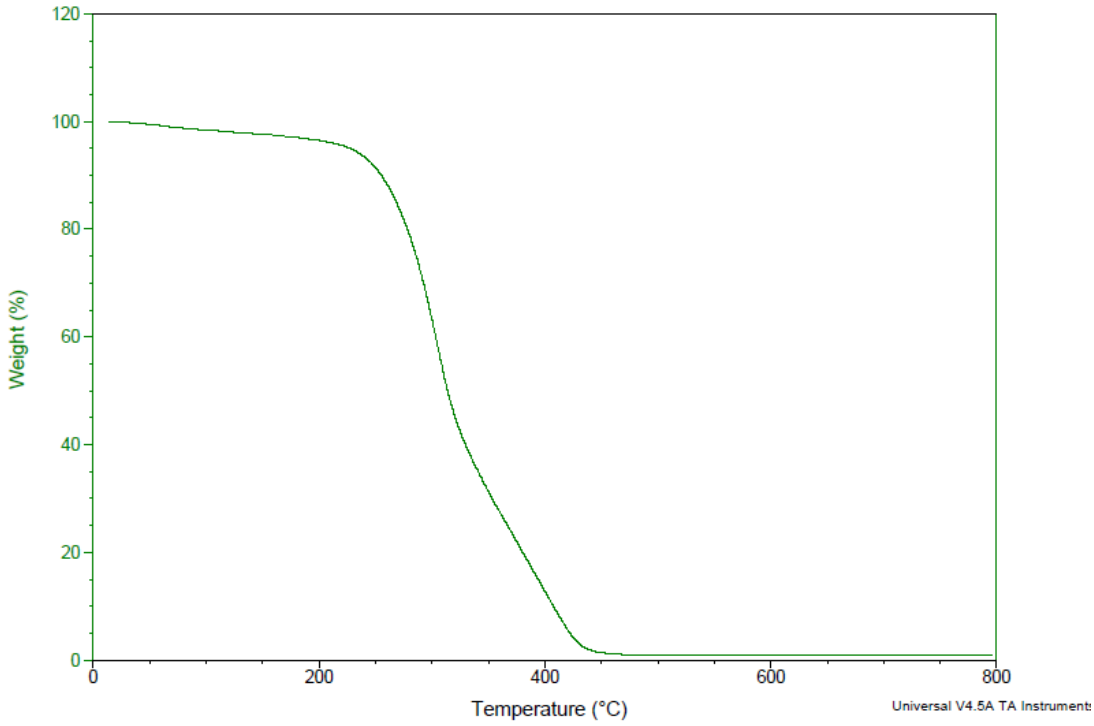

Figure 29. *TGA thermogram for PHU **54b**.*

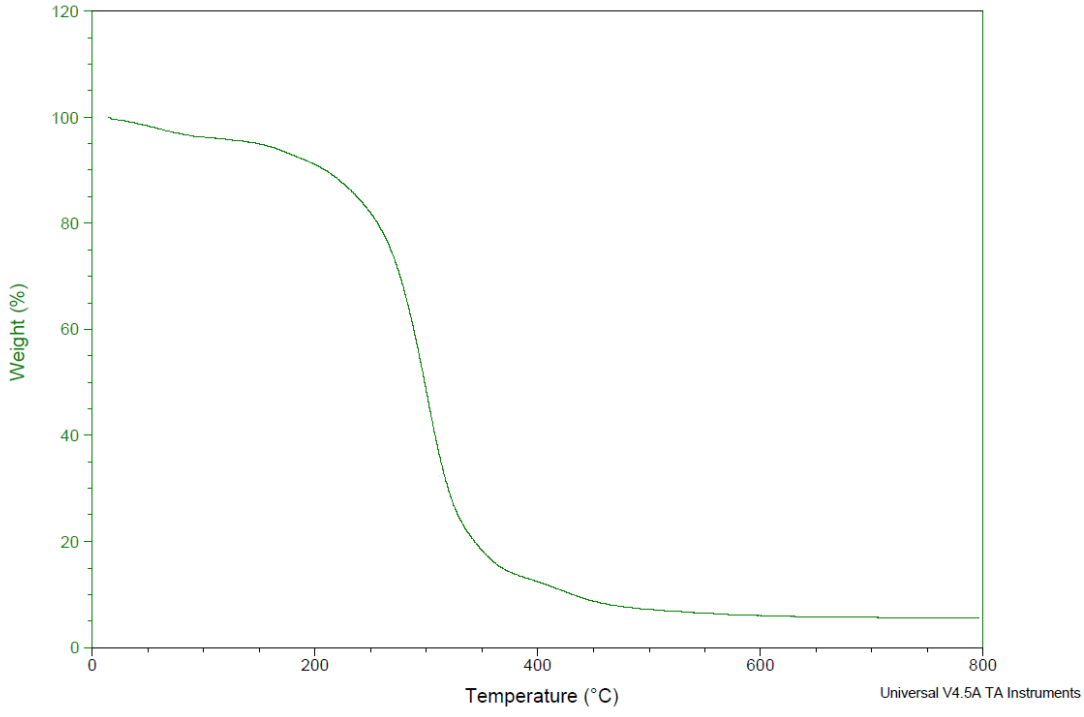

Figure 30. *TGA thermogram for PHU **55d**.*

*E*xperimental section

EXPERIMENTAL SECTION

1. Synthesis of starting materials

The epoxide 1,4-butanediol bis-glycidyl ether (BGDE), alkene (–)-carvyl acetate and glutaryl chloride were purchased from SIGMA-ALDRICH. Hydroxy-containing imidazole organocatalyst and [$AlMe_2(\kappa^2$-bpzbdeape)] were prepared according to previously reported procedure.[87,95] The rest of the epoxides and cyclic carbonates derived from the commercial reagents were prepared as follows.

1.1 Synthesis of starting epoxides

*1.1.1. Synthesis of glutaryl bis epoxide (**50**)*[96]

In a 250 cm^3 round bottom flask, glycidol (4.5 mL, 67.5 mmol), diisopropylethylamine (12.9 mL, 74.3 mmol) and glutaryl chloride (4.75 mL, 37.2 mmol) were added, and the resulting solution was left stirring for two hours at room temperature. After that time, 50 mL of an aqueous solution of NaOH (50%) were added and the solution was left stirring for further two hours at room temperature. Then, the reaction mixture was extracted with 100 mL of Et_2O and the organic layer was washed 3 x 20 mL of water. The organic layer was then dried over $MgSO_4$, filtered and the solvent removed under vacuum obtaining a brownish oil, which, after purification by column chromatography (EtOAc/Hex 1:6), afforded epoxide **50** as a yellowish oil in 81% yield.

*1.1.2. Synthesis of carvyl acetate bis epoxide (**51**)*[95]

In a 500 cm^3 round bottom flask, (–)-carvyl acetate (15.0 mL, 75.0 mmol) was dissolved in 200 mL of CH_2Cl_2 and the solution was cooled down to 0 ºC. Then, 3-chloroperbenzoic acid (22.8 g, 0.17 mol) was added in small portions, maintaining the resulting mixture 24 hours at room temperature. After that time, the mixture was washed with 50 mL of an aqueous solution of NaOH 1M, 50 mL of a saturated solution of $NaHCO_3$ and 50 mL of a saturated solution of NaCl. The organic layer was then dried over $MgSO_4$ and the solvent removed under vacuum, obtaining a yellowish oil, which, after purification by column chromatography (EtOAc/Hex 1:6) afforded epoxide **53** in 93% yield.

1.2. Synthesis of starting bis(cyclic carbonates)

*1.2.1. Synthesis of BGDC (**46**)*

1,4-butanediol diglycidyl ether (10.0 g, 49.5 mmol) and hydroxy-containing imidazole organocatalyst (0.2 g, 0.5 mmol) were placed in a stainless reactor equipped with a stirring bar. The reactor was then pressurised at 10 bar of CO_2 and the reaction mixture was stirred at 80 ºC for 2 h. After that time, the remaining sample was filtered through a plug of silica, eluting with CH_2Cl_2 to remove the catalyst used. The eluent was then removed in *vacuo* affording a white solid corresponding to 2,4-butanediol diglycidyl carbonate (BGC, **46**).

*1.2.2. Synthesis of BGLBC (**52**)*[95]

In the glovebox, glutaryl bis-epoxide (7.4 g, 30.1 mmol), [$AlMe_2$(κ^2-bpzbdeape)] (43.8 mg, 75.0 μmol) and tetrabutylammonium bromide (TBAB) (24.2 mg, 75.0 μmol) were placed in a stainless reactor equipped with a stirring bar. The reactor was then pressurised at 10 bar and the mixture was stirred for 3 hours at 80 ºC. After that time, the remaining sample was filtered through a plug of silica eluting with CH_2Cl_2 to remove the catalyst used. The eluent was then removed in *vacuo* affording a white solid corresponding to glutaryl bis-carbonate (BGLBC, **52**).

*1.2.3. Synthesis of CABC (**53**)*[94]

The synthesis of CABC (**53**) was carried out in a similar way to BGLBC (**52**), using carvyl acetate bis-epoxide (**51**) (15.8 g, 69.8 mmol), [$AlMe_2$(κ^2-bpzbdeape)] (0.4 g, 0.70 mmol) and tetrabutylammonium chloride (TBAC) (1.0 g, 3.5 mmol) and stirring the mixture for 66 h. After that time, the remaining sample was purified by flash chromatography using as solvent system of first hexane, then hexane:EtOAc (9:1), then hexane:EtOAc (6:1), then hexane:EtOAc (3:1),then EtOAc to afford a white solid corresponding to CABC (**53**) in 38% yield.

2. Synthesis of poly(hydroxyurethane)s (PHUs) and hydroxycarbamates

2.1. General procedure for the synthesis of PHUs 47a-e

As a mode of example, the synthesis of polyurethane **47a** is described. In a 10 mL Schlenk equipped with a small stir bar, BGDC (**46**) (250.0 mg, 0.86 mmol), 1,4-diaminobutane (86 μL, 0.86 mmol) and 0.75 mL of MeCN, were added. The

reaction mixture was then warmed up at 80 ºC and left stirring for 16 hours. After that time, solvent was removed in *vacuo* affording the corresponding PHU as a rubbery material or a solid depending on the diamine used in 80-95% yields.

2.2. Synthesis of PHU 47f

The synthesis of PHU **47f** was carried out in a similar manner to PHUs **47a-e**, using BGDC (**46**) (250.0 mg, 0.86 mmol), *L*-lysine (126.0 mg, 0.86 mmol) and TBD (120.0 mg, 0.86 mmol) or DBU (131 mg, 0.86 mmol), and was obtained as a white-yellowish solid in 93 % yield.

2.3. General procedure for the synthesis of PHUs 54a-e

As a mode of example, the synthesis of polyurethane **54a** is described. In a 10 mL Schlenk equipped with a small stir bar, BGLBC (**52**) (250.0 mg, 0.75 mmol), 1,4-diaminobutane (76.0 μL, 0.75 mmol) and 0.75 mL of DMF, were added. The reaction mixture was then warmed up at 80 ºC and left stirring for 16 hours. After that time, solvent was removed in *vacuo* affording the corresponding PHU as a rubbery material or a solid depending on the diamine used in 80-95% yields.

2.4. General procedure for the synthesis of PHUs 55a,d,e

As a mode of example, the synthesis of polyurethane **55a** is described. In a 10 mL Schlenk equipped with a small stir bar, CABC (**53**) (250.0 mg, 0.80 mmol), 1,4-diaminobutane (80.5 μL, 0.80 mmol) and 0.75 ml of MeCN, were added. The reaction mixture was then warmed up at 80 ºC and left stirring for 16 hours. After that time, solvent was removed in *vacuo* affording the corresponding PHU as a white solid in 90-95% yields.

2.5. Synthesis of PHUs 55f

The synthesis of PHU **55f** was carried out in a similar manner to PHUs **55a,d,e**, using CABC (**53**) (250.0 mg, 0.80 mmol), *L*-lysine (111.0 mg, 0.80 mmol) and TBD (120.0 mg, 0.80 mmol) or DBU (122 mg, 0.80 mmol) and was obtained as a white-yellowish solid in 93 % yield.

2.6. General procedure for the synthesis of hydroxycarbamates 48, 56a,d

In a 10 mL Schlenk equipped with a small stir bar, BGDC (**46**)/CABC (**53**) (0.90 mmol), the corresponding diamine (0.45 mmol) and 0.75 ml of MeCN, were added. The reaction mixture was then warmed up at 80 ºC and left stirring for 16 hours. After that time, solvent was removed in *vacuo* affording the corresponding hydroxycarbamate as a rubbery material or a solid depending on the bis(cyclic carbonate)/diamine used in 85-90% yields.

2.7. General procedure for the synthesis of hydroxycarbamates 49, 57a,d,e

In a 10 mL Schlenk equipped with a small stir bar, BGDC (**46**)/CABC (**53**) (0.90 mmol), the corresponding diamine (1.80 mmol) and 0.75 ml of MeCN, were added. The reaction mixture was then warmed up at 80 ºC and left stirring for 16 hours. After that time, solvent was removed in *vacuo* affording the corresponding hydroxycarbamate as a rubbery material or a solid depending on the bis(cyclic carbonate)/diamine used in 85-90% yields.

3. Structural characterisation of PHUs

The synthesised PHUs and hydroxycarbamates were characterised by IR, ^{1}H-NMR, ^{13}C-NMR and DOSY-NMR spectroscopy, MALDI-ToF analysis, DSC, TGA and GPC.

PHU 47a: ^{1}H-NMR (500 MHz, DMSO-d_6): 7.11 (d, $J_{H\text{-}H}$ = 5.7Hz, 1H, *NH*$_{urethane}$), 4.89 (d, $J_{H\text{-}H}$ = 5.1 Hz, 1H, *secondary OH*), 4.75 (t, $J_{H\text{-}H}$ = 5.5 Hz, 1H, *primary OH*), 4.67 (m, 1H), 3.89 (m, 2H), 3.73 (dd, $J_{H\text{-}H}$ = 10.4, 5.2 Hz, 1H), 3.46 (m, 2H,), 3.39 (m, 4H, $CH_2^{\alpha}{}_{BGDC}$), 3.33 (m, 4H), 2.96 (s, 4H,$CH_2^{\alpha}{}_{BDA}$), 1.51 (s, 4H, $CH_2^{\beta}{}_{BGDC}$), 1.37 (s, 4H, $CH_2^{\beta}{}_{BDA}$). ^{13}C-NMR (500 MHz, DMSO-d_6): 156.7 (C=O$_{urethane}$), 73.6 (5), 72.4 (6), 70.9 ($C^{\alpha}{}_{BGDC}$), 69.7 (3), 68.3 (4), 66 (7), 60.6 (3), 40.4 ($C^{\alpha}{}_{BDA}$), 27.2 ($C^{\beta}{}_{BDA}$), 26.4 ($C^{\beta}{}_{BGDC}$). IR: ν (C=O)$_{amide}$ = 1699 cm; ν (NH) $_{amide}$ = 1533 cm^{-}1, ν (C–O)$_{urethane}$= 1252 cm^{-}1.

PHU 47b: ^{1}H-NMR (400 MHz, DMSO-d_6): 7.11 (s, 1H, NH$_{urethane}$), 4.90 (s, 1H, OH), 4.67 (s, 1H), 3.88 (m, 2H), 3.74 (s, 2H), 3.57 (s, 1H, CH^{α}-NH$_{isophorone}$), 3.46 (s, 2H), 3.39 (s, 2H, $CH_2^{\alpha}{}_{BGDC}$), 3.32 (s, 2H), 2.72 (d, $J_{H\text{-}H}$ = 5.7 Hz, 2H, CH^{β}-NH$_{isophorone}$), 1.52 (s, 2H, $CH_2^{\beta}{}_{BGDC}$), 0.93 (m, 11H, CH_3, CH_2 $_{isophorone}$). ^{13}C-NMR (400 MHz, DMSO-

d_6): 157 ($C{=}O_{urethane}$), 73.7, 72.4, 70.9 (C^{α}_{BGDC}), 69.7, 68.3, 66, 60.6, 55 (C^{η}-$NH_{isophorone}$), 47.4 ($C_{isophorone}$), 43.9 (C^{α}-$NH_{isophorone}$), 35.5 ($C_{isophorone}$), 28.4 ($C_{isophorone}$), 26.4(C^{β}_{BGDC}), 23.7 ($C_{isophorone}$). IR: ν $(C{=}O)_{amide}$ = 1695 cm^{-1}; ν $(NH)_{amide}$ = 1537 cm−1, ν $(C{-}O)_{urethane}$ = 1243 cm−1.

PHU 47c: ^{1}H-NMR (500 MHz, DMSO-d_6): 7.11 (s, 1H, $NH_{urethane}$), 4.89 (s, 1H, *secondary OH*), 4.75 (s, 1H, *primary OH*), 4.67 (m, 1H), 3.88 (ddd, , $J_{H\text{-}H}$ = 15.2, 10.9, 6 Hz), 3.73 (m, 2H), 3.46 (s, 2H), 3.39 (s, 2H, $CH_2^{\alpha}{}_{BGDC}$), 3.32 (s, 2H), 2.95 (d, $J_{H\text{-}H}$ = 5.1 Hz, 1H), 2.80 (d, $J_{H\text{-}H}$ = 3.6 Hz, 4H, CH^{σ}-$NH_{diamine}$), 1.67 (d, $J_{H\text{-}H}$ = 12.9 Hz, 2H), 1.51 (d, $J_{H\text{-}H}$= 5.9 Hz, 4H, $CH_2^{\beta}{}_{BGDC}$), 1.37 (s, 2H, CH_2^{β}-$NH_{diamine}$), 1.27 (dd, $J_{H\text{-}H}$ = 13, 8.1Hz, 1H), 1.13 (m, 1H), 0.73 (m, 1H), 0.47 (q, $J_{H\text{-}H}$ = 12.2 Hz, 1H). ^{13}C-NMR (500 MHz, DMSO-d_6): 156.9 ($C{=}O_{urethane}$), 73.5, 72.4, 70.9 (C^{α}_{BGDC}), 69.7, 68.3, 66, 60.6, 47.3 (C^{α}-$NH_{diamine}$), 38 (C^{β}-$NH_{diamine}$), 30.8 ($C_{diamine}$), 26.4 (C^{β}_{BGDC}). IR: ν $(C{=}O)_{amide}$ = 1695 cm^{-1}; ν $(NH)_{amide}$ = 1538 cm−1, ν $(C{-}O)_{urethane}$ = 1251 cm−1.

PHU 47d: ^{1}H-NMR (400 MHz, DMSO-d_6): 7.67 (s, 1H, $NH_{urethane}$), 7.26 (t, $J_{H\text{-}H}$ = 7.7Hz, 1H, $Ph_{\eta\text{-}xylene}$), 7.13 (d, $J_{H\text{-}H}$ = 7.2 Hz, 3H, $Ph_{\eta\text{-}xylene}$), 4.92 (s, 1H, *secondary OH*), 4.78 (s, 1H, *primary OH*), 4.72 (m, 1H), 4.16 (d, $J_{H\text{-}H}$ = 5.8 Hz, 2H, CH_2^{α}-$NH_{\eta\text{-}xylene}$), 3.93 (ddd, , $J_{H\text{-}H}$ = 17.2, 11, 5.3 Hz, 2H), 3.76 (s, 1H), 3.48 (s, 2H), 3.39 (s, 2H, $CH_2^{\alpha}{}_{BGDC}$), 3.34 (s, 2H), 1.52 (s, 4H, $CH_2^{\beta}{}_{BGDC}$). ^{13}C-NMR (500 MHz, DMSO-d_6): 157 ($C{=}O_{urethane}$), 140.3 ($Ph_{\eta\text{-}xylene}$), 128.7 ($Ph_{\eta\text{-}xylene}$), 126.7 ($Ph_{\eta\text{-}xylene}$), 126 ($Ph_{\eta\text{-}xylene}$), 73.9, 72.4, 70.9 (C^{α}_{BGDC}), 69.7, 68.3, 66.2, 60.6, 44.3 (C^{α}-$NH_{\eta\text{-}xylene}$), 26.4 (C^{β}_{BGDC}). IR: ν $(C{=}O)_{amide}$ = 1695 cm^{-1}; ν $(NH)_{amide}$ = 1533 cm−1, ν $(C{-}O)_{urethane}$ = 1247 cm−1.

PHU 47e: ^{1}H-NMR (500 MHz, DMSO-d_6): 7.15 (s, 1H, $NH_{urethane}$), 4.68 (dt, $J_{H\text{-}H}$ = 10; 4.9 Hz, 1H), 3.90 (ddd, , $J_{H\text{-}H}$ = 17.8, 10, 7 Hz, 2H), 3.75 (m, 1H), 3.46 (s, 2H), 3.39 (s, 2H, $CH_2^{\alpha}{}_{BGDC}$), 3.32 (d, $J_{H\text{-}H}$= 5.4Hz, 2H), 3.01 (d, $J_{H\text{-}H}$= 5.6Hz, 4H, CH_2^{α}-$NH_{urethane}$), 2.55 (m, 2H, CH_2^{α}-$NH_{triamine}$), 2.45 (m, 4H, CH_2^{β}-$NH_{urethane}$), 2.38 (dd, $J_{H\text{-}H}$ = 13.1, 6.7 Hz, 2H, CH_2^{β}-$NH_{triamine}$), 1.52 (m, 2H, $CH_2^{\beta}{}_{BGDC}$). ^{13}C-NMR (500 MHz, DMSO-d_6): 156.9 ($C{=}O_{urethane}$), 73.9, 72.4, 70.9 (C^{α}_{BGDC}), 69.7, 68.2, 66.2, 60.6, 58.4 (C^{β}-$NH_{urethane}$), 54.4 (C^{β}-$NH_{triamine}$), 40 (C^{α}-$NH_{triamine}$), 39.5(CH_2^{α}-$NH_{urethane}$), 26.4 (C^{β}_{BGDC}). IR: ν $(C{=}O)_{amide}$ = 1696 cm^{-1}; ν $(NH)_{amide}$ = 1532 cm−1, ν $(C{-}O)_{urethane}$ = 1251 cm−1.

PHU 47f: ^{1}H-NMR (500 MHz, DMSO-d$_6$): 7.13 (s, 1H, *NH*$_{urethane}$), 6.21 (s, 1H, *NH*$_{urea}$), 4.65 (s, 1H), 3.86 (m, 2H), 3.82 (m, 1H, *CH*$^{\alpha}$-NH$_{L\text{-}lysine}$), 3.75 (m, 1H), 3.46 (s, 2H), 3.39 (s, 2H, *CH*$_2{}^{\alpha}$$_{BGDC}$), 3.32 (d, J$_{H\text{-}H}$= 5.4Hz, 2H), 3.26-3.3.20 (m, 8H, *DBU*), 2.91 (d, J$_{H\text{-}H}$ = 5.4 Hz, 4H, *CH*$_2{}^{\alpha}$-NH$_{L\text{-}lysine}$), 2.61 (d, J$_{H\text{-}H}$ = 5.4 Hz, 2H, *DBU*), 1.85 (m, 2H, *DBU*), 1.64-1.60 (m, 4H, *DBU*), 1.51 (s, 2H, *CH*$_2{}^{\beta}$$_{BGDC}$), 1.32 (m, 4H, *CH*$_2{}^{\beta}$-NH$_{L\text{-}lysine}$), 1.19 (s, 2H, *CH*$_2{}^{\gamma}$-NH$_{L\text{-}lysine}$) . ^{13}C-NMR (500 MHz, DMSO-d$_6$): 174.1(*C*=*O*$_{L}$-lysine), 164.7 (*DBU*), 156.7 (*C*=*O*$_{urethane}$), 155.8 (*C*=*O*$_{urea}$), 73.9, 72.4, 70.9 (*C*$^{\alpha}$$_{BGDC}$), 69.7, 68.2, 66.0, 60.6, 56.0 (*C*$^{\alpha}$-NH$_{L\text{-}lysine}$), 53.4 (*DBU*), 48.22 (*DBU*), 40.9 (*C*$^{\alpha}$-NH$_{L\text{-}lysine}$), 32.9 (*C*$^{\beta}$-NH$_{L\text{-}lysine}$), 32.7 (*DBU*), 30.0 (*C*$^{\beta}$-NH$_{L\text{-}lysine}$), 27.0(*DBU*), 26.4 (*C*$^{\eta}$$_{BGDC}$), 24.5 (*DBU*), 22.8 (*C*$^{\gamma}$-NH$_{L\text{-}lysine}$), 20.2 (*DBU*). IR: ν (C=O)$_{amide}$ = 1697 cm^{-1} ; ν (C=O)$_{urea}$ = 1646 cm^{-1}, ν (NH)$_{amide}$ = 1537 cm−1, ν (C–O)$_{urethane}$ = 1245 cm−1.

PHU 54a: ^{1}H-NMR (500 MHz, DMSO-d$_6$): 7.99; 7.76 (s, 1H, *NH*$_{amide}$), 7.14, 7.09 (s, 1H, *NH*$_{amide}$), *6*.79 (s, 1H, *NH*$_{urea}$), 5.18 (s, 1H), 4.91 (s, OH), 4.76 (s, OH), 4.64-4.04 (m, *chain ends and residual monomers*), 3.95 (m, 2H), 3.84 (m, 1H), 3.49 (s, 1H), 3.34 (s, 2H), 2.96 (s, 4H, *CH*$_2{}^{\alpha}$-NH$_{BDA}$), 2.37 (m, 4H, *CH*$_2{}^{\alpha}$-COO$_{BGLDC}$), 1.78 (m, 4H, *CH*$_2{}^{\beta}$-COO$_{BGLDC}$), 1.37 (s, 4H, *CH*$_2{}^{\beta}$-NH$_{BDA}$). ^{13}C-NMR (500 MHz, DMSO-d$_6$): 172.9-171.8 (*C*=*O*$_{ester\ BGLDC}$), 161.4 (C=O$_{amide}$), 156.9-156.6 (*C*=*O*$_{urethane}$), 155.8 (*C*=*O*$_{urea}$), 77.5, 72.4, 70.3, 69.7, 67.0, 66.0-65.2, 63.5-63.1, 61.0, 60.6, 40.4 (*C*$^{\alpha}$$_{BDA}$), 32.9 (*C*$^{\alpha}$$_{BGLDC}$), 27.2 (*C*$^{\beta}$$_{BDA}$), 20.2 (*C*$^{\beta}$$_{BGLDC}$). IR: ν (C=O)$_{ester}$ = 1722 cm^{-1}, ν (C=O)$_{amide}$ = 1660 cm^{-1}; ν (NH)$_{amide}$ = 1544 cm−1, ν (C–O)$_{urethane}$ = 1237, 1042 cm−1.

PHU 54b: ^{1}H-NMR (400 MHz, DMSO-d$_6$): 8.05-7.63 (s, 1H, *NH*$_{amide}$), 7.19-7.06 (s, 1H, *NH*$_{urethane}$), 5.20 (s, 1H, OH), 4.90 (s, 1H, OH), 4.78 (s, 1H), 4.67 (s, 1H), 4.64-4.04 (m, *chain ends and residual monomers*), 3.91 (m, 2H), 3.60 (s, 2H), 3.49 (s, 1H, *CH*$^{\alpha}$-NH$_{isophorone}$), 2.72 (d, J$_{H\text{-}H}$ = 5.1 Hz, 2H, *CH*$^{\alpha}$-NH$_{isophorone}$), 2.35 (m, 4H, *CH*$_2{}^{\alpha}$-COO$_{BGLDC}$), 1.76 (m, 4H, *CH*$_2{}^{\alpha}$-COO$_{BGLDC}$), 1.09-0.87 (m, 11H, *CH*$_3$, *CH*$_{2,isophorone}$). ^{13}C-NMR (400 MHz, DMSO-d$_6$): 172.9 (C=O$_{ester}$), 160.4 (C=O$_{amide}$), 73.0, 69.7, 67.1, 66.1, 65.7, 63.5-63.1, 55 (*C*$^{\alpha}$-NH$_{isophorone}$), 47.4 (*C*$_{isophorone}$), 44.3 (*C*$^{\alpha}$-NH$_{isophorone}$), 35.4 (*C*$_{isophorone}$), 32.9 (*C*$^{\alpha}$$_{BGLDC}$), 28.0 (*C*$_{isophorone}$), 23.7 (*C*$_{isophorone}$), 20.2 (*C*$^{\beta}$$_{BGLDC}$). IR: ν (C=O)$_{ester}$ = 1720 cm^{-1}, ν (C=O)$_{amide}$ = 1665 cm^{-1}; ν (NH)$_{amide}$ = 1533 cm−1, ν (C–O)$_{urethane}$ = 1236, 1045 cm−1.

PHU 54c: ^{1}H-NMR (500 MHz, DMSO-d$_6$): 8.00-7.78 (s, 1H, *NH*$_{amide}$) 7.18 (s, 1H, *NH*$_{urethane}$), 5.80 (s, 1H, *NH*$_{urea}$), 5.20 (s, 1H, *OH*), 4.92 (s, 1H, *OH*), 4.78 (d, J$_{H\text{-}H}$ = 4.6

Hz, 1H), 4.60-4.05 (m, *chain ends and residual monomers*), 3.88 (m, 4H), 3.46 (s, 2H), 3.32 (s, 2H), 2.91 (m, 1H), 2.80 (s, 4H, CH^{σ}-$NH_{diamine}$), 2.37 (m, 4H, CH_2^{α}-COO_{BGLDC}), 1.75 (m, 4H, CH_2^{β}-COO_{BGLDC}), 1.67 (d, J_{H-H} = 12.9 Hz, 2H), 1.37 (s, 2H, CH_2^{β}-$NH_{diamine}$), 1.27 (s, 1H), 1.13 (s, 1H), 0.73 (m, 1H), 0.47 (m, 1H). ^{13}C-NMR (500 MHz, DMSO-d_6): 172.8-171.8($C{=}O_{ester}$), 161.4 ($C{=}O_{amide}$), 156.7 ($C{=}O_{urethane}$), 73.0, 72.1, 69.7, 67.0, 66.1-65.2, 63.5-63.1, 60.6, 47.3 (C^{α}-$NH_{diamine}$), 43.8, 37.7 (C^{β}-$NH_{diamine}$), 32.8 ($C^{\alpha}{}_{BGLDC}$), 30.8 ($C_{diamine}$), 25.4, 20.3 ($C^{\beta}{}_{BGLDC}$). IR: ν $(C{=}O)_{ester}$ = 1715 cm^{-1}, ν $(C{=}O)_{amide}$ = 1660 cm^{-1}; ν $(NH)_{amide}$ = 1540 $cm^{-}1$, ν $(C{-}O)_{urethane}$ = 1239, 1052 $cm^{-}1$.

PHU 54d: ^{1}H-NMR (400 MHz, DMSO-d_6): 8.50-8.13 (s, 1H, NH_{amide}) 7.75-7.67 (s, 1H, $NH_{urethane}$), 7.26 (s, 1H, $Ph_{\eta\text{-}xylene}$), 7.13 (s, 3H, $Ph_{\eta\text{-}xylene}$), 5.23 (s, 1H, *OH*), 4.92 (s, 1H, *OH*), 4.81 (s, 1H), 4.70-4.30 (m, *chain ends and residual monomers*), 4.29-4.23 (m, 2H), 4.16 (d, J_{H-H} = 5.7 Hz, 2H, CH_2^{α}-$NH_{\eta\text{-}xylene}$), 3.95 (d, , J_{H-H} = 4.8 Hz, 2H), 3.65 (s, 1H), 3.51 (s, 1H), 3.34 (s, 2H), 2.37 (s, 4H, CH_2^{α}-COO_{BGLDC}), 1.75 (m, 4H, CH_2^{β}-COO_{BGLDC}). ^{13}C-NMR (500 MHz, DMSO-d_6): 173.2-172.0 ($C{=}O_{ester}$), 161.5 ($C{=}O_{amide}$), 157.1-156.9 ($C{=}O_{urethane}$), 139.5 ($Ph_{\eta\text{-}xylene}$), 128.8-125.8 ($Ph_{\eta\text{-}xylene}$), 73.9, 72.4, 70.3, 69.7, 67.0-66.5, 63.5-63.1, 44.3 (C^{α}-$NH_{\eta\text{-}xylene}$), 32.8 ($C^{\alpha}{}_{BGLDC}$), 20.3 ($C^{\beta}{}_{BGLDC}$). IR: ν $(C{=}O)_{ester}$ = 1718 cm^{-1}, ν $(C{=}O)_{amide}$ = 1662 cm^{-1}; ν $(NH)_{amide}$ = 1539 $cm^{-}1$, ν $(C{-}O)_{urethane}$ = 1233, 1043 $cm^{-}1$.

PHU 54e: ^{1}H-NMR (500 MHz, DMSO-d_6): 8.01-7.71 (s, NH_{amide}), 7.05 (s, 1H, $NH_{urethane}$), 5.93 (s, 1H, NH_{urea}), 5.28 (s, *OH*), 4.91 (s, *OH*), 4.66 (t, J_{H-H} = 5.1 Hz, 2H), 4.49 (d, J_{H-H} = 5.1 Hz, 2H), 4.41 (t, J_{H-H} = 5.3 Hz, 2H), 3.96 (m, 6H), 3.65 (m, 2H), 3.46 (m, 2H), 3.29 (d, J_{H-H}= 5.4Hz, 2H), 3.07 (m, 4H, CH_2^{α}-$NH_{urethane}$), 2.59 (m, 2H, CH_2^{α}-$NH_{triamine}$), 2.45 (m, 4H, CH_2^{β}-$NH_{urethane}$), 2.36 (dd, J_{H-H} = 7.2, 2.9 Hz, 2H, CH_2^{β}-$NH_{triamine}$), 2.34 (m, 4H, CH_2^{α}-COO_{BGLDC}), 2.08 (dd, J_{H-H}= 12.8, 7.3 Hz, 2H), 1.77 (m, 4H, CH_2^{β}-COO_{BGLDC}). ^{13}C-NMR (500 MHz, DMSO-d_6): 173.2-172.9 ($C{=}O_{ester}$), 161.6 ($C{=}O_{amide}$), 158.7 ($C{=}O_{urethane}$), 157.0 ($C{=}O_{urea}$), 73.0, 70.2, 69.7, 67.0-66.1, 65.4, 63.5, 63.1, 61.1, 60.2, 54.6 (C^{β}-$NH_{urethane}$), 53.6 (C^{β}-$NH_{triamine}$), 38.0 (C^{α}-$NH_{triamine}$), 37.2 (CH_2^{α}-$NH_{urethane}$), 35.9, 35.2, 34.7, 33.1-32.6 ($C^{\alpha}{}_{BGLDC}$), 22.0, 21.1, 20.4 ($C^{\beta}{}_{BGLDC}$), 17.0. IR: ν $(C{=}O)_{ester}$ = 1722 cm^{-1}, ν $(C{=}O)_{amide}$ = 1662 cm^{-1}; ν $(NH)_{amide}$ = 1542 $cm^{-}1$, ν $(C{-}O)_{urethane}$ = 1249, 1045 $cm^{-}1$.

PHU 55a: ^{1}H-NMR (400 MHz, DMSO-d_6): 7.85-7.31 (s, *NH*$_{amide}$), 7.13 (s, 1H, *NH*$_{urethane}$), 5.88 (s, *NH*$_{urea}$), 5.01 (s, *OH*), 4.75 (s, *OH*), 4.67-4.40 (m, 3H), 3.85 (m, 2H), 3.73 (dd, J_{H-H} = 10.4, 5.2 Hz, 1H), 3.46 (m, 2H,), 3.39-3.33 (m, 4H), 3.02 (s, 4H,*CH*$_2^{\alpha}$$_{BDA}$), 2.11 (s, 3H, *CH*$_{3,carvyl}$), 1.61 (s, 4H, *CH*$_2^{\beta}$$_{BDA}$), 1.46 (s, 3H, *CH*$_{3,carvyl}$), 1.06 (s, 3H, *CH*$_{3,carvyl}$). ^{13}C-NMR (400 MHz, DMSO-d_6): 170.4-169.4 (C=O$_{ester, amide}$), 156.8 (C=O$_{urethane}$), 154.6 (C=O$_{urea}$), 85.5, 84.3, 82.4, 80.8, 76.5, 75.6, 73.8, 72.9, 71.7, 69.7-69.4, 41.8 (*C*$^{\alpha}$$_{BDA}$), 31.7-30.9, 27.4-27.2 (*C*$^{\beta}$$_{BDA}$), 26.6, 23.1 (*C*H$_{3, carvyl}$), 22.0 (*C*H$_{3, carvyl}$), 21.3. IR: ν (C=O)$_{amide}$ = 1696 cm^{-1}; ν (NH)$_{amide}$ = 1539 cm−1, ν (C–O)$_{urethane}$ = 1245, 1026 cm−1.

PHU 55d: ^{1}H-NMR (400 MHz, DMSO-d_6): 8.33 (s, *NH*$_{amide}$), 7.63 (s, 1H, *NH*$_{urethane}$), 7.21 (m, 4H, *Ph*$_{\eta\text{-}xylene}$), 4.83-4.34 (m, 4H), 4.19 (m, 2H, *CH*$_2^{\alpha}$-NH$_{\eta\text{-}xylene}$), 3.85 (m, 2H), 3.76 (s, 1H), 3.48-3.34 (m), 2.03 (s, 3H, *CH*$_{3, carvyl}$), 1.39 (s, 3H, *CH*$_{3, carvyl}$), 1.04 (s, 3H, *CH*$_{3, carvyl}$). ^{13}C-NMR (400 MHz, DMSO-d_6): 170.6-169.5 (C=O$_{ester, amide}$), 157.1 (C=O$_{urethane}$), 144.2 (*Ph*$_{\eta\text{-}xylene}$), 140.1-139.8 (*Ph*$_{\eta\text{-}xylene}$), 128.7-128.2 (*Ph*$_{\eta\text{-}xylene}$), 126.5-125.4 (*Ph*$_{\eta\text{-}xylene}$), 85.9, 73.6, 72.9, 71.6, 69.9, 46.1 (*C*$^{\alpha}$-NH$_{\eta\text{-}xylene}$), 44.3 (*C*$^{\alpha}$-NH$_{\eta\text{-}xylene}$), 42.6, 23.0 (*C*H$_{3, carvyl}$), 22.5 (*C*H$_{3, carvyl}$), 21.4. IR: ν (C=O)$_{amide}$ = 1699 cm^{-1}; ν (NH)$_{amide}$ = 1535 cm−1, ν (C–O)$_{urethane}$ = 1243, 1042 cm−1.

PHU 55e: ^{1}H-NMR (400 MHz, DMSO-d_6): 7.88-7.79 (s, *NH*$_{amide}$), 7.08-6.74 (s, 1H, NH$_{urethane}$), 4.74-4.29 (m, *opening CABC*), 3.81-3.77 (m, 4H), 3.07 (m, 4H, *CH*$_2^{\alpha}$-NH$_{urethane}$), 2.56 (m, 2H, *CH*$_2^{\alpha}$-NH$_{triamine}$), 2.40 (m, 4H, *CH*$_2^{\beta}$-NH$_{urethane}$), 2.35 (m, 2H, *CH*$_2^{\beta}$-NH$_{triamine}$), 2.08 (s, 2H), 2.04 (s, 3H, *CH*$_{3,carvyl}$), 1.56 (s, 3H, *CH*$_{3,carvyl}$), 1.01 (s, 3H, *CH*$_{3,carvyl}$). ^{13}C-NMR (400 MHz, DMSO-d_6): 170.4-169.5 (C=O$_{ester}$), 156.9-156.7 (C=O$_{urethane}$), 77.2-75.8, 73.7-72.9, 71.7, 69.7-69.5, 58.4-58.0 (*C*$^{\beta}$-NH$_{urethane}$), 54.4-54.1 (*C*$^{\beta}$-NH$_{triamine}$), 37.8 (*C*$^{\alpha}$-NH$_{triamine}$), 37.6 (*CH*$_2^{\alpha}$-NH$_{urethane}$), 23.1 (*C*H$_{3, carvyl}$), 22.0 (*C*H$_{3, carvyl}$), 21.3. IR: ν (C=O)$_{amide}$ = 1690 cm^{-1}; ν (NH)$_{amide}$ = 1538 cm−1, ν (C–O)$_{urethane}$ = 1247, 1070 cm−1.

PHU 55f: ^{1}H-NMR (400 MHz, DMSO-d_6): 7.72, 7.36 (s, *NH*$_{amide}$), 6.97 (s, 1H, *NH*$_{urethane}$), 6.23 (s, 1H, *NH*$_{urea}$), 4.90-4.10 (m, *opening CABC*), 3.70 (m, 1H, *CH*$^{\alpha}$-NH$_{L\text{-}lysine}$), 3.55 (s, 2H), 3.29 (s, 2H), 3.16 (d, J_{H-H} = 5.2 Hz, 4H, *TBD*), 3.06 (d, J_{H-H} = 4.8 Hz, 4H, *TBD*), 2.85 (s, 4H, *CH*$_2^{\alpha}$-NH$_{L\text{-}lysine}$), 1.95 (s, 3H, *CH*$_{3,carvyl}$), 1.79 (d, J_{H-H} = 4.7 Hz, 4H, *TBD*), 1.58 (s, 3H, *CH*$_{3,carvyl}$), 1.31 (m, 4H, *CH*$_2^{\beta}$-NH$_{L\text{-}lysine}$), 1.12 (s, 2H, *CH*$_2^{\gamma}$-NH$_{L\text{-}lysine}$), 0.93 (s, 3H, *CH*$_{3,carvyl}$). ^{13}C-NMR (400 MHz, DMSO-d_6): 174.1

(*C*=$O_{L\text{-lysine}}$), 170.5-169.3 (*C*=O_{ester}), 156.8 (*C*=$O_{urethane}$), 154.8 (*C*=O_{urea}), 151.6 (*TBD*), 77.0, 75.7, 73.6-73.1, 72.4, 71.8, 70.8, 69.7, 68.2, 66.0, 60.6, 56.0 (C^{α}-$NH_{L\text{-}lysine}$), 46.4 (*TBD*), 40.9 (C^{α}-$NH_{L\text{-}lysine}$), 37.6 (*TBD*), 32.9 (C^{β}-$NH_{L\text{-}lysine}$), 30.0 (C^{β}-$NH_{L\text{-}lysine}$), 23.1 ($CH_{3,\ carvyl}$), 22.5 (C^{γ}-$NH_{L\text{-}lysine}$), 21.4 ($CH_{3,\ carvyl}$), 21.0 (*TBD*). IR: ν $(C{=}O)_{amide}$ = 1695 cm^{-1}; ν $(NH)_{urea}$ = 1639 cm^{-1}, ν $(NH)_{amide}$ = 1538 cm^{-1}, ν $(C{-}O)_{urethane}$ = 1247, 1055 cm^{-1}.

4. Structural characterisation of hydroxycarbamates

Hydroxycarbamate 48: ^{1}H-NMR (400 MHz, DMSO-d_6): 7.11 (d, $J_{H\text{-}H}$ = 5.5Hz, 1H, $NH_{urethane}$), 4.94 (m, 2H, $CH_{\ cyclic\ carbonate}$), 4.75 (t, $J_{H\text{-}H}$ = 5.5 Hz, 1H, *primary OH*), 4.67 (m, 1H), 4.52 (t, $J_{H\text{-}H}$= 8.4Hz, 2H, $CH_{2,cyclic\ carbonate}$), 4.25 (dd, $J_{H\text{-}H}$= 8.2, 5.9Hz, 2H, $CH_{2,cyclic\ carbonate}$), 4.09 (q, $J_{H\text{-}H}$ = 5.2 Hz, 1H, *secondary OH*), 3.89 (dd, $J_{H\text{-}H}$= 27.1, 5.3Hz, 2H), 3.74 (m, 1H), 3.59 (ddd, $J_{H\text{-}H}$= 15.6, 11.5, 3.4Hz, 4H), 3.46 (m, 2H), 3.39 (m, 4H, $CH_2{}^{\sigma}{}_{BGDC}$), 3.33 (m, 2H), 2.95 (s, 4H, $CH_2{}^{\alpha}{}_{BDA}$), 1.53 (s, 4H, $CH_2{}^{\beta}{}_{BGDC}$), 1.37 (s, 4H, $CH_2{}^{\eta}{}_{BDA}$). ^{13}C-NMR (400 MHz, DMSO-d_6): 156.7 (*C*=$O_{urethane}$), 155.4 (*C*=$O_{cyclic\ carbonate}$), 76 ($CH_{cyclic\ carbonate}$), 73.6, 72.4, 71.0, 70.9 ($C^{\sigma}{}_{BGDC}$), 70, 68.3, 66.6 ($CH_{2,\ cyclic\ carbonate}$), 66.0, 60.6, 40.4 ($C^{\alpha}{}_{BDA}$), 27.2 ($CH_2{}^{\beta}{}_{BDA}$), 26.1 ($CH_2{}^{\beta}{}_{BGDC}$). IR: ν $(C{=}O)_{cyclic\ carbonate}$ = 1787 cm^{-1}, ν $(C{=}O)_{amide}$ = 1692 cm^{-1}; ν $(NH)_{amide}$ = 1525 cm^{-1}, ν $(C{-}O)_{urethane}$ = 1249, 1049 cm^{-1}.

Analysis found:	C: 50.5 %	H: 7.5 %	N: 3.9 %
Calculated:	C: 50.3 %	H: 7.2 %	N: 4.2 %

Hydroxycarbamate 49: ^{1}H-NMR (400 MHz, DMSO-d_6): 7.11 (s, 1H, $NH_{urethane}$), 4.68 (m, 1H), 3.88 (ddd, , $J_{H\text{-}H}$= 17.1, 11, 5.4Hz, 4H, 2), 3.73 (m, 1H), 3.46 (m, 2H, 11), 3.39 (m, 4H, $CH_2{}^{\alpha}{}_{BGDC}$), 3.32 (m, 4H), 2.95 (dd,$J_{H\text{-}H}$= 12.6, 6.5Hz, 4H, $CH_2{}^{\alpha}{}_{BDA}$), 2.5 (m, 4H, $CH_2{}^{\alpha}{}_{BDA,urethane}$), 1.51 (d, $J_{H\text{-}H}$= 4.6Hz, 4H, $CH_2{}^{\beta}{}_{BGDC}$), 1.35 (m, 4H, $CH_2{}^{\beta}{}_{BDA,BDA\ urethane}$ 3). ^{13}C-NMR (400 MHz, DMSO-d_6): 156.7 ($C{=}O_{urethane}$), 73.5, 72.4, 70.9 ($C^{\alpha}{}_{BGDC}$), 69.7, 68.3, 66.0, 60.6, 41.9 ($C^{\alpha}{}_{BDA,\ urethane}$), 40.4 ($C^{\alpha}{}_{BDA}$), 31.1 ($C^{\beta}{}_{BDA,\ urethane}$) 27.5 ($C^{\beta}{}_{BDA}$), 26.4 ($C^{\beta}{}_{BGDC}$). IR: ν (O–H) = 3340 cm^{-1}, ν $(C{=}O)_{amide}$ = 1687 cm^{-1}; ν $(NH)_{amide}$ = 1535 cm^{-1}, ν $(C{-}O)_{urethane}$ = 1248, 1109 cm^{-1}.

Analysis found:	C: 52.7 %	H: 9.5 %	N: 11.4 %
Calculated:	C: 52.5 %	H: 9.2 %	N: 11.7 %

Hydroxycarbamate 56a: ^{1}H-NMR (400 MHz, DMSO-d$_6$): 7.84; 7.54 (s, *NH*$_{amide}$), 7.13; 6.84 (s, 1H, *NH*$_{urethane}$), 5.77 (s, *NH*$_{urea}$), 5.11 (m, 1H, *CH* $_{cyclic\ carbonate}$), 5.02 (q, J$_{H-H}$ = 5.5 Hz, 1H, *CH* $_{cyclic\ carbonate}$), 4.90-4.70 (m, *opening CABC*), 4.66 (m, 2H, *CH*$_{,cyclic\ carbonate}$), 4.50 (m, 2H, *CH*$_{2,cyclic\ carbonate}$), 4.42 (m, 2H, *CH*$_{2,cyclic\ carbonate}$), 4.25 (dd, J$_{H-H}$= 8.2, 4.5 Hz, 2H, *CH*$_{2,cyclic\ carbonate}$), 3.86 (s, 2H), 3.40 (d, J$_{H-H}$= 4.6Hz, 4H), 3.02 (s, 4H, *CH*$_2^{\alpha}$$_{BDA}$), 2.14-2.11 (s, 3H, *CH*$_{3,\ carvyl}$), 1.84 (s, 3H, *CH*$_{3,carvyl}$), 1.78-1.50 (m, 4H), 1.49 (s, 3H, *CH*$_{3,carvyl}$), 1.46 (s, 4H, *CH*$_2^{\eta}$$_{BDA}$), 1.08 (s, 3H, *CH*$_{3,carvyl}$). ^{13}C-NMR (400 MHz, DMSO-d$_6$): 170.0-169.5 (*C*=*O*$_{amide}$), 156.7 (*C*=*O*$_{urethane}$), 155.6 (*C*=*O*$_{urea}$), 154.2 (*C*=*O*$_{cyclic\ carbonate}$), 85.5, 84.3, 82.4, 80.8, 80 (*C*H$_{cyclic\ carbonate}$), 75.3, 74.6, 72.9-72.7, 72.0; 71.7 (*C*H$_{2,\ cyclic\ carbonate}$), 70.8, 69.4-69.1, 40.1 (*C*$^{\alpha}$$_{BDA}$), 27.2 (*C*$^{\beta}$$_{BDA}$), 23.1 (*C*H$_{3,\ carvyl}$), 22.0 (*C*H$_{3,\ carvyl}$), 21.1. IR: ν (C=O)$_{cyclic\ carbonate}$ = 1794 cm^{-1}, ν (C=O)$_{amide}$ = 1708 cm^{-1}; ν (NH)$_{amide}$ = 1526 cm^{-}1, ν (C–O)$_{urethane}$ = 1236, 1024 cm^{-1}.

Analysis found:	C: 53.9 %	H: 7.1 %	N: 3.7 %
Calculated:	C: 53.6 %	H: 6.8 %	N: 3.9 %

Hydroxycarbamate 56d: ^{1}H-NMR (400 MHz, DMSO-d$_6$): 8.32; 7.98 (s, *NH*$_{amide}$), 7.65 (s, 1H, *NH*$_{urethane}$), 7.20 (m, 4H, *Ph*$_{\eta\text{-}xylene}$), 5.57 (s, *NH*$_{urea}$), 5.05 (m, 1H, *CH* $_{cyclic\ carbonate}$), 4.98 (m, 1H, *CH* $_{cyclic\ carbonate}$), 4.90-4.75 (m, *opening CABC*), 4.70 (m, 4H, *CH*$_{,cyclic\ carbonate}$), 4.44 (m, 2H, *CH*$_{2,cyclic\ carbonate}$), 4.21 (dd, J$_{H-H}$= 8.8, 4.5 Hz, 2H, *CH*$_{2,cyclic\ carbonate}$), 4.17 (m, 2H, *CH*$_2^{\alpha}$-NH$_{\eta\text{-xylene}}$), 3.70 (s, 2H), 3.35 (m, 2H), 2.08-2.05 (s, 3H, *CH*$_{3,\ carvyl}$), 1.87 (s, 3H, *CH*$_{3,carvyl}$), 1.80-1.50 (m, 4H), 1.43-1.41 (s, *CH*$_{3,carvyl}$), 1.04 (s, 3H, *CH*$_{3,carvyl}$). ^{13}C-NMR (400 MHz, DMSO-d$_6$): 170.0-169.5 (*C*=*O*$_{amide}$), 156.9-156.7 (*C*=*O*$_{urethane}$), 155.6-154.2 (*C*=*O*$_{cyclic\ carbonate}$), 144.6 (*Ph*$_{\eta\text{-}xylene}$), 140.3 (*Ph*$_{\eta\text{-}xylene}$), 128.7-128.5 (*Ph*$_{\eta\text{-}xylene}$), 126.2-125.4 (*Ph*$_{\eta\text{-}xylene}$), 85.5-85.2, 82.8-82.4, 80.8, 80 (*C*H$_{cyclic\ carbonate}$), 75.3, 75.0, 72.9-72.7, 72.0; 71.7 (*C*H$_{2,\ cyclic\ carbonate}$), 70.8, 69.4-69.1, 46.1-44.2 (*C*$^{\alpha}$-NH$_{\eta\text{-xylene}}$), 23.1 (*C*H$_{3,\ carvyl}$), 22.0 (*C*H$_{3,\ carvyl}$), 21.1. IR: ν (C=O)$_{cyclic\ carbonate}$ = 1795 cm^{-1}, ν (C=O)$_{amide}$ = 1697 cm^{-1}; ν (NH)$_{amide}$ = 1521 cm^{-}1, ν (C–O)$_{urethane}$ = 1237, 1037 cm^{-1}.

Analysis found:	C: 56.8 %	H: 6.6 %	N: 3.5 %
Calculated:	C: 56.5 %	H: 6.3 %	N: 3.7 %

Hydroxycarbamate 57a: ^{1}H-NMR (500 MHz, DMSO-d$_6$): 7.79 (s, *NH*$_{amide}$), 7.07; 6.78 (s, 1H, *NH*$_{urethane}$), 4.73 (s, 1H), 4.60 (s, 1H), 4.48 (d, J$_{H-H}$= 7.2 Hz, 1H), 4.34 (d, J$_{H-H}$= 7.0 Hz, 1H), 4.28 (d, J$_{H-H}$= 7.4 Hz, 1H), 3.79 (s, 2H), 2.99 (m, 4H, *CH*$_2^{\alpha}$$_{BDA}$),

2.50 (s, 4H, $CH_2^{\alpha}{}_{BDA}$), 2.04 (s, 3H, $CH_{3,\ carvyl}$), 1.78 (s, 3H, $CH_{3,carvyl}$), 1.60-1.30 (m, 4H), 1.39 (m, 4H, $CH_2^{\eta}{}_{BDA}$), 1.33 (m, 4H, $CH_2^{\eta}{}_{BDA}$), 1.08-1.00 (s, 3H, $CH_{3,carvyl}$). ^{13}C-NMR (500 MHz, DMSO-d_6): 170.0-169.3 ($C{=}O_{amide}$), 156.7 ($C{=}O_{urethane}$), 76.5-75.7, 73.8, 72.9, 71.7, 69.6, 49.1, 42.1; 41.9 ($C^{\alpha}{}_{BDA}$), 38.9; 38.7 ($C^{\alpha}{}_{BDA}$), 31.0; 27.2 ($C^{\beta}{}_{BDA}$), 23.1 (CH$_{3,\ carvyl}$), 22.1 (CH$_{3,\ carvyl}$), 21.1. IR: ν (O–H) = 3306 cm^{-1}, ν (C=O)$_{amide}$ = 1693 cm^{-1}; ν (NH)$_{amide}$ = 1536 cm^{-}1, ν (C–O)$_{urethane}$ = 1243, 1023 cm^{-1}.

Analysis found:	C: 54.1 %	H: 8.8 %	N: 11.3 %
Calculated:	C: 53.9 %	H: 8.6 %	N: 11.4 %

Hydroxycarbamate 57d: ^{1}H-NMR (500 MHz, DMSO-d_6): 8.31; 7.98 (s, NH_{amide}), 7.64 (s, 1H, $NH_{urethane}$), 7.21 (m, 4H, $Ph_{\eta\text{-}xylene}$), 4.75 (s, 1H), 4.64 (s, 1H), 4.51 (s, 1H), 4.41 (s, 1H), 4.23; 4.16 (m, 4H, $CH_{,cyclic\ carbonate}$), 3.86 (s, 1H), 3.70 (s, 2H), 2.05-2.01 (s, 3H, $CH_{3,\ carvyl}$), 1.88 (s, 3H, $CH_{3,carvyl}$), 1.70-1.40 (m, 4H), 1.04 (s, 3H, $CH_{3,carvyl}$). ^{13}C-NMR (400 MHz, DMSO-d_6): 170.4-169.6 ($C{=}O_{amide}$), 157.1-156.9 ($C{=}O_{urethane}$), 144.6 ($Ph_{\eta\text{-}xylene}$), 140.3 ($Ph_{\eta\text{-}xylene}$), 128.7-128.3 ($Ph_{\eta\text{-}xylene}$), 126.2-125.3 ($Ph_{\eta\text{-}xylene}$), 84.5, 79.7, 76.3, 73.8, 71.8, 69.9-69.6, 46.1-44.2 (C^{α}-NH$_{\eta\text{-}xylene}$), 23.1 (CH$_{3,\ carvyl}$), 22.0 (CH$_{3,\ carvyl}$), 21.3. IR: ν (O–H) = 3260 cm^{-1}, ν (C=O)$_{amide}$ = 1694 cm^{-1}; ν (NH)$_{amide}$ = 1540 cm^{-}1, ν (C–O)$_{urethane}$ = 1245, 1029 cm^{-1}.

Analysis found:	C: 61.7 %	H: 7.4 %	N: 9.4 %
Calculated:	C: 61.4 %	H: 7.2 %	N: 9.6 %

Hydroxycarbamates 57e: ^{1}H-NMR (400 MHz, DMSO-d_6): 7.93; 7.83 (s, NH_{amide}), 7.10; 6.74 (s, 1H, NH$_{urethane}$), 4.63 (s, 2H), 4.28 (s, 2H), 3.81-3.77 (m, 4H), 3.24; 3.07 (m, 4H, CH_2^{α}-NH$_{urethane}$), 2.56 (m, 2H, CH_2^{α}-NH$_{triamine}$), 2.42 (m, 4H, CH_2^{β}-NH$_{urethane}$), 2.40 (m, 2H, CH_2^{β}-NH$_{triamine}$), 1.81 (s, 3H, $CH_{3,carvyl}$), 1.56 (s, 3H, $CH_{3,carvyl}$), 1.09; 1.00 (s, 3H, $CH_{3,carvyl}$). ^{13}C-NMR (400 MHz, DMSO-d_6): 169.6 (C=O$_{ester}$), 156.9 (C=O$_{urethane}$), 79.7, 76.7, 75.0, 72.9, 71.9, 69.7, 57.7 (C^{β}-NH$_{urethane}$), 54.4-54.2 (C^{β}-NH$_{triamine}$), 37.7 (C^{α}-NH$_{triamine}$), 37.5 (CH_2^{α}-NH$_{urethane}$), 23.1 (CH$_{3,\ carvyl}$), 22.5 (CH$_{3,\ carvyl}$), 21.3. IR: ν (O–H) = 3280 cm^{-1}, ν (C=O)$_{amide}$ = 1697 cm^{-1}; ν (NH)$_{amide}$ = 1551 cm^{-}1, ν (C–O)$_{urethane}$ = 1257, 1044 cm^{-}1.

Analysis found:	C: 51.7 %	H: 9.1 %	N: 18.3 %
Calculated:	C: 51.5 %	H: 8.9 %	N: 18.5 %

Bibliography

BIBLIOGRAPHY

(1) *Plastics-the Facts 2019: An analysis of European plastics production, demand and waste data.* https://www.plasticseurope.org (access 14 May 2021).

(2) Z. Rafiee and V. Keshavarz, *Prog. Org. Coat.*, **2015**, *86*, 190.

(3) K. M. Zia, S. Anjum, M. Zuber, M. Mujahid, T. Jamil, *Int. J. Biol. Macromol.*, **2014**, *66*, 26.

(4) S. A. Madbouly, J. U. Otaigbe, *Prog. Polym. Sci.*, **2009**, *34*, 1283.

(5) Patrick. Vermette, *Landes Biosci.*, **2001**.

(6) G. T. Howard, *Int. Biodeter. Biodegr.*, **2002**, *49*, 245.

(7) D. K. Chattopadhyay, K. V. S. N. Raju, *Prog. Polym., Sci.*, **2007**, *32*, 352.

(8) A. Llevot, M. Meier, *Polym. Int.*, **2019**, *68*, 826.

(9) F. E. Golling, R. Pires, A. Hecking, J. Weikard, F. Ritcher, K. Danielmeier, D. Dijkstra, *Polym. Int.*, **2019**, *68*, 848.

(10) *Szycher's handbook of Polyurethanes Second edition*, **2013**, CRC Press, Taylor and Francis Group, New York.

(11) A. F. T. Li, *Angew. Chem.*, **1947**, *9*, 257.

(12) I. Labunska, E. Greenpeace Research Laboratories (Exeter, *The Bhopal legacy : toxic contaminants at the former Union Carbide factory site, Bhopal, India : 15 years after the Bhopal accident*, Greenpeace Research Laboratories, Dept. of Biological Sciences, University of Exeter, **1999**.

(13) L. Maisonneuve, O. Lamarzelle, E. Rix, E. Grau, H. Cramail, *Chem. Rev.*, **2015**, *115*, 12407.

(14) R. D. Katsarava, T. M. Kartvelishvili, D. P. Kharadze, M. M. Zaalishvili, M. M. Patsuriya, *Polym. Sci. U.S.S.R*, **1987**, *29*, 2268.

(15) S. L. Kwolek, P. W. Morgan, *J. Polym. Sci.*, **1964**, *2*, 2693.

(16) E. K. Drechsel, *United States Patent Office 2806017*, **1957**.

(17) A. Y. Yuen, A. Bossion, A. Veloso, D. Mecerreyes, J. L. Hedrick, A. P. Dove, H. Sardon, *Polym. Chem.*, **2018**, *9*, 2458.

(18) T. Baba, A. Kobayashi, T. Yamauchi, H. Tanaka, S. Aso, M. Inomata, Y. Kawanami, *Catal. Lett.*, **2002**, *82*, 193.

(19) D. Zhang, Y. Zhang, Y. Fan, M. N. Rager, V. Guérineau, L. Bouteiller, M. H. Li, C. M. Thomas, *Macromolecules*, **2019**, *52*, 2719.

(20) B. M. Bhanage, S. I. Fujita, Y. Ikushima, M. Arai, *Green Chem.*, **2003**, *5*, 340.

(21) E. F. V. Scriven, K. Turnbull, *Chem. Rev.*, **1988**, *88*, 297.

(22) A. K. Ghosh, A. Sarkar, M. Brindisi, *Org. Biomol. Chem.*, **2018**, *16*, 2006.

(23) T. Tada, Y. Ishida, K. Saigo, *Synlett*, **2007**, 235.

(24) V. V. Sureshbabu, B. S. Patil, R. Venkataramanarao, *J. Org. Chem.*, **2006**, *71*, 7697.

(25) H. Lebel, O. Leogane, *Org. Lett.*, **2006**, *8*, 5717.

(26) D. Sawada, S. Sasayama, H. Takahashi, S. Ikegami, *Tetrahedron*, **2008**, *64*, 8780.

(27) E. Riva, S. Gagliardi, C. Mazzoni, D. Passarella, A. Rencurosi, D. Vigo, M. Martinelli, *J. Org. Chem.*, **2009**, *74*, 3540.

(28) D. Chaturvedi, A. K. Chaturvedi, N. Mishra, V. Mishra, *Org. Biomol. Chem.*, **2012**, *10*, 9148.

(29) A. M. Tafesh, J. Weiguny, *Chem. Rev.*, **1996**, *96*, 2035.

(30) W. B. Hardy, R. P. Bennett, *Tetrahedron Lett.*, **1967**, *11*, 961.

(31) C. Hahn, H. Keul, M. Möller, *Polym. Int.*, **2012**, *61*, 1048.

(32) E. Delebecq, J. P. Pascault, B. Boutevin, F. Ganachaud, *Chem. Rev.*, **2013**, *113*, 80.

(33) J. Guan, Y. Song, Y. Lin, X. Yin, M. Zuo, Y. Zhao, X. Tao, Q. Zheng, *Ind. Eng. Chem. Res.*, **2011**, *50*, 6517.

(34) M. S. Kathalewar, P. B. Joshi, A. S. Sabnis, V. C. Malshe, *RSC Adv.*, **2013**, *3*, 4110.

(35) S. H. Pyo, P. Persson, M. Amin Mollaahmad, K. Sörensen, S. Lundmark, R. Hatti-Kaul, *Pure Appl. Chem.*, **2012**, *84*, 637.

(36) R. D. Lundberg, S. Albans, D. R. Mont, *United States Patent Office 3523924*, **1970**.

(37) O. Ihata, Y. Kayaki, T. Ikariya, *Angew. Chem. Int. Ed.*, **2004**, *43*, 717.

(38) K. Soga, W.-Y. Chiang, S. Ikeda, *J. Polym. Sci.: Polym. Chem. Ed.*, **1974**, *12*, 121.

(39) H. Blattmann, M. Fleischer, M. Bähr, R. Mülhaupt, *Macromol. Rapid Commun.*, **2014**, *35*, 1238.

(40) B. Nohra, L. Candy, J. F. Blanco, C. Guerin, Y. Raoul, Z. Mouloungui, *Macromolecules*, **2013**, *46*, 3771.

(41) M. Jayakannan, D. Puthanparambil, *United States Patent US 2007/0117950*, **2007**.

(42) U. Romano, R. Tesel, M. Massi Mauri, P. Rebora, *Ind. Eng. Chem. Prod. Res. Dev.*, **1980**, *19*, 396.

(43) W. Peng, N. Zhao, F. Xiao, W. Wei, Y. Sun, *Pure Appl. Chem.*, **2012**, *84*, 603.

(44) S. Carloni, D. E. de Vos, P. A. Jacobs, R. Maggi, G. Sartori, R. Sartorio, *J. Catal.*, **2002**, *205*, 199.

(45) B. Sharma, H. Keul, H. Höcker, T. Loontjens, R. van Benthem, *Polymer*, **2005**, *46*, 1775.

(46) B. Sharma, L. Ubaghs, H. Keul, H. Höcker, T. Loontjens, R. van Benthem, *Polymer*, **2004**, *45*, 5427.

(47) R. W. McCabe, A. Taylor, *Green Chem.*, **2004**, *6*, 151.

(48) B. Elizabeth Dyer, H. Scott, *J. Am. Chem. Soc.*, **1957**, *79*, 672.

(49) Y. Deng, S. Li, J. Zhao, Z. Zhang, J. Zhang, W. Yang, *RSC Adv.*, **2014**, *4*, 43406.

(50) C. Li, S. Li, J. Zhao, Z. Zhang, J. Zhang, W. Yang, *J. Polym. Res.*, **2014**, *21*, 498.

(51) B. Sharma, L. Ubaghs, H. Keul, H. Höcker, T. Loontjens, R. van Benthem, *Macromol. Chem. Phys.*, **2004**, *205*, 1536.

(52) M. Firdaus, M. A. R. Meier, *Green Chem.*, **2013**, *15*, 370.

(53) S. J. Groszos, E. K. Drechsel, *United States Pattent Office 2802022*, **19541**.

(54) O. Figovsky, L. Shapovalov, A. Leykin, O. Birukova, R. Potashnikova, *Chem. Chem. Technol.*, **2013**, *7*, 79.

(55) O. Bunco, S. Yuriko, E. Takeshi, *J. Polym. Sci., Part A: Polym. Chem.*, **2009**, *47*, 4629.

(56) H. Büttner, L. Longwitz, J. Steinbauer, C. Wulf, T. Werner, *Top. Curr. Chem.*, **2017**, *375*.

(57) M. North, R. Pasquale, C. Young, *Green Chem.*, **2010**, *12*, 1514.

(58) R. R. Shaikh, S. Pornpraprom, V. D'Elia, *ACS Catal.*, **2018**, *8*, 419.

(59) H. Tomita, F. Sanda, T. Endo, *J. Polym. Sci. Part A: Polym. Chem.*, **2001**, *39*, 3678.

(60) R. M. Garipov, V. V. Mikheev, T. R. Deberdeev, V. I. Irzhak, Al. Berlin, *Doklady Phys. Chem.*, **2003**, *392*, 649.

(61) R. M. Garipov, V. A. Sysoev, V. V. Mikheev, A. I. Zagidullin, R. Ya. Deberdeev, V. I. Irzhak, Al. Al. Berlin, *Doklady Phys. Chem.*, **2003**, *393*, 61.

(62) B. Ochiai, S. Inoue, T. Endo, *J. Polym. Sci., Part A: Polym. Chem.*, **2005**, *43*, 6282.

(63) G. Prömpers, H. Keul, H. Höcker, *Des. Monomers Polym.*, **2005**, *8*, 547.

(64) S. Guillaume, M. Helou, J. F. Carpentier, *Patent WO2012/007254A1*, **2012**.

(65) B. Ochiai, Y. Satoh, T. Endo, *Green Chem.*, **2005**, *7*, 765.

(66) L. Annunziata, A. K. Diallo, S. Fouquay, G. Michaud, F. Simon, J. M. Brusson, J. F. Carpentier, S. M. Guillaume, *Green Chem.*, **2014**, *16*, 1947.

(67) L. Maisonneuve, A. L. Wirotius, C. Alfos, E. Grau, H. Cramail, *Polym. Chem.*, **2014**, *5*, 6142.

(68) X. Sheng, G. Ren, Y. Qin, X. Chen, X. Wang, F. Wang, *Green Chem.*, **2015**, *17*, 373.

(69) H. Tomita, F. Sanda, T. Endo, *J. Polym. Sci. Part A: Polym. Chem.*, **2001**, *39*, 860.

(70) N. Kihara, Yuuji Kushida, T. Endo, *J. Polym. Sci. Part A: Polym. Chem.*, **1996**, *34*, 2173.

(71) M. Blain, L. Jean-Gérard, R. Auvergne, D. Benazet, S. Caillol, B. Andrioletti, *Green Chem.*, **2014**, *16*, 4286.

(72) N. Kihara, T. Endo, *J. Polym. Sci. Part A: Polym. Chem.*, **1993**, *31*, 2765.

(73) T. Blirgel, M. Fedtke and M. Franzke, *Polym. Bull.*, **1993**, *30*, 155.

(74) A. Boyer, E. Cloutet, T. Tassaing, B. Gadenne, C. Alfos, H. Cramail, *Green Chem.*, **2010**, *12*, 2205.

(75) A. Bossion, R. H. Aguirresarobe, L. Irusta, D. Taton, H. Cramail, E. Grau, D. Mecerreyes, C. Su, G. Liu, A. J. Müller, H. Sardon, *Macromolecules*, **2018**, *51*, 5556.

(76) O. Lamarzelle, P. L. Durand, A. L. Wirotius, G. Chollet, E. Grau, H. Cramail, *Polym. Chem.*, **2016**, *7*, 1439.

(77) B. Tamami, S. Sohn, G. L. Wilkes, *J. App. Polym. Sci.*, **2004**, *92*, 883.

(78) M. Bähr, R. Mülhaupt, *Green Chem.*, **2012**, *14*, 483.

(79) A. Z. Yu, R. A. Setien, J. M. Sahouani, J. Docken, D. C. Webster, *J. Coat. Technol. Res.*, **2019**, *16*, 41.

(80) L. Poussard, J. Mariage, B. Grignard, C. Detrembleur, C. Jéroîme, C. Calberg, B. Heinrichs, J. de Winter, P. Gerbaux, J. M. Raquez, L. Bonnaud, P. Dubois, *Macromolecules*, **2016**, ***49***, 2162.

(81) S. Doley, S. K. Dolui, *Eur. Polym. J.*, **2018**, *102*, 161.

(82) M. Malik, R. Kaur, *Polym. Adv. Technol.*, **2018**, *29*, 1078.

(83) J. H. Clark, T. J. Farmer, I. D. V. Ingram, Y. Lie, M. North, *Eur. J. Org. Chem.*, **2018**, *31*, 4265.

(84) V. Schimpf, B. S. Ritter, P. Weis, K. Parison, R. Mülhaupt, *Macromolecules*, **2017**, *50*, 944.

(85) M. Bähr, A. Bitto, R. Mülhaupt, *Green Chem.*, **2012**, *14*, 1447.

(86) V. Besse, R. Auvergne, S. Carlotti, G. Boutevin, B. Otazaghine, S. Caillol, J. P. Pascault, B. Boutevin, *React. Funct. Polym.*, **2013**, *73*, 588.

(87) J. A. Castro-Osma, J. Martinez, F. de la Cruz-Martínez, M. P. Caballero, J. Fernández-Baeza, J. Rodríguez-López, A. Otero, A. Lara-Sánchez, J. Tejeda, *Cat. Sci. Technol*., **2018**, *8*, 1981.

(88) R. H. Lambeth, T. J. Henderson, *Polymer*, **2013**, *54*, 5568.

(89) A. Steblyanko, W. Choi, F. Sanda, T. Endo, *J. Polym. Sci. Part A: Polym. Chem.*, **2000**, *38*, 2375.

(90) S. Benyahya, J. P. Habas, R. Auvergne, V. Lapinte, S. Caillol, *Polym. Int.*, **2012**, *61*, 1666.

(91) S. Benyahya, B. Boutevin, S. Caillol, V. Lapinte, J. P. Habas, *Polym. Int.*, **2012**, *61*, 918.

(92) L. Xu, J. H. Fu, J. R. Schlup, *J. Am. Chem. Soc.*, **1994**, *116*, 2821.

(93) F. A. Saddique, A. F. Zahoor, S. Faiz, S. A. R. Naqvi, M. Usman, M. Ahmad, *Synth. Commun.*, **2016**, *46*, 831.

(94) B. Lee, K. H. Lee, B. W. Lim, J. Cho, W. Nam, N. H. Hur, *Adv. Synth. Cat.*, **2013**, *355*, 389.

(95) F. de la Cruz-Martínez, M. Martínez de Sarasa Buchaca, J. Martínez, J. Fernández-Baeza, L. F. Sánchez-Barba, A. Rodríguez-Diéguez, J. A. Castro-Osma and A. Lara-Sánchez, *ACS Sust. Chem. Eng.*, **2019**, *7*, 20126.

(96) T. Andrew, *Dow Chemical CO*, US5036154 (A), **1991**.

Chapter 5.

Synthesis of bis(1,2,3-triazol-1-yl)methane-derived heteroscorpionate complexes.

Introduction

In this Chapter of the dissertation, the results obtained in the design of different nitrogen ligands derived from bis(1,2,3-triazol-1-yl)methane moiety and their coordination to different metal centres such as aluminium, zinc and iridium, will be described. Before focusing on the synthesis and characterisation of these compounds, a brief introduction about triazole-derived ligands will be covered.

1. Ligands derived from 1,2,3-triazole

The ability of nitrogen compounds to act as polydentate ligands in organometallic and coordination chemistry has led to great interest in the development of highly efficient methods for the preparation of structurally diverse nitrogen-based ligands.[1]

The key feature of the different synthetic routes to develop nitrogen-based ligands lies on the versatility to prepare a broad range of new compounds with tuneable electronic and steric properties. Diversity-oriented synthesis (DOS) offers unexpected possibilities in this area for the easy and quick preparation of novel libraries of structurally diverse compounds.[2] In this context, triazole-derived nitrogen-ligands have received considerable attention due to their multiple applications in biological, pharmaceutical, agrochemical and textile industries.[3-9]

One of the most prominent reaction to synthesise 1,4 disubstituted 1,2,3-triazole compounds is the “click chemistry” regiospecific cooper(I)-catalysed alkyne/azide cycloaddition (CuAAC) reaction, characterised by high yields, mild conditions and excellent functional group tolerance (Scheme 1).[10-11]

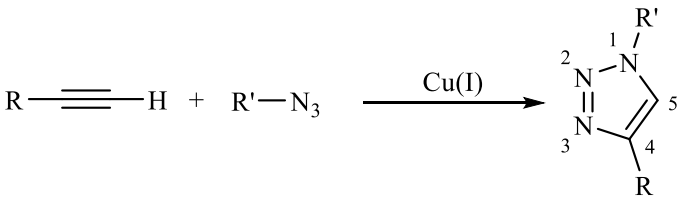

Scheme 1. *CuAAC click reaction.*

The 1,2,3-triazole moiety, through its ease of preparation and the ability to include a wide range of functional groups in the substituents, provides an excellent route for ligand design. 1,2,3-triazole compounds possess two nitrogen atoms capable of metal coordination, the N3-position being the more basic (Figure 1). Introduction of other donor functions into the R and R’ groups of the alkyne and azide precursors allows

access to a wide range of chelating ligands (Scheme 1). In addition, the 5-position C–H moiety affords the formation of anionic triazolides through C–H activation. Also, alkylation of the N3-position followed by deprotonation of the already mentioned acidic C–H[5] bond leads to the formation of *abnormal* mesoionic N-heterocyclic carbenes (*aNHC*s).[12] Whilst initially slow, the last decade has seen an explosion in the utilisation of CuAAC for the design of new ligand systems for metal complexes.[13]

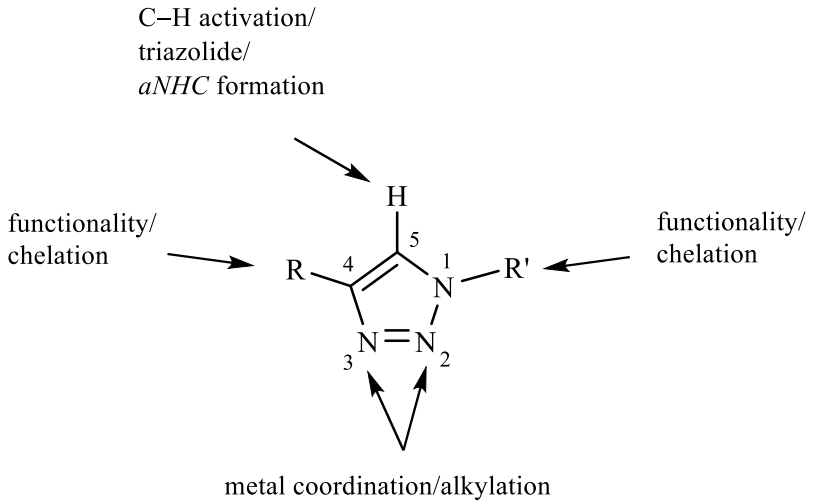

Figure 1. *Functionalisation potential of 1,2,3-triazoles for coordination chemistry.*

Following this synthetic route, different 1,2,3-triazole-derived tridentate ligands have been prepared by click chemistry from phenylazide and ethynylphosphine oxide (Scheme 2). In these compounds, a phosphorous atom acts as bridging atom between the triazole rings. These compounds are very similar to tris(pyrazol-1-yl)methane since they act as neutral ligands, although they are not included within the heteroscorpionate ligand definition. As an example, by their reaction with $RhCl_3$, the rhodium complex shown in Scheme 2 was obtained, where the 1,2,3-triazole-based ligand acts as a tridentate neutral ligand exhibiting a κ^3-NNN coordination mode.[14]

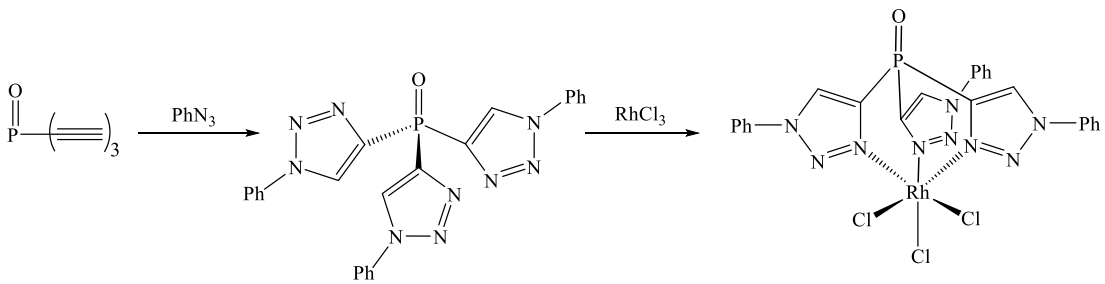

Scheme 2. *Synthesis of Rh (III) complex with a tridentate 1,2,3-triazole-based ligand.*

Since the first isolation of a free imidazole-based N-heterocyclic carbene (NHC), these ligands have become ubiquitous in organometallic chemistry (Figure 2). A rapidly expanding area was the development of so-called "*abnormal*" or mesoionic NHCs (*a*NHCs). In this case, the carbonic centre is formed at the C4 or C5 positions and as a result there is no neutral canonical form that can be drawn (Figure 2b,c). A new sub-class of *a*NHCs, derived from CuAAC derived triazolium salts has emerged and different metal complexes have been synthesised (Figure 2c).[15-18]

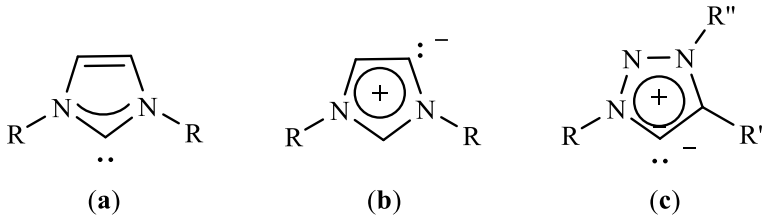

Figure 2. *a) normal imidazole-2-ylidene, b)" abnormal" imidazole-4-ylidene, c) "abnormal" 1,3,4-trisubstituted 1,2,3-triazol-5-ylidene.*

The first complex with this new class of *a*NHCs was isolated by reaction of a 1,3,4-trisubstituted 1,2,3-triazolium salt with Ag_2O to yield an *a*NHC silver complex. Transmetalation reaction with chloride 1,5-cyclooctadiene iridium (I) dimer afforded the first *a*NHC iridium (I) complexes (Figure 3a,b).[16] More recently, 1,2,4-trisubstitued 1,2,3-triazol-5-ylidene ligands synthesised by a non-CuAAC route have been employed to generate "normal" NHC iridium (I) complexes, also by transmetalation reaction using silver oxide as transmetalating agent (Figure 3c).[17]

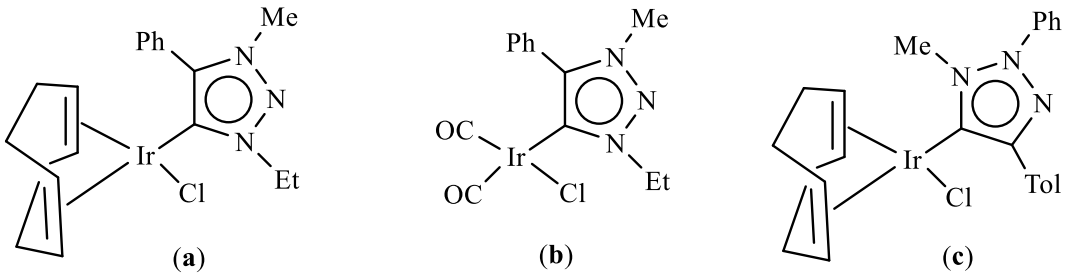

Figure 3. *a,b) aNHC Iridium (I) complexes; c) NHC Iridium (I) complex.*

1.1. Heteroscorpionate ligands derived from 1,2,3-triazole

As it has been previously mentioned in Chapter 1, heteroscorpionate ligands represent one of the most versatile ligands reported. Amongst them, bis(pyrazol-1-yl)methane derivatives have received great attention since they exhibit great versatility and capacity to coordinate to a wide range of elements. With the aim to design new heteroscorpionate ligands with different electronic and steric properties, different ligand precursors using other heterocycles such as 1,2,3-triazole have been prepared.[19,20]

The first heteroscorpionate ligands based on 1,2,3-triazole moieties were reported in 2010 by Burzlaff and co-workers.[19] In these ligands, 2H-benzotriazole was used as precursor, which led to three different isomers in different proportions; *(a)* bis(1*H*-benzotriazol-1-yl)methane, *(b)* bis(1*H*-benzotriazol-1-yl)(2*H*-benzo-triazol-2-yl) methane and *(c)* bis(2*H*-benzotriazol-2-yl)methane. Isomer *c* was employed for the synthesis of a heteroscorpionate ligand functionalised with a carboxylate group by reaction with ^{n}BuLi and CO_2, which, after hydrolysis, afforded the bis(2*H*-benzotriazol-2-yl)methane acetic acid (Scheme 3). This ligand was coordinated to different metal centres such as Mn and Ru by reaction with $[MnBr(CO)_5]$ and $[RuCl_2(PPh_3)_3]$, obtaining the organometallic complexes shown in Scheme 4. In these complexes, the 1,2,3-triazole-derived heteroscorpionate ligand acted as an anionic monofacial ligand, adopting a κ^3-NNO coordination mode (Scheme 4). The resulting complexes found applications in the preparation of metal-organic frameworks (MOFs) and in medicinal chemistry as structural mimics for the active site of metalloenzymes.

More recently, our research group developed a new synthetic route for the preparation of 1,2,3-triazole-derived heteroscorpionate ligands.[20] Thus, by reaction between a 1,1-bis(azide) and two equivalents of alkyne, innovative neutral bis(4-substituted 1,2,3-triazol-1-yl)methane compounds were synthesised (Scheme 5). These bis(1,2,3-triazol-1-yl)methane compounds were functionalised with acetamidate and thioacetamidate groups in the methine group bridging both triazole rings following the same procedure as for their bis(pyrazol-1-yl)methane analogues (Scheme 6). In addition, they were further employed for the preparation of alkyl zinc complexes by protonololysis reactions, as depicted in Scheme 7.[20]

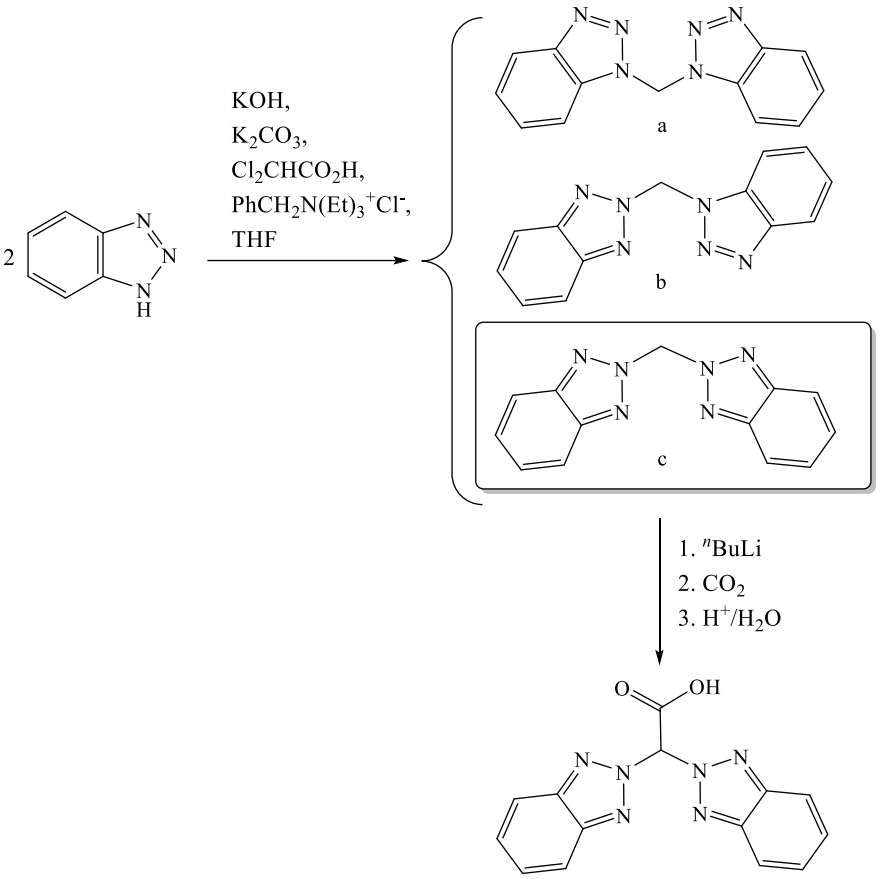

Scheme 3.

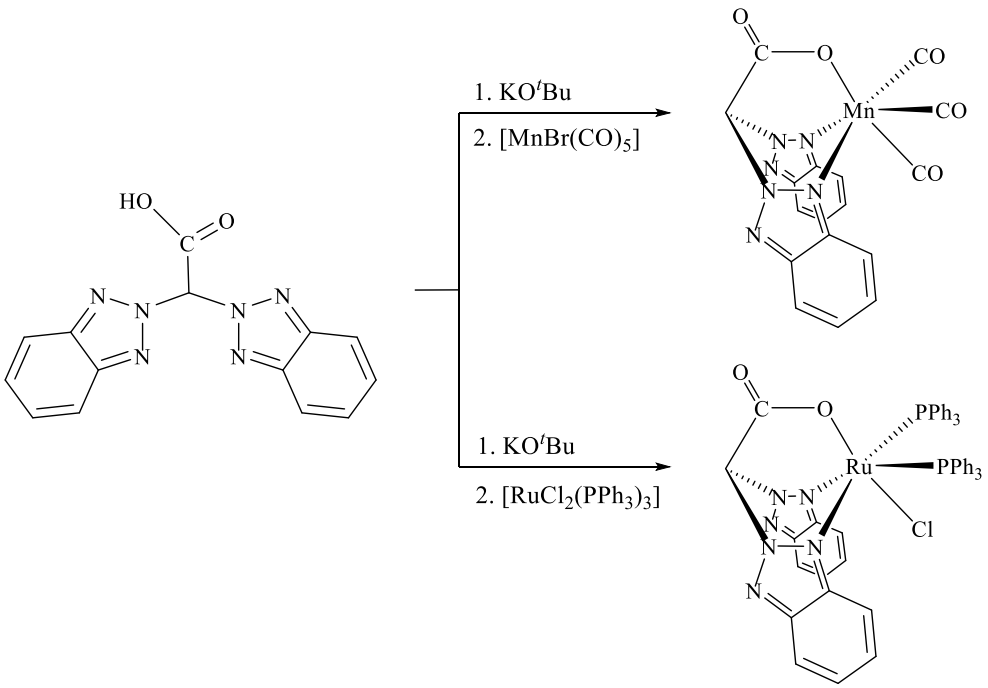

Scheme 4.

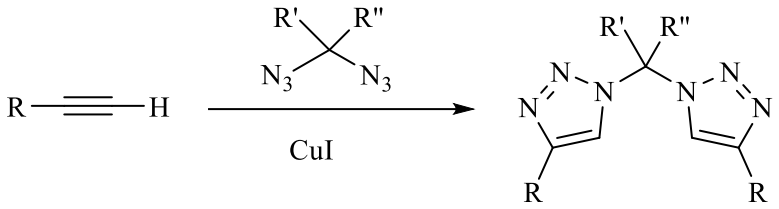

Scheme 5. *Synthesis of the bis(triazol-1-yl)methane derivates.*

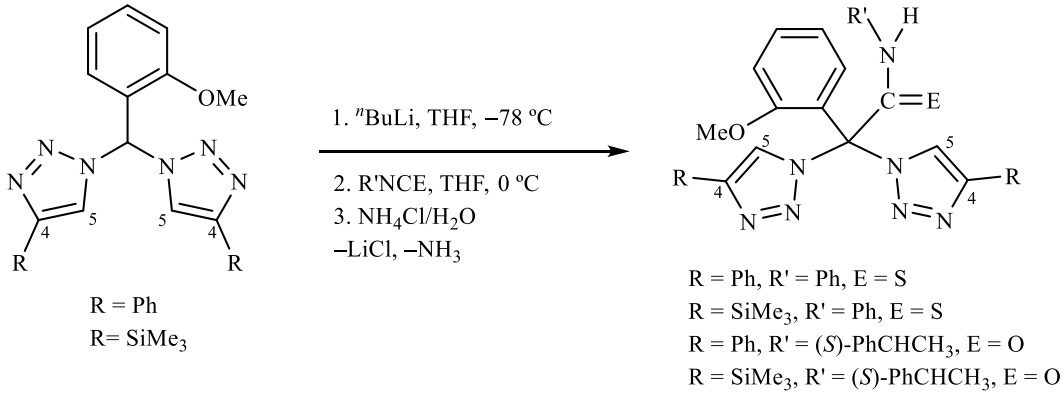

Scheme 6. *Synthesis of acetamide and thioacetamidate bis(triazol-1-yl)methane-derived heteroscorpionate ligands.*

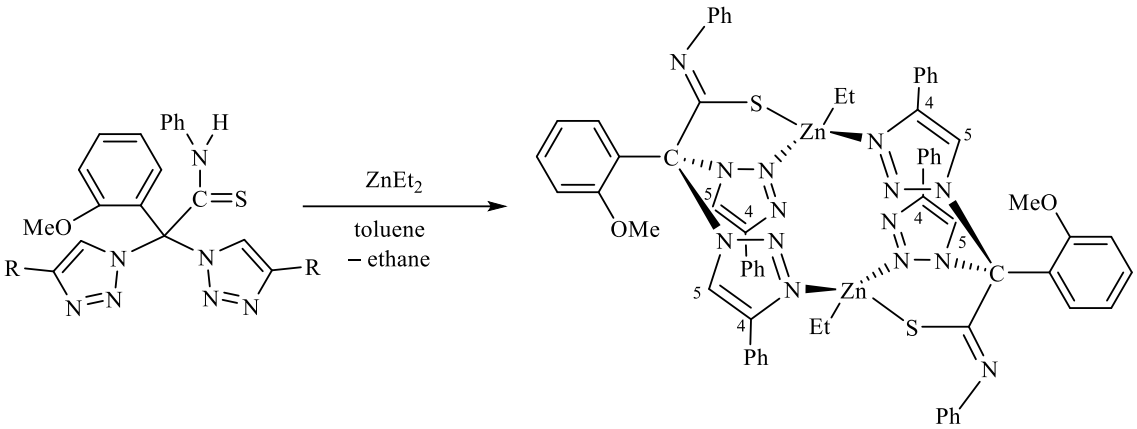

Scheme 7. *Dinuclear alkyl zinc complex supported by thioacetamidate bis(triazol-1-yl)methane-derived heteroscorpionate ligand.*

Results and discussion

As it has been previously commented in the introduction of this Chapter, there is a great interest in the design of new polyfunctional heteroscorpionate ligands with different electronic and steric properties. Thus, in order to contribute to this field, new neutral heteroscorpionate ligand precursors derived from bis(1,3,3-triazol-1-yl)methane (btzm) have been prepared.

1. Synthesis of bis(1,2,3-triazol-1-yl)methane derivatives

As previously mentioned in the introduction, the synthesis of the different bis(1,2,3-triazol-1-yl)methane derivatives has been carried out by "click" reaction, using organic diazides and terminal alkynes as substrates and Cu(I) as catalyst, as shown in Scheme 8.[20] Thus, the corresponding bis(triazol-1-yl) methane derivates: bptzpm, [bptzpm = 1,1'-((4-methoxyphenyl)methylene)bis(4-phenyl-1H-1,2,3-triazole)], bttzpm, [bttzpm = 1,1'-((4-methoxyphenyl)methylene)bis(4-(trimethylsilyl)-1H-1,2,3-triazole), bptzom, [bptzom = 1,1'-((2-methoxyphenyl)methylene)bis(4-phenyl-1H-1,2,3-triazole) and bttzom, [bttzom = 1,1'-((2-methoxyphenyl)methylene)bis(4-(trimethylsilyl)-1H-1,2,3-triazole) were obtained as white solids in high yields (Scheme 8).

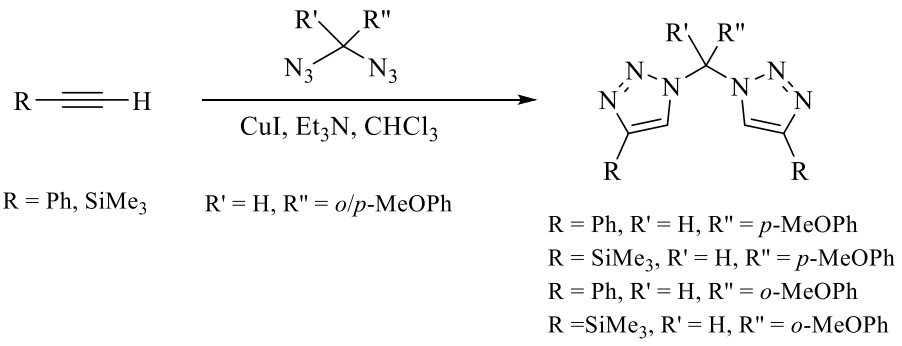

Scheme 8. *Synthesis of bis(1,2,3-triazol-1-yl)methane precursors.*

2. Synthesis of bis(1,2,3-triazol-1-yl)methane-derived compounds functionalised with alcohol groups

The synthesis of these compounds was carried out by reaction of the corresponding bis(1,2,3-triazol-1-yl)methane derivative with ^{n}BuLi in THF at −70 ºC during one hour, followed by the addition of the corresponding aldehyde compound (Schemes 9 and 10). Finally, the protonolysis reaction of the generated lithiated adduct with saturated aqueous NH_4Cl afforded the corresponding alcohol neutral compound **58**-**67**

as white solids in good yields. The products obtained in this reaction showed to be different depending on the aldehyde used. Thus, when aldehydes with aromatic substituents were used (Scheme 9), the deprotonation took place at the methine carbon bridging both triazole rings, affording compounds bptzpmmabzeH [bptzpmmabzeH = 1-(4-(dimethylamino) phenyl)-2-(4-methoxyphenyl)-2,2-bis(4-phenyl-1H-1,2,3-triazol-1-yl)ethan-1-ol] (**58**), bttzpmmabzeH, [bttzpmmabzeH = 1-(4-(dimethylamino)phenyl)-2,2-bis(4-(trimethylsilyl)-1H-1,2,3-triazol-1-yl)ethan-1-ol (**59**), bptzpmteH [bptzpmteH =2-(4-methoxyphenyl)-2,2-bis(4-phenyl-1H-1,2,3-triazol-1-yl)-1-(*p*-tolyl) ethan-1-ol] (**60**), bttzpmteH [bttzpmteH =2-(4-methoxyphenyl)-1-(*p*-tolyl)-2,2-bis(4-(trimethylsilyl)- 1H1,2,3-triazol-1-yl) ethan-1-ol] (**61**), bttzomteH [bttzomteH =2-(2-methoxyphenyl)-1-(*p*-tolyl)-2,2-bis(4-(trimethylsilyl)-1H-1,2,3-triazol-1-yl) ethan-1-ol] (**62**) and bptzomteH [bptzomteH = 2-(2-methoxyphenyl)-2,2-bis(4-phenyl-1H-1,2,3-triazol-1-yl)-1-(*p*-tolyl)ethan-1-ol] (**63**).

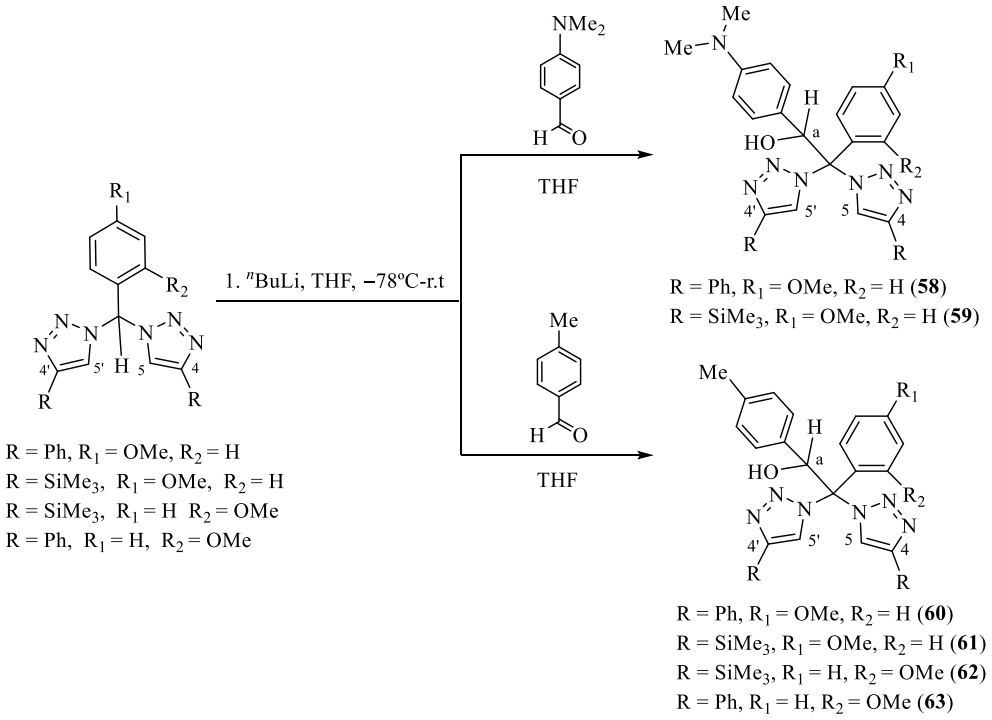

Scheme 9. *Synthesis of bis(triazol-1-yl)methane-derived compounds **58-63**.*

On the other hand, when aldehydes with aliphatic substituents such as trimethylacetaldehyde were used (Scheme 10), the deprotonation occurred at the C^5 carbon of the triazole rings, affording compounds bptzpmbeH [bptzpmbeH = 1-(1-((4-methoxyphenyl)(4-phenyl-1H-1,2,3-triazol-1-yl)methyl)-4-phenyl-1H-1,2,3-triazol-5

-yl)-2,2-dimethylpropan-1-ol] (**64**), bttzpmbeH [bttzpmbeH =1-(1-((4-methoxyphenyl)(4-(trimethylsilyl)-1H-1,2,3-triazol-1-yl) methyl)-4-(trimethylsilyl)-1H-1,2,3-triazol-5-yl)-2,2-dimethylpropan-1-ol] (**65**), bttzombeH [bttzombeH = 1-(1-((2-methoxyphenyl) (4-(trimethylsilyl)-1H-1,2,3-triazol-1-yl)methyl)-4-(trimethylsilyl)-1H-1,2,3-triazol-5-yl)- 2,2-dimethyl propan-1-ol] (**66**) and bptzombeH [bptzombeH = 1-(1-((2-methoxyphenyl)(4-phenyl-1H-1,2,3-triazol-1-yl)methyl)-4-phenyl-1H-1,2,3-triazol-5-yl)-2,2-dimethylpropan-1-ol] (**67**).

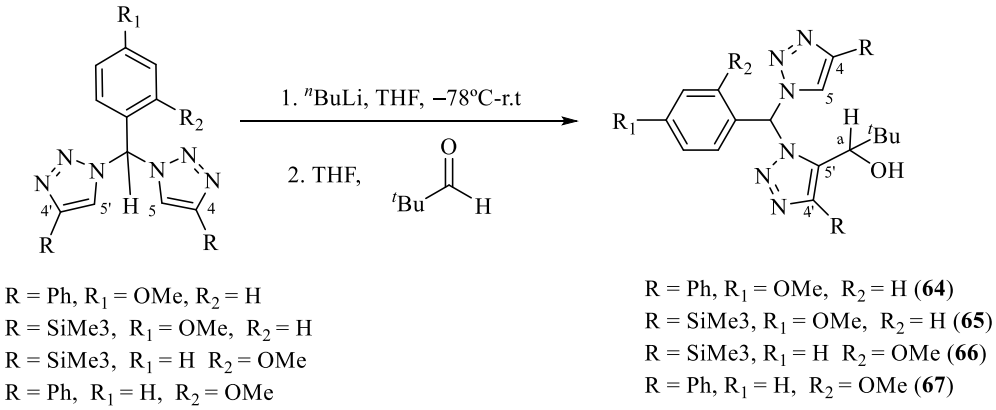

Scheme 10. *Synthesis of bis(triazol-1-yl)methane-derived compounds **64-67**.*

These results confirmed that upon deprotonation with ^{n}BuLi of the corresponding bis(1,2,3-triazol-1-yl)methane derivatives, two possible lithiated intermediates can be generated depending on the position at which the deprotonation occurs, either at the methine carbon bridging both triazole rings or the C^5 carbon of one triazole ring (Scheme 11).

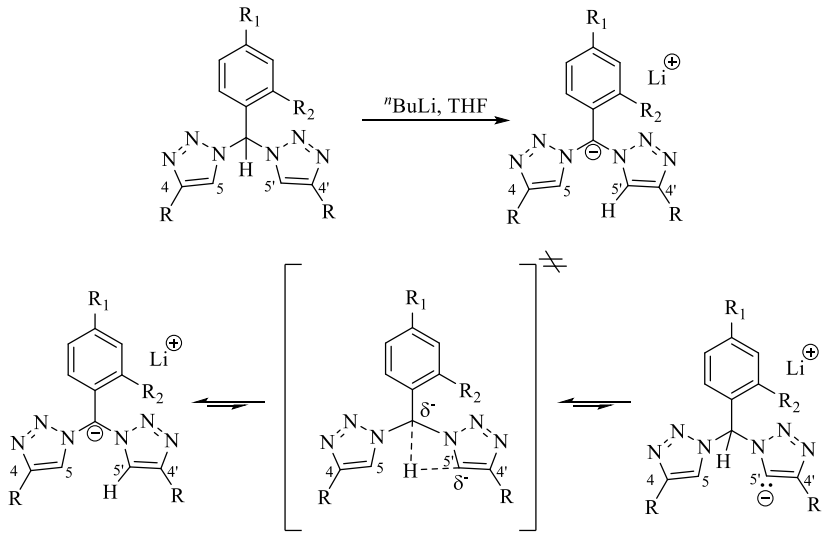

Scheme 11. *Deprotonation of bis 1,2,3-(triazol-1-yl) methane precursors using ^{n}BuLi.*

Structural Characterisation

The structural characterisation of compounds **58-67** was performed by ^{1}H-NMR and ^{13}C{^{1}H}-NMR spectroscopy (Tables 1-6) and X-Ray diffraction analysis. The ^{1}H-NMR and ^{13}C{^{1}H}-NMR spectra for compounds **58-63** exhibited two distinct sets of triazole resonances, showing two singlets for the H^{5} triazole protons and carbons due to the presence of the C^{a} stereogenic centre from the alcohol moiety (Figures 4 and 5). On the other hand, the ^{1}H-NMR and ^{13}C{^{1}H}-NMR spectra for compounds **64-67** exhibited only one proton resonance in the $H^{5'}$ region and another more acidic proton resonance in the region between 9.08-9.62 ppm, which was assigned to the methine proton bridging both triazole rings (Figure 6). These NMR data are consistent with the proposed structures in Schemes 9 and 10. When planar aldehydes such as 4-dimethylaminobenzaldehyde or *p*-tolualdehyde were used, the functionalisation occurred at the methine carbon bridging both triazole rings. However, when non-planar and bulkier aldehydes such as trimethylacetaldehyde were used, the functionalisation took place at one C^{5} carbon of one of the triazole rings. Figure 7 shows a comparison between the ^{1}H-NMR spectra for compounds **59**, **62** and **65** in the region of the H^{5} and methine protons.

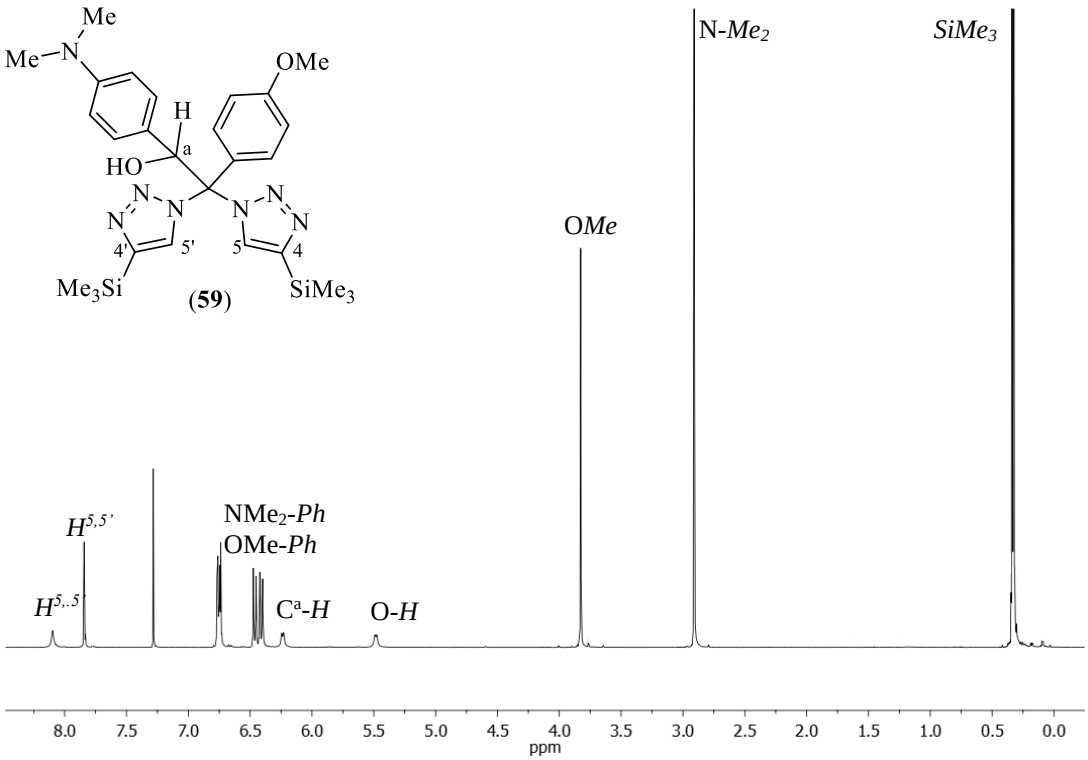

Figure 4. *^{1}H-NMR spectrum for compound **59** in $CDCl_3$.*

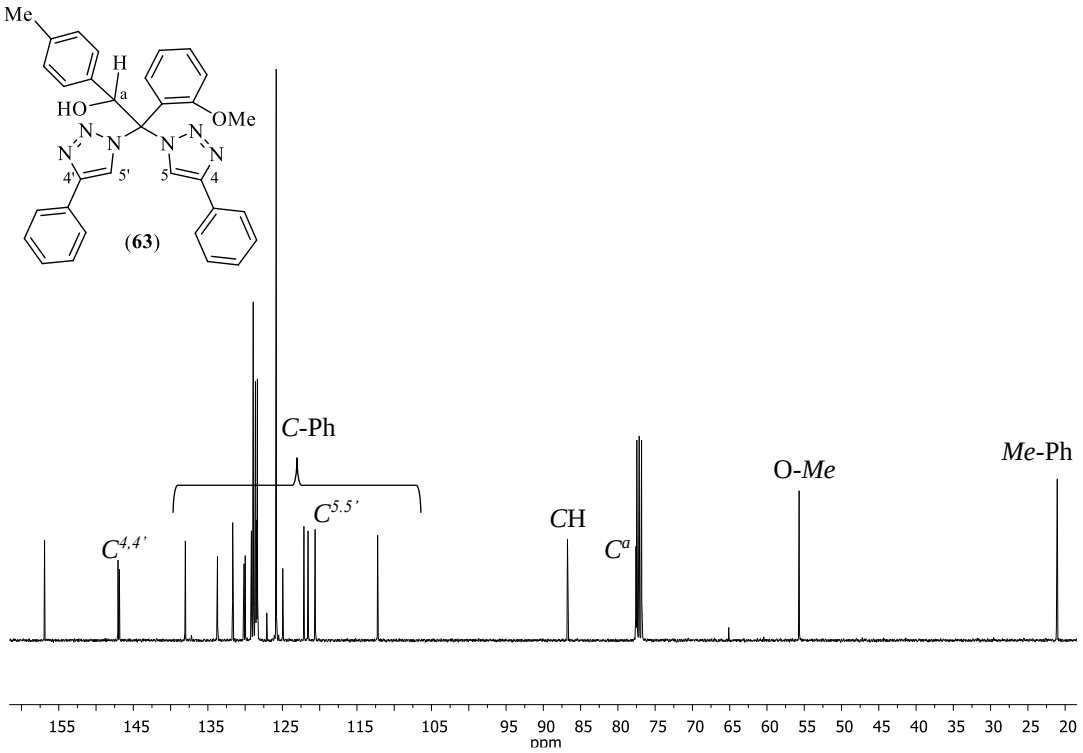

Figure 5. *^{13}C-{^{1}H}-NMR spectrum for compound **63** in $CDCl_3$.*

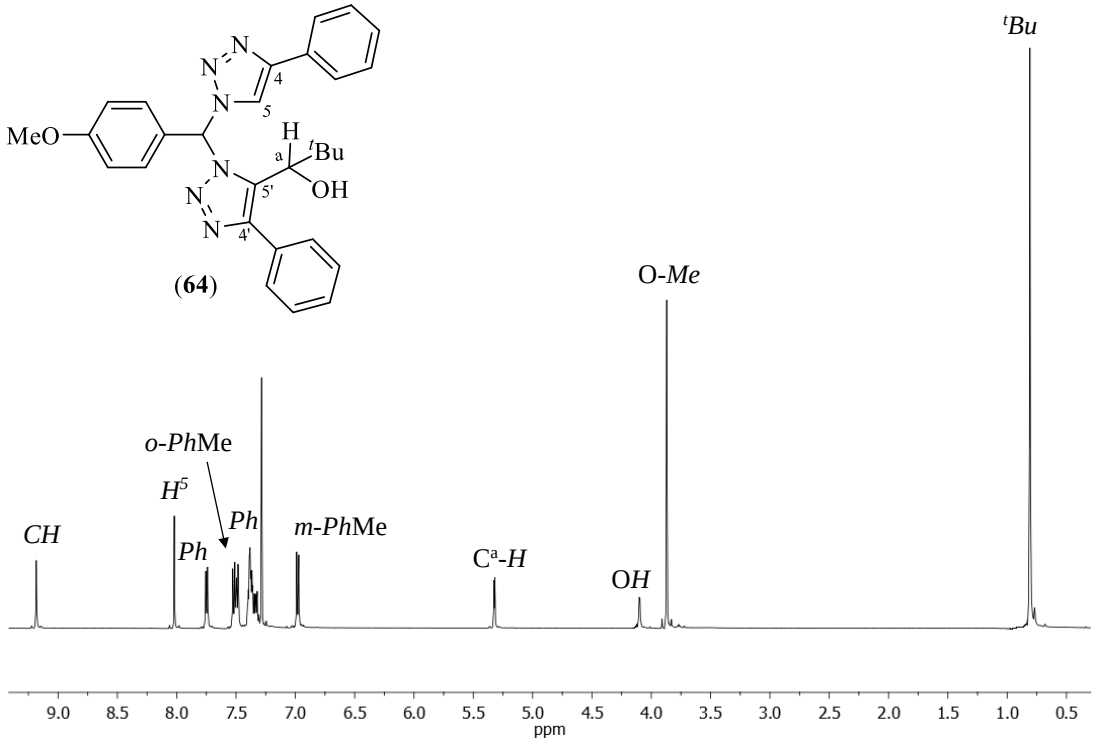

Figure 6. *^{1}H-NMR spectrum for compound **64** in $CDCl_3$.*

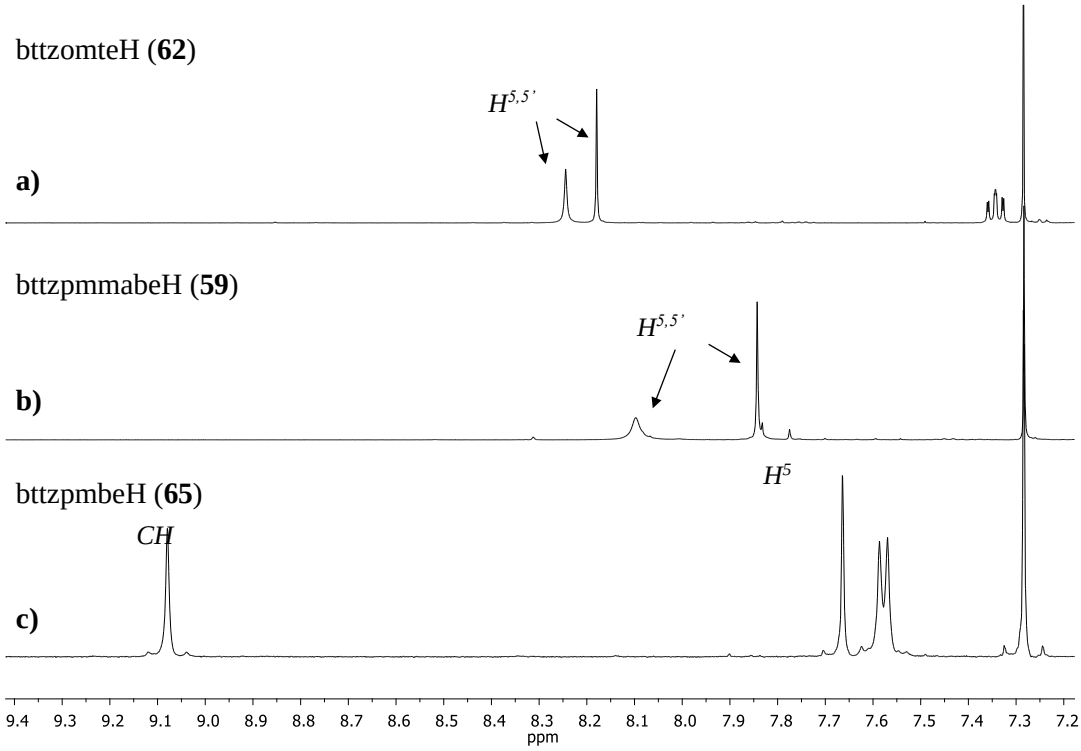

Figure 7. *Comparison of the ^{1}H-NMR spectra in $CDCl_3$ for compounds **62**, **59** and **65** in the CH and H^5 region.*

In order to gain further insight into the reaction mechanism, deuteration experiments were also carried out. Thus, after deprotonation of the bis-triazole precursor, D_2O was added to the solution (Scheme 12). Figure 8 shows the comparison between the ^{1}H-NMR spectrum of the bis-triazole precursor before (Figure 8a) and after deprotonation (Figure 8b). As it can be seen from Figure 8, the signal corresponding to the methine group has almost disappeared, while the signals corresponding to the H^5 protons remain unchanged, giving proof that the deprotonation occurred in a greater extent in the methine position. However, the ^{2}D-NMR spectrum of the generated specie (Figure 9) exhibited two different signals which were assigned to the higher deuteration of the methine group (CH) bridging both triazole rings (8.35 ppm) and the lower deuteration at the H^5 from the triazole rings (7.91 ppm). Thus, when using planar aldehydes such as *p*-tolualdehyde or 4-N,N-dimethylaminobenzaldehyde, the insertion of the aldehyde occurred at the C–*H* group since there is not much steric repulsion between the methoxybenzene substituent and the incoming aromatic substituent from the aldehyde. However, when using aldehydes with bulkier substituents such as trimethylacetaldehyde, the steric hindrance between

the methoxybenzene and the *tert*-butyl group from the incoming aldehyde makes it impossible for it to insert in this carbon, thus, giving the insertion product at the H^5 of one of the triazole rings.

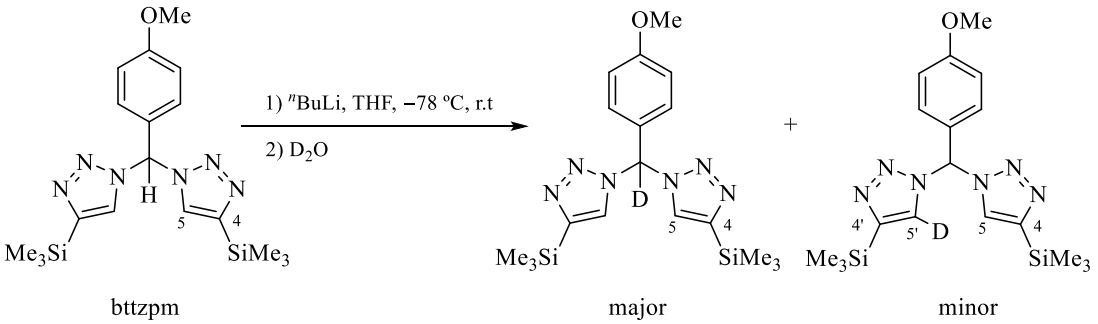

Scheme 12. *Deprotonation of bttzpm and subsequent deuteration using D_2O.*

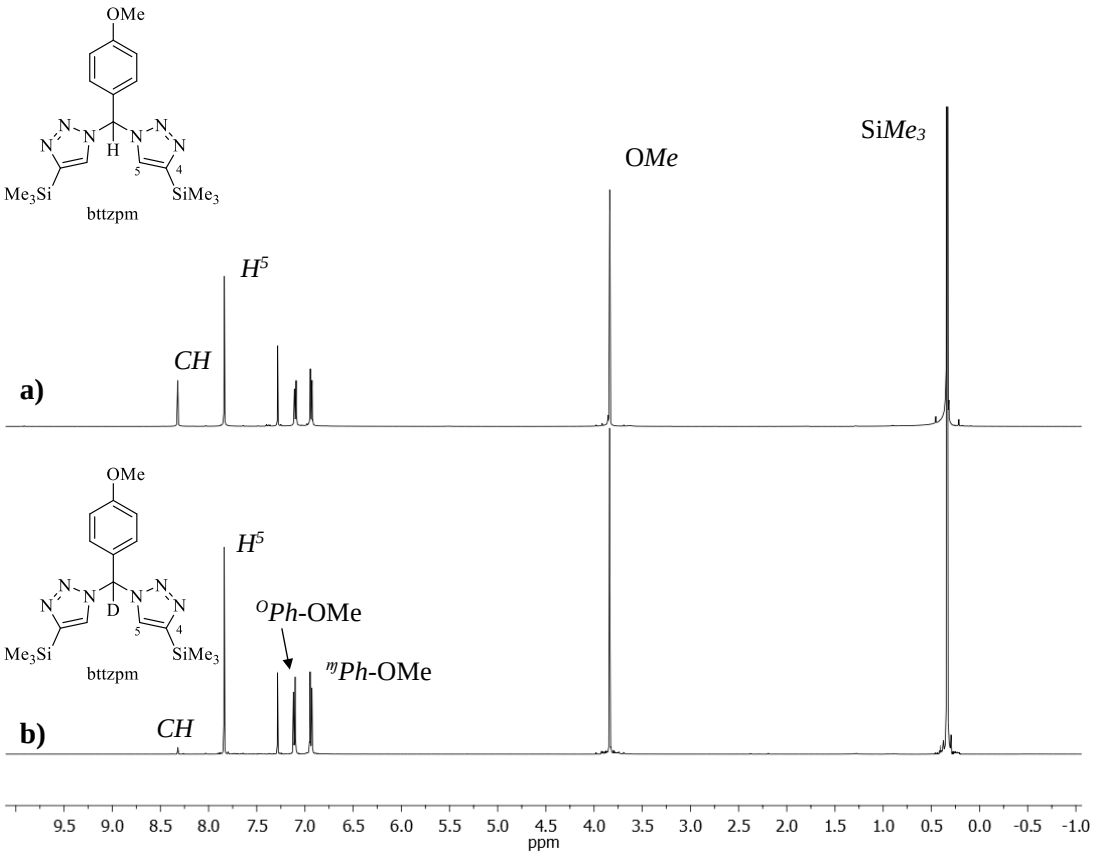

Figure 8. *^{1}H-NMR spectrum of a)bttzpm before and b) after adding D_2O to the deprotonated specie in $CDCl_3$.*

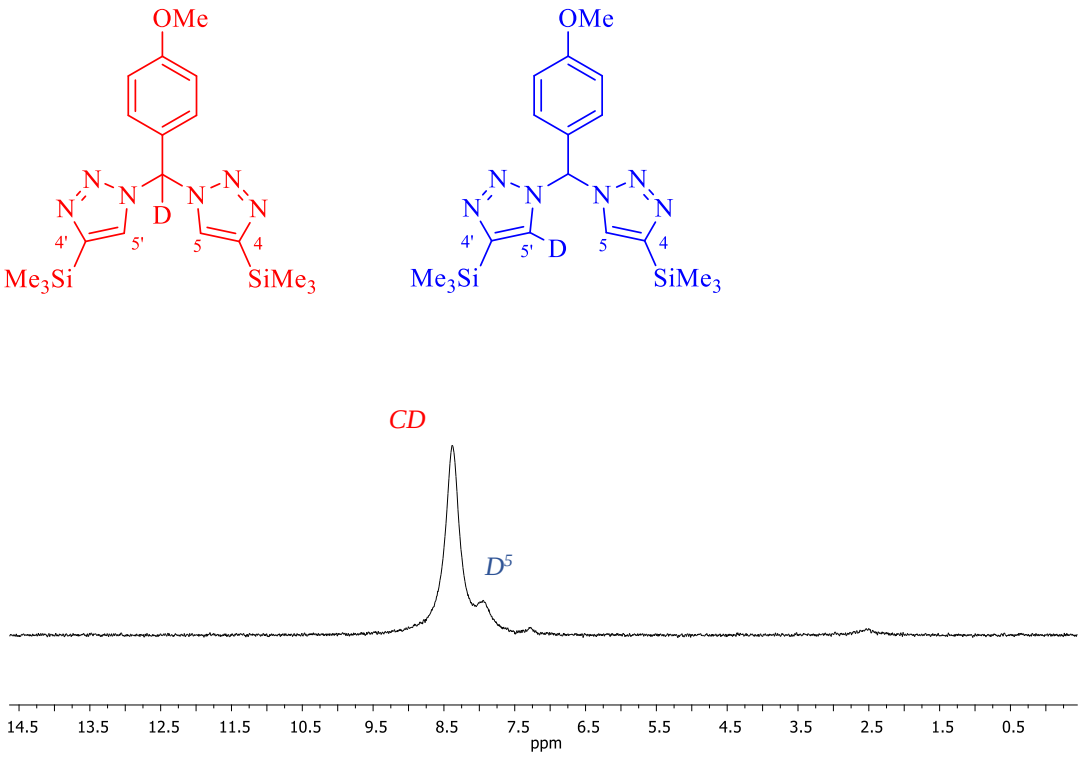

Figure 9. *^{2}D-NMR spectrum of deuterated precursor bttzpm in $CDCl_3$.*

Table 1. *^{1}H-NMR data for compounds **58** and **59**.*

Compound	$R^{4,4'}$	$H^{5,5'}$	MeOPh	*p*-N(Me)$_2$Ph	CH[a]	OH
bptzpmmabeH (**58**)	Ph 7.48-7.33 (m, 6H) 7.83 (d, J_{HH} = 1.1 Hz, 1H) 7.84 (d, J_{HH} = 1.4 Hz, 1H) 7.87 (d, J_{HH} = 1.1 Hz, 1H) 7.89 (d, J_{HH} = 1.4 Hz, 1H)	8.06 (s, 1H) 8.56 (s, 1H)	3.84 (s, 1H, O-*CH$_3$*) 6.58 (d, J_{HH} = 8.9 Hz, 2H, Ph) 6.78 (d, J_{HH} = 9.0 Hz, 2H, Ph)	2.91 (s, 6H, *CH$_3$*) 6.49 (d, J_{HH} = 9.0 Hz, 2H, Ph) 6.83 (d, J_{HH} = 8.8 Hz, 2H, Ph)	6.39 (s, 1H)	5.23 (s, 1H)
bttzpmmabeH (**59**)	$CH_3)_3Si$ 0.34(s, 9H, CH_3) 0.33(s, 9H, CH_3)	7.84 (s, 1H) 8.10 (s, 1H)	3.83 (s, 1H, O-*CH$_3$*) 6.46 (d, J_{HH} = 8.9 Hz, 2H, Ph) 6.74 (d, J_{HH} = 9.0 Hz, 2H, Ph)	2.91 (s, 1H, *CH$_3$*) 6.41 (d, J_{HH} = 9.0 Hz, 2H, Ph) 6.76 (d, J_{HH} = 8.9 Hz, 2H, Ph)	6.23 (s, 1H)	5.50 (s, 1H)

Spectra recorded in $CDCl_3$.

Table 2. *^{13}C-{^{1}H}-NMR data for compounds **58** and **59**.*

Compound	$C^{4,4'}$	$R^{4,4'}$	$C^{5,5'}$	MeOPh	*p*-N(Me)$_2$Ph	N-C-N	C[a]
bptzpmmabeH (**58**)	147.4 147.7	Ph 125.8-129.9	121.2	55.4 O-CH_3 113.0-160.4 Ph	40.3 N-$(CH_3)_2$ 111.4-150.5 Ph	87.6	79.1
bttzpmmabeH (**59**)	146.0 146.3	$(CH_3)_3Si$ -1.2	130.1 131.4	55.4 O-CH_3 112.9-160.2 Ph	40.3 N-$(CH_3)_2$ 111.2-150.3 Ph	86.8	79.5

Spectra recorded in $CDCl_3$.

Table 3. *^{1}H-NMR data for compounds **60-63**.*

Compound	$R^{4,4'}$	$H^{5,5'}$	MeOPh	*p*-MePh	CH[a]	OH
bptzpmteH (**60**)	Ph 7.48-7.33 (m, 6H) 7.83 (d, J_{HH} = 1.1 Hz, 1H) 7.84 (d, J_{HH} = 1.4 Hz, 1H) 7.86 (d, J_{HH} = 1.1 Hz, 1H) 7.88 (d, J_{HH} = 1.4 Hz, 1H)	8.07 (s, 1H) 8.52 (s, 1H)	3.84 (s, 3H, O-*CH*$_3$) 6.56 (d, J_{HH} = 9.0 Hz, 2H, Ph) 6.78 (d, J_{HH} = 9.0 Hz, 2H, Ph)	2.31 (s, 3H, CH_3) 6.88 (d, J_{HH} = 8.2 Hz, 2H, Ph) 6.98 (d, J_{HH} = 8.1 Hz, 2H, Ph)	6.47 (s, 1H)	5.40 (s, 1H)
bttzpmteH (**61**)	$(CH_3)_3Si$ 0.34 (s, 9H, CH_3) 0.33 (s, 9H, CH_3)	7.85 (s, 1H) 8.07 (s, 1H)	3.83 (s, 1H, O-*CH*$_3$) 6.39 (d, J_{HH} = 9.0 Hz, 2H, Ph) 6.74 (d, J_{HH} = 9.0 Hz, 2H, Ph)	2.29 (s, 3H, CH_3) 6.80 (d, J_{HH} = 8.1 Hz, 2H, Ph) 6.94 (d, J_{HH} = 8.0 Hz, 2H, Ph)	6.30 (s, 1H)	5.66 (s, 1H)
bttzomteH (**62**)	$(CH_3)_3Si$ 0.35 (s, 9H, CH_3) 0.33 (s, 9H, CH_3)	8.24 (s, 1H) 8.18 (s, 1H)	3.37 (s, 1H, O-*CH*$_3$) 6.13 (dd, J_{HH} = 8 Hz; 1.4 Hz, 1H, Ph) 6.74 (t, J_{HH} = 7.7 Hz, 1H, Ph) 6.85 (d, J_{HH} = 8.3 Hz, 1H, Ph) 7.34 (m, 1H, Ph)	2.24 (s, 3H, CH_3) 6.91 (d, J_{HH} = 8.0 Hz, 2H, Ph) 7.00 (d, J_{HH} = 8.2 Hz, 2H, Ph)	6.43 (brs, 1H)	5.93 (brs, 1H)
bptzomteH (**63**)	Ph 7.48-7.34 (m, 6H) 7.85 (d, J_{HH} = 7.1 Hz, 2H) 7.89 (d, J_{HH} = 7.1 Hz, 2H)	8.50 (s, 2H)	3.43 (s, 1H, O-*CH*$_3$) 6.45 (d, J_{HH}= 7.8 Hz, 1H, Ph) 6.80 (m, 1H, Ph) 6.90 (m, 1H, Ph) 7.39 (m, 1H, Ph)	2.27 (s, 3H, CH_3) 6.96 (d, J_{HH} = 8.1 Hz, 2H, Ph) 7.09 (d, J_{HH} = 8.2 Hz, 2H, Ph)	6.61 (brs, 1H)	5.82 (brs, 1H)

Spectra recorded in $CDCl_3$.

Table 4. *^{13}C-{^{1}H}-NMR data for compounds **60-63**.*

Compound	$C^{4,4'}$	$R^{4,4'}$	$C^{5,5'}$	MeOPh	*p*-MePh	N-C-N	C^{a}
bptzpmteH (**60**)	147.6 147.8	Ph 125.8-129.7	121.1 121.9	55.4 O-CH_3 113.1-160.6 Ph	21.1 (CH_3)-Ph 126.5 -138.6 Ph	87.4	79.1
bttzpmteH (**61**)	146.2 146.5	$(CH_3)_3Si$ -1.2	130.6	55.4 O-CH_3 113.0-160.4 Ph	21.1 (CH_3)-Ph 127.5-138.2 Ph	86.6	79.6
bttzomteH (**62**)	145.4 145.5	$(CH_3)_3Si$ -1.1 -1.2	130.7 131.5	55.5 O-CH_3 112.1-156.7 Ph	21.0 (CH_3)-Ph 125.7-137.7 Ph	85.8	77.7
bptzomteH (**63**)	146.9 147.1	Ph 125.8-130.2	121.6	55.7 O-CH_3 112.2-156.9 Ph	21.1 (CH_3)-Ph 127.1-138.0 Ph	86.8	77.6

Spectra recorded in $CDCl_3$.

Table 5. *^{1}H-NMR data for compounds **64-67**.*

Compound	$R^{4,4'}$	H^{5}	MeOPh	^{t}Bu	CH	CH^{a}	OH
bptzpmbeH (**64**)	Ph 7.43-7.30 (m, 6H) 7.49 (d, J_{HH} = 6.9 Hz, 2H) 7.75 (d, J_{HH} = 7.1 Hz, 2H)	8.02 (s, 1H)	6.98 (d, J_{HH} = 8.9 Hz, 2H, *m*-OMe, Ph) 7.52 (d, J_{HH} = 8.8 Hz, 2H, *o*-OMe, Ph) 3.87 (s, 3H, O-CH_3)	0.81 (s, 9H)	9.18 (s, 1H)	5.32 (s, 1H)	4.10 (s, 1H)
bttzpmbeH (**65**)	$(CH_3)_3Si$ 0.38 (s, 9H, CH_3) 0.27 (s, 9H, CH_3)	7.66 (s, 1H)	6.98 (d, J_{HH} = 8.4 Hz, 2H, ^{m}H-OMePh) 7.58 (d, J_{HH} = 8.6 Hz, 2H, ^{o}H-OMePh) 3.87 (s, 3H, O-CH_3)	0.98 (s, 9H)	9.08 (s, 1H)	5.05 (s, 1H)	3.41 (s, 1H)
bttzombeH (**66**)	$(CH_3)_3Si$ 0.37 (s, 9H, CH_3) 0.29 (s, 9H, CH_3)	7.63 (s, 1H)	8.11-6.96 (m, 4H, Ph) 3.79 (s, 3H, O-CH_3)	0.88 (s, 9H)	9.46 (s, 1H)	5.04 (s, 1H)	3.75 (s, 1H)
bptzombeH (**67**)	Ph 8.10-7.77 (m, 10H)	7.94 (s, 1H)	8.04-6.96 (m, 4H, Ph) 3.78 (s, 3H, O-CH_3)	0.71 (s, 9H)	9.62 (s, 1H)	5.44 (s, 1H)	3.72 (s, 1H)

Spectra recorded in $CDCl_3$.

Table 6. *^{13}C-{^{1}H}-NMR data for compounds **64**-**67**.*

Compound	$C^{4,4'}$	$R^{4,4'}$	$C^{5,5'}$	OMePh	^{t}Bu	CH	C^{a}
bptzmbeH (**64**)	145.8 147.9	Ph 128.3-131.4	120.0 125.7	55.41 O-CH_3 114.4-160.6 Ph	26.1 $(CH_3)_3$ 37.9 C-^{t}Bu	73.3	74.0
bttzpmbeH (**65**)	144.4 146.8	$(CH_3)_3$Si –1.1 –0.3	129.0 142.9	55.37 O-CH_3 114.4-160.5 Ph	26.7 $(CH_3)_3$ 36.6 C-^{t}Bu	72.4	74.2
bttzombeH (**66**)	145.2 144.5	$(CH_3)_3$Si 0.0 –1.0	131.9	56.0 O-CH_3 157.0-111.3 Ph	26.5 $(CH_3)_3$ 36.8 C-^{t}Bu	68.3	74.2
bptzombeH (**67**)	145.5 147.0	Ph 125.8-131.6	120.1	55.7 O-CH_3 156.9-111.0 Ph	26.7 $(CH_3)_3$ 36.6 C-^{t}Bu	68.3	73.3

Spectra recorded in $CDCl_3$.

The proposed structures in solution for compounds **59**, **60** and **62** were further confirmed in solid state by X-Ray diffraction studies. The ORTEP diagrams for compounds **59**, **60** and **62** are represented in Figures 10, 11 and 12 respectively. In these compounds, the triazole rings are oriented in anti-parallel manner respect each other, possibly to minimise the intramolecular steric repulsion between the pyridinic nitrogen atoms. These conformation is in agreement with the one found for the bis(pyrazol-1-yl)methane based heteroscorpionate ligands functionalised with alcohol groups.

Bond distances between C–C atoms (Table 7) in triazole rings adopt values between 1.338(7) Å and 1.393(8) Å. These distances are consistent with the characteristic C–C double bond distances. On the other hand, bond distances between N(1)–N(2) and N(4)–N(5) adopt values from 1.344(6) Å to 1.369(7) Å and from 1.342(6) Å to 1.364(6) Å respectively, which are higher than those found for N(2)–N(3) and N(5)–N(6), with values from 1.302(3) Å to 1.327(6) Å and from 1.293(7) Å to 1.312(3) Å respectively. This finding confirms the simple bond character for N(1)–N(2) and N(4)–N(5) bonds and a double bond character for the N(2)–N(3) and N(5)–N(6) bonds of the triazole rings.

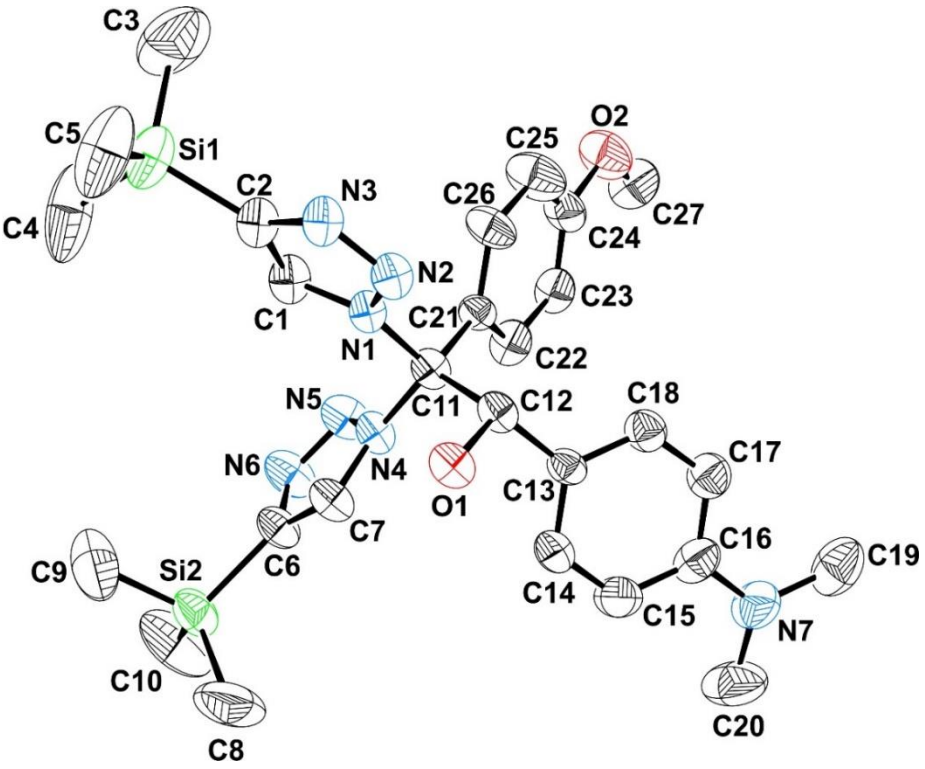

Figure 10. *ORTEP diagram for compound **59**.*

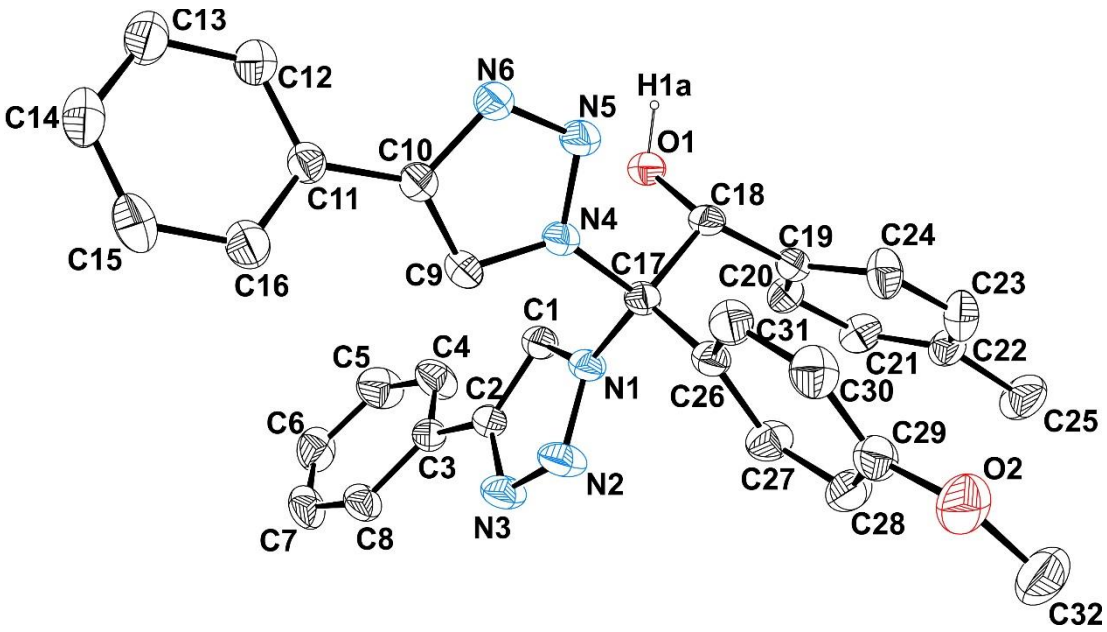

Figure 11. *ORTEP diagram for compound **60**.*

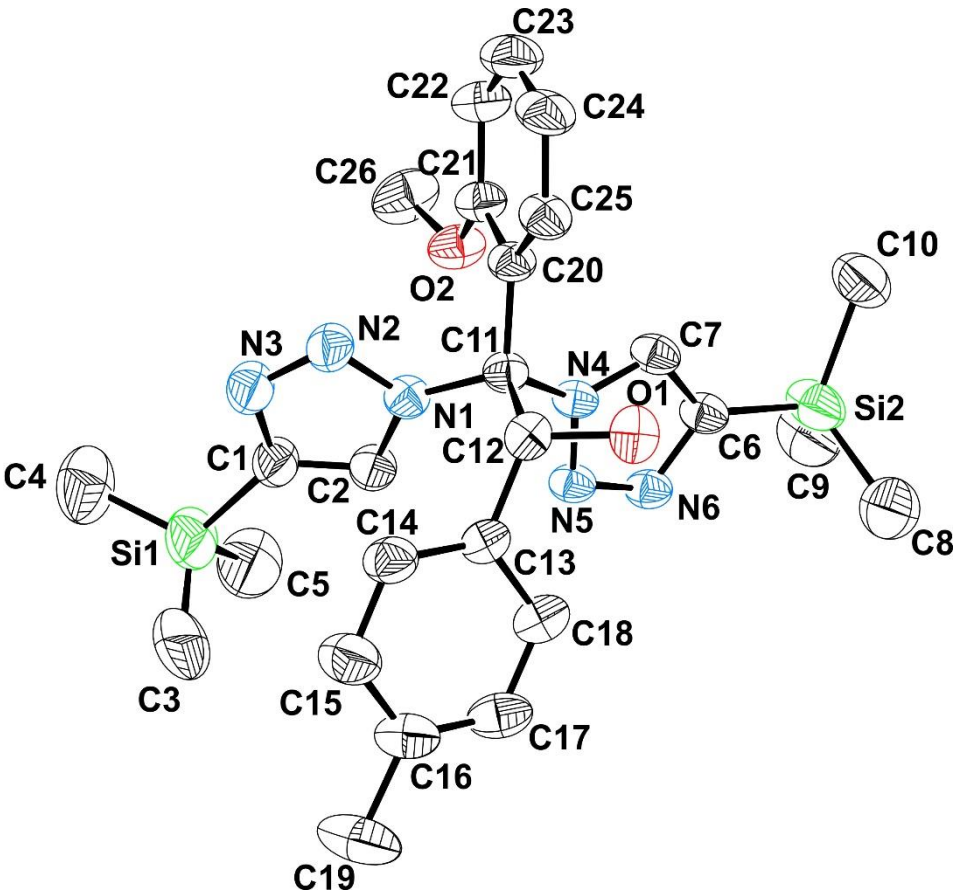

Figure 12. *ORTEP diagram for compound **62**.*

Table 7. *Bond distances and angles for compounds bttzpmmabzeH (**59**), bptzpmteH (**60**) and bttzomteH (**62**).*

Distances (Å)		**Angles (º)**	
*bttzpmmabzeH (**59**)*			
N(1)–N(2)	1.344(6)	C(1)–C(2)–Si(1)	130.5(5)
N(2)–N(3)	1.327(6)	C(7)–C(6)–Si(2)	130.6(6)
N(4)–N(5)	1.364(6)	N(4)–C(11)–N(1)	104.4(5)
N(5)–N(6)	1.300(6)	N(3)–N(2)–N(1)	105.7(5)
C(1)–C(2)	1.367(8)	N(6)–N(5)–N(4)	106.9(5)
C(6)–C(7)	1.338(7)		
*bptzpmteH (**60**)*			
N(1)–N(2)	1.359(3)	C(4)–C(3)–C(2)	120.7(2)
N(2)–N(3)	1.302(3)	C(9)–C(10)–C(11)	131.2(2)
N(4)–N(5)	1.344(3)	N(1)–C(17)–N(4)	104.97(16)
N(5)–N(6)	1.312(3)	N(3)–N(2)–N(1)	107.52(19)
C(1)–C(2)	1.362(3)	N(6)–N(5)–N(4)	107.08(17)
C(6)–C(7)	1.363(4)		
*bttzomteH (**62**)*			
N(1)–N(2)	1.369(7)	C(1)–C(2)–Si(1)	128.4(6)
N(2)–N(3)	1.314(7)	C(7)–C(6)–Si(2)	133.8(6)
N(4)–N(5)	1.342(6)	N(1)–C(11)–N(4)	109.4(5)
N(5)–N(6)	1.293(7)	N(3)–N(2)–N(1)	107.1(5)
C(1)–C(2)	1.365(9)	N(6)–N(5)–N(4)	106.8(5)
C(6)–C(7)	1.393(8)		

3. Synthesis of quaternised bis(1,2,3-triazol-1-yl)methane-derived compounds

With the aim to increase the versatility of bis(1,2,3-triazol-1-yl)methane-derived compounds and study their potential ability to generate carbene complexes, the quaternisation of the neutral bttzpm and bptzom precursors was explored.

The synthesis of these compounds was carried out by reaction of the corresponding bis(1,2,3-triazol-1-yl)methane precursors bttzpm and bptzom with methyl triflate ($MeOSO_2CF_3$) in CH_2Cl_2 at room temperature for 16 hours, which, after the appropriate work-up, afforded the quaternised salt-type compounds bttz(NMe_2)pm, [bttz(NMe_2)pm = 1,1'-((2-methoxyphenyl)methylene)bis(3-methyl-4-(trimethylsilyl)-1H-1,2,3-triazol-3-ium)triflate] (**68**) and bptz(NMe_2)om [bptz(NMe_2)om = 1,1'- ((4-methoxyphenyl)methylene)bis(3-methyl-4-phenyl-1H-1,2,3-triazol-3-ium) triflate] (**69**) as pale-yellow solids (Scheme 13). Compounds **68** and **69** were obtained in good yields and are soluble in polar solvents.

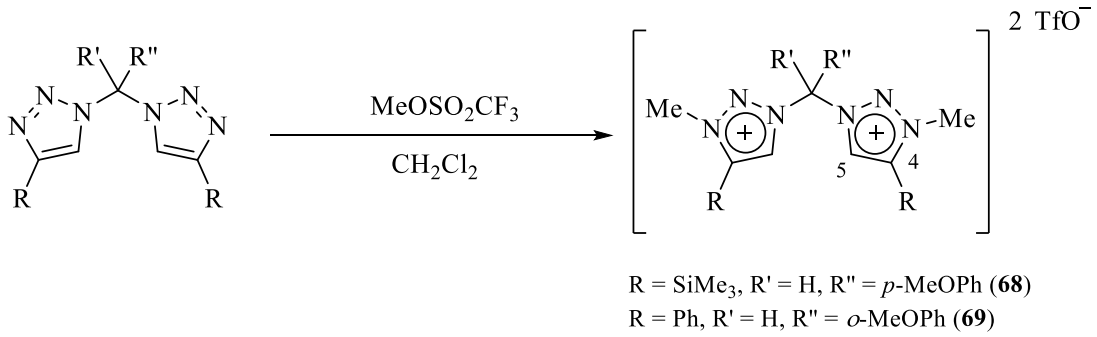

Scheme 13. *Synthesis of compounds **68** and **69**.*

Structural Characterisation

The structural characterisation of compounds **68** and **69** was performed by ^{1}H-NMR and $^{13}C\{^1H\}$-NMR spectroscopy (Tables 8 and 9). The ^{1}H-NMR and $^{13}C\{^1H\}$-NMR spectra for compounds **68** and **69** are similar to the ones corresponding to the starting materials. However, the presence of a new signal in the ^{1}H-NMR at 4.40 ppm corresponding to the methyl groups N-Me from the triazole rings confirmed the reaction (Figure 13). In addition, the $^{13}C\{^1H\}$-NMR spectra exhibited a signal close to 40 ppm, which can be assigned to the N-Me group, giving further proof of the desired product (Figure 14). The spectroscopic data obtained from the ^{1}H-NMR and $^{13}C\{^1H\}$-NMR confirmed that both triazole rings are equivalent.

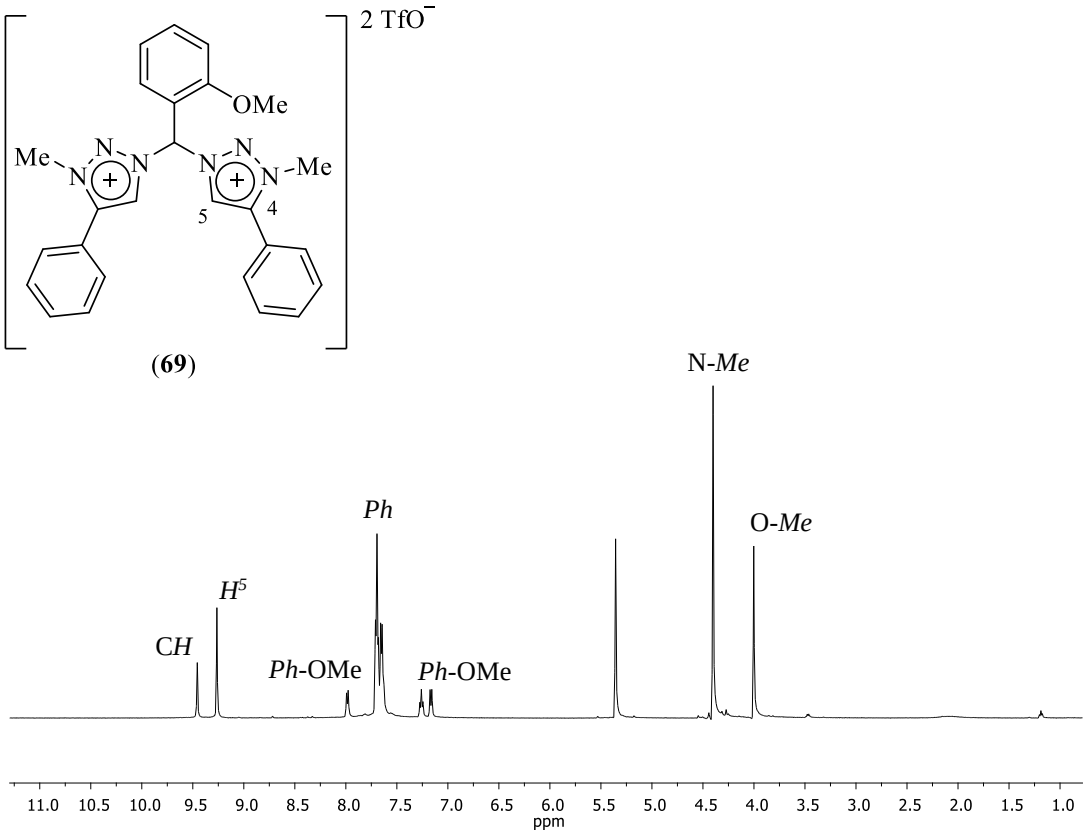

Figure 13. *^{1}H-NMR of compound **69** in CD_2Cl_2.*

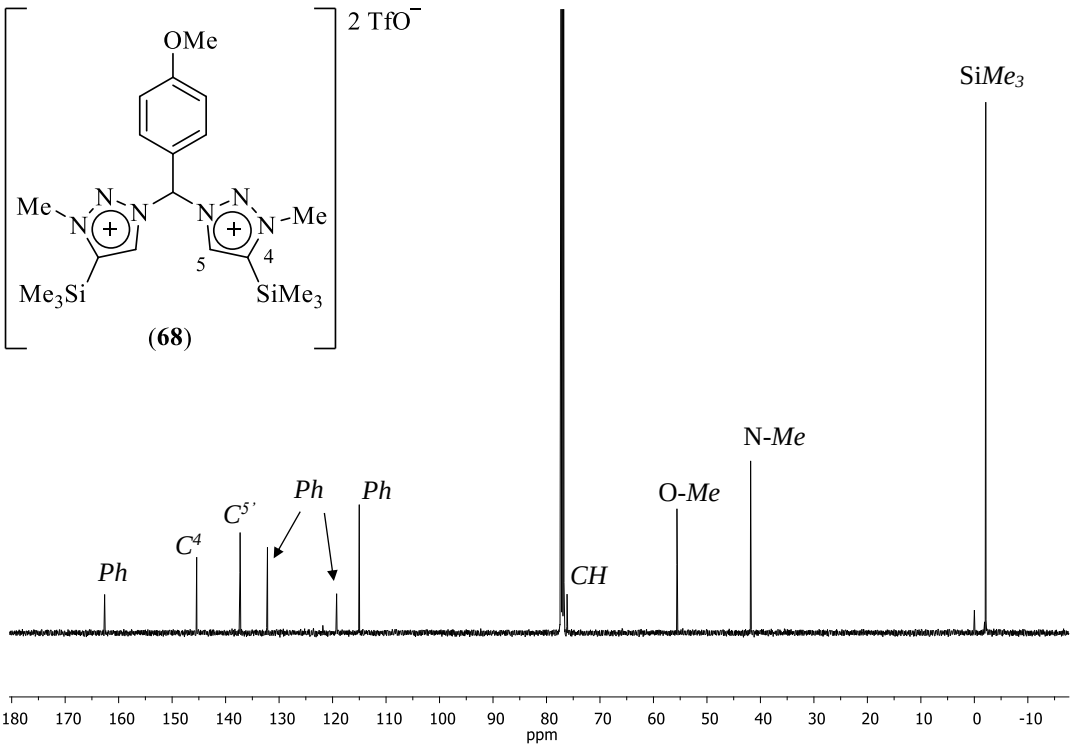

Figure 14. *^{13}C-{^{1}H}-NMR of compound **68** in $CDCl_3$.*

Table 8. *^{1}H-NMR data for compounds **68** and **69**.*

Compound	$R^{4,4'}$	$H^{5,5'}$	MeOPh	N-Me	CH
bttz(NMe)$_2$pm (**68**)[a]	$(CH_3)_3Si$ 0.50 (s, 18H, *CH_3*)	9.00 (s, 2H)	3.88 (s, 3H, O-*CH_3*) 7.06 (d, J_{HH} = 8.6 Hz, 2H, Ph) 8.07 (d, J_{HH} = 8.0 Hz, 2H, Ph)	4.42 (s, 6H)	9.20 (s, 1H)
bptz(NMe)$_2$om (**69**)[b]	Ph 7.71-7.80 (m, 10H)	9.25 (s, 2H)	3.88 (s, 1H, O-*CH_3*) 7.21 (td, J_{HH} = 7.7, 0.8 Hz, 1H, Ph) 7.35 (d, J_{HH} = 8 Hz, 1H, Ph) 7.54 (dd, J_{HH} = 7.9, 1.4 Hz, 1H, Ph) 7.71 (1H)	4.40 (s, 6H)	9.46 (s, 1H)

Spectra recorded in a) $CDCl_3$ and b) CD_2Cl_2.

Table 9. *^{13}C-{^{1}H}-NMR data for compounds **68** and **69**.*

Compound	$C^{4,4'}$	$R^{4,4'}$	$C^{5,5'}$	MeOPh	N-Me	CH
bttz(NMe)$_2$pm (**68**)[a]	145.5	$(CH_3)_3Si$ -2.13	137.3	55.1 O-CH_3 119.2-160.4 Ph	41.8	76.2
bptz(NMe)$_2$om (**69**)[b]	144.4	Ph 129.7-134.4	130.0	56.2 O-CH_3 112.0-157.6 Ph	39.7	74.1

Spectra recorded in a) $CDCl_3$ and b) CD_2Cl_2.

4. Synthesis of alkyl complexes

The coordination ability of bis(1,2,3-triazol-1-yl)-derived ligands functionalised with alcohol groups was studied *via* protonolysis reaction with different alkyl zinc and aluminium precursors. In this section, the synthesis and characterisation of alkyl zinc and aluminium complexes will be discussed.

4.1. Synthesis of alkyl zinc complexes

The synthesis of alkyl zinc complexes was carried out by reacting the neutral heteroscorpionate precursor bttzombeH (**66**) with ZnR_2 (R = Me, Et) in toluene for two hours at 0 ºC in a 1:1 molar ration (Scheme 14). The corresponding alkyl zinc complexes supported by heteroscorpionate ligands functionalised with alkoxide group $[ZnMe\{(\kappa^2\text{-bttzombe})(\mu\text{-O})\}]_2$ (**70**) and $[ZnEt\{(\kappa^2\text{-bttzombe})(\mu\text{-O})\}]_2$ (**71**) were obtained in good yields and isolated as white solids. These complexes are soluble in aliphatic and aromatic hydrocarbons and are thermally stable.

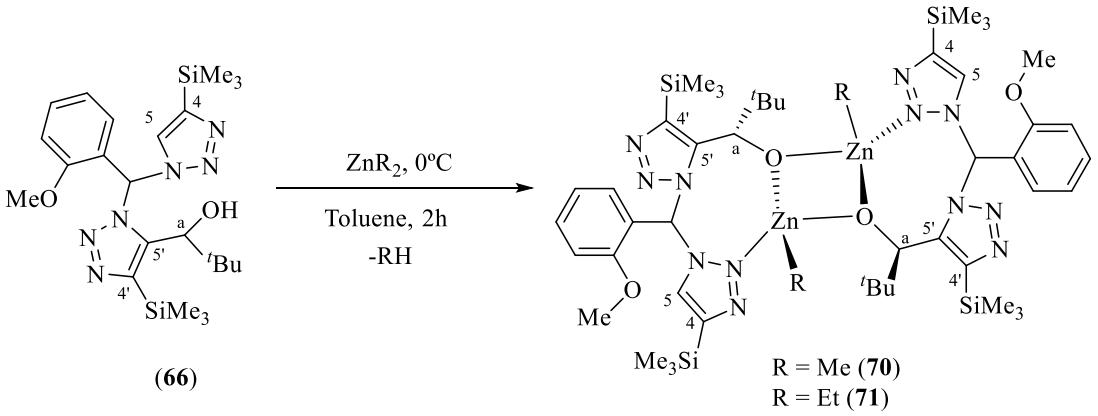

Scheme 14. *Synthesis of alkyl zinc complexes **70** and **71**.*

Structural Characterisation

The structural characterisation of complexes **70** and **71** were performed by ^{1}H-NMR and $^{13}C\{^1H\}$-NMR spectroscopy (Tables 10 and 11) and X-Ray diffraction analysis. As previously commented, due to the functionalisation at the C^5 of one of the triazole rings, a stereogenic centre is generated in the methine group (CH) bridging both triazole rings. Thus, these ligands exhibited two different chiral centres which can lead to the formation of different diastereoisomers in solution. Figure 15 shows the ^{1}H-NMR and $^{13}C\{^1H\}$-NMR for complex **71**, where the presence of two diastereoisomers in different proportions can be observed.

NOESY-1D and heteronuclear correlation ^{1}H-^{13}C-g-HSQC experiments allowed the unequivocal assignment of the triazole and the alkoxide moiety resonances.

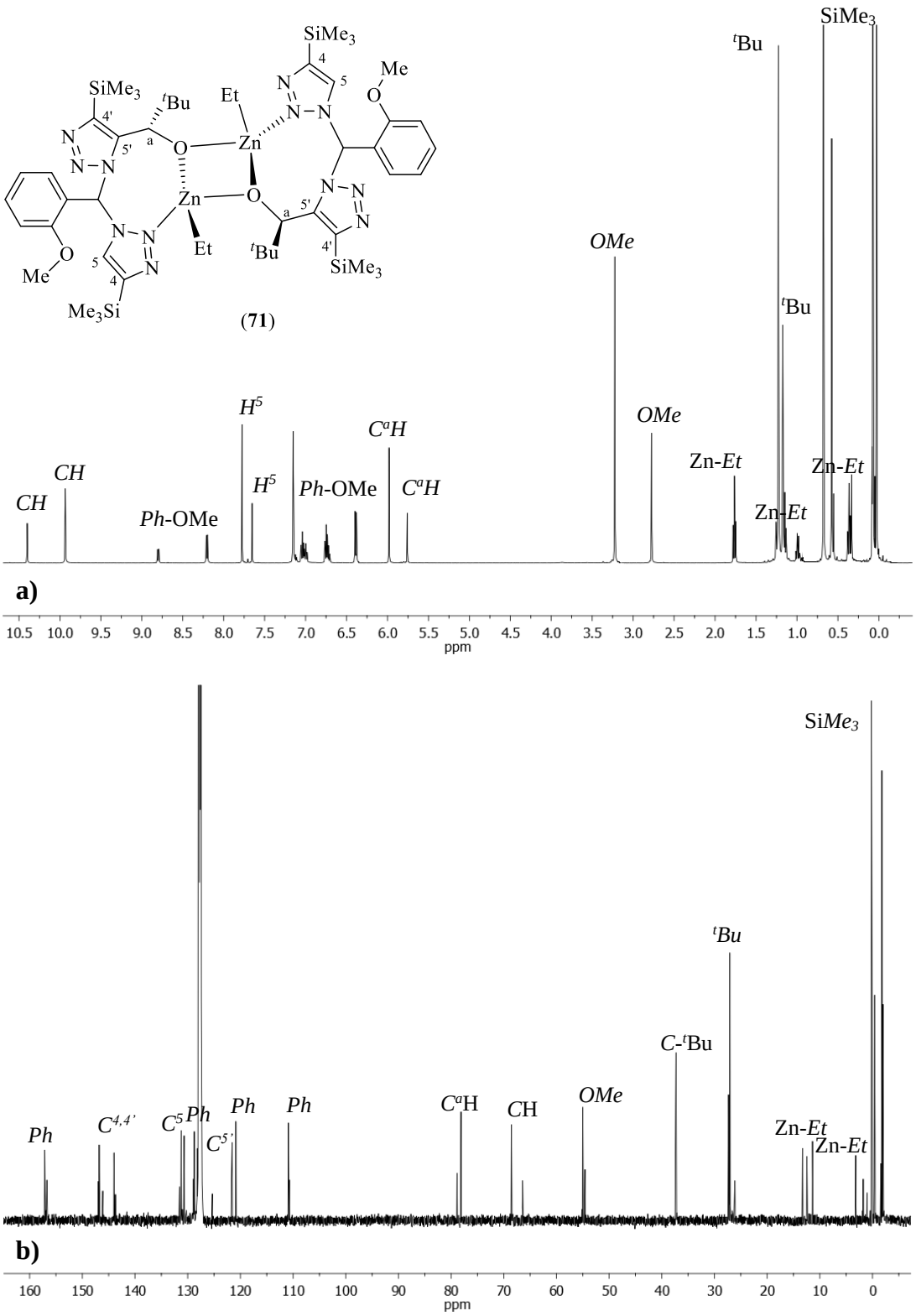

Figure 15. *a) ^{1}H-NMR and b) ^{13}C-{^{1}H}-NMR spectra for alkyl zinc complex **71** in C_6D_6.*

Table 10. *^{1}H-NMR data for zinc complexes **70** and **71**.*

Complex	$SiMe_3$	H^5	MeOPh	^{t}Bu	CH	CH^a	Zn-R
[ZnMe{(κ^2-bttzpmbe)(μ-O)}]$_2$ (**70**)	0.10 (s, 9H) 0.73 (s, 9H)	7.85 (s, 1H)	8.15 (dd, J_{H-H} = 7.5, 1.2 Hz, 1H, *Ph*-OMe) 7.02 (td, J_{H-H} = 7.3, 1.4 Hz, 1H, *Ph*-OMe) 6.75 (m, 1H, *Ph*-OMe) 6.32 (d, J_{H-H} = 8.2 Hz, 1H, *Ph*-OMe) 3.25 (s, 3H, O-*CH_3*)	1.31 (s, 9H)	9.97 (s, 1H)	6.04 (s, 1H)	-0.20 (s, 3H, Zn-*Me*)
[ZnEt{(κ^2-bttzpmbe)(μ-O)}]$_2$ (**71**)	0.07 (s, 9H) 0.67 (s, 9H)	7.78 (s, 1H)	8.2 (dd, J_{H-H} = 7.8, 0.9Hz, 1H, *Ph*-OMe) 7.04 (td, J_{H-H} = 8.3, 1.5Hz, 1H, *Ph*-OMe) 6.75 (m, 1H, *Ph*-OMe) 6.39 (d, J_{H-H} = 8.3 Hz, 1H, *Ph*-OMe) 3.22 (s, 3H, O-*CH_3*)	1.23 (s, 9H)	9.93 (s, 1H)	5.98 (s, 1H)	0.35 (m, 3H, Zn-CH_2-*CH_3*) 1.15 (m, 2H, Zn-*CH_2*-CH_3)

Spectra recorded in C_6D_6.Chemical shifts corresponding to the major isomer in solution.

Table 11. *^{13}C-{^{1}H}-NMR data for zinc complexes **70** and **71**.*

Complex	$C^{4,4'}$	$SiMe_3$	$C^{5,5'}$	MeOPh	^{t}Bu	CH	C^a	Zn-R
[ZnMe{(κ^2-bttzpmbe)(μ-O)}]$_2$ (**70**)	146.8 146.9	-1.8 0.2	121.6 128.7	157.1-110.9 (*Ph*-OMe) 55.0 (O-*Me*)	27.1 (CH_3)$_3$ 37.3 C-^{t}Bu	68.5	78.1	3.2 (Zn-Me) 11.4 (Zn-Me)
[ZnEt{(κ^2-bttzpmbe)(μ-O)}]$_2$ (**71**)	146.8 146.9	-1.8 0.2	121.6 128.7	157.1-110.9 (*Ph*-OMe) 55.0 (O-*Me*)	27.1 (CH_3)$_3$ 37.3 C-^{t}Bu	68.5	78.1	3.2 (Zn-*CH_2*-CH_3) 11.4 (Zn-CH_2-*CH_3*)

Spectra recorded in C_6D_6.Chemical shifts corresponding to the major isomer in solution.

The proposed structure for alkyl zinc complex **71** in solution was further confirmed by X-Ray diffraction analysis. The corresponding ORTEP diagram is given in Figure 16. This complex shows a dimeric structure in which each zinc centre exhibits a distorted tetrahedral geometry with the bis(1,2,3-triazol-1-yl)methane heteroscorpionate ligand coordinated in a κ^2-NO fashion, one ethyl group and the oxygen atom from the alkoxide moiety of the other zinc centre, which acts as a bridging group between both zinc centres. The crystal structure is consistent with the one proposed in Scheme 14 on the basis of solution-state NMR spectroscopy. In solid state, complex **71** crystallises as a racemic mixture of a single diastereoisomer *SSSS/RRRR* and the structure for enantiomer *SSSS* is depicted in Figure 16.

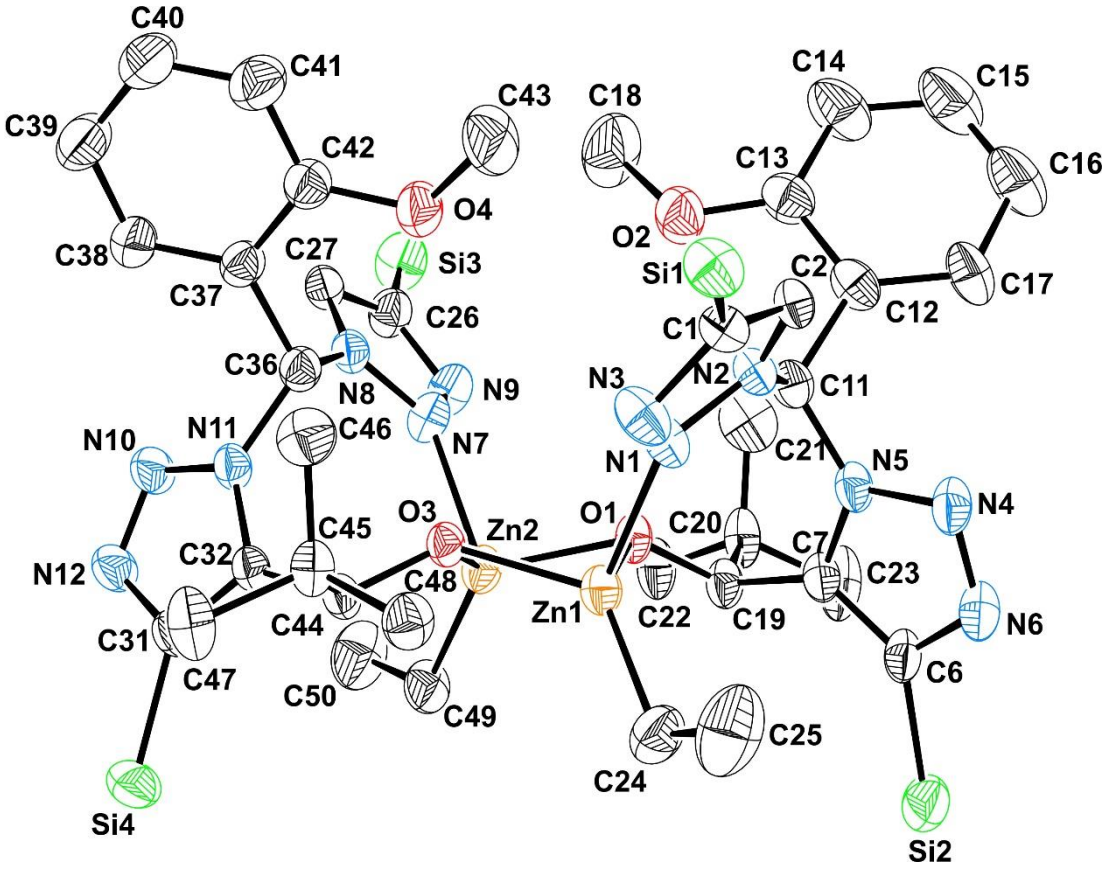

Figure 16. *ORTEP diagram for alkyl zinc complex **71**.*

Bond distances (Table 12) between zinc centres and carbon atoms from the ethyl groups exhibit values of 1.916(10) Å and 1.933(10) Å respectively, which are slightly shorter than the with the ones found for other ethyl zinc derivatives.[20] On the other hand, the bond distances between zinc centres and pyridinic nitrogens from both triazole rings, Zn(1)–N(1) and Zn(2)–N(7) of 2.133(8) Å and 2.169(8) Å respectively,

are slightly longer than the ones found for other bis(1,2,3-triazol-1-yl)methane-derived zinc complexes.[20] Finally, the bond distances between the zinc centres and the oxygen atoms of the alkoxide moiety from the heteroscorpionate ligands of Zn(1)–O(1) and Zn(2)–O(3) of 2.055(6) Å and 2.046(6) Å respectively are longer than the ones found for other zinc alkoxide complexes.[21,22]

Bond angles (Table 12) confirmed the distorted tetrahedral geometry for the zinc centres, with distorted values with respect to an ideal tetrahedron (Table 12), with the maximum distortion observed for the angles between O(3)–Zn(1)–O(1) and O(1)–Zn(2)–O(3) of 84.4(2)º and 84.1(2)º respectively. The dihedral angle between O(3)–Zn(1)–O(1) and C(24)–Zn(1)–N(1) for Zn(1) centre and the dihedral angle between O(1)–Zn(2)–O(3) and C(49)–Zn(1)–N(7) for Zn(2) centre display values of 87.85º and 87.89º respectively.

Table 12. *Bond distances and angles for alkyl zinc complex **71**.*

Distances (Å)		**Angles (º)**	
[ZnEt{(κ^2-bttzpmbe)(μ-O)}]$_2$ (**71**)			
Zn(1)–C(24)	1.916(10)	C(24)–Zn(1)–O(3)	129.1(4)
Zn(1)–O(3)	1.974(6)	C(24)–Zn(1)–O(1)	122.4(4)
Zn(1)–O(1)	2.055(6)	O(3)–Zn(1)–O(1)	84.4(2)
Zn(1)–N(1)	2.133(8)	C(24)–Zn(1)–N(1)	114.4(4)
Zn(2)–C(49)	1.933(10)	O(3)–Zn(1)–N(1)	102.1(3)
Zn(2)–O(1)	1.994(6)	O(1)–Zn(1)–N(1)	97.1(3)
Zn(2)–O(3)	2.046(6)	C(49)–Zn(2)–O(1)	129.3(4)
Zn(2)–N(7)	2.169(8)	C(49)–Zn(2)–O(3)	122.8(4)
		O(1)–Zn(2)–O(3)	84.1(2)
		C(49)–Zn(2)–N(7)	113.6(4)
		O(1)–Zn(2)–N(7)	102.6(3)
		O(3)–Zn(2)–N(7)	97.4(3)

4.2. Synthesis of alkyl aluminium complexes

The synthesis of alkyl aluminium complexes was carried out by reacting the corresponding neutral heteroscorpionate precursors bttzpmmabeH (**59**), bttzpmteH (**61**) and bttzombeH (**66**) with alkyl aluminium derivatives AlX_3 (X = Me, Et) in toluene for two hours at 0 ºC in a 1:1 molar ratio (Scheme 15). The corresponding dialkyl aluminium complexes supported by heteroscorpionate ligands functionalised with alkoxide groups $[AlMe_2\{(\kappa^2\text{-bttzpmmabe})(\mu\text{-O})\}]_2$ (**72**), $[AlMe_2\{(\kappa^2\text{-bttzpmte})(\mu\text{-O})\}]_2$ (**73**) and $[AlMe_2\{(\kappa^2\text{-bttzombe})(\mu\text{-O})\}]_2$ (**74**) were obtained in 80% yield and isolated as white solids. These complexes are soluble in aliphatic and aromatic hydrocarbons and are thermally stable.

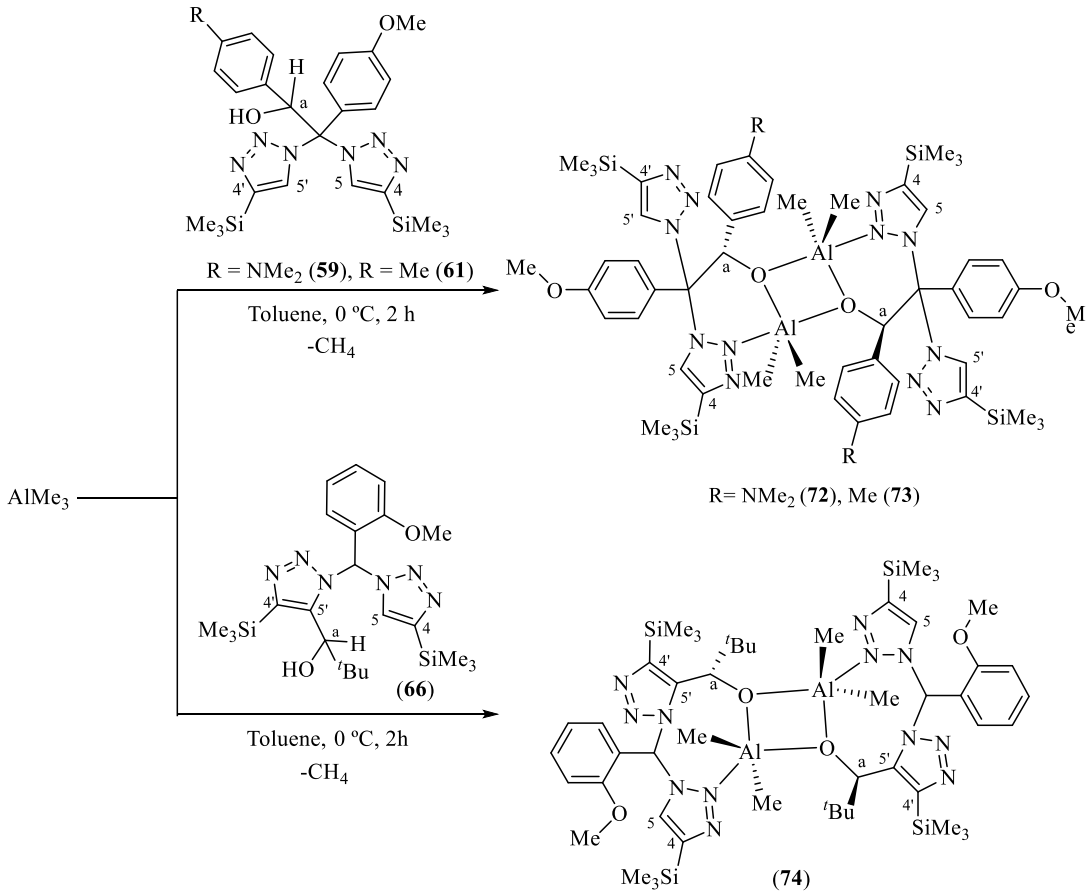

Scheme 15. *Synthesis of alkyl aluminium complexes **72-74**.*

Structural Characterisation

The structural characterisation of compounds **72-74** was performed by ^{1}H-NMR and $^{13}C\{^1H\}$-NMR spectroscopy (Tables 13 and 14) and X-Ray diffraction analysis. The ^{1}H-NMR and $^{13}C\{^1H\}$-NMR spectra for complexes **72** and **73** exhibited broad

signals at room temperature and only one isomer was present in solution (Figure 17). In addition, two different sets of signals for H^5 protons were observed, indicating the non-equivalence between both triazole rings, due to coordination of only one of them to the aluminium centre, which generates a stereogenic centre at the carbon atom bridging both triazole rings. On the other hand, ^{1}H-NMR and $^{13}C\{^1H\}$-NMR spectra for complex **74** exhibit two different sets of signals for each resonance indicating the presence of two different isomers in solution. In this case, only one signal for the H^5 protons of the triazole rings and another signal for the methine group bridging both triazole moieties were observed due to functionalisation in one of the triazole rings (Figure 18).

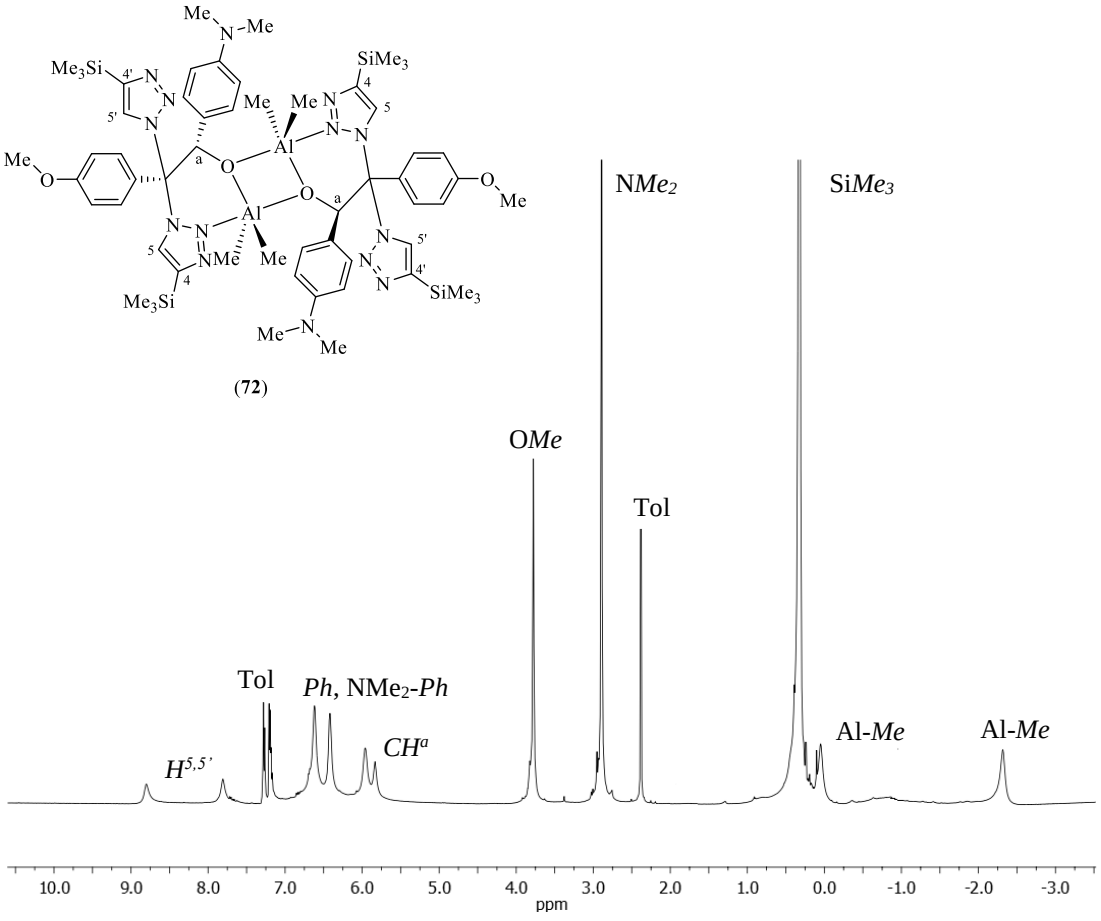

Figure 17. *^{1}H-NMR of alkyl aluminium complex **72** in $CDCl_3$.*

^{13}C-$\{^1H\}$-NMR signals were assigned by ^{1}H-^{13}C g-HSQC NMR experiments. Figure 19 shows the ^{1}H-^{13}C-g-HSQC spectrum for complex **74**.

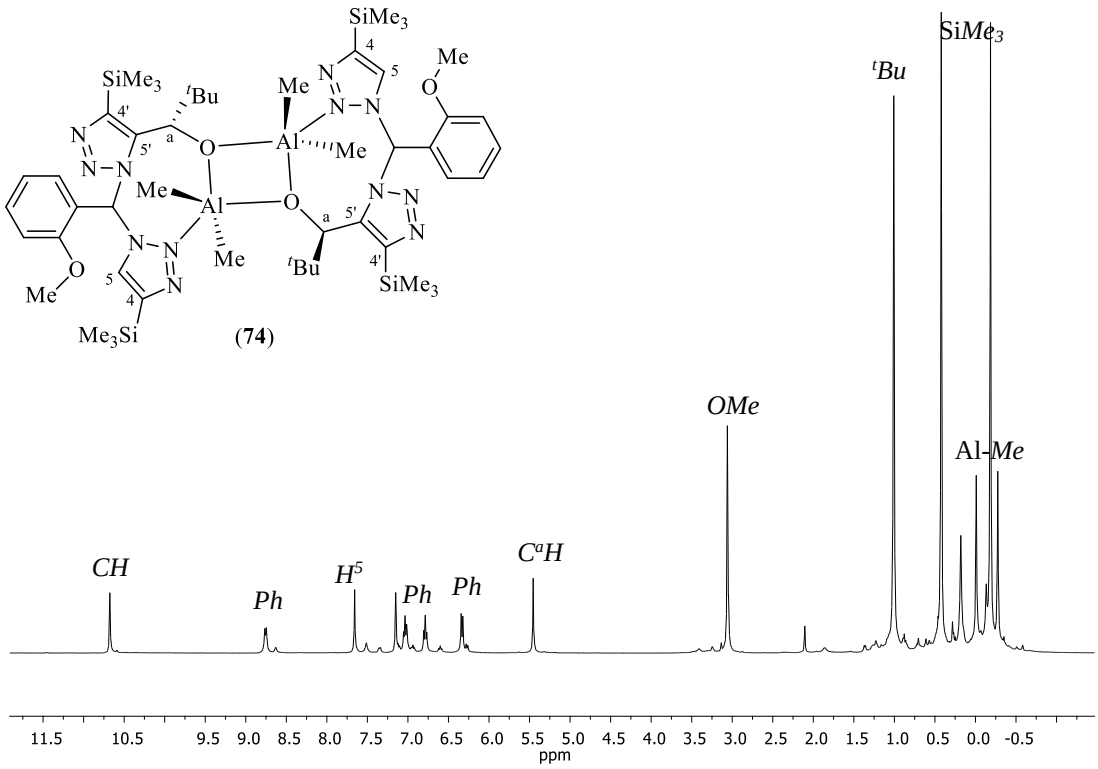

Figure 18. *^{13}C-{^{1}H}-NMR of alkyl aluminium complex **74** in C_6D_6.*

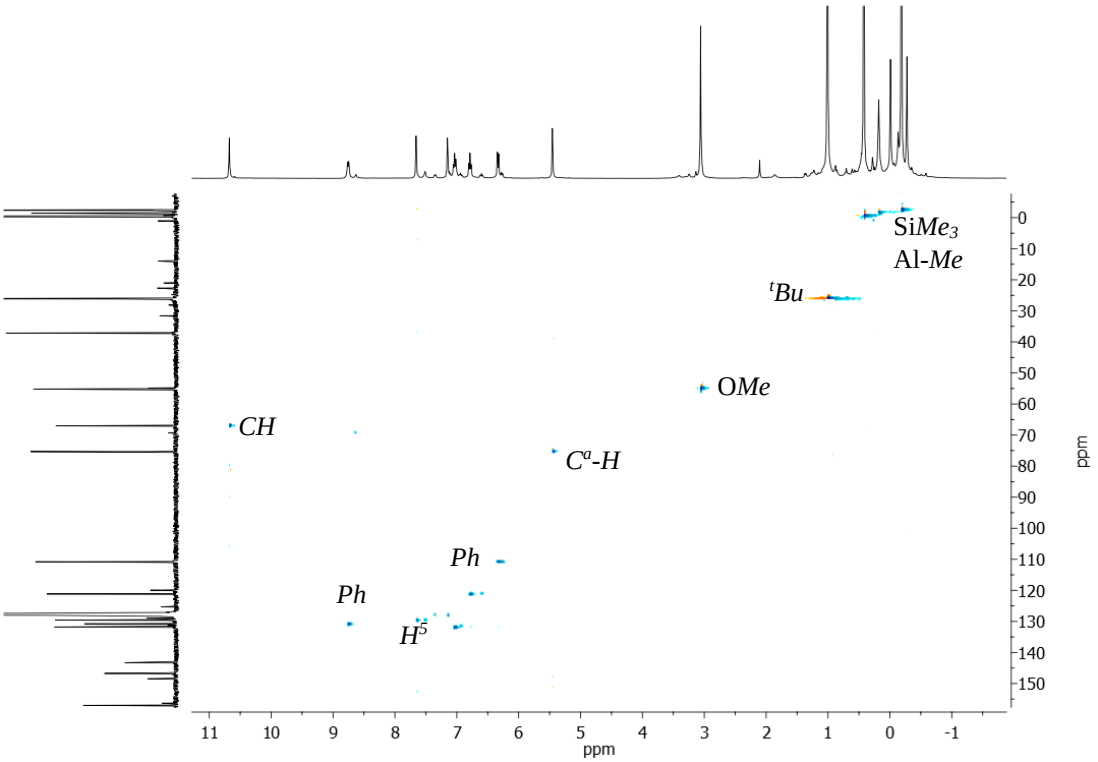

Figure 19. *Correlation spectrum ^{1}H-^{13}C-gHSQC for alkyl aluminium complex **74** in C_6D_6.*

Table 13. *^{1}H-NMR data for aluminium complexes **72-74**.*

Complex	$SiMe_3$	$H^{5',5}$	MeOPh	R	CH	CH[a]	Al-Me
$[AlMe_2\{(\kappa^2\text{-bttzpmmabe})(\mu\text{-O})\}]_2$ (**72**)	0.32 (s, 18H)	8.80 (s, 1H) 7.81 (s, 1H)	6.62 (s, 4H, *Ph*-OMe) 3.78 (s, 3H, O-CH_3)	6.42 (s, 1H, *Ph*-NMe_2) 5.96 (s, 1H, *Ph*-NMe_2) 2.89 (s, 6H, N-Me_2)	-	5.83 (s, 1H)	0.05 (s, 3H) -2.32 (s, 3H)
$[AlMe_2\{(\kappa^2\text{-bttzpmte})(\mu\text{-O})\}]_2$ (**73**)	0.32 (s, 18H)	8.75 (s, 1H) 7.83 (s, 1H)	6.60 (s, 2H, H^{σ}-*Ph*OMe) 5.97 (s, 2H, H^{m}-*Ph*OMe) 3.81 (s, 3H, O-CH_3)	6.90 (s, 2H, H^{σ}-*Ph*OMe) 6.70 (s, 1H, H^{m}-*Ph*OMe) 2.26 (s, 3H, Ph-*Me*)	-	5.97 (s, 1H)	0.05 (s, 3H) -2.40 (s, 3H)
$[AlMe_2\{(\kappa^2\text{-bttzombe})(\mu\text{-O})\}]_2$ (**74**)*	0.42 (s, 9H) -0.19 (s, 9H)	7.66 (s, 1H)	8.76 (dd, $J_{H\text{-}H}$ = 7.4 Hz, 1H, H^{σ}-*Ph*OMe) 7.03 (m, 1H, H^{m}-*Ph*OMe) 6.79 (t, $J_{H\text{-}H}$ = 7.6 Hz, 1H, H^{p}-*Ph*OMe) 6.33 (d, $J_{H\text{-}H}$= 8.2 Hz, 1H, H^{m}-*Ph*OMe) 3.06 (s, 3H, O-CH_3)	^{t}Bu 1.01 (s, 9H)	10.68 (s, 1H)	5.46 (s, 1H)	0.01 (s, 3H) -0.28 (s, 3H)

Spectra recorded in $CDCl_3$ and C_6D_6. Chemical shifts corresponding to the major isomer in solution.*

Table 14. *^{13}C-{^{1}H}-NMR data for aluminium complexes **72-74**.*

Complex	$C^{4,4'}$	$SiMe_3$	$C^{5,5'}$	MeOPh	R	CH	C^{a}	Al-Me
$[AlMe_2\{(\kappa^2$-bttzpmmabe)(μ-O)$\}]_2$ (**72**)	137.9	-1.23	130.6	*Ph* 160.2-112.5 55.4 (O-*Me*)	*Ph*NMe_2 150.2-111.6 40.3 (N-*Me_2*)	81.2	87.2	-0.83
$[AlMe_2\{(\kappa^2$-bttzpmte)(μ-O)$\}]_2$ (**73**)	146.2 146.5	-1.20	130.6	*Ph* 160.4-113.0 55.4 (O-*Me*)	*Ph*Me 138.2-127.5 21.1(Ph-*Me*)	79.6	86.6	-1.00
$[AlMe_2\{(\kappa^2$-bttzombe)(μ-O)$\}]_2$ (**74**)*	146.7	0.4 -2.4	120.0 130.8	*Ph* 157.0-110.8 55.2 (O-*Me*)	26.2 $(CH_3)_3$ 37.2 C-^{t}Bu	67.0	75.3	-1.46

Spectra recorded in $CDCl_3$ and C_6D_6. Chemical shifts corresponding to the major isomer in solution.*

The proposed structure for alkyl aluminium complex **73** in solution was further confirmed by X-Ray diffraction analysis. The corresponding ORTEP diagram is given in Figure 20. This complex shows a dimeric structure in which each aluminium centre exhibits a distorted trigonal-bipyramid geometry with the heteroscorpionate ligand coordinated in a κ^2-NO fashion, two methyl groups and the oxygen atom from the alkoxide moiety of the other aluminium centre, which acts as a bridging group between both aluminium centres. The crystal structure is consistent with the one proposed in Scheme 15 on the basis of solution-state NMR spectroscopy. In solid state, complex **73** crystallises as a racemic mixture of a single diastereoisomer *SSSS/RRRR* and the structure for enantiomer *SSSS* is depicted in Figure 20.

The τ value for complex **73** is 0.58, which indicates that the geometry around the aluminium centre can be described as a distorted trigonal-bipyramid, with the highest distortion at the O(1A)-Al(1)-N(2) angle (Table 15) with a value of 159.14º with respect the 180º of a perfect trigonal-bipyramid.

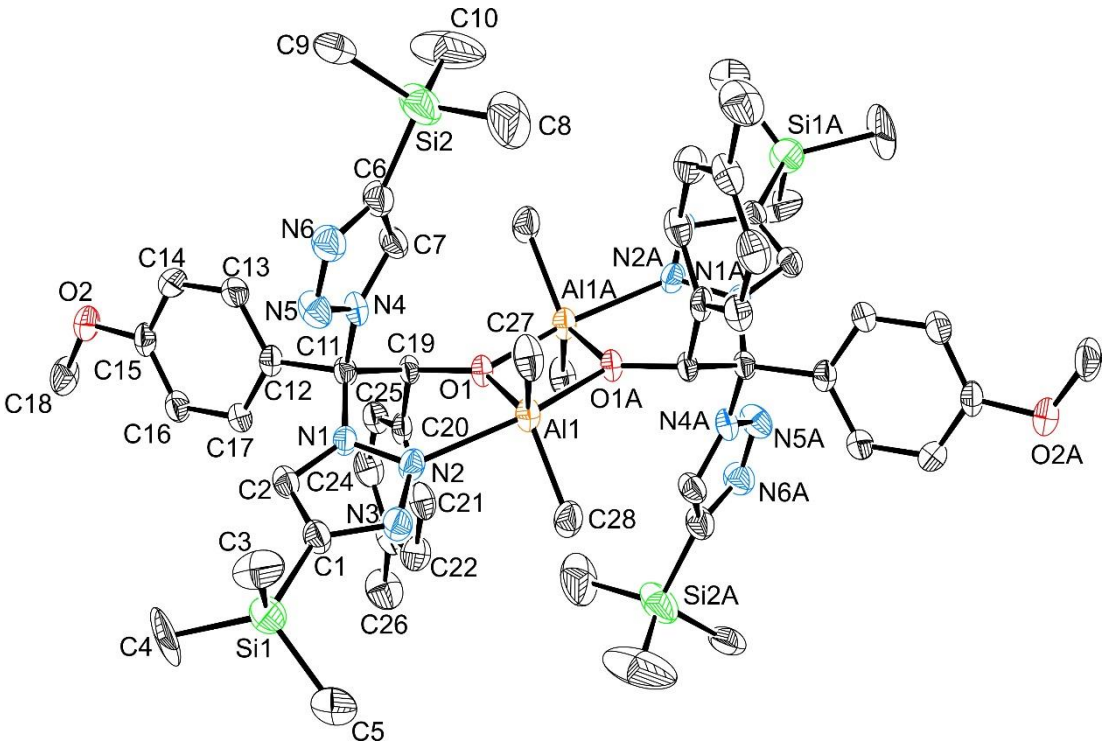

Figure 20. *ORTEP diagram for alkyl aluminium complex **73**.*

The bond distance (Table 15) between the aluminium centre of complex **73** and the methyl ligands Al(1)-C(27) and Al(1)-C(28) of 1.937(7) Å and 1.963(7) Å

respectively are slightly shorter than that found for other alkyl aluminium complexes.[23,24] On the other hand, bond distance between the aluminium centre and the nitrogen of the triazole ring Al(1)–N(2) of 2.231(5) Å is slightly longer than the one found for other bis(3,5-dimethyl-pyrazol-1-yl)methane based ligand aluminium complexes.[24]

Table 15. *Bond distances and angles for alkyl aluminium complex **73**.*

Distances (Å)		**Angles (º)**	
[$AlMe_2$\{(κ^2-bttzpmte)(μ-O\}]$_2$ (**73**)			
Al(1)–O(1)	1.834(4)	O(1)–Al(1)–C(27)	117.9(3)
Al(1)–C(27)	1.937(7)	O(1)–Al(1)–C(28)	124.5(3)
Al(1)–C(28)	1.963(7)	C(27)–Al(1)–C(28)	117.3(3)
Al(1)–O(1A)	2.008(4)	O(1)–Al(1)–O(1A)	75.73(17)
Al(1)–N(2)	2.231(5)	C(27)–Al(1)–O(1)	102.4(2)
		C(28)–Al(1)–O(1A)	98.2(2)
		O(1)–Al(1)–N(2)	84.39(17)
		C(27)–Al(1)–N(2)	92.4(2)
		C(28)–Al(1)–N(2)	87.8(2)
		O(1A)–Al(1)–N(2)	159.14(18)

5. Synthesis of carbene iridium carbene complexes

The versatility of the bis(1,2,3-triazol-1-yl)methane-derived compounds has been tested for the synthesis of carbene iridium complexes, which was carried out by reaction of the chloride 1,5-cyclooctadiene iridium (I) dimer precursor with the corresponding quaternised bis(triazol-1-yl)methane derivative bttz(NMe_2)pm (**68**) and bptz(NMe_2)om (**69**) in EtOH and in the presence of a strong base, NaH (Scheme 16). After the appropriate work-up, the corresponding iridium carbene complexes [Ir(OEt){bttz(NMe_2)pm}]$_2$ (**74**) and [Ir(OEt){bptz(NMe_2)om}]$_2$ (**75**) were obtained as brown solids in good yields. These complexes are soluble in polar solvents such as CH_2Cl_2 and DMSO and are thermally stable.

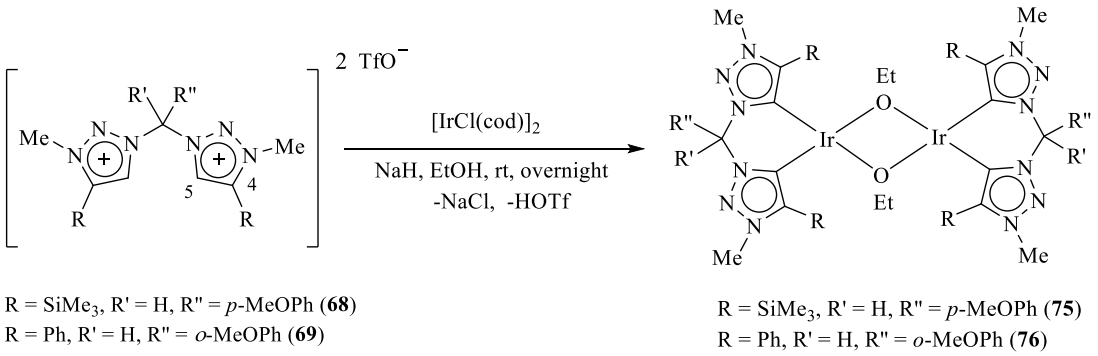

Scheme 16. *Synthesis of iridium carbene complexes **75** and **76**.*

Structural Characterisation

The structural characterisation of complexes **75** and **76** was performed by ^{1}H-NMR and ^{13}C{^{1}H}-NMR spectroscopy (Tables 16 and 17) and MALDI-ToF analysis. The ^{1}H-NMR and ^{13}C{^{1}H}-NMR spectra for complexes **75** and **76** exhibited no signals for H^{5} protons of the triazole rings, indicating the formation of the carbene specie (Figure 21). In addition, *CH* signal in ^{13}C{^{1}H}-NMR spectra shifted downfield from 76.2 ppm to 113.5 ppm and from 74.1 ppm to 133.1 ppm for complexes **75** and **76** respectively, giving further proof of the formation of carbene iridium complexes (Figure 22).

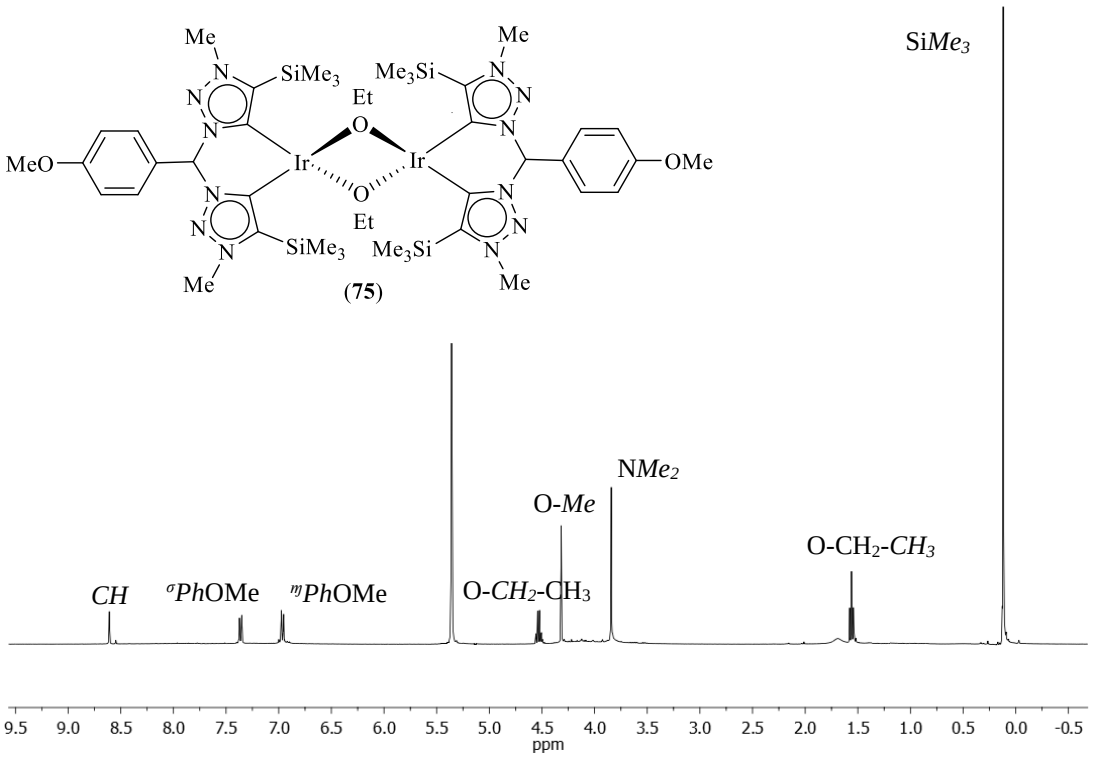

Figure 21. *^{1}H-NMR spectrum for iridium complex **75** in CD_2Cl_2.*

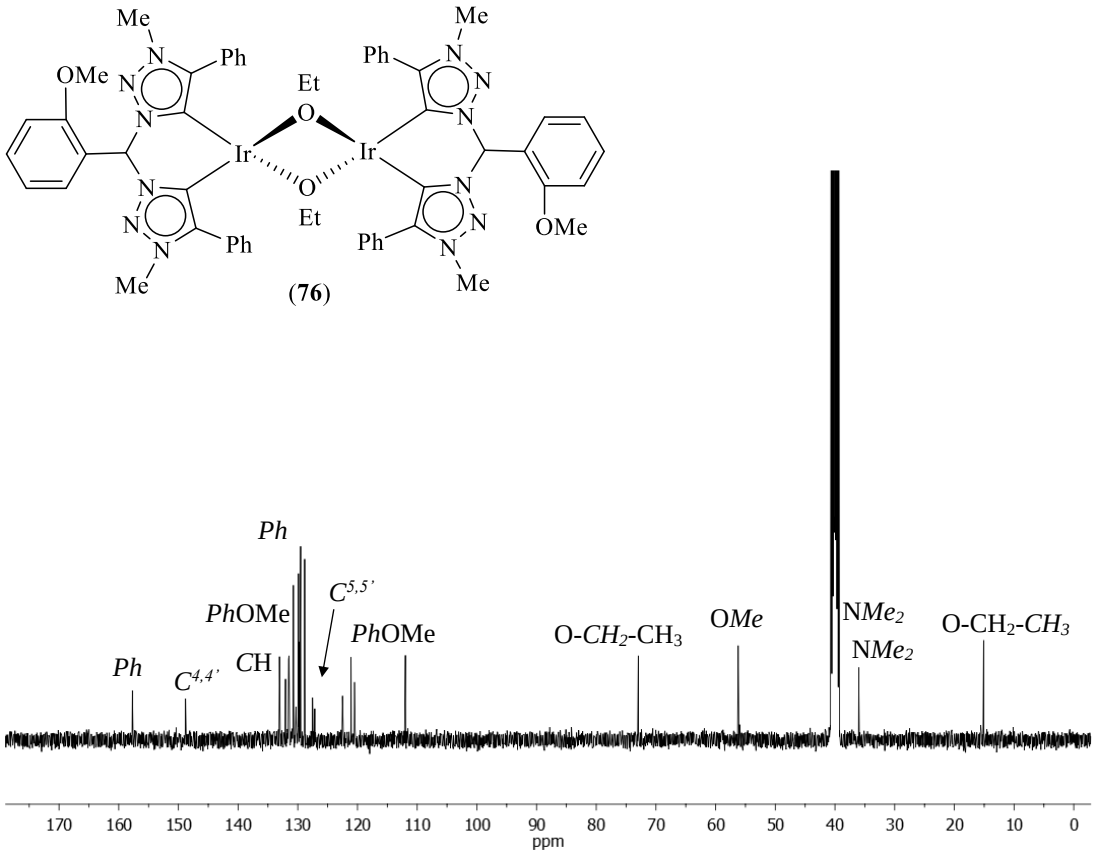

Figure 22. ^{13}C-{^{1}H}-NMR spectrum for iridium complex ***76*** *in DMSO.*

Table 16. *^{1}H-NMR data for iridium complexes **75** and **76**.*

Compound	R^4	MeOPh	N-Me	CH	Ir-OEt
[Ir(OEt){bttz(NMe)$_2$pm}]$_2$ (**75**)[a]	$(CH_3)_3Si$ 0.12 (s, 18H, *CH_3*)	4.32 (s, 3H, O-*CH_3*) 6.96 (d, J_{HH} = 8.8 Hz, 2H, Ph) 7.36 (d, J_{HH} = 8.8 Hz, 2H, Ph)	3.84 (s, 6H)	8.61 (s, 1H)	1.56 (t, J_{HH} = 7 Hz, 3H, O-CH_2-*CH_3*) 4.53 (q, J_{HH} = 7 Hz, 2H, O-*CH_2*-CH_3)
[Ir(OEt){bptz(NMe)$_2$om}]$_2$ (**76**)[b]	Ph 7.71-7.25 (m, 10H)	3.84 (s, 3H, O-CH_3) 7.05 (td, J_{HH} = 7.5 Hz; 1.0 Hz, 1H, Ph) 7.13 (dd, J_{HH} = 8.7 Hz; 0.7 Hz, 1H, Ph) 7.45 (m, 2H, Ar)	4.06 (s, 3H) 4.08 (s, 3H)	7.92 (s, 1H)	1.56 (t, J_{HH} = 7 Hz, 3H, O-CH_2-*CH_3*) 4.53 (q, J_{HH} = 7 Hz, 2H, O-*CH_2*-CH_3)

Spectra recorded in a) CD_2Cl_2 and b) DMSO.

Table 17. *^{13}C-{^{1}H}-NMR data for iridium complexes **75** and **76**.*

Compound	$C^{4,4'}$	R^4	C^5	MeOPh	N-Me	CH	Ir-OEt
[Ir(OEt){bttz(NMe)$_2$pm}]$_2$ (**75**)[a]	152.3	$SiMe_3$ 0.74	123.0	160.8-114.6 (Ph) 41.2 (O-*CH_3*)	55.4	113.5	14.1 (O-CH_2-*CH_3*) 72.8 (O-*CH_2*-CH_3)
[Ir(OEt){bptz(NMe)$_2$om}]$_2$ (**76**)[b]	148.8	Ph 138.0-127.2	127.2 127.5	157.7-112.0 (Ph) 56.2 (O-*CH_3*)	36.0 40.3	133.1	15.1 (O-CH_2-*CH_3*) 73.0 (O-*CH_2*-CH_3)

Spectra recorded in a) CD_2Cl_2 and b) DMSO.

Experimental section

EXPERIMENTAL SECTION

1. Synthesis of precursors

The starting materials bptzpm, bptzom, bttzpm and bttzom have been prepared as previously described in bibliography.[20]

2. Synthesis of bis(1,2,3-triazol-1-yl)methane compounds 58-67

*2.1. Synthesis of bptzpmmabzeH (**58**)*

In a 250cm^3 Schlenk tube, bptzpm (1.50 g, 3.67 mmol) was dissolved in 40 mL of dry THF and cooled down to −78 ºC. Then a solution of ^{n}BuLi (2.40 mL, 3.86 mmol, 1.6M in hexanes) was added, and the mixture was stirred for one hour. The resulting cloudy solution was added dropwise via cannula to a pre-cooled solution containing 4-(dimethylamino)benzaldehyde (0.52 mL, 3.86 mmol) in THF. The mixture was then allowed to warm up at room temperature and left stirring for one hour. After that time, the product was hydrolysed with 15 mL of saturated aqueous NH_4Cl. The organic layer was extracted, dried over $MgSO_4$ and filtered. Removal of the volatiles *in vacuo* afforded a yellowish oil. The oil was further purified by flash chromatography using as eluent hexane/EtOAc in 9:1, 6:1, 3:1 and 1:1 ratio. Compound **58** was isolated as white solid in 70 % yield.

Analysis found:	C: 71.5 %	H: 6.0 %	N: 17.2 %
Calculated:	C: 71.1 %	H: 5.8 %	N: 17.6 %

*2.2 Synthesis of bttzpmmabzeH (**59**)*

The synthesis of compound **59** was carried out following the same experimental procedure as compound **58** using bttzpm (1.5 g, 3.74 mmol), ^{n}BuLi (2.46 ml, 3.93 mmol) and 4-(dimethylamino)benzaldehyde (0.53 mL, 3.93 mmol). Compound **59** was obtained as a white solid in 85% yield. Suitable crystals for X-Ray analysis were obtained from a hexane/EtOAc (1:2) solution.

Analysis found:	C: 59.5 %	H: 7.6 %	N: 17.5 %
Calculated:	C: 59.0 %	H: 7.2 %	N: 17.8 %

*2.3 Synthesis of bptzpmteH (**60**)*

The synthesis of compound **60** was carried out following the same experimental procedure as compound **58** using bptzpm (1.50 g, 3.67 mmol), ^{n}BuLi (2.40 mL, 3.86 mmol) and *p*-tolualdehyde (0.46 mL, 3.86 mmol). Compound **60** was obtained as a white solid in 75% yield. Suitable crystals for X-Ray analysis were obtained from a hexane/EtOAc (1:2) solution.

Analysis found:	C: 72.8 %	H: 5.5 %	N: 15.5 %
Calculated:	C: 72.7 %	H: 5.3 %	N: 15.9 %

*2.4 Synthesis of bttzpmteH (**61**)*

The synthesis of compound **61** was carried out following the same experimental procedure as compound **58** using bttzpm (1.50 g, 3.74 mmol), ^{n}BuLi (2.46 mL, 3.93 mmol) and *p*-tolualdehyde (0.57 mL, 3.93 mmol). Compound **61** was obtained as a white solid in 72% yield.

Analysis found:	C: 60.5 %	H: 7.4 %	N: 15.8 %
Calculated:	C: 60.0 %	H: 7.0 %	N: 16.1 %

*2.5 Synthesis of bttzomteH (**62**)*

The synthesis of compound **62** was carried out following the same experimental procedure as compound **58** using bttzom (1.50 g, 3.74 mmol), ^{n}BuLi (2.46 mL, 3.93 mmol) and *ρ*-tolualdehyde (0.47 mL, 3.93 mmol). Compound **62** was obtained as a white solid in 77% yield. Suitable crystals for X-Ray analysis were obtained from a hexane/EtOAc (1:2) solution.

Analysis found:	C: 60.4 %	H: 7.3 %	N: 15.9 %
Calculated:	C: 60.0 %	H: 7.0 %	N: 16.1 %

*2.6 Synthesis of bptzomteH (**63**)*

The synthesis of compound **63** was carried out following the same experimental procedure as compound **58** using bptzom (1.50 g, 3.67 mmol), ^{n}BuLi (2.40 mL, 3.86 mmol) and *p*-tolualdehyde (0.46 mL, 3.86 mmol). Compound **63** was obtained as a white solid in 69% yield.

Analysis found:	C: 72.9 %	H: 5.7 %	N: 15.6 %
Calculated:	C: 72.7 %	H: 5.3 %	N: 15.9 %

*2.7 Synthesis of bptzpmbeH (**64**)*

The synthesis of compound **64** was carried out following the same experimental procedure as compound **58** using bptzpm (1.50 g, 3.67 mmol), ^{n}BuLi (2.40 mL, 3.86 mmol) and trimethylacetaldehyde (0.42 mL, 3.86 mmol). Compound **64** was obtained as a white solid in 78% yield.

Analysis found:	C: 70.8 %	H: 6.5 %	N: 16.6 %
Calculated:	C: 70.4 %	H: 6.1 %	N: 17.0 %

*2.8 Synthesis of bttzpmbeH (**65**)*

The synthesis of compound **65** was carried out following the same experimental procedure as compound **58** using bttzpm (1.5 g, 3.74 mmol), ^{n}BuLi (2.46 mL, 3.93 mmol) and trimethylacetaldehyde (0.43 mL, 3.93 mmol). Compound **65** was obtained as a white solid in 80% yield.

Analysis found:	C: 57.1 %	H: 8.3 %	N: 17.0 %
Calculated:	C: 56.7 %	H: 7.9 %	N: 17.3 %

*2.9 Synthesis of bttzombeH (**66**)*

The synthesis of compound **66** was carried out following the same experimental procedure as compound **58** using bttzom (1.50 g, 3.74 mmol), ^{n}BuLi (2.46 mL, 3.93 mmol) and trimethylacetaldehyde (0.43 mL, 3.93 mmol). Compound **66** was obtained as a white solid in 75% yield.

Analysis found:	C: 57.2 %	H: 8.4 %	N: 16.9 %
Calculated:	C: 56.7 %	H: 7.9 %	N: 17.3 %

*2.10 Synthesis of bptzpmbeH (**67**)*

The synthesis of compound **67** was carried out following the same experimental procedure as compound **58** using bptzom (1.5 g, 3.67 mmol), ^{n}BuLi (2.40 mL, 3.86 mmol) and trimethylacetaldehyde (0.42 mL, 3.86 mmol). Compound **67** was obtained as a white solid in 81% yield.

Analysis found:	C: 70.6 %	H: 6.4 %	N: 16.5 %
Calculated:	C: 70.4 %	H: 6.1 %	N: 17.0 %

3. Synthesis of quaternised bis(1,2,3-triazol-1-yl)methane compounds

*3.1. Synthesis of bttz(NMe$_2$)pm (**68**)*

To a stirred solution containing bttzpm (0.70 g, 1.75 mmol) in CH_2Cl_2 (30 mL), previously cooled down to −78 ºC, trifluoromethanesulfonate (0.46 mL, 4.10 mmol) was added. The reaction mixture was warmed up to room temperature and left stirring for 16 h. After that time, the solvent was evaporated *in vacuo* affording a yellow-greenish sticky oil. Addition of Et_2O prompted the precipitation of a light green solid corresponding to compound **68**, which was isolated in 80 % yield.

Analysis found:	C: 37.5 %	H: 5.0 %	N: 11.1 %
Calculated:	C: 37.2 %	H: 4.8 %	N: 11.3 %

*3.2. Synthesis of bptz(NMe$_2$)om (**69**)*

The synthesis of compound **69** was carried out following the same experimental procedure as compound **68** using bptzom (0.70 g, 1.72 mmol) and trifluoromethanesulfonate (0.45 mL, 3.94 mmol). Compound **69** was obtained as a light green solid in 87% yield.

Analysis found:	C: 46.6 %	H: 3.8 %	N: 10.9 %
Calculated:	C: 46.5 %	H: 3.6 %	N: 11.2 %

4. Synthesis of alkyl complexes

4.1. Synthesis of alkyl zinc complexes

*4.1.1. Synthesis of [ZnMe{(κ^2-bttzombe)(μ-O)}]$_2$ (**70**)*

In a 100cm^3 Schlenk tube, bttzombeH (**66**) (0.40 g, 0.82 mmol) was dissolved in dry toluene (15 mL) and cooled down to 0 ºC. A solution of $ZnMe_2$ (0.41 mL 0.82 mmol, 2M in hexanes) was then added and the resulting mixture was allowed to warm up to room temperature and stirred for 2 h. The solvent was removed *in vacuo* and the remaining sticky oil was further triturated with *n*-hexane. Alkyl zinc complex **70** was isolated as a white solid in 80% yield.

Analysis found:	C: 50.9 %	H: 7.1 %	N: 14.8 %
Calculated:	C: 50.7 %	H: 6.9 %	N: 15.0 %

*4.1.2. Synthesis of [ZnEt{(κ^2-bttzombe)(μ-O)}]$_2$ (**71**)*

The synthesis of alkyl zinc complex **71** was carried out following the same experimental procedure as complex **70** using bttzombeH (0.40 g, 0.82 mmol) and $ZnEt_2$ (0.82 mL, 1M in hexanes). Complex **71** was obtained as a white crystalline solid in 60% yield. Suitable crystals for X-Ray analysis were obtained from a toluene solution.

Analysis found:	C: 52.0 %	H: 7.4 %	N: 14.3 %
Calculated:	C: 51.8 %	H: 7.3 %	N: 14.5 %

4.2. Synthesis of alkyl aluminium complexes

*4.2.1. Synthesis of [AlMe$_2$}(κ^2-bttzpmmabe)(μ-O)}]$_2$ (**72**)*

In a 100cm^3 Schlenk tube, bttzpmmabeH (**59**) (0.40 g, 0.73 mmol) was dissolved in dry toluene (15 mL) and cooled down to 0 ºC. A solution of $AlMe_3$ (0.37 mL, 0.73 mmol, 2M in hexanes) was then added and the resulting mixture was allowed to warm up at room temperature and stirred for 2 h. The volatiles were then removed *in vacuo* and the resulting solid was washed with *n*-hexane. Alkyl aluminium complex **72** was isolated as a white solid in 70% yield.

Analysis found:	C: 57.7 %	H: 7.5 %	N: 16.0 %
Calculated:	C: 57.5 %	H: 7.3 %	N: 16.2 %

*4.2.2. Synthesis of [AlMe$_2$}(κ^2-bttzpmte)(μ-O}]$_2$ (**73**)*

The synthesis of alkyl aluminium complex **73** was carried out following the same experimental procedure as complex **72** using bttzpmteH (0.40 g, 0.77 mmol) and 0.40 mL of $AlMe_3$ (0.39 mL, 0.77 mmol). Complex **73** was obtained as a white crystalline solid in 65% yield. Suitable crystals for X-Ray analysis were obtained from a toluene/hexane (9:1) solution.

Analysis found:	C: 58.4 %	H: 7.4 %	N: 14.5 %
Calculated:	C: 58.3 %	H: 7.2 %	N: 14.6 %

*4.2.3. Synthesis of [AlMe$_2${(κ^2-bttzombe)(μ-O)}]$_2$ (**74**)*

The synthesis of alkyl aluminium complex **74** was carried out following the same experimental procedure as complex **72** using bttzombeH (0.41 g, 0.82 mmol) and AlMe$_3$ (0.41 mL, 0.82 mmol). Complex **74** was obtained as a white solid in 71% yield.

Analysis found:	C: 55.5 %	H: 8.3 %	N: 15.2 %
Calculated:	C: 55.3 %	H: 8.0 %	N: 15.5 %

5. Synthesis of carbene iridium complexes

*5.1. Synthesis of [Ir(OEt){bttz(NMe$_2$)pm}]$_2$ (**75**)*

A solution of NaH (23.00 mg, 0.95 mmol) in EtOH (10 mL) was transferred via cannula to a suspension of [IrCl(cod)]$_2$ (124.50 mg, 0.18 mmol) in EtOH (10 mL). The reaction mixture was stirred for 30 min at room temperature. Then, bttz(NMe$_2$)pm (**68**) (0.28 g, 0.38 mmol) was added to the mixture at −78 ºC, warmed to room temperature after 10 min, and stirred overnight for 16 h. After that time, volatiles were removed *in vacuo* and the remaining solid was taken up in 50 mL of dichloromethane to extract complex **75**. The resulting suspension was filtered, and the solvent removed affording complex **75** as a brown solid in 80% yield.

Analysis found:	C: 40.0 %	H: 5.9 %	N: 12.4 %
Calculated:	C: 39.7 %	H: 5.6 %	N: 12.6 %

*5.2. Synthesis of [Ir(OEt){bptz(NMe$_2$)om}]$_2$ (**76**)*

The synthesis of iridum carbene complex **76** was carried out following the same experimental procedure as complex **75** using NaH (23.00 mg, 0.95 mmol), [IrCl(cod)]$_2$ (124.50 mg, 0.18 mmol), bptz(NMe$_2$)om (**69**) (0.28 g, 0.38 mmol) and 20 mL of EtOH. Complex **76** was obtained as a brown solid in 75% yield.

Analysis found:	C: 50.2 %	H: 4.4 %	N: 12.4 %
Calculated:	C: 49.9 %	H: 4.3 %	N: 12.5 %

Bibliography

BIBLIOGRAPHY

(1) A. Togni, L. M. Venanzi, *Angew. Chem. Int. Ed.*, **1994**, *33*, 497; *(b)* F. Fache, E. Schulz, M. L. Tommassino, M. Lemaire, *Chem. Rev.*, **2000**, *100*, 2159; *(c)* A. A. Mohamed, *Coord. Chem. Rev.*, **2010**, *254*, 1918.

(2) *(a)* R. Breinbauer, I. R. Vetter, H. Waldmann, *Angew. Chem. Int. Ed.*, **2002**, *41*, 2878; *(b)* I. Paterson, E. A. Anderson, *Science*, **2005**, *310*, 451; *(c)* D. J. Newman, G. M. Cragg, *J. Nat. Prod.*, **2007**, *70*, 461; *(d)* F. E. Koehn, G. T. Carter, *Nat. Rev. Drug Discov.*, **2005**, *4*, 206.

(3) M. Whiting, J. Muldoon, Y. C. Lin, G. Cauvi, C. H. Wong, D. E. McRee, J. H. Elder, C. D. Stout, B. E. TTorbett, *J. Med. Chem.*, **2008**, *51*, 1435.

(4) H.Liu, D. Audisio, L. Plougastel, E. Decuypere, D. A. Buisson, O. Koniev, S. Kolodych, A. Wagner, M. Elhabiri, A. Krzyczmonik, S. Forsback, O. Solin, V. Gouverneur, F. Taran, *Angew. Chem.*, **2016**, *128*, 12252.

(5) S. Sampaio, T. M. R. Miranda, J. G. Santos, G. M. B. Soares, *Polym. Int.*, **2011**, *60*, 1737.

(6) S. Rana, H. J. Yoo, J. W. Cho, B. C. Chun, J. S. Park, *J. App. Polym Sci.*, **2011**, *119*, 31.

(7) L. Xu, W. Wang, D. Yu, *RSC Adv.*, **2017**, *7*, 2044

(8) A. H. Yap, S. M. Weinreb, *Tetrahedron Lett.*, **2006**, *47*, 3035.

(9) J. Hou, X. Liu, J. Shen, G. Zhao, P. G. Wang, *Expert Opin. Drug Discov.*, **2012**, *7*, 489.

(10) R. Huisgen, *Angew. Chem.*, **1963**, *75*, 604.

(11) *(a)* L. Liang, D. Astruc, *Coord. Chem. Rev.*, **2011**, *255*, 2933; *(b)* L. M. Stanley, M. P. Sibi, *Chem. Rev.*, **2008**, *108*, 2887.

(12) M. Albrecht, *Chem. Commun.*, **2008**, 3601.

(13) J. D. Crowley, D. A. McMorran, *Top. Heterocycl. Chem.*, **2012**, *28*, 31.

(14) S. G. A. van Assema, C. G. J. Tazelaar, G. Bas de Jong, J. H. van Maarseveen, M. Schakel, M. Lutz, A. L. Spek, J. C. Slootweg, K. Lammertsma, *Organometallics*, **2008**, *27*, 3210.

(15) K. F. Donelly, A. Petronilho, M. Albretch, *Chem. Commun*., **2013**, *49*, 1145.

(16) P. Mathew, A. Neels, M. Albretch, *J.Am. Chem. Soc*., **2008**, *130*, 13534.

(17) L. A. Schaper, K. Oefele, R. Kadryov, B. Bechlars, M. Drees, M. Cokoja, W. A. Herrmann, F. E. Kuhn, *Inorg. Chem*., **2013**, *52*, 6142.

(18) G. Guisao-barrios, M. Soleilhavoup, G. Bertrand, *Acc. Chem. Res*., **2018**, *51*, 3236.

(19) E. Hübner, N. V. Fischer, F. W. Heinemann, U. Mitra, V. Dremov, P. Müller, N. Burzlaff, *Eur. J. Inorg. Chem*., **2010**, *26*, 4100.

(20) J. A. Castro-Osma, A. Lara-Sanchez, A. Otero, A. M. Rodríguez, M. C. de la Torre, M. A. Sierra, *Eur. J. Org. Chem*., **2016**, *4*, 682.

(21) M. Honrado, S. Sobrino, J. Fernández-Baeza, L. F. Sánchez-Barba, A. Garcés, A. Lara-Sánchez, A. M. Rodríguez, *Chem. Commun*., **2019**, *55*, 8947.

(22) F. de la Cruz-Martínez, M. Martínez de Sarasa Buchaca, J. Fernández-Baeza, L. F. Sánchez-Barba, Ana. M Rodríguez, J. A. Castro-Osma, A. Lara-Sánchez, *Inorg. Chem*., **2021**, *60*, 5322.

(23) M. A. Gaona, F. de la Cruz-Martínez, J. Fernández-Baeza, L. F. Sánchez-Barba, C. Alonso-Moreno, A. M. Rodríguez, A. Rodríguez-Diéguez, J. A. Castro-Osma, A. Otero, A. Lara-Sánchez, *Dalton. Trans*., **2019**, *48*, 4218.

(24) J. Martínez, M. Martínez de Sarasa Buchaca, F. de la Cruz-Martínez, C. Alonso-Moreno, L. F. Sánchez-Barba, J. Fernández-Baeza, A. M. Rodríguez, A. Rodríguez-Diéguez, J. A. Castro-Osma, A. Otero, A. Lara-Sánchez, *Dalton Trans*., **2018**, *47*, 7471.

Conclusions

1. A wide variety of synthetic processes for the preparation of new organometallic entities of group 13 metals such as aluminium, indium and gallium, supported by alkoxide ligands based on the bis(pyrazol-1-yl)methane unit with different ancillary ligands, such as chloride, alkyl, amide and isopropoxide, have been developed.

2. The different families of isolated organometallic group 13 complexes have been characterised by spectroscopic IR and NMR methods. The molecular structures of some of the organometallic complexes have been determined by X-ray diffraction studies.

3. Reactions of the alcohol heteroscorpionate protio-ligands with 1 equivalent of MCl_3 (M = Ga, In) proceed in very high yields to give the neutral alkoxide heteroscorpionate aluminium/gallium complexes $[Al(\kappa^2\text{-NO})]^+[AlCl_4]^-$ (**2**-**5**) and $[Ga(\kappa^3\text{-NNO})]^+[GaCl_4]^-$ (**6**-**9**) with elimination of LiCl.

4. Reactions of the alcohol heteroscorpionate protio-ligands with 1 equivalent of $InCl_3$ proceed in very high yields to give the neutral alkoxide heteroscorpionate indium complexes $[InCl_2\{(\kappa^3\text{-NNO})(\mu\text{-O})\}]_2$ (**10**-**13**) with elimination of LiCl. Crystallization of complex $[InCl_2\{(\kappa^3\text{-bpzbe})(\mu\text{-O})\}]_2$ (**10**) affords the formation of a new complex with one water molecule bridging both indium centres $[\{InCl_2(\kappa^3\text{-bpzbe})\}_2(\mu\text{-}H_2O)]$ (**14**) which was attributed to the presence of small traces of water in solvent.

5. Reactions of the alcohol heteroscorpionate protio-ligand bpzFerrH with 1 equivalent of AlX_3 (X = Me, Et) proceed in very high yields to give the neutral alkoxide heteroscorpionate alkyl aluminium complexes $[AlX_2(\kappa^2\text{-bpzFerr})]$ (**15** and **16**) with vigorous elimination of the corresponding alkane.

6. In-situ reaction of MCl_3 (M = Ga, In) with 3.3 equivalents of MeLi and subsequent reaction with the corresponding alcohol heteroscorpionate protio-ligands proceed in very high yields to afford the neutral alkoxide heteroscorpionate heterobimetallic complexes $[\{Li(\kappa^3\text{-NNO})(Et_2O)\}(\mu\text{-O})\{MMe_2Cl\}]$ (**17**-**20**).

7. In-situ reaction of $GaCl_3$ with 2.2 equivalents of MeLi and subsequent reaction with the corresponding alcohol heteroscorpionate protio-ligands proceed in high yields to afford the neutral alkoxide heteroscorpionate complexes [GaMeCl(κ^3-NNO)] (**21** and **22**).

8. In-situ reaction of $InCl_3$ with 2.2 equivalents of MeLi and subsequent reaction with the corresponding alcohol heteroscorpionate protio-ligands proceed in high yields to afford the neutral alkoxide heteroscorpionate complexes [$InMe_2Cl$(κ^3-NNO)] (**23** and **24**).

9. Reactions of the alcohol heteroscorpionate protio-ligands with 1 equivalent of AlO^iPr_3 proceed in moderate yields to give the neutral alkoxide heteroscorpionate alkoxide aluminium complexes [Al(O^iPr)(κ^2-NO)] (**25** and **26**). X-Ray diffraction studies for complexes **25** and **26** have shown a trigonal bipyramidal structure around aluminium atom.

10. Alkoxide heteroscorpionate amido indium complex [InCl{$N(SiMe_3)_2$}{(κ^3-bpzbe)(μ-O)}]$_2$ (**28**) has been synthetised by reaction of the alcohol heteroscorpionate protio-ligand bpzbeH with 1 equivalent of the corresponding amide indium precursor (**27**).

11. Previously reported heteroscorpionate alkyl aluminium alkoxide (**30**-**35**) and acetamidate (**37**-**40**) complexes have been proven to be effective catalyst for the ring opening copolymerisation (ROCOP) of epoxides and cyclic anhydrides using low catalyst loadings under mild reaction conditions. Thus, different polyesters have been prepared, including poly(limonene succinate), which has never been reported before.

12. The synthesis of polycarbonate materials from epoxides and CO_2 has been studied using some of the complexes synthesised in this dissertation as catalysts. Thus, chloride complexes **2**-**14** and indium complexes **18**, **23** and **28** have been found active for the ROCOP of cyclohexene oxide and CO_2 without the use of a co-catalyst under mild reaction conditions and low pressure of CO_2. Amongst them, complex **10** has been found to be the most active and selective for the process.

13. Complex **10** has also been tested as catalyst for the terpolymerisation of epoxides, CO_2, and phthalic anhydride or *L*-lactide. It has shown no activity towards the synthesis of polycarbonate when phthalic anhydride was used. On the other hand, it afforded the synthesis of block copolymers poly(cyclohexene carbonate)-polylactide with different compositions in the polymer structure.

14. The polyaddition reaction of petroleum-based bis(glycidyl ether carbonate) and a wide range of diamines with different steric and electronic properties to synthesise non-isocyanate polyurethanes has been carried out. Similarly, reactions using different bis(cyclic carbonate) and diamine ratios have been carried out affording the formation of hydroxycarbamates compounds.

15. The polyaddition reaction of bio-based bis(glutaryl carbonate) and bis(carvyl acetate carbonate) and different diamines has also been explored. Thus, different firstly reported PHUs have been synthesised and characterised. Similarly, hydroxycarbamates derived from bis(carvyl acetate carbonate) have also been synthesised using different bis(carvyl acetate carbonate)/diamine ratios.

16. New alcohol heteroscorpionate protio-ligands based on bis(1,2,3-triazol-1-yl)methane moieties (**58**-**67**) have been synthesised and their coordination ability as NNO donors has been tested against ZnR_2 (R= Me, Et) and $AlMe_3$ for the preparation of alkyl zinc [ZnMe{(κ^2-bttzombe)(μ-O}]$_2$ (**70**) and [ZnEt{(κ^2-bttzombe)(μ-O}]$_2$ (**71**) complexes and alkyl aluminium [$AlMe_2${(κ^2-NO)(μ-O}]$_2$ (**72**-**74**) complexes with vigorous elimination of the corresponding alkane.

17. Two bis(1,2,3-triazol-1-yl)methane compounds have been reacted with methyl triflate affording quaternised compounds **68** and **69**. The coordination ability of these compounds has been studied for the preparation of *abnormal* N-heterocyclic carbene iridium [Ir(OEt){bttz(NMe_2)pm}] (**75**) and [Ir(OEt){bptz(NMe_2)om}] (**76**) complexes.